



National Library
of Canada

Acquisitions and
Bibliographic Services Branch

395 Wellington Street
Ottawa, Ontario
K1A 0N4

Bibliothèque nationale
du Canada

Direction des acquisitions et
des services bibliographiques

395, rue Wellington
Ottawa (Ontario)
K1A 0N4

Your file *Votre référence*

Our file *Notre référence*

NOTICE

The quality of this microform is heavily dependent upon the quality of the original thesis submitted for microfilming. Every effort has been made to ensure the highest quality of reproduction possible.

If pages are missing, contact the university which granted the degree.

Some pages may have indistinct print especially if the original pages were typed with a poor typewriter ribbon or if the university sent us an inferior photocopy.

Reproduction in full or in part of this microform is governed by the Canadian Copyright Act, R.S.C. 1970, c. C-30, and subsequent amendments.

AVIS

La qualité de cette microforme dépend grandement de la qualité de la thèse soumise au microfilmage. Nous avons tout fait pour assurer une qualité supérieure de production.

S'il manque des pages, veuillez communiquer avec l'université qui a conféré le grade.

La qualité d'impression de certaines pages peut laisser à désirer, surtout si les pages originales ont été dactylographiées à l'aide d'un ruban usé ou si l'université nous a fait parvenir une photocopie de qualité inférieure.

La reproduction, même partielle, de cette microforme est soumise à la Loi canadienne sur le droit d'auteur, SRC 1970, c. C-30, et ses amendements subséquents.

UNIVERSITY OF ALBERTA

DESIGN OF TUNNELS CONSTRUCTED USING PRESSURIZED SHIELD
METHODS

by

OMAR YOUSSEF EZZELDINE



A THESIS

SUBMITTED TO THE FACULTY OF GRADUATE STUDIES AND RESEARCH IN
PARTIAL FULFILLMENT OF THE REQUIREMENTS FOR THE DEGREE OF
DOCTOR OF PHILOSOPHY

DEPARTMENT OF CIVIL ENGINEERING

EDMONTON, ALBERTA

Spring 1995



National Library
of Canada

Acquisitions and
Bibliographic Services Branch

395 Wellington Street
Ottawa, Ontario
K1A 0N4

Bibliothèque nationale
du Canada

Direction des acquisitions et
des services bibliographiques

395, rue Wellington
Ottawa (Ontario)
K1A 0N4

Your file *Voire référence*

Our file *Notre référence*

THE AUTHOR HAS GRANTED AN IRREVOCABLE NON-EXCLUSIVE LICENCE ALLOWING THE NATIONAL LIBRARY OF CANADA TO REPRODUCE, LOAN, DISTRIBUTE OR SELL COPIES OF HIS/HER THESIS BY ANY MEANS AND IN ANY FORM OR FORMAT, MAKING THIS THESIS AVAILABLE TO INTERESTED PERSONS.

L'AUTEUR A ACCORDE UNE LICENCE IRREVOCABLE ET NON EXCLUSIVE PERMETTANT A LA BIBLIOTHEQUE NATIONALE DU CANADA DE REPRODUIRE, PRETER, DISTRIBUER OU VENDRE DES COPIES DE SA THESE DE QUELQUE MANIERE ET SOUS QUELQUE FORME QUE CE SOIT POUR METTRE DES EXEMPLAIRES DE CETTE THESE A LA DISPOSITION DES PERSONNE INTERESSEES.

THE AUTHOR RETAINS OWNERSHIP OF THE COPYRIGHT IN HIS/HER THESIS. NEITHER THE THESIS NOR SUBSTANTIAL EXTRACTS FROM IT MAY BE PRINTED OR OTHERWISE REPRODUCED WITHOUT HIS/HER PERMISSION.

L'AUTEUR CONSERVE LA PROPRIETE DU DROIT D'AUTEUR QUI PROTEGE SA THESE. NI LA THESE NI DES EXTRAITS SUBSTANTIELS DE CELLE-CI NE DOIVENT ETRE IMPRIMES OU AUTREMENT REPRODUITS SANS SON AUTORISATION.

ISBN 0-612-01688-9

Canada

Name OMAR YOUSSEF FZELDINE

Dissertation Abstracts International is arranged by broad, general subject categories. Please select the one subject which most nearly describes the content of your dissertation. Enter the corresponding four-digit code in the spaces provided.

CIVIL ENGINEERING

SUBJECT TERM

0543

SUBJECT CODE

U·M·I

Subject Categories

THE HUMANITIES AND SOCIAL SCIENCES

COMMUNICATIONS AND THE ARTS

Architecture	0729
Art History	0377
Cinema	0900
Dance	0378
Fine Arts	0357
Information Science	0723
Journalism	0391
Library Science	0399
Mass Communications	0708
Music	0413
Speech Communication	0459
Theater	0465

EDUCATION

General	0515
Administration	0514
Adult and Continuing	0516
Agricultural	0517
Art	0273
Bilingual and Multicultural	0282
Business	0688
Community College	0275
Curriculum and Instruction	0272
Early Childhood	0518
Elementary	0524
Finance	0277
Guidance and Counseling	0519
Health	0680
Higher	0745
History of	0520
Home Economics	0278
Industrial	0521
Language and Literature	0279
Mathematics	0280
Music	0522
Philosophy of	0998
Physical	0523

Psychology	0525
Reading	0535
Religious	0527
Sciences	0714
Secondary	0533
Social Sciences	0534
Sociology of	0340
Special	0529
Teacher Training	0530
Technology	0710
Tests and Measurements	0288
Vocational	0747

LANGUAGE, LITERATURE AND LINGUISTICS

Language	
General	0679
Ancient	0289
Linguistics	0290
Modern	0291
Literature	
General	0401
Classical	0294
Comparative	0295
Medieval	0297
Modern	0298
African	0316
American	0591
Asian	0305
Canadian (English)	0352
Canadian (French)	0355
English	0593
Germanic	0311
Latin American	0312
Middle Eastern	0315
Romance	0313
Slavic and East European	0314

PHILOSOPHY, RELIGION AND THEOLOGY

Philosophy	0422
Religion	
General	0318
Biblical Studies	0321
Clergy	0319
History of	0320
Philosophy of	0322
Theology	0469

SOCIAL SCIENCES

American Studies	0323
Anthropology	
Archaeology	0324
Cultural	0326
Physical	0327
Business Administration	
General	0310
Accounting	0272
Banking	0770
Management	0454
Marketing	0338
Canadian Studies	0385
Economics	
General	0501
Agricultural	0503
Commerce-Business	0505
Finance	0508
History	0509
Labor	0510
Theory	0511
Folklore	0358
Geography	0366
Gerontology	0351
History	
General	0578

Ancient	0579
Medieval	0581
Modern	0582
Black	0328
African	0331
Asia, Australia and Oceania	0332
Canadian	0334
European	0335
Latin American	0336
Middle Eastern	0333
United States	0337
History of Science	0585
Law	0398
Political Science	
General	0615
International Law and Relations	0616
Public Administration	0617
Recreation	0814
Social Work	0452
Sociology	
General	0626
Criminology and Penology	0627
Demography	0938
Ethnic and Racial Studies	0631
Individual and Family Studies	0628
Industrial and Labor Relations	0629
Public and Social Welfare	0630
Social Structure and Development	0700
Theory and Methods	0344
Transportation	0709
Urban and Regional Planning	0999
Women's Studies	0453

THE SCIENCES AND ENGINEERING

BIOLOGICAL SCIENCES

Agriculture	
General	0473
Agronomy	0285
Animal Culture and Nutrition	0475
Animal Pathology	0476
Food Science and Technology	0359
Forestry and Wildlife	0478
Plant Culture	0479
Plant Pathology	0480
Plant Physiology	0817
Range Management	0777
Wood Technology	0746
Biology	
General	0306
Anatomy	0287
Biostatistics	0308
Botany	0309
Cell	0379
Ecology	0329
Entomology	0353
Genetics	0369
Limnology	0793
Microbiology	0410
Molecular	0307
Neuroscience	0317
Oceanography	0416
Physiology	0433
Radiation	0821
Veterinary Science	0778
Zoology	0472
Biophysics	
General	0786
Medical	0760
EARTH SCIENCES	
Biogeochemistry	0425
Geochemistry	0996

Geodesy	0370
Geology	0372
Geophysics	0373
Hydrology	0388
Mineralogy	0411
Paleobotany	0345
Paleoecology	0426
Paleontology	0418
Paleozoology	0985
Palaology	0427
Physical Geography	0368
Physical Oceanography	0415

HEALTH AND ENVIRONMENTAL SCIENCES

Environmental Sciences	0768
Health Sciences	
General	0566
Audiology	0300
Chemotherapy	0992
Dentistry	0567
Education	0350
Hospital Management	0769
Human Development	0758
Immunology	0982
Medicine and Surgery	0564
Mental Health	0347
Nursing	0569
Nutrition	0570
Obstetrics and Gynecology	0380
Occupational Health and Therapy	0354
Ophthalmology	0381
Pathology	0571
Pharmacology	0419
Pharmacy	0572
Physical Therapy	0382
Public Health	0573
Radiology	0574
Recreation	0575

Speech Pathology	0460
Toxicology	0383
Home Economics	0386

PHYSICAL SCIENCES

Pure Sciences	
Chemistry	
General	0485
Agricultural	0749
Analytical	0486
Biochemistry	0487
Inorganic	0488
Nuclear	0738
Organic	0490
Pharmaceutical	0491
Physical	0494
Polymer	0495
Radiation	0754
Mathematics	0405
Physics	
General	0605
Acoustics	0986
Astronomy and Astrophysics	0606
Atmospheric Science	0608
Atomic	0748
Electronics and Electricity	0607
Elementary Particles and High Energy	0798
Fluid and Plasma	0759
Molecular	0609
Nuclear	0610
Optics	0752
Radiation	0756
Solid State	0611
Statistics	0463
Applied Sciences	
Applied Mechanics	0346
Computer Science	0984

Engineering	
General	0537
Aerospace	0538
Agricultural	0539
Automotive	0540
Biomedical	0541
Chemical	0542
Civil	0543
Electronics and Electrical	0544
Heat and Thermodynamics	0348
Hydraulic	0545
Industrial	0546
Marine	0547
Materials Science	0794
Mechanical	0548
Metallurgy	0743
Mining	0551
Nuclear	0552
Packaging	0549
Petroleum	0765
Sanitary and Municipal	0554
System Science	0790
Geotechnology	0428
Operations Research	0796
Plastics Technology	0795
Textile Technology	0994

PSYCHOLOGY

General	0621
Behavioral	0384
Clinical	0622
Developmental	0620
Experimental	0623
Industrial	0624
Personality	0625
Physiological	0989
Psychobiology	0349
Psychometrics	0632
Social	0451



UNIVERSITY OF ALBERTA

RELEASE FORM

NAME OF AUTHOR	Omar Youssef Ezzeldine
TITLE OF THESIS	Design of Tunnels Constructed using Pressurized Shield Methods
DEGREE FOR WHICH THESIS WAS PRESENTED	Doctor of Philosophy
YEAR THIS DEGREE GRANTED	Spring 1995

Permission is hereby granted to THE UNIVERSITY OF ALBERTA LIBRARY to produce single copies of this thesis and to lend or sell such copies for private, scholarly or scientific research purposes only.

The author reserves other publication rights, and neither the thesis nor extensive extracts from it may be printed or otherwise reproduced without the author's written permission.

.....*Omar Y Ezzeldine*.....

PERMANENT ADDRESS:
3- Mossadak Street, Giza, Cairo
Egypt

DATED ..*November, 9th*..... 1994

UNIVERSITY OF ALBERTA
FACULTY OF GRADUATE STUDIES AND RESEARCH

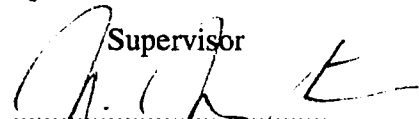
The undersigned certify that they have read, and recommend to the Faculty of Graduate Studies and Research, for acceptance, a thesis entitled *Design of Tunnels Constructed using Pressurized Shield Methods* submitted by Orr - Youssef Ezzeldine in partial fulfillment of the requirements for the degree of Doctor of Philosophy

Dr. Z. Eisenstein




Supervisor

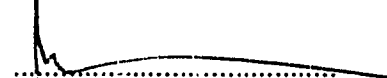
Dr. N. Morgenstern



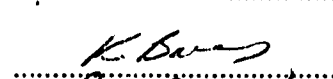
Dr. D. Chan



Dr. A. Elwi



Dr. K. Barron



Dr. B. Ladanyi



External Examiner

Date: October 12th, 1994

ABSTRACT

Pressurized tunnelling methods have reached a satisfactory degree of achievement as they provide a support to all the boundaries of the excavation during the entire construction process. Three methods constitute the main branches of the pressurized tunnelling technology: the compressed air method, the bentonite slurry shield method, and the earth pressure balanced shield method.

The applicability of these methods extends over a wide range of construction conditions. Through various site conditions, the objectives of pressurized tunnelling methods are to provide adequate control of the displacement at the ground surface, to maintain the integrity of the excavation boundaries, and to select the lining system adequate for the loading conditions imposed on it.

In general, the control over ground conditions during excavation is achieved through two phases: the stability of the face of the excavation, and the ground control behind the shield. A finite element analysis is carried out to assess the required pressure to be applied at the face for different mechanical properties of the ground. Three-dimensional and axisymmetric schemes are used in the study. The results of the analysis are compared, with satisfactory degree of agreement, with experimental studies, with other similar numerical analyses, and with actual case histories.

The stress-strain field related to the construction process is analyzed using three-dimensional finite element analysis. Along with parameters affecting soil behaviour, two main straining actions are related to the construction process: the grout pressure and the liner pressure. The purpose of the grout pressure is to fill the void behind the tail of the shield. The liner pressure is the longitudinal pressure applied by the shield on the liner as a reaction to the advance of the excavation. While the liner pressure enhances the face stability, high liner pressure may result in an excessive ground movement behind the shield tail.

The results of the two analyses are presented in a generalized form using the framework previously established by Eisenstein-Negro's method of tunnel design. The proposed design method is compared to an actual case history in Edmonton.

DEDICATION

I dedicate this work to my mother,
Prof. Amira Matar

ACKNOWLEDGMENTS

I am indebted to my supervisor, Prof. Z. Eisenstein, for his support and guidance throughout this research programme. His continuous encouragement made this work possible.

The research was supported by a grants from the National Sciences and Engineering Research Council of Canada to Prof. Eisenstein.

I wish to thank Dr. D. Chan for his invaluable help by providing me with the computer code necessary for the implemented numerical analysis. I also thank him for his numerous suggestions regarding the various numerical simulations.

Prof. N.R. Morgenstern is to be credited for his suggestions and for directing my interest on the effect of the initial stress field in the ground on the face stability on the tunnels. Such effect was noticed from actual case history.

Dr. Flavio Kuwajima was kind enough to offer me his sincere help both technically and at the personal level. I am proud and thrilled with his friendship and I wish to maintain it despite the long distances separating us.

Dr. Heinrich Heinz helped me with his advises in revising some parts of the thesis. His suggestions had major effect in essential direction of the line of research. The moral support he provided me was immensely helpful to me during the long period of research.

Mrs. Isobel Mailloux undertook the heavy task of editing the thesis. She was fantastic in coming to my help in such a short notice and correcting my first draft. Her excellent work cannot be appreciated unless one could see the first versions of this thesis which is, unfortunately (and fortunately to me), now, impossible.

My friend Sam Proskin, his wife Moira and his daughter Bryna provided me an unconditional friendship and were, during my long period of estrangement, a second family to me. I especially remember with gratitude their support to me during some very difficult moment. I remember also with pleasure their initiatives in showing me different part of the immense Canada. While I was discovering the greatness of the space, I was also discovering the greatness of the people.

Dr. F. El-Nahas and Mr. G.R. Flint were kind enough to provide me with the data regarding the Cairo Tunnel Project. I am especially grateful to Dr. F. El-Nahas for

personally presenting our paper at the Cairo Conference in 1991 when special circumstances precluded Prof. Eisenstein and me from going to Egypt.

Dr. R.N. Taylor , from the City University, G.B., kindly responded to me and provided me with the data regarding the Tilbury tunnel.

Finally, I wish to thank my mother, Prof. Amira Matar, and my sister, Dr. Manar Ezzeldine, for their support to me and their uninterrupted love and care they managed to send to me across the very long distances.

TABLE OF CONTENTS

Chapter	Page
1. INTRODUCTION.....	1
2. METHODS OF PRESSURIZED SHIELD TUNNELLING.....	4
2.1 Introduction.....	4
2.2 Historical Background-Brunel's Tunnel.....	4
2.3 Classification of Pressurized Tunnelling Shield Methods.....	5
2.3.1 Basic Features of different Pressurized Shield Methods.....	6
2.3.2 Equipment of Tunnelling Methods.....	6
2.3.2.1 Equipment of the Bentonite Slurry Shield.....	7
2.3.2.1.1 The Shield.....	10
2.3.2.1.2 The Lining System.....	10
2.3.2.1.3 The Tail Seal.....	14
2.3.2.1.4 The Slurry.....	14
2.3.2.1.5 The Grout.....	16
2.3.2.1.6 The Treatment Plant.....	17
2.3.2.1.7 The Control System.....	17
2.3.2.2 The Earth Pressure Balanced Shield.....	19
2.3.2.2.1 The Shield.....	19
2.3.2.2.2 The Auger.....	22
2.3.2.2.3 The Lining System and the Tail Void.....	23
2.3.2.2.4 The Control System.....	23
2.3.2.3 The Compressed Air Shield.....	24
2.3.2.3.1 The Shield.....	24
2.3.2.3.2 The Locks.....	26
2.3.2.3.3 The Compressor Plant.....	28
2.3.2.3.4 The Control System.....	28
2.3.2.3.5 Tail Seal, Lining System and Grout.....	28
2.3.2.4 Other Methods.....	29
2.3.2.4.1 Pipe-jacking.....	29
2.3.2.4.2 The Multiface Method.....	39
2.3.2.4.3 The Injectoshield Method.....	39
2.4 Performance of Pressurized Shields.....	40

2.4.1	Requirements for Satisfactory Tunnelling.....	40
2.4.2	Applicability of Pressurized Shields.....	41
2.4.2.1	The Bentonite Slurry Shield.....	42
2.4.2.1.1	Historical Background.....	42
2.4.2.1.2	The Hydrosield.....	43
2.4.2.1.3	The Japanese Bentonite Shield.....	47
2.4.2.2	The Earth Pressure Balanced Shield.....	49
2.4.2.2.1	Historical Background.....	49
2.4.2.2.2	The Conventional EPBS.....	50
2.4.2.2.3	The Mud Pressurized Shield.....	52
2.4.2.3	the Compressed Air Shield.....	53
2.5	Factors Affecting the Selection of Tunnelling Methods.....	55
2.5.1	Comparison between Pressurized Shields and other Tunnelling Methods.....	55
2.5.2	Comparison between Pressurized Shields.....	56
2.6	Conclusions.....	57
3.	FACE STABILITY OF TUNNELS CONSTRUCTED USING PRESSURIZED SHIELD METHODS.....	59
3.1	Introduction.....	59
3.2	Safety Requirements for the Face of Excavation.....	60
3.3	Idealized Face Stability.....	60
3.3.1	Concept of Stress Relief.....	60
3.3.1.1	Stress Path Associated with Stress Relief.....	61
3.3.1.2	Effect of Confinement on Stress Relief.....	63
3.3.2	Methods of Face Support.....	67
3.3.2.1	The Bentonite Slurry Shield.....	68
3.3.2.2	The Earth Pressure Balanced Shield.....	69
3.3.2.3	The Compressed Air Shield.....	69
3.3.4	Stress Paths for Different Face Support Techniques.....	72
3.4	Face Stability Analyses.....	75
3.4.1	Empirical Analysis.....	77
3.4.2	Physical Models.....	78
3.4.3	Limit Theorems of Plastic Analysis.....	83
3.4.3.1	Lower-Bound Solutions.....	83
3.4.3.2	Upper-Bound Solutions.....	88

3.4.3.3	Comparisons between Limit Theorems of Plastic Analyses and Physical Models.....	88
3.4.4	Stability Analysis.....	95
3.4.5	Numerical Analyses.....	95
3.5	Applied Numerical Models.....	97
3.5.1	Statement of the Problem.....	97
3.5.2	Finite Element Models.....	97
3.5.2.1	Axisymmetric Models.....	98
3.5.2.2	Three-dimensional Models.....	102
3.5.3	Analysis of the Results.....	115
3.5.3.1	Degree of Overstressing.....	118
3.5.3.2	Stress Path.....	136
3.5.3.3	Confinement Ratio.....	146
3.5.3.4	Design Criterion.....	148
3.5.4	Verification of Results.....	152
3.5.4.1	Comparison with Experimental results.....	152
3.5.4.2	Comparison with Case Histories.....	156
3.6	The Effect of the Initial Stress Field.....	163
3.6.1	The St. Clair River Project.....	163
3.6.1.2	Ground Conditions.....	164
3.6.1.3	Construction Details.....	164
3.6.2	Numerical Analysis.....	164
3.6.2.1	Ground Model.....	165
3.6.2.2	Computational Work.....	165
3.6.3	Results.....	174
3.7	Conclusions.....	174
4.	STRESS AND STRAIN FIELDS AROUND TUNNELS EXCAVATED USING PRESSURIZED SHIELD METHODS.....	177
4.1	Introduction.....	177
4.2	Concept of Volume Loss.....	178
4.2.1	Volume Loss at the Tunnel.....	178
4.2.2	Displacement and Strains Induced by Volume Loss at the Tunnel.....	178
4.2.2.1	Empirical Description of Settlement Trough.....	179
4.2.2.2	Semi-Empirical Analyses.....	179

4.2.3	Evaluation of Parameters Describing	
	Volume Losses at and around the Tunnel.....	181
4.2.3.1	Volume Loss at the Tunnel.....	184
4.2.3.2	The Trough Width.....	187
4.2.3.3	Volume of Settlement Trough at The ground surface.....	188
4.3	Idealized Stress Field around an Opening.....	189
4.3.1	The Effect of Tunnel Depth.....	189
4.3.2	The Effect of the Delay Distance.....	190
4.3.3	Stress Paths related to Tunnel Excavation.....	192
4.4	Idealized Strain Field around an Opening.....	192
4.4.1	Strain Field near Excavation Boundary.....	194
4.4.2	Strain Field around the Fxcavation.....	196
4.5	Stress Strain Modeling.....	200
4.5.1	Ground Reaction Curves for	
	Conventional Tunnelling-Eisenstein Negro Method.....	200
4.5.2	Ground Reaction Curves for Tunnels Constructed	
	using Pressurized Shield Methods.....	203
4.6	Concept of Interaction at Construction Phase.....	206
4.6.1	Overall Equilibrium of Forces.....	207
4.6.2	Internal Equilibrium of Forces of the Excavation.....	209
4.7	Numerical Analysis.....	210
4.7.1	Statement of the Problem.....	210
4.7.2	Background.....	210
4.7.3	Description of computational work.....	212
4.7.3.1	Choice of Parameters.....	212
4.7.3.2	Finite Element Meshes.....	214
4.7.3.3	Simulation of Excavation Steps.....	214
4.7.4	Results.....	221
4.7.4.1	Ground Deformation.....	221
4.7.4.2	Mean Stress Changes.....	238
4.7.4.3	Mobilized Shear Strengths.....	238
4.7.4.4	Stress Paths.....	253
4.7.5	Analysis.....	272
4.7.5.1	Methodology.....	272
4.7.5.2	Surface Displacement.....	272
4.7.5.2	Displacement at the Crown.....	272

4.7.5.3	Stress Ratio.....	274
4.7.5.4	The Deviatoric Stress Ratio.....	274
4.7.6	Verification.....	279
4.8	Conclusions.....	279
5.	DESIGN METHOD FOR TUNNELS CONSTRUCTED USING PRESSURIZED SHIELD METHODS.....	292
5.1	Introduction.....	292
5.2	Framework.....	293
5.3	Tunnel Lining Design.....	293
5.3.1	Loading Conditions before Ground-liner interaction Stage.....	294
5.3.2	Structural Models for Tunnel Design.....	300
5.3.2.1	Elastic Continuum Model.....	300
5.3.2.2	Elastic Continuum Model with Predefined Mode of Deformation (Muir Wood's model).....	306
5.3.2.3	Ring-and-Spring Model.....	306
5.3.3	Adaptation of Hartmann's Solution to Eisenstein-Negro Method of Tunnel Design.....	307
5.4	Two Dimensional Stress and Strain Fields due to Tunnelling: Twice Normalized Ground Reaction Curves according to the Eisenstein-Negro Method.....	307
5.5	Ground-Liner Interaction.....	313
5.6	Design Method for Tunnels Constructed using Pressurized Shield Methods.....	314
5.6.1	The Three-dimensional Effects.....	315
5.6.1.1	The Three-dimensional Effect on Stress Changes.....	315
5.6.1.2	The Three-dimensional Effect on Surface Movement.....	324
5.6.1.3	Limitations of the Evaluations of the Three-dimensional Effects.....	324
5.6.2	Evaluation of Stress Changes and Surface Displacement at Plane Strain Condition.....	327
5.6.3	The use of Eisenstein-Negro Method in the Design Method... ..	328
5.6.4	The Plane Strain Model.....	329
5.6.5	The Design Method.....	330
5.7	Application: Edmonton LRT Tunnel.....	334
5.7.1	Ground Conditions.....	334

5.7.2	Construction Details.....	337
5.7.3	Algorithm of the Design Method.....	343
5.7.4	Detailed Numerical Example.....	345
5.7.5	Validation of the Results.....	347
5.8	Conclusions.....	351
6.	CONCLUSIONS.....	352
	REFERENCES.....	357
	Appendix A: Lower and Upper Bound	
	Solutions for Face Stability Problems	372
	Appendix B: Distribution of Normalized	
	Surface Movement due to Three-dimensional	
	Action in the Transversal Plane.....	376
	Appendix C: Input File for the Edmonton LRT Example.....	395
	Appendix D: Output File for the Edmonton LRT Example.....	396
	Appendix E: FORTRAN Program for the	
	Design of Shallow Tunnels constructed	
	using Pressurized Shield Methods.....	403

LIST OF TABLES

Table		Page
2.1	Case Histories of Tunnelling Projects using Pressurized Shields.....	30
3.1	Values of Paramete N_{γ} in Equation 3.14 (Leca and Dormieux, 1990: Figure 7).....	89
3.2	Comparison between Predicted and Measured Pressures at Failure- Upper Bound Solution. (Leca and Dormieux, 1990: Table 2).....	92
3.3	Comparison between Predicted and Measured Pressures at Failure- Two-Spiral Plane Strain Configuration (Chambon and Corté, 1990: Figure 15).....	93
3.4	Comparison between Predicted and Measured Pressures at Failure- One-Spiral Plane Strain Configuration (Chambon and Corté, 1990: Figure 4).....	93
3.5	Parameters used for Axisymmetric Finite Element Analysis of Tunnel Face Stability.....	100
3.6	Parameters used for Three-dimensional Finite Element Analysis of Tunnel Face Stability.....	101
3.7	Assessment of Factors of Safety of some Case Histories in Cohesive Soils.....	159
3.8	Assessment of Factors of Safety of some Case Histories in Frictional Soils.....	160
3.9	Steps Performed at the 3-D Analysis of St. Clair River Tunnel.....	170
4.1	Executed Finite Element Runs of Three-dimensional Analysis of a Tunnel Constructed using a Pressurized Shield Method.....	213
4.2	Regression Coefficients for Ground Movement Expressions w_s and w_c	275
4.3	Regression Coefficients for Stress Ratio, S.R. Expression	276
4.4	Regression Coefficients for Deviatoric Stress Ratio, D.S.R. Expression	280

Table		Page
5.1	Curve Fitting Coefficients <i>ar</i> of the Stress Ratio, S.R.....	316
5.2	Curve Fitting Coefficients <i>ad</i> of the Deviatoric Stress Ratio, D.S.R.....	317
5.3	Curve Fitting Coefficients $\bar{\omega}_s$ of Ground Surface Displacement.....	325
5.4	Soil Properties at Edmonton LRT Site (after PCL- Hochtief 1988).....	338

LIST OF FIGURES

Figure		Page
2.1	The Bentonite Slurry Shield.....	8
2.2	The Bentonite Slurry Shield-the Hydrosield.....	9
2.3	Precast Concrete Segmental Liner.....	12
2.4	Construction Sequence of Reinforced Extruded Concrete Liner.....	13
2.5	Tail Seals for Bentonite Slurry Shields.....	15
2.6	Treatment Plant for the Hydrosield.....	18
2.7	The Earth Pressure Balanced Shield.....	20
2.8	Some Mechanical Arrangements of Earth Pressure Balanced Shields (modified after Nishitake, 1990).....	21
2.9	The Compressed Air Shield.....	25
2.10	Compressed Air Locks used in Tunnelling Works.....	27
2.11	Grain Size Distribution of Granular Materials encountered during Tunnel Construction using the Bentonite Slurry Shield.....	45
3.1	Two Different Stress Paths (modified after Burland and Fouries, 1985).....	62
3.2	Stress Paths Investigated by Medeiros and Eisenstein (1983).....	62
3.3	Stress Paths related to various degrees of Confinement.....	65
3.4	Movement at the Face of an EPBS (modified Finno, 1983).....	70
3.5	Estimation of Air Front Zone during Tunnelling with Compressed Air, Cairo Sewage Project.....	73
3.6	Effect of Bentonite Slurry on the Stress Distribution at the Tunnel Face.....	74
3.7	Effect of Face Support Method on the Stress Distribution at the Tunnel Face for Cases of Compressed Air Shield and Earth Pressure Balanced Shield.....	76
3.8	Overload Factor, OF versus the Depth Ratio from Physical Models on Cohesive Soils.....	80

Figure		Page
3.9	Failure Mechanisms at the Tunnel Face in Cohesive and Frictional Materials according to Experimental Results.....	81
3.10	a) Critical Face Pressure versus Depth Ratio from Centrifuge Tests on Non Cohesive Soils (after Chambon et. al. 1991). b) Critical Face Pressure versus Tunnel Diameter from Centrifuge Tests on Non Cohesive Soils (after Chambon et. al. 1991).....	82
3.11	Different Configurations of Limit Theorems of Plastic Analysis used to Estimate Face Stability.....	84
3.12	Upper Bound Solutions for Non Cohesive Soils.....	90
3.13	Upper and Lower Bound Solutions for Cohesive Soils (modified after Heinz 1988).....	91
3.14	Comparison between Centrifuge Results and Lower Bound Solutions for Non Cohesive Soils (Loose Sand).....	94
3.15	Comparison between Centrifuge Results and Lower Bound Solutions for Non Cohesive Soils (Dense Sand).....	94
3.16	Some Axisymmetric Finite Element Meshes used for Tunnel Face Stability Analyses.....	99
3.17	Parameter of Face Displacement, Ω , versus Face Pressure Ratio, PF, for various values of Angle of Internal Friction, ϕ , $\gamma= 10 \text{ kN/m}^3$, $K_0= 0.6$ and $H/D= 1.5$	103
3.18	Parameter of Face Displacement, Ω , versus Face Pressure Ratio, PF, for various values of Angle of Internal Friction, ϕ , $\gamma= 10 \text{ kN/m}^3$, $K_0= 0.8$ and $H/D= 1.5$	103
3.19	Parameter of Face Displacement, Ω , versus Face Pressure Ratio, PF, for various values of Angle of Internal Friction, ϕ , $\gamma= 20 \text{ kN/m}^3$, $K_0= 0.6$ and $H/D= 1.5$	104
3.20	Parameter of Face Displacement, Ω , versus Face Pressure Ratio, PF, for various values of Angle of Internal Friction, ϕ , $\gamma= 20 \text{ kN/m}^3$, $K_0= 0.8$ and $H/D= 1.5$	104

Figure		Page
3.21	Parameter of Face Displacement, Ω , versus Face Pressure Ratio, PF, for various values of Angle of Internal Friction, ϕ , $\gamma= 20 \text{ kN/m}^3$, $K_o= 0.8$ and $H/D= 2.0$	105
3.22	Parameter of Face Displacement, Ω , versus Face Pressure Ratio, PF, for various values of Angle of Internal Friction, ϕ , $\gamma= 20 \text{ kN/m}^3$, $K_o= 0.8$ and $H/D= 2.5$	105
3.23	Parameter of Face Displacement, Ω , versus Face Pressure Ratio, PF, for various values of K_o , $\gamma= 10 \text{ kN/m}^3$, $H/D= 1.5$	106
3.24	Parameter of Face Displacement, Ω , versus Face Pressure Ratio, PF, for various values of K_o , $\gamma= 20 \text{ kN/m}^3$, $H/D= 1.5$	106
3.25	Parameter of Face Displacement, Ω , versus Face Pressure Ratio, PF, for various values of K_o , $\gamma= 20 \text{ kN/m}^3$, $H/D= 2.0$	107
3.26	Parameter of Face Displacement, Ω , versus Face Pressure Ratio, PF, for various values of K_o , $\gamma= 20 \text{ kN/m}^3$, $H/D= 2.5$	107
3.27	Parameter of Face Displacement, Ω , versus Face Pressure Ratio, PF, for various values of ν , $\gamma= 20 \text{ kN/m}^3$, $K_o= 0.6$, $H/D= 1.5$	108
3.28	Parameter of Face Displacement, Ω , versus Face Pressure Ratio, PF, for various values of ν , $\gamma= 20 \text{ kN/m}^3$, $K_o= 0.7$, $H/D= 1.5$	108
3.29	Parameter of Face Displacement, Ω , versus Face Pressure Ratio, PF, for various values of ν , $\gamma= 20 \text{ kN/m}^3$, $K_o= 0.8$, $H/D= 1.5$	109
3.30	Parameter of Face Displacement, Ω , versus Face Pressure Ratio, PF, for various values of ν , $\gamma= 20 \text{ kN/m}^3$, $K_o= 0.8$, $H/D= 2.5$	109
3.31	Parameter of Face Displacement, Ω , versus Face Pressure Ratio, PF, for various values of Cohesion, c , $\phi= 0^\circ$, $H/D= 1.5$	110

Figure	Page	
3.32	Parameter of Face Displacement, Ω , versus Face Pressure Ratio, PF, for various values of Cohesion, c , $\phi = 10^\circ$, $H/D = 1.5$	110
3.33	Parameter of Face Displacement, Ω , versus Face Pressure Ratio, PF, for various values of Cohesion, c , $\phi = 20^\circ$, $H/D = 1.5$	111
3.34	Parameter of Face Displacement, Ω , versus Face Pressure Ratio, PF, for various values of Cohesion, c , $\phi = 30^\circ$, $H/D = 1.5$	111
3.35	Parameter of Face Displacement, Ω , versus Face Pressure Ratio, PF, for various values of Cohesion, c , $\phi = 0^\circ$, $H/D = 2.0$	112
3.36	Parameter of Face Displacement, Ω , versus Face Pressure Ratio, PF, for various values of Cohesion, c , $\phi = 10^\circ$, $H/D = 2.0$	112
3.37	Parameter of Face Displacement, Ω , versus Face Pressure Ratio, PF, for various values of Cohesion, c , $\phi = 20^\circ$, $H/D = 2.0$	113
3.38	Parameter of Face Displacement, Ω , versus Face Pressure Ratio, PF, for various values of Cohesion, c , $\phi = 30^\circ$, $H/D = 2.0$	113
3.39	Parameter of Face Displacement, Ω , versus Face Pressure Ratio, PF, for various values of Cohesion, c , $\phi = 0^\circ$, $H/D = 2.5$	114
3.40	Parameter of Face Displacement, Ω , versus Face Pressure Ratio, PF, for various values of Cohesion, c , $\phi = 10^\circ$, $H/D = 2.5$	114
3.41	Parameter of Face Displacement, Ω , versus Face Pressure Ratio, PF, for various values of Cohesion, c , $\phi = 20^\circ$, $H/D = 2.5$	115
3.42	Parameter of Face Displacement, Ω , versus Face Pressure Ratio, PF, for various values of Cohesion, c , $\phi = 30^\circ$, $H/D = 2.5$	115
3.43	Three-dimensional Finite Element Mesh used for Tunnel Face Stability Analyses.....	116

Figure		Page
3.44	Longitudinal Displacement at the Vertical Axis of the Face for various Face Pressure Ratios, Non Cohesive Soil.....	117
3.45	Longitudinal Displacement at the Vertical Axis of the Face for various Face Pressure Ratios, Cohesive Soil.....	117
3.46	Parameter of Face Displacement, Ω , versus Face Pressure Ratio, PF, for Non Cohesive Soils, $\phi = 20^\circ$	119
3.47	Parameter of Face Displacement, Ω , versus Face Pressure Ratio, PF, for Non Cohesive Soils, $\phi = 30^\circ$	119
3.48	Parameter of Face Displacement, Ω , versus Face Pressure Ratio, PF, for Non Cohesive Soils, $\phi = 40^\circ$	120
3.49	Parameter of Face Displacement, Ω , versus Face Pressure Ratio, PF, for Cohesive Soils, $\phi = 0^\circ$	120
3.50	Parameter of Face Displacement, Ω , versus Face Pressure Ratio, PF, for c- ϕ Soils, $\phi = 10^\circ$	121
3.51	Displacement at the Centre Point of the face, δ_x , versus the Face Pressure Ratio, PF, for Non Cohesive Soils, $\phi = 20^\circ$	122
3.52	Displacement at the Centre Point of the face, δ_x , versus the Face Pressure Ratio, PF, for Non Cohesive Soils, $\phi = 30^\circ$	122
3.53	Displacement at the Centre Point of the face, δ_x , versus the Face Pressure Ratio, PF, for Non Cohesive Soils, $\phi = 40^\circ$	123
3.54	Displacement at the Centre Point of the face, δ_x , versus the Face Pressure Ratio, PF, for Cohesive Soils, $c = 40$ kPa and $\phi = 0^\circ$	124
3.55	Displacement at the Centre Point of the face, δ_x , versus the Face Pressure Ratio, PF, for c- ϕ Soils, $c = 10$ kPa and $\phi = 10^\circ$	124
3.56	Displacement at the Centre Point of the face, δ_x , versus the Face Pressure Ratio, PF, for c- ϕ Soils, $c = 20$ kPa and $\phi = 10^\circ$	125
3.57	Contour Lines of Degree of Overstressing, OS, in percent, due to Stress Relief at the Face of a Tunnel, Axisymmetric Analysis, $c = 0$, $\phi = 30^\circ$	126

Figure	Page
3.58	Contour Lines of Degree of Overstressing, OS, in percent, due to Stress Relief at the Face of a Tunnel, Axisymmetric Analysis, $c= 10$, $\phi= 30^\circ$ 128
3.59	Contour Lines of Degree of Overstressing, OS, in percent, due to Stress Relief at the Face of a Tunnel, Axisymmetric Analysis, $c= 20$ kPa, $\phi= 0^\circ$ 129
3.60	Contour Lines of Degree of Overstressing, OS, in percent, due to Stress Relief at the Face of a Tunnel, Axisymmetric Analysis, $c= 20$ kPa, $\phi= 10^\circ$ 130
3.61	Contour Lines of Degree of Overstressing, OS, in percent, due to Stress Relief at the Face of a Tunnel, Axisymmetric Analysis, $c= 20$ kPa, $\phi= 20^\circ$ 132
3.62	Contour Lines of Degree of Overstressing, OS, in percent, due to Stress Relief at the Face of a Tunnel, Axisymmetric Analysis, $c= 40$ kPa, $\phi= 0^\circ$ 134
3.63	Contour Lines of Degree of Overstressing, OS, in percent, due to Stress Relief at the Face of a Tunnel, Three-dimensional Analysis, $c= 0$ kPa, $\phi= 30^\circ$ 137
3.64	Contour Lines of Degree of Overstressing, OS, in percent, due to Stress Relief at the Face of a Tunnel, Three-dimensional Analysis, $c= 40$ kPa, $\phi= 0^\circ$ 139
3.65	Mohr-Coulomb Failure Criterion..... 141
3.66	Stress Paths at the Centre Point of Tunnel Face during Gradual Stress Relief, Three-dimensiona Analysis, $c= 0$ kPa, $\phi= 30^\circ$ 143
3.67	Stress Paths at the Centre Point of Tunnel Face during Gradual Stress Relief, Three-dimensiona Analysis, $c= 40$ kPa, $\phi= 0^\circ$ 144
3.68	Stress Paths at various Points of Tunnel Circumference during Gradual Stress Relief, Three-dimensiona Analysis, $c= 0$ kPa, $\phi= 30^\circ$ 145
3.69	Stress Paths at various Points of Tunnel Circumference during Gradual Stress Relief, Three-dimensiona Analysis, $c= 40$ kPa, $\phi= 0^\circ$ 147

Figure		Page
3.70	Contour Lines of Nondimensional Confinement Ratio, CR', in percent due to Stress Relief at the Face of a Tunnel, Axisymmetric Analysis, $c= 0, \phi= 30^\circ$	149
3.71	Contour Lines of Nondimensional Confinement Ratio, CR', in percent due to Stress Relief at the Face of a Tunnel, Axisymmetric Analysis, $c= 40, \phi= 0^\circ$	151
3.72	Influence Factor of Frictional Resistance, I_ϕ versus Angle of Internal Friction, ϕ , for various values of Depth Ratio, H/D.....	153
3.73	Influence Factor of Frictional Resistance, I_ϕ versus K_ϕ for various values of Depth Ratio, H/D.....	154
3.74	Influence Factor of Frictional Resistance, I_ϕ versus ν for various values of Depth Ratio, H/D.....	154
3.75	Influence Factor of Frictional Resistance, I_ϕ versus Angle of Internal Friction, ϕ , for various values of Depth Ratio, H/D for $c-\phi$ Soils.....	155
3.76	Influence Factor of Cohesive Resistance, I_c versus Angle of Internal Friction, ϕ , for various values of Depth Ratio, H/D for $c-\phi$ Soils.....	155
3.77	Comparison between Centrifuge Results and Finite Element Results for Non Cohesive Soils, $\phi= 40^\circ$	157
3.78	Parameters used in the Finite Element Analysis of the St. Clair River Tunnel.....	166
3.79	Transversal Section of the 3-D Mesh used in the Analysis of the St. Clair River Tunnel.....	167
3.80	Longitudinal Cross Section of the 3-D Mesh used in the Analysis of the St. Clair River Tunnel.....	168
3.81	Mobilized Maximum Shear Stress versus the Distance ahead of the Tunnel Face for various Face Pressure Ratios.....	171
3.82	Mobilized Maximum Shear Stress versus the Distance ahead of the Tunnel Face for various Face Pressure Ratios (Strain Softening Case).....	172

Figure		Page
3.83	Upper and Lower Bounds of the Propagation of the Yield Zone ahead of the Tunnel Face versus the Face Pressure Ratio	173
4.1	Normal Probability Curve Describing the Transversal Settlement Trough (after Peck 1969).....	180
4.2	Displacement and Strain Fields around an Excavation.(After Attewell et al. , 1986).....	182
4.3	Volume Loss versus Overload Factor.....	185
4.4	Three-dimensional Aspects of Ground Reaction Curves at the Crown Level of the Tunnel (after Eisenstein et al., 1984).....	191
4.5	Stress Paths Resulting from Numerical Simulation of Conventional Tunnelling (after Negro, 1988).....	193
4.6	Displacement at Crown Level versus Longitudinal Distance at Frankfurt Tunnel (after Eisenstein et al., 1984).....	195
4.7	Displacement at Crown Level versus Longitudinal Distance at Two Locations at Edmonton LRT Tunnel (after Thurber, 1990).....	195
4.8	Displacement at Crown Level at Cairo Sewage Tunnel- Location MPX I (after Shalaby 1990).....	197
4.9	Displacement at Crown Level at Tilbury Tunnel at Two Locations (after De Moor and Taylor, 1989).....	197
4.10	Shear and Volumetric Strains around Edmonton Experimental Tunnel (modified after El-Nahhas 1980).....	199
4.11	Shear and Volumetric Strains around Tilbury Tunnel Site B (after De Moor and Taylor, 1989).....	201
4.12	Ground Conditions and Locations of Convergence Point Measurements at Edmonton LRT Tunnel.....	204
4.13	Displacement versus Radial Pressure at the Crown of Edmonton LRT Tunnel (after Eisenstein and Ezzeldine (1990)).....	205
4.14	Ground Reaction Curves at Edmonton LRT Tunnel (after Eisenstein and Ezzeldine (1990)).....	205
4.15	Parameters affecting the Stress and Strain Fields around a Tunnel Excavated using Pressurized Shield Method.....	208

Figure		Page
4.16	Finite Element Mesh for a Tunnel (Depth Ratio= 1.0).....	215
4.17	Finite Element Mesh for a Tunnel (Depth Ratio= 1.5).....	216
4.18	Finite Element Mesh for a Tunnel (Depth Ratio= 2.5).....	217
4.19	Finite Element Mesh for a Tunnel (Depth Ratio= 3.5).....	218
4.20	Steps used in the Finite Element Simulation of a Tunnel Excavated using a Pressurized Shield Method.....	220
4.21	Nodes Locking used in the Three-dimensional Numerical Simulation of a Tunnel Excavated using a Pressurized Shield Method.....	222
4.22	Three Dimensional View of Vertical Movement (G.R.= 30.0% and L.R.= 0.0%).....	223
4.23	Three Dimensional View of Vertical Movement (G.R.= 75.0% and L.R.= 0.0%).....	224
4.24	Three Dimensional View of Vertical Movement (G.R.= 112.5% and L.R.= 0.0%).....	225
4.25	Three Dimensional View of Vertical Movement (G.R.= 150.0% and L.R.= 0.0%).....	226
4.26	Three Dimensional View of Vertical Movement (G.R.= 225.0% and L.R.= 0.0%).....	227
4.27	Three Dimensional View of Vertical Movement (G.R.= 30.0% and L.R.= 45.0%).....	228
4.28	Three Dimensional View of Vertical Movement (G.R.= 30.0% and L.R.= 90.0%).....	229
4.29	Three Dimensional View of Vertical Movement (G.R.= 30.0% and L.R.= 135.0%).....	230
4.30	Surface Displacement at Longitudinal Axis for various Grout Ratios (L.R.= 0.0%).....	231
4.31	Surface Displacement at Longitudinal Axis for various Grout Ratios (L.R.= 45.0%).....	231
4.32	Surface Displacement at Longitudinal Axis for various Grout Ratios (L.R.= 90.0%).....	232
4.33	Surface Displacement at Longitudinal Axis for various Grout Ratios (L.R.= 135.0%).....	232
4.34	Surface Displacement at Longitudinal Axis for various Grout Ratios (L.R.= 180.0%).....	233

Figure		Page
4.35	Surface Displacement at Longitudinal Axis for various Poisson's Ratios (G.R.= 30.0% and L.R.= 0.0%).....	234
4.36	Surface Displacement at Longitudinal Axis for various Poisson's Ratios (G.R.= 112.5% and L.R.= 0.0%).....	234
4.37	Surface Displacement at Longitudinal Axis for various Poisson's Ratios (G.R.= 30.0% and L.R.= 180.0%).....	235
4.38	Surface Displacement at Longitudinal Axis for various Poisson's Ratios (G.R.= 112.5% and L.R.= 180.0%).....	235
4.39	Surface Displacement at Longitudinal Axis for various values of K_0 (G.R.= 30.0% and L.R.= 0.0%).....	236
4.40	Surface Displacement at Longitudinal Axis for various values of K_0 (G.R.= 112.5% and L.R.= 0.0%).....	236
4.41	Surface Displacement at Longitudinal Axis for various values of K_0 (G.R.= 30.0%).....	237
4.42	Surface Displacement at Longitudinal Axis for various values of K_0 (G.R.= 112.5%).....	237
4.43	Contour Plot of Stress Ratio, S.R., at the Central Longitudinal Plane (G.R.= 30% and L.R.= 0.0%).....	239
4.44	Contour Plot of Stress Ratio, S.R., at the Central Longitudinal Plane (G.R.= 30% and L.R.= 45%).....	240
4.45	Contour Plot of Stress Ratio, S.R., at the Central Longitudinal Plane (G.R.= 30% and L.R.= 90%).....	241
4.46	Contour Plot of Stress Ratio, S.R., at the Central Longitudinal Plane (G.R.= 30% and L.R.= 135%).....	242
4.47	Contour Plot of Stress Ratio, S.R., at the Central Longitudinal Plane (G.R.= 30% and L.R.= 180%).....	243
4.48	Contour Plot of Stress Ratio, S.R., at the Transversal Plane at the Point of Lining Activation (G.R.= 30% and L.R.= 0.0%).....	244

Figure		Page
4.49	Contour Plot of Stress Ratio, S.R., at the Transversal Plane at the Point of Lining Activation (G.R.= 75% and L.R.= 0.0%).....	245
4.50	Contour Plot of Stress Ratio, S.R., at the Transversal Plane at the Point of Lining Activation (G.R.= 112.5% and L.R.= 0.0%).....	246
4.51	Contour Plot of Stress Ratio, S.R., at the Transversal Plane at the Point of Lining Activation (G.R.= 150% and L.R.= 0.0%).....	247
4.52	Contour Plot of Stress Ratio, S.R., at the Transversal Plane at the Point of Lining Activation (G.R.= 225.5% and L.R.= 0.0%).....	248
4.53	Contour Plot of Stress Ratio, S.R., at the Transversal Plane at the Point of Lining Activation (G.R.= 30% and L.R.= 45%).....	249
4.54	Contour Plot of Stress Ratio, S.R., at the Transversal Plane at the Point of Lining Activation (G.R.= 30% and L.R.= 90%).....	250
4.55	Contour Plot of Stress Ratio, S.R., at the Transversal Plane at the Point of Lining Activation (G.R.= 30% and L.R.= 135%).....	251
4.56	Contour Plot of Stress Ratio, S.R., at the Transversal Plane at the Point of Lining Activation (G.R.= 30% and L.R.= 180%).....	252
4.57	Contour Plot of Stress Ratio, S.R., at the Transversal Plane at the Point of Lining Activation (G.R.= 30% and L.R.= 0.0%).....	254
4.58	Contour Plot of Mobilized Friction Angle, ϕ , at the Central Longitudinal Plane (G.R.= 30% and L.R.= 45%).....	255
4.59	Contour Plot of Mobilized Friction Angle, ϕ , at the Central Longitudinal Plane (G.R.= 30% and L.R.= 90%).....	256
4.60	Contour Plot of Mobilized Friction Angle, ϕ , at the Central Longitudinal Plane (G.R.= 30% and L.R.= 135%).....	257
4.61	Contour Plot of Mobilized Friction Angle, ϕ , at the Central Longitudinal Plane (G.R.= 30% and L.R.= 180%).....	258

Figure		Page
4.62	Contour Plot of Mobilized Friction Angle, ϕ , Transversal Plane at the Point of Lining Activation (G.R.= 30% and L.R.= 0%).....	259
4.63	Contour Plot of Mobilized Friction Angle, ϕ , Transversal Plane at the Point of Lining Activation (G.R.= 75% and L.R.= 0%).....	260
4.64	Contour Plot of Mobilized Friction Angle, ϕ , Transversal Plane at the Point of Lining Activation (G.R.= 112.5% and L.R.= 0%).....	261
4.65	Contour Plot of Mobilized Friction Angle, ϕ , Transversal Plane at the Point of Lining Activation (G.R.= 150% and L.R.= 0%).....	262
4.66	Contour Plot of Mobilized Friction Angle, ϕ , Transversal Plane at the Point of Lining Activation (G.R.= 30% and L.R.= 45%).....	263
4.67	Contour Plot of Mobilized Friction Angle, ϕ , Transversal Plane at the Point of Lining Activation (G.R.= 30% and L.R.= 135%).....	264
4.68	Contour Plot of Mobilized Friction Angle, ϕ , Transversal Plane at the Point of Lining Activation (G.R.= 30% and L.R.= 180%).....	265
4.69	Stress Ratio versus the Normalized Shear Stress (G.R.= 30% and L.R.= 0%).....	266
4.70	Stress Ratio versus the Normalized Shear Stress (G.R.= 112.5% and L.R.= 0%).....	267
4.71	Stress Ratio versus the Normalized Shear Stress (G.R.= 112.5% and L.R.= 135%).....	268
4.72	Stress Ratio versus the Mobilized Friction Angle, ϕ , (G.R.= 30% and L.R.= 0%).....	269
4.73	Stress Ratio versus the Mobilized Friction Angle, ϕ , (G.R.= 112.5% and L.R.= 0%).....	270
4.74	Stress Ratio versus the Mobilized Friction Angle, ϕ , (G.R.= 30% and L.R.= 135%).....	271
4.75	Regression Coefficients for Surface Movement ω_s	273
4.76	Regression Coefficients for Stress Ratio, S.R.....	277

Figure		Page
4.77	Regression Coefficients for Deviatoric Stress Ratio, D.S.R.....	281
4.78	Calculated values of Normalized Surface Displacement, \bar{w}_s , versus Interpolated values.....	283
4.79	Calculated values of Normalized Crown Displacement, \bar{w}_c , versus Interpolated values.....	284
4.80	Calculated values of Stress Ratio, S.R. at the Crown versus Interpolated values.....	285
4.81	Calculated values of Stress Ratio, S.R. at the Spring Line versus Interpolated values.....	286
4.82	Calculated values of Stress Ratio, S.R. at the Floor versus Interpolated values.....	287
4.83	Calculated values of Deviatoric Stress Ratio, D.S.R. at the Crown versus Interpolated values.....	288
4.84	Calculated values of Deviatoric Stress Ratio, D.S.R. at the Spring Line versus Interpolated values.....	289
4.85	Calculated values of Deviatoric Stress Ratio, D.S.R. at the Floor versus Interpolated values.....	290
5.1	Influence of Compressed Air Pressure on the Ground Reaction Curve (after Peck, 1969).....	296
5.2	Ground Reaction Curve for the Earth Pressure Balanced Shield (after Eisenstein 1993).....	297
5.3	Loading Conditions for Different Structural Models of Circular Tunnels.....	299
5.4	Centrifuge Test Results on Rigid Pipe in Dense Sand (after Tohda et al. 1988).....	301
5.5	Hartmann's Solutions (after Negro 1988: Figure 7.1).....	304
5.6	Flow Chart of Eisenstein-Negro's Method of Design of Shallow Tunnels.....	308
5.7	The Hyperbolic Model.....	309
5.8	Hartmann's Solutions (after Negro 1988: Figure 7.1).....	312
5.9	Calculated and Curve Fitted values of ar_g versus the Normalized Tunnel Depth.....	318
5.10	Calculated and Curve Fitted values of ar_l versus the Normalized Tunnel Depth.....	318

Figure		Page
5.11	Calculated and Curve Fitted values of ar_{n2} versus the Normalized Tunnel Depth.....	319
5.12	Calculated and Curve Fitted values of ar_{n1} versus the Normalized Tunnel Depth.....	319
5.13	Calculated and Curve Fitted values of ar_k versus the Normalized Tunnel Depth.....	320
5.14	Calculated and Curve Fitted values of ar_o versus the Normalized Tunnel Depth.....	320
5.15	Calculated and Curve Fitted values of ad_{g2} versus the Normalized Tunnel Depth.....	321
5.16	Calculated and Curve Fitted values of ad_{g1} versus the Normalized Tunnel Depth.....	321
5.17	Calculated and Curve Fitted values of ad_{n2} versus the Normalized Tunnel Depth.....	322
5.18	Calculated and Curve Fitted values of ad_{n1} versus the Normalized Tunnel Depth.....	322
5.19	Calculated and Curve Fitted values of ad_k versus the Normalized Tunnel Depth.....	323
5.20	Calculated and Curve Fitted values of ad_o versus the Normalized Tunnel Depth.....	323
5.21	Calculated and Curve Fitted values of as versus the Normalized Tunnel Depth.....	326
5.22	Coefficients A1, A2, A3, and A4 Calculated Based on Hartmann's Solution.....	331
5.23	Flow Chart of a Design Method of Tunnels Constructed using Pressurized Shield Methods.....	332
5.24	Site Plan of the Edmonton LRT Project.....	335
5.25	Simplified Geological Profile for the Edmonton LRT Project.....	336
5.26	Grout Pressure Ratio used at the Edmonton LRT Project.....	340
5.27	Excess Grout Volume used at the Edmonton LRT Project.....	341
5.28	Limer Pressure Ratio, L.R. used at the Edmonton LRT Project.....	342

Figure		Page
5.29	Profile of Ground Parameters at the LRT Project versus the Design Parameters.....	344
5.30	Measured and Estimated Maximum Ground Surface Settlement versus the Grout Ratio at the Edmonton LRT Project, Material Parameters of Profile 1.....	348
5.31	Measured and Estimated Maximum Ground Surface Settlement versus the Grout Ratio at the Edmonton LRT Project, Material Parameters of Profile 2.....	348
5.32	Measured and Estimated Settlement Trough at Ground Surface at the Edmonton LRT Project, Material Parameters of Profile 2.....	349
5.33	Calculated Normal Forces at the Liner Edmonton LRT Project, Material Parameters of Profile 2.....	350
5.34	Calculated Bending Moment at the Liner Edmonton LRT Project, Material Parameters of Profile 2.....	350

LIST OF SYMBOLS

A_i	Constants.
ac_i	Constants related to vertical displacement near the tunnel's crown.
ad_i	Constants related to deviatoric stress ratio.
ar_i	Constants related to stress ratio.
as_i	Constants related to surface displacement.
B	Constant.
c	Cohesion.
C	Compressibility ratio
C^*	Compressibility ratio including the effect of excavation
CR	Confinement ratio.
CR'	Normalized confinement ratio.
c_u	Undrained cohesion.
D	Tunnel diameter (external).
D_i	Inside tunnel diameter.
DIF	Difference between radial and tangential stresses at the liner.
E	modulus of deformation.
E_u	Undrained elastic modulus.
E_l	Elastic modulus of the liner.
E_t	Tangential modulus of deformation.
E_{ti}	Initial tangential modulus of deformation of the liner.
F	Flexibility ratio
F^*	Flexibility ratio including the effect of excavation
G	Shear modulus.
$G.R.$	Grout pressure ratio.
H	Cover depth.
H_l	Depth of rigid layer under the tunnel floor.
H_o	Depth of tunnel axis.
i	Settlement trough width.
$I_1, I_2, I_3.$	Stress invariants.
I_c	Influence factor of cohesive resistance.

I_{ϕ}	Influence factor of frictional resistance.
J'_1, J'_1	Parameters relating shear and volumetric effects.
J_1, J_2, J_3	Deviatoric Stress invariants.
K	Bulk modulus.
$(K)_h$	Janbu's constant used in the hyperbolic model.
K_a	Active coefficient of lateral earth pressure.
K_o	Coefficient of lateral earth pressure at rest (initial).
K_p	Passive coefficient of lateral earth pressure.
L	Unsupported tunnel length- delay distance.
$L.R.$	Liner pressure ratio.
LDI	Longitudinal Distortion Index.
L_s	Shield length.
L_s	Shield length.
m	constant.
n	constant relating the depth with the width of tunnel trough.
$(n)_h$	Janbu's constant used in the hyperbolic model.
N	Stability ratio.
N_d	Size coefficient.
N_f	Face coefficient.
N_o	Depth coefficient.
N_s	Surcharge coefficient.
OF	Overstress factor.
OS	Degree of overstraining.
p	Mean stress.
p_c	Collapse face pressure.
PF	Face pressure ratio.
p_f	Face pressure.
p_g	Grout pressure.
p_{ho}	Initial horizontal pressure at tunnel axis.
p_l	Longitudinal liner pressure.
p_i	Initial mean stress.
p_o	Initial vertical pressure at tunnel axis.
p_s	Surcharge pressure.
p_y	Yield face pressure.
q	Deviatoric stress.
q_i	Initial deviatoric stress.

$(R_f)_h$	Stress ratio in the hyperbolic model relating the deviator stress at failure to the ultimate deviator stress .
R_o	Tunnel radius.
$S.R.$	Stress ratio.
s_u	Shear strength.
SUM	Summation of radial and tangential stresses at the liner.
t	Liner thickness.
U	Normalized radial displacement.
u_r	Radial displacement.
u, v, w	Longitudinal, transversal and vertical displacements respectively.
V	Tunnel volume.
V'	Relative volume loss.
V_b	Bead volume loss.
V_f	Volume loss at the tunnel face.
V_g	Postgrout volume loss.
V_p	Pitch volume loss.
V_s	Volume of settlement trough.
V_t	Total volume losses at the tunnel.
V_u	Postshield/Pregrout volume loss.
W_e	Weight of soil excavated.
W_l	Weight of liner.
w_s	Surface displacement.
W_s	Weight of shield.
w_c	Vertical displacement near tunnel's crown.
w_{cl}	Displacement at the centre of line of the surface settlement trough.
α	Ratio of radial stress release.
$\dot{\alpha}$	Incompressibility ratio.
β	Rigidity ratio.
ΔV	Total volume losses at the tunnel.
δ_x	Longitudinal movement at the centerpoint of the face.
$\epsilon_1, \epsilon_2, \epsilon_3.$	Principal strains.
ϵ_a	Axial strain.
ϵ_r	Radial strain.
ϵ_s	Shear strain.

ϵ_v	Volumetric strain.
$\epsilon_x, \epsilon_y, \epsilon_z$	Longitudinal, transversal and vertical strains respectively.
ϕ	Angle of internal friction.
ϕ_a	Approximated angle of internal friction to include the effect of cohesion.
Γ	Integration function of normal probability curve.
η	Empirical constant expressing the reduction of tunnel loading due to arching.
γ	Soil unit weight.
ν	Poisson's ratio.
ν_l	Poisson's ratio of the liner.
θ	Angle of similitude.
λ	parameter of the twice normalized ground reaction curve NNGRC.
ρ	Deviatoric stress invariant.
$\sigma_1, \sigma_2, \sigma_3$	Principal stresses.
σ_a	Axial stress in the triaxial configuration.
σ_c	Stress representing the normal pressure during an unconfined loading condition.
σ_h	Horizontal stress.
σ_{h0}	Initial horizontal stress.
σ_r	Radial stress.
σ_{r0}	Initial radial stress.
σ_v	Vertical stress.
Σ	Radial stress ratio (= $1-\alpha$).
Ω	Parameter of face displacement.
ω_s	Normalized surface displacement.
ω_c	Normalized vertical displacement near tunnel's crown.
ξ	Hydrostatic stress invariant.

CHAPTER 1

INTRODUCTION

New tunnelling technologies are being designed and improved upon to accommodate the needs of contemporary urban planning. Safety and economy are still the two major conditions that have to be examined when comparing between the methods of construction for underground projects. In the case of tunnelling in modern cities, these two factors acquire new dimensions. Also, time is becoming an increasingly important factor that influences the economical feasibility of the project, therefore, the rate of advance of the project is crucial for the success of the project. In addition, as the conventional cut-and-cover method of construction of underground projects proves, in many instances, to be obstructive in practice in congested cities, tunnelling represents an attractive alternative. Thus, there is a high demand to develop a tunnelling method capable of achieving high ground control standards in relatively soft and shallow ground conditions. Furthermore, an additional important requirement of a successful modern tunnelling method is the efficiency of the technology applied to cope with ground water problems during the excavation. To date, pressurized shield tunnelling methods have proven to answer these requirements as they have been implemented successfully in many projects during recent years.

The study of the geotechnical implications of the use of pressurized shield methods in tunnelling is fundamentally based on the current analyses of conventional tunnelling with a certain number of adaptations regarding three major points. First, the safety requirements of the project should include relatively restrictive conditions on the amount of resultant deformation at the ground surface. Therefore, settlement at the ground surface and its gradient are required to be estimated with a high degree of reliability. Secondly, site conditions which are predominantly in shallow ground, stiffness is low compared to the lining system that is usually constituted of a precast-segmented-concrete liner. It follows

that the boundaries of the excavation acquire structural properties and the tunnel interacts with the surrounding soil. This is expected to result in changing the initial concept of tunnelling being a monotonic stress release in the ground mass. Finally, the construction method is expected to have an effect on the anticipated failure mechanisms because of the imposed support conditions at the boundaries of the excavation.

Bearing in mind the above special conditions, a study of a design method for constructing tunnels using pressurized shield tunnels is required to have the following objectives:

- (1) to provide a better understanding of the pressurized shield methods of construction by identifying their different aspects, the specific constructional and mechanical characteristics involved in each method, and the actual field performance of each method with respect to the economy and the safety requirements of the project;
- (2) to investigate the stress-and-strain fields related to tunnel construction using pressurized shield methods in light of current state-of-the-art of shallow tunnel analyses, and thus to estimate the specific features of the developed stress field related to these methods. Special emphasis is directed toward the expected mechanisms of failure, displacement at the ground surface, and straining actions on the liner;
- (3) to identify soil parameters that affect the ground response to tunnelling activity and the stress paths that are expected to take place at different construction stages;
- (4) to develop a design method that takes into account the new construction techniques and that enables the evaluation of the resulting ground deformation and the straining actions in the liner;
- (5) to validate the proposed design method by comparing it with actual case histories;
- (6) to put the results of the analysis within the perspective of current developments in construction methods and of the prospective developments in the near future and, at the same time, to take into account the emerging requirements of successful tunnelling practices in modern urban areas; and
- (7) to present the formulated design method in a comprehensive manner and in a way that enables it to be used by practitioners.

The approach followed during this study is selected based on actual case histories, the available computer system, and the already formulated design methods. Recently, the southern extension of the Light Rail Transit (LRT) System in the city of Edmonton was

completed and extends to the University area. In a particular part of the project, severe soil conditions have raised concerns about the safety of the neighbouring structures. A pressurized shield method, the Hydroshield was used in this portion of the tunnel and its performance was deemed satisfactory. Also, an extensive monitoring program was applied around the excavation. The results of the instrumentation measurements, along with the construction records, represent a unique opportunity to better understand the characteristics of this new method of construction. Meanwhile, accelerating advances in computer systems have enabled the production of more potent machines with respect to their speed and their storage capacity, and this has produced the availability of more efficient software material for engineering calculations, data handling, and for graphic representations. A design method for shallow tunnel construction using conventional methods has been developed at the University of Alberta by Negro (1988). The method, known as the Eisenstein-Negro method, is based on finite element analyses in two and in three-dimensions and on a closed form solution to evaluate the safety of the tunnel, movement at the ground surface, and stresses in the liner. The method has proven to be reliable and effective in tunnel design, as long as, it is used within the predefined limits of application. The basic advantages are that the method takes into account to a certain degree the effect of gravity, strain softening, and ground liner interaction and at the same time it is simple and, it is presented in a generalized form that permits its application to a wide range of ground and construction conditions. Nevertheless, the method does not include the effect of the use of a pressurized shield method in the tunnelling construction, itself. The review of the method, along with other analyses of tunnelling in general, constitutes the theoretical background of the intended design method. The results obtained are ultimately verified against field data collected from the LRT Edmonton project, and from other field data obtained from the literature.

CHAPTER 2

METHODS OF PRESSURIZED SHIELD TUNNELLING

2.1 Introduction

Pressurized shield methods are proving themselves as safe and effective methods of tunnelling in shallow ground conditions through various projects around the world. The evolution of technologies in use during the last two decades has led to the improvement of the performance of the machinery, especially, regarding the stability of the surrounding ground, as well as, the stability of the excavation itself. It is, therefore, of interest to identify the basic characteristics of the various pressurized shield methods with respect to the equipment and sequence of construction. The applicability of each method is reviewed through the inspection of a number of published case histories. The examination also takes into account the historical background of each method, as well as, the future prospects of its development. Finally, the advantages and the disadvantages of each method are presented in order to identify the comparative merits that each method has against the others and that the pressurized shield methods, in general, have against other tunnelling methods in shallow soil conditions.

2.2 Historical Background--Brunel's Tunnel.

For a long time, tunnelling activity was confined to dealing with self-supported ground conditions with respect to excavation work. From a civil engineering point of view, the ability of the ground to maintain its stability was a prerequisite for successful tunnelling. Up till the past hundred years, the emphasis was upon the efficiency and the speed with which the rock could be excavated and removed. Tunnelling in soft ground and below the groundwater table represented a challenge to early excavation techniques; a challenge that has now been met by more modern tunnelling techniques.

A landmark in the history of soft ground tunnelling was the birth of shield tunnelling during the construction of the Thames Tunnel (1824-1842) by Sir Marc Brunel. Brunel invented a rectangular shield 11.43 m wide and 6.78 m high. The shield is divided

into twelve independent units protected by an iron roof and side plates. Each unit consists of three floors and is propelled against the brickwork lining by screw jacks. Thus the shield is equivalent to 36 simultaneous headings in which the tunnel face is supported by horizontal boards which were 154 mm high and 76 mm thick. In each heading, a miner excavates the face, one board at a time, and reapplies the board on the advanced portion of the face using screw jacks until the whole face has been taken. Strong iron plates extend beyond the shield to overlap the part of the tunnel already constructed with the assembled liner.

The construction of the tunnel began by going through layers of sand and gravel alternating with impervious material. Difficulties started when a decision was made to double the shield advance pitch. As the work reached pervious layers, excessive ground movement took place through the ends of the face boards. In several instances, soil and water burst through flooding the tunnel. Furthermore, river water irrupted into the gallery and clay bags had to be dumped at the bottom of the river to stem water flow.

The Brunel tunnel reveals many principles of modern shield tunnelling in conditions of difficult soft ground near the water table. Face support is a necessity. The horizontal boards used to cover most of the face, at all times, is an early adaptation of the closed face excavation scheme. Soil removal was only allowed to take place through limited opening in the face while the major part of the face is kept under stable conditions by providing rigid support. Technical details in the excavation scheme, such as, the rate of advance of the shield appeared to have a great influence on the success of the operation. A less than cautious approach may have resulted in ground losses, and eventually, the shield-ground-water balance could have been disrupted. In many instances special provisions were needed to be taken in order to impede water flow and reduce ground permeability. An important constituent of this tunnelling method was to provide an appropriate transition from the shield support to a permanent liner support: the tail design. The permanent support acquire a new function: that of providing a longitudinal reaction to the shield; thus, there was a need for a lining system both rigid enough and capable of progressing with the same speed as the shield. Added to the above principles, modern tunnelling technology is required to provide an adequate, practical, and environmentally accepted way of muck disposal. Finally, a powerful system of pumping is required to accommodate the worst expected conditions.

2.3 Classification of Pressurized Tunnelling Shield Methods

Various shield tunnelling methods have been developed based on insuring the stability of the works by keeping the excavated boundaries under constant pressure. As

new construction conditions were met, applied technologies became diversified. Three major methods are now recognized:

- (1) the Bentonite Slurry Shield method (BSS);
- (2) the compressed air method; and
- (3) the Earth Pressure Balanced Shield method (EPBS).

2.3.1 Basic Features of different Pressurized Shield Methods

Face support measures are constantly being developed and improved upon to respond to practical site conditions, it is becoming harder to distinctively identify new tunnelling methods. Thus, three basic features are examined in order to distinguish the methods of pressurized shield tunnelling: face pressure, ground treatment, and muck disposal techniques.

In the case of the bentonite slurry shield method, the face pressure is applied following a distribution close to the hydrostatic distribution because of slurry injection. The ground treatment takes place ahead of the face as the cake layer is formed, and the muck disposal is achieved hydraulically through the slurry circuit. The earth pressure balanced shield method relies on applying mechanical pressure at the face by using the shield's face stiffness and the forward propelling movement of the shield to shove the ground. The ground treatment, if necessary, takes place inside the excavation chamber to control water pressure. Muck is disposed of in the form of solid matter. The compressed air method applies face pressure in the form of seepage forces at the face. Usually, air seepage balances water pressure within a certain volume inside the ground mass, and ground treatment takes place inside the dry space as soil properties improve because of capillary forces. Muck disposal is achieved in a way similar to that of the earth pressure balanced shield method.

2.3.2 Equipment of Tunnelling Methods

The design and production of different components of the excavation progress in a direct way in response to market demands. In many instances, this strong link weakens the geotechnical engineering role in the making of project decisions, especially, those concerning the choice of tunnelling methods, excavation trajectory, and special ground treatment procedures. On the one hand, the inclusion of geotechnical opinion in decision making will have many positive results, both regarding ground control and machinery performance of the. On the other hand, the geotechnical engineering point of view has to be based on a complete understanding of the machinery options in the market, machine performance, capability to accommodate difficult conditions, and the history of machinery

and construction success in a variety projects.

2.3.2.1 Equipment of the Bentonite Slurry Shield

The bentonite slurry shield method depends upon applying slurry pressure to enhance face stability. Figures 2.1 and 2.2 show the major components of two bentonite slurry shields. A *cutter head* is equipped with two systems of cutters: face cutters and edge cutters. The number and the shape of face cutters are selected depending on the soil stiffness and the required speed and degree of mixture with the slurry. Edge cutters produce an overbreak around the shield to facilitate its movement forward: the bead thickness. Abrasion, earth pressure, and heat sensors are commonly used to monitor the functioning of the cutting system from the control room. The structure of the cutter head and the projection of the cutter bits influence the thickness and the quality of the slurry-soil mixture layer at the face: the cake. As the cutter head rotates, the excavation proceeds. The reversible mode of rotation of the cutter head has proven to be of practical value. In addition, a pressure *bulk head* maintains the required slurry pressure in the working chamber which is in front of it, and face pressure and pressure needed to advance the shield are transmitted to the already constructed liner through a number of *hydraulic jacks*. As the excavated soil is mixed with slurry, it acquires a certain degree of fluidity, therefore, a *slurry transportation circuit* is designed: to feed the slurry to the excavation chamber under the required pressure, to transport the excavated material from the excavation chamber, to treat the muck by separating coarse material using a special system of successive screening, to extract the colloidal material, and to remake the slurry so that it will be reinjected in the excavation chamber. A *lining system* is designed to sustain, in addition to ground pressures, the handling loads, and the longitudinal shield reaction. Thus, the advance of the lining construction must be synchronized with the rate of advance of the excavation. The required rate of liner construction, as well as, the required ability of the early constructed liner rings to withstand longitudinal forces from the shield, favor the precast segmented concrete liner system over the cast in place liner system. The assembly of the segments is undertaken inside the shield using special liner *erectors*. A gap between the already assembled liner and the shield extrados: the tail void, is unavoidably created. The tail void is grouted to limit soil movement behind the shield and to provide the required adhesion between the liner and ground. The *grout system* and the grout material used vary depending on the site conditions. Cement and cement based grouts behind the segmented liner are commonly used. An important detail in the system is the *tail seal* that prevents the fluid grout from penetrating into the working space. In many instances the success of the tunnelling method depends on the effectiveness of the tail seal.

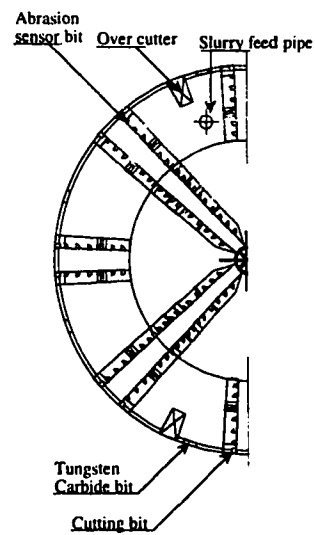
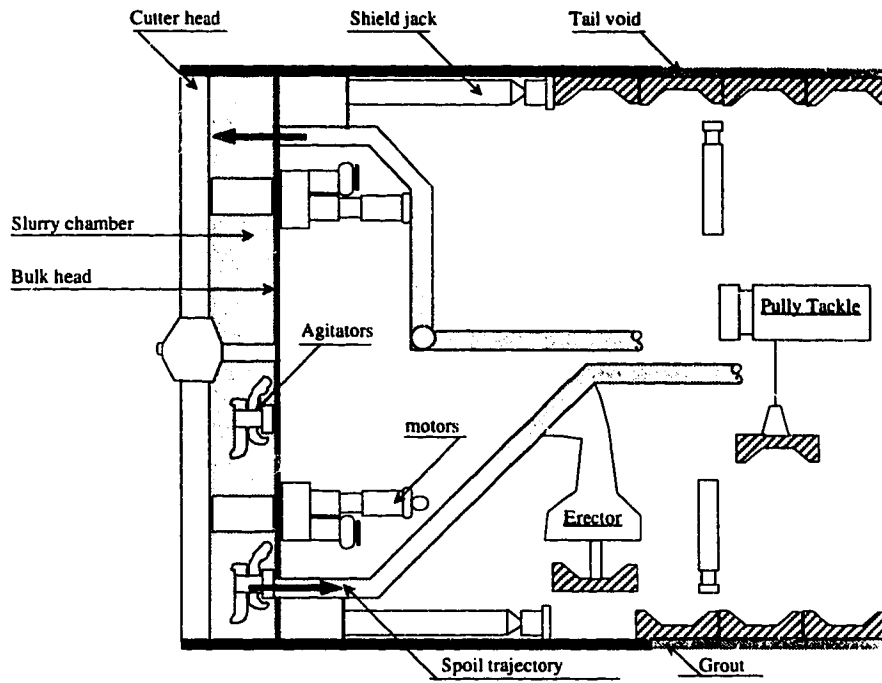


Figure 2.1: the Bentonite Slurry Shield

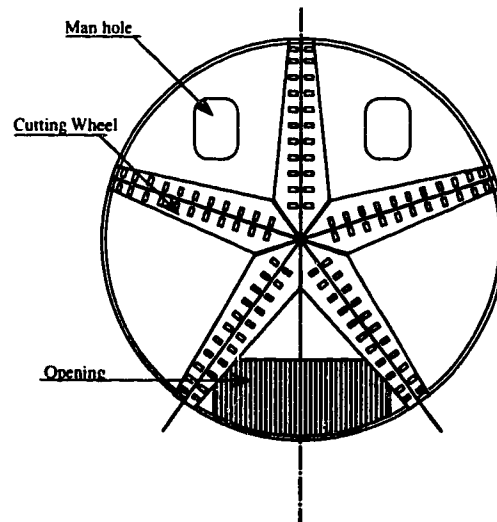
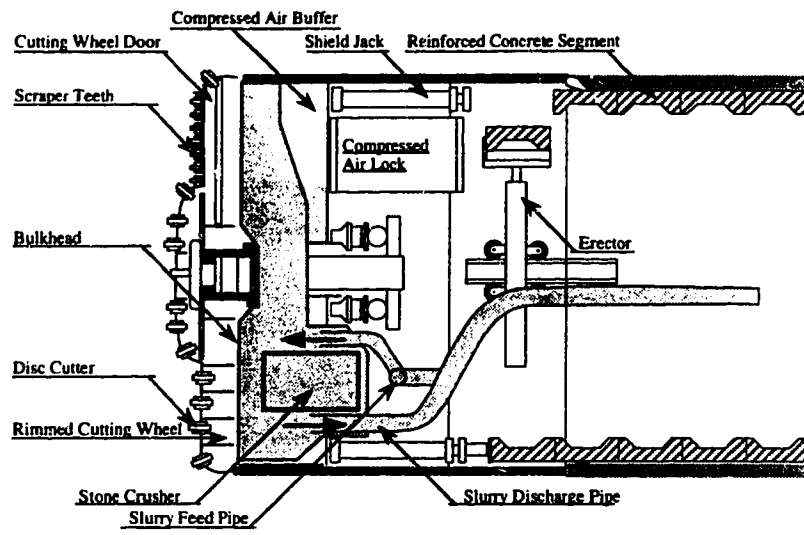


Figure 2.2: the Bentonite Slurry Shield- the Hydroshield

2.3.2.1.1 The Shield

Japanese bentonite slurry boring machines have been widely used during the last decade. Figure 2.1 is based on the description provided by Hashimoto et al. (1985) of the machinery used in excavating a large stormwater tunnel (11.22 m diameter) in Osaka, Japan, in 1981 and that provided by Hurpin and Bousset (1988) of the equipment used for the construction of an 8 m subway tunnel in Lille, France in 1985.

One or several types of agitators are used in the slurry chamber to prevent the adhesion of colloids with the mechanical parts of the chamber. Water jets also may be used for the same reason. Fluctuations in slurry pressure may take place because of the blocking of the slurry discharge system or because of sudden change in ground permeability. As a consequence, collapse of the face may ensue. Slurry pressure is controlled by means of a variable displacement pump and a control valve inside the tunnel.

The German bentonite slurry boring machine, also known as the Hydroschild, uses compressed air to regulate slurry pressure in the excavation chamber. Figure 2.2 shows data from machinery used in the shield based on a description of the equipment used in the Edmonton subway system in 1989 which is provided by Jones (1990). An air compressor insures constant slurry pressure at the excavation chamber. In case of emergency, compressed air may clear the chamber and working personnel may inspect the chamber and the excavated face.

Additional measures may be taken depending on working conditions. In the Osaka project, the use of an articulating two body type shield reduced the minimum radius of curvature in the horizontal plan from 50 times the diameter to 20. Further, an injection unit may be added to the system to improve the properties of the excavated ground ahead of the face by chemical grouts. According to Wallis (1990), a stone crusher was included inside the excavation chamber to allow excavation and removal of boulders during the construction of the Berlin metro (1988-1989). While in the case of Cairo's sewerage project, boulders were dealt with by using more efficient cutting bits (Wallis, 1987).

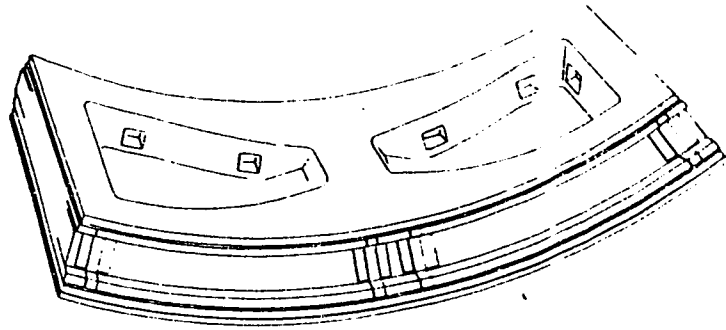
2.3.2.1.2 The Lining System

Because the propelling movement of the shield requires a solid liner to offer longitudinal support, a segmental lining is the preferred lining system. Typically, the number of segments is between 5 and 8 and the longitudinal dimension of the assembled ring is about 1.1 m, and a small segment, the key, is often included in the system. The segment shape is usually rectangular although trapezoidal segments have been used with success in some projects. Concrete strength and reinforcement of the segments are designed to sustain ground and functional loads, as well as, loads due to construction and

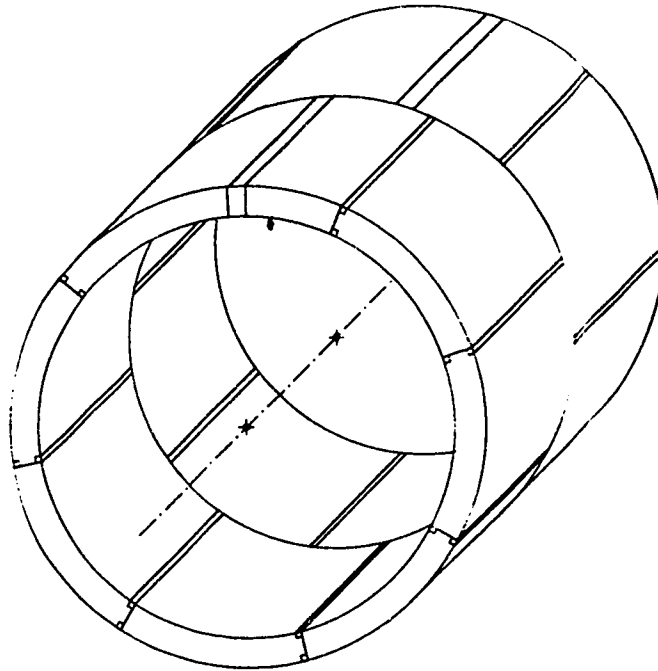
handling operations. The assembly of the lining system takes place inside the shield in a staggered scheme. Special care is addressed toward joint insulation, joint compressibility and flexibility, and interaction between individual segments. Bituminous packing or rubber gaskets are usually used for the joint filling in the insulation layer. Precast concrete segments assembled either by a tongue-and-groove interlocking system or by bolting. The completely assembled liner section is provided with a certain degree of compression due to the expansion of the ring toward the ground due to the grout pressure inside the gap void. Figure 2.3 shows a typical lining system using the segmental concrete liner in the Edmonton Light Rail Transit (LRT) system, based on a description provided by Krywiak and Morison (1990).

An extruded concrete liner has been used in the Lyon metro Line D project and proved to have a number of advantages as it produces good control of the ground movement behind the shield. Also, the newly cast concrete is in direct contact with the ground which precludes the use of grout and provides better ground-liner interaction. The major difficulty of designing a cast in place reinforced concrete system is that the rate of progress in casting concrete has to be compatible with the rate of advance of the shield, since the shield reaction is transmitted to and from the forms and, eventually, to the cured liner and then to the ground mass behind it. Another problem encountered in the case of casting a reinforced concrete liner is that in installing a steel cage for reinforcement the support for the newly cast concrete provided by the shield has to be temporarily removed. Figure 2.4(a) shows the construction sequence given by Okada (1989) where the concrete end is able to sustain itself when the press ring is removed. Another solution is presented by Sato (1989) and is shown in Figure 2.4(b) where the reinforcement system includes pressure holding rings and tie rods to maintain the pressure inside the freshly casted concrete when the thrust transmission ring is not in contact with the lining following the shield advance. Here, a special seal is designed to keep the fresh concrete under a higher pressure than the ground pressure. Also, an extruded concrete liner using steel fibers has proven to be of a practical advantage as there is no assembly of a reinforcement cage is required during construction. Furthermore, a special design for the stop end ensures that the extruded concrete remains under constant pressure regardless of the cycle of the shield movement. As explained by Babendererde (1987), the stop end is connected with the shield through an elastic spring and hydraulic jacks that are linked together to a gas pressure vessel that regulates the concrete pressure.

Special care must be directed toward the quality of extruded concrete as it has to respond to operational and long-term design requirements, especially, with respect to the following points:

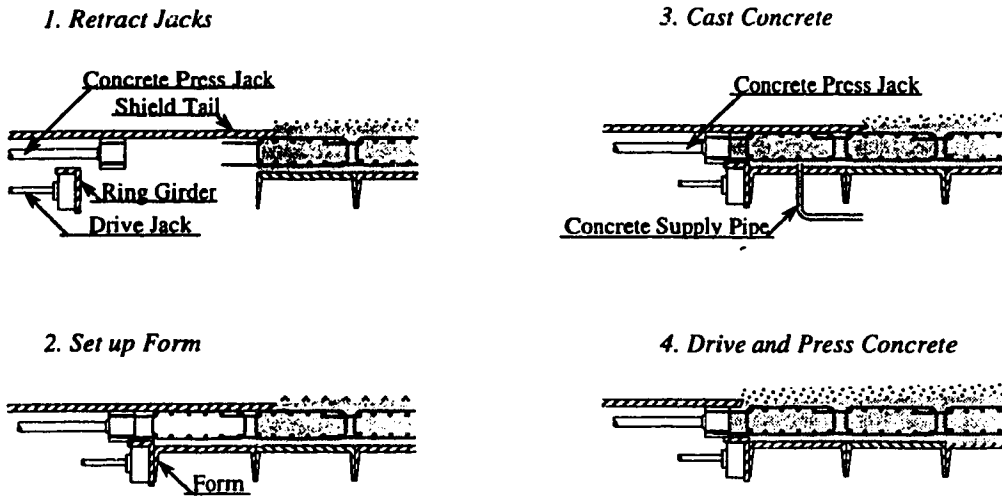


Typical Precast Concrete Segment

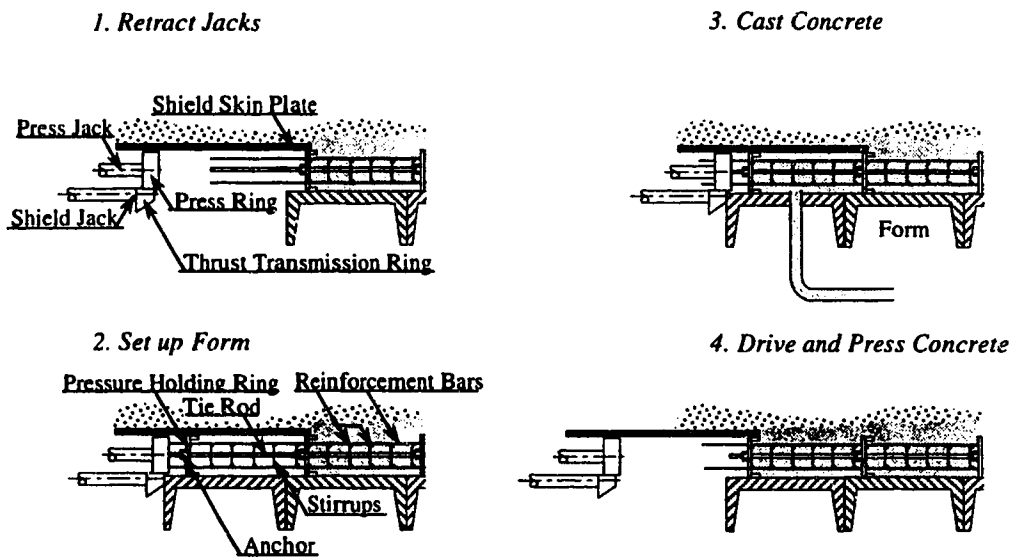


Typical Arrangement of Staggered Precast Concrete Segmental Liner
(after Krywiak and Morison 1990)

Figure 2.3: Precast Concrete Segmental Liner



a) Extruded Reinforced Concrete Liner using Self Sustained Concrete (after Okada 1989)



b) Extruded Reinforced Concrete Liner using Rings and Tie Rods (after Sato 1989)

Figure 2.4: Construction Sequence of Reinforced Extruded Concrete Liner

- (1) the concrete mix must have high workability in order to insure that the forms and the tail void are adequately filled;
- (2) the forms are expensive and the space is very limited inside the tunnel, therefore, the concrete mix that develops high early strength is of great benefit since it reduces the required number of forms; and
- (3) no additional insulating layers are provided between the liner and the ground, therefore, the concrete must have excellent long term water tightness, cracking resistance, and durability.

Further details about the extruded concrete lining system used in the Lyon metro Line D project are found in Babendererde (1989).

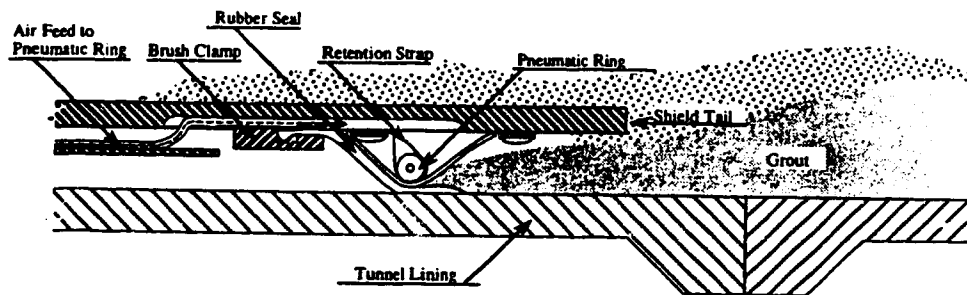
2.3.2.1.3 The Tail Seal

The basic engineering function of the tail seal is to provide a buffer between two zones: the tail void, kept under grout pressure, and the excavation chamber with normal pressure conditions. Furthermore, the seal is required to have enough flexibility to allow the movement of the tail skin with respect to the lining, and to accommodate the expected irregularities in the lining surface while maintaining the pressure gradient. Figure 2.5(a) shows a typical rubber tail seal (Bartlett et al., 1973). As explained by Babendererde (1991), the effectiveness of rubber seals depends on their flexibility and the accuracy of the liner construction. Japanese technology commonly uses, with a fair amount of success, steel brush seals, Figure 2.5(b). A number of rows of steel brushes, between three and five, are placed one behind the other. Grease is injected between the rows under different pressures to allow a gradual pressure transition.

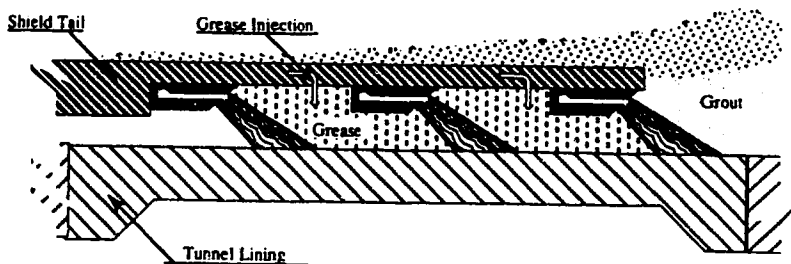
In the case of the extruded concrete lining, the tail seal is a part of the tubing. It consists of a steel ring connected to the shield by a hydraulic jack. Two rubber seals close the ring to the shield skin from one side, and to the concrete forms from the other side. Pressure inside the extruded concrete is regulated by a special jacking system. Figure 2.5(c) shows the tail seal used in the construction of the Lyon metro Line D project, based on the description provided by Ferrand and Bouyat (1985).

2.3.2.1.4 The Slurry

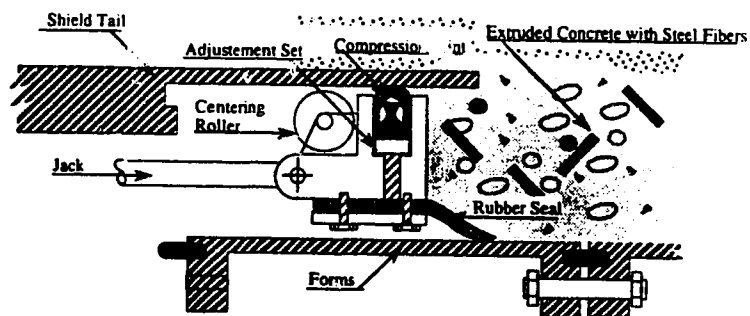
The two main functions of the slurry is to maintain face stability and to transport the excavated soil. Interaction between the slurry and the ground material is characterized by a continuous process of building and destroying the cake layer. Under a designated face pressure, the slurry is supposed to mix with soil particles and to infiltrate the ground up to a certain depth. The thixotropic property of the bentonite provides the cake layer with a



a. Rubber Seal



b. Steel Brush Seal



c. Sealing for Extruded Concrete Liner

Figure 2.5: Tail Seals for Bentonite Slurry Shields

certain degree of cohesion and at the same time the ground permeability is reduced. As the excavation advances, the cake layer, or a major part of it, is destroyed and the newly exposed face undergoes a process of mixing with the slurry. The time required for the new cake layer to be built and to acquire its properties is crucial to the success of the face stability. After excavation, the muck, which is a mixture of soil and bentonite, is supposed to be cleared from the excavation chamber and to be pumped in to a treatment plant. This requires that the slurry has an adequate degree of fluidity. Bouyat et al. (1985) presented results of a laboratory study investigating the effect of the slurry mix composition on the required properties of the slurry. During the construction of Lyon metro Line D project, about 60 kg of dry bentonite per cubic meter of water was used for ground conditions consisting mainly of gravel. In some instances the amount of bentonite was increased to 70 and 80 kg in order to achieve better watertightness.

2.3.2.1.5 The Grout

Grout injection is designed to fill the tail void between the liner and the ground while the tail seal keeps the grout under constant pressure until it cures. The manual technique of application consists of injecting the grout sequentially behind each segment of the cross sectional ring. Thus, uneven grout distribution may result because of the relatively long trajectory from the grout hole to the segment borders and because the injection is not carried out simultaneously throughout the section. Automated grout, as described by Borttscheller (1990) is performed longitudinally through the tail of the shield. Thus, it produces a good distribution of pressure and the grout material is evenly distributed both radially and longitudinally because all injection nozzles at the lining ring are activated within a short period of time. On the other hand, the placement of the grout pipe under the tail requires that the tail void be of greater thickness than if the grout pipe was not placed under the tail. Also, grout material is transported to the tunnel using a silo car and an agitator prepares the mix while a thick matter pump presses the grout simultaneously into the nozzles. A rotor distributor is designed to inject all nozzles with the grout mix according to a predetermined cycle. Then, operation controls insure that a certain grout volume is evenly distributed around each section at appropriate levels of pressure.

Grout material is composed, in general, of a cement clay mixture. The cement-water ratio is directly related to the mechanical properties of the mortar. Fillers, such as natural sand are added to the mixture and have the effect of improving the consistency of the mixture. Clay or bentonite is added in order to improve the penetration and watertightness of the grout and to reduce the aggregate segregation and water filtration processes that are responsible of the loss of grout efficiency. A detailed description of

grout materials and grout methods are presented by AFTES (160)¹.

2.3.2.1.6 The Treatment Plant

The main purpose of the treatment plant is to build up the slurry circuit to insure the continuity of the excavation. The need to provide a spacious area above ground for the plant in proximity of the excavation is one of the drawbacks of the bentonite slurry shield method when used in congested cities. Figure 2.6 shows a typical treatment plant for a bentonite slurry shield as described by J. J. Vanheuser (1985). An air compressor is only required for the Hydroshield type and can be mounted on the ground (as shown in the figure) or inside the tunnel. Here, the slurry circuit inside the tunnel consists of feeding and discharging tubes, and a short circuit pipe (used in case of emergency to empty the feeding pipe) and the discharging pump. In some cases, a primary screening system extracts large-sized particles from the discharging pipe before they reach the pump. Inside the tunnel, a pumping system evacuates the slurry chamber and conveys the excavated material with the slurry. Above the ground surface, the discharged muck undergoes successive steps of screening in order to dispose of the coarse grained materials and to reconstitute the slurry. The figure shows three steps in the process: the vibrating screen, then two cyclones with different capacities. The screening system is able to separate soil particles as small as 100 μm , while high performance cyclones may sort materials reaching a lower size limit of 25 μm . Centrifugal systems may separate up to 10 μm . A mixer plant prepares the slurry mix to the designated mixture and sends it to the reservoir, where feeding pump conveys the slurry to the tunnel.

2.3.2.1.7 The Control System

The complexity of the control system results from the numerous objectives that have to be met during construction. The control system includes a collection of measurements, data processing, and construction controls. Measurements are taken to cover a number of items that may exceed 50. Basic information includes data related to the ground movements, shield alignment, face slurry pressure, discharging slurry flow, slurry specific weight at feeding and discharging, excavated dry soil weight, cutter torque and rotation, shield jack speed and propelling force, mechanical performance of the shield equipment, and so forth. Data processing requires the identification of management items in a sequential list of priority, and establishing of target values within allowable limits for each item. Construction involves the evaluation of the processed data and the possible changes in the priority list depending on the progress of the construction.

¹Association Française des Travaux en Souterrain

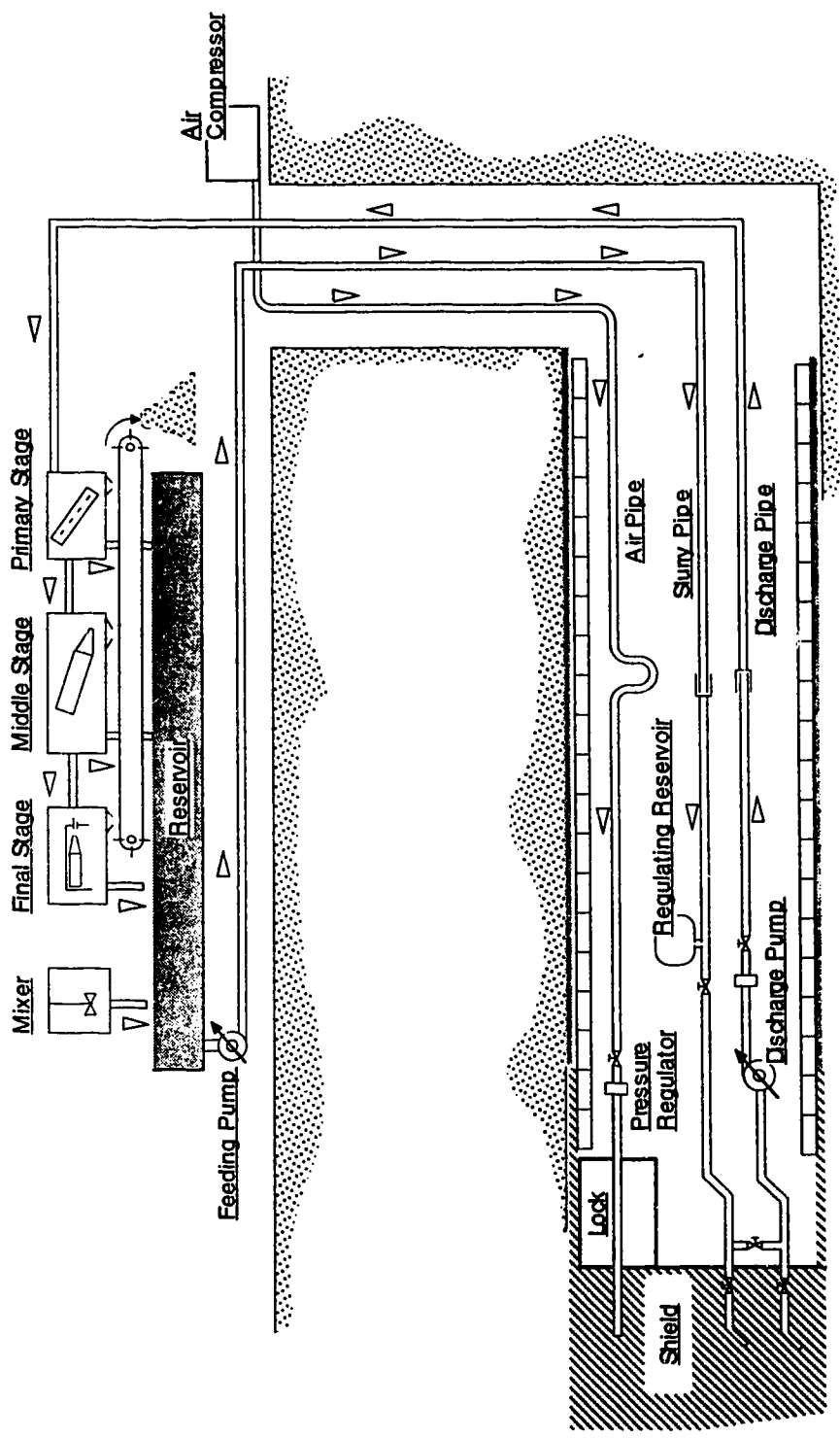


Figure 2.6: Treatment Plant for the Hydroschild (after Anheuser 1985)

2.3.2.2 The Earth Pressure Balanced Shield

The basic principle behind the Earth Pressure Balanced Shield (EPBS) is to stabilize the face by controlling the volume of the excavated soil, and that evacuated from it. As a result, the shield is comprised of a chamber where soil is kept under pressure to equalize ground pressure at the face. Figure 2.7 shows a typical shield based on the description provided by Kasali and Clough (1983). From the figure, a bulk head is placed behind the cutter head of the shield to form a closed space: the excavating chamber. Cutting bits at the face direct the loosened soil through slots in the face into the spoil area. A screw conveyor then evacuates the spoil chamber in a controlled manner according to the rotational speed of the auger. Finally, a conveyor belt disposes of the muck to the mucking cars. The basic features of the overall movement encountered in the case of BSS are met in EPBS: shield jacks are responsible for moving the shield forward and for providing the necessary reaction for the face stability by pressing on the already constructed solid liner. Furthermore, the tail void and the grouting system are similar to those of the BSS.

2.3.2.2.1 The Shield

The cutting system of the EPBS is supposed to have a high degree of endurance and effectiveness since the excavation proceeds generally without additives to increase the fluidity of the ground and because the cutting system is supposed to drive the excavated soil through an almost completely closed face. Cutter-bit performance depends on its hardness and fracture resistance to operational conditions. Early detection of worn cutter bits has an impact on improving the construction performance. The cutter head is supported by the main bearing, and reliable performance of the bearing requires complete sealing from water, as well as, regular rotation of the cutter head. Various design schemes for the excavation chamber and the cutter head are adopted to achieve certain performance requirements. Also, the dimensions of the excavation chamber have a direct impact on the stability of the face as a larger excavation chamber offers more constant and uniform support to the face. Different schemes are developed to optimize the performance of the cutting head and the excavation chamber for different ground conditions together with the structural system of the shield, Nishitake (1990). As shown in Figure 2.8, Scheme (1) provides good space distribution although an extra large, high reliability bearing is required. Scheme (2) is suitable for harsh working conditions as the seal has a small diameter and more rugged construction. Scheme (3) allows a smooth flow of excavated soil and the installation of a relatively large, ribbon-type auger. According to Nishitake (1987), an auger of this type can handle boulders up to 250 mm in size. Scheme (4) has the advantage of preventing sticky soil from adhering to the centre area. In a case where

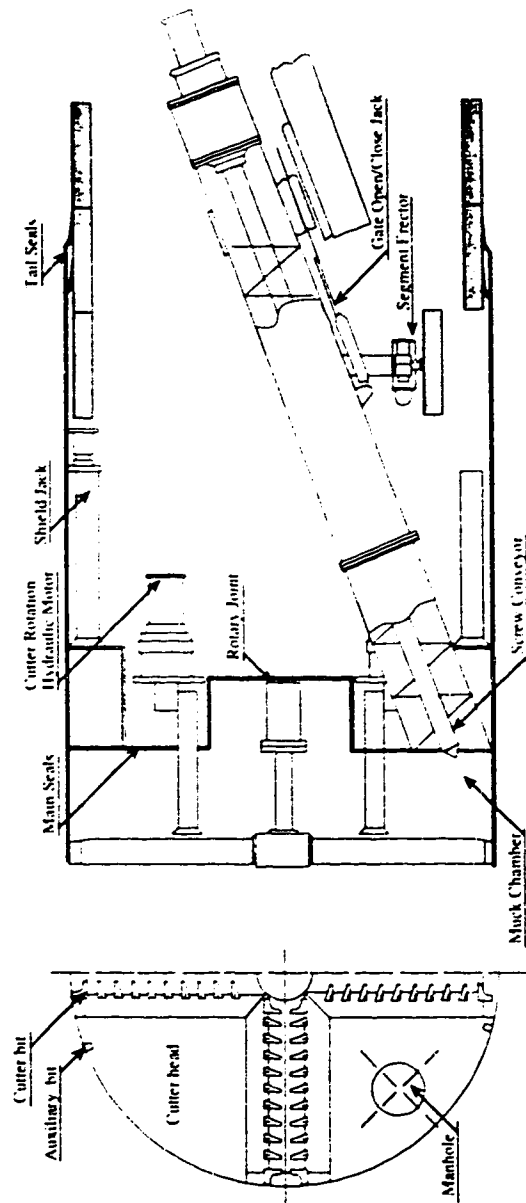
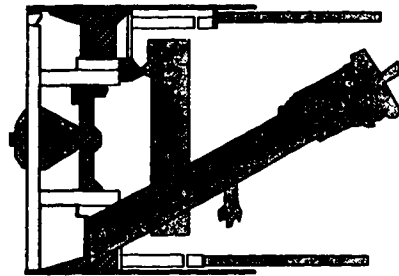
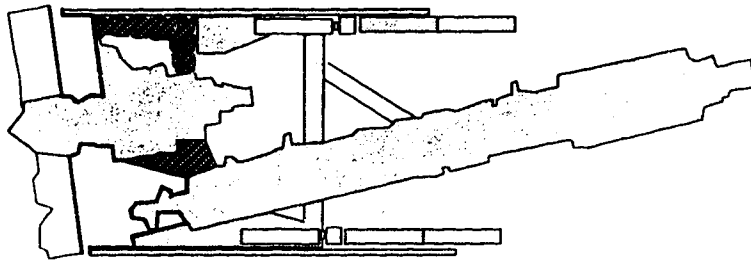


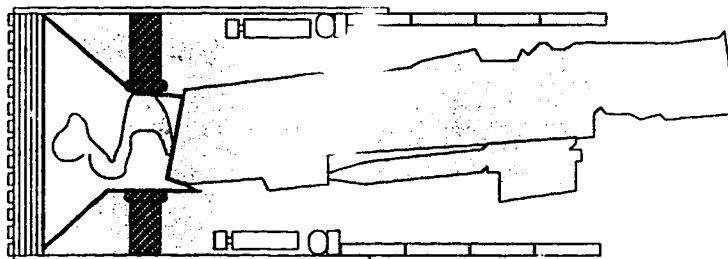
Figure 2.7: The Earth Pressure Balanced Shield



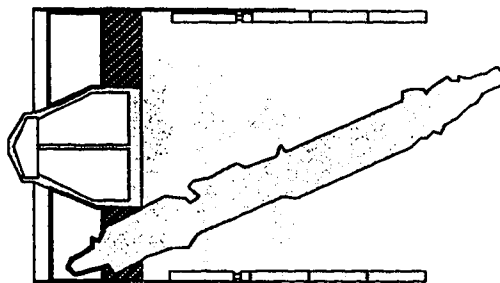
1. Intermediate Cutter Support System



2. Cutter Shaft Support System



3. Cutter Drum Support System



4. Centre Cone Support System

Figure 2.8: some Mechanical Arrangements of Earth Pressure Balanced Shields
(modified after Nishitake, 1990)

boulders encountered are of a size larger than the auger can handle, a crushing process is required either at the cutter head using roller cutter bits, or inside the excavation chamber using a stone crusher device. Nishitake (1990) shows different stone crushing methods and devices.

Pressure inside the chamber is supposed to equilibrate the face pressure, so special pressure sensors are supplied inside the excavation chamber to measure the chamber pressure. The accuracy of these sensors depends on their quality, number, and position. Typically, two to three sensors are mounted on the cutter head and four to six sensors are mounted on the bulk head. Also, homogeneity of the mixture is necessary to insure that the chamber is under uniform pressure. The method used in conveying and transporting the muck requires that the excavated soil has a certain amount of consistency. Groundwater may expose the excavation process to two possible problems: water intrusion through the auger and into the tunnel which may cause flooding of the tunnel; and work interruption, or in the case of highly plastic soils mud formation may plug the excavation and material handling devices. Frequently, special additives are used in the excavation chamber to control the mix quality, thus, new tunnelling methods are being developed based on the principles of the EPBS but with special agents added to the mixture (such as soil plasticizing shields or a mud pressurized shield). An example of a soil plasticizing shield in gravely subaqueous ground conditions is presented by Sasanbe and Matsubara (1986) in the construction of the Nagoya Municipal Subway . A clay-bentonite-water mix takes the place of the void water in the ground and thus improves the properties of the excavated soil with respect to its fluidity and its impermeability. Tamai et al. (1989) describe the use of a super-absorbent polymer in the control of groundwater during the construction of an EPBS tunnel passing through a highly pervious layer under a river. Nishitake (1990) noted that high density slurry may even be injected from the face to improve the properties of the unexcavated ground.

2.3.2.2.2 The Auger

The auger plays the key role in controlling the pressure in the excavation chamber. The rate of muck evacuation is related to the rate of advance of the shield. If the volume of soil removed from the excavation chamber exceeds the volume of ground entering it from the face at a certain time period, pressure drops in the chamber and vice versa. At the same time, a smooth pressure transition from the inside of the auger to the tunnel space is achieved as results of a specifically designed rotation speed which is chosen depending on the auger dimensions. Water tightness of the discharge mechanism is achieved by adding special devices to the gate of the auger. Nishitake (1990) describes a number of water cut

off devices commonly used including the two stage screw conveyor, casing rotator, and rotary hopper.

2.3.2.2.3 The Lining System and the Tail Void

There is no noticeable difference in practice between the lining system and tail void grouting and sealing processes for EPBS and those used for the bentonite slurry shield. Precast concrete segments are the most common lining systems in actual conditions although extruded reinforced concrete liners and extruded fiber concrete liners are adopted as well. Rubber and steel-brush tail seals are commonly used to support the shield tail.

2.3.2.2.4 The Control System

The data collection stage of the control system includes a number of aspects which affect the construction operation:

- (1) pressure inside the excavation chamber- Direct measurement of the chamber pressure is provided by pressure sensors. A certain shoving speed is preselected. Accordingly, the cutter disc operation and the thrust forces in the shield jacks are adjusted. Direct regulation of the chamber pressure is achieved through the speed of the screw conveyor;
- (2) the amount of displaced soil mass- The volume of soil entering the shield may be calculated as the speed of shield advance by cross-sectional area. The volume of discharging soil is calculated from the speed and the capacity of the screw auger. Excavated soil density is determined, also, by means of integrating a continuously calibrated load cell inside the conveyor belt and/or by weighing the muck car;
- (3) machinery monitoring- Detection of worn cutter bits is achieved through a number of ways: using a supersonic thickness meter, monitoring hydraulic pressure of the pipe buried inside the bit, or by checking the insulation condition in an electric wire. The load acting on the main bearing is measured through the load cell and this gives an indication of the state of the bearing system; and
- (4) underground investigation- Occasionally, data related to ground conditions may also be collected through different means, in order, to detect ground cavities or ground obstacles ahead of the face. A drilling probe attached at the cutter head to measures stiffness of the ground before excavation, while installation of a number of probes gives a picture of the distribution of soil strength at the face. Also, the ultrasonic-wave method is used to determine the overcut volume and, thus, to provide an early estimation of the grout volume required for the back filling. Seismic waves may also be used to detect obstacles in the ground, and the specific

electric resistivity methods may provide information about existing cavities.

Changes in the pressure chamber and in the speed of revolution of the screw conveyor with respect to time are monitored during construction as part of the data processing stage. Depending on the method of control of the auger, a certain tolerance in the variation of pressure is established. Also, manual control of the auger demands higher tolerance than automatic control. After a certain operational time, a pattern of relationships between the three parameters(the pressure in the chamber, the auger speed, and the speed of the screw conveyor) is established and any deviation from this pattern may signify a sudden change of site conditions, a mechanical problem, or an irregularity at the face. Data processing also is intended to cover mechanical performance of the machinery, control of grout material, alignment of the shield, and so forth . The sorting of the data processing items in priority order is regularly reviewed during the construction control stage depending on their urgency or whether a new element in site condition has been met.

2.3.2.3 The Compressed Air Shield

Compressed air was used for long time in construction works dealing with water bearing ground conditions. The first attempt to use compressed air in tunnelling took place in the Hudson River Tunnel-Part One, in 1878-1882 between New York and New Jersey. In addition, Greathead was the first to use compressed air in conjunction with a shield during the construction of the City & South London Railway in 1886. Since then, the basic constituents of the tunnelling method have started to emerge and a tradition of practices has established itself. In practice, a plant including a system of compressors feeds air to the face of the tunnel where excavation proceeds in dry conditions. Then, a system of bulkheads and air locks control the movement of machinery and personnel to the tunnel face.

2.3.2.3.1 The Shield

Figure 2.9 shows an arrangement for a compressed air shield used in the construction of the Cairo sewerage system as demonstrated by El Nahhas et al. (1992). Basically, air pressure is supposed to inhibit water intrusion into the gallery, and ground properties in the dried region are supposed to improve enough to sustain face stability. Therefore, open face excavation may proceed using cutting equipment that is suitable to the ground. In many instances, dried soil strength is increased by pregrouting either from the ground surface or from the face itself. In the case of pervious granular soils, air losses are limited by the application of bentonite or a bentonite-cement mixture at the face. A shoving system using a number of hydraulic jacks and a segmented precast concrete lining system

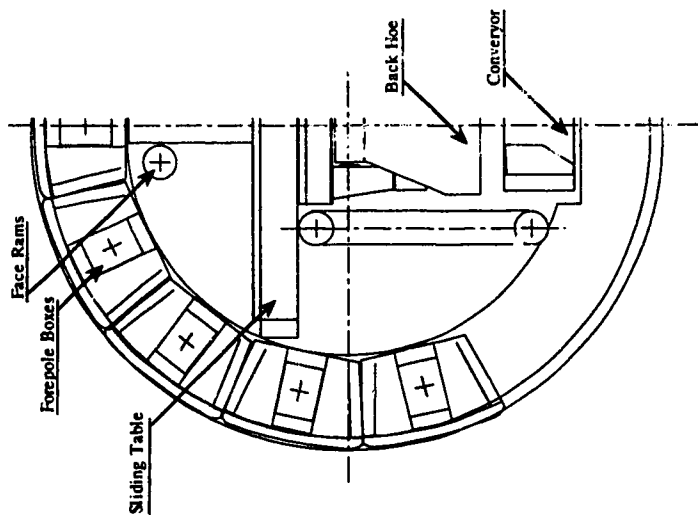
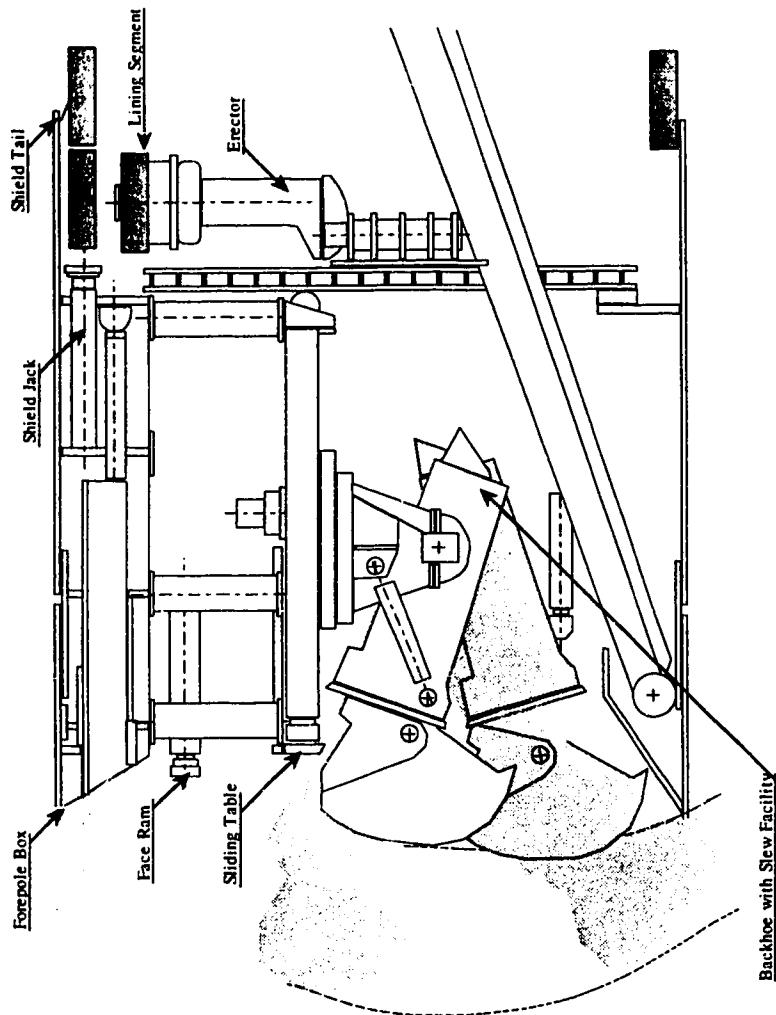


Figure 2.9: the Compressed Air Shield

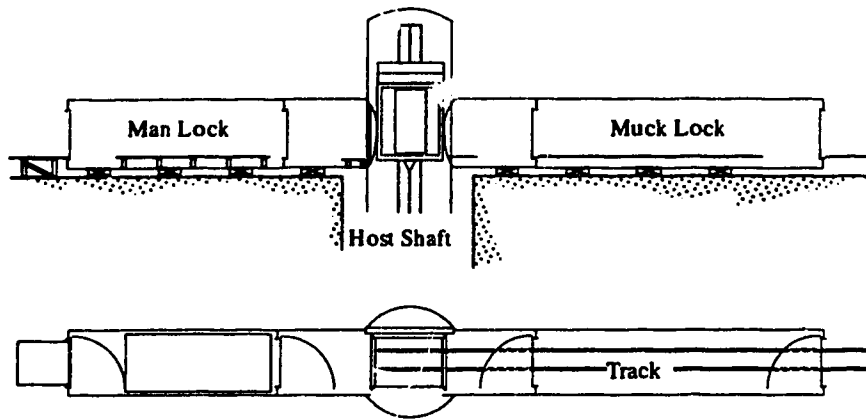
were used and are similar to those used for the EPBS method and BSS method.

2.3.2.3.2 The Locks

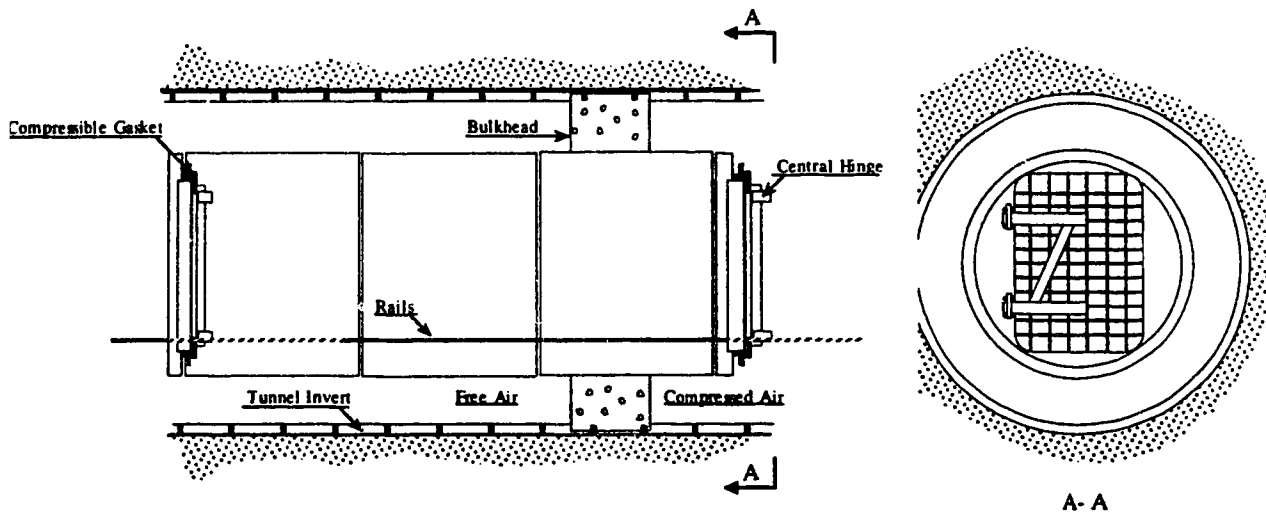
The most important part of compressed air tunnelling method equipment is the bulkhead. The purpose of the bulkhead is to seal off the working space from outside air. Usually the amount of force resulting from the difference of pressure at the cross section of the tunnel is substantial, therefore, a well built structure is necessary. Mass concrete is the most common material used in building bulkheads. Here, a decision has to be made either to transmit the reaction to the surrounding ground by shear or to the lining system behind the bulkhead into the ground. The design of the bulkhead, therefore, must include locks for material and personnel passage to the face. In addition, all services necessary to the pressurized working area have to pass through the bulkhead including low pressure and high pressure air pipes, the water supply, the required electric power, the light and control cables, the telephone cables, the pumping mains, the slurry supply and pumping equipment, and so forth. . Concrete must be fabricated with great care in order to insure that no voids are left for air to escape through joints around pipes passing through, and to insure good contact with the lining for transfer of shield thrust force.

Figure 2.10(a) shows a typical boiler lock, based on the description provided by Megaw and Bartlett (1988). The figure shows that the bulkhead is closer to the pressurized zone so that the steel-cylinder skin of the lock comes under tension when the pressure inside the chamber is raised. The lock consists of two airtight doors for passage from the atmosphere into the lock and from the lock into the working space. In order to pass from the atmosphere to the working space which is at a pressure higher than the atmosphere, a worker enters the lock chamber and closes the door behind him/her. Air pressure is feed into the lock until it is equal to that of the working space, then the worker is free to proceed into the pressurized area. Two separate types of locks are necessary: locks for personnel and for materials. For hygienic reasons, the rate of air decompression of the personnel lock is regulated to be slower than that required for the material lock. Additional locks may be needed for special purposes. As the period of time required for air decompression is considerable, in some instances, workers may pass rapidly through the personnel lock and then go to the decanting lock where air is recompressed and slowly decompressed. In the case of air sickness, medical treatment may be provided in a special lock.

In some instances locks are more convenient on the ground. In this case, a T-lock may be placed at the shaft entrance as shown in Figure 2.10(b). Thrust forces act vertically upward and may be equilibrated by the dead weight of the locks.



Section and Plan of T-Lock at Shaft Head



Boiler Lock inside the Tunnel

Figure 2.10: Compressed Air Locks used in Tunnelling Works

2.3.2.3.3 The Compressor Plant

The compressor plant is located above the ground surface. The plant is comprised of different types of low and high pressure compressors units which are used for supplying compressed air to maintain the face pressure, providing power supply to air tools for excavation, drilling, air winching, and other purposes. A cooling system is incorporated into the compressor to release the generated heat from the compressed air and to reduce its humidity by condensation. This is, especially, important as working conditions in a tunnel usually consist of high humidity which may result in fog in the working chamber.

2.3.2.3.4 The Control System

Besides aspects of the control systems which deal with ground conditions and machinery performance that are discussed in Sections 2.3.2.1.7 and 2.3.2.2.4 and which are applicable to a certain extent in to the compressed air tunnelling method, medical control of the effect of decompression on crew members is of great concern when compressed air is used in construction. As mentioned by Jardine (1991), decompression sickness is classified into two types. Type I includes joint pains and skin disorders while Type II includes symptoms such as dizziness, sensory impairment, vertigo respiratory disorder, vomiting, paralysis of the limbs, and/or partial or complete unconsciousness. Also, the disease related to air decompression is Hyperbaric osteonecrosis: the death of areas of tissue within the limbs that may occur at the hip or the shoulder joints and may result in collapse of the joint and loss of function or a disability. Thus codes of practice are formulated to provide guidelines for compressed-air usage in the industry. In Great Britain, "Blackpool Tables" establish limits on working periods and periods of exposure to compressed air. The limitations imposed to prevent decompression sickness have a substantial impact on work organization. For example, according to the Tables, at a maximum pressure of 3.4 bar, exposure exceeding 4 hours requires 6 hours and 35 minutes of decompression time to follow. As a 12 hour limit for shift work is scheduled for exposure time plus decompression time, this allows a maximum actual working period of 5 hours and 25 minutes at this pressure level.

2.3.2.3.5 Tail Seal, Lining System and Grout

The major difference between the compressed air shield and the other two shields is that the pressurized zone extends from the tunnel face backward up to the rigid bulkhead at some distance behind the shield while in the BSS or the EPBS the bulkhead is inside the shield. At the shield tail the ground surface is under air pressure which limits the possibility of ground or water intrusion into the working zone. Therefore, the importance

of the role played by the grout and the tail seal is diminished as they are needed to deal with ground under supportive air pressure. A conventional grouting system may be regarded as sufficient in many instances. In these cases, pea gravel is used as the primary grout material followed by mortar sometime later.

As a result of having the bulkhead behind the shield, air pressure is not transmitted to the ground through the liner. Furthermore, as the design of the cutting system and the muck disposal system are not restricted by pressure zoning inside the shield, a rotary cutterhead for excavating the full face is not indispensable. As a matter of fact, manual digging may be used (see Vinnel and Herman, 1969). Because of the above two reasons, the required longitudinal reaction from the lining system is relatively low. Segmented steel liners may be used in addition to the precast concrete segmented liner.

2.3.2.4 Other Methods

The classification of pressurized tunnelling methods as expressed in Section 2.3 embraces the major design requirements of construction technology and, hence, most of the tunnelling methods compiled from the literature may be tabulated into the three major categories as shown in Table 2.1 . However, some excavation methods may be classified, at least for the present state-of-the-art, as "other methods". The main reason behind this exemption is to stress a certain aspect of the construction method that may have an effect on the further developments currently taking place in the three main tunnelling methods.

2.3.2.4.1 Pipe-jacking

Pipe-jacking is a well known technique in microtunnelling and small-diameter tunnelling. Its main feature is that the thrust force of the shield is transmitted through hydraulic jacks to thrust rings in the lining system which consists of pipe segments and from the pipes to a bearing frame which is installed against a rigid rear wall at the beginning of the pipe line. Compared to other small diameter tunnelling techniques, like auger boring methods, pipe-jacking is characterized by a shield protecting the face of the excavation and the main function of the auger, if used, is to remove the excavated soil. The propelling of the pipe line follows the excavation in order to advance the shield. In auger boring methods, pipe propelling is part of the excavation process through which a cutter shoe is placed at the front edge of the leading pipe segment. Thus, the face stability is controlled by the forward movement of the pipe and by the capacity and position of the auger. Because of the availability of a wide variety of shield types, the pipe-jacking method which was applied in the construction of tunnels of diameters reaching 3.25 m in Alexandria, Egypt, (McCusker, T.G. in Sinha, 1989) is competitive with the compressed air shield, the

#	Shield Type	Description	Project	Ground Conditions	Purpose	Length (km)	H (m)	D (m)	date	Lining	References
1	BSS, Hydroshield		Antwerp-Metro Line 2	Fine sand	Subway	4.40	9-18	6.4	77-81	7 PCS+ key	1, 2, 3, 4, 5
2	BSS, Hydroshield		Antwerp-Metro under Scheldt River.	Heavy clay (Boom clay) under GWT.	Subway	2.01	-11	6.8	85	6 PCS+ Key	6
3	BSS, Hydroshield		Berlin	Mixed face: boulder clay, with sand lenses, under GWT.		2x1.077	6-10	6.6	88-89	7 PCS+ key	86
4	BSS, Hydroshield		Berlin	Sand with cobbles under GWT.		1.10	7.5- 12	6.4		PCS	1
5	BSS		Bordeaux	Sandy clay		0.24		1.4	81		4
6	BSS		Cairo	Silty sand with some boulders and cobbles under GWT.	Sewage	1.34		5.15	87	PCS	7, 81
7	BSS, Hydroshield		Cairo	Silty sand with some boulders and cobbles under GWT.	Sewage	2.30		6.11	87	PCS	7, 81
8	BSS		Cheshire, Warrington	Mixed: sand, sandstone, bouldery gravel at GWT.	Sewage	1.17	4-5	2.87	75	5 PCS	4, 8
9	BSS, Hydroshield		Edmonton	Variable: bedrock, sand and gravel, sand. All above GWT.	Subway	0.31	15.00	6.56	89	7 PCS+ key	9, 10, 11
10	BSS, Thixshield	Excavation face is supported by a bentonite suspension under pressure. Soil is loosened by a cutting arm with a cutting head in the bulkhead wall. Dredging pump evacuates the soil-slurry mixture from the chamber.	Gelsenkirchen	Mixed face: sand, silty sand, and chalk marl under GWT.	Railway	2x0.63	>3.5	7.29	79	6 SS (w)	12, 5

Table 2.1: Case Histories of Tunneling Projects Constructed using Pressurized Shields

#	Shield Type	Description	Project	Ground Conditions	Purpose	Length (km)	H (m)	D (m)	date	Lining	Reference
11	BSS, Mixshield, Hydroshield	The machine is allowed to change from bentonite slurry shield method into an other tunnelling method, stone crusher is added into the slurry chamber of the hydroshield to cut boulders.	Grauholtz	Variable: from silty clay to pure gravel, boulders are encountered in many occasions. Most of the tunnel is below GWT.		Bentonite: 14.34 Water: 4.63 Dry: 9.00	Variable	11.6	91	6 PCS+ key	13, 14, 15
12	BSS, Hydrojetshield	Hydroshield	Hamburg-sewer Bluhmstraße Hamburg	Medium Sand	Sewage			1.96-3		Concrete pipes	1
13	BSS, Thixshield			Variable: sand or clay containing sea silt under variable GWT due to Tides.	Sewage	0.36	4.00	4.18	78		5
14	BSS, Hydroshield		Hamburg-wilhelmsburg	Coarse to fine sand below GWT.	Sewage	4.56		4.32	74		4, 5
15	BSS, Hydroshield		Hamburg-Wilhelmsburg	Sand and gravel under River, under GWT.	Sewage	0.54	16.50	4.35		PCS	1
16	BSS		Hiroshima	Medium fine sand under river.	Sewage		2.6-4.9 (ground)	3.48	83-84	PCS	16
17	BSS		Kaohsiung	Sand under GWT.	Sewage	3.36	7.5-11	3.27	81	PCS	17
18	BSS, Hydroshield		Lille, Lille Metro, Lot3	Mixed: alluvium silty sand and chalk under GWT..	Subway	1.77	8-12	7.7	86	7 PCS+ key	18, 19
19	BSS		Lille, Lille Metro, Lot8	Variable: Fissured chalk or silty sand under GWT.	Subway	0.99	7-10	7.65	87	5 PCS+ key	20
20	BSS		London	Gravel at GWT.	Test	0.14	8.00	4.1	72	CIS	4
21	BSS, Hydroshield		Lyon, metro line-D	Gravel under River.	Subway	0.96		6.5	84-85	EF C	4, 21, 22, 23, 24, 25, 26, 27

Table 2.1: Case Histories of Tunnelling Projects Constructed using Pressurized Shields (continued)

#	Shield Type	Description	Project	Ground Conditions	Purpose	Length (km)	H (m)	D (m)	date	Lining	Reference
22	BSS		Mexico City	Highly compressible clay under GWT.	Sewage	5.34	9.70	4	84-86	6 PCS	28
23	BSS, Mixshield		Mulheim	Alternating vertical bands of sandstone and limestone with boulders under River.	Subway	2.40	>7.5	6.9	89	6 PCS	29
24	BSS, Hydrosield		Mulheim/Ruhr	Variable: solid rock to loose rock (sand)					86	PCS	30
25	BSS		Nagoya	Variable: hard silt and fine sand- sand- sandy gravel and clay- sand and soft clay. Under sea.	Water	2.11	11-14	3.85	78	SS	31
26	BSS		Osaka	Sandy Gravel under sea		1.33	35.00	5.4	84	6 SS+ key	84
27	BSS		Osaka	Sandy Gravel under sea.	Gas	2.13	10-15 (sea)	3.84		6 PCS	32
28	BSS		Osaka Stormwater 1	Complex alternate strata of very hard dilluvium sand and gravel.	Sormwater	1.28	22.00	11.22	85	PCS	33, 34
29	BSS		Osaka Stormwater 2	Complex alternate strata of very hard dilluvium sand and gravel.	Sormwater	0.63	24.60	11.22	88	PCS	33,34
30	BSS, Hydrosield		Rome, Galleria Aurelia	Variable: Hard clay, silty sand, sand with gravel, or silty sand. All below GWT.	Railway	1.50	-30	10.6	89	8 PCS+ key	35, 36, 2, 37, 38, 17
31	BSS, mudwater	Bentonite Slurry Shield	Shikawa, Tokyo	Noncohesive, well compacted gravel, under GWT.	Railway	0.89	22-26	8.1		PCS	85
32	B'S		Takaido	Gravel with sand under GWT.		0.79	26.00	2.4			39

Table 2.1: Case Histories of Tunnelling Projects Constructed using Pressurized Shields (continued)

#	Shield Type	Description	Project	Ground Conditions	Purpose	Length (km)	H (m)	D (m)	date	Lining	Reference
33	BSS		Tokyo	Gravel and Sand below GWT.	Railway	2x.844		10	80		4
34	BSS		Tokyo	Variable: sandy soil or clayey soils. Under river		1.59	38.6-33.7	3.73			82
35	BSS		Tokyo, Shinuzaki	Sandy soil under GWT	Sewage	1.13	7.05	3.92			72
36	BSS		trunk sewer			0.62		2.4			39
37	BSS, Hydroshield		Ushiku	Sand under GWT		2x4.8	50.00	9.25	84-88	6 PCS+ 2Kc/s	42, 43, 41, 2, 44
38	BSS		Villejust	Fine dense sand at and above GWT.	Railway	0.83		2.4			39
39	Compressed Air		Yotsugi	Sand under GWT			3.62	2.74	77	5 PCS	40
40	Compressed Air		Belfast	Mixed face: organic silt and soft silty clay (sleech). Under GWT.	Sewage	2.50		5.15	86	PCS	45, 83, 87
41	Compressed Air		Cairo	Mixed face: sandy silt and sand. Below GWT.	Sewage	1.03	6.00	3	79- 81	PCS	46
42	Compressed Air		Crimstby	Soft organic silty clay under GWT.	Sewage		16.00	5.65		6 SSS	47
43	Compressed Air		Oakland, California. BART Project	Recent Soil Marine Silty clay (Bay mud)	Subway	0.57	5.9	4	82- 85	4-6 PCS	48
44	Compressed Air		Shanghai	Soft clay under GWT	Railway (test)	0.76		5.4		PCS	49
45	EPBS, DK		Singapore	Soft Clay and permeable sand under G WT	Subway	1.26		2.10			50
46	EPBS, DK		Akshima	Variable: sand with gravel or silty clay				1.60			50
47	EPBS, DK		Amagasaki	Sand				1.6			50
48	FPBS		Amagasaki Bristol, England	Variable: very soft clay, then silty clay, then running sand under Avon River.	Bulk handling conveyor	0.56	6.00	3.4	11/92	6 PCS	52

Table 2.1: Case Histories of Tunnelling Projects Constructed using Pressurized Shields (continued)

#	Shield Type	Description	Project	Ground Conditions	Purpose	Length (km)	H (m)	D (m)	date	Lining	Reference
49	EPBS		Cairo	sand under GWT.	Sewage	6.60	~ 1.5	3.24-2.54	90	6 PCS	53, 54
50	EPBS, DK		Chigasaki	Fine sand							50
51	EPBS, LOVAT		Caracas metro 1	Variable: loamy sand, sandy loam, or gravelly sand, under GWT.	Subway	2x1.6	5-10	5.77	86	5 PCS+ key	55
52	EPBS, LOVAT		Caracas metro 2	Variable: hard shale or fissured shale with gravel inclusions.	Subway	4.30	6-11	5.77	88	5 PCS+ key	55
53	EPBS, LOVAT		Caracas metro 3	Variable: hard shale or fissured shale with gravel inclusions.	Subway		<50	5.77	88	5 PCS+ key	55
54	EPBS, DK		Hanamatsu	Sand with gravel under GWT.	0.526	0.85	7.70	2.00			50
55	EPBS, DK		Higashi-Osaka City	Silty clay							50
56	EPBS, DK		Hiroshima	Variable: silt or silty sand.	1.196			2.12			50
57	EPBS, DK		Ichihara	Variable: fine sand or coarse sand with clay				2.27			50
58	EPBS, Soil Plasticizing Shield	Super absorbent polymer; hydrogel absorbing several hundred times its weight in water, is added to the excavation chamber of the EPBS to control soil homogeneity inside the chamber.	Japan	Alluvium gravel then alluvium clay, under GWT and under a river.	Sewage	0.45	6.00	3.28		PCS	56
59	EPBS, DK		Kaohsiung-Taiwan	Sand under sea.		2.04	7.75 (ground) + 12.5 (sea)	3.91			50
60	EPBS, DK		Kobe	Sand							50

Table 2.1: Case Histories of Tunneling Projects Constructed using Pressurized Shields (continued)

#	Shield Type	Description	Project	Ground Conditions	Purpose	Length (km)	H (m)	D (m)	date	Lining	Reference
61	EPBS, Soil Plasticizing Shield	A Plasticizer (Kaoline clay- Bentonite- water mix) is injected by pushing at the face of the ground which lowers the permeability of excavated soil and improves its fluidity	Nagoya Municipal Subway	Loose, water bearing, gravelly soil, containing boulders.	Subway	0.88	13.00	7.43		PCS	57
62	EPBS, DK	A mud- making agent is added to the excavated soil in the excavation chamber to improve its properties: impermeability and fluidity.	Okayama			0.44		3.27			50
63	EPBS, DK		Osaka			1.566		2.86			50
64	EPBS		San Francisco	Soft sandy clay under GWT (Recent Eay Mud)	Water	0.92	9.10	3.7	81	6 SS	58, 59, 60, 61, 62, 63
65	EPBS		Shanghai	Mixed face: silty clay and silty sand under GWT.	Sewage	2.00	4.00	4.33		4 PCS	64
66	EPBS, DK		Shiga	Coarse sand				3.28			50
67	EPBS		Singapore	Soft Clay and permeable sand	Subway	0.76		5.4			65
68	EPBS	Compressed air was used for temporary works	Sprogø, Great Denmark	Mixed face: till (silty sand) and marl with boulders under sea	Railway	2x 6.9	15 m (minimum cover under sea)	7.7 (D)	91	6 PCS+ key	66, 67

Table 2.1: Case Histories of Tunnelling Projects Constructed using Pressurized Shields (continued)

#	Shield Type	Description	Project	Ground Conditions	Purpose	Length (km)	H (m)	D (m)	date	Lining	Reference
69			Taipei- Taiwan	Sandy silty or silty clay under GWT	Sewage	0.81	6-9	4.35	79-81	PCS	68
70	EPBS		Taipei- Taiwan	Silty sand or sandy silt under GWT.	Sewage	1.44	7.5-8.5	4.35	82	PCS	68
71	EPBS, DK		Tamamatsu	Silt	test	0.50	18.00	3.55	86	ERC	50
72	EPBS		Tokyo	Silty clay		12.80	12.80	3.68			69
73	EPBS		Tokyo	Sand with gravel		1.13		4.66			70
74	EPBS, DK		Tokyo	Silt		1.35		3.28			50
75	EPBS, DK		Tokyo	Sandy silt and fine sand under GWT.	Sewage	0.92	16.00	3.68	87-88	PCS	50
76	EPBS, Mud Pressurized Shield	In a closed excavation chamber, soil excavated by the cutter is mixed with additives by the mixing wing behind the cutter and the mud which has plastic fluidity and impermeability is retained inside the chamber.	Tokyo Sewer System(Omoni trunk)								71
77	EPBS, Soil Plasticizing Shield	Mud is injected under pressure into the excavation chamber to counteract soil and water pressure. Screw conveyor and mud chamber are kept full and muck is disposed of in form of mud with a certain consistency.	Tokyo, Ohta trunk sewer	Silt under GWT	Sewage	0.56	16.00	8.21		PCS	71
78	EPBS, Mud Pressurized Shield		Tokyo, Shin-Omori trunk sewer	Silt and sand under GWT	Sewage	1.21	16.00	5.84		PCS	71

Table 2.1: Case Histories of Tunnelling Projects Constructed using Pressurized Shields (continued)

#	Shield Type	Description	Project	Ground Conditions	Purpose	Length (km)	H (m)	D (m)	date	Lining	Reference
79	EPBS		Tokyo, Shinozaki	Cohesive soil under GWT	Sewage	1.11	12.80	8.48			72
80	EPBS		Tokyo, Shinozaki	Sandy soil under GWT	Sewage	1.63	10.30	5.24			72
81	EPBS		Tokyo, Shinozaki	Sandy soil under GWT	Sewage	1.55	9.70	4.44-4.69			72
82	EPBS		Tokyo, sewer between Arakawa and	Variable: dense sand or weak silt under GWT.	Sewage	1.04	13.00	8.48	77-78	8 PCS	73
83	EPBS, DK		Wakayama	Silty sand				2.58			50
84	EPBS, DK		Yokohama	Fine sand				5.03			50
85	MF	Excavating bentonite slurry shield machine to construct a double track tunnel at the same time.	Tokyo, Keiyo line	Variable: sandy clay or gravel, under GWT	Subway	0.62	24-27	7.2	90	PCS	74, 75
86	Pipe Jacking	Commercial name: Crushingmole	Tilbury, Essex	Mixed face: peat and sandy clayey silt under GWT.	Sewage		10.00	2.1			76, 77, 78
87	Injectoshield				Lab test						79
88	Spiral (H-V)										80

References

- 1: Anheuser (1982)
- 2: Anheuser (1985)
- 3: Cloquet (1985)
- 4: West (1988)
- 5: ITA (1981)
- 6: Wittmans and Bonvoisin (1988)
- 7: Wallis (1987)
- 8: Walsh and Biggart (1976)
- 9: Krywiak and Morison (1990)
- 10: Jones (1990)
- 11: Eisenstein and Ezzeldine (1992:a)
- 12: Hollstegge and Meseck (1989)
- 13: Steiner (1989)
- 14: Steiner and Becker (1991)
- 15: Steiner (1992)
- 16: Morimoto et al. (1985)
- 17: Becker (1985)
- 18: Briglia et al. (1988)
- 19: Kongrad and Anheuser (1988)
- 20: Hupin (1988)
- 21: Chaffois et al. (1988)
- 22: Bouyat et al. (1985)
- 23: Ferrand and Morcrette (1988)
- 24: Ferrand and Bouyat (1985)
- 25: Babendererfe (1987)
- 26: Morcrette and Bouyat (1986)
- 27: Morcrette (1988)
- 28: Schmitter et al. (1988)
- 29: Wallis (1991)
- 30: Gebower and Frohlich (1985)
- 31: Ohta et al. (1978)
- 32: Yamashita et al. (1988)
- 33: Hashimoto et al. (1988)
- 34: Hashimoto et al. (1985)
- 35: Cassinis et al. (1985)
- 36: Pandolofa (1986)

Table 2.1: Case Histories of Tunnelling Projects Constructed using Pressurized Shields (continued)

- References**
- 37: Capellani and Ottaviani
 38: Wallis (1984)
 39: Miki et al. (1977)
 40: Glossop and Farmer (1979)
 41: Piquant and Gesta (1986)
 42: Leblais and Bochon (1991)
 43: Guillaume (1989)
 44: Wallis (1986)
 45: El-Nahas et al. (1991)
 46: O'Reilly et al. (1991)
 47: Kuesel (1972)
 48: Maidl (1988)
 49: Shirlaw (1991)
 50: Hagimoto and Kashima (1985)
 51: Krause (1991)
 52: Darling (1992)
 53: Flint (1992)
 54: Darling (1991)
 55: Paulus (1988)
 56: Tamai et al. (1989)
 57: Sasanbe and Matsubara (1986)
 58: Clough et al. (1985)
 59: Clough et al. (1983:1)
 60: Rowe and Kack (1983)
 61: Finno (1983)
 62: Kasali and Clough (1983)
- 63: Clough et al. (1983:2)
 64: Maidl et al. (1990)
 65: Shirlaw and Doran (1991)
 66: Ostenfeld and Curtis (1992)
 67: Wallis (1992:a)
 68: Chi et al. (1985)
 69: Matsumoto et al. (1986)
 70: Murata et al. (1990)
 71: Matsuzaki et al. (1986)
 72: Magata et al. (1982)
 73: Saito and Kobayashi (1979)
 74: Matsumoto et al. (1989)
 75: Matsumoto et al. (1991)
 76: DeMoor and Taylor (1991)
 77: Mair and Taylor (1993)
 78: DeMoor and Taylor (1993)
 79: Mohkam (1989)
 80: Sonoda et al. (1992)
 81: Safwat (1983)
 83: Flint and Foreman (1992)
 82: Murakami et al. (1990)
 84: Ono et al. (1989)
 85: Shimizu and Maeda (1989)
 86: Wallis (1990)
 87: Ahmed (1990)
- Abbreviations**
 GWT: Ground Water Table
 ID: Internal Diameter
 PCS: Precast Concrete Segments
 SS: Steel Segments
 CIS: Cast Iron Segments
 EFC: Extruded Concrete with Steel Fibres
 ERC: Extruded Reinforced Concrete
 (w): welded
 MF: Multiface Shield

Table 2.1: Case Histories of Tunneling Projects Constructed using Pressurized Shields (continued)

EPBS, and the BSS. The method used for excavation and face support may involve any of the techniques of the compressed air or EPBS or BSS methods. Thus, in a sense, pipe-jacking is a pressurized tunnelling method where the reaction to the shield force is provided through pipe segments to a rigid supporting structure. An example of a pipe-jacking project is provided by De Moor and Taylor (1993) where a tunnelling machine, named the "Crushingmole" is employed which uses an excavation technique close to that of the EPBS method and which disposes of the muck using a slurry transport system.

2.3.2.4.2 The Multiface Method

The twin-tunnel arrangement needed for tunnels used for transportation purposes poses a number of problems, especially, with respect of the width of the ground surface trough movement and the stability of the ground between the two tunnels. Multiface tunnels have the advantage of being constructed of the twin tunnels with the smallest possible area and with the smallest possible excavated volume, thus, limiting the extent and the amount of ground deformation around the tunnels. A commuter line-the new JR Keiyo Line-was constructed in Tokyo, Japan, in 1990 over a length of 519 m with a height of 7.2 m and a width of 11.97 m as described by Matumoto et al. (1989). Special precast concrete segments were designed to fit the "one twin gallery section". The excavation method was accomplished using the BSS method.

When comparing the advantages and disadvantages of horizontal and vertical arrangements of twin tunnels, a clear final conclusion is not easily reached. Thus, combining the two methods in a Horizontal and Vertical tunnel (H&V Tunnel) was effected in a test tunnel in Japan, 1989, (Sonoda et al., 1992). Along the tunnel length of 70.5 m, two Slurry tunnelling machines, each of a 2.12 m diameter, allowed the construction of a phase with two separate vertical galleries and a phase with two horizontal galleries and the two phases are connected through joined spiral galleries. Special precast concrete segments were designed for the different arrangements and a detachable diaphragm was installed between the tails of the two bodies for assembly of either joined or separate segments.

2.3.2.4.3 The Injectoshield Method

An innovation that may be classified between the compressed air shield method and the Hydroshield is the "injectoshield". As described by Mohkam (1989), the method consists of injecting ground face with a slurry which is fed through the core of a cutter arm and which has appropriate characteristics for the ground condition. Through the nozzles at the tip of the cutter head, slurry under pressure penetrates the interstices of the soil over some depth and it also coats the face and, thus, forms a cake simultaneously with the

excavation. The confining pressure is compressed air which is then mobilized by the cake. The Injectoshield has the advantageous aspects of the Hydroshield that of forming a consistent cake layer at the face and using the improved impermeability property of this layer to confine air pressure that supports the face. At the same time, the process of destroying the cake layer for tunnel advance is accomplished in a controlled manner by using one telescopic cutter arm instead of the cutter head that excavates the whole face area at one time. This method is still at the stage of laboratory testing according to recent literature.

2.4 Performance of Pressurized Shields

Over the past fifteen years, shield tunnelling methods have been carried out around the world with a degree of success and they are considered highly competitive with other tunnelling methods such as the New Austrian Tunnelling Method (NATM), also called the Sequential Excavation Method (SEM), or with cut and cover construction schemes. Furthermore, the choice between different pressurized shield methods results in stronger competition. Table 2.1 shows some data collected from the literature regarding a number of excavating machines used in recent tunnelling projects. Inspection of these cases and the performance of the machines in these projects gives information about the terms and the means of the competition.

2.4.1 Requirements for Satisfactory Tunnelling

Requirements for successful tunnelling in soft ground as pointed out by Peck (1969) are :

- (1) the tunnel is feasible. Using an adopted construction scheme the excavation is able to be advanced safely and efficiently;
- (2) excessive damage to surroundings is prevented; and
- (3) the tunnel has the ability to withstand, during its lifetime, all the influences to which it may be subjected.

Even though the new innovations in tunnelling technology were not realized yet, Peck (1969) discusses the performance of machine-driven excavations compared to hand-mined tunnels and reaches the above stated conclusions which are still applicable for pressurized shield methods. Regarding the feasibility requirements, excavating machines provided with shields may reach appreciable levels of performance in firm and slowly raveling ground, while in the case of flowing or running ground conditions, improvement measures like predrainage, compressed air, or injections are imperative. The disadvantage of closed face shield methods is that they attack the entire face without allowing for visual inspection

which increases the damage risks when compared to hand mining where selective digging is adopted. The strain field induced around the excavation is highly dependent on the construction sequence and the degree of soil homogeneity. Settlement estimation should rely on previous records of settlements in comparable conditions, as well as, on statical calculations. Finally, the long-term requirements rely on the ability of the lining system to readjust and to withstand the earth pressure associated with the resultant deformation pattern.

Pressurized shield tunnelling methods have achieved considerable improvement with regard to the feasibility requirements. External measures to enhance face stability are effected from inside the shield and they include a variety of techniques besides using compressed air. Ground deformation around the excavation is not attributed only to ground loss but include new factors such as stress redistribution due to the movement and rigidity of the shield, grout performance, and the effect of lining systems even on the frontal part of the displacement trough at the ground surface. Therefore, Peck's recommendation regarding the importance of reviewing the performance of comparable tunnelling projects is even more appropriate in the case of pressurized shield methods. The complexity of the stress-and-strain fields induced by pressurized shields, together, with the complexity of the soil conditions and soil behaviour makes it harder to use calculations based on the principles of static mechanics to predict the expected ground movement within a practical margin of error.

2.4.2 Applicability of Pressurized Shields

Advances in pressurized shield tunnelling can be classified into two categories: advances in the tunnel design which imply the optimization of the selected construction method to achieve the best tunnelling performance, and advances in the construction method, itself, by improving the performance of the mechanical details involved in the project. Therefore, tunnelling practitioners are supposed to keep pace of the progress in the two domains of the technology when making choices about the method of excavation, the details of the ground control measures, and the economical evaluation of the construction scheme. The general rule is that every new project has its own peculiarities regarding its various aspects, such as the construction and the structural details, the economy, the environment, the machinery, the workmanship, and so forth. The final design scheme is supposed to be based on an evaluation of the recent performances of selected tunnelling methods in comparable conditions. Meanwhile, the various construction details involved in the project have to be sufficiently adaptable to unexpected site conditions. The performance of the three tunnelling technologies: the BBS, the EPBS, and the compressed air shield is

reviewed throughout the literature in order to compare their suitability to various site conditions and their prospects for improvement in the near future. The final assessment of a project is based on the integrity of the excavation and on the rate of progress.

2.4.2.1 The Bentonite Slurry Shield

Two types of technologies are increasingly competitive in the international market. The Hydroschild, a German concept of a bentonite supported face shield, represents the results of research efforts throughout Europe to produce a reliable and economically feasible machine to construct a safe excavation in difficult ground conditions. Japanese bentonite slurry shields were developed earlier and have been used extensively in Japan. More recently the Japanese technology has proven itself through being used in several projects around the world with a degree of success comparable to that of the German technology.

2.4.2.1.1 Historical Background

The general concept of the BSS may be viewed in the light of the historical background of the invention. The idea of the BSS started as an improvement to the compressed air shield. The health hazards of high air pressure made it desirable to minimize the compressed air zone, therefore the bulkhead is placed inside the shield rather than being rigidly constructed somewhere behind the face. This was first implemented in 1962 in Paris, France, at the construction for the La Folie and Etoile 10 m diameter tunnel. Although the operation was a success, workers had to enter the pressurized chamber to remove the spoil which failed the basic principle of avoiding work in compressed air conditions. The first BSS was designed by John Vernon Bartlett in 1964 having the basic features described in Section 2.3.2.1 and was applied in 1972 during the construction of an experimental tunnel in London (Table 2.1: 20). The ground conditions in the part excavated consisted of water bearing gravels and sands. The ultimate evaluation of the experiment was positive which encouraged the use of the method in Cheshire, England, in 1976 (Table 2.1: 8). The second project was not as successful as the first mainly due to the existence of large granitic cobbles and boulders up to 500 mm diameter. An improvement to Bartlett's idea was made by Erich Jacob from Germany who invented the Hydroschild. An "air accumulator" regulates the slurry instead of an automatic valve, therefore, losses of the face pressure due to sudden loss of slurry into the ground are immediately compensated for by compressed air. The first Hydroschild was operated in the construction of a sewage tunnel in Wilhelmsburg, Hamburg in 1974 (Table 2.1: 14) with a satisfactory advance rate. However, the principle of the BSS was not fully implemented in the project as the tail seal

was not considered reliable and compressed air was supplied from a shaft at the ground surface; therefore, the role of the slurry was confined to spoil removal. The complete principle of the Hydroschild was fully implemented in Antwerp, Belgium, in 1977 (Table 2.1: 1) during the construction of the subway system.

The development of the BSS in Japan has taken a different path. The method was first applied for small diameter sewage tunnels. According to Jacob (1976), Mitsubishi Heavy Industry constructed two slurry supported driving systems as early as 1961. In some instances, the mole was converted into pipe-jacking or used in conjunction with a pipe-jacking system. In 1970 a large diameter tunnel (7.3 m) was successfully constructed at the undersea section of the Haneda Tunnel of the Keiyo Railway Line. Since then, an increasing number of machines have been constructed, with the small diameter shields being used as drill heads for the pipe-jacking method while the larger ones (higher than 2.5 m diameter) are being used as conventional type BSS which are propelled against a segmented concrete liner.

2.4.2.1.2 The Hydroschild

Historical background has a direct impact on the applicability of the BSS. As shown in the previous section, drawbacks of the European technology, especially the German Hydroschild, were related to the tail seal and to the existence of boulders in the excavated ground. Also, as the nature of the ground in the early projects was mainly water-bearing sandy ground, tunnel designers were uncertain regarding the applicability of the Hydroschild in cohesive ground or in dry soil conditions. Inspection of Table 2.1 shows how this primary idea has been reinforced or changed during the last years.

Among the eighteen Hydroschildes, Thixshields or British designed shields referred to in Table 2.1, only three were constructed in cohesive soil conditions, namely the tunnels in Antwerp, Berlin, and Mexico City (Table 2.1: 2, 3, and 22). The most noticeable case is Antwerp's Metro as it was constructed in well known highly plastic ground, where the subway system included the use of a 6.4 external diameter Hydroschild under the Scheldt River in Antwerp, Belgium. According to Wittmans and Bonvoisin (1988), the excavation had to proceed through a tertiary layer of dense lime sand containing shells and shell fragments. Then the tunnel trajectory had to go deeper under the river through tertiary clay known as the Boom Clay. The clay is described as heavy clay containing large solid septaria of sizes reaching 2 m. The main difficulty occurred at the interface between the two layers where the clay adhered to the cutter wheel and stuck to the walls of the excavation chamber which required the emptying and cleaning of the excavation chamber under compressed air. A solution to the problem was reached by increasing the capacity of

the discharge pump, changing the design of the intake of the discharge pipe, and by modifying the direction of bentonite injection holes. As a result, higher turbulence was generated in the excavation chamber. Large-sized boulders were treated at the cutter head using 23 roller bits and inside the excavation chamber using a special stone crusher. Work was not interrupted due to the existence of boulders. Final assessment of the project was positive as the ground movement was within acceptable limits.

An ideal case of the Hydroshield was the twin tunnel for a high speed railway link to the Atlantic at Villejust, France, (Table 2.1: 37). Soil conditions consisted of fine dense sand, known as Fontainebleau sand. The groundwater table was at the tunnel axis in some parts of the trajectory while most of the work was carried out above the groundwater table. As described by Guillaume (1989) work progress was exceptionally high; 7.5 m/day and 15.4 m/day for the first and the second line, respectively, (as a rule of thumb, 3 m/day advance is a critical limit). Only two work interruptions were reported and both were related to mechanical problems at the cutter head. Measurements of ground movements and straining actions in the liner were presented by Leblais and Bochon (1991) and proved to be within an acceptable range.

The Cairo Sewerage project (Table 2.1:7) used two Hydroshields to deal with wet and running sand, and gravel soil conditions, (Flint, 1993). As described by Wallis (1987) the major problem facing the construction was the inadequacy of the rubber seal. The problem was solved by using a wire-brush seal of the same type as used by the Japanese company working on the same project. The operational rule was to maintain bentonite pressure higher than groundwater pressure. Occasionally, a drop in face pressure cavities may develop above the face and they may work their way to the ground surface within a few hours or days.

Tunnelling in Rome (Table 2.1: 30) represented a challenge to the Hydroshield technology because of its exceptionally large diameter (about 11 m) and because of the wide range of soil particles encountered along the trajectory, see Figure 2.11. As reported by Wallis (1984), interbedding of cohesive and noncohesive layers under the groundwater table resulted in the development of localized artesian water pressure pockets. Since the first part of the project consisted of overconsolidated clay, bentonite pressure was not necessary and the shield operated in "dry mode". Changing from dry to wet modes posed some problems as plastic cohesive material still had to be excavated. As in the case of Antwerp, colloids plugged the intake pipes and the operation was interrupted until pipes were manually flushed. High water pressure with sandstone formations required high slurry pressure to support the face which exposed the tail seal to the danger of breaking. The average rate of progress was about 9 m/day which is comparable to the capacity of the

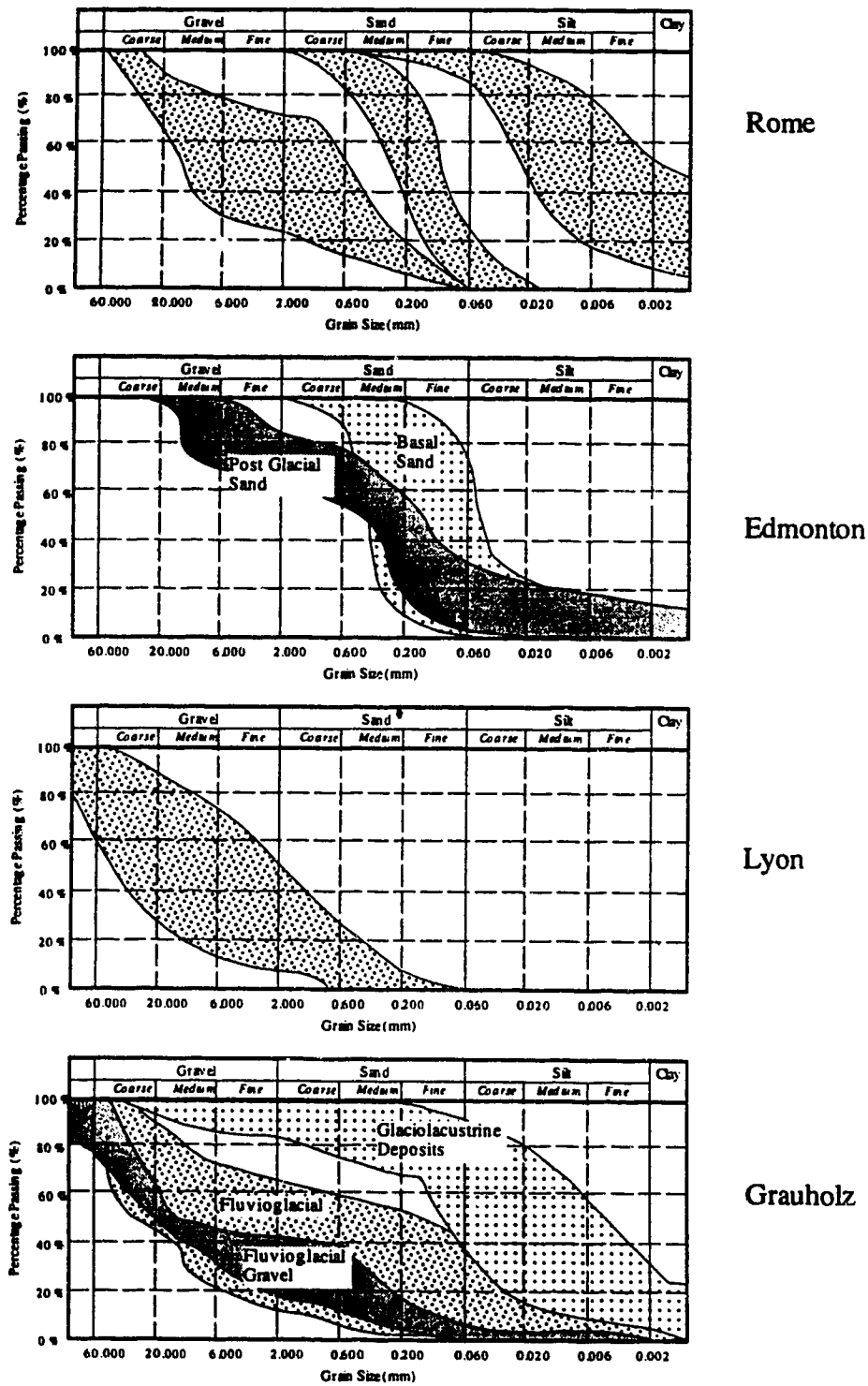


Figure 2.11: Grain Size Distribution of Granular Materials encountered during Tunnel Construction using the Bentonite Slurry Shield

cutting mucking and grouting system for a tunnel of this size. Maximum surface settlement was 7 mm which was considered satisfactory. The problem of cohesive soil plugging the mechanical parts of the machine resulting in interruption of work were also encountered in other projects, such as, in the Lille Metro-Lot 3 of Line 1 (Table 2.1: 18) according to Kongrad and Anheuser (1988).

The Grauholz Tunnel (Table 2.1: 11) represents new construction conditions in response to the variability of ground conditions en route which required changing the excavation method using the same shield. The machine, commonly known as the *Mixshield* uses the bentonite slurry shield technology, along, with other shield technologies in different phases of the same project. As shown by Steiner (1989) and Steiner and Becker (1991), the tunnel passed through fluvio-glacial deposits with a wide range of particle sizes, then, through rocky ground followed by fluvio-glacial silty gravel and fine grained glaciolacustrine deposits. The bentonite slurry mode (wet mode) was used during the passage through the soft ground and when the rock cover was relatively small. In the glaciolacustrine formation grain sizes were no bigger than 6 mm, and as a result, the portion of fines in the spoil was very high. The discharged mixture overcharged the secondary circuit of the separation plant while the primary plant was almost not utilized. Measures were taken to increase the capacity of the circuit by adding one more filter and a bigger centrifuge. Rocky particles caused an unexpectedly and unacceptable high rate of wear in the cutter bits, and very pervious strings of gravel caused the total collapse of the face. The face collapse directed attention to a certain important detail, as the excavation chamber had to be emptied from time to time to allow manual maintenance and repair operations at the cutting wheel, the face became fully supported by compressed air. In many instances, especially, when permeable ground conditions prevail, the face support depends almost entirely on the air tightness of the cake layer. It has been shown that the interaction mechanism between the cake layer and the compressed air deteriorates with time. Therefore, construction rules have to be set limiting the time of exposure of the face to compressed air. If the repair work requires a longer period, then the chamber has to be refilled with bentonite and re-emptied again for another session of working under compressed air. Following such a process was not practical considering the substantial wear on tools which required frequent access to the chamber. Ground freezing was used to enhance the stability of the face.

The Light Rail Transit (LRT) subway in Edmonton, Canada (Table 2.1: 9), used the Hydroschild method through layers of bedrock formation, post-glacial deposits of highly heterogeneous grain size distribution, basal sand and glacial clay till layers. In many instances, excavation was carried out in a mixed face, and the mechanical properties of the

ground layers are described by Hardy (1988). As shown by Eisenstein and Ezzeldine (1992: a), excavation was carried out in dry mode in the bedrock while bentonite was used on the remainder of the project. Occasionally the excavation chamber had to be emptied to remove large size cobbles. Limitations on the working period under compressed air were applied and tolerated without the need for external ground improvement measures. Except for a number of incidences where the rubber tail seal failed and had to be replaced, settlement at the ground surface was within tolerable limits. Throughout the project, no damage to neighbouring structures was recorded and the shield performance was satisfactory.

The case of the Lyon Metro, Line-D (Table 2.1: 21) is an example of using the Hydrosshield in ground conditions consisting of gravels where the particle size has a highly uniform distribution. The seriousness of the situation is increased due to the fact that the excavation was designed to take place under a very shallow cover under the Rhône River and because of a pioneering use of an extruded-steel-fiber concrete liner. A number of severe problems interrupted the work, especially, at the beginning of the project. As described by Morcrette (1988), four face collapses took place in a critical section under the Rhône where the ground cover was as thin as 2 to 3 metres. Direct contact with the river water necessitated dropping sand bags to the bottom of the river and using barges while heavy bentonite and PVC sheets were used in the excavation chamber to plug the very permeable face. In many instances, it was not possible to empty the excavation chamber and the work inside it had to be carried out by divers. Special measures were undertaken to prevent such problems: using vibroflotation at the river bottom, adopting a concrete mix more suitable to site conditions, and increasing the number of concrete injection pipes from 4 to 6. As a result, the rate of advance increased from 3.32 m/working day to 8.32 m/working day.

2.4.2.1.3 The Japanese Bentonite Shield

The fundamental difference between the Japanese BSS and the Hydrosshield is in the method of adjusting the face pressure, especially, in the case of sudden change in ground conditions. While the Hydrosshield depends on the air accumulator device to compensate for sudden drops in face pressure, the Japanese BSS relies on the machine face to offer adequate ground support through the closeness of the cutter head, the effectiveness of cutting bits and adjustment of slit devices, and the speed of rotation and advance of the cutter head. Although the cutting face is equipped with manholes to allow access to the face in case of emergency, the absence of compressed air necessitates dealing with large-sized obstacles using special roller cutters and stone crushers. Finally, the performance of

the system depends on very sensitive data collection and automatic control to detect any sudden change in ground conditions. Agitators are supplied in the excavation chamber to prevent separation of large-sized particles from the slurry.

Osaka's stormwater tunnels (Table 2.1: 28 and 29) as described by Hashimoto et al. (1988) and Hashimoto et al. (1985) represent a remarkable accomplishment for the Japanese slurry shield technology as the shield diameter was a record high of 11.22 m. Soil conditions included dense sand and gravel with a percentage of fine grained material. During the first part of the excavation, problems of high cutter torque and jack thrust were noticed because of clogging of the centre cutter head and wear and loss of cutter bits. As a solution to the problem, cutter speed were increased, as well as, slurry circulation which resulted in reducing the torque to half. Additional measures were adopted to eliminate adhesion of excavated muck on the cutter centre by using an agitator and water jets.

The Cairo sewerage project (Table 2.1: 6) represents an example of the Japanese technology working side by side with the German technology in wet-running sandy ground conditions. As shown by Wallis (1987), three Okumura designed shields were used: two 5.15 m Outside Diameter (O.D.) and one 6.11 m O.D. . Typically, the face was almost completely closed except for 250 mm wide slots with hydraulic gates to control the flow of material to the excavation chamber. An important drawback of the shield was that the system is less adaptable than the Hydrosshield to unexpected site conditions as the access to the face is limited. Unfortunately, large boulders of, up to 900 mm were found in the Japanese type shield trajectory. As the excavation tools were designed primarily to cope with boulders of about 250 mm, it was necessary to interrupt the work to allow the change in the design of the cutting face; cutting teeth were changed to more effective ones, roller disc cutters were added to the face, and slot gates were strengthened. Unlike the Hydrosshield that had problems with the rubber tail seal, the steel-brush tail seal proved to be reliable and adequate for the site conditions. Advance rates of the two types of BSS has proven to be comparable. The maximum rate of advance when all was going well reached 11 m/ 11 h shift and 14 m/ 12 h shift for the Okumura type shield and for the Hydrosshield, respectively. Meanwhile, as the bentonite slurry is pressure controlled in the case of the Hydrosshield, the rate of consumption of slurry was lower in the case of the Japanese shield.

Special conditions showed that a Japanese Kawasaki designed shield was best suited to the Metro of Lille-Lot 8, Line 1 (Table 2.1: 19). As described by Hurpin and Bousset (1988), the tunnel had to pass through ground conditions consisting either of lightly fissured chalk containing some fire stones or of altered highly fissured chalk. Excavation had to be carried out under the groundwater table, and the hydrostatic pressure,

as well as, the cover depth varied significantly along the trajectory. The advantage of the chosen shield was that it offered slurry support necessary for the altered chalk ground at the same time that it provided a rugged cutter head capable of excavating through the fissured chalk. Execution of the first part of the project showed excellent control of the face stability while in some instances, the bentonite-chalk interaction failed resulting in sudden losses of slurry and relatively high settlement at the ground surface (50 mm on average). Therefore, it was decided to increase the slurry pressure and at the same time, to improve the bentonite-chalk interaction. Chalk additives were added to the bentonite to produce an impermeable slurry for the site conditions. As a result, surface settlement during the second part of the project was remarkably reduced to 15 mm.

From the above review, BSS was successfully used for sewerage and transportation purposes in soil conditions varying from fine grained soil up to bouldery soil. The degree of success is dependent on the ability to preinvestigate the encountered ground conditions and to take them into consideration when designing the excavation scheme and when selecting the mechanical parts. Construction may be carried out in difficult ground conditions such as running and flowing soil conditions, or under sea or river tunnels, or tunnels with large size openings (up to 11 m in diameter), or tunnels constructed under a small soil cover, and so forth. The general impression formed is that reliability of the BSS is increasing according to the most recent publications.

2.4.2.2 The Earth Pressure Balanced Shield

The Earth Pressure Balanced Shield method is based on the principle of reducing volume losses by maintaining a balance between the volume of removed soil and the rate of advance. Unlike the BSS, there is no significant difference between the density and stiffness of the ground and the material inside the excavation chamber. This restricts soil intrusion into the machine. A screw-soil conveyor operating on the Archimedes principle removes the required amount of soil in order to keep the excavation chamber under pressure. The operation relies to great extent on a sophisticated computerized system for data collection and operational control.

2.4.2.2.1 Historical Background

According to Murayama, in ITA (1981), the first EPBS was applied in 1974 in Japan to an aqueduct of 3.35 m diameter. Since then, the method has proven acceptable and shields up to 8.48 m O.D. have been assembled and used. The inclination and the length of the screw are designed to provide gradual change in earth pressure to allow operating the discharge gate under free air conditions. Therefore, soil in the conveyor is

consolidated and seals out water. In 1976, another system, the pressurized mud shield which originated with the D.K. shield, was developed by the Daiho Company, Japan, and was used in the construction of a 2.4 m O.D. tunnel, see Hagimoto and Kashima (1985). The system may be regarded as a hybrid between the EPBS and the BSS. Here too, bentonite slurry is added to the excavation chamber to increase the muck fluidity inside the excavation chamber and the screw conveyor. An open face allows the muddy mixture to press directly against the face ground. Thus, improved management and control of the earth pressure is achieved in the excavation chamber and a more impermeable property of the muck is realized.

2.4.2.2.2 The Conventional EPBS

According to Flint (1992) and Darling (1991), two LOVAT Earth Pressure Balanced Shields were used in Contracts 3, 4, and 12 in the Cairo Sewerage Project (Table 2.1: 49). Due to the considerable length of the project (about 6.6 km total), EPBS method was selected instead of the compressed air method. It was believed that the change of groundwater pressure resulting from application of the compressed air might cause damage to the neighbouring structures, as well as, causing a certain degree of inconvenience to the public and the working crew. The tunnel trajectory passes through recent alluvial sandy deposits with occasional silt and clay layers. Properties of the excavated ground differ considerably through the length of the tunnel depending on the geological history. Experience gained during the construction of other parts of the project showed that wire-brush-type tail seals gave the best performance for the ground conditions so they were again selected for this part. The lining system consisted of newly designed trapezoidal precast concrete segments bolted together in a scattered scheme and has proven to give excellent quality of ring building (ovality). Except for several instances where excessive settlement took place, average settlement ranged between 15 and 35 mm. The relatively wide range of settlement could be due to changes in soil conditions. In general the EPBS performance has proven to be satisfactory in the project and a rate of advance of up to 138 m/ week was achieved.

The Caracas Metro, in Venezuela, (Table 2.1: 51 through 53) demonstrated the ability of the LOVAT EPBS to accommodate different ground conditions. As described by Paulus (1988) the project included three phases. In the first phase, ground conditions at the tunnel level consisted of sandy silt, silty sand, and gravely sand of medium density. In the second phase, the tunnel section was situated generally between a lower layer of stiff shale or fissured shale and a layer of silty sand with gravel inclusions. One part of the third phase is similar to the second one while the remaining ground conditions at the tunnel

section consisted of stiff to very stiff shale. The groundwater table was close to the ground surface and the cover depth varied between 5 and 11 m for the first two phases and increased up to 50 m for the third phase. The cutter head was designed with a bulging shape to cope with the stiff ground. In the case of compressible ground, a protecting ring with cutting devices was allowed to propel ahead of the face to prevent lateral movement and two ailerons operating through hydraulic jacks provided the necessary reactional torque to the rotational movement of the cutter head. Problems of ground movements were encountered due to soil heterogeneity and the existence of a number of artificially filled thawlegs. Predrainage and jet grouting were necessary for soil stabilization.

The Sprogø Tunnel (Table 2.1: 68) shows the ability of EPBS to cope with undersea excavation in heterogeneous ground under a relatively small depth cover. The tunnel is constructed for railway purposes as a part of the Great Belt Project in Denmark. According to Ostenfeld and Curtis (1992), soil conditions at the extremities of this tunnel consist of till while marl is encountered in the deep middle part. The till consists of clayey silt and sand and is laid into two geologically separate layers: lower and upper till. In some parts of the project the excavation was carried out in a mixed face between the two till formations. The lower layer represented a considerably difficult tunnelling condition as it contained solid granitic boulders of up to 3 m diameter, as well as, frequent pure sand bodies. A persistent meltwater silt and sand body existed at the interface of the two layers. Shield design took into consideration the existence of boulders and the need to control high water pressure. A considerably long two phase screw conveyor (24 m long) provided the necessary pressure gradient to keep the excavation chamber under pressure and to impede water flow. The discharge gate was equipped with a pressure regulator to control muck evacuation. Meanwhile, the relatively large cross section of the screw permitted the transportation of boulders after they passed through the special disc cutter bits. A compressed air system with a decompression man lock was incorporated into the shield to allow maintenance work at the face under water bearing ground. Construction problems took several forms: progressive raveling of ground material at the crown, piping in the sand layer, sand washing into the gallery, and losing of air pressure during operation stoppage. As a remedial measure, dewatering wells were included to reduce the hydraulic head.

The San Francisco N-2 clean water tunnel (Table 2.1: 64) is a landmark case as it represented the first application of the EPBS method in North America. A detailed analysis of the project was carried out by Finnø (1983), Kasali and Clough (1983), and Clough et al. (1983). Ground conditions consist of a stratum of soft interbedded silts, clays, and sands known locally as the Bay Mud soil layer, and the water head is about 3 m at crown

level. The major difficulty in the construction was the existence of wooden piles along the alignment, therefore, special carbide teeth were fitted on the cutterhead to cut through the piles. Soil response to the excavation, as shown from the monitoring program reveals typical aspects of the performance of the EPBS in soft ground. As the shield face approaches the instrumented point, soil heaves at the ground surface. Subsequently, downward movement is recorded as the tail void approaches the monitored section. Some problems were encountered as wooden pile fragments partially clogged the screw auger causing some disturbance in soil removal and a sudden increase in earth pressure at the face. Surface settlement was, in general, less than anticipated as it varied between 5 and 76 mm with an average of 33 mm. The larger settlement usually took place during the period of operation stoppage as the face support mechanism was negated. General assessment of the EPBS performance was largely positive as the project was accomplished ahead of its time schedule. The method gained approval due to good ground control and because the excavation proceeded with minimal disturbance to the groundwater table.

2.4.2.2.3 The Mud Pressurized Shield

A soil plasticizing shield can be used for excavation in water-bearing gravely soil containing boulders as was the case in part of the Nagoya Municipal Subway (Table 2.1: 61). According to Sasanbe and Matsubara (1986), the project represented a challenge regarding the difficult ground conditions and the large size of the tunnel (7.43 m O.D.). The "plasticizer" is defined as the additive injected into the excavation chamber to improve the excavated soil properties. The composition of the plasticizer is selected in order to produce a mixture with the excavated soil satisfying required limiting values of permeability and consistency (slump test). Meanwhile, viscosity of the plasticizer should be low enough to accommodate the pumping system transporting the additive to the excavation face. A mix of kaolinite clay, bentonite and water was selected and was expected to reduce ground permeability from 10^{-3} m/sec to less than 10^{-8} m/sec and the slump value was shown to increase as the percentage of plasticizer increased. The plasticizer was advantageous as it resulted in reducing the necessary torque at the cutter face. At the same time, excessive amounts of plasticizer may result in segregation of excavated soil particles and uneven distribution of face pressure. Additional measures were undertaken to control soil movement at the ground surface. These measures included the construction of diaphragm walls to protect important structures, and the advance of inclined boring rods from the ground surface to detect and to fill in advance any cavities ahead of the face. Simultaneous tail grouting and quick setting grout material contributed to the reduction the ultimate ground settlement. Final assessment of the performance was encouraging as the

resultant ground movement was within the range of 20 mm and did not exceed one tenth the originally estimated settlement.

2.4.2.3 the Compressed Air Shield

A number of factors are still limiting the applicability of the compressed air shield method as compared to the other pressurized shield methods. As face pressure relies on compressed air, only the pore pressure of the surrounding ground is affected, therefore, the method is not applicable under dry soil conditions and difficulties are encountered in cases of irregular pore water pressure distribution. Health concerns, as mentioned before, put a limitation on the applicability of the method where high air pressure is required. Finally, the interaction between the compressed air and groundwater is often unpredictable regarding the extent of the compressed air zone and the possibility of air losses which result in piping and face collapse. On the other hand, the method has some advantages. It allows the work through the open face which permits visual inspection of the face and it provides a wide range of choices for the most suitable excavation scheme. As the bulkhead is placed at the lock section behind the shield tail, soil at the tail section is under compressed air. This enhances the stability at this critical section and precludes the damages related to the tail seal failure often encountered in the other methods.

O'Reilly et al. (1991) provide a description of an excavation of a sewage tunnel in Grimsby (Table 2.1: 41) through a soft to very soft clay layer. The soil formation at the tunnel section is locally known as Marine Warp; a very soft marine clay of recent origin. Excavation was carried out manually through an open face. The water head above the tunnel axis was about 6 m and a compressed air of 41 kPa was used as considerable difficulties were experienced when excavation proceeded under free air conditions. Soil movement at the ground surface was relatively high and ranged between 79 and 48 mm. Some damage to the neighbouring services and structures were recorded. Due to the effect of air pressure on pore pressure of the relatively impervious ground, soil movement was found to be highly time dependent. A prolonged monitoring program showed that settlement at the ground surface, as well as, the width of the settlement trough took about ten years to reach its ultimate value.

The construction of a twin tunnel for the Bay Area Rapid Transit (BART) subway system along Lower Market Street in Oakland, California (Table 2.1: 42) is another example of the performance of the compressed air tunnelling method in compressible cohesive soil. As mentioned by Kuesel (1972), ground conditions consisted in this part of the project of soft plastic clay known as the Bay Mud. Ground cover varied along the tunnel trajectory and in some points reached a minimum of 2.1 m (7 feet). Relatively

shallow working conditions allowed the use of air pressure within reasonable limits (average 84 kPa air pressure was used) and resulted in high ground movement at the ground surface in some instances. Excavation had to pass through a large number of timber piles that were cut manually which had an effect on soil deformation around the tunnels. Open-faced shields allowed the excavation to be carried out manually. Two methods of grouts were followed with satisfactory results: one step grouting by injecting liquid grout as the shield was being jacked, and two phase grout where pea gravel was injected immediately behind the shield followed by the grout some 45 m behind the heading. As the rigid support to the advancing shield is provided, according to the excavation method, by the rigid bulkhead, a flexible tunnel liner was an acceptable option. Six welded steel segments and a tapered key made up the lining system. Ground settlement was about two inches (50.8 mm) and reached 99 mm in some points. The settlement pattern showed a clear trend of time dependency as ring deformation measurements showed that the maximum deformation occurred about five months after erection.

The sewerage project in Cairo (Table 2.1: 40) is an example of the performance of a compressed air tunnelling method in noncohesive ground conditions. The project included the construction of a 5.15 m tunnel using the compressed air method. Details of the projects are found in El-Nahas et al. (1991), El-Nahas et al. (1992), Shalaby (1990), and Ahmed (1990). Ground conditions at the tunnel section consisted mainly of a mixed face where the lower part was excavated through a layer of dense to very dense graded sand and the upper part was sandy clayey silt. A fill layer, predominantly silt, overtopped the sandy clayey silt, and the groundwater head was about 9 m from the tunnel crown. An open-faced shield machine using a semi-mechanical excavation scheme was adopted. The tunnelling machine is described in Section 2.3.2.3.1. A major concern was the possibility of air losses through the noncohesive sandy layer. The monitoring program included a number of piezometers which register the changes in pore pressure around the advancing shield. The movement pattern at the ground surface monitoring points was characterized by three distinct phases: (1) ahead of the face a slight upward movement of the ground surface resulted due to the application of compressed air; (2) a sudden downward movement followed the passage of the shield tail due to the effect of the tail void; and (3) an additional downward movement took place after the release of air pressure. Because of the existence of the sandy layer, time dependency of soil movement was not as obvious as in the Oakland or Grimsby projects. Piezometer measurements showed that, except for a period of sudden disturbance during the passage of the shield, pore water pressure fluctuated around its original level which indicated that the compressed air zone was confined around the tunnel. The average the ground surface movement was about 25 mm

and which was considered a satisfactory performance.

2.5 Factors Affecting the Selection of Tunnelling Methods

Recent advances in tunnelling technologies usually provides the decision makers of any tunnelling project with a number of acceptable options. The three objectives of tunnelling projects from the civil engineering point of view as pointed out by Peck (1969) are considered fundamental requirements: tunnelling feasibility, safety of neighbouring structures, and long term serviceably. The decision to choose a pressurized shield method as opposed to other methods involves a number of factors such as the operational cost of the project, the availability of supporting services to the project, the degree of confidence in the safety of the works, the experience and skill of the workmanship, and the performance of methods in similar but previous projects.

2.5.1 Comparison between Pressurized Shields and other Tunnelling Methods

Competition to pressurized shield methods in shallow tunnelling projects is generally from cut and cover, or the New Austrian Tunnelling Method (NATM)-also known in North America as the Sequential Excavation Method (SEM). As shown in the previous section, pressurized tunnelling methods were used in a wide range of difficult ground conditions. In some cases of under sea or under river excavation they were a unique solution. The prominent advantage of pressurized shield methods over the other two methods is that they allow the construction of the tunnel, with the ground treatment and support if necessary, to be undertaken completely from the excavated gallery. Consequently, the undertaken measures are more effective as they are localized around the cavity and disruption of activities and services along the tunnel trajectory during the construction period is minimized. Meanwhile, some soil treatments from the ground surface, although they improve ground properties at the excavation level, may result in damages to neighbouring structures and services. Predrainage is an obvious example. Another advantage of the pressurized shield method is that, unlike the SEM, the construction sequence goes through only one phase, therefore, it is more effective and has proven to be of economic advantage especially for long tunnels.

The Edmonton LRT tunnelling project is an example of the use of the Hydroshield method along with SEM and open shield with jet pile grout, see Wallis (1992:b). Tunnelling in competent, self supported glacial till ground using the SEM has proven to be successful. In the part of the project where excavation had to be carried out through raveling sandy soil, the open face shield with jet pile grouting method was shown to cause some damage at the ground surface due to imperfections in the jet pile intersection. The use

of the Hydrosshield in the same ground conditions yielded a very satisfactory performance both regarding the safety and the economy of the works.

It could, therefore, be believed that the ability of the pressurized shield to perform satisfactorily in difficult ground conditions without external ground improvement measures is a requirement for its ability to compete with other tunnelling methods. Inspection of the above mentioned case histories proves that this requirement has not always been fulfilled, especially in pioneering project cases such as the Great Belt Project and Lyon Line-D Project where severe constructional problems necessitated intervention from the ground surface by predrainage and by consolidating the bottom of the river respectively.

2.5.2 Comparison between Pressurized Shields

While certain site requirements and subsurface conditions make the choice between pressurized shield methods and other tunnelling methods generally simple, a considerable amount of comparison is commonly needed for the selection of a certain pressurized shield method among the others. The most important feature considered when weighting the advantages and the disadvantages of each method is the way the excavation method handles the anticipated difficult conditions.

Difficult conditions usually refer to changes or irregularity of groundwater pressure, existence of a raveling or running soil formation, existence of large-sized boulders and cobbles or non homogeneity of the excavated cross section. Furthermore, mechanical problems related to sudden failure of the ground support system or weekend shutdown have to be taken into consideration. Traditionally, the designer prefers to deal with these situations with the highest potential for of visual inspection and physical contact between the workmanship and the excavated ground. This is a strong point for the compressed air method and the Hydrosshield. On the other hand, modern technology of in site monitoring and evaluation of various aspects of the excavation process enables the control of the mechanical or ground support system to accommodate sudden difficult conditions. This trend is especially obvious in Japanese technology based shields.

Large-sized boulders and cobbles are handled differently between the BSS and the EPBS. In the case of the BSS, boulder trajectory passes downward into the excavation chamber where it will be evacuated or crushed through a special stone crusher while in the case of the EPBS stone fragments have to be evacuated upward through the screw driver. Since the diameter of the screw driver is always limited to a certain size, stones are required to be crushed at the cutting face through special cutter bits. Wooden Piles were encountered in the way of the EPBS used in the construction of the San Francisco N2 project and emptying the excavation chamber could be avoided. In the case of the BSS

used in the Osaka Stormwater project, chemical injection from inside the chamber helped stabilize the face before cutting through reinforced concrete piles. As the compressed air shield allows access to the face during the excavation, large-sized obstacles could be replaced manually.

Site planning has to be considered when comparing different pressurized shield methods. The BSS method requires the establishment of a treatment plant near the excavation site which may be a concern when working in congested cities. At the same time, the method relies on pumping the spoil through slurry pipes which is considered a more practical transport system than the use of mechanical means for spoil disposal.

An example of the performance of the Hydroshield in extreme conditions related to seepage forces has been given in Lyon Metro Line-D case history. The intrusion of the Rhône River water into the Hydroshield required stoppage the excavation and exceptional measures to be undertaken both at the river bottom and inside the chamber to plug the seepage passage. Difficult conditions related to ground properties were encountered in the construction of the Antwerp Metro under the Scheld River where clay adhesion to mechanical parts of the excavation chamber required, in many instances, the emptying of the chamber to clean it. In the Edmonton LRT project the excavation had to be stopped in many instances to evacuate large-sized boulders. On the other hand, in the Cairo sewerage project, the discovery of boulders at the cross section of the BSS required changing the cutter bits to more effective ones as it would have been inconvenient to empty the chamber to evacuate the stones in the shield of the Japanese based technology.

2.6 Conclusions

The application of pressurized shield methods (the bentonite slurry shield, the earth pressure balanced shield, and the compressed air shield methods) in tunnelling engineering allows excavation through difficult field conditions. A satisfactory degree of success for the new technology has been detected in urban areas where, in general, the tunnel is relatively shallow and the prevailing ground conditions consist of deformable soils of low shearing resistance and with groundwater tables above the crown level. The criteria of success for the construction technique are determined as being the integrity of the excavation boundaries, as well as, the safety of the neighbouring structures.

Compressed air shields have been used since the last century in order to control water intrusion into the excavation and to limit seepage forces that may result in face collapse. The Hydroshield is a European type of BSS that has been designed mainly to provide face support by injecting a slurry into the exposed face. The slurry is controlled by a compressed air cushion. The main objective of the method is to limit the compressed air

zone in order to eliminate health hazards to the personnel, as well as, to provide better ground control. Further developments of the method allow it to be implemented in new ground conditions such as through bouldery or impermeable soils or above the groundwater table. The earth pressure balanced shield was originally designed in Japan as an adaptation to microtunnelling technology to large sized tunnels. The ability of the shield to preclude water intrusion is enhanced by additives which have led the way to new types of shields. These shields are named depending on the additive used in the excavation chamber, such as the Soil Plasticizing Shields and the Mud Pressurized Shields and so forth . The Japanese BSS is, thus, constructed as the excavation chamber is filled with pressurized bentonite slurry which acts at the same time as a face support, as well as, a muck transporting agent. Unlike the Hydrosshield, the Japanese BSS does not use compressed air to regulate the slurry pressure.

An important feature of installation used in the compressed air shield method is the air locks. Generally two types of air locks are used, one for the material and one for the personnel. The position and the performance of the locks have direct implications for ground control and for the progress of the project, as well as, for the safety of the workers. The installation of the BSS requires the assignment of a substantial area on the ground for the treatment plant and slurry recycling operations. Meanwhile, the performance of the shield has proven to be dependent on the adopted pressure levels of the slurry and that of the grout behind the liner, as well as, on the performance of the tail seal at the back of the shield. Ground control using the EPBS relies mainly on the tightness and the performance of the cutter wheel and those of the auger. A precast concrete segmental lining system represents the most common lining system used in association with the pressurized shield methods. In some cases the precast, bolted or welded, steel segments are used. Extruded concrete methods, using either a steel reinforcing cage or steel fibre additives, represents an important innovation in tunnel lining systems. Its application in some of the recent projects reveals a number of advantages and disadvantages that the system has against the precast concrete segmental lining system.

A review of a number of case histories of tunnelling using pressurized shield tunnels underlines the technical features of the applied methods specifically with respect to the integrity of the excavation, the safety of the neighbouring structures, the performance of the critical components of the excavation system, the innovations introduced facing emerging problems, and with respect to the rate of progress of excavation.

CHAPTER 3

FACE STABILITY OF TUNNELS CONSTRUCTED USING PRESSURIZED SHIELD METHODS

3.1 Introduction

The developmental needs of modern cities require the construction of drainage and sewer works, mass rail transit and road tunnels beneath densely developed areas. Although the problems encountered in the construction of these projects are diverse, some common trends may be identified and the methods used to solve these problems can be added to the designer's experience. For obvious practical reasons which include accessibility, serviceability, and economy, tunnels in urban areas are constructed at shallow depths. Problems of groundwater control are commonly present and concerns are raised about the soil's capacity to sustain the imposed stress changes related to the excavation. A successful excavation scheme would preserve the integrity of the project against shear failure and seepage forces and it would preclude excessive ground movements that may endanger neighbouring structures.

The principle of ground control using shield methods is to provide an uninterrupted support to the excavation boundaries. A rigid shield followed by an adequate lining system restricts soil movement at the circumference of the tunnel. However, face support remains a major concern in the excavation design. A variety of methods are used to improve the face stability either by dividing the face into partially self-supported subdivisions (New Austrian Tunnelling Method, NATM, also known as the Sequential Excavation Method, SEM) or by ameliorating soil conditions using external agents such as freezing, grouting, dewatering, and so forth. Positive ground control methods such as the compressed air, the bentonite slurry shield (BSS), or the earth pressure balanced shield (EPBS) methods rely on minimizing the disturbance at the face so that: (1) induced stress changes conform to the resistance capacity of the existing soil conditions; and (2) the resulting ground movements are within acceptable limits imposed by the site conditions.

3.2 Safety Requirements for the Face of Excavation

Safety requirements for the excavation face are similar to those of diaphragm walls. As pointed out by Bathaus (1989) they comprise the following safety features against:

- (1) intrusion of groundwater;
- (2) movement of single grains (local stability);
- (3) excessively low support pressure (global stability); and
- (4) formation of slip surfaces (collapse of tunnel face).

Additional features are attributed to the cases where face pressure exceeds the initial soil pressure, such as safety against:

- (1) heaving of the overburden; and
- (2) blow out failure.

Examination of different mechanisms of face collapse showed that the above mentioned items are often interdependent. A pattern of uncontrolled movement of single grains may propagate into the soil mass until there is the development of a slip surface. Water intrusion into the tunnel, besides being, itself, a threat to the excavation process creates seepage forces that may result in global stability problems. On the other hand, blow out failure is generally associated with the loss of the supportive material (generally, compressed air) and, thus, the loss of face pressure.

3.3 Idealized Face Stability

The concept of face stability for the pressurized shield tunnelling method is based on the assumption that an infinitely extended half space is initially under gravitational force effects. A cylindrical cavity is introduced at a certain depth such that the circumference of the excavation is protected. At the face a certain amount of pressure is applied in the normal and tangential directions. If the resultant stress field exhibits a reduction of mean normal pressure, the process of face relief takes place. Then, face stability is achieved if the soil movement associated with the induced stress changes is within acceptable limits, and face failure takes place as a collapse mechanism is developed.

3.3.1 Concept of Stress Relief

Burland and Fourie (1985) define the path of "*passive stress relief*" as a simultaneous reduction of the two principal stresses as the soil element moves into a state of passive failure. As one principal stress is steadily reduced, the other one manifests changes until the soil element reaches a state of limit equilibrium on the passive failure line. The authors argue that the resultant stress trajectory and its sign during the early stages of stress relief, as well as, during stages of yield and failure are not unique as they depend on

many factors such as the stiffness of the surrounding ground and on the support system. Figure 3.1 shows two cases of passive stress relief that the authors used to demonstrate the effect of boundary conditions on the resultant stress path. A triaxial test was conducted using Bishop and Wesley (1975) stress path apparatus on undisturbed and reconstituted London clay samples and on undisturbed Claygate beds at the site of a cut and cover tunnel at Bell Common project, (Hubbard et al., 1984). After subjecting the samples to stresses corresponding to the initial site conditions, axial stress was steadily and slowly reduced followed by reduction of cell pressure. The amount of reduction in the cell pressure is adjusted according to the apparatus installation such that it is linearly dependent on the axial strain. Results showed that for the selected test conditions, the resultant stress path, as well as, the resultant volumetric strain were influenced by drained shear strength parameters and by the dilation potential of the clay.

3.3.1.1 Stress Path Associated with Relief

The effect of the stress path on the stress-and-strain fields around the excavation has been acknowledged and investigated by many authors and for various types of excavation problems and constitutive models. Medeiros and Eisenstein (1983) conducted laboratory investigations of stress-strain behavior of two typical soil formations encountered in Edmonton: glacial till and Saskatchewan sand. Both, drained triaxial, as well as, plane strain tests were carried out. Various stress paths were investigated as shown in Figure 3.2:

- (1) passive compression stress path, **PC**: increasing the major principal stress σ_1 while maintaining the minor principal stress σ_3 constant;
- (2) active compression stress path, **AC**: decreasing the minor principal stress σ_3 while maintaining the major principal stress σ_1 constant;
- (3) active extension stress path, **AE**: decreasing the major principal stress σ_1 while maintaining the minor principal stress σ_3 constant; and
- (4) proportional unloading stress path, **PU**: decreasing simultaneously the two principal stresses following the same ratio as the coefficient of lateral pressure at rest K_0 .

The study shows that for both types of soils the passive compression case yielded stiffness parameters (modulus of deformation, E) lower than those obtained from the other cases. Following the experimental study, Eisenstein and Medeiros (1983) used the obtained soil parameters to simulate a case of a deep supported wall using the finite element method as a back analysis at the Churchill Square Station in the LRT system in Edmonton. Three regions were identified as having different stress paths: active compression beside

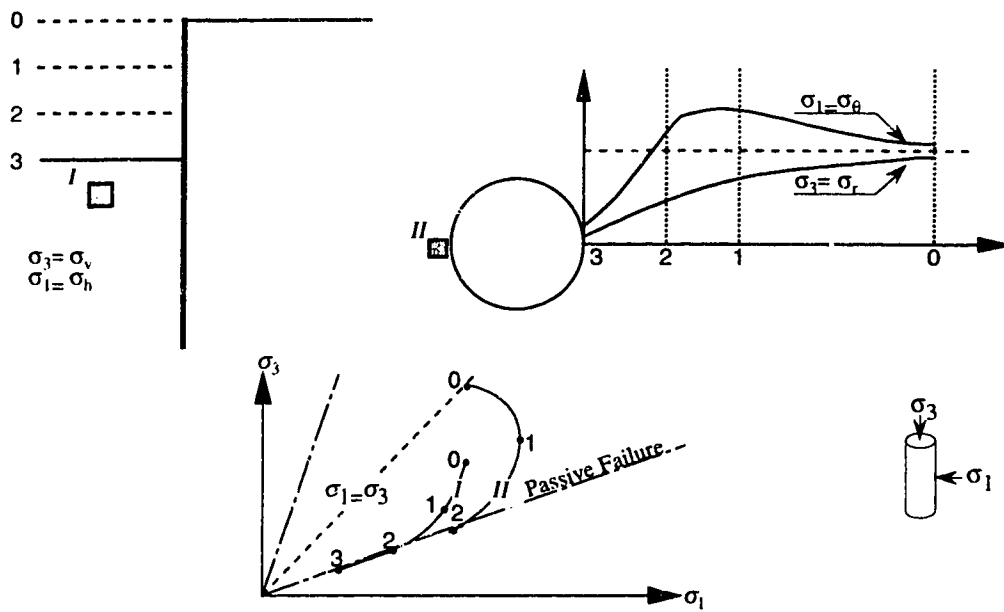


Figure 3.1: Two Different Stresses (modified after Burland and Fourie, 1985)

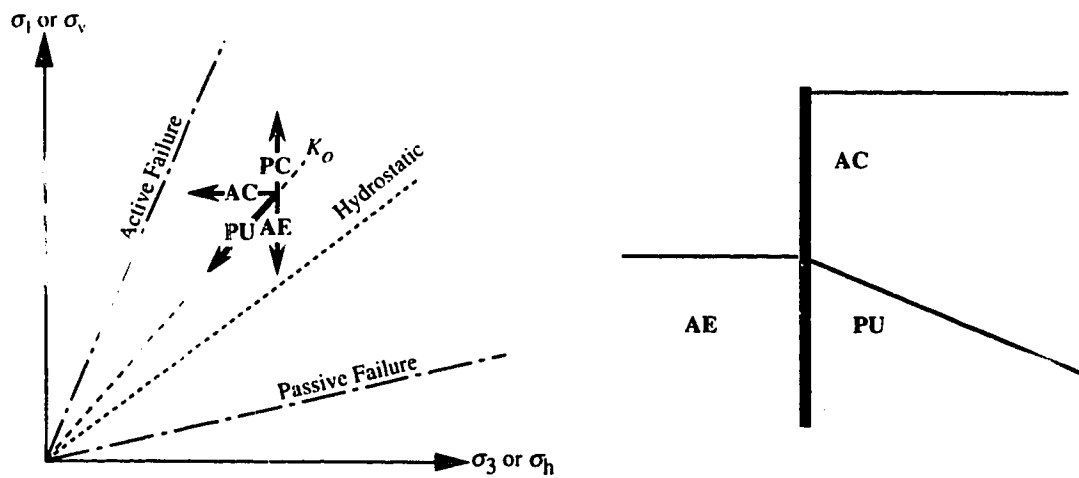


Figure 3.2: Stress Paths investigated by Medeiros and Eisenstein (1983)

the excavation, active extension under the excavation, and proportional unloading between the two regions. Comparisons between different simulation techniques showed that the hyperbolic model based on plane strain stress path dependent parameters gave the most realistic results.

3.3.1.2 Effect of Confinement on Stress Relief

The effect of the stress path on the deformation characteristics of the soil can be qualitatively described if we consider an idealized material constitutive relationship in terms of the incremental stress and strain invariants:

$$\begin{Bmatrix} \delta \varepsilon_v \\ \delta \varepsilon_s \end{Bmatrix} = \begin{bmatrix} \frac{1}{K} & J'_2 \\ J'_1 & \frac{1}{3G} \end{bmatrix} \begin{Bmatrix} \delta p \\ \delta q \end{Bmatrix}, \quad (3.1)$$

where:

ε_v is the volumetric strain,

ε_s is the deviator strain,

p is the mean normal stress,

q is the deviator stress, and

K is the bulk modulus,

J'_1 and J'_2 are parameters relating shear and volumetric effects, and

G is the shear modulus.

For a triaxial sample, axial and radial stresses, σ_a and σ_r , respectively, are expressed as:

$$\sigma_a = p + \frac{2q}{3}, \quad (3.2.a)$$

and

$$\sigma_r = p - \frac{q}{3}, \quad (3.2.b)$$

and axial and radial strains, ε_a and ε_r , respectively, are expressed as:

$$\varepsilon_a = \varepsilon_s + \frac{\varepsilon_v}{3}, \quad (3.3.a)$$

and

$$\varepsilon_r = \frac{\varepsilon_v}{3} - \frac{\varepsilon_s}{2} \quad (3.3.b)$$

If we consider the ratio between the change of confining pressure and the change of axial strain as an indication of confinement, then the confinement ratio **CR** is defined as:

$$CR = -\frac{\delta p}{\delta \varepsilon_a} = -\left(\left(J'_1 + \frac{1}{3K} \right) + \frac{\delta q}{\delta p} \left(\frac{1}{3G} + \frac{J'_2}{3} \right) \right)^{-1} \quad (3.4)$$

from Equations 3.1 and 3.4 the variation of deviator stress due to change of mean normal stress may be expressed as:

$$\frac{\delta q}{\delta p} = \frac{1/CR - A}{B} \quad (3.5)$$

where:

$$A = J'_1 + \frac{1}{3K} \quad ,$$

and

$$B = \frac{1}{3G} + \frac{J'_2}{3} \quad .$$

Figure 3.3 shows an idealized illustration of different stress trajectories with respect to all possible values of **CR**. As the conventional notation of stresses and strains assigns a positive sign in the case of compression, stress relief is expected to produce extensive strain in the axial direction. Therefore, the increment $\delta \varepsilon_a$ is negative. If the mean effective stress is, consequently, reduced, δp is negative. Due to the negative sign in Equation 3.4, **CR** would be negative and the process is termed "*negative confinement*". On the other hand, if there is a negative change in mean effective pressure because of a reduction of axial strain (extension), a positive value for **CR** results and the process is termed "*positive confinement*". The following trajectories may be identified:

- (1) Trajectory **a**- the reduction of axial pressure σ_a is associated with increase of radial pressure, σ_r , which results in an increase in the mean effective pressure,

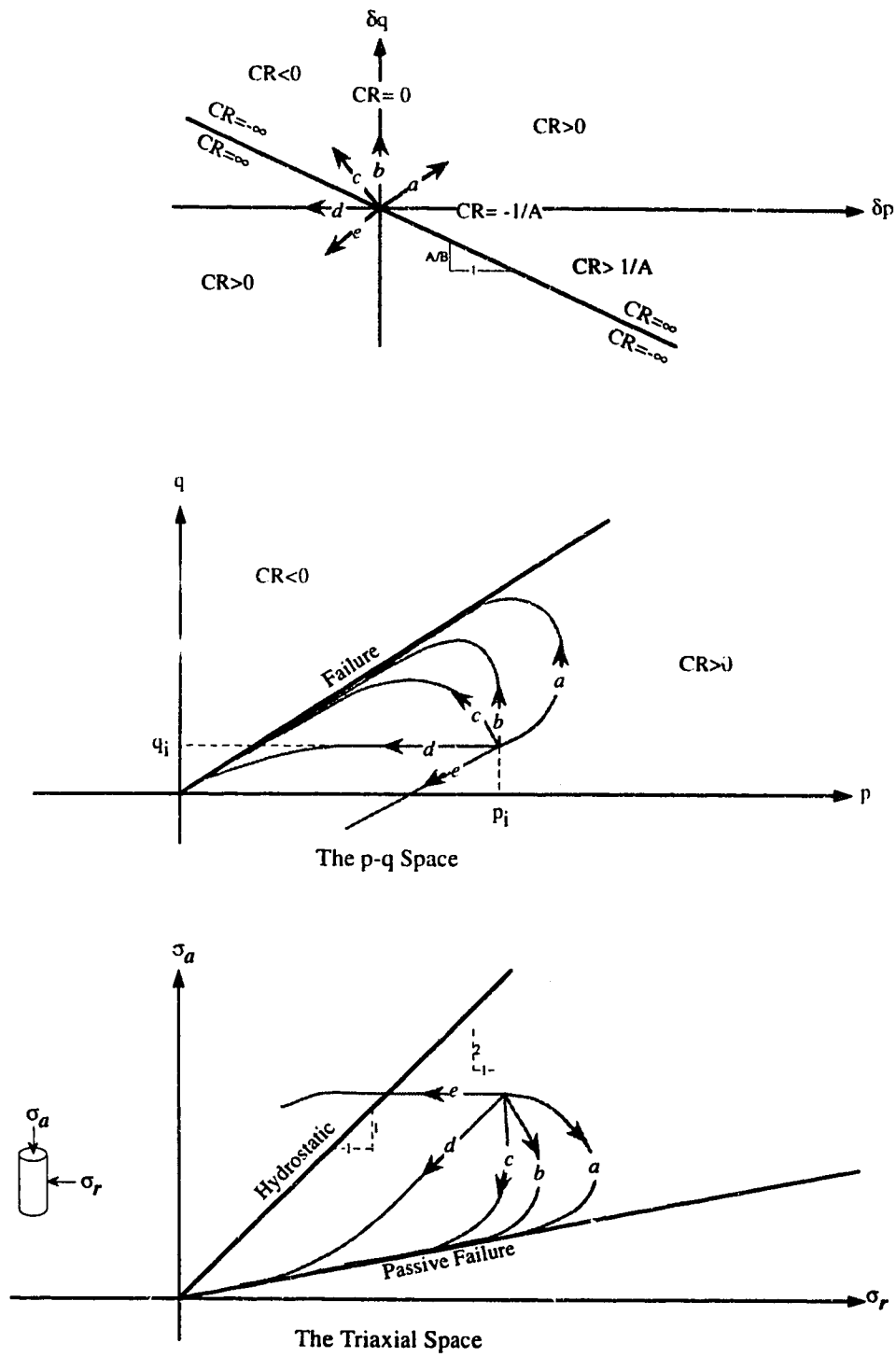


Figure 3.3: Stress Paths related to various degrees of Confinement

- p ;
- (2) Trajectory **b**- the reduction of axial pressure, σ_a , is associated with an increase in radial pressure σ_r which results in a constant mean effective pressure, p ;
 - (3) Trajectory **c**- the reduction of axial pressure, σ_a , is associated with no change in radial pressure σ_r which results in a reduction in the mean effective pressure, p ;
 - (4) Trajectory **d**- the reduction of axial pressure, σ_a , is associated with an equal reduction in radial pressure, σ_r , which results in a reduction in the mean effective pressure p while the deviator stress q remains constant; and
 - (5) Trajectory **e**- the reduction of axial pressure, σ_a , is associated with larger reduction in radial pressure, σ_r , which results in a reduction in the mean effective pressure, p , as well as, a reduction of the deviator stress, q .

The Region (**ab**) represents a case of positive confinement which is attributed to a high dilation tendency. The effect of the boundary conditions is to restrain volume changes and, thus, to increase the radial pressure. The Path (**b**) represents a conventional case of the active extension of the triaxial test (Path **AE** in Figure 3.2). The Region (**bc**) represents a case of negative confinement where the soil element expands at a rate higher than the rate of volume increase because of stress relief. At Path (**d**) the soil element follows a path parallel to the hydrostatic axis while Path (**e**) represents a case where the soil element may cross the hydrostatic axis and then it undergoes a rotation of the principal stresses. In this case, active failure may develop. Burland and Fourie (1985) following a constant confinement ratio related to their laboratory installation showed that the effect of material nonlinearity is to increase the ratio of increment of the mean deviatoric stress to the mean normal stress ($\delta q/\delta p$). It could be suggested, therefore, that the effect of material nonlinearity is to decrease soil confinement. Such an assumption is affirmed by inspection of the stress path in Case (II) (Figure 3.1).

The concept of confinement highly influences face stability as it affects the shear strength within the soil mass in the case of drained ground condition and it affects the distribution of pore water pressure and seepage patterns in the case of undrained ground conditions. A case of positive confinement (Region (**ab**) in Figure 3.3) will increase the mean effective stress during the passive stress relief process which will result in increasing the frictional resistance. At the same time, only relatively small amounts of reduction in axial stress is required to cause failure in the soil element. As a result, for an excavation problem with positive confinement, failure zones develop quickly, but their propagation remains restricted behind the face. On the other hand, if the soil follows a stress path of negative confinement during passive stress relief, deviator stress increases slowly and a

high reduction of axial stress is allowed before the soil element reaches failure. At the same time, as the mean effective pressure is in a decreasing trend, soil layers near the excavation are no longer able to support the ground weight above it, thus, failure zones propagate deeply inside the soil mass before failure takes place. It is to be remembered that the mobility of the face of the pressurized shield excavation does not necessarily imply the occurrence of failure since the cutting process is, in fact, a process that brings soil elements at the face to yield and then failure conditions. Therefore, the function of the face support is to control soil mobility toward the excavation and at the same time it restrains the extent of the stress relief zones from reaching the ground surface so that it does not create excessive settlement.

An extreme case of positive confinement may result in early failure and high pressure at the face. Such field conditions are likely to develop in dilative material and provoke an uncontrolled material flow toward the face. At the same time, an extreme case of negative confinement will result in developing a large failure zone due to low mobilized frictional resistance. In this case, stress release zones extend upward behind and ahead of the face and produces, although face collapse may not take place, excessive deformation and instability problems to the face and to the neighbouring structures.

3.3.2 Methods of Face Support

A practical approach of classifying problems of face support is proposed by Peck (1969) where ground conditions are distinguished based on their mobility when subjected to stress relief. According to Peck:

- (1) *firm* ground permits excavation advance without the need for additional support;
- (2) *raveling* ground produces an excessive degree of loosening near the excavation boundary as soil particles flake into the heading, and an unstable zone can progress through the soil mass and endanger the integrity of the project;
- (3) *running* ground can penetrate into the heading and bury the lower part of the shield;
- (4) *flowing* ground can take place if seepage pressure develops in a raveling or running ground condition, and the shield may be totally buried;
- (5) *squeezing* ground can produce a high degree of deformation at the boundaries.

Accommodation of the above field conditions is achieved either by improving ground conditions through grouting, draining, or freezing, or by providing the exposed face with adequate support. Although the performance of face support methods is attributed to various factors besides the suitability of the technology to ground conditions,

such as, the workmanship and the quality of machines and material applied, three distinct methods may be identified:

- (1) the bentonite slurry shield method;
- (2) the earth pressure balanced shield method; and
- (3) the compressed air method.

A description of the technologies adopted in these methods is provided by Eisenstein and Ezzeldine (1992:b).

3.3.2.1 The Bentonite Slurry Shield

Slurry methods for face support have been used for a wide variety of soil conditions during the last fifteen years with a substantial degree of success and their advantages render them as attractive alternatives to either of the above two methods. Bentonite slurry is injected under pressure at the face of an excavation. In order to fulfill its function as a counterbalance to earth and water pressure, slurry pressure has to build up over a layer of finite thickness. This layer, called "the cake", which is formed from a mix of bentonite slurry and soil particles has improved shear strength properties and low permeability. The effectiveness of the cake layer as a supporting layer is dependent basically upon the composition of the slurry and the soil, the slurry pressure and the rate of excavation. Mohkam and Bouyat (1985) and Bouyat et al. (1985) demonstrated experimentally the physical aspects of the cake formation in gravely soil corresponding to a site condition at Lyon, France. The discharge volume of slurry supplied to the soil passes through three stages: penetration where the filtrate volume increases steadily and reaches an optimum value, then accumulation of colloidal particles causes blocking of slurry flow and the discharge reduces sharply until it reaches a state of steady filtration. Then, support pressure is transmitted to the ground through the thickness of the cake. Therefore, the thinner, the faster, the stiffer, the cake is, the more efficiently the support function of the slurry is met. A "*membrane cake*" takes place if the blocking process develops quickly and up to a limited ground thickness which gives an efficient face support. On the other hand, an "*impregnation cake*" is formed if the blocking occurs at slow rates and up to high extent of ground thickness behind the face. In this case, the support constancy throughout the excavation stages is better achieved as the rate of propagation of cake layer is synchronized with the rate of advance of excavation. As the progress of the excavation requires a continuous process of forming and destroying the cake layer, the design of the composition of the slurry must take into account the change of cake thickness. Meanwhile, the slurry acts as a transporting agent for the excavated muck through a specially designed cycle. German and Japanese technologies used in building bentonite slurry shields represent two

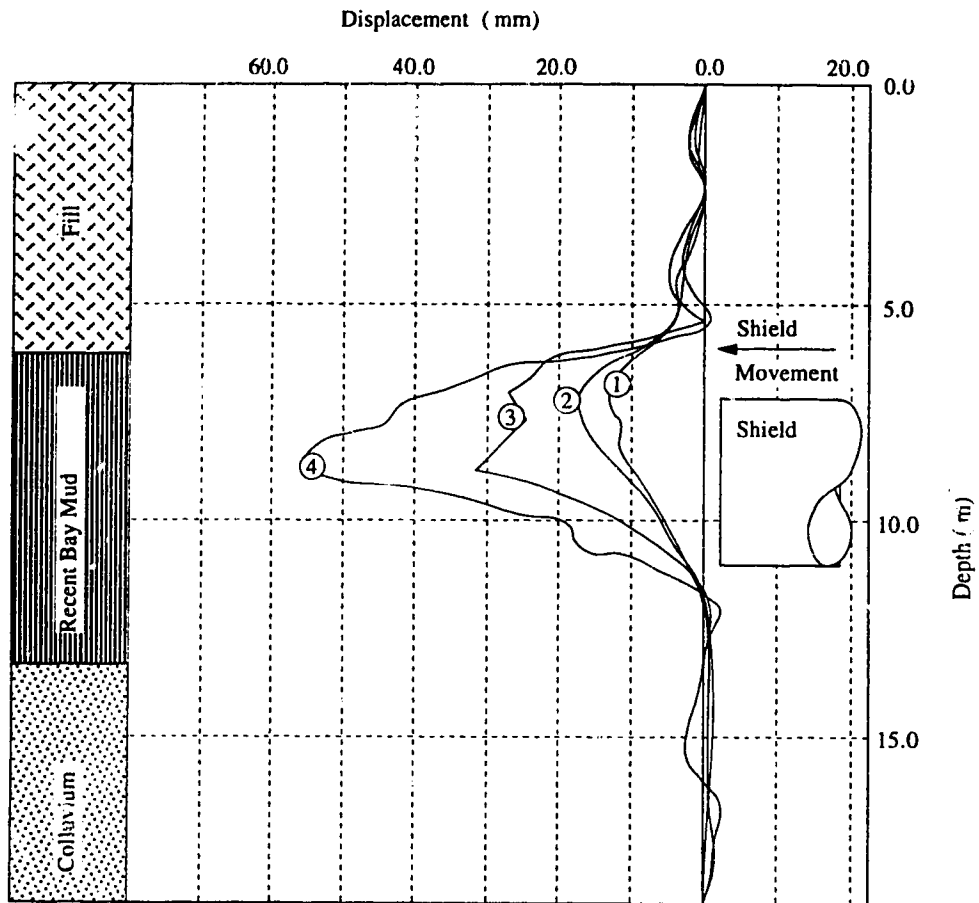
distinctive ways in applying the method. German boring machines, also known as the Hydroschild, rely on a compressed air reservoir to maintain constant support pressure inside a slurry chamber. A description of the technicalities of this method is provided by Babendererde (1991) and by Anheuser (1985), and Japanese boring machines are used with comparable degree of success. While air pressure is not used to regulate the bentonite pressure, the continuity of face support is guaranteed by the effectiveness of the face openings and the adequacy of the cutter bits in use. Kurosawa (1985) provides a description of recent Japanese technology.

3.3.2.2 The Earth Pressure Balanced Shield

The earth pressure balanced shield method consists in providing a rigid support to the face by regulating the amount of excavation. The rate of advance of the shield is related to the volume of transported muck through a controlled screw conveyor from a closed spoil retaining area. This retaining area acts as a rigid support and controls the movement of the face toward the excavation. A more thorough description of the earth pressure balanced shield method is provided by Clough et al. (1983). In order to transmit the required pressure to the face from the shield jacks located at the tail, the shield has to overcome the adhesion developed along its skin by keeping its relative movement toward the advancing direction. This yields, in general a thrust pressure at the face higher than the initial horizontal pressure and results in an inward movement at the face. Such idealization is confirmed by Finno (1983) who used rigid face support to numerically simulate an EPBS used in the construction of the N-2 San Francisco Tunnel, (Section 2.4.2.2.2). As shown in Figure 3.4, a measured soil response related to the shield advance during the excavation through the soft clay Bay mud formation resulted in soil movement away from the tunnel face which indicated that the face pressure exceeded the initial horizontal pressure. Control measures employed in this method are described by Xi (1990). As a development of the earth pressure balanced shield, the muddy soil pressure balanced shield was developed, or the D. K. shield (Hagimoto and Kashima, 1985). Instead of controlling earth pressure by regulating muck displacement, a mud making agent is added to the soil in the retaining area in order to provide the excavated soil with fluidity and impermeability, and to improve the uniformity of the support pressure.

3.3.2.3 The Compressed Air Shield

The use of compressed air for sub-aquatic constructions has been practiced since the sixteen century. Application of this method to tunnelling projects started in 1871 during the construction of the New York tunnel under the Hudson River. Successes and failures



- 1- Shield 5.40 m from Inclinometer Line
- 2- Shield 3.30 m from Inclinometer Line
- 3- Shield 2.40 m from Inclinometer Line
- 4- Shield 1.20 m from Inclinometer Line

Figure 3.4: Movement at the Face of an EPBS (modified after Finno 1983)

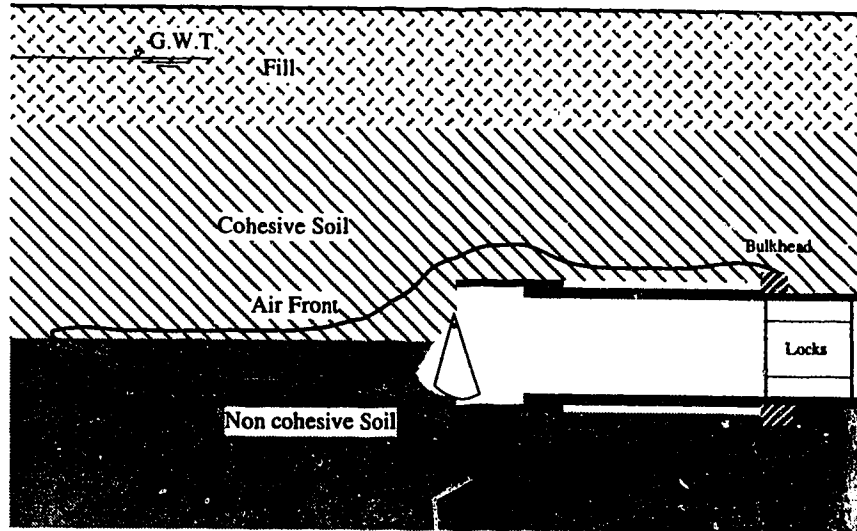
of the method have been noted during the construction of London's underground railway system between 1886 and 1900 (Kirkland, 1984). Until now, compressed air has been considered as an acceptable face support alternative which is attributed to its major advantage in controlling groundwater pressure. On the other hand, health and safety concerns impose restrictions on the application of the method (Jardine et al., 1991 and Anderson et al., 1991). The basic idea of compressed air support is to control seepage forces by applying fluid air pressure to interact with the fluid pore pressure. As air pressure is supposed to be higher than the water pressure, air advances into the soil expelling pore water from a certain region around the excavation. A pattern of air seepage is thus created in the soil to counteract the water seepage pattern that would have been created had the face not been supported. At a certain point, the equilibrium between the two forces is established creating an air front surface. The propagation of the air front depends mainly on the permeability, air tightness, and the capillary forces in the soil formations at the air front. The air-water interaction has a positive effect on face stability because it excludes ground movement driven by seepage forces into the excavation and because it increases soil strength due to capillary forces. At the same time, the exposed face of the excavation, under the new state of pore pressure, is required to support itself. Failure of the face is generally related to loss of air pressure. If such a condition occurs under water areas, air pockets burst through the ground and then up to the water surface pushing with them soil particles in a process known as "*blow out*" of the tunnel face. The mechanism of blow out is initiated by excessive ground movement at the face that may result in loosening the soil and increasing its porosity. As the movement progresses into the ground, it affects the air front equilibrium leading to air losses. Then, compressed air in the ground changes its formation from being confined in the gallery to air streams trying to escape. Once air trajectories have been established to the free air at the ground surface, the supporting effort dissipates through piping.

Shalaby (1990) presents a detailed study of data collected at an instrumented section of the Cairo wastewater project (Section 2.4.2.3). Compressed air was applied at a mixed cross-section where a relatively porous predominantly noncohesive soil layer underlies an impervious cohesive layer. Two stand pipe piezometers were installed in the noncohesive soil at different distances from the tunnel centerline. The purpose of the piezometers was to measure the changes in pore pressure due to the tunnel construction. A drop in water pressure would indicate a loss of air pressure and a groundwater seepage toward the tunnel. Measurements showed that fluctuations in pore water pressure were minimum until a certain point where air pressure interfered with the piezometers and disrupted any further measurements until the compressed air was released. Figure 3.5 shows a sketch of a

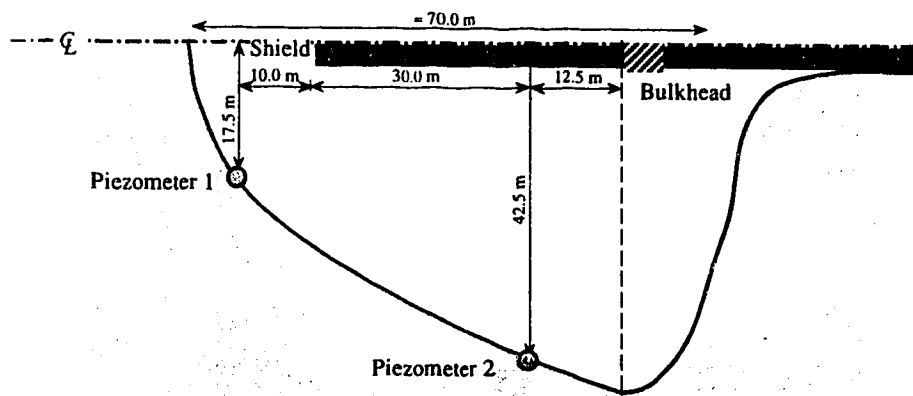
reconstituted air front at the instrumented section based on comparing the location and the time of the position of the face when air pressure reached the piezometers. From the figure it can be concluded that the air front can extend to relatively large dimensions and still perform its function of controlling seepage forces as long as the tightness of the ground stratification prohibits piping to take place.

3.3.4 Stress Paths for Different Face Support Techniques

Let us consider the case of an unsupported face excavation with positive confinement. Figure 3.6 shows the changes in axial and radial stresses in a cylindrical element at the centre of the face and along the axis of the tunnel behind the face. Stress relief starts at a Point (1) far enough from the excavation. Axial stress decreases while radial stress increases until Point (2) where yield starts and radial stress deviates from its initial incremental trend. The failure zone starts at Point (3) where the ultimate shear strength is reached at the passive mode of failure. The application of bentonite slurry pressure in the form of a membrane cake will have the effect of reducing the extent of the face relief zone due to limiting the axial stress reduction to a value equal to the applied face pressure and due to imposing a higher state of confinement to the soil behind the face. A successful application of face pressure results in mobilizing shear stress lower than the allowable shear strength at the cake surface as shown by Path (1-5) in the figure. Meanwhile, the initial shear strength is expected to increase by a certain amount (Δc) due to the cohesion of the new mixture. Inside the membrane cake thickness, axial stresses increase sharply from a state of almost no effective pressure at the face of the excavation to the required face pressure at the surface of the membrane, and radial stress undergoes even a sharper increase until it reaches equilibrium at the membrane surface. The ability of the bentonite to accumulate a pressure gradient and to mobilize the associated shear strength depends on its thixotropic property. Cake cohesion increases with time until the layer is disturbed by the face advance. Therefore, the stress path of a newly formed membrane would be likely to follow Path (1-4) in the figure while it follows Path (1-6) if the cake is allowed to settle. It is, therefore, imperative to select the cutting speed, cutting effort, and rate of advance that are compatible with the ability of the cake to regenerate the required support so that as the soil particles at the face alternate between the two stress paths through the excavation cycle, global failure of the face is prohibited. An impregnation cake is illustrated in the same figure. Compared to the membrane cake, pressure changes inside the cake layer are more gradual which is related to a bentonite type of higher fluidity. As a result, the extent of stress release zone created is larger, and there is a smaller difference between the two stress Paths (1-4) and (1-6). On the other hand, because of its larger

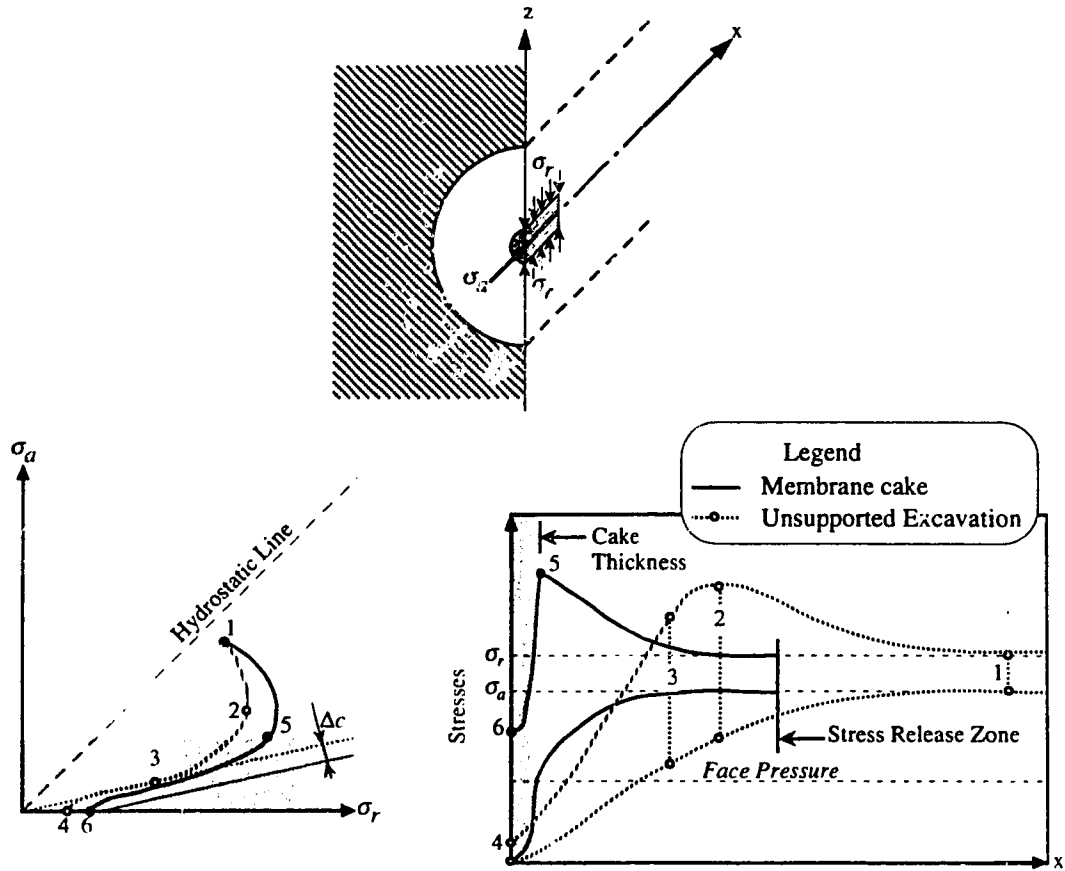


Ground Conditions at Cairo Sewage Project

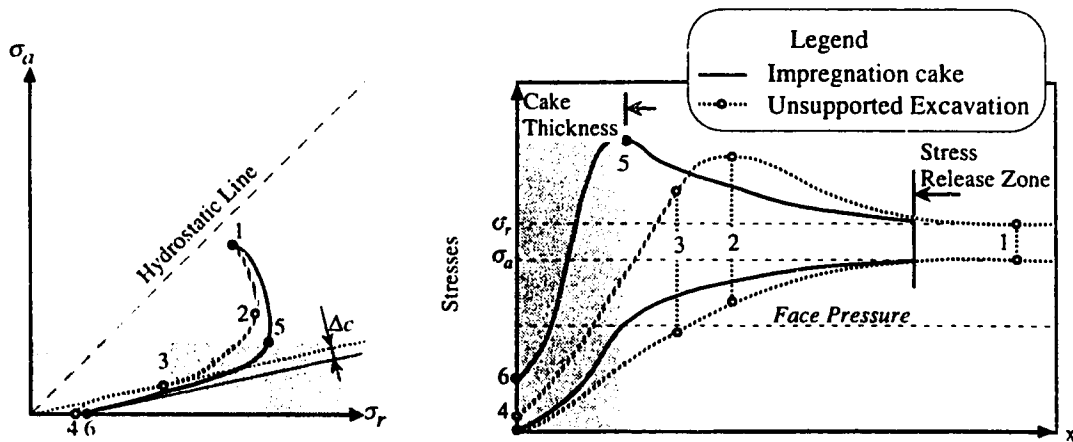


Plan

Figure 3.5: Estimation of Air Front Zone during Tunnelling with Compressed Air. Cairo Sewage Project



Bentonite Slurry Shield: Membrane cake



Bentonite Slurry Shield: Impregnation cake

Figure 3.6: Effect of Bentonite Slurry on the Stress Distribution at the Tunnel Face

thickness, the range of fluctuation of the pressure gradients related to the excavation cycle is considerably smaller which may enhance the stability of the face if the appropriate excavation scheme is followed.

Figure 3.7 (a) shows a case where the face pressure exceeds the initial axial pressure which is close to representing the EPBS method. The new stress path crosses the hydrostatic line and the element undergoes reversal of the principal stresses. In this case, high face pressure failure may take place on the active state side. Depending on the boundary conditions and the soil formations around the excavation, ground heave may result. As long as the surface movement gradient is within an allowable range, this type of failure could be considered not to jeopardize face stability. However, the nature of the applied pressure is related to the advance of the excavation. It is, therefore, important to consider the effect of stopping excavation during the weekends or for other reasons on the integrity of the face. As pointed out by Clough et al. (1983) the maximum settlement of the N-2 Project occurred because of stopping the excavation for a 15-day period.

It could be argued that the case of compressed air is closer to that of an impregnation cake where the cake thickness is large enough to comprise the zone of initial stress relief. For the sake of comparison, Figure 3.7 (b) shows the same initial stress path presented in the former two figures. Neglecting the effect of the seepage forces on the state of the effective pressure of the ground, the application of air pressure exceeding the initial pore water pressure will result in reducing both the radial and axial pressures and an additional cohesion (Δc) will be added to the soil shear strength because of capillary forces. As long as, the ground formation precludes any air losses and the soil conditions do not change along the tunnel length, the new stress Path (5-6) may be expected to remain constant and independent of the excavation scheme which is a major advantage of the compressed air Tunnelling method.

3.4 Face Stability Analyses

The question of face stability has received special consideration as the safety of the construction is a primary concern in the excavation design. The problem is three-dimensional and is dependent on a number of factors besides the shear strength of the supported soils. Such factors include the method of support, soil permeability, compressibility, soil ability to produce volume changes due to the mobilization of shear strength, and soil interaction with the additives. Furthermore, the macroscopic view of the problem and the boundary conditions are important in determining the extent of the failure zones and the overall mobility of the ground. Therefore, methods used for studying face stability are diverse as they include empirical, experimental, analytical, or numerical

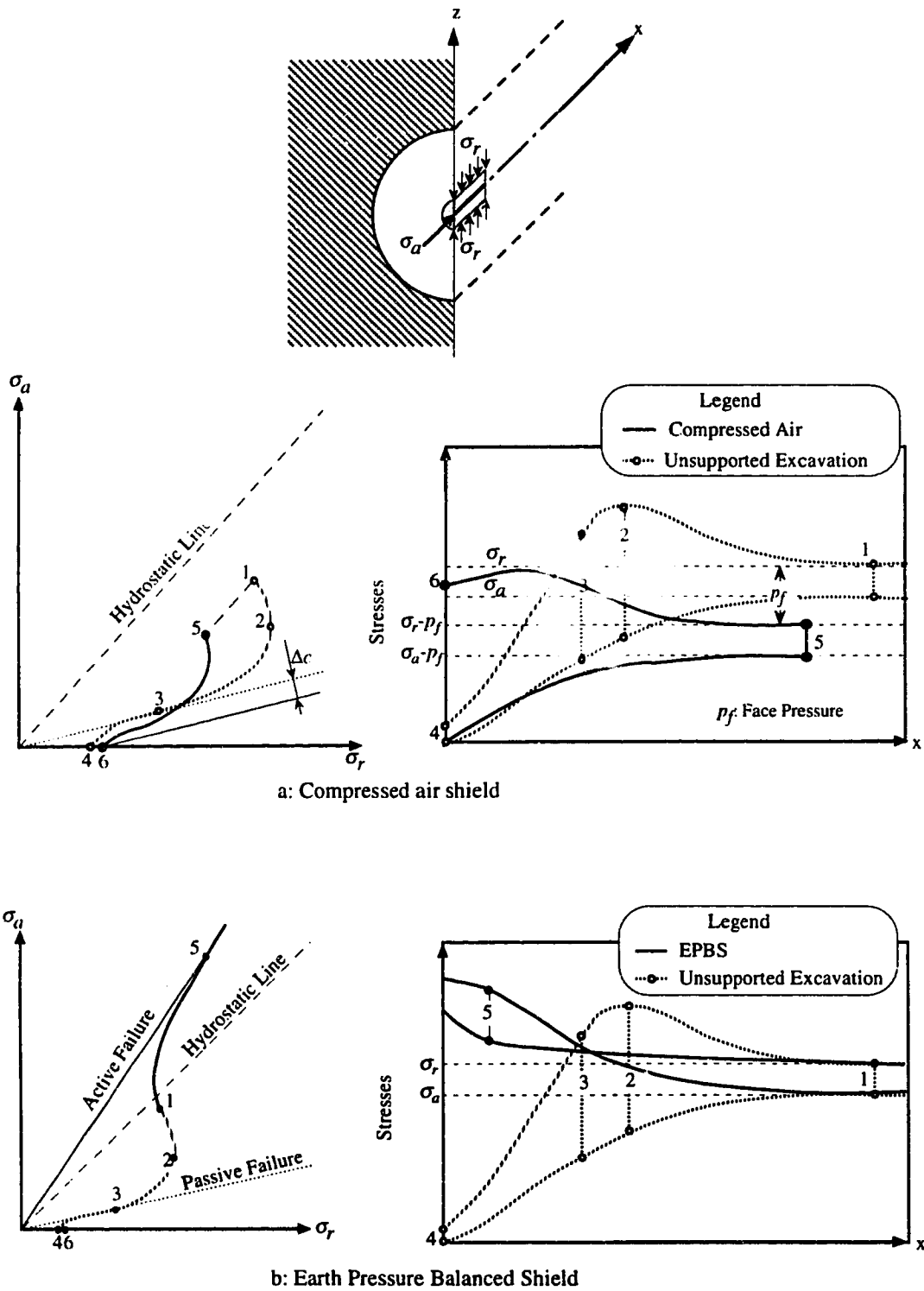


Figure 3.7: Effect of Face Support Method on the Stress Distribution at the Tunnel Face for Cases of Compressed Air Shield and Earth Pressure Balanced Shield.

approaches. It is expected that a global design requirement will not ensue from a certain type of analysis but that comparisons between different analyses collected from the literature is expected to provide guidelines on the quantitative and qualitative aspects of the problem, and at the same time this would enable the determination of the limitations and advantages of the various methods of analyses.

3.4.1 Empirical Analysis

Stability of the face in cohesive soil has been investigated by Broms and Bennermark (1967). The basis for development of the stability criterion which is widely used, thereafter, is the undrained shear strength. The approach followed by the authors include an experimental analysis in which face instability is simulated using extrusion tests. A number of compiled case histories were examined and the corresponding values of undrained cohesion, c_u , were assessed using the unconfined compressive test, the lab vane test, and the Swedish fall cone test. The following expression is suggested:

$$OF = \frac{p_o - p_f}{c_u} \quad , \quad (3.6)$$

where:

p_o is the total initial vertical pressure in the ground at the tunnel axis level,

p_f is the total pressure applied at the face, and

OF is the overload factor.

The overload factor at failure is known as the "*Stability Ratio*" or the "*Stability Number*", N . According to the authors, a value of N equal to six may be suggested as a safe limit for the design of a vertical excavation (which includes a vertical cut, as well as, a tunnel face) and the value of the shear strength, as well as, the geometry of the problem does not have much influence on the suggested stability criterion.

The Broms and Bennermark formula has become a 'rule of thumb' to evaluate the face stability in cohesive material. However, the extension of the use of the formula to design tunnel stability in the transversal section is been questioned by many authors. Heinz (1988) used analytical plastic solutions to demonstrate that at the transversal section the stability number at collapse depends on the depth of the tunnel and on the support system near the face. According to the author's proposed solution for a fully supported length of tunnel, the Broms and Bennermark criterion overestimates tunnel safety as long as the *depth ratio* (cover to diameter ratio, H/D) is higher than 2.0 while it is on the unsafe side

for lower depth ratios or less supported length near the face. It is to be noted also that changes in undrained shear strength due to changes in pore pressure at the face have to be considered if the Broms and Bennermark formula is used. It could even be suggested that drained analysis will provide a better estimation of safety than the undrained analysis as it takes into account pore pressure changes and variation of the mean confining pressure related to the excavation and to the face support process. Finally, extrusion tests performed by Broms and Bennermark were carried out under high mean effective pressure which corresponds to a deep tunnel in a state of positive confinement.

3.4.2 Physical Models

Physical models have an advantage over analytical models in the sense that no assumptions are to be made with respect to the material constitutive relationship. Galle and Wilhoit (1962) investigated stress distribution around a wellbore using epoxy-resin models. Axisymmetric and three-dimensional initial stress fields were applied to a cubic model representing a half space with a cylindrical hole of finite length inside. Stresses at the end of the borehole are comparable to stresses at the tunnel face. A three-dimensional photoelasticity technique was used to determine stresses inside the model material. Then contour lines of the stresses were plotted for different loading conditions. Since elastic behavior is expected in the material, superposition of the different contour lines gave a generalized assessment of stresses around a finite circular excavation.

Casarin and Mair (1981) used an experimental model to simulate face stability of a tunnel heading in an overconsolidated cohesive soil. Radiographic images of lead shots inside the clay model were used to monitor soil displacement around the tunnel. Initial stress was applied as surcharge pressure at the top surface of the model while failure was introduced by quickly removing supporting pressure inside the tunnel. The experimental program included different values of cover to a diameter ratio (H/D) and of an unsupported tunnel length (L). Results showed that for a fully supported length of tunnel, the stability ratio increased with the cover to diameter ratio and the Broms and Bennermark criterion may be considered as an upper-bound for a deep tunnel (cover to diameter ratio higher than 3.0).

While physical models simulate soil weight as a surcharge at the ground surface, centrifuge models provide a more realistic simulation of gravity forces by increasing the unit weight because of an increase of the centrifuge acceleration related to the model scale. Additionally, time for centrifuge model tests is reduced as the scale is reduced which helps in monitoring long term effects. On the other hand, soil behaviour at the particle level is not accurately simulated by the tests. Furthermore, vertical movement may undergo a

certain amount of distortion depending on the direction and velocity of the sample rotation. Such an effect is referred to as the Coriolis effect (Schofield, 1988).

Mair (1979) used centrifuge tests to model stability of the tunnel heading in soft clay. The experimental program included various values of H/D and L . Results showed that the stability ratio increases with H/D and that, contrary to the Casarin and Mair (1981) results, Broms and Bennermark criterion may be considered as a lower-bound for shallow tunnels where the excavation length is fully supported as shown in Figure 3.8. Nevertheless, both studies agreed on the shape of the failure zone: a semi spherical segment starting at the floor of the face with its central sphere at the crown level and expanding in a funnel shape until reaching the ground surface where signs of failure are detected as excessive movement at the ground surface ahead of the face as shown in Figure 3.9. The Casarin and Mair tests also showed that failure takes place associated with high amounts of displacement at the face, the crown, and at the ground surface. For a small ratio of unsupported length ($L/D=0.1$) a soil movement at the face of the excavation of 1.0% the tunnel diameter would take place before any failure shape can be developed while failure may be identified for a face displacement of about 8.0% tunnel diameter. Also, an increase of the slope of deformation associated with the removal of face pressure is gradual.

Chambon et al. (1991) investigated the face stability of shallow tunnels in granular soils using centrifuge models performed in LCPC¹, France on dry clean silica sand (Fontainebleau sand) with different densities at Bochum, Germany. A description of the installation is provided by Chambon and Corté (1989). Layers of colored sand were laid horizontally at regular intervals inside the sand in order to show the movement associated with face pressure reduction. An experiment program included different values of supporting length, cover to diameter ratio, and diameter sizes. Failure mechanisms as sketched in Figure 3.10(a) were found to exhibit a consistent degree of similitude and could be described as follows: as face pressure decreases, face movements are almost negligible until a certain pressure is reached, the yield pressure, p_y . Then the slope of face deformation with the stress relief increases constantly until collapse pressure, p_c , is reached. At this point uncontrolled face displacement takes place characterized by a sudden rise of air pressure inside the model tunnel. Figures 3.10(a) and 3.10(b) show the obtained yield and collapse pressures for various tunnel diameters and depth ratios, respectively. Based on the same figures it can be concluded that the effect of depth ratio and the tunnel diameter is more obvious on the collapse pressure than it is on the yield pressure. Figure 3.9(b) shows failure zones as described by the authors. The yield starts in a region of limited thickness in the longitudinal direction and takes a bulb shape in the transversal

¹Laboratoire Central des Ponts et Chaussées

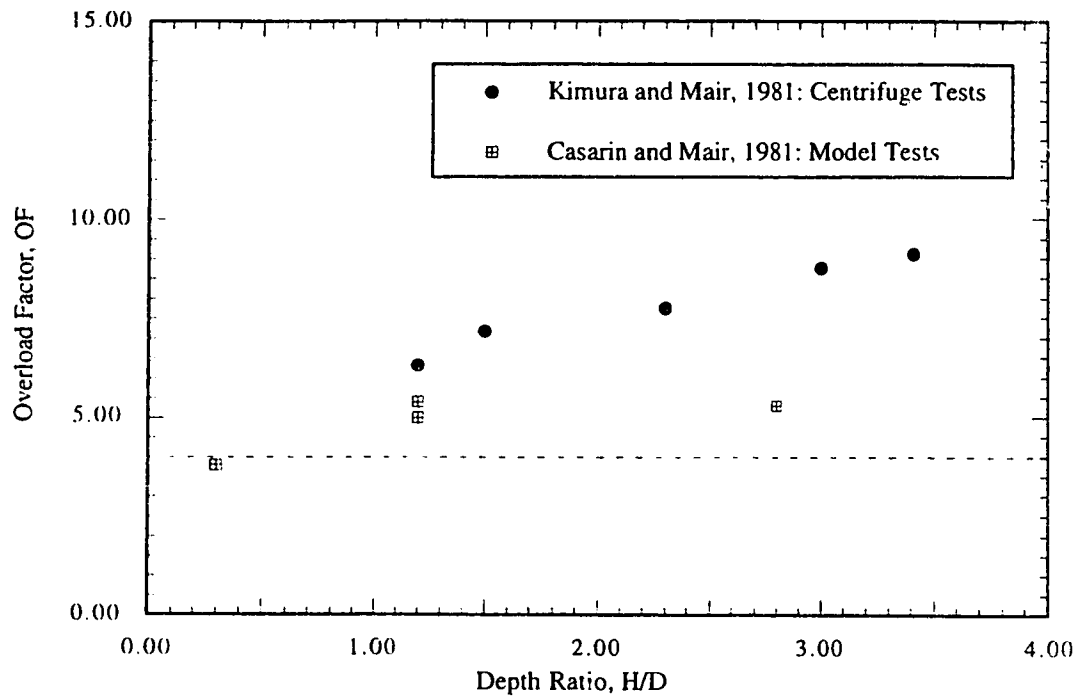
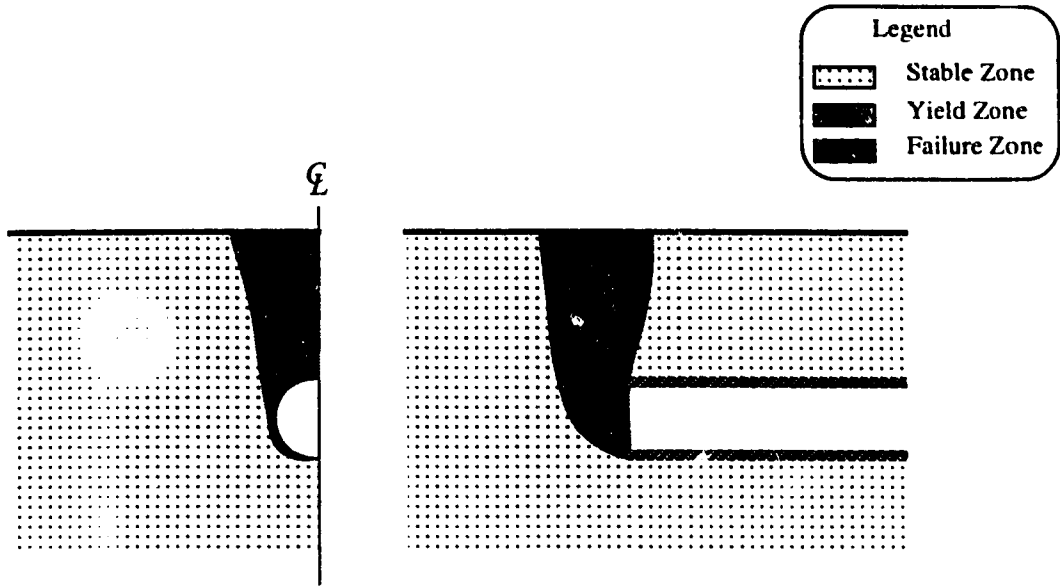
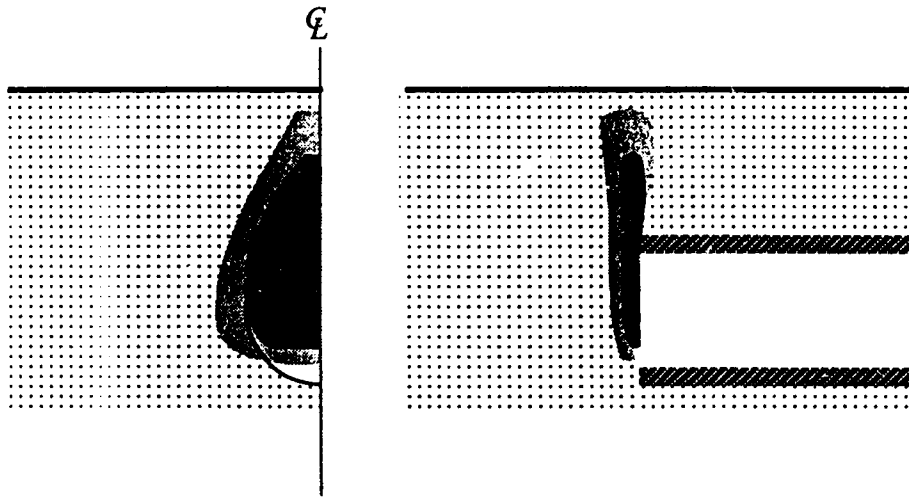


Figure 3.8: Overload Factor, OF versus the Depth Ratio from Physical Models on Cohesive Soils.



a: Failure Mechanism in Cohesive Material (after Kimura and Mair, 1981)



b: Failure Mechanism in Frictional Material (after Chambon et. al., 1991)

Figure 3.9: Failure Mechanisms at the Tunnel Face in Cohesive and Frictional Materials according to Experimental Results.

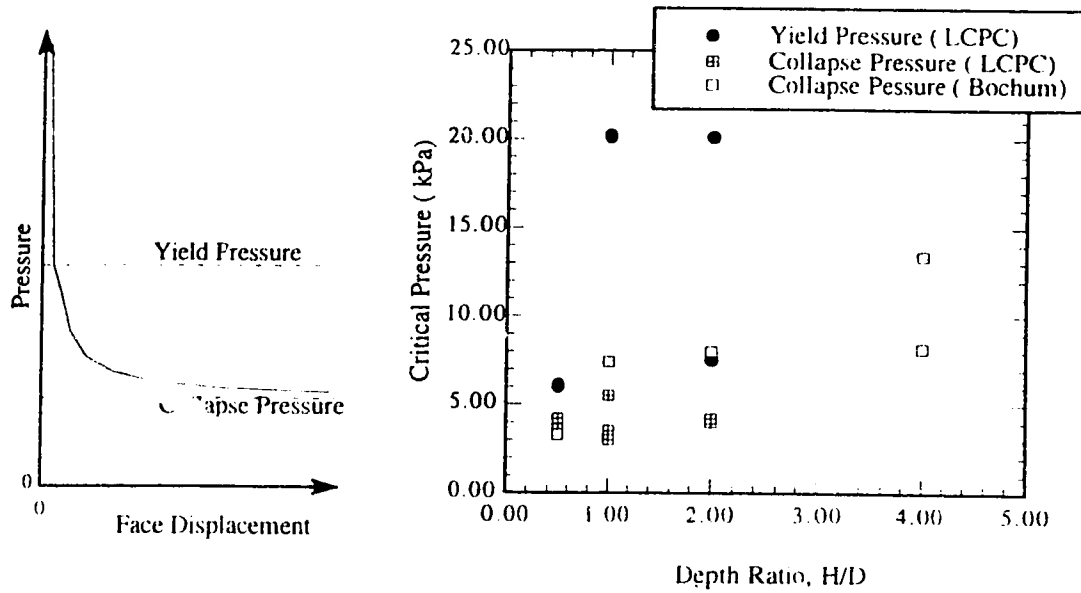


Figure 3.10 a: Critical Face Pressure versus Depth Ratio from Centrifuge Tests on Non Cohesive Soils (after Chambon et. al. 1991).

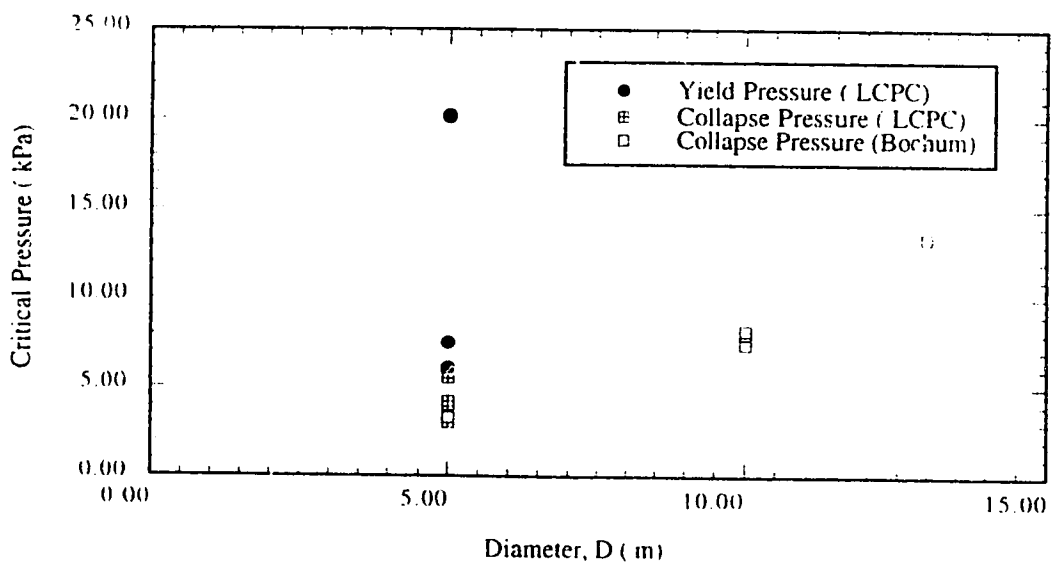


Figure 3.10 b: Critical Face Pressure versus Tunnel Diameter from Centrifuge Tests on Non Cohesive Soils (after Chambon et. al. 1991).

direction. Unless the depth ratio is very low, collapse occurs before the failure zones reach the ground surface, and then failure propagates rapidly upward. Besides, the results showed that the depth ratio has little influence on the limit collapse pressure.

3.4.3 Limit Theorems of Plastic Analysis

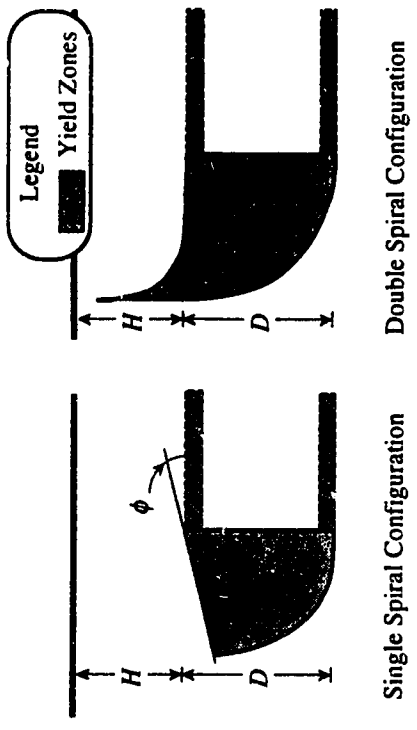
Face instability may be idealized as a result of the development of a mechanism of failure along a certain defined failure surface. Plastic analyses consider the strain compatibility and stress equilibrium separately to accommodate boundary conditions and failure criterion. Results of the analyses are represented in the form of lower- and upper-bound solutions that are supposed to bracket the idealized failure conditions. The analyses have the advantages of being simple and in a generalized form, however, comparisons with other types of analyses is required to evaluate the accuracy of the results.

3.4.3.1 Lower-Bound Solutions

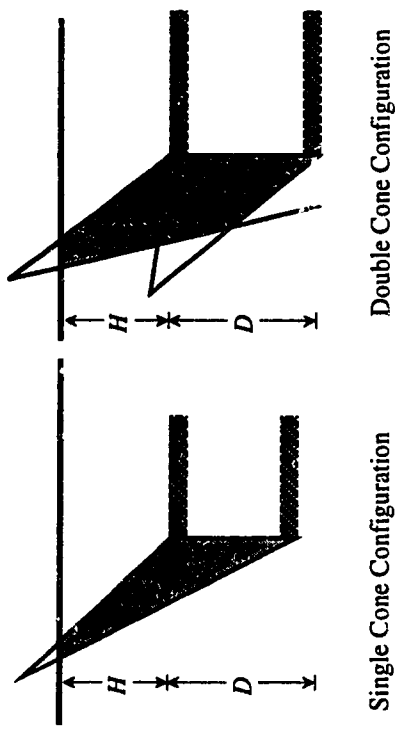
The principle of a lower-bound solution has been used in a number of static problems and has proved to have the ability of providing simple estimations of failure loads for an idealized plastic material. The validity of each solution has to be examined by comparison with other solutions, especially with the upper-bound solution and solutions from physical models. The principle of a lower-bound solution consists of finding for a certain system in equilibrium a statically admissible stress distribution which satisfies the equilibrium equations, the stress boundary conditions, and that in nowhere violates the yield condition. Therefore, yield and equilibrium conditions are considered while the kinematics of the problem is not necessarily taken into account. The lower-bound method gives, therefore, a lower estimation of the collapse load or a "*safe solution*".

Davis et al. (1980) used the lower-bound solution to investigate the stability of a tunnel face in cohesive soil. Three mathematical models were considered for a weightless material: plane strain heading, circular heading with a failure zone extending into a long cylindrical volume behind the face, and a circular heading with failure zone extending into a spherical volume behind the face. Inspection of the three solutions proved that the circular heading with spherical failure zone gives the most critical results (higher stability number) as long as the depth ratio is higher than 0.85.

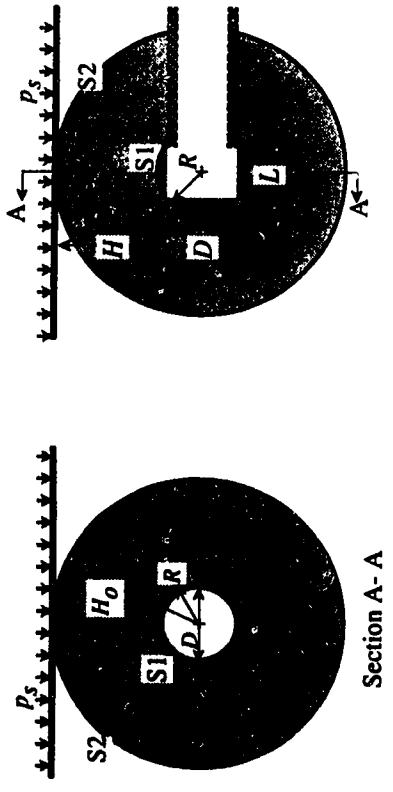
Mülhaus (1985) considered the lower-bound solution for a problem of face collapse using Davis' configurations and adding to them the effect of an unsupported length. Figures 3.11(a) and 3.11(b) show the geometrical configuration of the study. The tunnel is considered rigidly supported up to a distance L from the heading. Gravitational forces are not acting inside the soil mass and are substituted by applying an equivalent surcharge



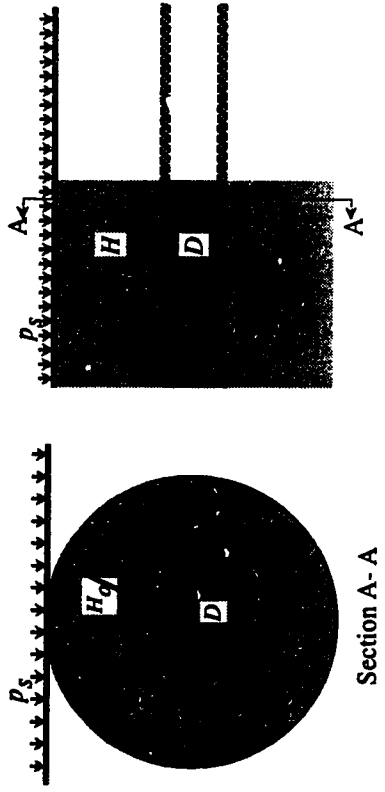
c: Plane Strain Configuration of Upper Bound Solution (Chambon and Corté, 1990)



d: Three Dimensional Configuration of Upper Bound Solution (Leca and Dormieux, 1990)



a: Spherical Configuration of Lower Bound Solution



b: Cylindrical Configuration of Lower Bound Solution

Figure 3.11: Different Configurations of Limit Theorems of Plastic Analysis used to estimate Face Stability

pressure at the ground surface. A spherically symmetric stress field is assumed outside of Sphere S2 while the surface of Sphere S1 is a free boundary. The Mohr-Coulomb criterion of failure is assumed for cohesive frictional material between the two spheres. Results of the analysis are expressed in terms of the unsupported length at which failure starts to take place:

$$L = D \sqrt{\frac{\left(1 + 2\frac{H}{D}\right)^2}{\left(\left(K_p - 1\right)\frac{p_s}{2\sigma_c} + 1\right)^{\frac{1}{K_p - 1}}} - 1} \quad (3.7)$$

where:

$$K_p = \frac{1 + \sin \phi}{1 - \sin \phi} \quad ,$$

$$\sigma_c = \frac{2c \cos \phi}{1 - \sin \phi} \quad , \text{ and}$$

p_s is the surcharge at the ground surface.

For purely cohesive material the above equation is reduced to:

$$L = D \sqrt{\left(\frac{1 + 2H/D}{\exp\left(\frac{p_s}{4c_u}\right)}\right)^2 - 1} \quad (3.8)$$

The above solution has been extended by Heinz (1988) and Leca and Panet (1988), separately, to include the face pressure effect simulated as applied pressure on the surface of Sphere S1. Results are reproduced, hereafter, with some modification of the symbols for consistency. The coefficients N_s , N_f , N_d , and N_o termed, respectively, as *the surcharge coefficient*, *the face pressure coefficient*, *the size coefficient*, and *the depth coefficient* are defined as follows:

$$N_s = \frac{P_s}{\sigma_c} \quad , \quad (3.9.a)$$

$$N_f = \frac{P_f}{\sigma_c} \quad , \quad (3.9.b)$$

$$N_d = \frac{\gamma D}{\lambda \sigma_c} \quad , \quad (3.9.c)$$

and

$$N_o = \frac{\bar{H}_o}{R} \quad , \quad (3.9.d)$$

where:

γ is the soil unit weight.

Special interest is addressed to the case where the tunnel length is a fully supported tunnel. Then the Sphere **S1** is tangent to the tunnel circumference and R reduces to the tunnel radius R_o . The extended solution is produced for a general cohesive frictional material as follows:

$$N_f = N_s N_o^{-2(K_p-1)} + \frac{1 - N_o^{2(K_p-1)}}{(K_p - 1)N_o^{2(K_p-1)}} \quad , \quad (3.10.a)$$

for purely cohesive material:

$$N_f = N_s - 2 \ln(N_o) \quad , \quad (3.10.b)$$

and for purely frictional material:

$$\frac{P_f}{P_s} = N_o^{-2(K_p-1)} \quad . \quad (3.10.c)$$

The above equations are referred to as the extended Mülhaus solution. Equation (3.10b) is

the same as the equation presented by Davis et al. (1980: Equation 9) if a fully supported tunnel length is considered ($L=0$). It is also interesting to note that for the same case, the Broms and Bennermark criterion corresponds to a tunnel depth ratio of about 1.7 ($N_o = e^{1.5}$).

Leca and Panet (1988) have extended Davis' configuration for plane strain analysis of the longitudinal tunnel section to include the effect of friction. The following expression is obtained for a general cohesive frictional material:

$$N_f = K_a (N_s + N_d(N_o + 1) - 1) \quad , \quad (3.11.a)$$

and for purely frictional material:

$$p_f = K_a (p_s + \gamma(H + D)) \quad , \quad (3.11.b)$$

where:

$$K_a = \frac{1 - \sin \phi}{1 + \sin \phi} \quad .$$

Equation 3.11.b is the same as the conventional Rankine's expression for active lateral earth pressure at a retaining wall where the height of the wall is equal to the depth of the tunnel floor. The same authors have used Davis' configuration for a circular heading with a cylindrical failure zone (Figure 3.11:b) to include the effect of friction. The following expression is obtained for a general cohesive frictional material:

$$N_f = \frac{N_s + 1}{K_p N_o^{(K_p - 1)}} - \frac{1}{K_p - 1} \quad , \quad (3.12.a)$$

for purely cohesive material:

$$N_f = N_s - 1 - \ln(N_o) \quad , \quad (3.12.b)$$

and for purely frictional material:

$$\frac{p_f}{p_s} = \frac{1}{K_p N_o^{(K_p - 1)}} \quad (3.12.c)$$

Equation (3.12.b) is the same as the equation presented by Davis et al. (1980: 7). The above equations are referred to as the extended Davis solution. It is to be noted also that the Broms and Bennermark criterion corresponds to a depth ratio of about 3.2 ($N_o = e^2$).

3.4.3.2 Upper-Bound Solutions

In an idealized failure condition, the strain values are indeterminate and the relationship between stress and plastic deformation is considered in terms of strain rates and velocities. The principle of upper-bound solution consists of finding for a certain system in failure a kinematically admissible velocity field that satisfies the strain and velocity compatibility conditions: the velocity boundary conditions. The load determined by equating the external rate of work to the internal rate of dissipation of energy of the assumed velocity field, is an upper estimation of the collapse load. Therefore, the compatibility condition of equilibrium of energy is considered while the stress distribution is not necessary in equilibrium. The upper-bound method gives, therefore, an upper estimation of the collapse load or an "*unsafe solution*".

The upper-bound theorem has been used by Davis et al. (1980) to estimate face pressure in a state of failure for a plane strain of a longitudinal section in cohesive material. The following expression is obtained:

$$N_f = N_s - \sqrt{2N_o - 1} \quad (3.13)$$

From the above equation, the Broms and Bennermark criterion corresponds to a depth ratio value of 2.0. The same authors have also presented a solution for a circular tunnel heading. As expected, the obtained critical face pressure is lower than that obtained from the plane strain analysis. For this case, the Broms and Bennermark criterion corresponds to a depth ratio of 0.488.

Chambon and Corté (1990) investigated the limit face pressure that satisfies the upper-bound requirements for frictional material. A two dimensional plane strain analysis was adopted. Failure patterns were chosen to follow log spiral curves. Two failure patterns are considered: a one-spiral mechanism and a two-spiral mechanism as shown in Figure 3.11 (c). The effect of gravity is included as the weight of the failure area while the influence of the free surface at ground level is not included, as long as, the ground surface

does not interfere with the extent of the zone of failure.

Leca and Dormieux (1990) have used three-dimensional configurations to assess face pressure at failure according to the upper-bound theorem. Failure zones are considered as one cone with the base as the tunnel face, or a composition of two cones as shown in Figure 3.11 (d). The effect of the free boundary at the ground surface is included as a truncation of the failure zone. The study shows that the difference between the two modes of failure is not considerable as long as the depth ratio is higher than 0.5 and the friction angle is higher than 20° provided the depth coefficient found does not influence the value of the necessary support pressure. The effect of the surcharge pressure is limited to cases of low depth ratio (H/D less than 0.5) for a friction angle higher than 20°. For a cohesive frictional material without surcharge at the ground surface, the following expression is proposed:

$$N_f = 2N_d N_\gamma - \frac{1}{K_p - 1} \quad , \quad (3.14)$$

where N_γ are parameters given in Table 3.1. Figure 3.12 shows a comparison between the results of Leca and Dormieux, and Chambon and Corté. It is to be noticed that Leca and Dormieux's results fall in between the two spiral failure mechanisms presented by Chambon and Corté with the single spiral failure mechanism giving the least required support pressure. Some of the above solutions are presented in Appendix A.

Table 3.1: Values of Parameter N_γ in Equation (3.14)
(Leca and Dormieux, 1990: Figure 7)

ϕ (°)	20	25	30	35	40	45
N_γ	0.210	0.151	0.112	0.087	0.066	0.050

3.4.3.3 Comparisons between Limit Theorems of Plastic Analysis and Physical Models

Physical models are used to verify analytical solutions as they are closer to the idealized soil conditions than real case histories. Heinz (1988) presented a comparison between analytical solutions, physical model results, and actual case histories. Figure 3.13 shows a comparison between the above lower- and upper-bound solutions and results of the physical models (Casarin, 1981) and the centrifuge test models (Mair, 1979). From the figure, the stability ratio appears to exhibit a substantial amount of dependency on the depth ratio. The Broms and Bennermark formula falls in between the two types of tests. Lower-bound solutions reveal an acceptable degree of accuracy as they provide an expected safe

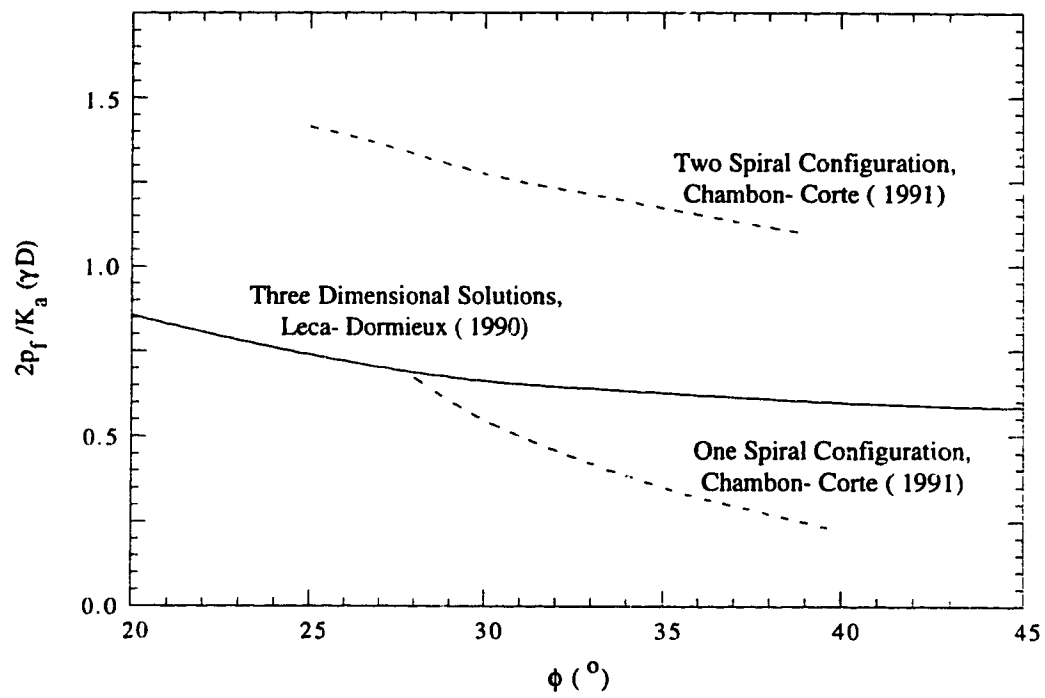


Figure 3.12: Upper Bound Solutions for Non Cohesive Soils.

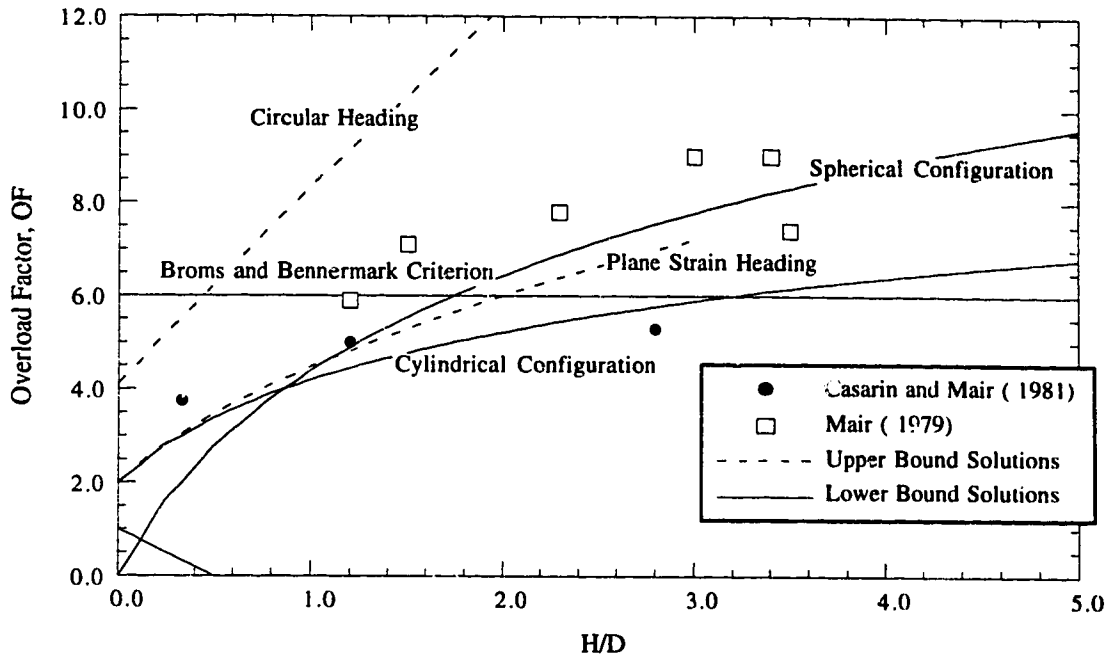


Figure 3.13: Upper and Lower Bound Solutions for Cohesive Soils (modified after Heinz 1988).

estimate of the stability ratio except for one or two points. The cylindrical configuration best fits the results of the physical model while the spherical configuration best fits the centrifuge model results. This may be attributed to the loading conditions. As gravitational pressure is compensated by a surcharge at the top surface of the clay model, a more extended yield zone results where centrifuge tests yield a failure zone that corresponds better to the spherical configuration. A lower-bound solution using plane-strain configuration may be considered as an oversimplification of the problem and may be disregarded. An upper-bound solution using a circular heading configuration provides an excessively high estimate of the stability ratio especially for depth ratios higher than 2.0. The plane strain configuration gives lower estimates to the stability ratio which is opposite to what is expected and may, therefore, be excluded.

Analytical solutions for frictional materials were verified by centrifuge tests carried out by Chambon and Cort e. Leca and Dormieux (1990) suggested that the upper-bound solutions (Equation 3.14) agreed closely with the centrifuge test results while lower-bound solutions yielded excessively high estimations of support pressure as shown in Table 3.2. While centrifuge tests were carried out using a clean dry sand, a certain amount of cohesion was considered by Leca and Dormieux (1990). This may be attributed to capillary tension. The method of shear strength measurement is not described by any of the authors.

Table 3.2: Comparisons between Predicted and Measured Pressures at Failure-Upper Bound Solution (Leca and Dormieux, 1990: Table 2)

<i>H/D</i>	γ (kN/m ³)	Critical Pressures Predicted from Limit Analyses (kPa)		Measured Pressure at Failure in the Centrifuge (kPa)
		Lower-bound	Upper-bound	
1.0	15.3	29	2	6
1.0	16.1	29	3	3
2.0	15.3	46	2	4
2.0	16.1	44	3	4

It is to be noted that the lower-bound solution referred to in Table 3.2 is based on the plane-strain configuration because it is the only configuration that includes gravitational forces. Spherical or cylindrical configurations (Equations 3.10 and 3.12, respectively) may be considered as they represent the gravitational stress at the tunnel axis as a surcharge at the ground surface ($p_s = p_o$) while the depth coefficient N_o is selected to be equal to that of the experimental configurations. The calculated critical face pressure, then, may be unrealistically low and in some cases of a negative sign. As such, the experimental result is

approached from the "unsafe side" which is opposite to what would be expected from a lower-bound solution. The reason behind that may be explained as the two solutions suggest that the failure zone extends to the ground surface. The same solutions may be reexamined with the gravitational stress represented as a surcharge at the ground surface and with a reduced value of N_o in order to represent the extent of the failure zone and not the geometrical configuration of the experiments. Figures 3.14 and 3.15 show a comparison between cylindrical and spherical lower-bound solutions and the experimental results. From the figure, a depth coefficient as low as 1.5 yields face pressure values comparable with the experimental results.

Chambon and Corté (1990) have used the same shear strength parameters as Leca and Dormieux to verify upper-bound solutions using one-spiral and two-spiral configurations with the centrifuge test results as shown in Table 3.3. From the table, the double-spiral mechanism yields higher estimations of collapse pressure which is opposite to what is expected from an upper-bound solution. Table 3.4 shows a comparison between predictions based on one spiral configuration and centrifuge results. The table shows that one-spiral-configuration results are more reliable than two-spiral-configuration results. Also, from Table 3.2, a three-dimensional configuration gives more accurate results than the other two configurations.

Table 3.3: Comparisons between Predicted and Measured Pressures at Failure-Two-Spiral Plane Strain Configuration (Chambon and Corté, 1990: Figure 15)

γ (kN/m ³)	H/D	c (kPa)	ϕ	Measured Limit Pressure (kPa)	Predicted Limit Pressure (kPa)
15.3	2	2.3	35.2	4.4	8.65
16.1	2	1.1	38.3	4	9.24

Table 3.4: Comparisons between Predicted and Measured Pressures at Failure-One-Spiral Plane Strain Configuration (Chambon and Corté, 1990: Figure 4)

γ (kN/m ³)	D (m)	c (kPa)	ϕ	Measured Limit Pressure (kPa)	Predicted Limit Pressure (kPa)
16.0	5	1.0	35.2	4.4	2.00
16.0	5	1.0	38.3	4.0	0.56

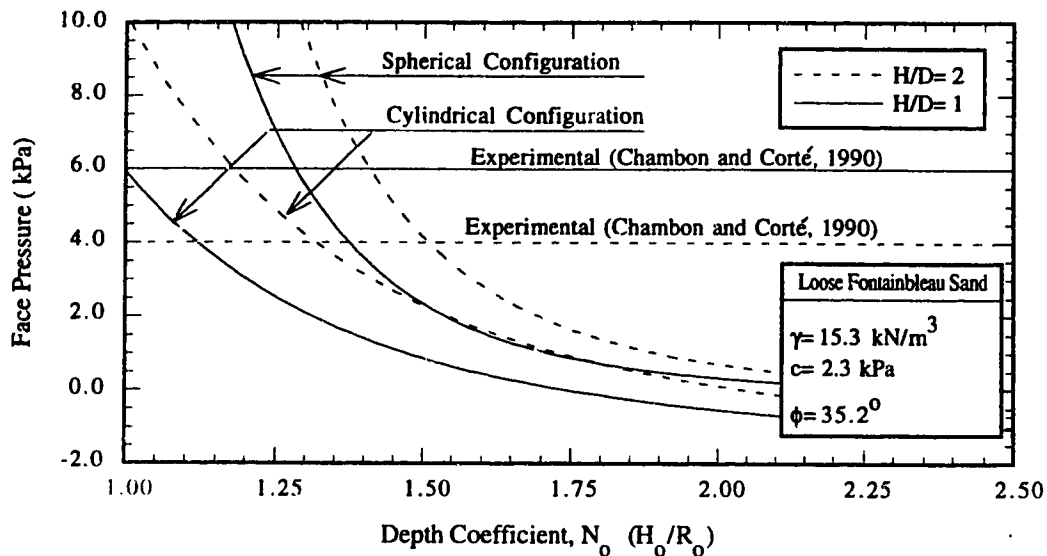


Figure 3.14: Comparison between Centrifuge Results and Lower Bound Solutions for Non Cohesive Soils (Loose Sand).

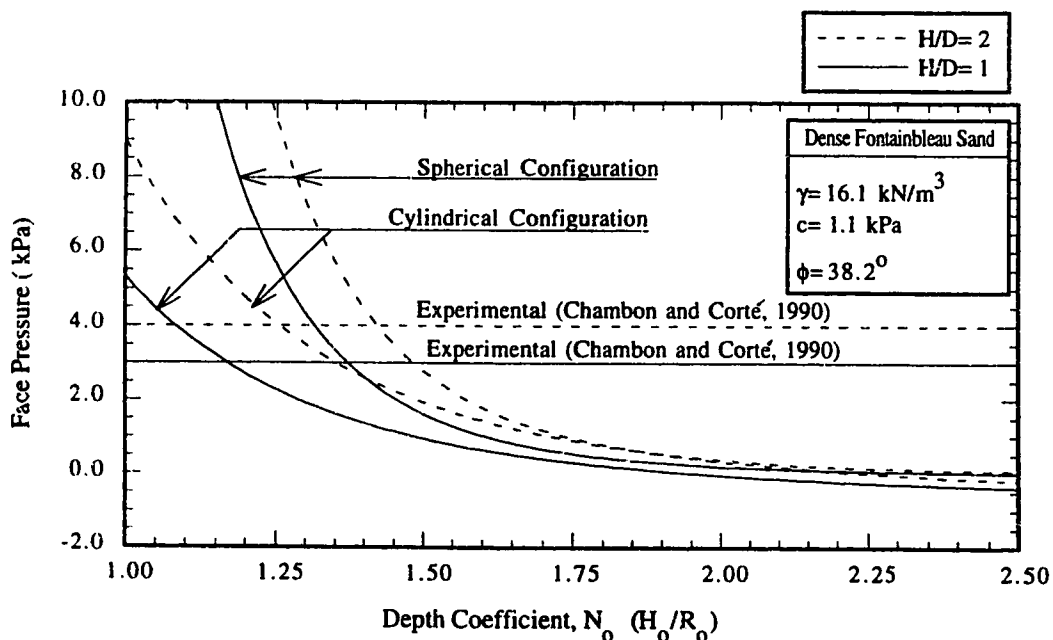


Figure 3.15: Comparison between Centrifuge Results and Lower Bound Solutions for Non Cohesive Soils (Dense Sand).

3.4.4 Stability Analysis

Stability analyses assume that a predefined soil mass undergoes a rigid body motion. At failure, resisting forces related to soil strength are in equilibrium with forces responsible for the motion. The moving soil mass that requires the least resisting forces to produce instability provides the most critical case. Stability analyses are similar to upper-bound-plastic solutions in the sense that they are optimized.

Mohkam and Wong (1988) have used an elaborate three-dimensional-limit-state solution to estimate the necessary face pressure to be applied at the face of a circular tunnel, in order to, maintain critical equilibrium of an assumed soil mass. A sliding soil mass is bounded by the tunnel face, a slip surface extending upward from the invert, and a horizontal surface at the crown level. Forces acting on the soil mass are: the weight of the soil inside the failure zone; overburden pressure above the tunnel level calculated according to Terzaghi's arching formula (Terzaghi, 1943); resisting forces acting at the slip surface, and face pressure due to air pressure acting uniformly and a slurry pressure increasing linearly with the depth. Solutions are obtained such that they satisfy Coulomb's failure criterion and equilibrium equations. Functions describing the geometry of the slip surface and normal stresses along it were optimized and air pressure resulting in a factor of safety of one was obtained. The problem considered consisted of an eight-metre-diameter tunnel with a depth ratio of 2.5. Two extreme cases are suggested: a completely immersed tunnel where the groundwater table is at the ground surface or a completely dry tunnel. As unit weights of either the soil or the slurry are not given, accurate comparisons between the given solutions and other results is not possible. However, if reasonable unit weights of the soil in its two cases are assumed the collected results are found to be closer to lower-bound solutions (Equations 3.11 or Equations 3.10 and 3.12 with reduced N_o) than it is to upper-bound solution (Equation 3.14).

3.4.5 Numerical Analyses

Elastoplastic constitutive models offer a more realistic simulation of the face stress relief process than do analytical plastic solutions as they include the effects of prefailure deformation and stress path dependency. Recent advances in numerical methods, especially the finite element method, and in the capacity of computing systems have allowed for further modeling of complicated configurations with respect to the geometry of the problem, field conditions, and material constitutive relationships. At the same time, the complexity of the performed analyses renders it difficult to develop a generalized model for the stress relief process.

Romo and Diaz (1981) have used a plane strain longitudinal finite element model based on hyperbolic stress strain relationship to obtain a safety factor for a certain depth ratio and face pressure. The following expressions are defined:

$$\text{safety factor} = \frac{\text{shear strength}}{\text{shear stress}} = \frac{c + \sigma_1 \tan \phi}{\tau} \quad , \quad (3.15)$$

and

$$\text{horizontal stability ratio} = \frac{p_{ho} - p_f}{(\sigma_c)_{ave}} \quad , \quad (3.16)$$

where:

σ_1 is the major principal stress,

τ is the shear stress at a certain point,

p_{ho} is the initial horizontal stress at the tunnel axis, and

$(\sigma_c)_{ave}$ is the mean compressive soil strength from the ground surface to the depth of the tunnel floor.

For different values of horizontal stability ratios, contour lines of the safety factors were plotted and the most critical failure surfaces were obtained, and then the average safety factors along these surfaces were computed. As a result, a relationship between the average factor of safety and the horizontal stability ratio was presented and this indicated that the factor of safety decreases with the horizontal stability ratio and reaches unity at a horizontal stability ratio of about 6.5.

Chaffois et al.(1988) have carried out a three-dimensional finite element analysis using an elasto-plastic constitutive relationship to model the behaviour of a sandy-gravelly soil. The purpose of the study is to investigate the effect of the applied face pressure on the stability of the excavation face for the D line of the Lyon subway, France. The study shows that soil movement at the centerpoint of the face increases linearly as the face pressure ratio, the ratio of face pressure p_f to the initial horizontal stress at the tunnel axis p_{ho} , decreases until a certain point where yielding takes place. At this point, the limit face pressure ratio is reached. Further decrease of face pressure results in an accelerating slope of soil movement with face pressure with face pressure until failure takes place. At this point, a plasticity area develops before the face. The volume of the failure zone

² Term changed from "stability ratio" in the original document for consistency.

corresponding to a relatively low face pressure ratio was found to be located in a semi-hemisphere concentric with the centre of the face and with a radius equal to that of the tunnel. The study shows that yield started at a face pressure ratio of 40% corresponding to a face movement as low as 0.05% of the tunnel diameter.

3.5 Applied Numerical Models

The purpose of the study carried out is to investigate ground behaviour with respect to stress reduction at the face of an excavation. Numerical analysis using the finite element method is found to be an appropriate tool of investigation as it provides a satisfactory simulation accuracy of the geometry and the constitutive model of the problem. Three-dimensional analysis, although exhaustive in its computational effort, has become more affordable because of recent advances in computer systems both regarding their speed and their storage capacity. The ability of the method to account for nonlinear material behaviour through iterative processes allows the simulation of realistic material behaviour. Meanwhile, the ability to divide the excavation process into several loading steps allows the inspection of the various stages of excavation and the observation of stress paths followed by different elements in the soil mass. As the obtained results are related to the specific geometrical and parametric configurations, analyses have to be repeated for a considerable number of times in order to obtain a generalized assessment of the face stability problem.

3.5.1 Statement of the Problem

Considering certain soil conditions, a single circular tunnel is excavated. The circumference of the cavity is supported by a rigid liner and its face is under normal pressure which is equal to the initial ground pressure. The face pressure then is gradually reduced creating a longitudinal displacement at the face toward the gallery. The critical state of the face stability is reached when the magnitude of face pressure is reduced such that the rate of increase of the face displacement associated with face pressure reduction follows an accelerating trend. At this point, yield pressure at the face is recorded.

3.5.2 Finite Element Models

The finite element program SAGE™ developed by Chan (1986) at the University of Alberta was employed in all the numerical analyses. Computational work was done on the RISC™ System/6000. A parametric analysis was carried out to investigate face stability problems. Also finite element meshes were constructed based on three-dimensional and axisymmetric configurations. Table 3.5 shows the parameters investigated for axisymmetric computer runs, and Table 3.6 shows those used for three-dimensional runs.

3.5.2.1 Axisymmetric Models

An elasto-plastic model based on the Mohr-Coulomb failure criterion with a non-associated flow rule is employed in the axisymmetric analyses. Figure 3.16 shows three of the five adopted meshes for the analyses and their boundary conditions. Eight node elements are selected for all the meshes. A constant tunnel diameter of 5.0 m is chosen for all analyses. Young's modulus for the elastic state is chosen to be 10.0 MPa.

Each run includes a number of steps ranging between 20 and 30. The first step consists of applying the initial state of the stresses. A linear-elastic model is assumed with a calculated Poisson's ratio, ν , based on the chosen coefficient of lateral earth pressure at rest K_0 . The second step consists of applying the actual material properties. In the case of pure frictional material, an elastic zone is assumed at the top elements of the mesh in order to save computer effort in the iteration process as this region is under low confining pressure and, thus, is expected to fail. However, this assumption has not been found to interfere with the calculated values of yield pressure at the face. The excavation of the tunnel region is simulated by eliminating the excavated elements from the global stiffness matrix and then by applying nodal forces at the boundaries of the excavation that are equivalent to the stresses at one side of the boundary. The supporting system at the circumference of the tunnel shaft (the shield and the liner) is assumed to be rigid and high stiffness parameters are selected for elements in this region. The following steps consist of gradually reducing the pressure applied at the face using about 25 equal steps and allowing an iteration strain tolerance of 10^{-4} . In cases where convergence is not met, the loading step is subdivided into smaller subload steps. Soil movement at the centre of the face is monitored and a non-dimensional parameter of face displacement, Ω , is calculated as:

$$\Omega = \frac{\delta_x E}{D(K_0 \gamma H_0 - p_f)} \quad (3.17)$$

where:

δ_x is the horizontal soil movement at the centerpoint of the face, and
 H_0 is the depth of the tunnel axis.

It should be noted that the parameter Ω is not the face displacement, but it is defined as a dimensionless ratio of soil movement at the face equal to the amount of stress reduction. As such, the parameter represents the slope of a pressure-face displacement curve. This rather complex form of definition of parameter Ω is used to obtain a dimensionless term and thus to make the results more applicable.

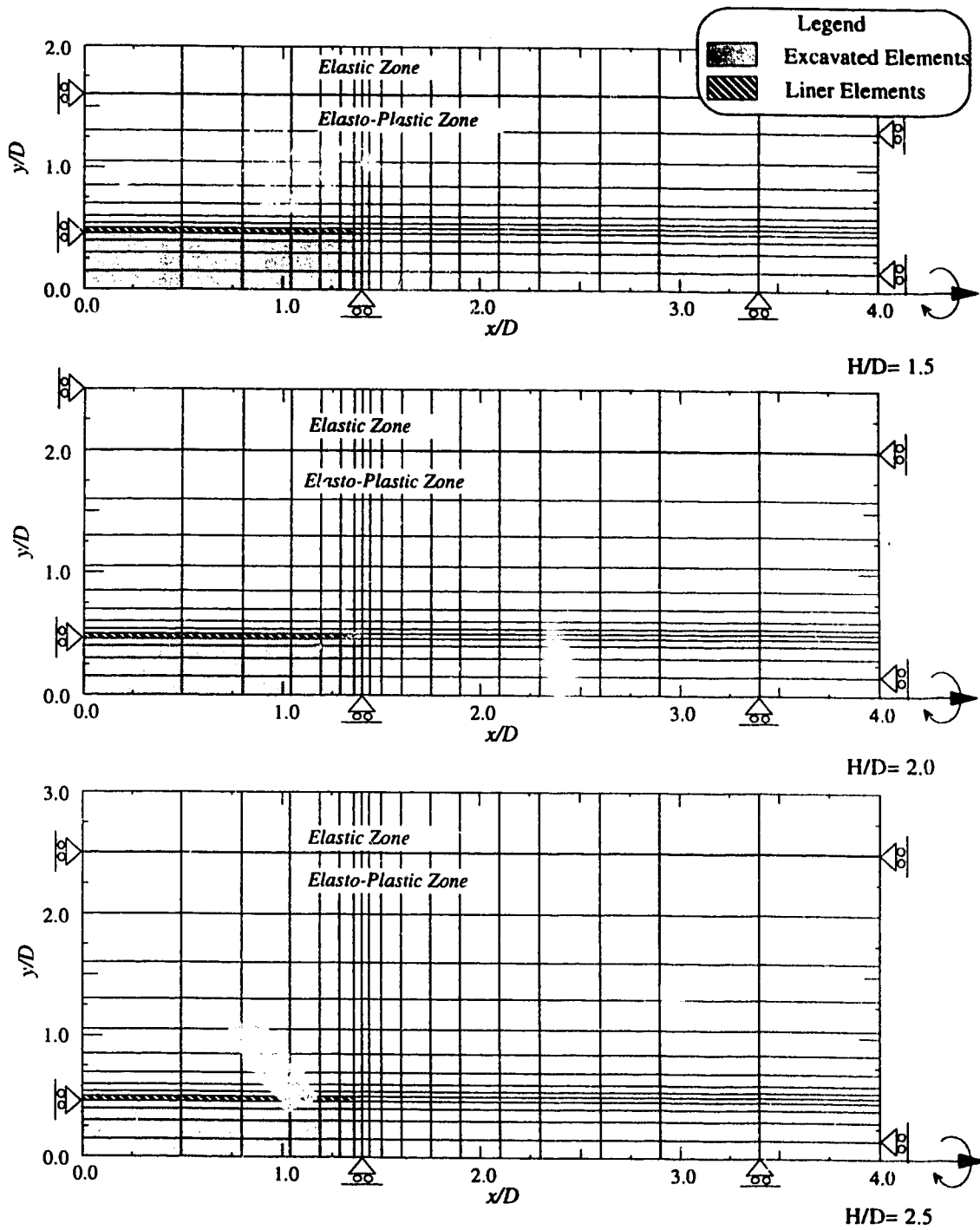


Figure 3.16: Some Axisymmetric Finite Element Meshes used for Tunnel Face Stability Analyses

#	K_0	H/D	γ	ν	ϕ	c
1	0.60	1.50	20	0.20	30	0
2	0.60	1.50	20	0.25	30	0
3	0.60	1.50	20	0.30	30	0
4	0.60	1.50	20	0.35	30	0
5	0.60	1.50	20	0.40	30	0
6	0.60	1.50	20	0.45	30	0
7	0.80	1.50	20	0.20	30	0
8	0.80	1.50	20	0.25	30	0
9	0.80	1.50	20	0.30	30	0
10	0.80	1.50	20	0.35	30	0
11	0.80	1.50	20	0.40	30	0
12	0.80	1.50	20	0.45	30	0
13	0.70	1.50	20	0.20	30	0
14	0.70	1.50	20	0.25	30	0
15	0.70	1.50	20	0.30	30	0
16	0.70	1.50	20	0.35	30	0
17	0.70	1.50	20	0.40	30	0
18	0.70	1.50	20	0.45	30	0
19	0.50	1.50	10	0.30	20	0
20	0.60	1.50	10	0.30	20	0
21	0.60	1.50	10	0.30	25	0
22	0.60	1.50	10	0.30	30	0
23	0.60	1.50	10	0.30	35	0
24	0.60	1.50	10	0.30	40	0
25	0.60	1.50	10	0.30	45	0
26	0.70	1.50	10	0.30	30	0
27	0.80	1.50	10	0.30	20	0
28	0.80	1.5	10	0.30	25	0
29	0.80	1.5	10	0.30	30	0
30	0.80	1.5	10	0.30	35	0
31	0.80	1.5	10	0.30	40	0
32	0.80	1.5	10	0.30	45	0
33	0.50	1.5	20	0.30	30	0
34	0.60	1.5	20	0.30	20	0
35	0.60	1.5	20	0.30	25	0
36	0.60	1.5	20	0.30	30	0
37	0.60	1.5	20	0.30	35	0
38	0.60	1.5	20	0.30	40	0
39	0.60	1.5	20	0.30	45	0
40	0.70	1.5	20	0.30	30	0
41	0.80	1.5	20	0.30	20	0
42	0.80	1.5	20	0.30	25	0
43	0.80	1.5	20	0.30	30	0
44	0.80	1.5	20	0.30	35	0
45	0.80	1.5	20	0.30	40	0
46	0.80	1.5	20	0.30	45	0
47	0.80	2.0	20	0.30	20	0
48	0.80	2.0	20	0.30	25	0
49	0.80	2.0	20	0.30	30	0
50	0.80	2.0	20	0.30	35	0
51	0.80	2.0	20	0.30	40	0
52	0.80	2.0	20	0.30	45	0
53	0.60	2.0	20	0.30	30	0
54	0.65	2.0	20	0.30	30	0
55	0.70	2.0	20	0.30	30	0
56	0.75	2.0	20	0.30	30	0
57	0.80	2.5	20	0.30	20	0
58	0.80	2.5	20	0.30	25	0
59	0.80	2.5	20	0.30	30	0
60	0.80	2.5	20	0.30	35	0
61	0.80	2.5	20	0.30	40	0
62	0.80	2.5	20	0.30	45	0
63	0.80	2.5	20	0.20	30	0
64	0.80	2.5	20	0.40	30	0
65	0.40	2.5	20	0.30	30	0
66	0.50	2.5	20	0.30	30	0
67	0.60	2.5	20	0.30	30	0
68	0.70	2.5	20	0.30	30	0
69	0.80	2.5	20	0.30	30	0
70	0.90	2.5	20	0.30	30	0
71	0.80	1.0	20	0.20	20	0
72	0.80	1.0	20	0.30	20	0
73	0.80	1.0	20	0.40	20	0
74	0.80	1.0	20	0.20	30	0
75	0.80	1.0	20	0.30	30	0
76	0.80	1.0	20	0.40	30	0
77	0.80	1.0	20	0.20	40	0
78	0.80	1.0	20	0.30	40	0
79	0.80	1.0	20	0.40	40	0
80	0.80	3.5	20	0.20	20	0
81	0.80	3.5	20	0.30	20	0
82	0.80	3.5	20	0.40	20	0

Table 3.5: Parameters used for Axisymmetric Finite Element Analysis of Tunnel Face Stability

#	K_o	H/D	γ	ν	ϕ	c
83	0.80	3.5	20	0.20	30	0
84	0.80	3.5	20	0.30	30	0
85	0.80	3.5	20	0.40	30	0
86	0.80	3.5	20	0.20	40	0
87	0.80	3.5	20	0.30	40	0
88	0.80	3.5	20	0.40	40	0
89	0.80	1.5	20	0.30	0	10
90	0.80	1.5	20	0.30	0	20
91	0.80	1.5	20	0.30	0	30
92	0.80	1.5	20	0.30	0	40
93	0.80	1.5	20	0.30	0	50
94	0.80	1.5	20	0.30	10	10
95	0.80	1.5	20	0.30	10	20
96	0.80	1.5	20	0.30	10	40
97	0.80	1.5	20	0.30	10	60
98	0.80	1.5	20	0.30	20	0
99	0.80	1.5	20	0.30	20	5
100	0.80	1.5	20	0.30	20	10
101	0.80	1.5	20	0.30	20	20
102	0.80	1.5	20	0.30	20	30
103	0.80	1.5	20	0.30	20	50
104	0.80	1.5	20	0.30	30	5
105	0.80	1.5	20	0.30	30	10
106	0.80	2.0	20	0.30	0	10
107	0.80	2.0	20	0.30	0	30
108	0.80	2.0	20	0.30	0	20
109	0.80	2.0	20	0.30	0	60
110	0.80	2.0	20	0.30	10	10
111	0.80	2.0	20	0.30	10	20

#	K_o	H/D	γ	ν	ϕ	c
112	0.80	2.0	20	0.30	10	40
113	0.80	2.0	20	0.30	10	60
114	0.80	2.0	20	0.30	20	10
115	0.80	2.0	20	0.30	20	20
116	0.80	2.0	20	0.30	20	40
117	0.80	2.0	20	0.30	20	30
118	0.80	2.0	20	0.30	20	60
119	0.80	2.0	20	0.30	20	50
120	0.80	2.0	20	0.30	30	10
121	0.80	2.5	20	0.30	0	20
122	0.80	2.5	20	0.30	0	30
123	0.80	2.5	20	0.30	0	40
124	0.80	2.5	20	0.30	10	10
125	0.80	2.5	20	0.30	10	20
126	0.80	2.5	20	0.30	10	40
127	0.80	2.5	20	0.30	20	10
128	0.80	2.5	20	0.30	20	20
129	0.80	2.5	20	0.30	20	30
130	0.80	2.5	20	0.30	30	5
131	0.80	2.5	20	0.30	30	10

Dimensions: c : kPa γ : kN/m³

Table 3.5: Parameters used for Axisymmetric Finite Element Analysis of Tunnel Face Stability (continued)

#	K_o	H/D	γ	ν	ϕ	c
1	0.80	1.5	20	0.30	20	0
2	0.80	1.5	20	0.30	30	0
3	0.80	1.5	20	0.30	40	0

#	K_o	H/D	γ	ν	ϕ	c
4	0.80	1.5	20	0.30	0	40
5	0.80	1.5	20	0.30	10	10
6	0.80	1.5	20	0.30	10	20

Table 3.6: Parameters used for Three Dimensional Finite Element Analysis of Tunnel Face Stability

Figures 3.17 through 3.22 show typical results of the relationship between the parameter of face displacement and the *face pressure ratio* PF for different cases of noncohesive soil where

$$PF = \frac{P_f}{K_o \gamma H_o} \quad (3.18)$$

At a face pressure ratio of 100%, the parameter of face displacement is an undefined number, therefore, a certain stress relief is required until the parameter reaches a constant value. At a certain degree of stress relief, the yield point, Ω starts to increase at an accelerating pattern. Figures 3.23 through 3.26 show the effects of the initial coefficient of lateral pressure at rest, K_o , on face stability. As expected, a small value of the initial lateral pressure results in higher intrinsic shear stresses and a higher amount of face pressure at yielding point is required. Figures 3.27 through 3.31 show that lower face pressure is required for a higher value of Poisson's ratio, ν , and this is attributed to lower soil compressibility which, in turn, limits soil movement at the face. Changes in Ω due to a reduction of PF in the case of cohesive materials are shown in Figures 3.32 through 3.42. In the case of frictional material, the yield point is well defined and the accelerating pattern of increase of Ω is clear while the increase is gradual for cohesive materials and geometrical construction sometimes is needed to select the yielding points. This behaviour is expected as was shown in the experimental results described in Section 3.4.2. As expected, the increase of shear strength parameters, c and/or ϕ , will result in decreasing the face pressure ratio required at the yield point.

3.5.2.2 Three-dimensional Models

The same constitutive model and loading process are used in the three-dimensional as in the axisymmetric analyses. The considerable computational effort needed for this type of analysis requires a reduction in the number of loading steps while the total number of steps ranging between 8 to 16 is used. Here a strain tolerance equals to that of the axisymmetric analyses is used. Figure 3.43 shows the constructed finite element mesh: it consists of 711 elements each which has 20 nodes making a total of 3,622 nodal points and a global stiffness matrix size of 14,429,094. As in the axisymmetric analyses, elements at the ground surface are assigned linear-elastic material properties in the case of frictional material.

Figures 3.44 and 3.45 show a typical deformation pattern at the centerline of the supported face for frictional and cohesive soils, respectively. Soil movement increases as

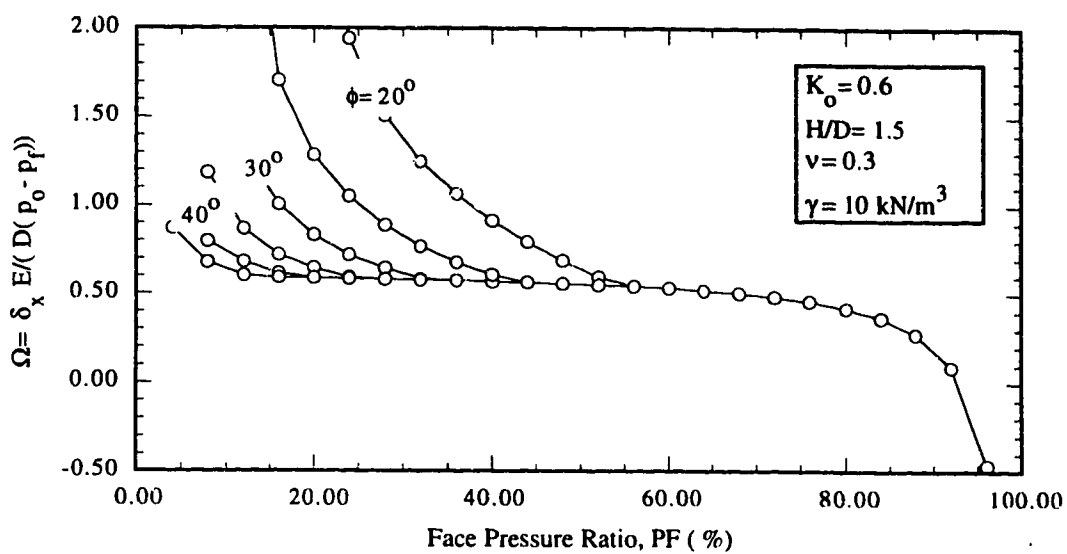


Figure 3.17: Parameter of Face Displacement, Ω , versus Face Pressure Ratio, PF, for various values of Angle of Internal Friction, ϕ , $\gamma = 10 \text{ kN/m}^3$, $K_o = 0.6$ and $H/D = 1.5$.

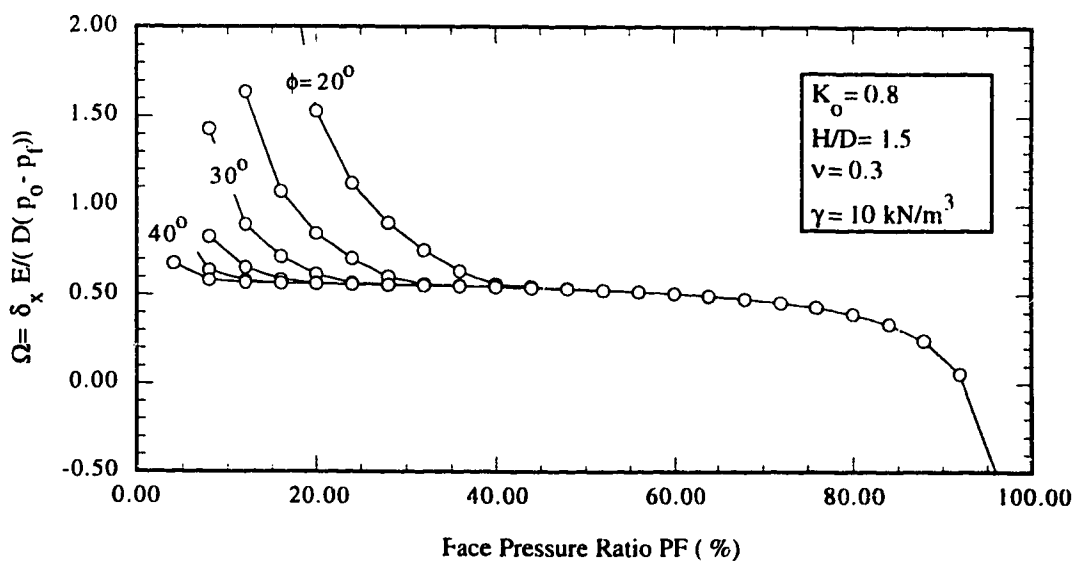


Figure 3.18: Parameter of Face Displacement, Ω , versus Face Pressure Ratio, PF, for various values of Angle of Internal Friction, ϕ , $\gamma = 10 \text{ kN/m}^3$, $K_o = 0.8$ and $H/D = 1.5$.

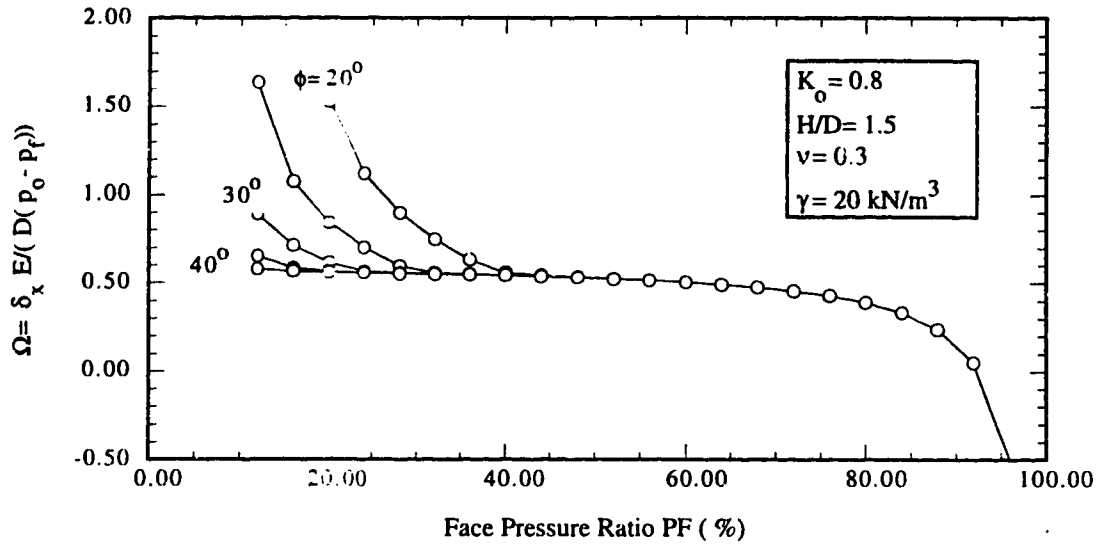


Figure 3.19: Parameter of Face Displacement, Ω , versus Face Pressure Ratio, PF, for various values of Angle of Internal Friction, ϕ , $\gamma = 20 \text{ kN/m}^3$, $K_0 = 0.6$ and $H/D = 1.5$.

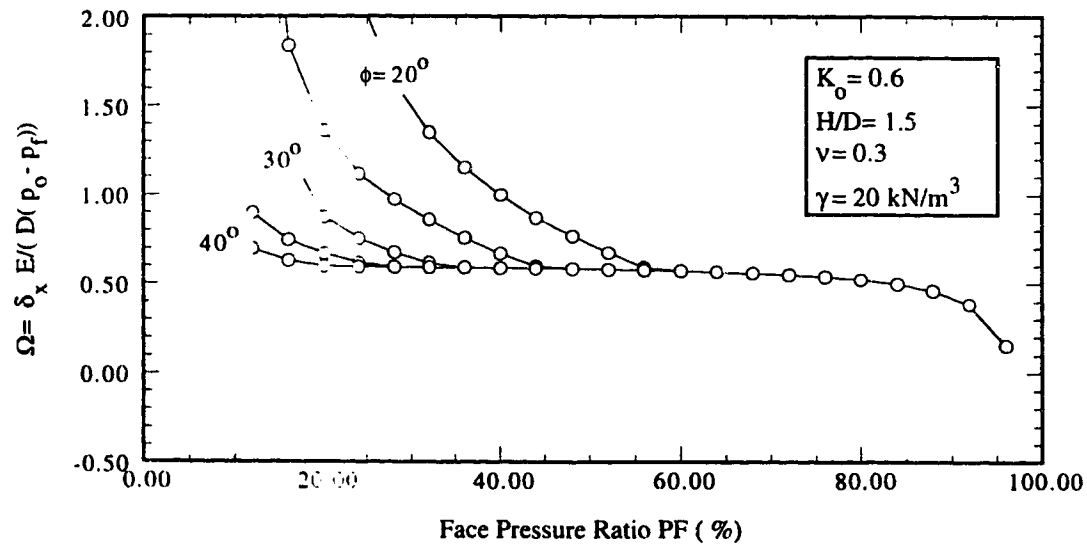


Figure 3.20: Parameter of Face Displacement, Ω , versus Face Pressure Ratio, PF, for various values of Angle of Internal Friction, ϕ , $\gamma = 20 \text{ kN/m}^3$, $K_0 = 0.8$ and $H/D = 1.5$.

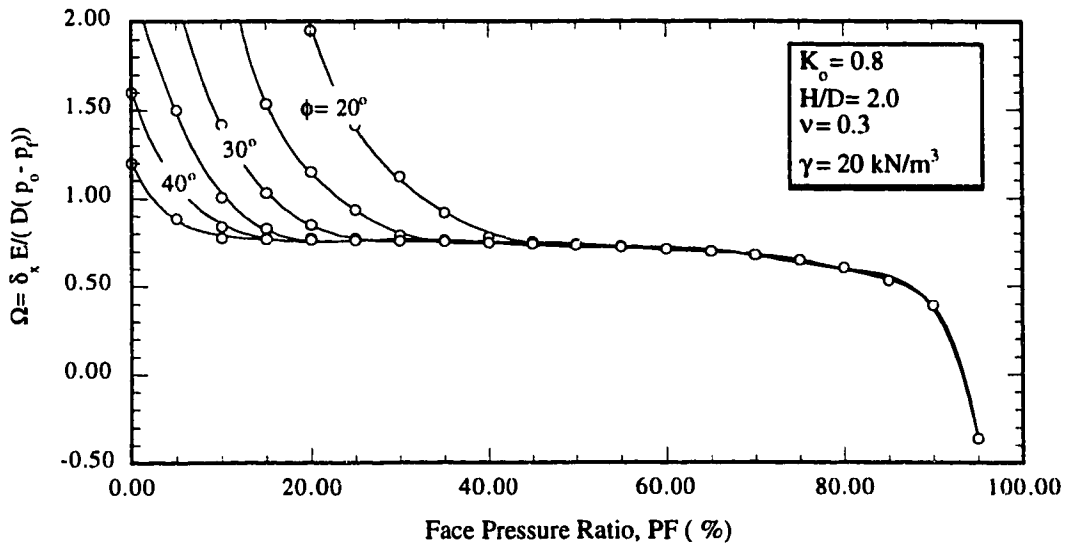


Figure 3.21: Parameter of Face Displacement, Ω , versus Face Pressure Ratio, PF, for various values of Angle of Internal Friction, ϕ , $\gamma = 20 \text{ kN/m}^3$, $K_0 = 0.8$ and $H/D = 2.0$.

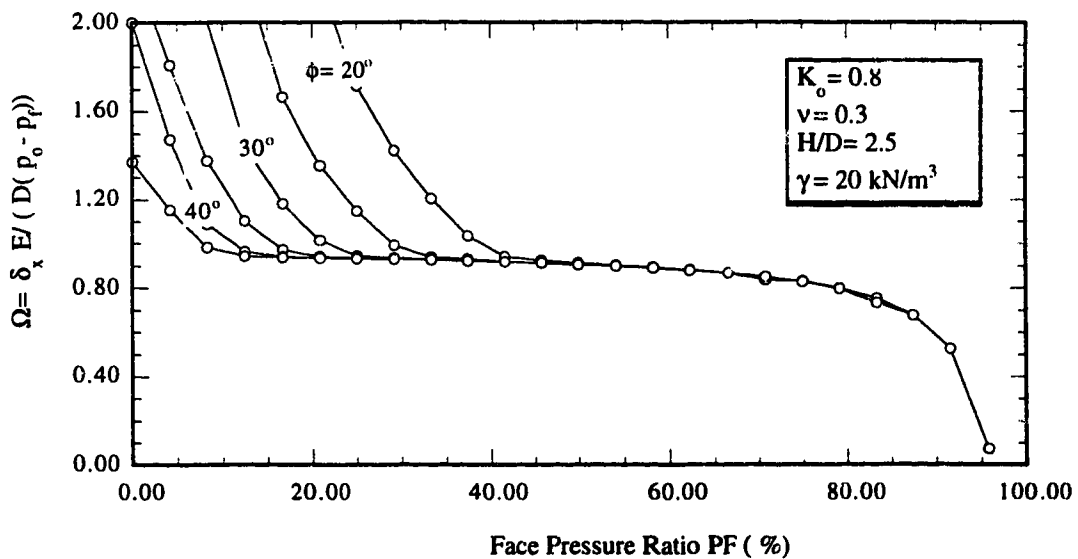


Figure 3.22: Parameter of Face Displacement, Ω , versus Face Pressure Ratio, PF, for various values of Angle of Internal Friction, ϕ , $\gamma = 20 \text{ kN/m}^3$, $K_0 = 0.8$ and $H/D = 2.5$.

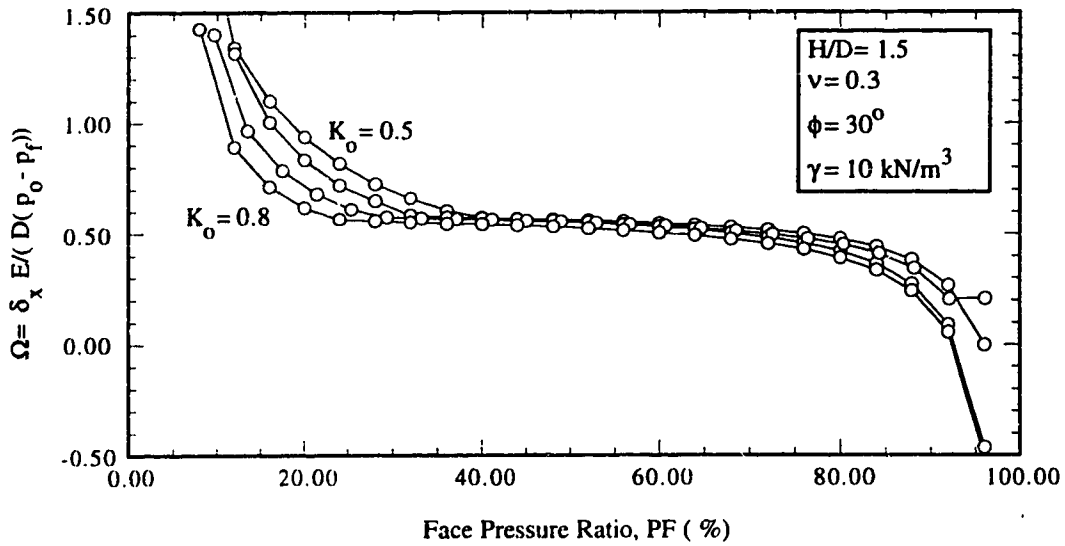


Figure 3.23: Parameter of Face Displacement, Ω , versus Face Pressure Ratio, PF, for various values of K_o , $\gamma = 10 \text{ kN/m}^3$, $H/D = 1.5$.

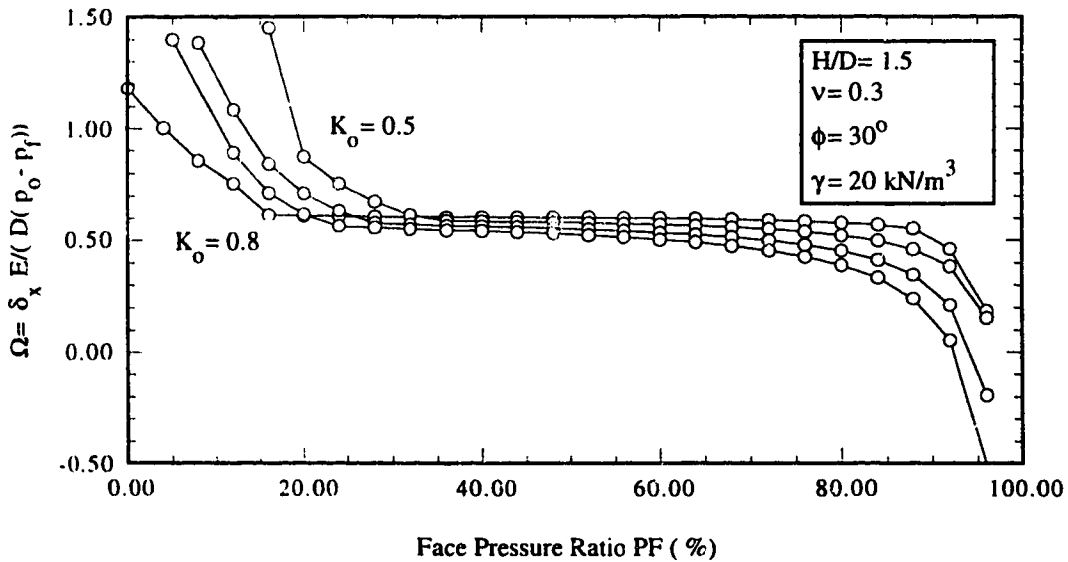


Figure 3.24: Parameter of Face Displacement, Ω , versus Face Pressure Ratio, PF, for various values of K_o , $\gamma = 20 \text{ kN/m}^3$, $H/D = 1.5$.

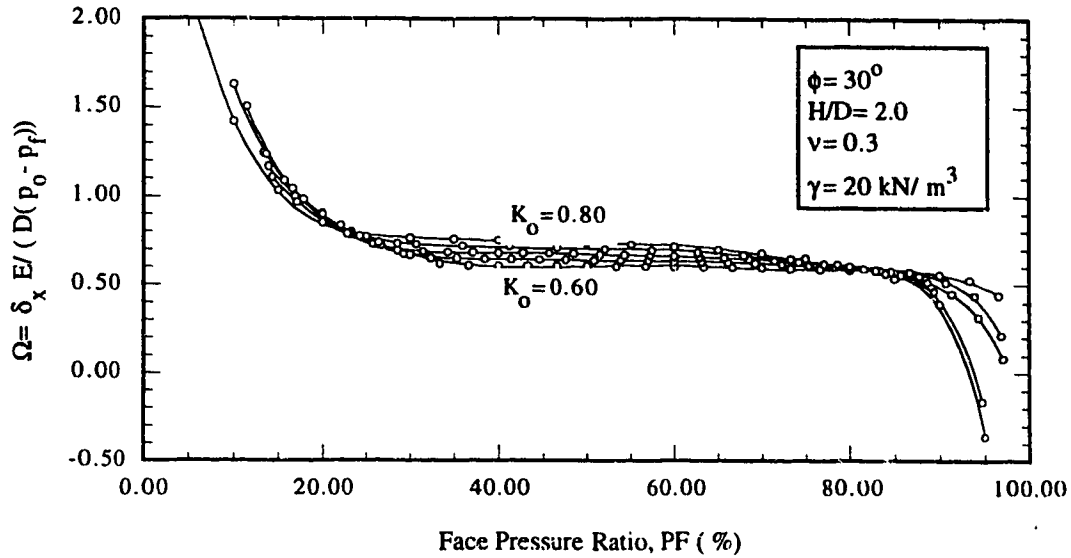


Figure 3.25: Parameter of Face Displacement, Ω , versus Face Pressure Ratio, PF, for various values of K_0 , $\gamma = 20 \text{ kN/m}^3$, $H/D = 2.0$.

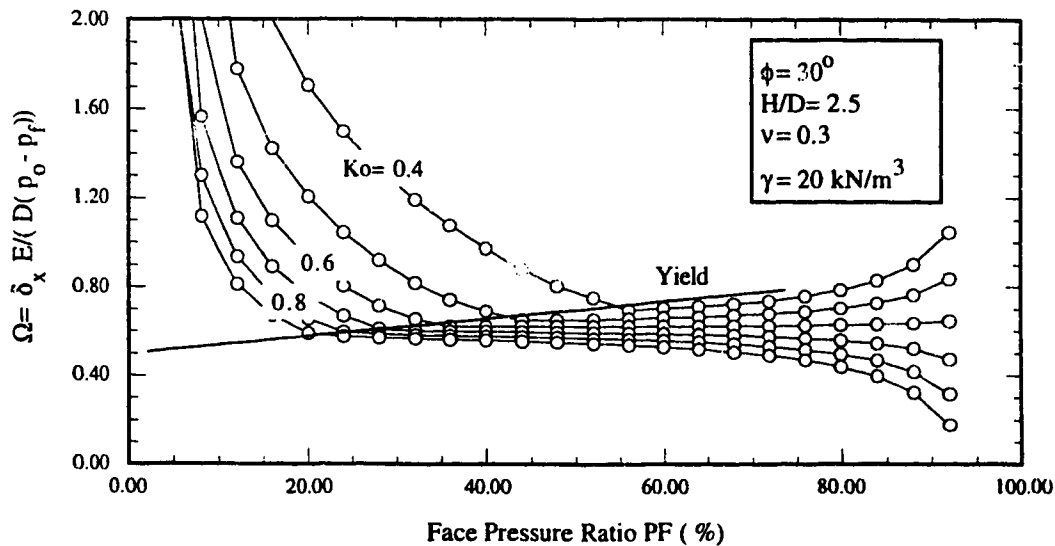


Figure 3.26: Parameter of Face Displacement, Ω , versus Face Pressure Ratio, PF, for various values of K_0 , $\gamma = 20 \text{ kN/m}^3$, $H/D = 2.5$.

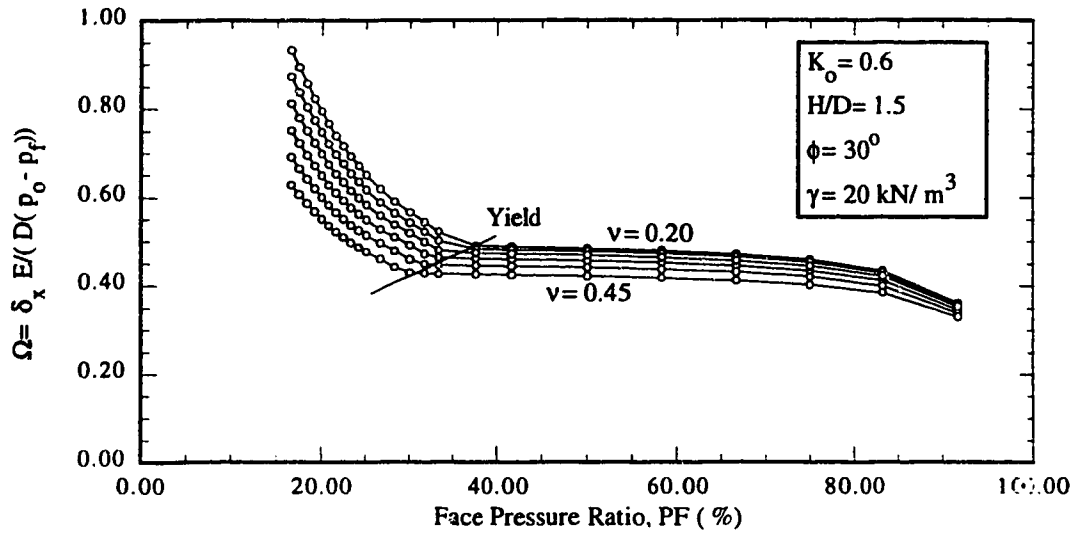


Figure 3.27: Parameter of Face Displacement, Ω , versus Face Pressure Ratio, PF, for various values of ν , $\gamma = 20 \text{ kN/m}^3$, $K_o = 0.6$, $H/D = 1.5$.

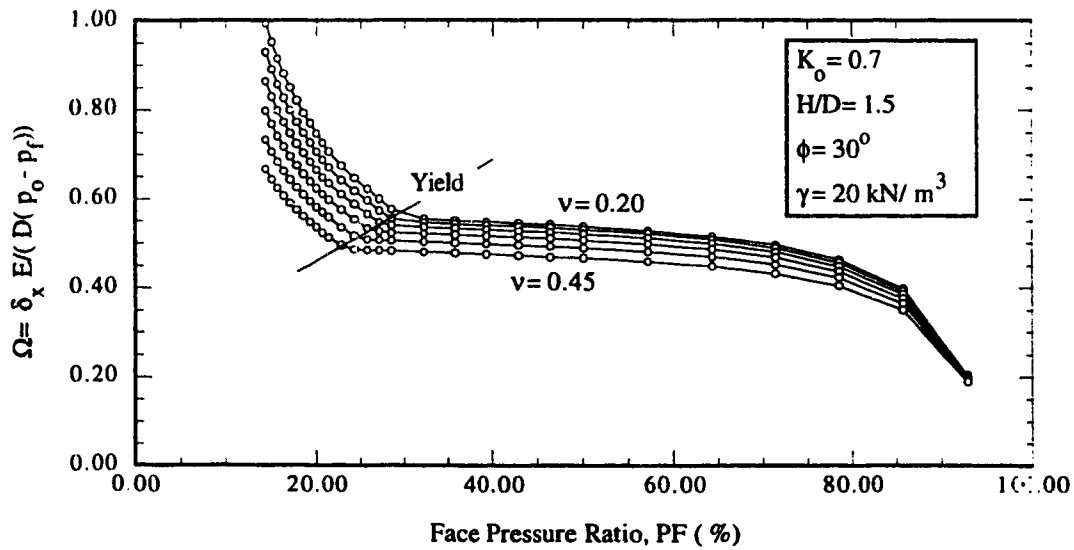


Figure 3.28: Parameter of Face Displacement, Ω , versus Face Pressure Ratio, PF, for various values of ν , $\gamma = 20 \text{ kN/m}^3$, $K_o = 0.7$, $H/D = 1.5$.

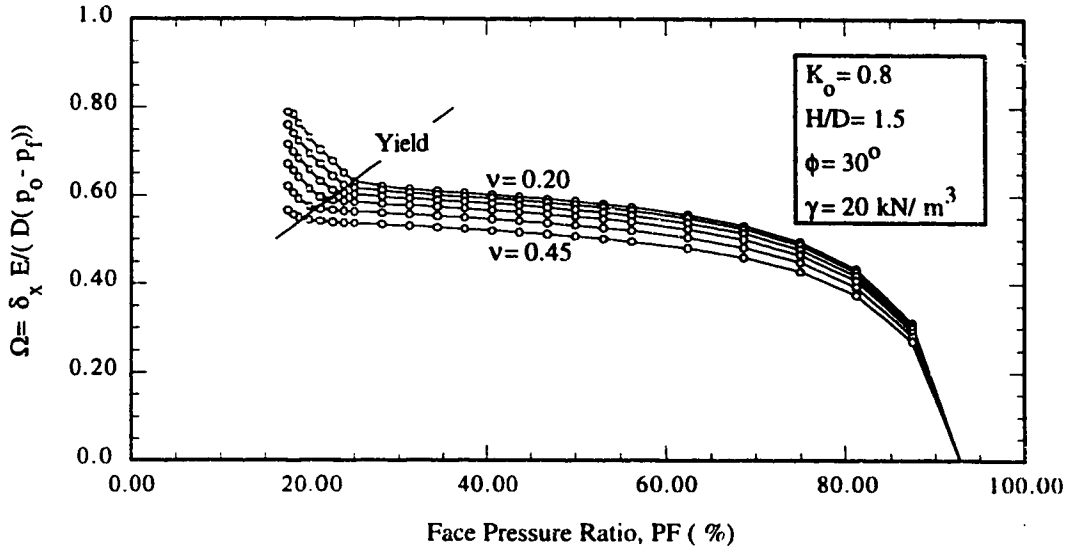


Figure 3.29: Parameter of Face Displacement, Ω , versus Face Pressure Ratio, PF, for various values of ν , $\gamma = 20 \text{ kN/m}^3$, $K_o = 0.8$, $H/D = 1.5$.

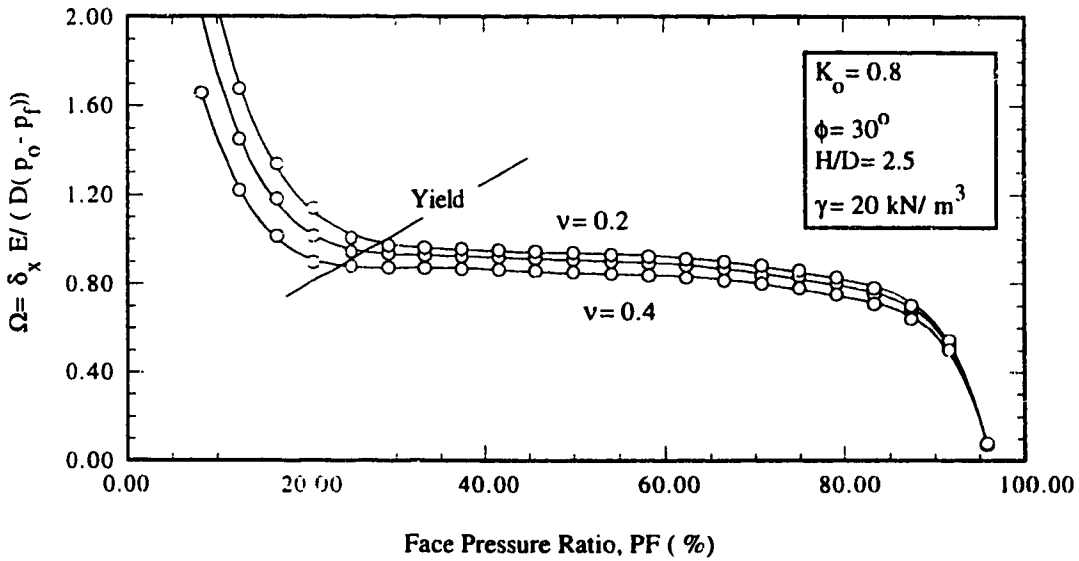


Figure 3.30: Parameter of Face Displacement, Ω , versus Face Pressure Ratio, PF, for various values of ν , $\gamma = 20 \text{ kN/m}^3$, $K_o = 0.8$, $H/D = 2.5$.

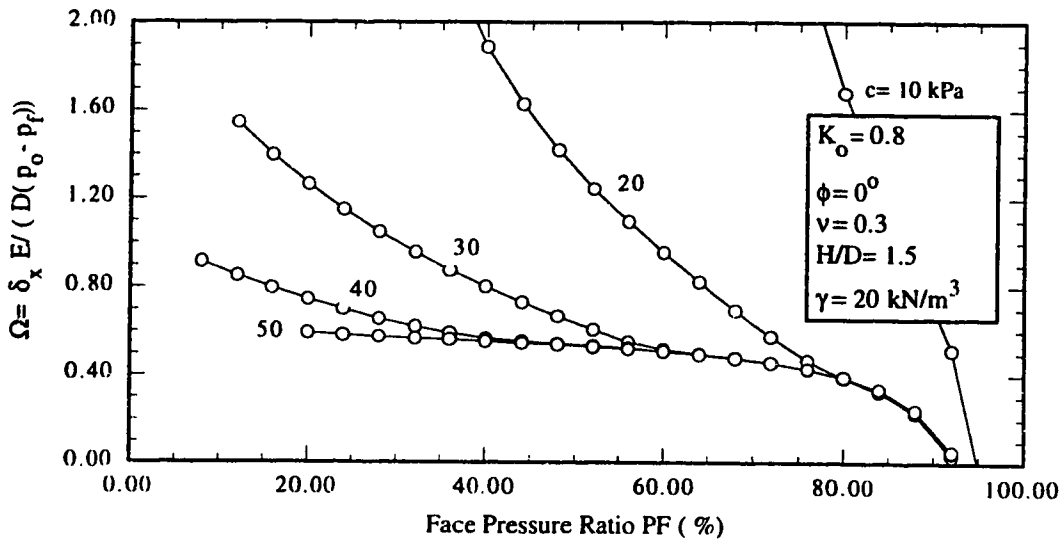


Figure 3.31: Parameter of Face Displacement, Ω , versus Face Pressure Ratio, PF, for various values of Cohesion, c , $\phi = 0^\circ$, $H/D = 1.5$.

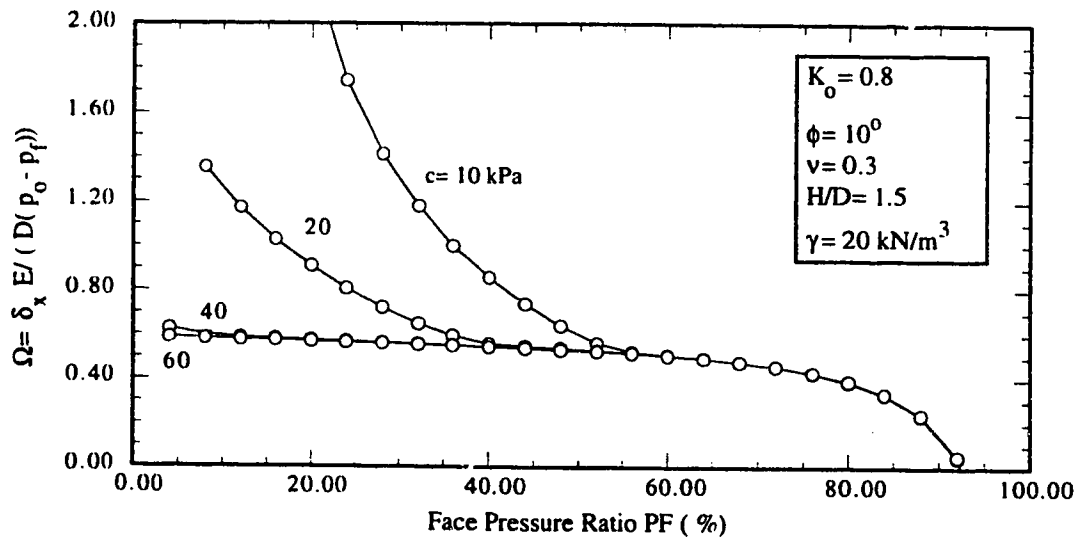


Figure 3.32: Parameter of Face Displacement, Ω , versus Face Pressure Ratio, PF, for various values of Cohesion, c , $\phi = 10^\circ$, $H/D = 1.5$.

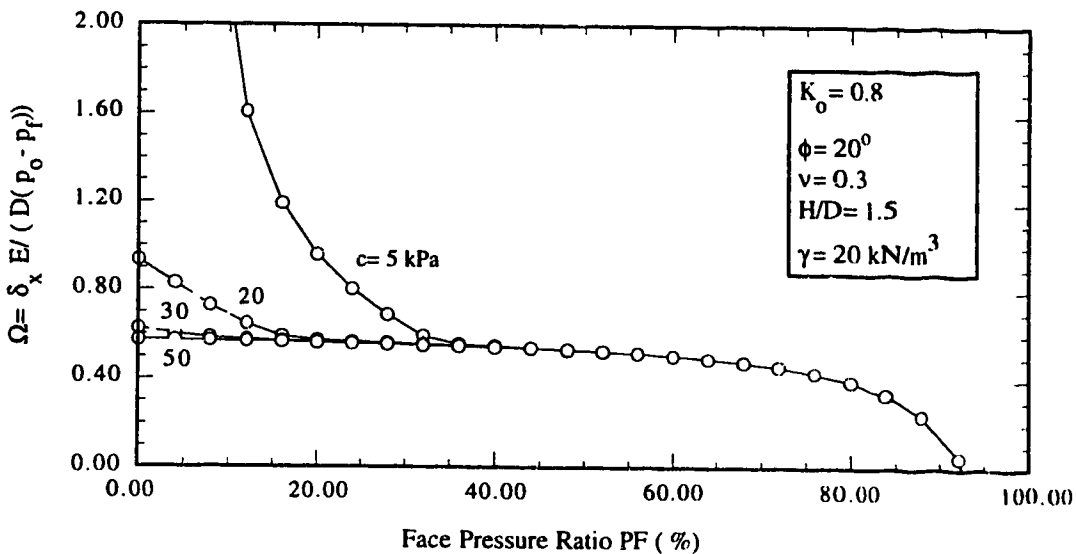


Figure 3.33: Parameter of Face Displacement, Ω , versus Face Pressure Ratio, PF, for various values of Cohesion, c , $\phi = 20^\circ$, $H/D = 1.5$.

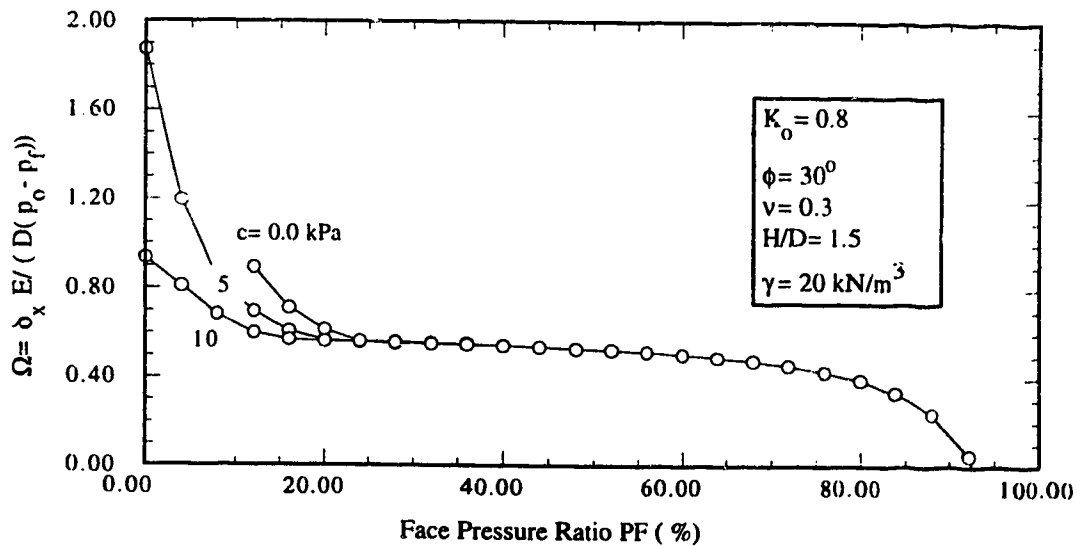


Figure 3.34: Parameter of Face Displacement, Ω , versus Face Pressure Ratio, PF, for various values of Cohesion, c , $\phi = 30^\circ$, $H/D = 1.5$.

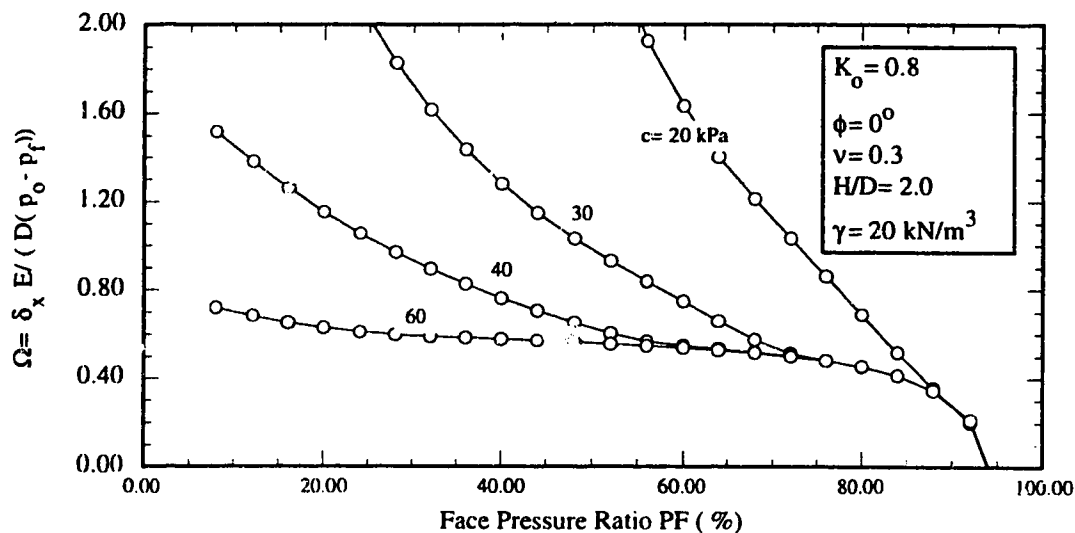


Figure 3.35: Parameter of Face Displacement, Ω , versus Face Pressure Ratio, PF, for various values of Cohesion, c , $\phi = 0^\circ$, $H/D = 2.0$.

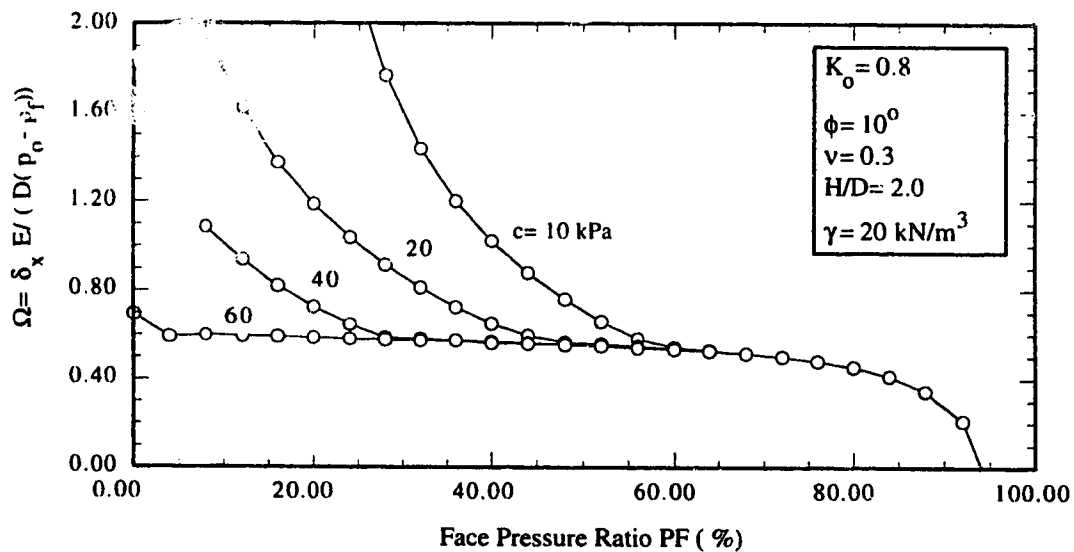


Figure 3.36: Parameter of Face Displacement, Ω , versus Face Pressure Ratio, PF, for various values of Cohesion, c , $\phi = 10^\circ$, $H/D = 2.0$.

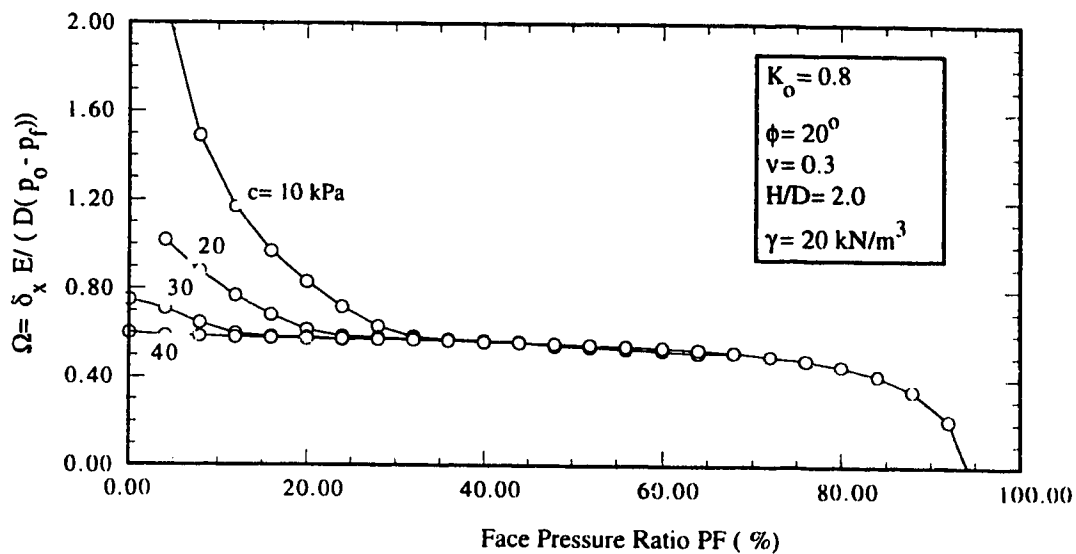


Figure 3.37: Parameter of Face Displacement, Ω , versus Face Pressure Ratio, PF, for various values of Cohesion, c , $\phi = 20^\circ$, $H/D = 2.0$.

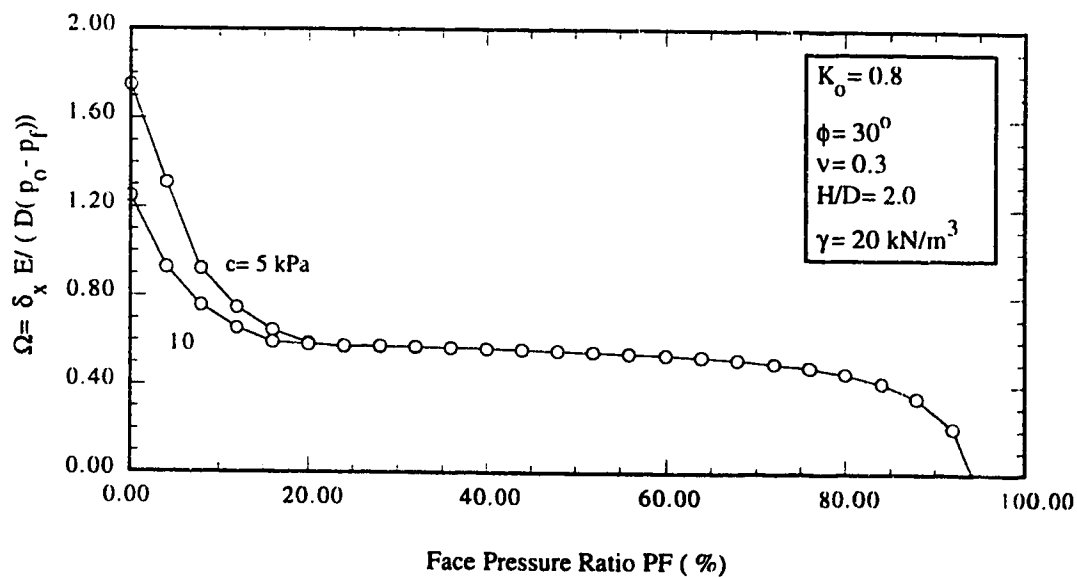


Figure 3.38: Parameter of Face Displacement, Ω , versus Face Pressure Ratio, PF, for various values of Cohesion, c , $\phi = 30^\circ$, $H/D = 2.0$.

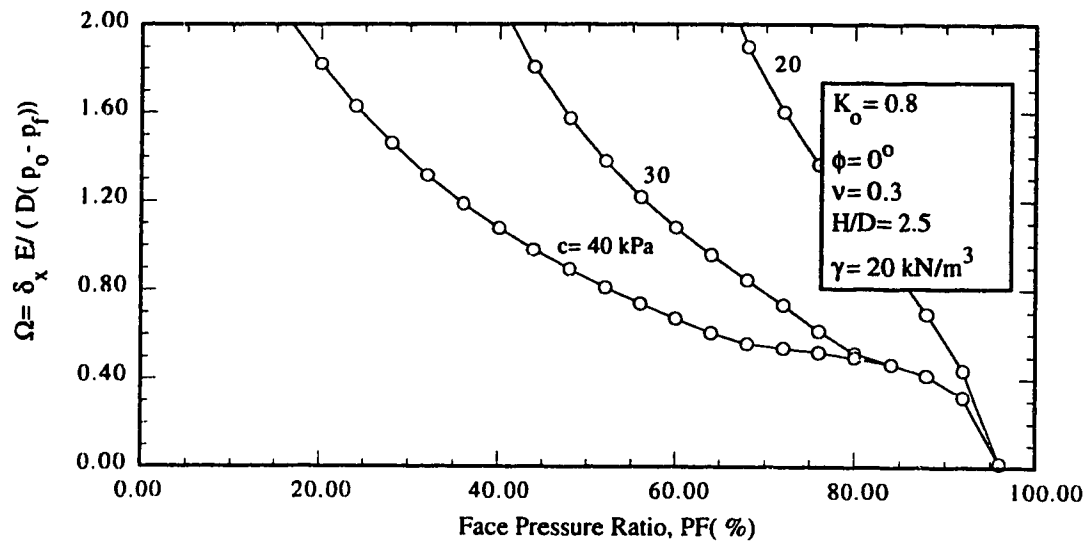


Figure 3.39: Parameter of Face Displacement, Ω , versus Face Pressure Ratio, PF, for various values of Cohesion, c , $\phi = 0^\circ$, $H/D = 2.5$.

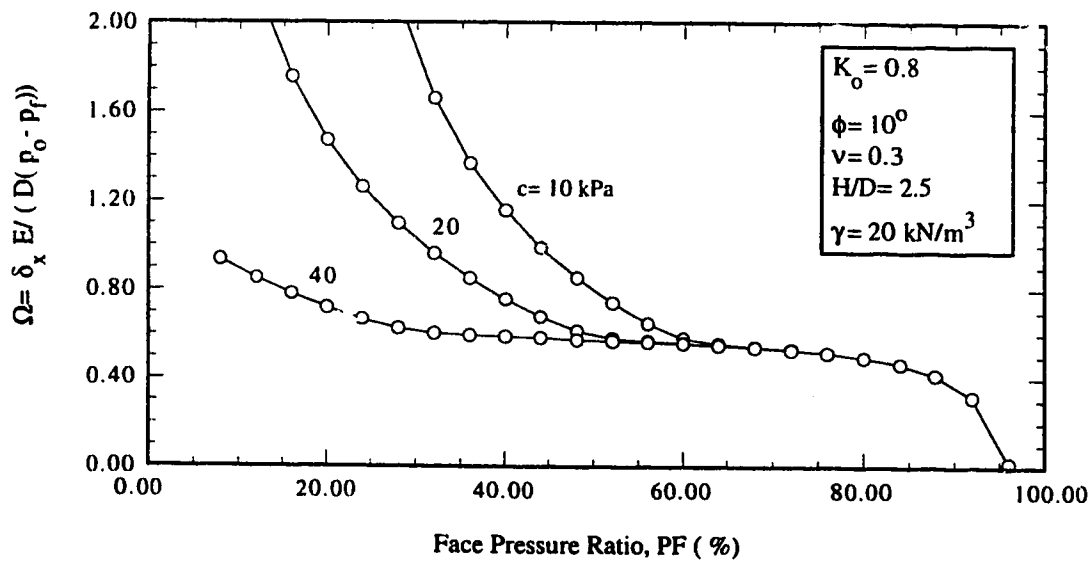


Figure 3.40: Parameter of Face Displacement, Ω , versus Face Pressure Ratio, PF, for various values of Cohesion, c , $\phi = 10^\circ$, $H/D = 2.5$.

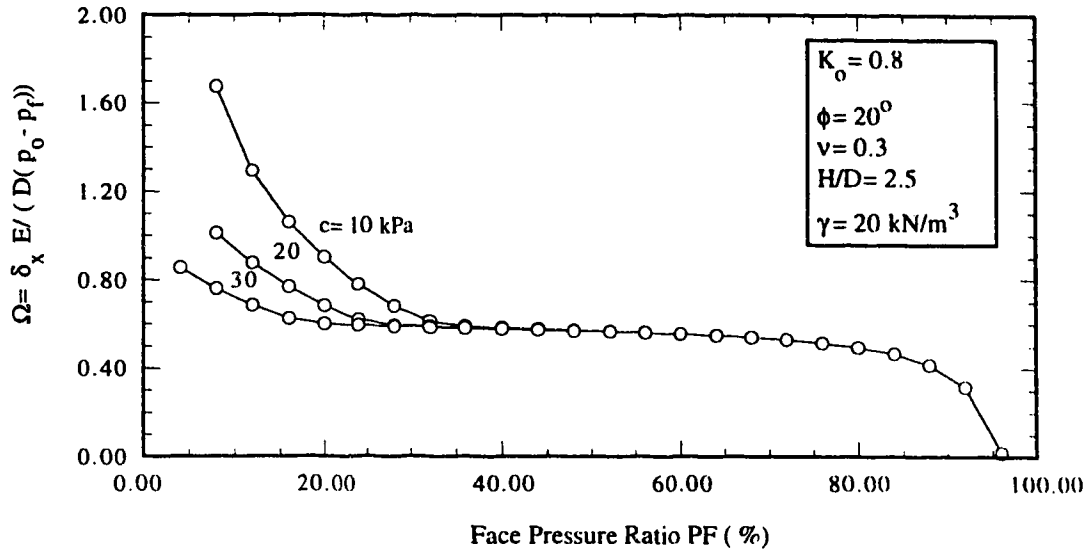


Figure 3.41: Parameter of Face Displacement, Ω , versus Face Pressure Ratio, PF, for various values of Cohesion, c , $\phi = 20^\circ$, $H/D = 2.5$.

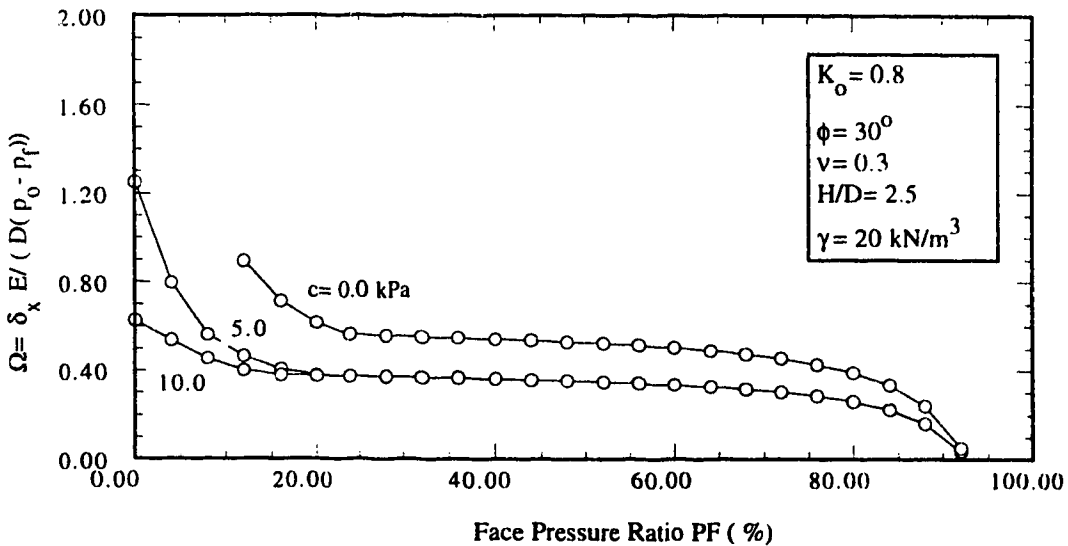
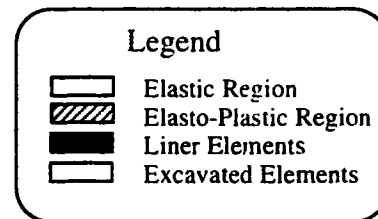
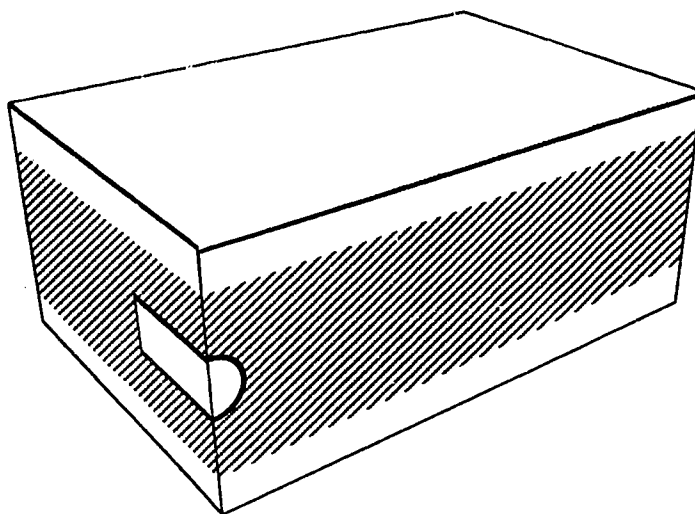
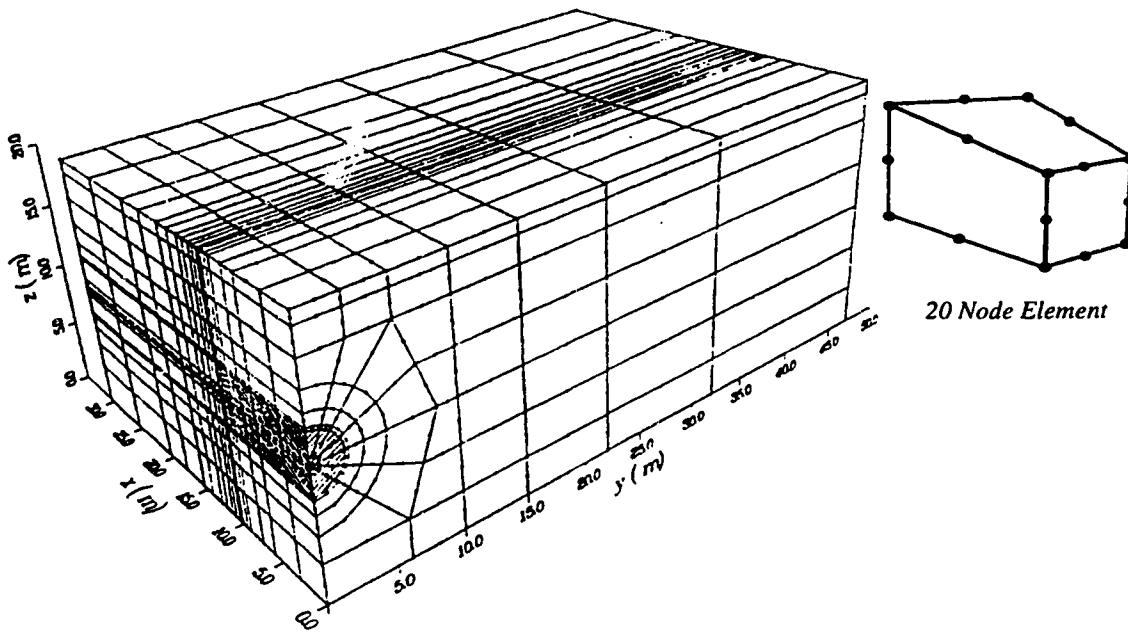


Figure 3.42: Parameter of Face Displacement, Ω , versus Face Pressure Ratio, PF, for various values of Cohesion, c , $\phi = 30^\circ$, $H/D = 2.5$.



2. Material Properties used for Face Stability of Non Cohesive Material

Figure 3.43: Three Dimensional Finite Element Mesh used for Tunnel Face Stability Analyses

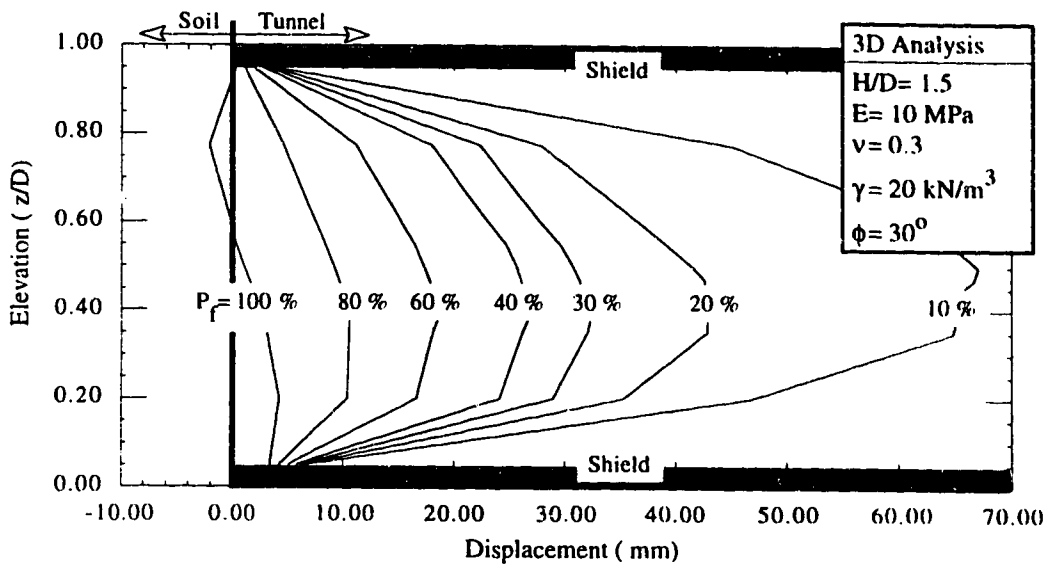


Figure 3.44: Longitudinal Displacement at the Vertical Axis of the Face for various Face Pressure Ratios, Non Cohesive Soil.

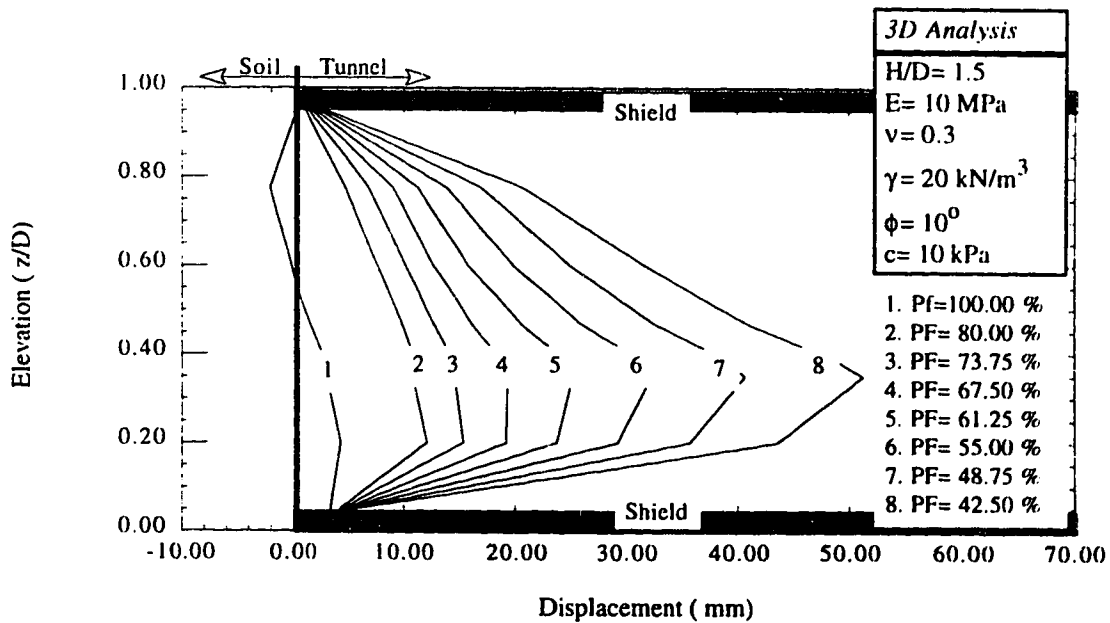


Figure 3.45: Longitudinal Displacement at the Vertical Axis of the Face for various Face Pressure Ratios, Cohesive Soil.

PF decreases with the maximum displacement taking place at the lower half of the face and its location gets higher as the face pressure is reduced. As shown in the figures, the elevation of the point of maximum displacement is close to the lower third of the face in the case of cohesive soil while it is closer to the centerpoint in the case of noncohesive soil. This is due to the higher vertical component of displacement in the case of cohesive soil. Figures 3.46 through 3.50 show a comparison between face movement curves of the axisymmetric and three-dimensional configurations for cases of frictional material. The simple, dimensional relationship between pressure reduction and face displacement is shown on Figures 3.51 through 3.56. The figures show, in general, close agreement in determining the critical face pressure ratio at which yield takes place.

3.5.3 Analysis of the Results

The objectives of the analysis of the obtained results is to qualitatively describe aspects of the stress- and-strain-fields related to the simulated passive stress relief process, to quantitatively assess face pressure at yielding point for different ground and geometrical conditions, and to verify some of the obtained results with the three-dimensional analyses. The differences between the behaviour of cohesive materials and that of frictional materials are studied in detail with respect to:

- (1) degree of overstressing;
- (2) stress path parameters; and
- (3) degree of confinement;

Generalization of the results is expressed through weighted coefficients of the conventional Rankine expression of lateral earth pressure.

3.5.3.1 Degree of Overstressing

The degree of overstressing could be considered as the inverse of the Safety Factor (Equation 3.15) and is defined as follows:

$$OS = \frac{\text{Maximum Shear Stress}}{\text{Shear Strength}} \quad (3.19)$$

Figures 3.57 through 3.62 show plots of contour lines of the degree of overstressing for axisymmetric cases of different shear strengths. It is to be noticed that the zone of influence due to the face stress release depends upon the type of ground resistance whether it is related to cohesion or friction. In cases of frictional material, the failure zone is a half circle extending approximately one radius ahead of the face. This observation is confirmed

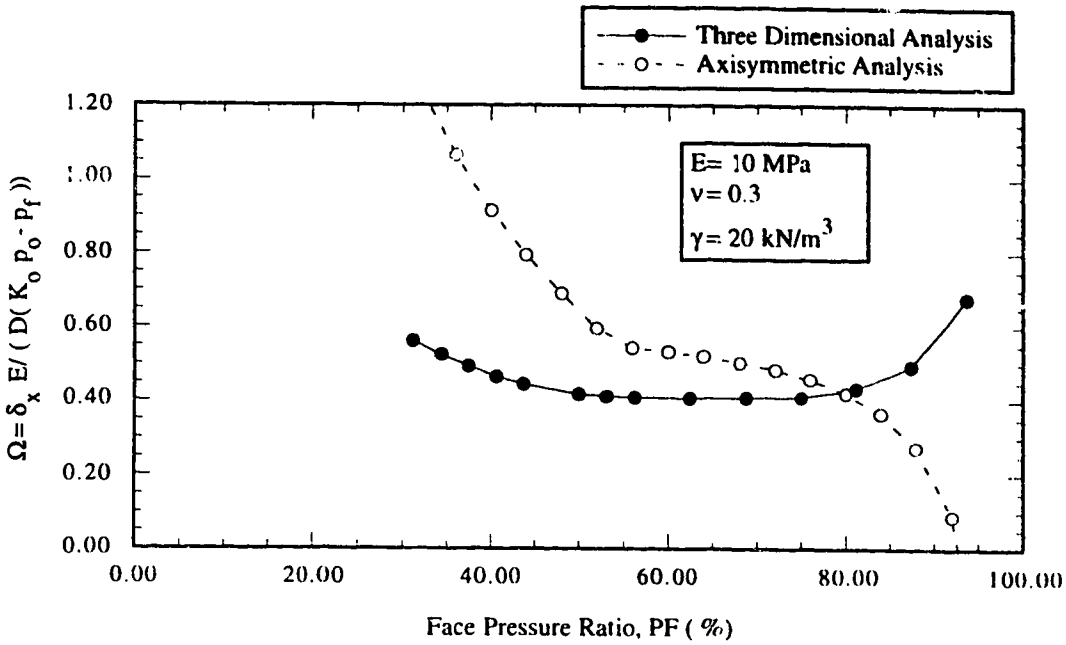


Figure 3.46: Parameter of Face Displacement, Ω , versus Face Pressure Ratio, PF, for Non Cohesive Soils, $\phi = 20^\circ$.

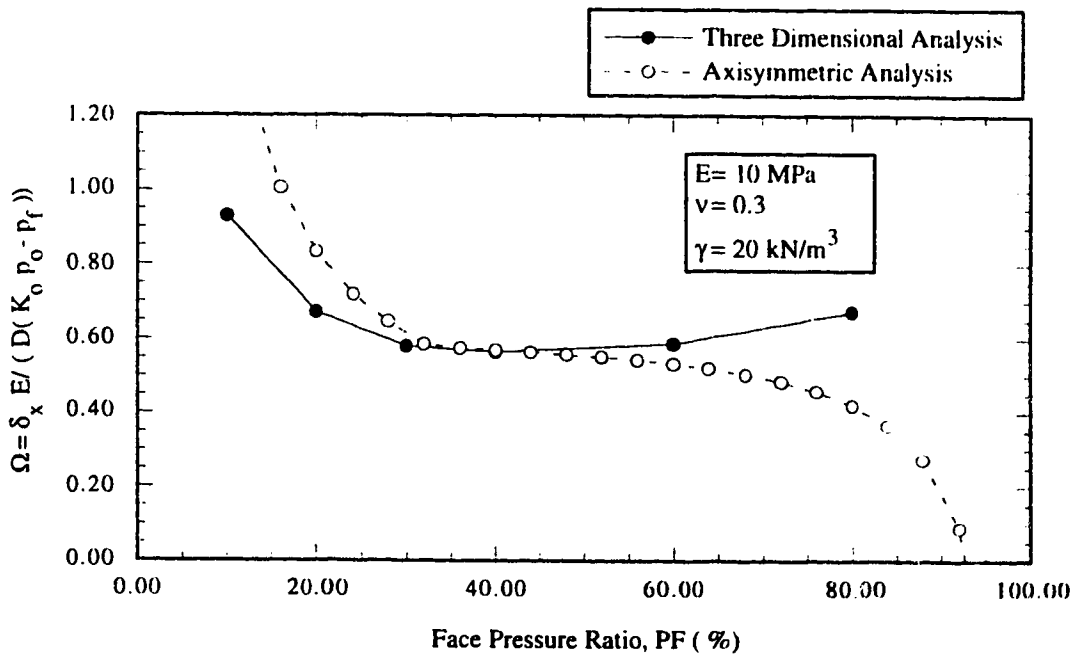


Figure 3.47: Parameter of Face Displacement, Ω , versus Face Pressure Ratio, PF, for Non Cohesive Soils, $\phi = 30^\circ$.

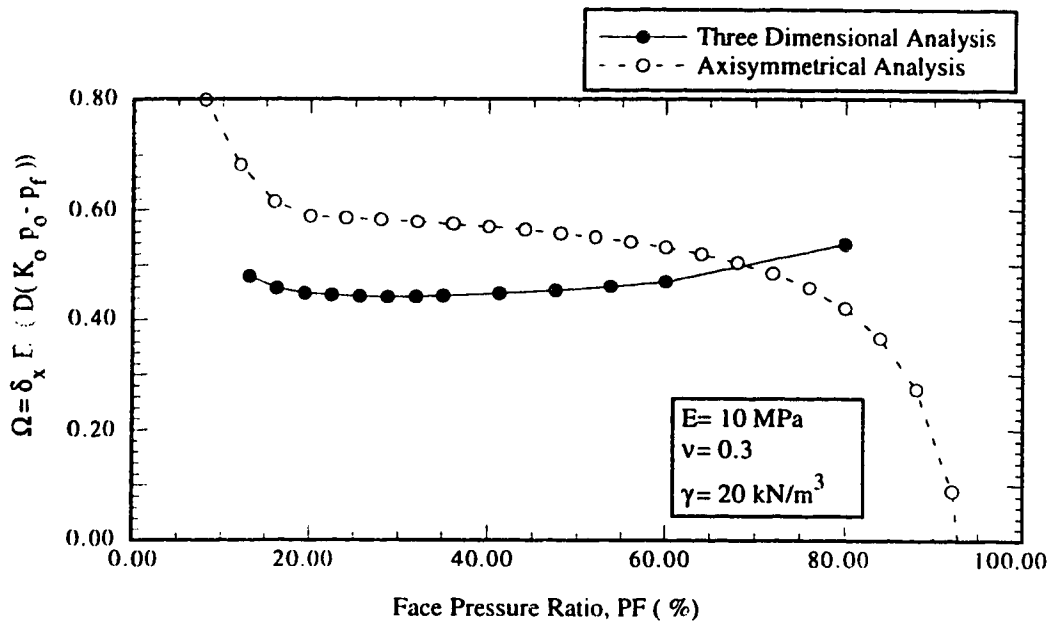


Figure 3.48: Parameter of Face Displacement, Ω , versus Face Pressure Ratio, PF, for Non Cohesive Soils, $\phi = 40^\circ$.

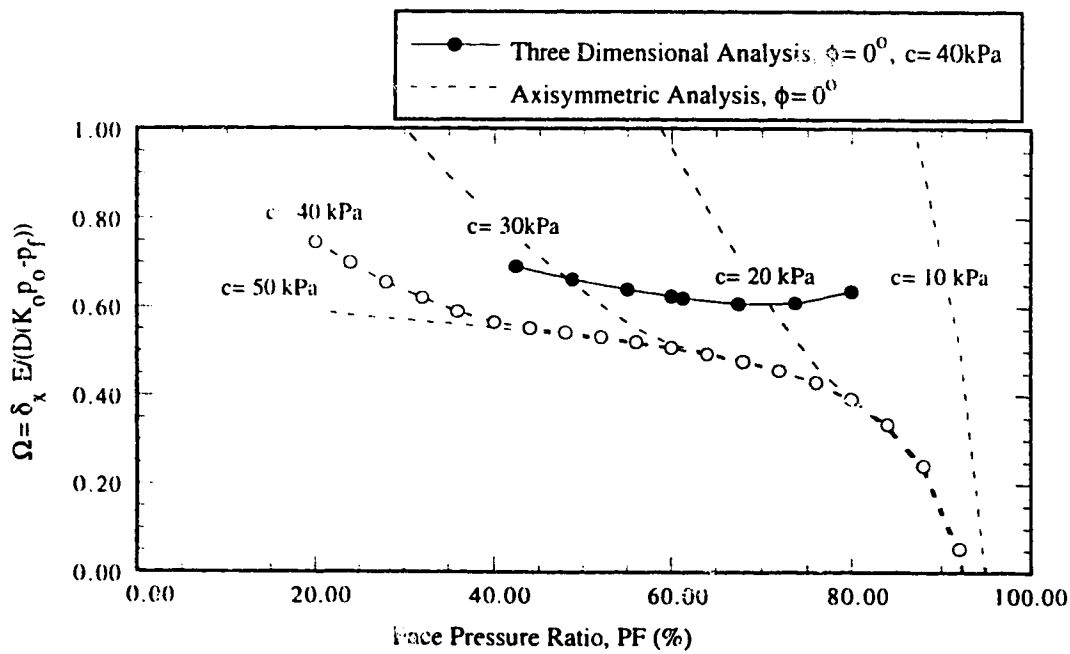


Figure 3.49: Parameter of Face Displacement, Ω , versus Face Pressure Ratio, PF, for Cohesive Soils, $\phi = 0^\circ$.

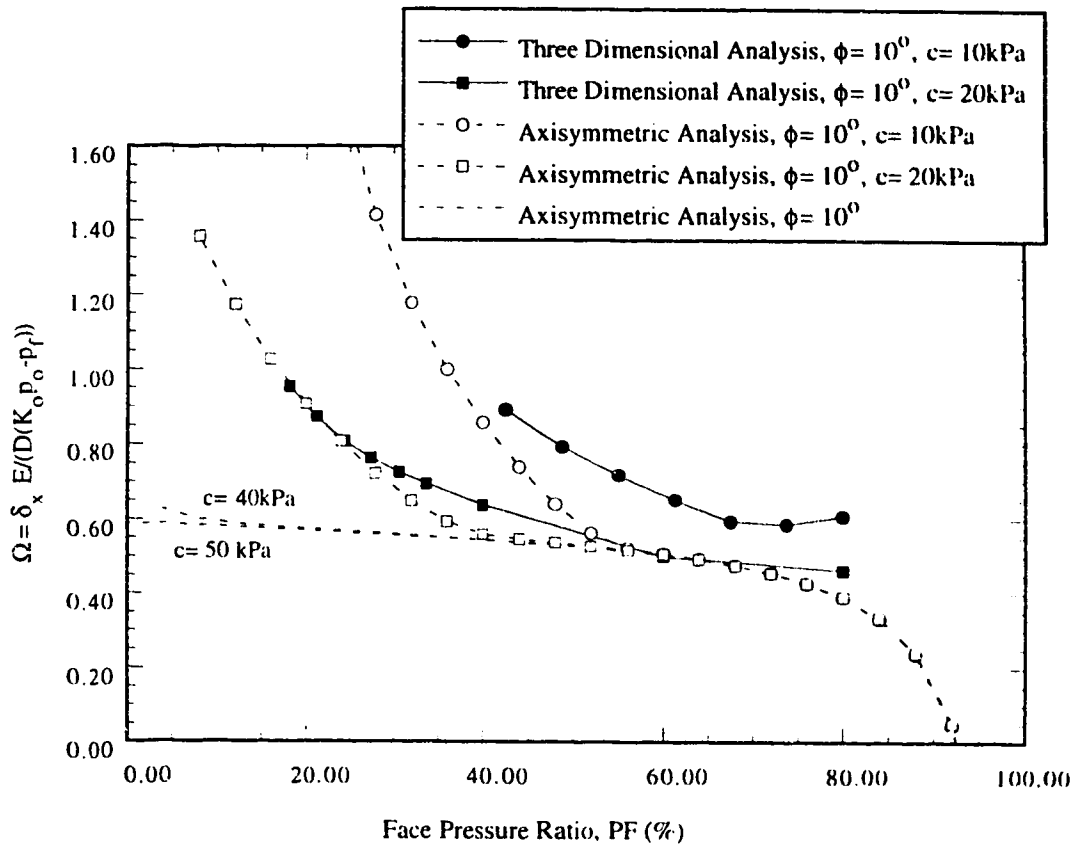


Figure 3.50: Parameter of Face Displacement, Ω , versus Face Pressure Ratio, PF, for c - ϕ Soils, $\phi = 10^\circ$.

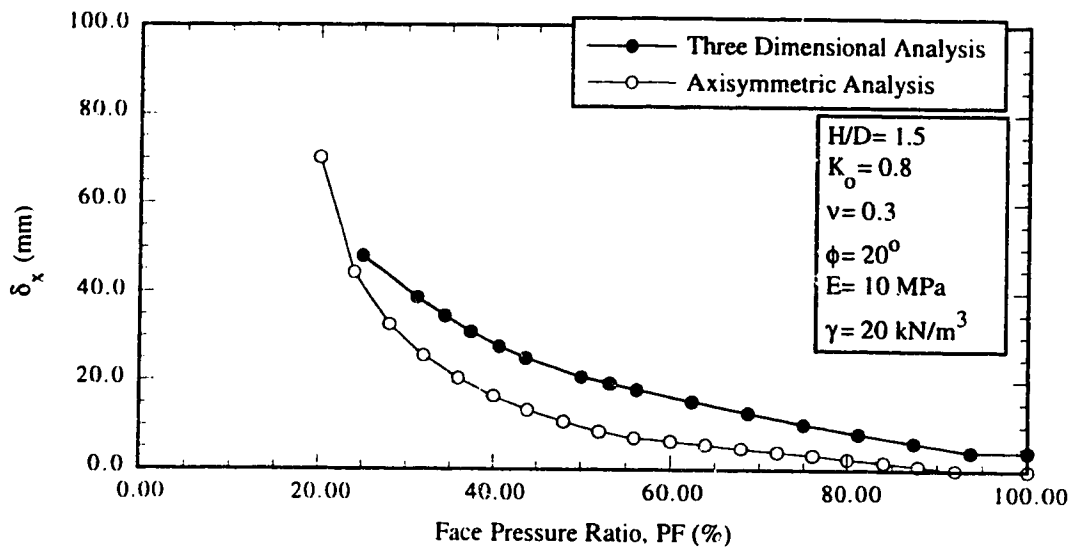


Figure 3.51: Displacement at the Centre Point of the face, δ_x , versus the Face Pressure Ratio, PF, for Non Cohesive Soils, $\phi = 20^\circ$.

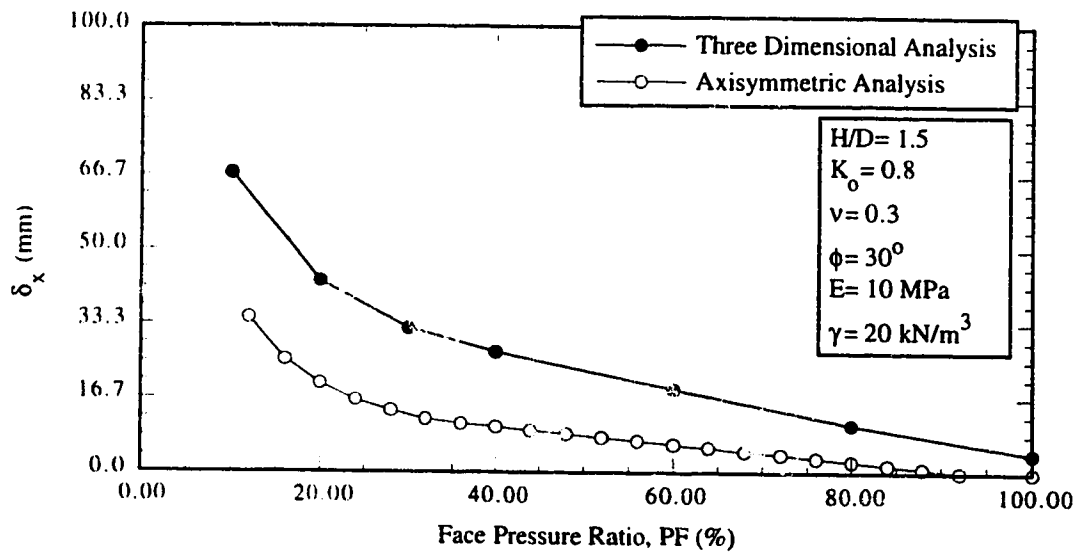


Figure 3.52: Displacement at the Centre Point of the face, δ_x , versus the Face Pressure Ratio, PF, for Non Cohesive Soils, $\phi = 30^\circ$.

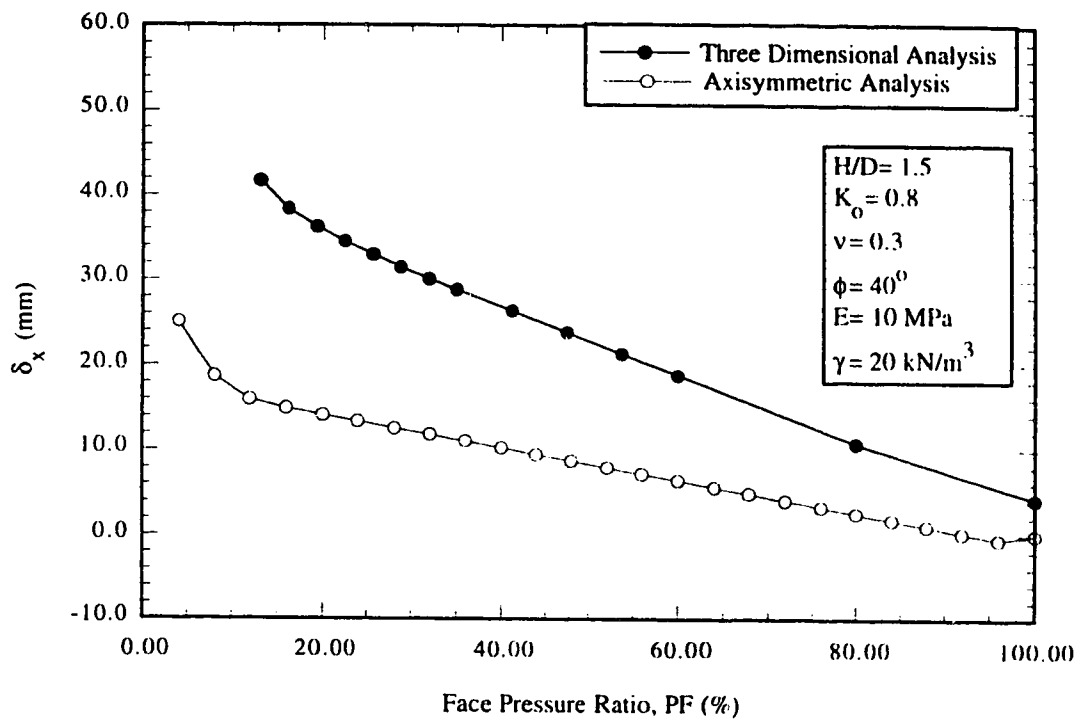


Figure 3.53: Displacement at the Centre Point of the face, δ_x , versus the Face Pressure Ratio, PF, for Non Cohesive Soils, $\phi = 40^\circ$.

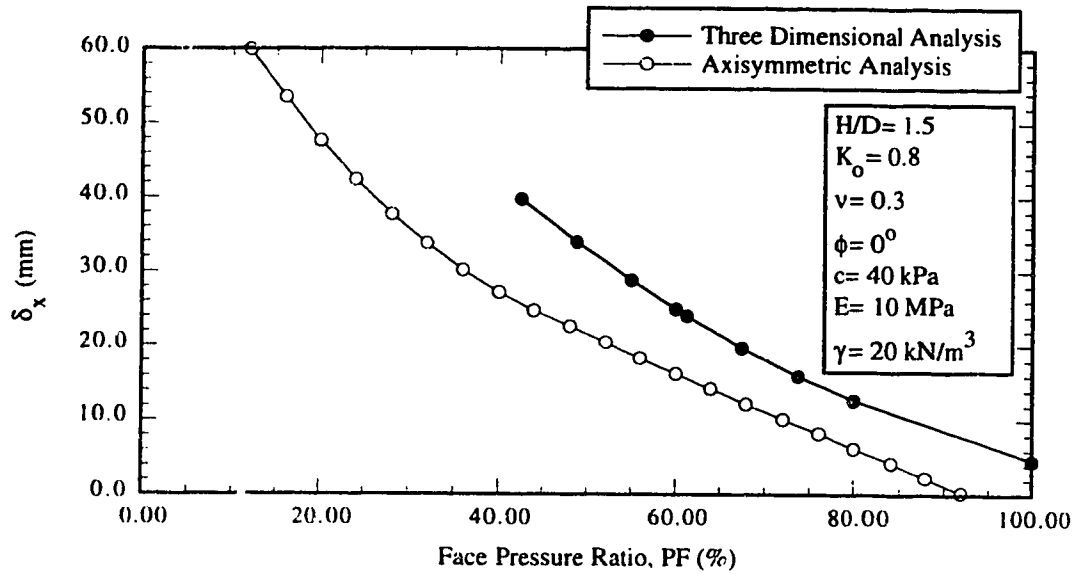


Figure 3.54: Displacement at the Centre Point of the face, δ_x , versus the Face Pressure Ratio, PF, for Cohesive Soils, $c= 40$ kPa and $\phi= 0^\circ$.

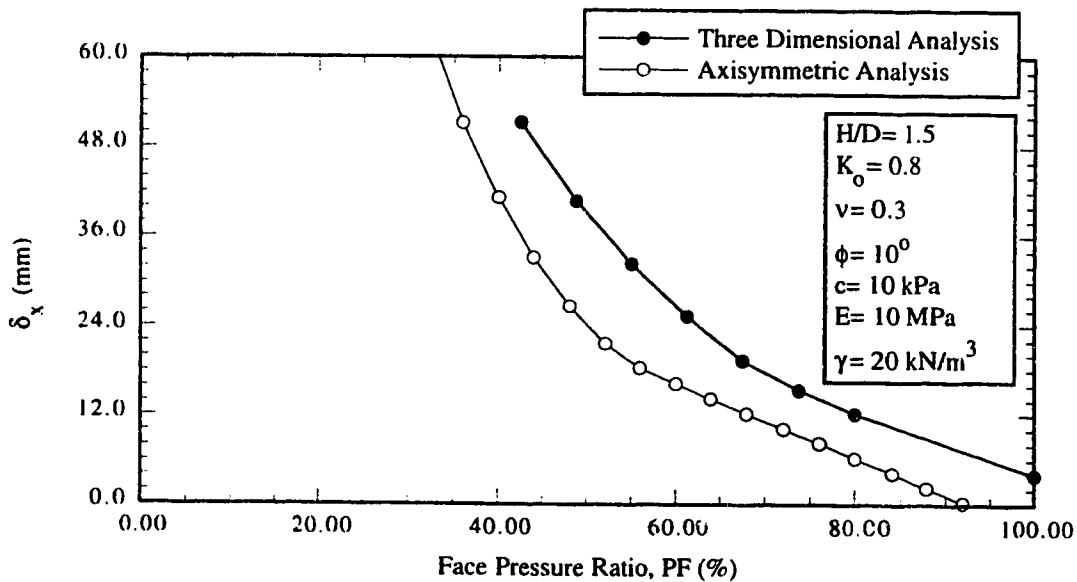


Figure 3.55: Displacement at the Centre Point of the face, δ_x , versus the Face Pressure Ratio, PF, for $c-\phi$ Soils, $c= 10$ kPa and $\phi= 10^\circ$.

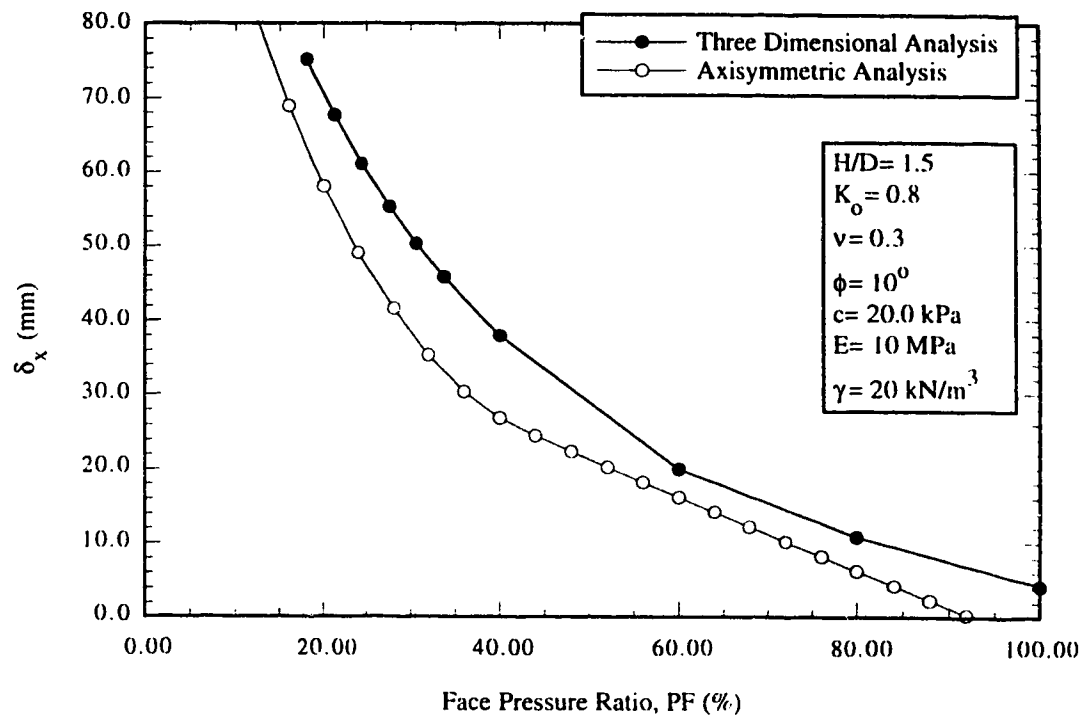


Figure 3.56: Displacement at the Centre Point of the face, δ_x , versus the Face Pressure Ratio, PF (%), for c - ϕ Soils, $c = 20 \text{ kPa}$ and $\phi = 10^\circ$.

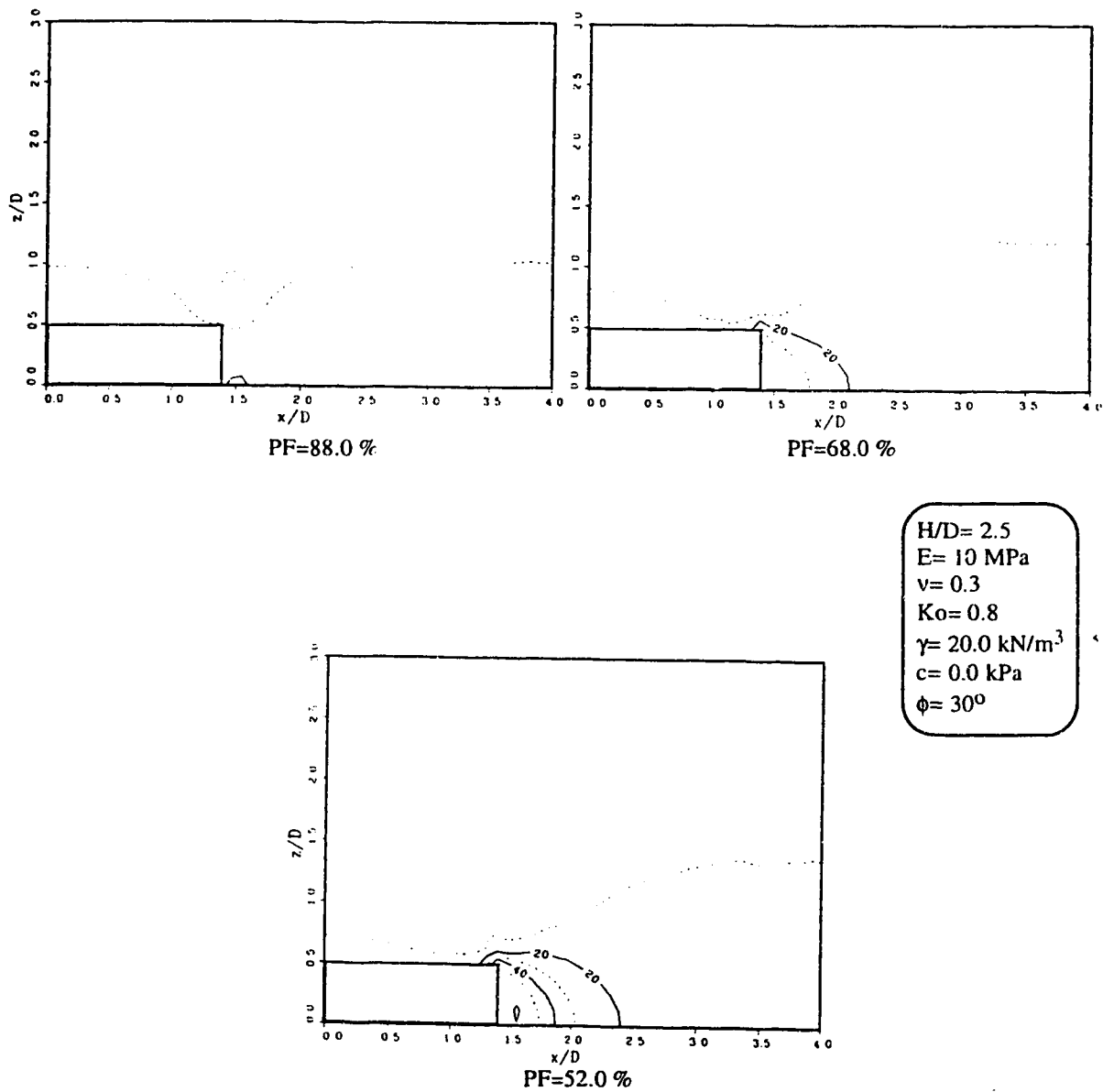
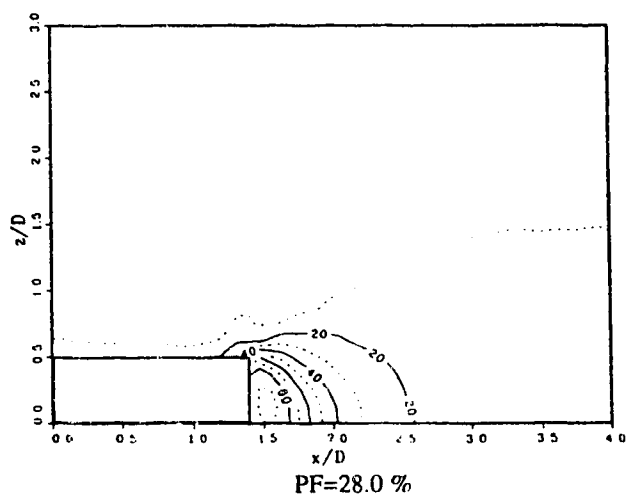


Figure 3.57: Contour Lines of Degree of Overstressing, OS, in percent, due to Stress Relief at the Face of a Tunnel, Axisymmetric Analysis, $c=0$, $\phi=30^\circ$.



$H/D = 2.5$
 $E = 10 \text{ MPa}$
 $\nu = 0.3$
 $K_0 = 0.8$
 $\gamma = 20.0 \text{ kN/m}^3$
 $c = 0.0 \text{ kPa}$
 $\phi = 30^\circ$

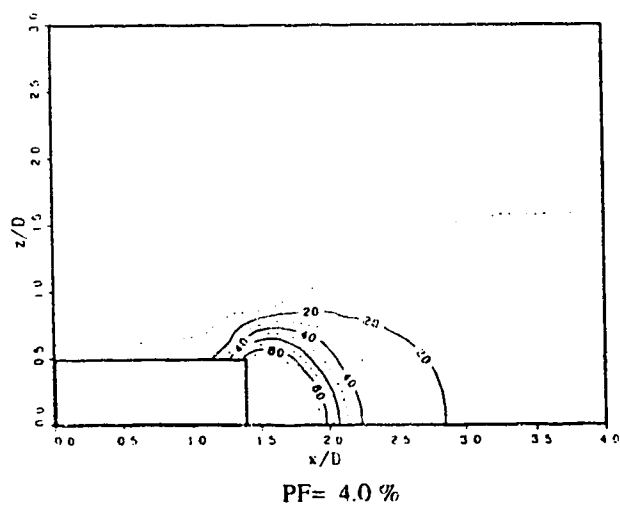


Figure 3.57: Contour Lines of Degree of Overstressing, OS, in percent, due to Stress Relief at the Face of a Tunnel, Axisymmetric Analysis, $c = 0$, $\phi = 30^\circ$ (continued).

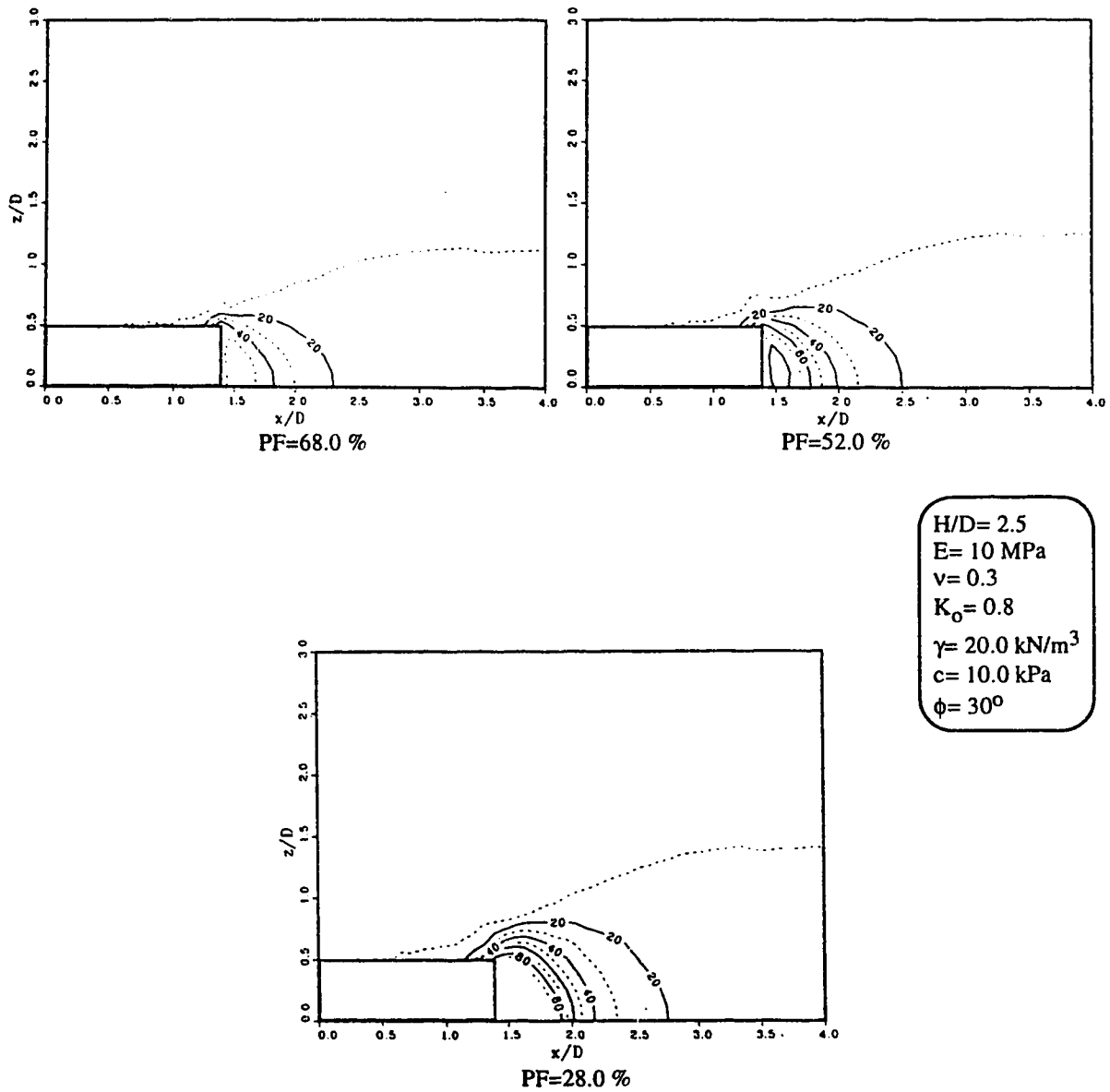


Figure 3.58: Contour Lines of Degree of Overstressing, OS, in percent, due to Stress Relief at the Face of a Tunnel, Axisymmetric Analysis, $c = 10 \text{ kPa}$, $\phi = 30^\circ$.

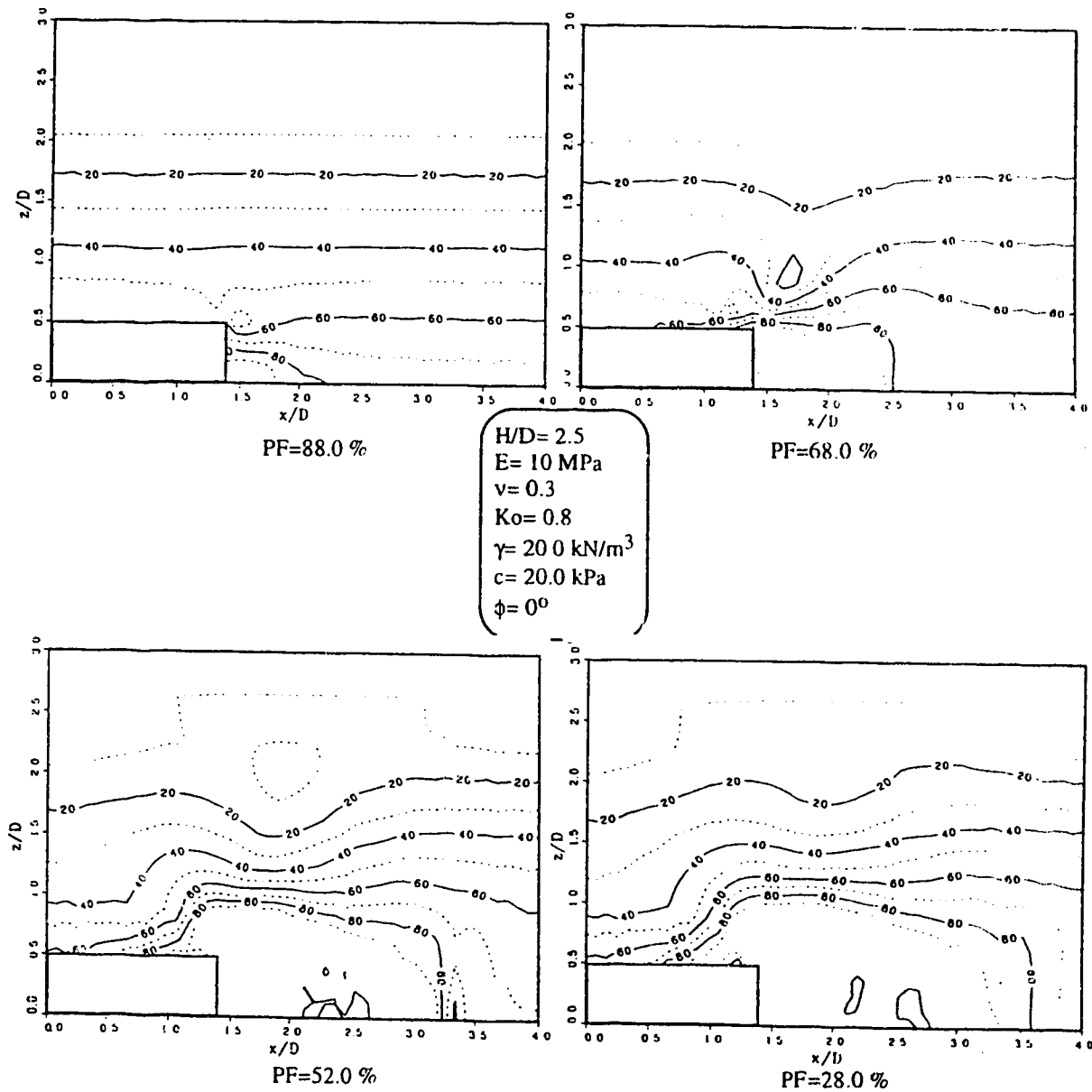


Figure 3.59: Contour Lines of Degree of Overstressing, OS, in percent, due to Stress Relief at the Face of a Tunnel, Axisymmetric Analysis, $c=20 \text{ kPa}$, $\phi=0^\circ$.

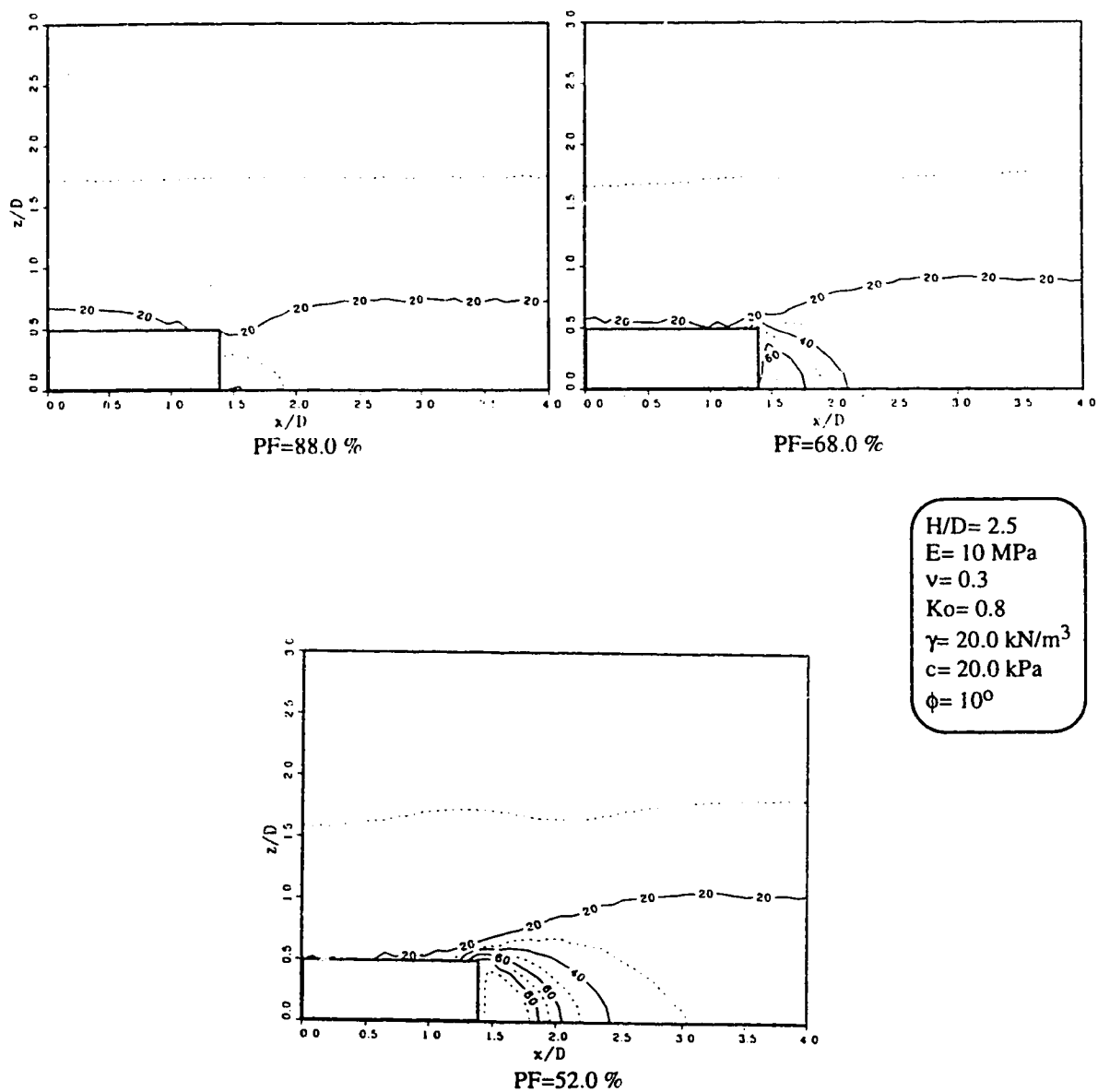
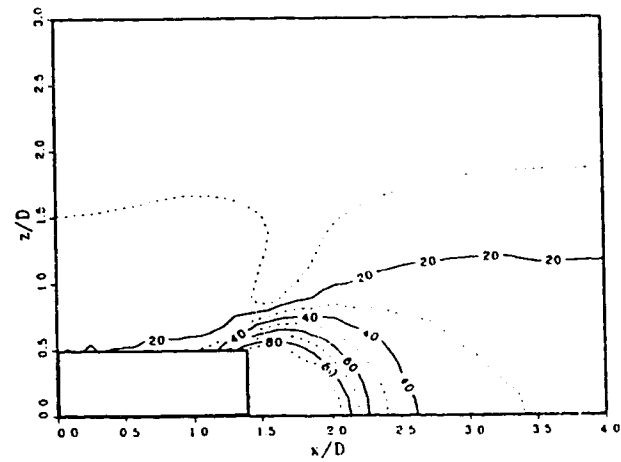
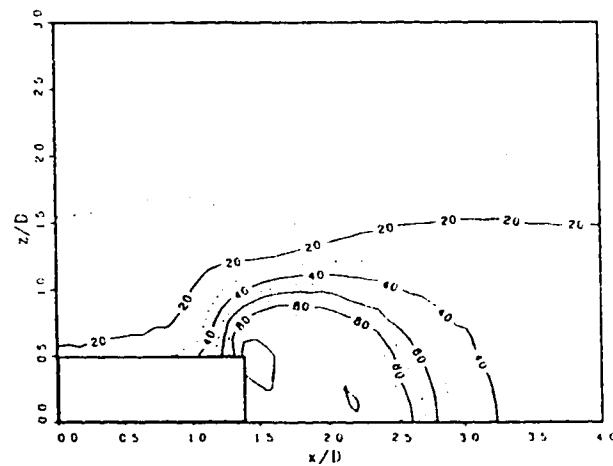


Figure 3.60: Contour Lines of Degree of Overstressing, OS, in percent, due to Stress Relief at the Face of a Tunnel, Axisymmetric Analysis, $c=20\text{ kPa}$, $\phi=10^\circ$.



PF=28.0 %

$H/D = 2.5$
 $E = 10 \text{ MPa}$
 $\nu = 0.3$
 $K_0 = 0.8$
 $\gamma = 20.0 \text{ kN/m}^3$
 $c = 20.0 \text{ kPa}$
 $\phi = 10^\circ$



PF= 4.0 %

Figure 3.60: Contour Lines of Degree of Overstressing, OS, in percent, due to Stress Relief at the Face of a Tunnel, Axisymmetric Analysis, $c = 20 \text{ kPa}$, $\phi = 10^\circ$ (continued).

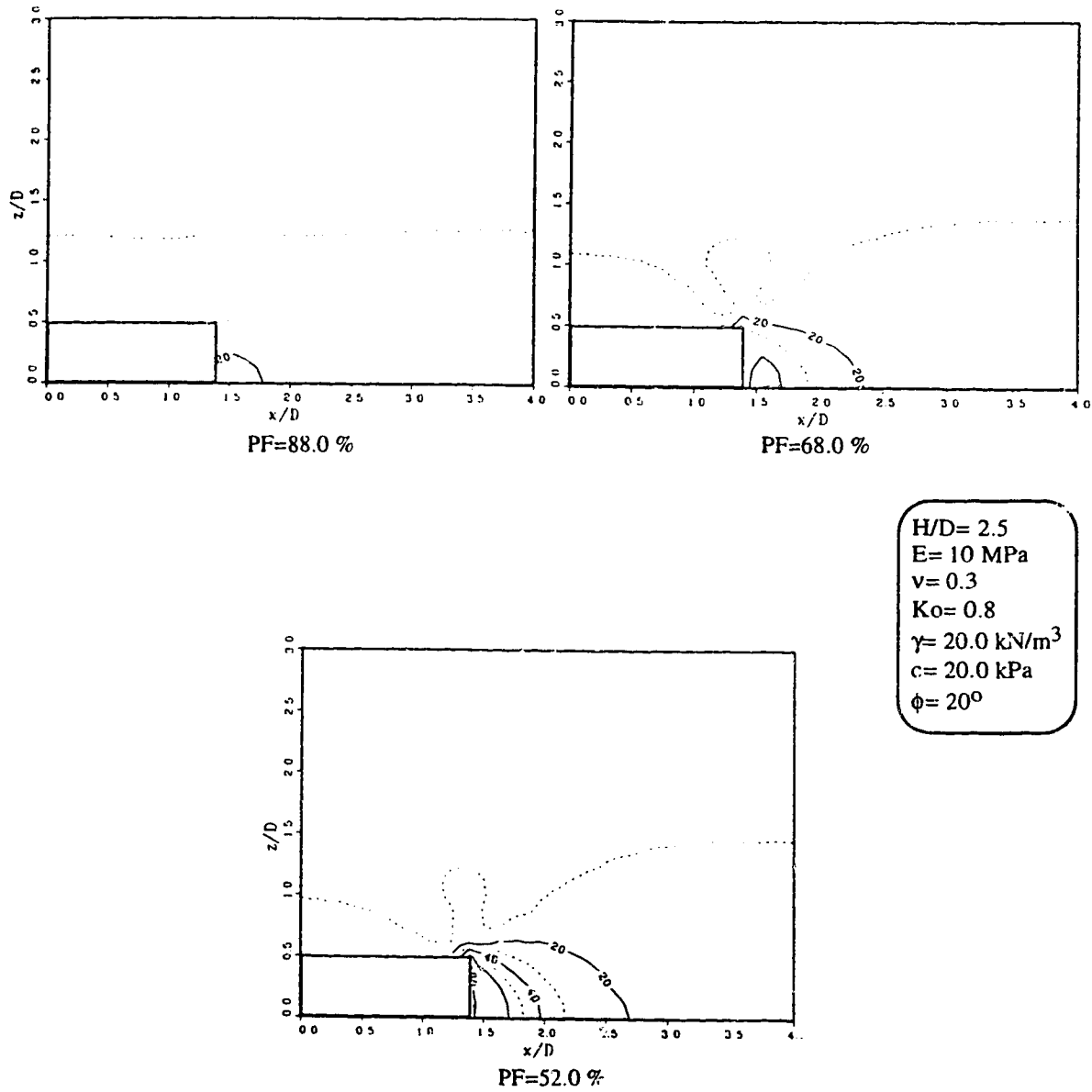
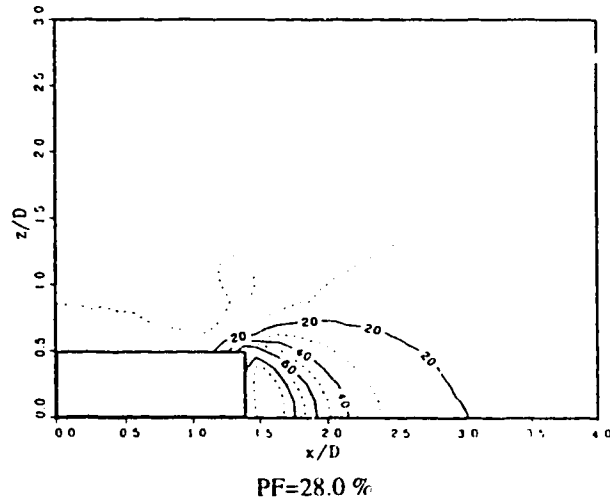


Figure 3.61: Contour Lines of Degree of Overstressing, OS, in percent, due to Stress Relief at the Face of a Tunnel, Axisymmetric Analysis, $c=20 \text{ kPa}$, $\phi=20^\circ$.



H/D= 2.5
 E= 10 MPa
 ν= 0.3
 K_σ= 0.8
 γ= 20.0 kN/m³
 c= 20.0 kPa
 φ= 20°

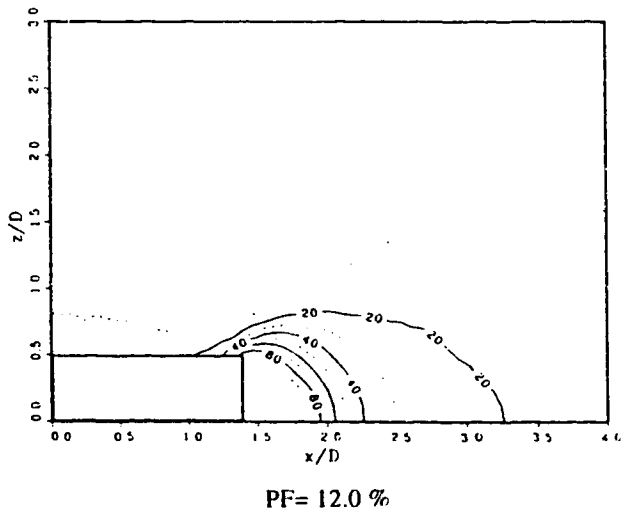


Figure 3.61: Contour Lines of Degree of Overstressing, OS, in percent, due to Stress Relief at the Face of a Tunnel, Axisymmetric Analysis, $c= 20 \text{ kPa}$, $\phi= 20^\circ$ (continued).

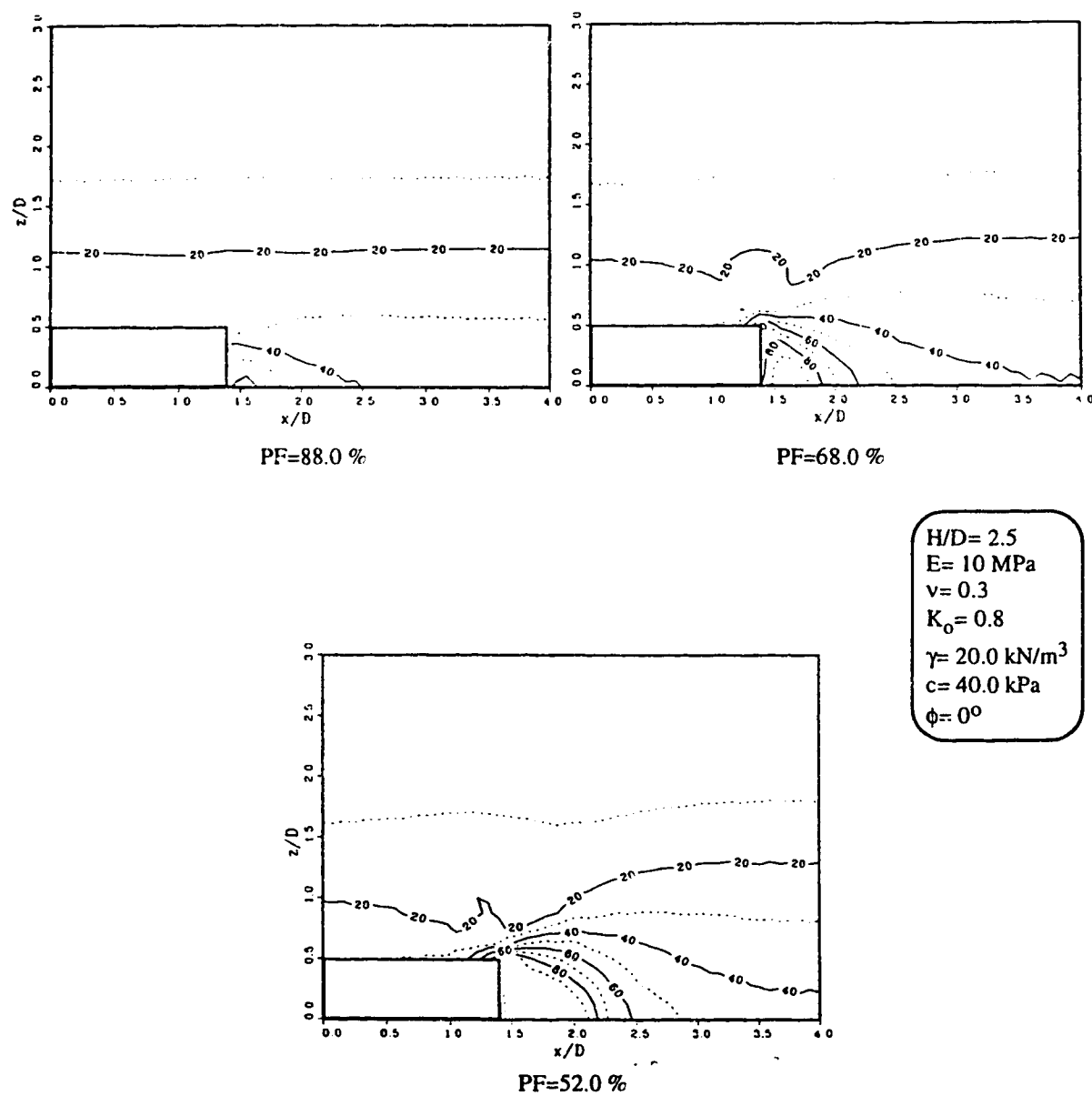
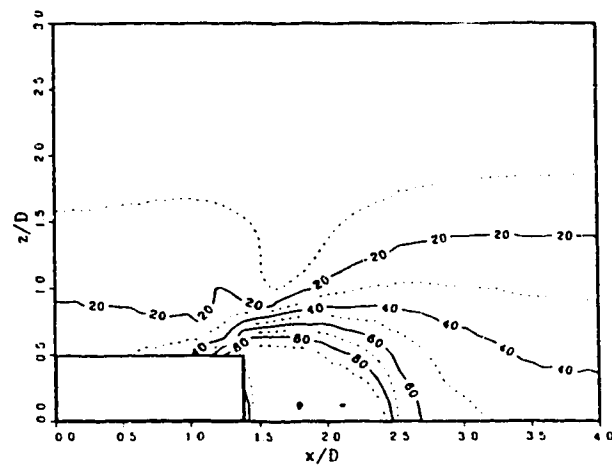
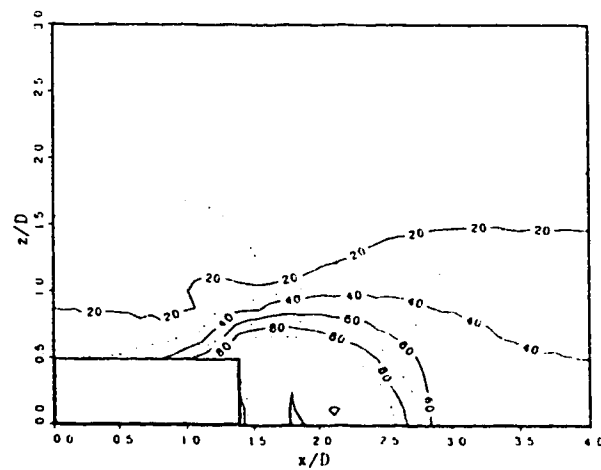


Figure 3.62: Contour Lines of Degree of Overstressing, OS, in percent, due to Stress Relief at the Face of a Tunnel, Axisymmetric Analysis, $c = 40 \text{ kPa}$, $\phi = 0^\circ$.



PF=28.0 %

$H/D = 2.5$
 $E = 10 \text{ MPa}$
 $\nu = 0.3$
 $K_o = 0.8$
 $\gamma = 20.0 \text{ kN/m}^3$
 $c = 40.0 \text{ kPa}$
 $\phi = 0^\circ$



PF=16.0 %

Figure 3.62: Contour Lines of Degree of Overstressing, OS, in percent, due to Stress Relief at the Face of a Tunnel, Axisymmetric Analysis, $c = 40 \text{ kPa}$, $\phi = 0^\circ$ (continued).

by Chaffois et al. (1988). Failure zones in cohesive material may extend even further ahead of the face. Their extent depends on the amount and the variation of cohesive resistance and also on initial lateral pressure.

Three-dimensional analyses represent a more complete description of the problem by adding the effect of the tunnel weight to the investigated problem. In all simulated cases, it is assumed that the tunnel weight is equal to the weight of the excavated soil. This assumption, although it may be considered as an overestimation with respect to actual cases, has the advantage of excluding the effect of upward heave of the whole tunnel because of weight loss inside the excavated gallery. As a matter of fact, the change of weight acts in combination with other factors related to the excavation method such as the tail gap, the grout pressure and the stiffness of the liner. The study of all such elements could add excessive complexity to the problem. Figure 3.63 shows plots of contour lines indicating the degree of overstressing for the three-dimensional case of frictional material. It can be noticed that a region of overstressing takes place near the ground surface because confinement pressure is very low in this area. Propagation of the overstressing zone ahead of the face takes almost a circular pattern with the highest overstressing zone near the centerpoint of the face.

Figure 3.64 shows the degree of overstressing due to mobilized shear stress in the three-dimensional case of cohesive soil which is the ratio between the mobilized shear stress (shear stress minus the initial shear stress) and the shear strength. Compared with the contour lines of the total degrees of overstressing (Figure 3.62), it is clear that the extent of the zones influenced is more limited. This indicates the effect the initial stress (K_0) has on the propagation of failure zone. It can be remarked, also, that the propagation of the influence zones starts from the lower part of the tunnel and propagates upward which explains the pattern of lateral displacement shown in Figure 3.45 where the maximum displacement is near the lower third of the face.

3.5.3.2 Stress Path

The stress path at the face depends on the adopted Mohr-Coulomb failure criterion. The criterion is represented in (ξ, ρ, θ) space in Figure 3.65 where ξ is the hydrostatic stress invariant, ρ , is the deviatoric stress invariant, and θ is the angle of similarity:

$$\xi = \frac{I_1}{\sqrt{3}} = \sqrt{3}p = \frac{(\sigma_1 + \sigma_2 + \sigma_3)}{\sqrt{3}} \quad , \quad (3.20.a)$$

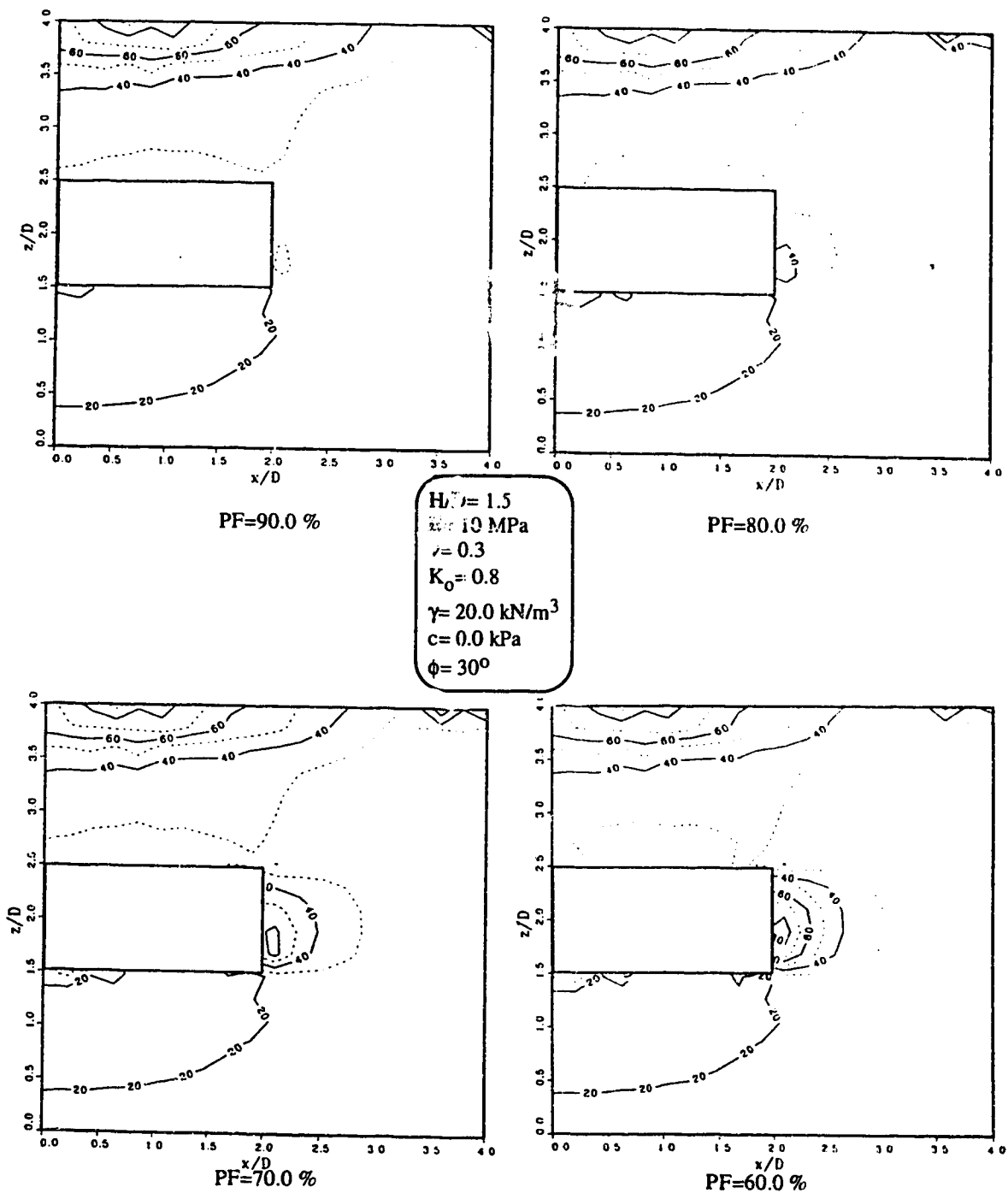


Figure 3.63: Contour Lines of Degree of Overstressing, OS, in percent, due to Stress Relief at the Face of a Tunnel, Three Dimensional Analysis, $c = 0 \text{ kPa}$, $\phi = 30^\circ$.

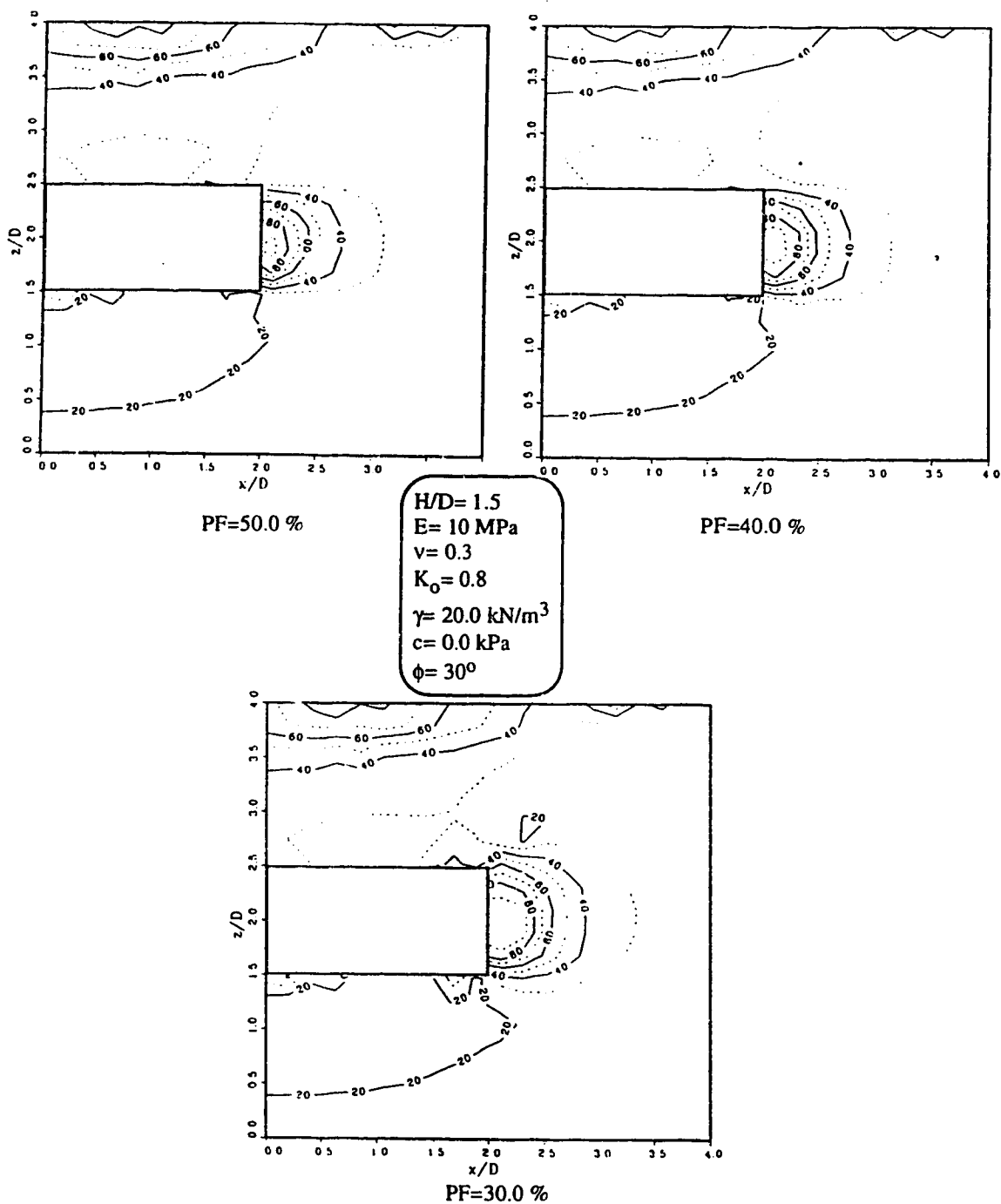


Figure 3.63: Contour Lines of Degree of Overstressing, OS, in percent, due to Stress Relief at the Face of a Tunnel, Three Dimensional Analysis, $c=0 \text{ kPa}$, $\phi=30^\circ$ (continued).

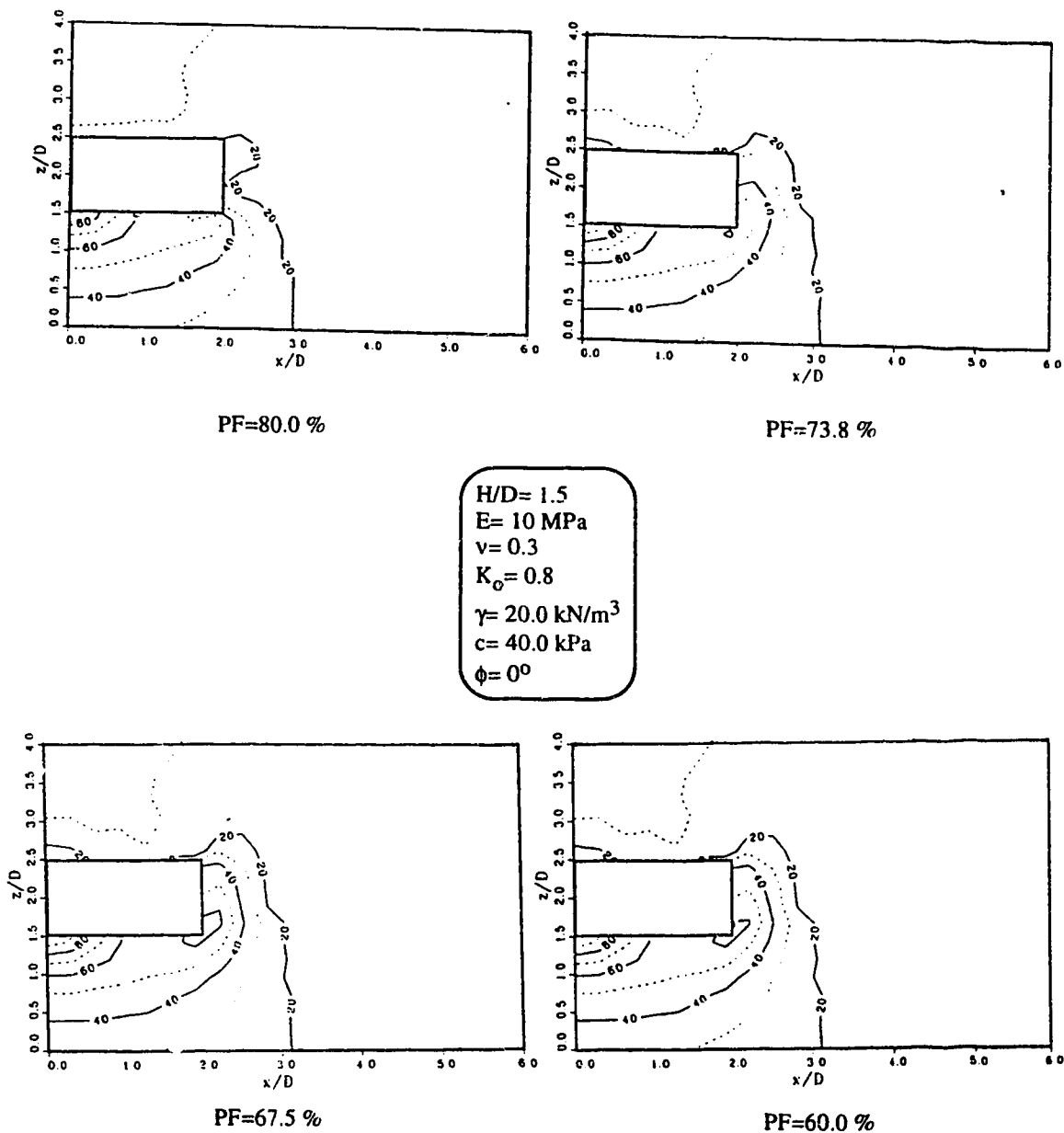


Figure 3.64: Contour Lines of Mobilized Degree of Overstressing, OS, in percent, due to Stress Relief at the Face of a Tunnel, Three Dimensional Analysis, $c = 40 \text{ kPa}$, $\phi = 0^\circ$.

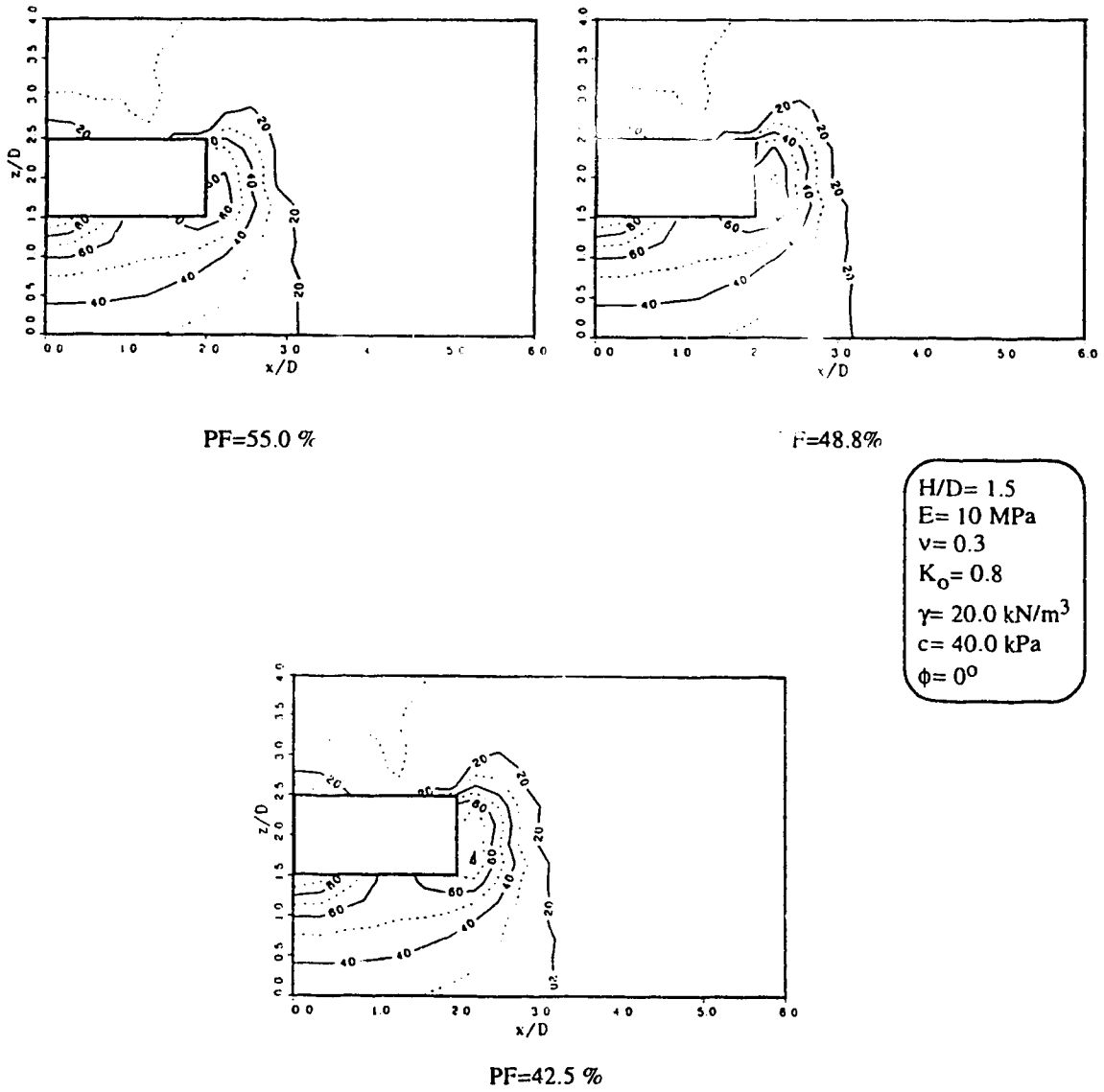


Figure 3.64: Contour Lines of Mobilized Degree of Overstressing, OS, in percent, due to Stress Relief at the Face of a Tunnel, Three Dimensional Analysis, $c = 40 \text{ kPa}$, $\phi = 0^\circ$, (continued).

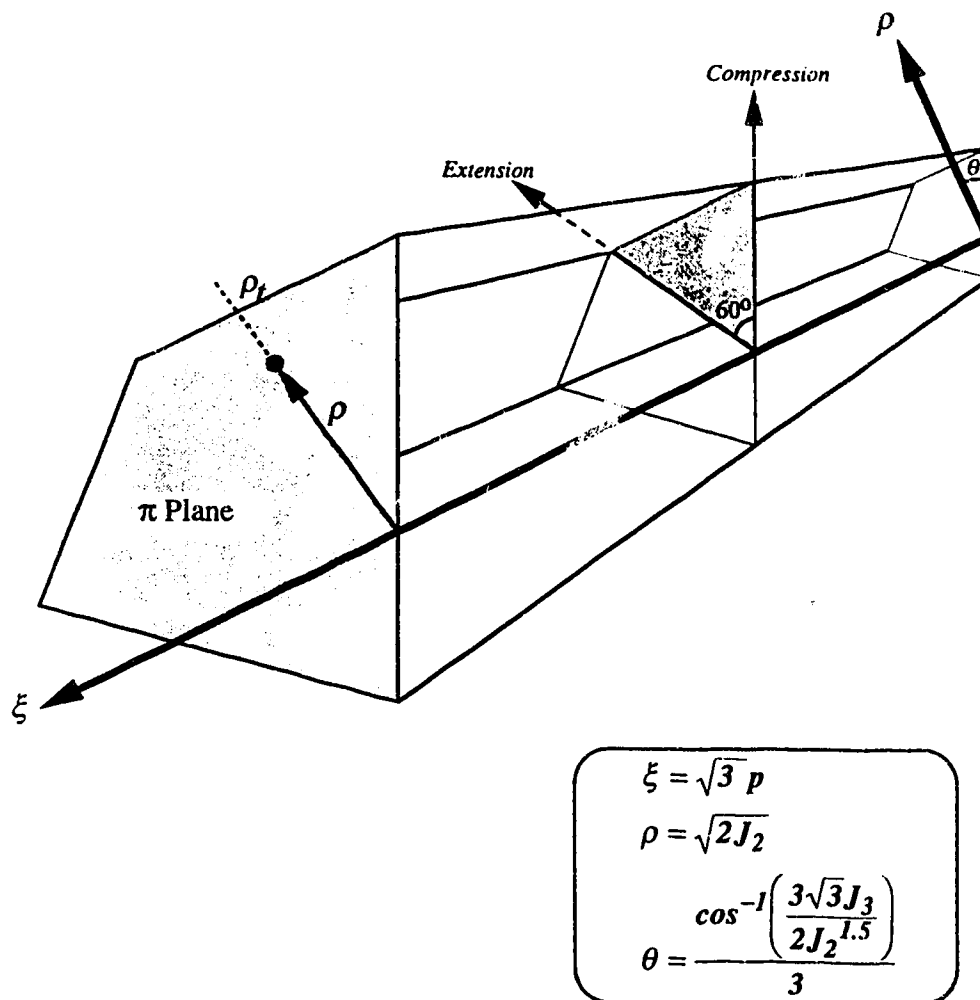


Figure 3.65: Mohr Coulomb Failure Criterion

$$\rho = \sqrt{2J_2} \quad , \quad (3.20.b)$$

and

$$\theta = \frac{\cos^{-1}\left(\frac{3\sqrt{3}J_3}{2J_2^{1.5}}\right)}{3} \quad . \quad (3.20.c)$$

where:

I_1 is the first invariant of stress tensor and

J_2 and J_3 are the second and third invariants of deviatoric stress tensor, respectively .

The meridian plan describes the relationship between ρ and ξ for a certain value of θ . The normalized meridian plan shows the relationship between the hydrostatic stress and the ratio between the deviatoric stress and maximum deviatoric stress, ρ_t , according to the failure criterion for a specific angle, θ . At a certain value of ξ , the relation between ρ and θ is described in the π plan. The normalized meridian plan represents the state of stress with respect to the maximum allowable stresses, and the π plan represents the state of the intermediate stress. At a point where $\theta=0^\circ$, the intermediate stress σ_2 is equal to the major principal stress which corresponds to a state of extension in the triaxial-stress configuration, and if $\theta=60^\circ$, σ_2 is equal to the minor principal stress corresponding to a state of compression.

Figure 3.66 shows the stress path of the centerline of the face in the three-dimensional case of frictional material. From the figure, the hydrostatic stress follows a constant trend of reduction because of the stress release which corresponds to a case of negative confinement. This is expected as a non-associated flow rule is adopted in the constitutive model with no dilation allowed. The stress path in the π plan starts from the initial state of compression and the departure from the initial state increases as stress reduction proceeds and as the centerline approaches the face. At failure, a similitude angle of 45° may be reached. Figure 3.67 shows that the stress path for a cohesive material follows a similar trend as that for the noncohesive material. It is to be observed that the departure from the initial compressive state is more limited for the investigated case.

The stress path at the tunnel circumference for the noncohesive case is represented in Figure 3.68. At the upper quarter, hydrostatic stress exhibits a slight increase until the yield point is reached. After yield, the stress path follows an accelerating trend toward

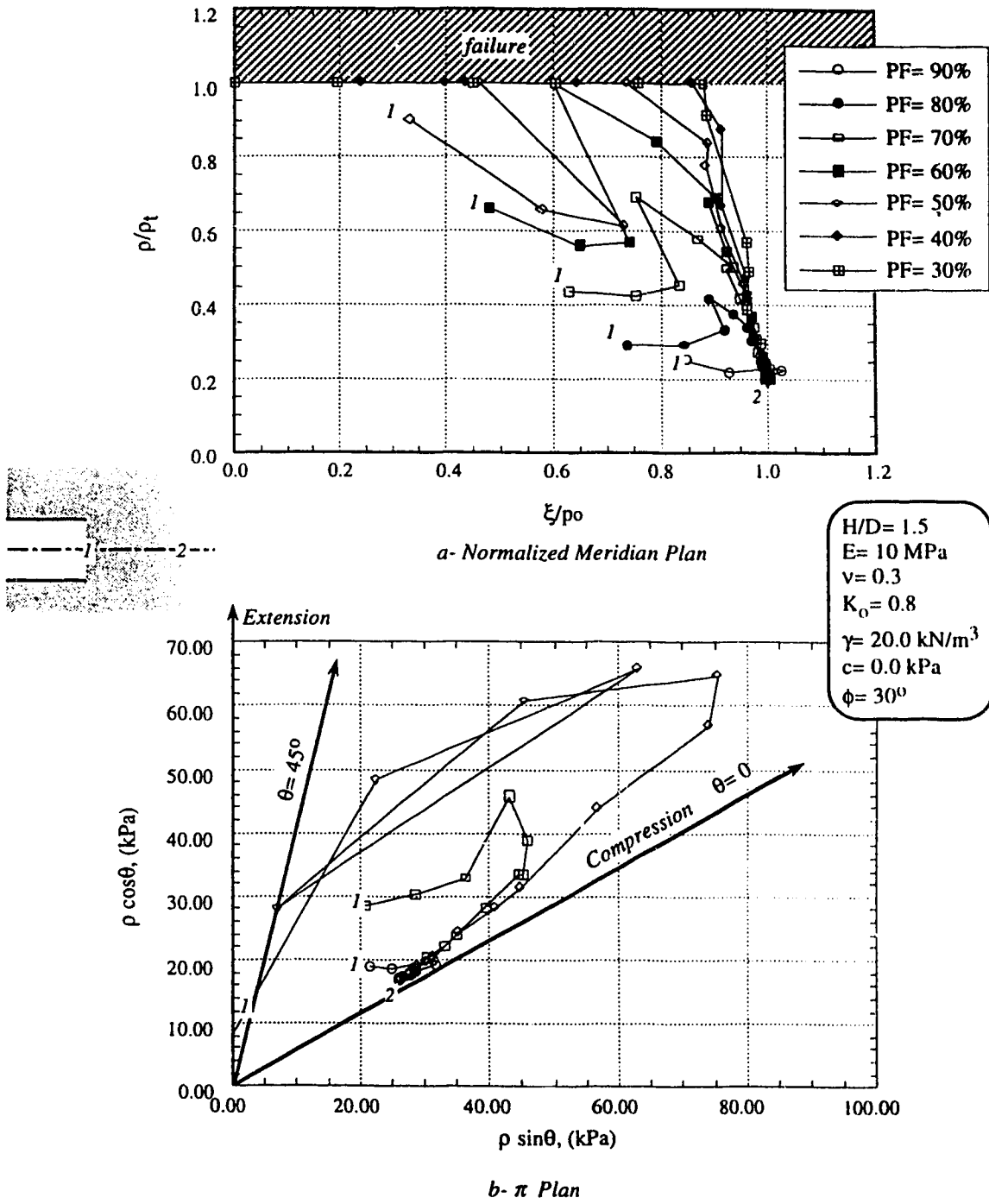


Figure 3.66: Stress Paths at the Centre Point of Tunnel Face during Gradual Stress Relief, Three Dimensional Analysis, $c = 0$ and $\phi = 30^\circ$.

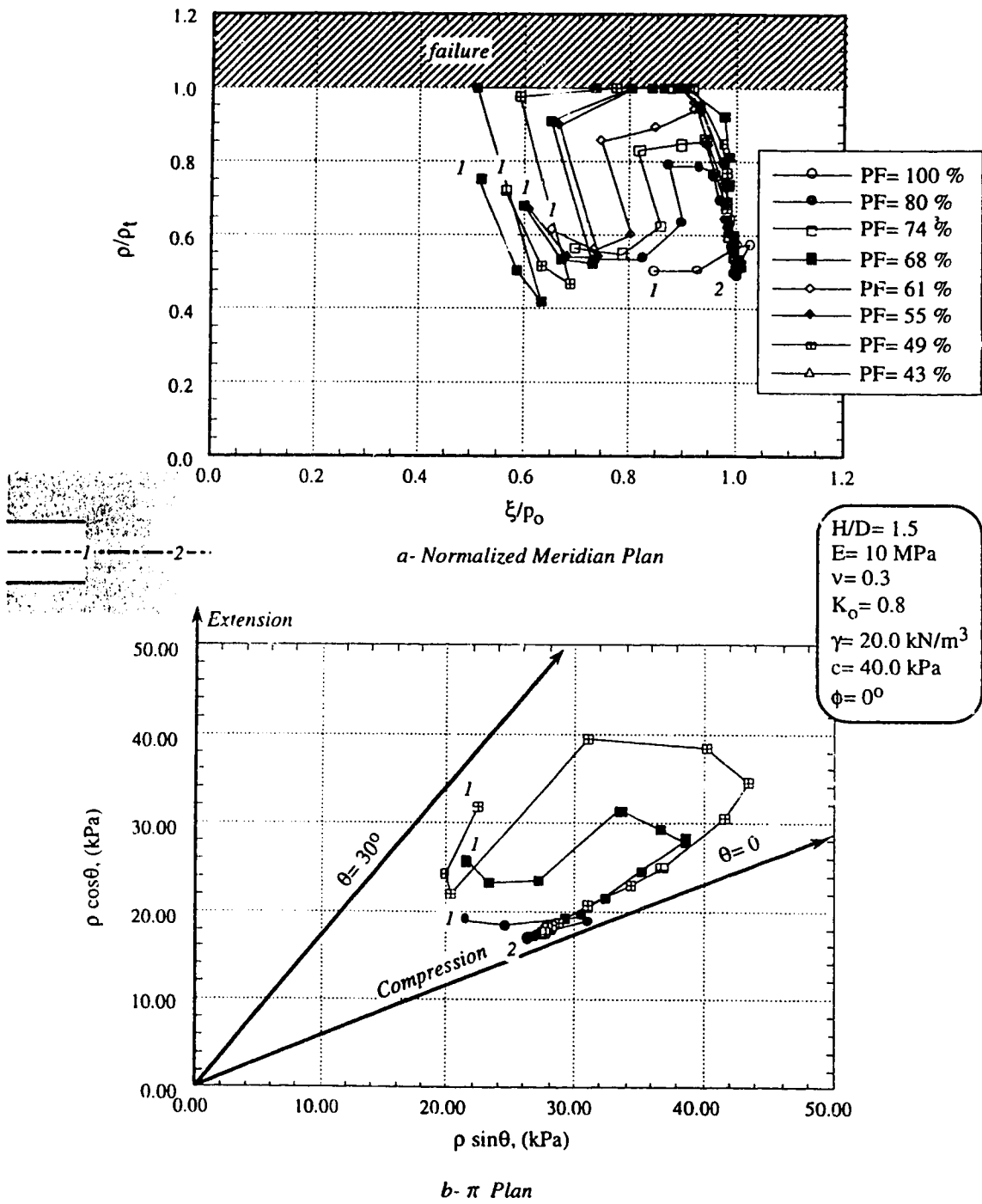


Figure 3.67: Stress Paths at the Centre Point of Tunnel Face during Gradual Stress Relief, Three Dimensional Analysis, $c = 40 \text{ kPa}$ and $\phi = 0^\circ$.

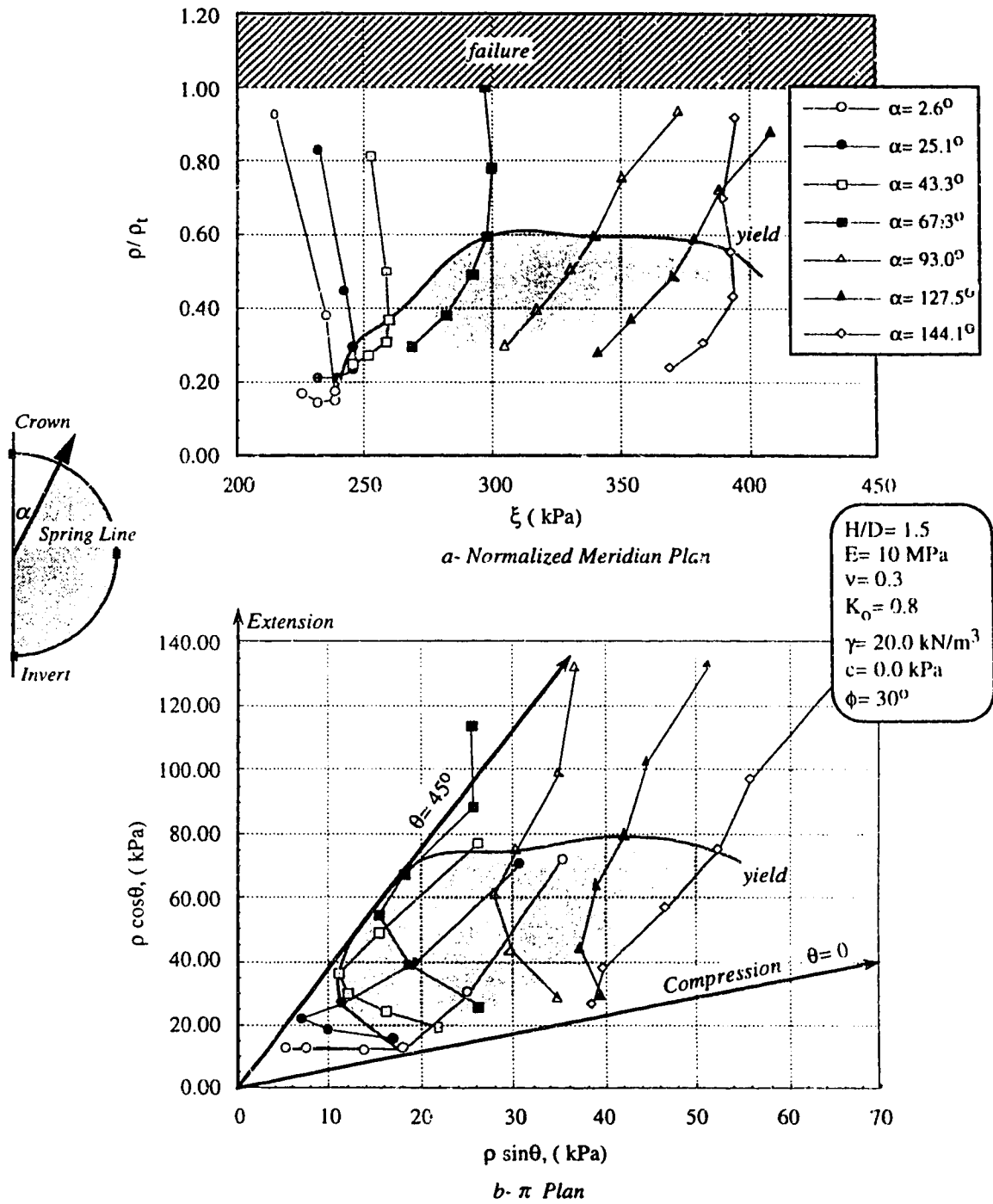


Figure 3.68: Stress Paths at various Points of Tunnel Circumference during Gradual Stress Relief at the Face, Three Dimensional Analysis, $c = 0$ and $\phi = 30^\circ$.

failure associated with a reduction in hydrostatic stress. The stress path in the remainder of the circumference, except for the lowest point, shows an increase in hydrostatic stress. The stress path at the π plan is characterized by a departure from the initial state of compression until the yield point is reached, then the departure reduces considerably. Also, the angle of similitude reaches a greater value than 45° . Figure 3.69 describes the stress path at the circumference in the case of cohesive soil. The meridian plane confirms that failure is initiated in the lower part of the face and an increase in hydrostatic stress takes place. Compared to the case of noncohesive soil, both changes in hydrostatic and the deviatoric stresses are very limited. The stress path in the π plan follows a path similar to that in the case of noncohesive soil with the maximum value of the angle of similitude being approximately 30° .

3.5.3.3 Confinement Ratio

The confinement ratio described in Equation 3.4 may be expressed for a three-dimensional case in a normalized form as CR' :

$$CR' = \frac{\delta p \varepsilon_3}{p \delta \varepsilon_3} \quad (3.21)$$

where:

ε_3 is the minor principal strain.

As the sign convention followed is positive for compression, the minor principal strain is at its maximum principal strain in the tensile direction. As the action imposed on the ground mass monotonically reduces the face pressure, ε_3 is always negative while the mean normal pressure, p , is always positive. Therefore, a positive value of CR' indicates that p increases because of the decrease of ε_3 which indicates a case of positive soil confinement which is discussed in Section 3.3.1.2 .

The normalized confinement ratio, CR' , is calculated at a section closest to the face (about 0.08 D from the face) following a scheme based on the finite difference principle:

$$CR' = \frac{((\varepsilon_3)_{i+1} - (\varepsilon_3)_i) \left(\frac{(p_{i+1} + p_i)}{2} \right)}{(p_{i+1} - p_i) \left(\frac{(\varepsilon_3)_{i+1} + (\varepsilon_3)_i}{2} \right)} \quad (3.22)$$

where:

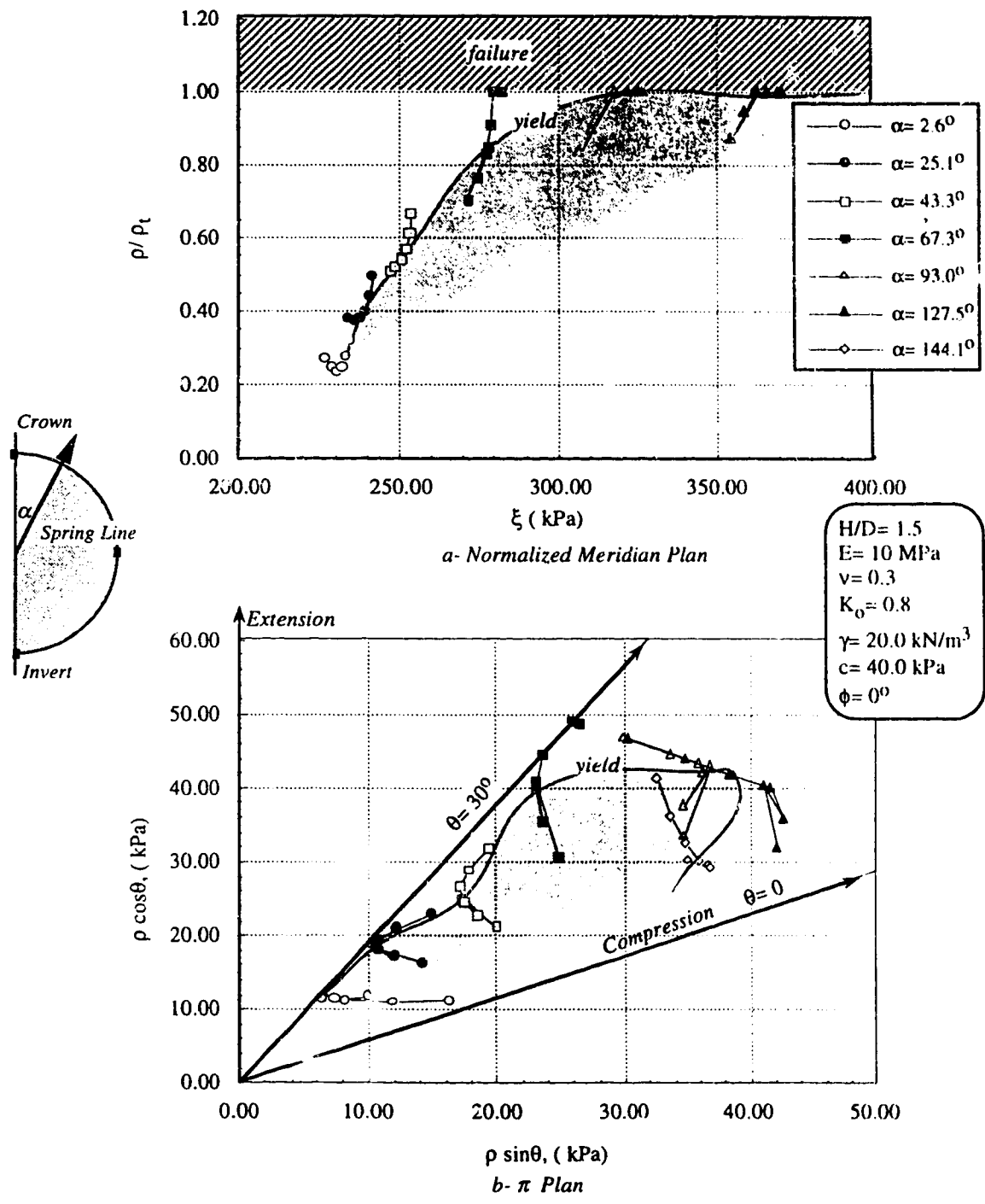


Figure 3.69: Stress Paths at various Points of Tunnel Circumference during Gradual Stress Relief at the Face, Three Dimensional Analysis, $c = 40.0 \text{ kPa}$ and $\phi = 0^\circ$.

p_i and $(\epsilon_3)_i$ are p and e_3 at step i , and
 p_{i+1} and $(\epsilon_3)_{i+1}$ are p and e_3 at step $i+1$.

Due to the approximation used in the calculation, the results presented may only be regarded as a general qualitative description of the stress-strain field in cohesive and noncohesive cases. Figure 3.70 shows contour lines of CR' for the noncohesive soil case between different loading steps. From the figure, a region of negative confinement takes place at the tunnel circumference separating the two zones of positive confinement inside the circumference and above the top quarter of it extending to the ground surface. As gradual stress release proceeds, the region of negative confinement progresses upward until it reaches the ground surface in failure. The existence of two separate blocks of positive confinement regions indicates that two different mechanisms are taking place. Inside the boundary of tunnel circumference, the increase of mean effective stress may be attributed to the applied face pressure. An arching mechanism is developed above the tunnel circumference which results in increasing the mean pressure at this zone. The upward propagation of the negative confinement zone is attributed to the displacement of the arching mechanism. The resemblance between the shape of the positive confinement area in Figure 3.70 ($PF=35\%$ which brings stress condition at the face close to the yield pressure) and the shape of the failure and yield zone described by the centrifuge test on sandy soil in Figure 3.9 should be noted. Figure 3.71 shows the contour lines of the normalized confinement ratio for a case of cohesive soil. Except at the early stage of stress release, the whole area above the tunnel is under negative confinement. This indicates that the ground mass above the tunnel circumference is supported mainly by the face pressure.

3.5.3.4 Design criterion

Processing of the results obtained from the axisymmetric analyses shows that the conventional Rankine expression for active earth pressure fits to a high degree the magnitudes of the required face pressure at yielding points with the introduction of the following two influence factors:

$$p_f = I_\phi (K_a \gamma H_o) - I_c (2c\sqrt{K_a}) \quad (3.23)$$

where:

I_ϕ is the influence factor of frictional resistance,
 I_c is the influence factor of cohesive resistance, and

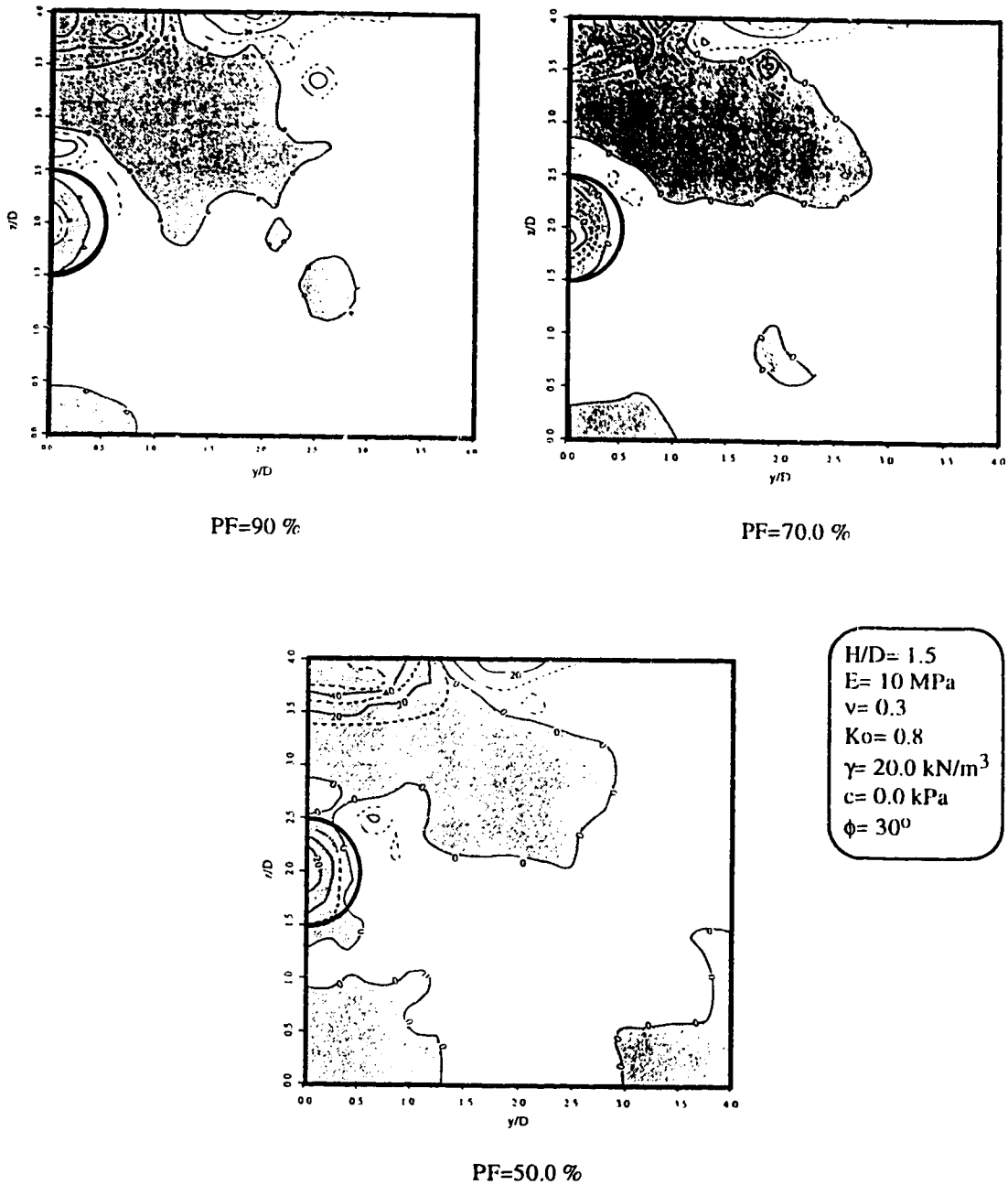
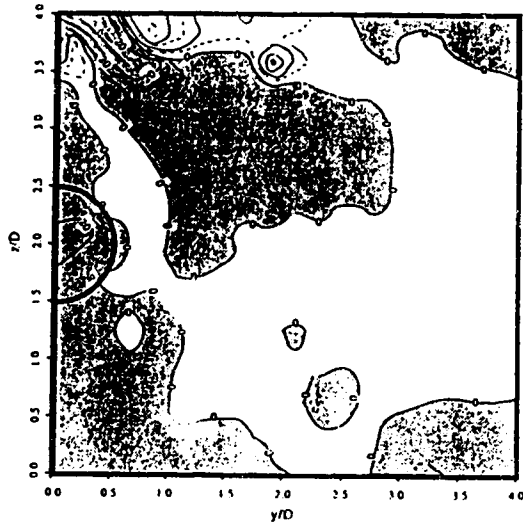
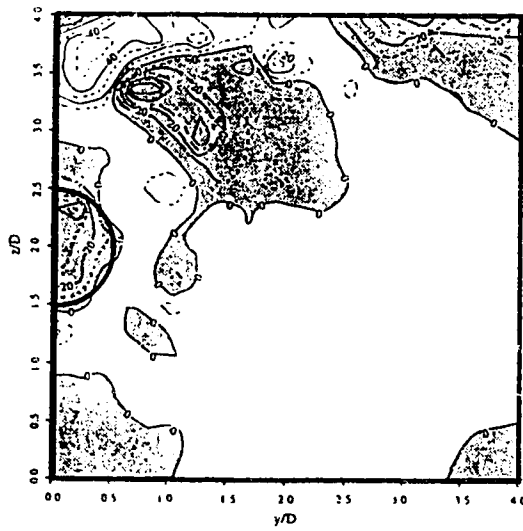


Figure 3.70: Contour Lines of the Nondimensional Confinement Ratio, CR', in percent, due to Stress Relief at the Face of a Tunnel, Axisymmetric Analysis, $c = 0$, $\phi = 30^\circ$.



PF=35.0%



PF=25.0 %

$H/D = 1.5$
 $E = 10 \text{ MPa}$
 $\nu = 0.3$
 $K_o = 0.8$
 $\gamma = 20.0 \text{ kN/m}^3$
 $c = 0.0 \text{ kPa}$
 $\phi = 30^\circ$

Figure 3.70: Contour Lines of the Nondimensional Confinement Ratio, CR' , in percent, due to Stress Relief at the Face of a Tunnel, Axisymmetric Analysis, $c = 0$, $\phi = 30^\circ$ (continued).

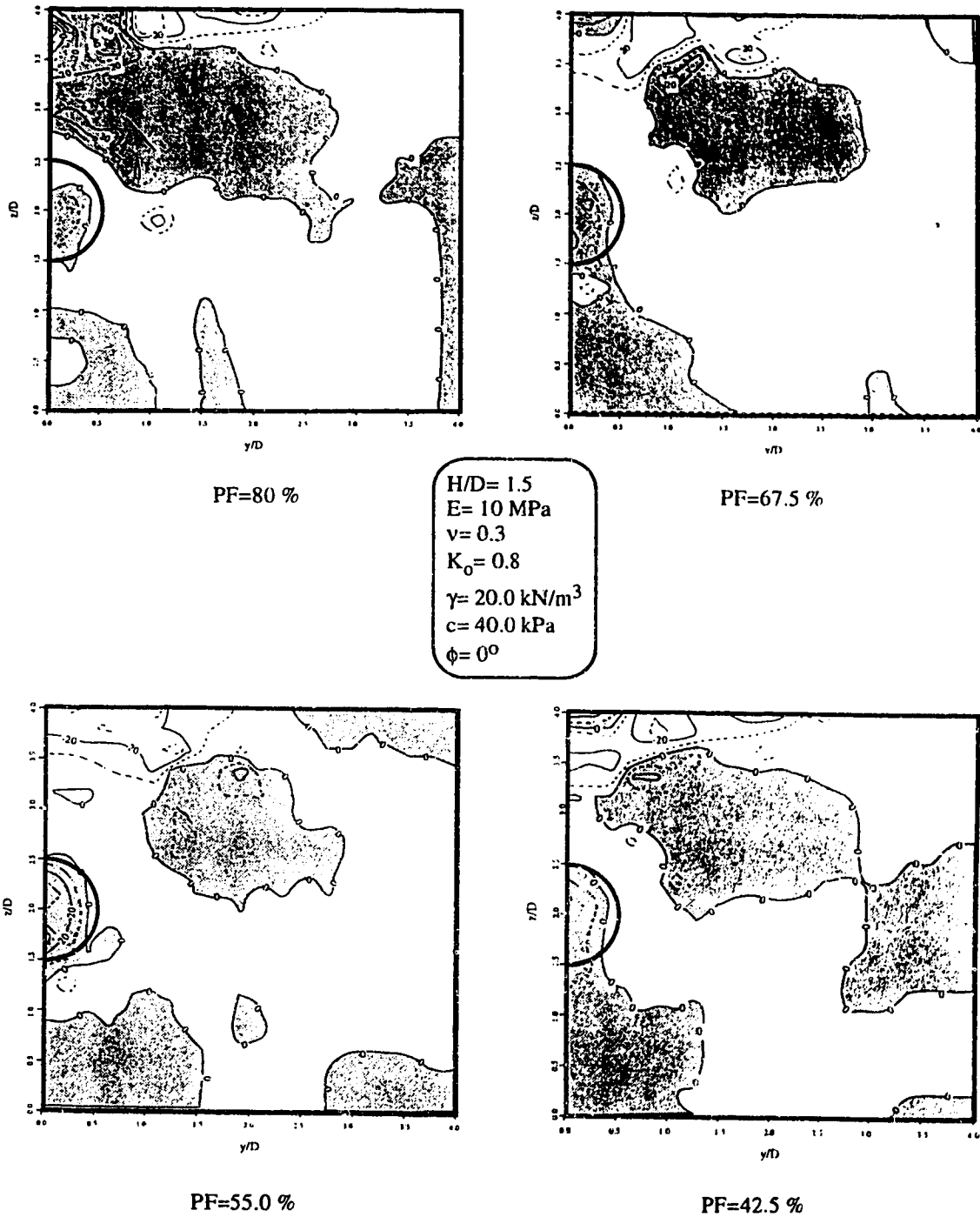


Figure 3.71: Contour Lines of the Nondimensional Confinement Ratio, CR' , in percent, due to Stress Relief at the Face of a Tunnel, Axisymmetric Analysis, $c = 40 \text{ kPa}$, $\phi = 0^\circ$.

Figures 3.72 through 3.74 show changes of I_ϕ for noncohesive material with respect to the angle of internal friction, the coefficient of lateral earth pressure at rest, and Poisson's ratio. The figures indicate that the angle of internal friction affects, to a high degree, the magnitude of the influence factor while K_o and ν have a lower impact on it. The scatter of the obtained values of I_ϕ may be referred to as the tolerance used in the iterative process and to the geometrical construction employed to define the value of critical face pressure. Figures 3.75 and 3.76 show the effect of the angle of internal friction on the influence factors for cohesive material. By inspection of Equation 3.23, for a purely cohesive soil ($K_a = 1.0$ and $I_\phi = 1.0$), I_c is equivalent to one half the stability ratio N (Equation 3.6). Figure 3.76 indicates that the critical stability ratio for this type of soil is equal to 4.0.

3.5.4 Verification of Results

The purpose of verifying the obtained results from the numerical study is to ensure that the suggested face pressure values are comparable to the safe pressure values obtained from the experimental results. At the same time, since the numerical study proposes a certain definition of face stability, it is necessary that case histories of pressurized shield tunnels be checked so that the proposed design criterion constitutes a lower-bound for face stability and that this lower-bound is acceptable and has been achieved in successful projects.

3.5.4.1 Comparison with Experimental results

Finite element results presented in the previous section are based on the assumption that critical face pressure is the yield pressure rather than the collapse pressure. Experimental determination of this pressure requires that accurate monitoring of the soil displacement be associated with a reliable estimation of the shear strength parameters. The purpose for comparison of the numerical and experimental works is to confirm that the calculated values predict to an acceptable degree of accuracy the actual yield pressure of the tested models.

In the case of cohesive soils, difficulties arise from the gradual increase in the slope of displacement at the face centerpoint with the face pressure. Therefore, the point at which the face displacement starts to follow an accelerating pattern with respect to the reduction of face pressure cannot be clearly identified. Meanwhile, the use of undrained strength as the basis of analysis has been, for a long time, the subject of discussion. Questions may be raised regarding whether the measured undrained cohesion is representative of the tested

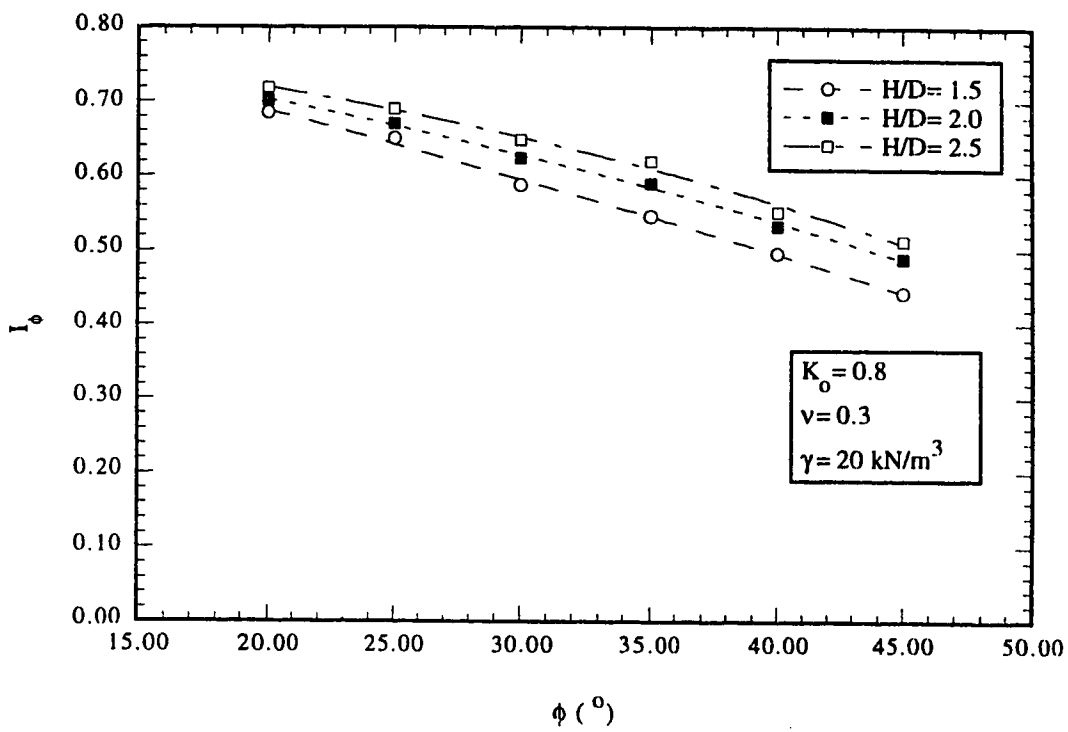


Figure 3.72: Influence Factor of Frictional Resistance, I_ϕ versus Angle of Internal Friction, ϕ , for various values of Depth Ratio, H/D .

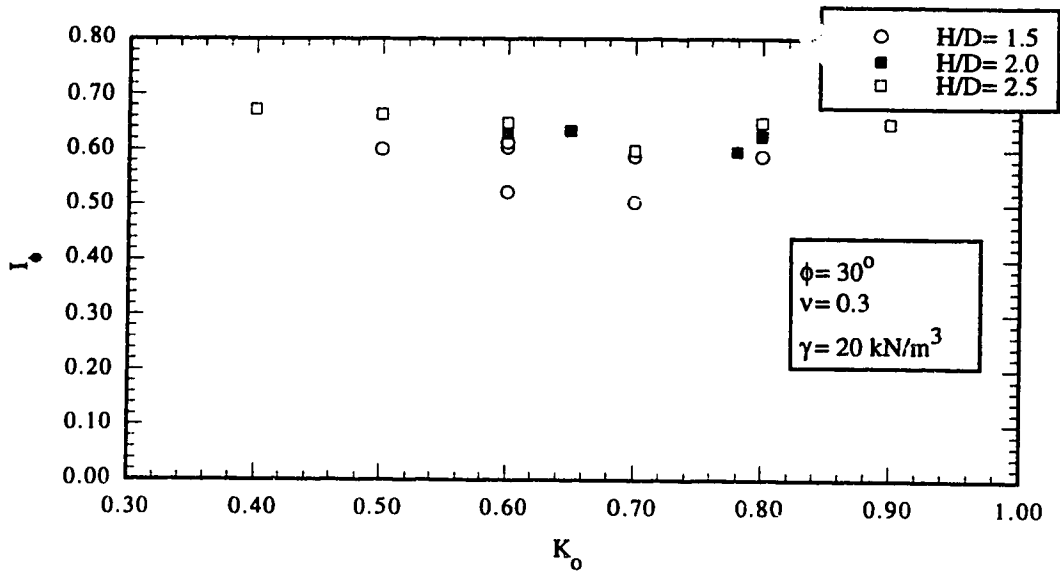


Figure 3.73: Influence Factor of Frictional Resistance, I_ϕ versus K_o for various values of Depth Ratio, H/D .

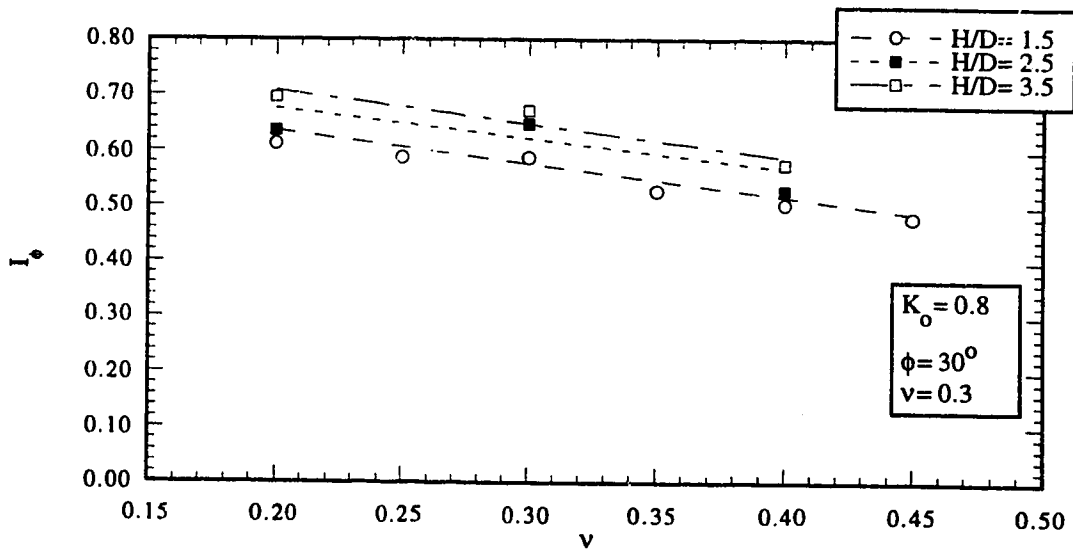


Figure 3.74: Influence Factor of Frictional Resistance, I_ϕ versus ν for various values of Depth Ratio, H/D .

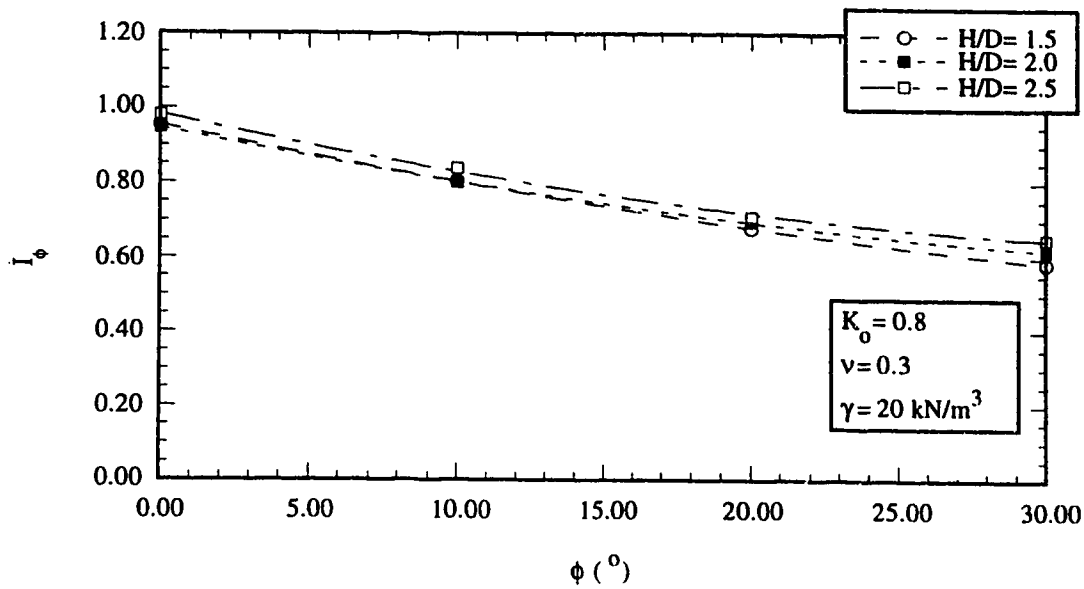


Figure 3.75: Influence Factor of Frictional Resistance, I_ϕ versus Angle of Internal Friction, ϕ , for various values of Depth Ratio, H/D for $c-\phi$ Soils.

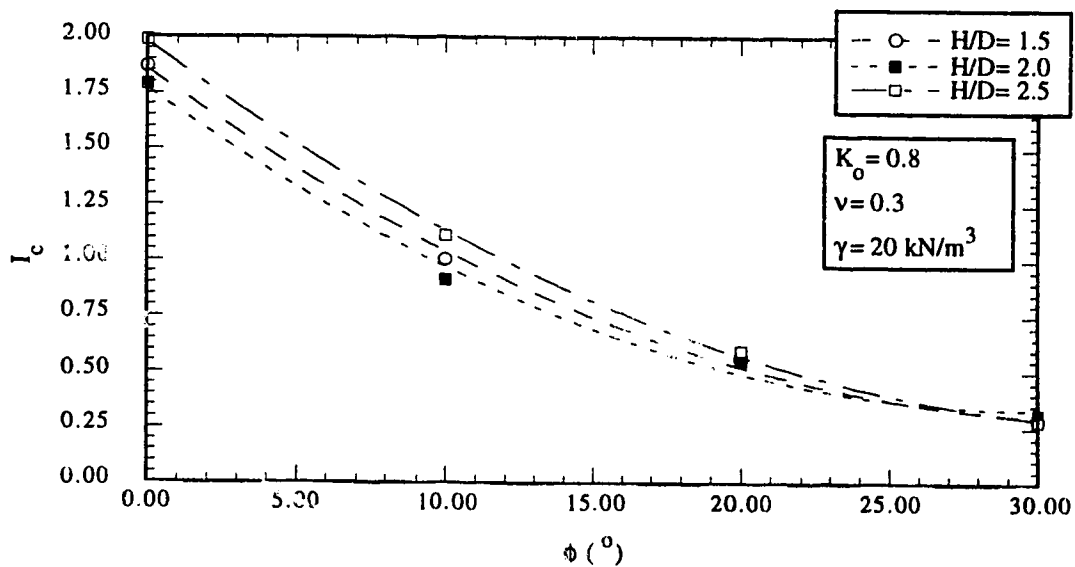


Figure 3.76: Influence Factor of Cohesive Resistance, I_c versus Angle of Internal Friction, ϕ , for various values of Depth Ratio, H/D for $c-\phi$ Soils.

soil, especially due to, the effects of loading rates and changes in pore water pressure. However, stability ratios measured in the experimental works are expected to be higher than those obtained from the numerical results. Referring to Figure 3.8, a stability ratio of 4 represents, in general, a lower-bound for the described experimental results.

Noncohesive soil tests permit the accurate detection of yield pressure as the sand follows two distinct deformation patterns before and after yielding. The major difficulty is the estimation of shear strength parameters as these parameters may be influenced by a number of factors such as changes in dry density, capillarity, homogeneity, and so forth. As stated by Chambon et al. (1991), the tested soil may be considered to be purely frictional sand of $\phi = 40^\circ$. Figure 3.77 shows a comparison between the experimental results presented by the authors and the performed numerical results. From the figures, numerical analyses results are close to the yield pressure while collapse pressures are of lower magnitude as is to be expected.

3.5.4.2 Comparison with Case Histories

The objective of comparing numerical results and actual case histories is to indicate that in practical experience there is reliance on the yield pressure as the minimum required pressure to support the face. As previously mentioned, methods of face support are of various types and each of these types generates a stress and a displacement field which is categorically different than those generated by the other types and some face support measure are used for purposes beyond the integrity of the face such as controlling water flow by compacting soil particles at the face, reducing surface settlement by pushing the ground forward as excavation proceeds, or improving the cutting performance of the machine.

In the case of a cohesive soil, Kirkland (1984) and Peck (1969) confirm that a stability ratio of 4 represents a general requirement in the use of compressive air to support a cohesive soil in an undrained case. As no reference was mentioned by the authors about the basis of this selection, it may be concluded that it is of an empirical nature. Tables 3.7 and 3.8 show case histories compiled from different projects using various types of face support for cohesive and noncohesive soils, respectively.

Belfast (Table 3.7: 1 and 2)- Glossop and Farmer (1979) present an investigation of the effect of compressed air in supporting the face of a tunnel excavated for sewerage purposes in Sydenham, Belfast, Ireland. Monitoring soil movement around the excavation gives a clear indication of a consolidation process resulting from applying and, then, releasing the supporting air pressure. Ground conditions around the excavation consist mainly of silt: dark gray organic clay. Values of undrained shear strength, measured

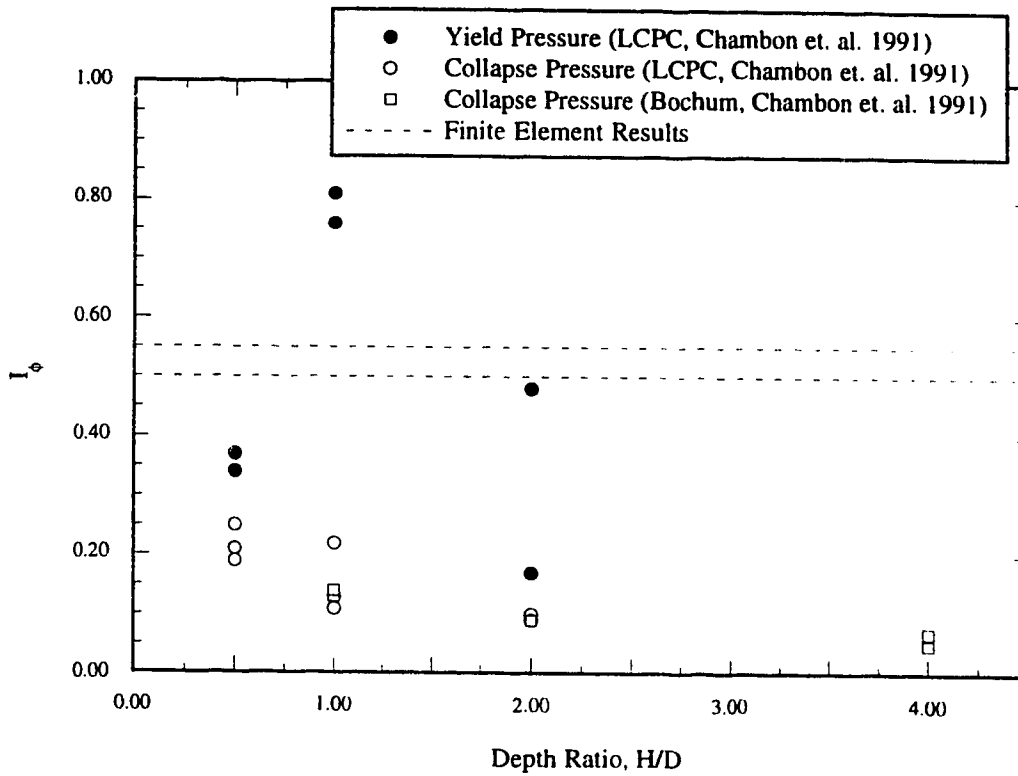


Figure 3.77: Comparison between Centrifuge Results and Finite Element Results for Non Cohesive Soils, $\phi = 40^\circ$.

using field vane and triaxial tests, and a typical ground stratigraphy are presented by the authors. During construction, initial applied air pressure is found to be unsatisfactory (Case 1) and was increased (Case 2). As the table shows, safe support of the excavation is only reached when the average I_c is lower than 2. The *actual factor of safety (FS)* is defined as the ratio between the actual face pressure and the face pressure required to support the face as calculated from Equation 3.23 and to neutralize groundwater pressure. An average factor of safety of 1.2 is expected to be satisfactory.

Cairo (Table 3.7: 3 and Table 3.8:1)- Greater Cairo wastewater project, as described by Safwat (1983), extends 33 km using bentonite slurry shields, earth pressure balanced shields, and compressed air shields. The compressed air method is used for a construction length of 2.5 km. In this part, the tunnel is excavated in mixed-face ground conditions consisting of a water bearing sandy layer overlying cohesive clayey silt soil. El-Nahhas et al. (1991) describes the results of a dewatering program applied in this part. Measurements include piezometric, and shallow and deep displacement readings. Pore water pressure rose in the cohesive material due to the use of compressed air which produced upward movement in front of the tunnel followed by downward displacement after the release of compressed air. The final settlement was found to be within tolerable settlement limits. If the tunnel section were considered totally imbedded in the cohesive layer, the actual I_c based on estimated undrained strength would be equal to 0.88. Using a value of $I_c = 2$, no face pressure is required to maintain the face stability and the only purpose of the compressed air is, then, to control seepage forces which results in factor of safety of 1.233. If the section were considered to be totally imbedded in sandy soil, then a factor of safety of less than unity would be obtained. It is believed that the stability of the lower half of the face is enhanced by the increase of shear strength of the sand because of capillary forces.

Grimsby (Table 3.7: 4 and 5 and Table 3.8: 3)- a sewer tunnel was constructed in Grimsby, as described by O'Reilly et al. (1991), from 1979 to 1981. Initially, the tunnel was excavated under free-air conditions. Ground conditions consisted of soft to very soft clay (marine warp) and in some instances a mixed face of marine warp and glacial till (stony clay). If the undrained cohesion of the marine warp is used to calculate I_c relative to the unsupported face, then a value exceeding 2 is obtained. Actually, the project suffered excessive settlement at the ground surface and there were major difficulties in maintaining face stability. Air pressure was then introduced and no further difficulties were encountered. Field monitoring described by the authors shows results at two sites A and B. Factors of safety calculated for the two sites are about 1.22. As pore water pressure measurements and effective shear strength parameters are provided, the influence factor for

#	Place	Time (yr)	Length (km)	H/D	c (kPa)	ϕ	I_c	I_ϕ	F.S.	Remarks	Reference
7.1	Belfast	74	C.A	1.32	8.8-10.6	0	1.86-2.24	-	0.91-1.08	Some Problems	1
7.2	Belfast 2	2.74	C.A	1.32	8.8-10.6	0	1.43-1.72	-	1.11-1.32	No Problems	1
7.3	Cairo(up)	5.15	C.A	2.23	60	0	0.88	-	1.233	Mixed Section	2, 3
7.4	Grimby(B)	79-81	C.A	2.21	18	0	1.23	-	1.23	No Problems, Total Stresses	4
7.5	Grimby(A)	79-81	C.A	2.21	26	0	1.87	-	1.21	Problems when $I_c = 2.66$	4
7.6	Mexico City	76-79	BSS	2.43	23-40	0	0.81-1.4	-	-	No Problems	5
7.7	Nagoya	3.85	BSS	5.71	40-45	0	0.26	-	-	Under sea	6
7.8	San Francisco	3.7	EPBS	2.46	27.4	0	(-)	-	3-4.23		7, 8, 9
7.9	Shanghai-up	4.33	EPBS	2	10	10.5	0.95	0.78	3.44	Upward movement	10
7.10	Shanghai-low	4.33	EPBS	2	3	12.5	0.82	0.76	3.29	Upward movement	10
7.11	Tokyo	3.73	BSS	10.27	78.48	0	1.325	-	1.36	No Problems	11
7.12	Unknown	4.13	D.K.	2.55	22.56	0	0.69-1.12	-	1.37		12

C.A.: Compressed Air

D.K.: D.K. Shield

References

- 1:Glossop and Farmer (1979)
2:El-Nahas et al. (1991)
3:Safwat (1983)
4:O'Reilly et al. (1991)
5:Schmitter et al. (1988)
6:Ohta et al. (1978)
7:Clough et al. (1983)
8:Clough et al. (1985)
9: Finno (1983)
10:Maidl et al. (1990)
11:Murakami et al. (1990)
12:Hagimoto and Kashima (1985)

Table 3.7: Assessment of Factors of Safety of some Case Histories in Cohesive Soils

#	Place	Time	D (m)	Method	Length (km)	H/D	c (kPa)	ϕ	I_c	I_ϕ	FS	Remarks	Reference
8.1	Cairo (low)		5.15	CA		2.23	-	30	-	0.55	0.88	Mixed Section	2, 3
8.2	Edmonton, SLRT	89-90	5	BSS	0.28	2	-	33.5	-	1.38	2.3	No Problems	13
8.3	Grimshy- Site B	79-81	3	CA		2.21	-	32	-	0.53- 1.41	1-2.66	No Problems	4
8.4	Hamamatsu		2	D.K.	0.526	3.85	-	40	-	0.33- 1	0.6- 1.82		12
8.5	Kaoshung-Taiwan		3.914	D.K.	1.224	1.98	-	30	-	1.06	3		12
8.6	Lyon_D	1984	6.5	BSS		1.87	-	33	-	0.59	1	Numerical Analysis	14, 15, 16, 17, 18, 19
8.7	Osaka	84-85	11.22	BSS		1.96	-	45	-	0.72- 1.68	1.44- 3.36		20
8.8	Rome	89	10.6	BSS	1.5	2.83	-	36	-	1.18	1.852	No Problems	21, 22, 23, 24, 25
8.9	Takaïdo		2.4	BSS	0.785	10.83	-	45	-	0.48	1		26
8.10	Unknown		5.22	D.K.	0.499	3.54	-	36	-		0.63- 2.72		12
8.11	Yotsugi		2.4	BSS	0.729	2.63	-	20	-	1.39	2		26

C.A.: Compressed Air
D.K.: D.K. Shield

References

- 2:El-Nahas et al. (1991)
3:Safwat (1983)
4:O'Reilly et al. (1991)
12:Hagimoto and Kashima (1985)
13:Eisenstein and Ezzeldine (1992:2)
14:Ferrand and Bouyat (1985)
15:Bouyat et al. (1985)
16:Ferrand and Morcrette (1988)
17:Mohkam and Bouyat (1989)
18:Morcrette and Bouyat (1986)
19:Chaffois et al. (1988)
20:Hashimoto et al. (1988)
21:Anheuser (1985)
22:Becker (1985)
23:Casisnis et al. (1985)
24:Capellari and Ottaviani (1982)
25:Pandolfo (1986)
26:Miki et al. (1977)

Table 3.8: Assessment of Factors of Safety of some Case Histories in Frictional Soils

frictional material, I_{ϕ} , is verified at Site B (Table 3.8: 3). The groundwater table varies between 1.6 to 3.8 which corresponds to a factor safety ranging between 1.0 and 2.66.

Mexico City (Table 3.7: 6)- a sewer tunnel of 5.3 km was constructed in Mexico City using a BSS. As described by Schmitter (1988), soil conditions consisted of highly compressible clay. The face pressure is almost equal to the initial pore water pressure at the tunnel axis. Considering total stresses, I_c has a value between 0.81 and 1.4 because of variations in shear strength. The effective stress calculations showed that for $I_c = 2.0$, no face pressure is required to support the face and the only purpose of the slurry pressure is to neutralize water pressure.

Nagoya (Table 3.7: 7)- the construction of a water supply tunnel under Nagoya Harbor, Japan, is designed to pass under the sea bed. Soil conditions, as described by Ohta (1978) at the face include in many places in the project highly permeable layers. As the tunnel is located considerably below the sea level, high bentonite slurry pressure is used to neutralize hydrostatic pressure. In spite of the high variation of shear strength along the tunnel trajectory the calculated pressure required for soil support has always been very small compared to the total face pressure.

San Francisco (Table 3.7: 8)- the first application of EPBS was used in the construction of the San Francisco clean water project (N2). A description of the project and numerical analysis of the obtained data is found in Clough et al. (1983 and 1986) and Finno (1983). The entire face was immersed in a normally consolidated clayey soil known locally as the Bay Mud. A number of wooden piles had to be cut as the excavation proceeds. As mentioned before, face pressure of the EPBS is usually higher than the initial horizontal pressure. Negative values of I_c are calculated for this project as the face pressure is higher than the initial horizontal pressure. The value of the factor of safety was higher than 3.0 and reached 4.23 at the section where the face pressure had to be increased to cut the wooden piles.

Shanghai (Table 3.7: 9 and 10)- a sewage tunnel was driven in Shanghai, China through soft and saturated soil. Soil conditions as described by Maidl et al. (1990) indicate that the tunnel section consisted of two layers of silty clay divided by a thin layer of silty sand passing almost at the tunnel axis. The average applied face force is calculated by subtracting the friction and adhesion forces along the shield skin from the applied force from the hydraulic jacks connecting the shield to the lining system. Face pressure is calculated by dividing the net face force by the shield cross-section. As in the previous case, high value of factor of safety is obtained. The values of I_c and I_{ϕ} presented in Table 3.7 are calculated assuming that fully shearing resistance is mobilized.

Tokyo (Table 3.7: 11)- a bentonite slurry shield machine was used in the

construction of a Tokyo cable tunnel which passed under two rivers. As described by Murakami (1990), the tunnel has a high depth ratio and mainly passes through a diluvium stratum of stiff clay. Total stress analysis resulted in a value of I_c of 1.325 and a factor of safety of 1.36.

D.K. Shield (Table 3.7: 12)- D.K. Shields may be considered a transition technique between the EPBS and the bentonite slurry shield. Here, the face stability is not directly achieved through shield jacking at the liner as in the case of EPBS. Also, the mix of mud with the spoil provides a better distribution for the support pressure inside the bulkhead and, thus, at the face. Hagimoto and Kashima (1985) show a case where the D.K. shield was constructed in a cohesive soil with a factor of safety considerably less than that of the EPBS.

Edmonton LRT (Table 3.8: 2)- the extension of Edmonton Light Rail Transit system has included the construction of a tunnel using the Hydroshield; a bentonite slurry machine based on German technology. Soil conditions at the tunnel section, as described by Eisenstein and Ezzeldine (1992:a) consist of a sandy postglacial outwash and gravel deposits with a very high degree of heterogeneity in one part of the project, while in the other part of the project the lower half of the cross-section passes through the Edmonton formation, a Cretaceous bedrock. The groundwater table is below the tunnel level. The function of the slurry pressure, therefore included, besides face support, the formation of a permanent and reliable cake thickness and mucking of the excavation spoil. A factor of safety of 2.3 is calculated.

Hamamatsu (Table 3.8: 4, 5 and 10)- the D.K. Shield described above by Hagimoto and Kashima (1985) was used in noncohesive soils in Hamamatsu, Japan, and in Kaoshung, Taiwan. The presented information shows a wide range of values for the factor of safety which may be attributed to the specific working conditions at these projects.

Lyon-D (Table 3.8: 6)- the construction of the Lyon metro Line D is described by Ferrand and Bouyat (1985) and Ferrand and Morcrette(1988) and Morcrette and Bouyat (1990). The tunnel trajectory was constructed in 1984 under the Rhône and the Saône rivers in sandy gravelly soils. Due to the importance of the project, a number of analyses were initiated in different domains. Bouyat et al. (1985) experimentally investigate the interaction between the slurry and the sandy soil, and Chaffois et al. (1988) used a three-dimensional analysis to determine the yield pressure. The resultant pressure compares very well with the current analysis.

Osaka (Table 3.8: 7)- a large diameter tunnel was constructed in Osaka City, Japan, for stormwater management using the bentonite slurry shield. The project which is described by Hashimoto et al. (1988) passes through a predominantly very hard diluvium

sand and gravel with a Standard Penetration Number exceeding 50. In some parts of the project, ground freezing was used to insure the face stability, and therefore, low slurry pressure was needed. In the part where no additional face protection was used, assuming an angle of internal friction $\phi = 40^\circ$, a value of I_ϕ very close to that suggested in Figure 3.72 is obtained.

Rome(Table 3.8: 8)- a large diameter railway tunnel was constructed in Rome, Italy. Excavation works as described by Casinis et al. (1985) and Pandolfo (1986) were carried out using the Hydroschild in a competent hard clay in a part of the project and in silty sand layers in other parts, and the entire project was constructed under the groundwater table. Face pressure was found necessary for the part constructed in the sandy layer and a factor of safety of 1.852 was calculated.

Takaido and Yotsui(Table 3.8: 9)- Miki et al. (1977) presents a description of the development of slurry shield technology in Japan and shows that the method of calculation of the support face pressure in cohesionless soils is close to Equation 3.23, except that they use K_a instead of K_a and an empirical factor instead of I_ϕ . The authors justified their method of calculation from three case histories of projects in Japan: Yotsugi, Ushiku, and Takaido. The three projects were carried out in sandy soils with, respectively, low, variable, and high Standard Penetration Test Numbers at the excavated sections. While it is difficult to estimate a reliable value for the angle of internal friction of the Ushiku project, $\phi = 20^\circ$ and $\phi = 45^\circ$ may be considered a realistic estimation for the Yotsugi and Takaido projects, respectively, which yields factors of safety as shown in Table 3.8.

3.6 The Effect of the Initial Stress Field

The preceding analysis shows the decisive effect of shear strength parameters on the stability of the face. Field conditions, however, do not allow the excavation to follow the idealized field conditions. An interesting case history has been examined and analyzed and has showed the importance of initial ground stress field on the face stability of the excavated tunnel, as well as, on the safety of the neighbouring structures.

3.6.1 The St. Clair River Project

A new tunnel is under construction to replace the old St. Clair tunnel connecting Sarnia (Ontario, Canada) to Port Huron (Michigan, USA). The EPBS method is selected to build a 8.4 m internal diameter tunnel. The tunnel trajectory is 1824 m of which 600 m is below the St. Clair River bed. Details of the project are described in a series of papers among which are Charalambu et al. (1993), Busbridge et al. (1993), and Kramer et al. (1993).

3.6.1.2 Ground Conditions

A review has been carried out of the geotechnical information for the St. Clair Till at the shaft location. Most of the geotechnical information is contained in the report by Golder Associates (1992), date August and November 1992. The St. Clair till is described as a silty clay with lenses of sand and gravel and with occasional silt to clayey silt seams. The clay is normally consolidated due to desiccation and ground water fluctuations in the upper 10 m or so. Below a depth of about 10 m, the clay is essentially normally consolidated.

Golder Associates (1992) reported an extensive laboratory and field tests which indicated that the undrained shear strength, s_u , is constant at the top 10 m and is equal to about 60 kPa. Below this level, s_u increases with the effective overburden pressure with a ratio of about 0.22. The field vane tests indicate a sensitivity of between 1.5 to 2.0.

Based on the given information and the previous experience in similar clays, the undrained modulus of deformation could be reasonably estimated to vary between 100 to 800 s_u and the coefficient of the in-situ at-rest lateral earth pressure, K_0 , is 0.55.

3.6.1.3 Construction Details

As described by Harrison et al. (1994), extreme weather conditions required the increase of the face pressure applied by the tunnelling machine. At Chainage 10+500, a check of the main bearing lubrication filters at the cutterhead revealed that the debris was entering the lubricating system. Further investigations indicated that the sealing system indicated that the seals of the cutterhead had been broached. It was decided, therefore to replace the cutterhead. This required the sinking of a shaft and the advance of the excavation, virtually without face support, toward the shaft position where it was possible to effect the needed replacements.

The shaft sinking scheme included a ring of interlocking concrete piles of 1.2 m diameter to provide the support around a pit of 10.5 x 4 m and at least 30 m deep. The piles were constructed using uncased augured excavation. At a certain point, it was found that it was impossible to advance the pile any further and that the problem is more critical at the region close to the excavated tunnel.

3.6.2 Numerical Analysis

The objective of the analysis is to estimate, using a numerical model the extent of the yield zone ahead of the tunnel face due to the effect of stress relief related to the excavation process. A number of points has to be taken into consideration in the selection of the type of the analysis:

- (1) the stress field and the boundary conditions of the problem require the

- numerical simulation to be carried out in three dimensions. Such type of analysis enables the accurate representation of the tunnel dimensions and, at the same time, allows the introduction of the effect of the gravitational stress field and the free boundary surface at the ground surface;
- (2) the presence of the shield and the lining system and it provides a protection to the cylindrical boundary of the tunnel shaft;
 - (3) the soil behaviour is considered undrained; and
 - (4) the propagation of the yield zone is dependent on the soil strength. Therefore, an elasto-plastic constitutive model has to be employed in the analysis.

The finite element method is chosen in the numerical simulation as it has been well recognized in the research and practical fields of geotechnical engineering. The finite element program, SAGE™, developed in the University of Alberta, is selected to be used in the computation as it permits the modeling of nonlinear material behaviour in three dimensional problems. The extensive use of the program in the University of Alberta throughout the recent years has proven that program is reliable and accurate. The calculations are carried out using an IBM RISC System/6000™. The system provides the computing speed and the storage capacity required to perform the analysis within reasonable ranges of computational time and accuracy.

3.6.2.1 Ground Model

Ground conditions are selected based on the official documentation of the project at Chainage 10+500. Figure 3.78 shows the profile of undrained shear strength, s_u , values adopted in the analysis based on the profile used in the tunnel design. The modulus of deformation of the soil, E , is believed to be related to the undrained shear strength of the ground and the ratio E/s_u is expected to vary between 500 and 1000. Analyses were carried out using the two extreme ratios shows that the effect of E/s_u on the propagation of the yield zone ahead of the tunnel face is minimal. A Poisson's ratio of 0.49 is selected for the soil elements. This represents a case of incompressible material due to undrained loading. Reasonable values of the deformation parameters of the simulated liner elements are adopted taking into consideration the effect of the joints between the liner segments.

3.6.2.2 Computational Work

The numerical model is based on the three dimensional finite element mesh shown Figures 3.79 and 3.80. The mesh is comprised of 1106 elements of twenty nodes each which bring the global number of nodes to 5542 and the size of the stiffness matrix exceeding 11 million. The boundary conditions are selected to represent a symmetrical

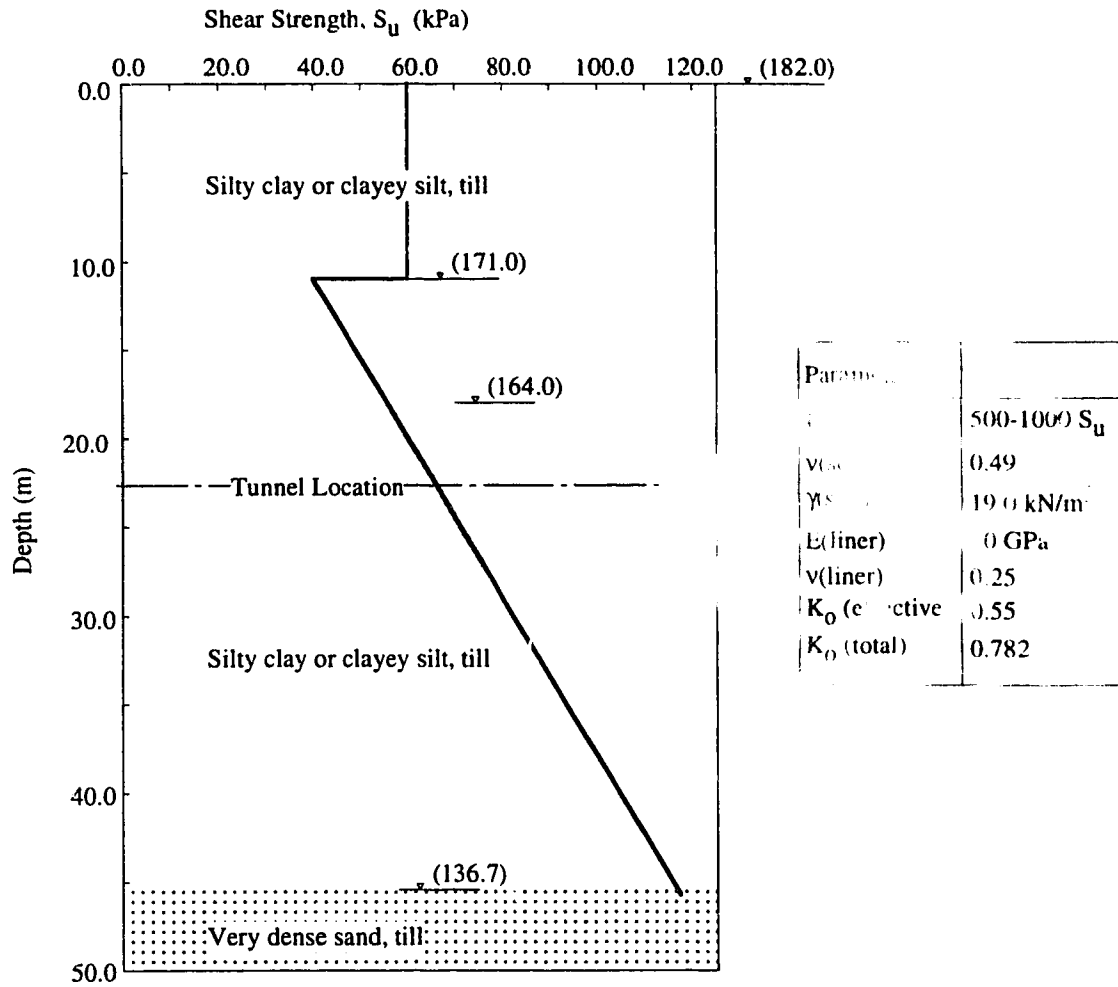


Figure 3.78: Parameters used in the Finite Element Analysis of the St. Clair River Tunnel

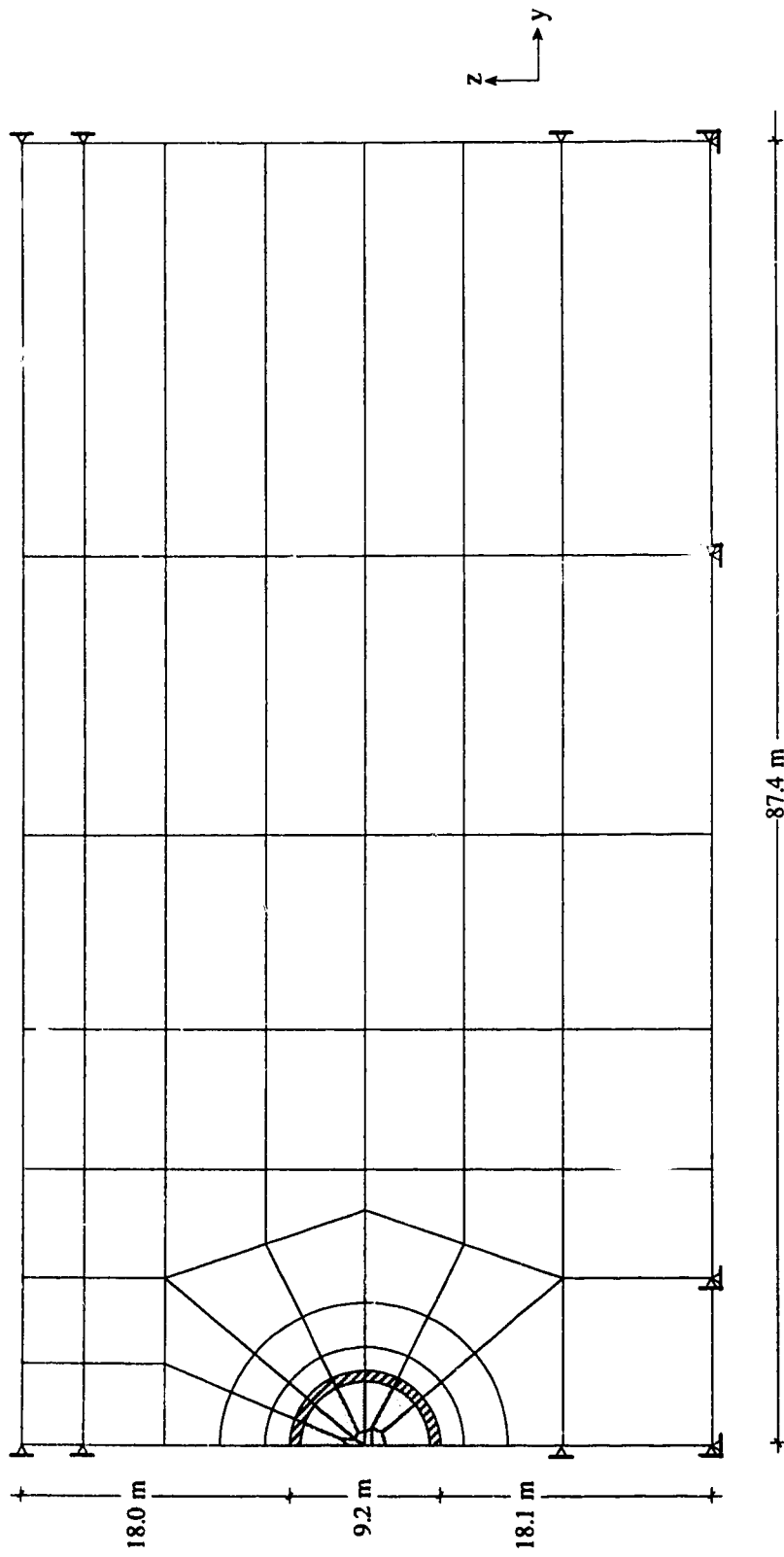


Figure 3.79: Transversal Section of the 3-D Mesh used in the Analysis of the St. Clair River Tunnel

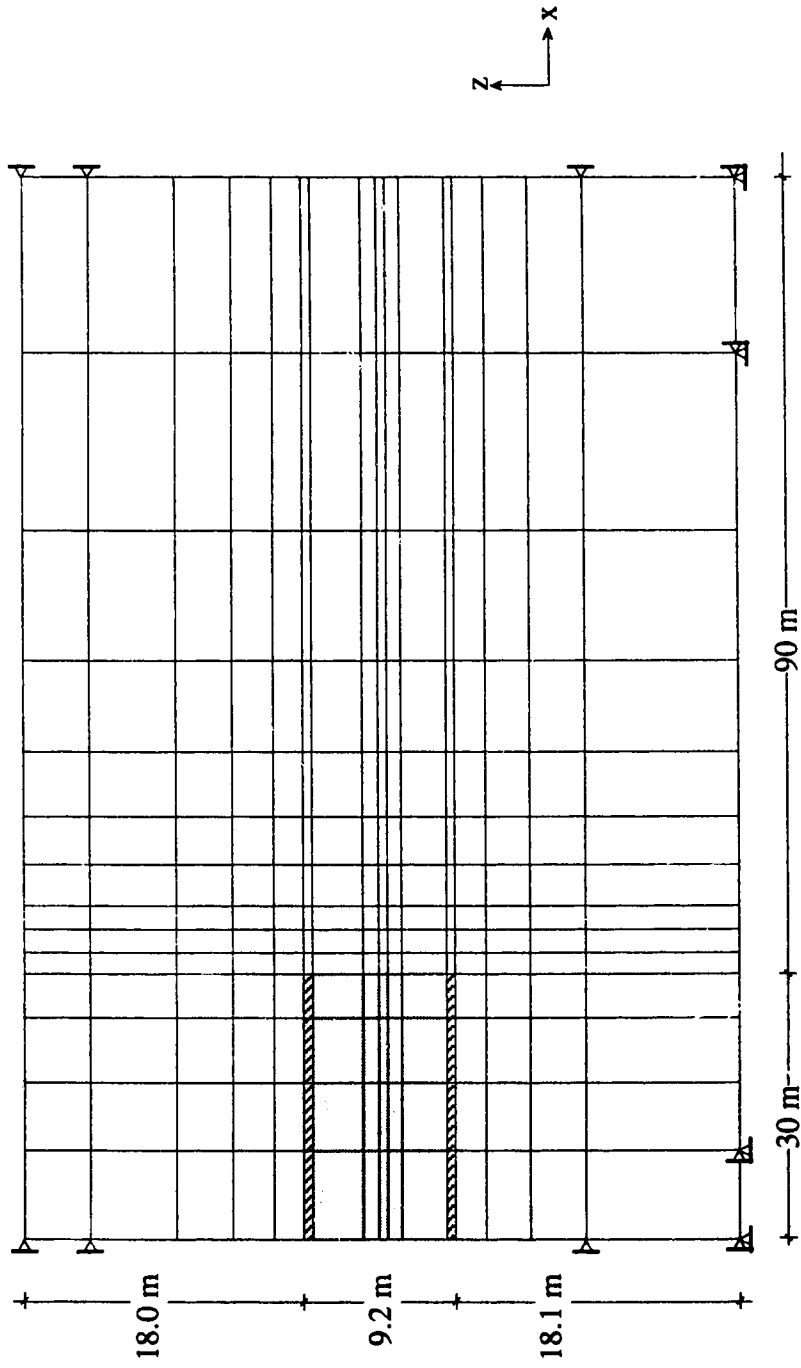


Figure 3.80: Longitudinal Cross Section of the 3-D Mesh used in the Analysis of the St. Clair River Tunnel

tunnel. As shown in Figure 3.79, at the plane of symmetry, only the horizontal displacement in the y -direction is restricted. Horizontal displacement in the x - and y -direction are restricted at remote vertical boundary plane. It has been verified that such condition does not interfere with the gravitational stress field. In the longitudinal cross section (Figure 3.80), horizontal displacements in the x -direction are restricted at the vertical boundary plane behind the tunnel face while the horizontal displacement in x - and y -directions are restricted at the boundary ahead of the face. Displacements in all directions at the lower plane are restricted to represent a rigid boundary and the upper plane is free to represent the ground surface.

The Tresca elasto-plastic model is selected to represent soil material. Two stress-strain curves are investigated: (1) no strain softening is allowed, thus, the peak shear strength is equal to the residual shear strength, (2) strain softening results in a brittle drop of the post-peak shear strength to one half the peak shear strength. Liner elements are elastic.

The first step in the numerical simulation consists in inducing the initial gravitational stress field. All the elements in the mesh are assigned elastic properties corresponding to the soil gravity and the initial coefficient of lateral pressure at rest (total). The second step consists of reassigning actual elasto-plastic properties to the soil elements, excavating the elements within the tunnel boundaries and reactivating elements representing the liner. The excavation process is simulated by removing the excavated elements from the assembled stiffness matrix and applying at the excavation boundaries traction forces corresponding to stress released during excavation. The magnitude of the traction forces is calculated such that the equilibrium of forces of the system is maintained. As such, excavation forces are acting on the liner elements and at the face of the excavation. In order to simulate a case of no stress release at this step, traction forces equal to the initial stresses are reapplied at the face. The face pressure ratio (PF) is defined as the ratio between the pressure applied at the face and the initial lateral earth pressure at the level of the tunnel axis. At this step, PF is equal to 100%. During the third step and the steps following it, PF is gradually reduced until it reaches 0% which corresponds to a case of complete stress release or an excavation using an open face shield.

Table 3.9 shows the computational work effected for the two cases corresponding to the two adopted stress-strain curves. The number of iterations performed in each step varies and may reach a maximum number of 12. Iteration tolerance in displacement error, in stress calculation, and in principal stresses are taken to be the same and equal to 0.001. An average step requires about two hours of computer time and about 12 M Bytes of storage capacity for the output files. A storage capacity of 50 M Bytes is required at the

Analysis 1: No Strain Softening

Step	PF	Remarks
1	100	Elastic: apply initial conditions
2	100	Elasto-plastic: excavate the tunnel and apply 100% PF
3	90	Elasto-plastic
4	80	Elasto-plastic
5	70	Elasto-plastic
6	60	Elasto-plastic
7	50	Elasto-plastic
8	45	Elasto-plastic
9	42.5	Elasto-plastic
10	40	Elasto-plastic
11	37.5	Elasto-plastic
12	35	Elasto-plastic
13	32.5	Elasto-plastic
14	31.25	Elasto-plastic
15	30	Elasto-plastic
16	27.5	Elasto-plastic
17	25	Elasto-plastic
18	20	Elasto-plastic
19	15	Elasto-plastic
20	10	Elasto-plastic
21	5	Elasto-plastic
22	0	Elasto-plastic

Analysis 2: Strain Softening-
Su (residual)= 0.5 Su Peak

Step	PF	Remarks
1		Elastic: apply initial conditions
2	100	Elasto-plastic: excavate the tunnel and apply 100% PF
3	90	Elasto-plastic
4	80	Elasto-plastic
5	70	Elasto-plastic
6	60	Elasto-plastic
7	50	Elasto-plastic
8	40	Elasto-plastic
9	30	Elasto-plastic
10	20	Elasto-plastic
11	10	Elasto-plastic
12	0	Elasto-plastic

Table 3.9: Steps Performed at the 3-D Analysis of St. Clair River Tunnel

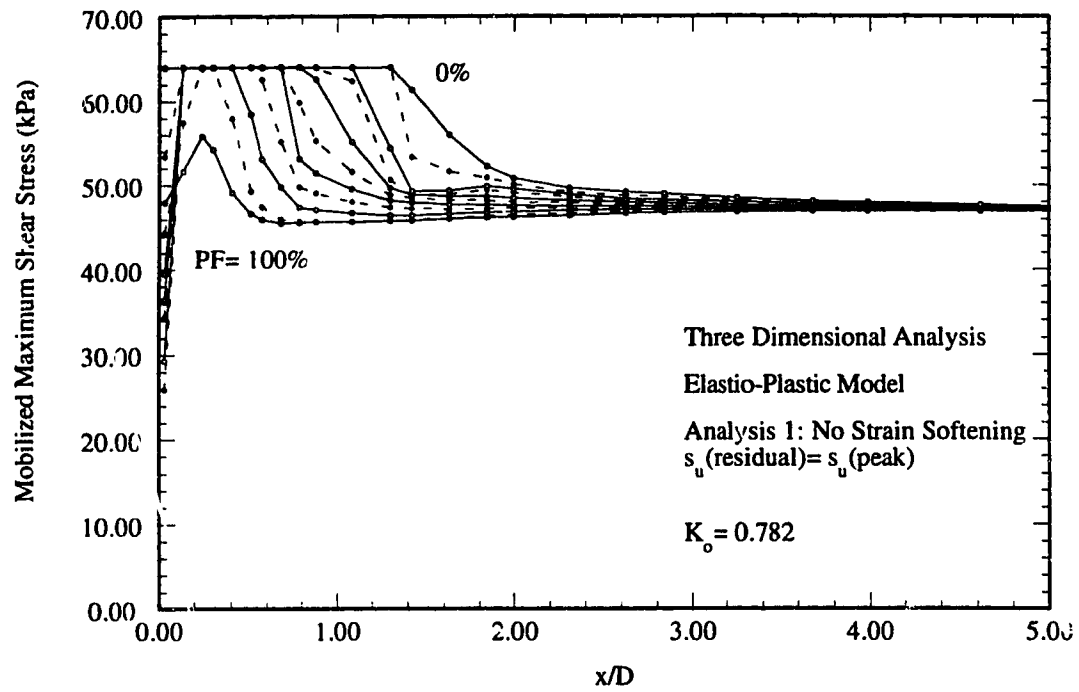


Figure 3.81: Mobilized Maximum Shear Stress versus the Distance ahead of the Tunnel Face for various Face Pressure Ratios

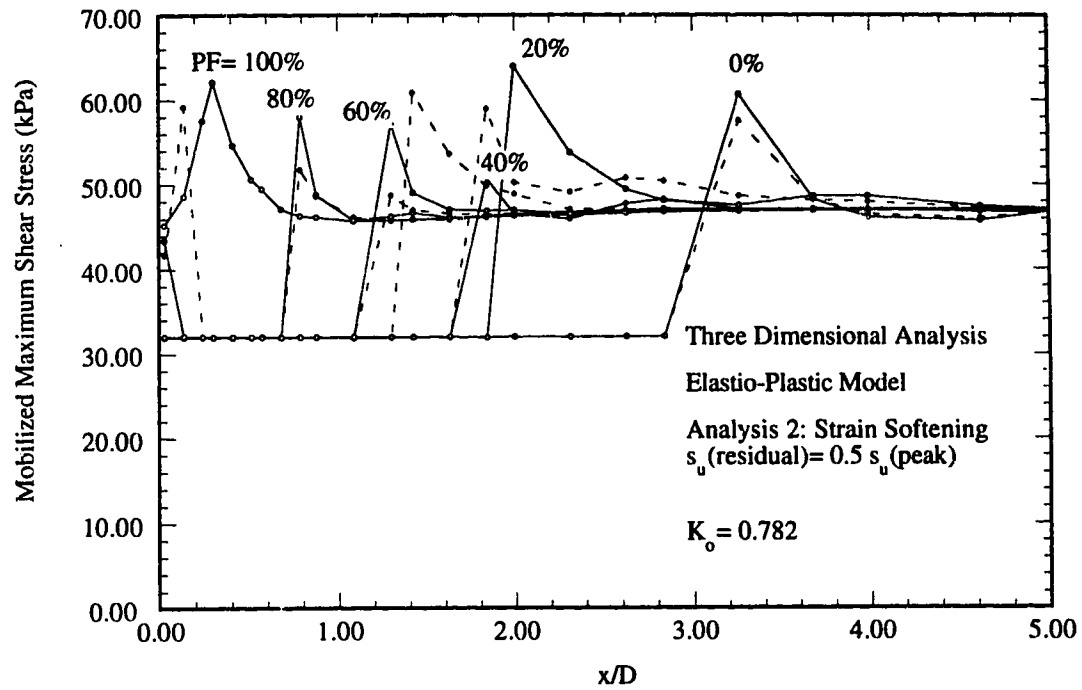


Figure 3.82: Mobilized Maximum Shear Stress versus the Distance ahead of the Tunnel Face for various Face Pressure Ratios (Strain Softening Case)

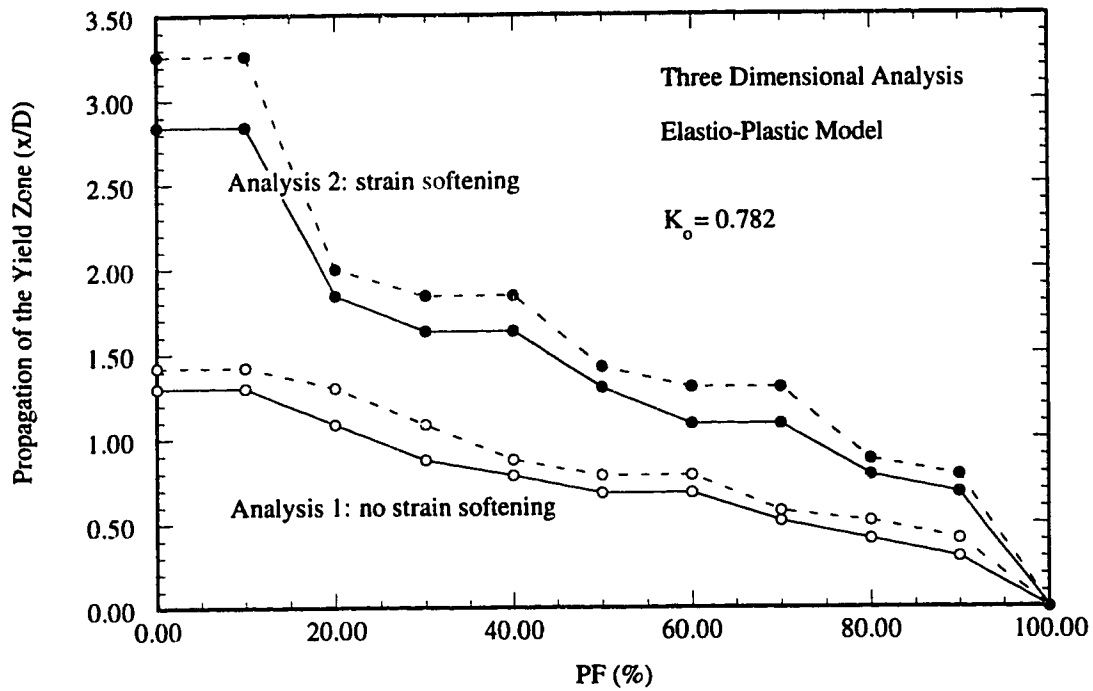


Figure 3.83: Upper and Lower Bounds of the Propagation of the Yield Zone ahead of the Tunnel Face versus the Face Pressure Ratio

machine in order to conduct the computational run.

3.6.3 Results

The major results from the analyses are summarized in Figures 3.81, 3.82, and 3.83. Figure 3.81 shows the propagation of the yield zone ahead of the face as the face pressure is reduced and the clay acts in a perfectly plastic manner. Figure 3.82 shows the same information but reflects the sensitivity of the clay. It is evident that the influence of sensitivity is to make the plastic zone extend further.

The results from both analyses are summarized in Figure 3.83. The two plots for each analysis arise from discretization and it is close enough to average them for practical purposes. The extent of yield propagation is essentially doubled as a result of strain weakening. When the EPBS exerts a face pressure of 10% the yield zone has propagated about $3D$ ahead of the face. Had the actual strength profile of the adjacent boring been included in the analysis, the extent of propagation would be greater.

3.7 Conclusions

The stability of the face of the tunnel constitutes the most critical element in the case of shielded excavation because of the rigidity of the shield and that of the liner inhibit the development of any failure mechanism in the transversal direction. A loading condition imposed on the face is described as the passive stress relief, and it is comprised of a monotonical reduction of the longitudinal stresses at the face from the initial state of stress to the actual pressure imposed by the shield. In the case of pressurized shield tunnelling using the bentonite slurry shield, the earth pressure balanced shield, or the compressed air shield, stress at the face depends on the method of application of face support. In the case of BSS, a layer comprised of a mixture of bentonite-ground, the cake, is formed and has improved properties regarding its shear strength and impermeability. Two types of cake layers can be formed: the membrane cake and the impregnation cake. The performance of these layers mainly depends on the rate of advance of the face. The earth pressure balanced shield provides a rigid support to the face and may result in an inward displacement of the soil particles. The compressed air shield creates an air pressurized zone covering a considerable volume of ground from the position of the locks behind the shield up to several metres ahead of the face. The distribution of the air pressurized zone mainly depends on the properties of the ground and on the applied air pressure.

Although the concept of face stress relief is simple and similar to the concept of the earth pressure behind a retaining wall, the stress path associated with it in the case of the shallow tunnel is of a certain degree of complexity because of the gravitational stress field

and the effect of several boundary conditions imposed on the ground which include a circular face under the stress relief condition and a horizontal stress free boundary at the ground surface. The effect of boundary conditions on the stress path followed during passive stress relief is demonstrated through a triaxial experimental setup and through the definition of a certain ratio: the confinement ratio.

Different methods of estimating the critical face pressure are examined. These methods include experimental models: physical models or centrifuge models, analytical analyses using limit theorems of plasticity or stability analyses, and numerical analyses mainly using the finite element method. Comparisons between the results of different methods show the advantages and the disadvantages of each method. Two different mechanisms of failure were determined for the cases of cohesive and noncohesive soils. In the case of cohesive soil, the yielding zone is developed following the funnel shape and it propagates up to the ground surface during the early stages of stress relief. The change of face movement associated with face pressure relief is gradual. In the case of noncohesive soil, the yield zone is generally close to the face, then the slope of face movement with the face pressure increases suddenly, and the yield zone reaches the ground surface only in the case of very shallow tunnels.

Numerical analyses using axisymmetric and three-dimensional finite element analyses were carried out in order to examine the stress and strain fields developed during cases of passive stress relief in cohesive or noncohesive soils. The critical face pressure is defined as the face pressure at which the slope of inward face movement associated with the gradual reduction of face pressure follows an increasing pattern and deviates from its initial constant state. The results of the analyses are compared with experimental results and with field data collected from several case histories. The calculated stress fields are found to conform with the estimated general configuration of failure mechanisms at the face. Comparisons of the results with case histories show that the presented results conform with some empirical design criteria actually in use. A detailed review of some case histories is carried out and show that the level of face pressure applied in successful tunnelling projects using pressurized shield method is higher than the proposed limit face pressure. The estimated margin of safety in these project is shown to be dependent on the method of face support. The EPBS, in general, provides the highest margin of safety while the BSS and the compressed air shields provide lower levels of face pressure.

An interesting case history involving the EPBS may be considered a practical examination of the stress relief at the face. Due to technical difficulties, the face pressure has been reduced to a low value. This could be believed to have resulted in causing instability to a nearby pile shaft. The undertaken numerical analysis has proven that for the

given estimated ground parameters, the yield zone could extend as far as 3 times the tunnel diameter. The analysis concludes on stressing on the major role that the prevailing initial stress field plays in affecting the face stability and the stability of neighbouring structures. This role is enhanced in the case where the intrinsic shear stress, created by the difference between the major principal stresses, is comparable to the ground shear strength.

CHAPTER 4

STRESS AND STRAIN FIELDS AROUND TUNNELS EXCAVATED USING PRESSURIZED SHIELD METHODS

4.1 Introduction

Stress and strain fields developed around a tunnel excavated using pressurized shield methods have a number of characteristics that differentiate them from those excavated using other methods of excavation. The basic idea behind pressurized methods of construction is to allow the erection of a lining system under favourable conditions both for the excavation and to the neighbouring structures. Consequently, the amount of change in the initial state of stress is reduced to a minimum by providing a system of rigid and pressurized support to the newly exposed excavation boundaries. Meanwhile, an additional enhancement to ground stability is achieved by material improvements (injection, grouting, or dewatering). Provided that the face stability is insured, the most critical phase in the control process takes place between the face and the point where the lining is activated, the delay distance. Stress changes that take place in this phase are affected by a number of factors among which are (1) the gravitational stress field; (2) the stress free boundary at the ground surface; (3) the longitudinal stresses applied at the shield and at the liner; and (4) the protection measures at the tail of the shield. Investigation of these factors shows that reliable estimation of soil movement at the ground surface, as well as, at the tunnel boundary requires the discretization of the different stress-strain actions in the three dimensions. Modern computer systems allow for the application of numerical methods, specifically, the finite element method, for these types of analyses that have been regarded, so far, as too exhaustive and too costly. A parametric investigation using three-dimensional finite element schemes is carried out in order to establish a relationship between the excavation method and the support system involved in it, and the geotechnical requirements of safety, specifically, settlement at the ground surface.

4.2 Concept of Volume Loss

The concept of volume losses has its logic derived from an ideal case of an unsupported excavation. In the ideal case, the removal of a certain volume of ground material within the excavation boundary results in soil movement toward the tunnel initiating new stress fields. Ultimately, a settlement trough develops at the ground surface such that its volume is related to the volume loss at the tunnel. Intensive application of the concept to case histories in the literature has led to the development of a number of methods of estimating surface movement based on empirical and stochastic models (see for example Sweet and Bogdanoff, 1965) for different soil conditions and excavation methods. The relative simplicity of the application of the proposed methods has rendered the concept increasingly popular while inadequate generalization of the principle may lead to inaccurate estimations. The general impression is that the reliability of empirical and stochastic methods based on the volume loss concept in estimating the settlement trough is higher in the case of cohesive soils rather than in the case of granular soils, and that the applicability of the methods depends largely on the availability of empirical data from cases similar to the case under study.

4.2.1 Volume Loss at the Tunnel

An ideal excavation consists of removing ground material within the cut profile without introducing changes to the state of stress of the surrounding soil. Typically, the changes inflicted to the ground are related to a loss of ground particles. Cording and Hansmire (1975) define the volume loss as the volume of soil that is displaced across the perimeter of the tunnel. It is expressed as a volume per unit length of tunnel. It is understood from the definition that volume losses are ultimate losses. Therefore, they are supposed to include volume losses at the face, as well as, at the circumference of the excavation. Furthermore, it may be argued that the final amount of volume losses is the resultant of all types of material changes related to the method of excavation which may include volume "gains" due to either forward movement at the face, grouting, or lining expansion.

4.2.2 Displacement and Strains Induced by Volume Loss at the Tunnel

The concept of volume loss is extended to the description of the propagation of losses within the soil mass that would ultimately be manifested as surface settlement. It is therefore essential to make certain assumptions regarding :

- (1) the distribution of the generated displacement field above the tunnel and up to the ground surface;

- (2) the shape of (vertical) displacement trough above the tunnel; and
- (3) the relationship between the volume of the settlement trough (volume loss at the ground surface, V_s) and the volume loss at the tunnel V_t .

The methodology used in formulating a displacement model induced by volume loss at the tunnel relies on adopting simple assumptions based on case histories of different tunnelling projects.

4.2.2.1 Empirical Description of Settlement Trough

Peck (1969) has proposed the normal error function to represent the transversal profile of settlement distribution at the ground surface. The expression, shown in Figure 4.1, relates the vertical displacement at the ground surface due to tunnel excavation, w , to two parameters V_s and i :

$$w = \frac{V_s}{i\sqrt{2\pi}} \cdot \exp\left(-\frac{y^2}{2i^2}\right), \quad (4.1)$$

where:

y is the transversal coordinate, and

i is the width of settlement trough, or the transversal distance between the point of maximum settlement and the inflexion point.

Other distributions of ground settlement are formulated based on empirical, theoretical, or probabilistic approaches (see for example Szechy, 1973: 870). However, Peck's distribution has gained a predominant acceptance among tunnel designers. The expression is acceptable logically as it is normally expected that the maximum settlement takes place above the tunnel crown and decreases away from the centerline of the tunnel in the transversal direction. Meanwhile, the introduction of two parameters to evaluate the settlement trough provides the expression with sufficient flexibility to accommodate different measured settlement profiles. As the pattern of surface displacement varies along the tunnel trajectory, collected settlement data from different tunnelling works is sufficiently consistent to challenge, correct or to definitively confirm the proposed expression.

4.2.2.2 Semi-Empirical Analyses

Attewell and Woodman (1982) and Attewell et al. (1986), have presented a mathematical model of soil strain and displacement around an excavation based on the assumption that, at the tunnel depth, H_o , a sink point exists producing a certain volume

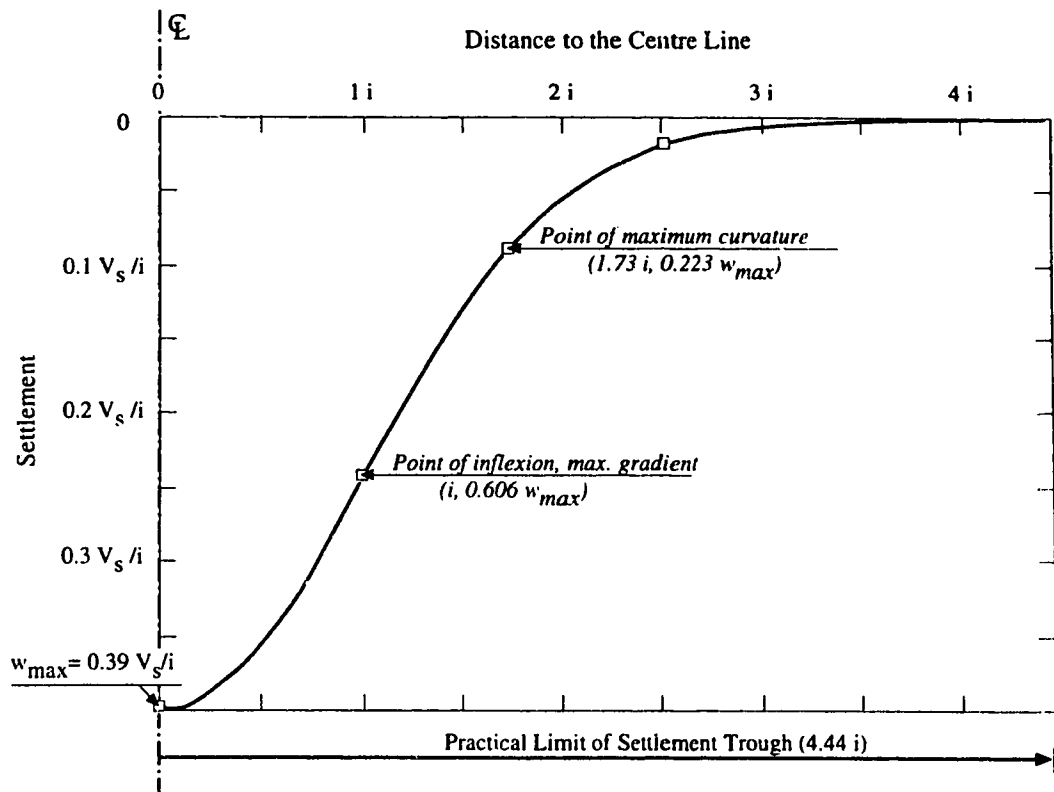


Figure 4.1: Normal Probability Curve Describing the Transversal Settlement Trough (after Peck 1969)

loss. Since the sink is dimensionless, vertical soil displacement at the sink is infinite while the horizontal movement is prohibited. Above the sink point, soil displacement follows the normal probability curve distribution described by Peck (1969) except that the distribution extends symmetrically around the vertical axis while passing through the sink. The volume of the trough anywhere above the sink point is constant based on the assumption of no volumetric strains. The width of the trough expressed by i is assumed to be proportional to the depth:

$$i \propto (H_0 - z')^n \quad , \quad (4.2)$$

where:

n is empirical parameter and

z' is vertical axis extending from the ground surface downward.

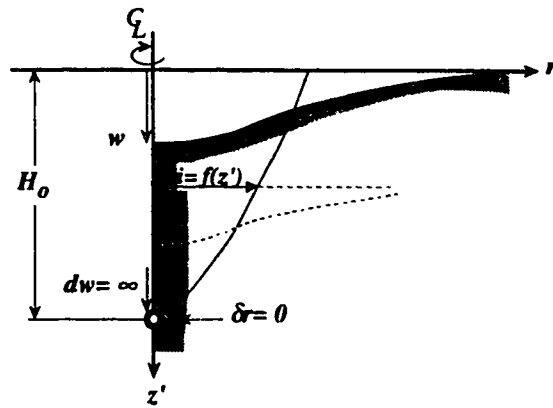
Or:

$$\frac{i}{a_1} = a_2 \left(\frac{H_0 - z'}{a_1} \right)^n \quad , \quad (4.3)$$

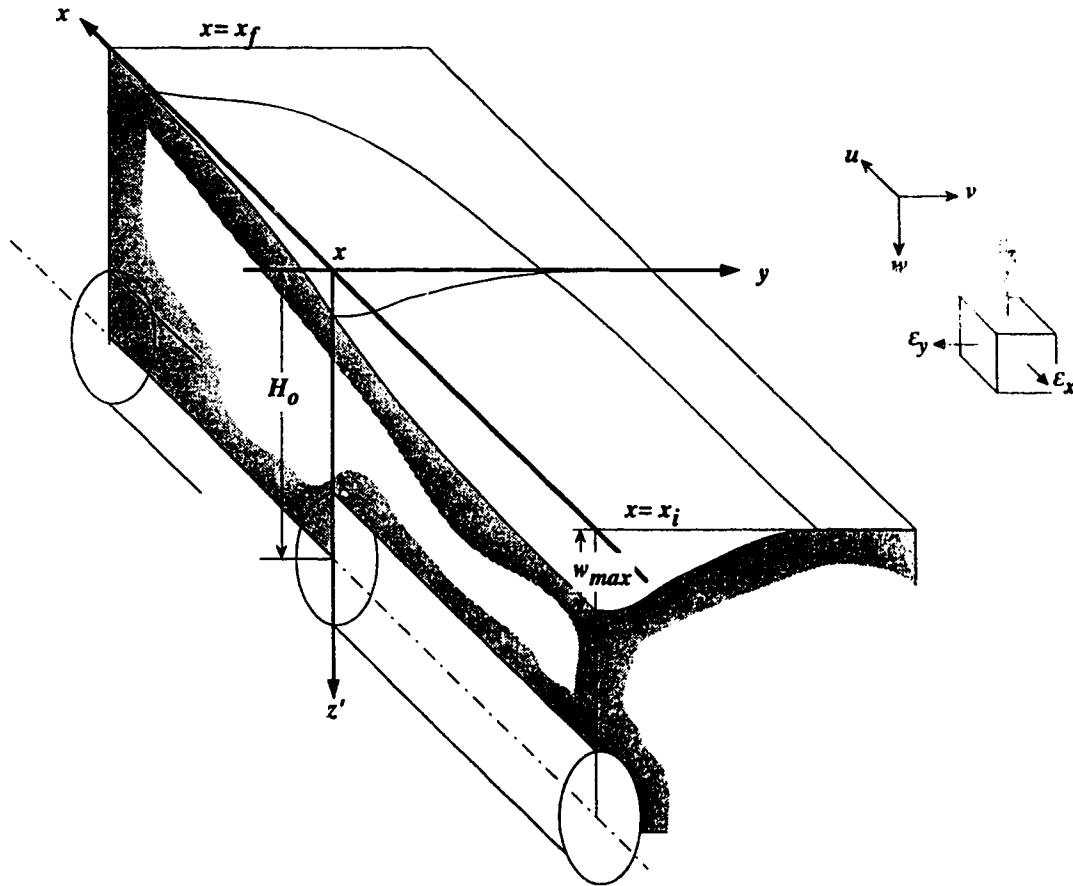
where a_1 is a constant with a length dimension and a_2 is a dimensionless constant. Vertical strain is obtained by differentiating the vertical soil movement in the vertical dimension. Integration of the equations for vertical displacements and strain in the longitudinal direction, x , yield the vertical displacement and strain due to a point sink advancing in a horizontal line. Conditions of compatibility of strains associated with the assumption of zero volumetric strains give the equations for strains and deformations in the transversal and longitudinal directions shown in Figure 4.2 . Values of displacement and strains are calculated for a case where the tunnel is excavated between two points x_i and x_f . The ultimate state may be calculated by using $x_i = -\infty$ and $x_f = +\infty$.

4.2.3 Evaluation of Parameters Describing Volume Losses at and around the Tunnel

The implementation of the concept of volume loss based on the above formulae constitutes a framework which needs continuous adaptations and re-evaluations based on case histories of different tunnelling projects. The reliability of the results is mainly dependent on the reliability of the parameters used rather than that of the framework itself.



1. Displacement Field before Integration



2. Symbols and Problem Configuration

Figure 4.2: Displacement and Strain Fields around an Excavation (after Attewell et. al. 1986)

$$w = \frac{V_s}{i\sqrt{2\pi}} \left[\Gamma\left(\frac{x-x_i}{i}\right) - \Gamma\left(\frac{x-x_f}{i}\right) \right] \exp\left(\frac{-y^2}{2i^2}\right)$$

$$v = \frac{-n}{(H_0 - z')} y w$$

$$u = \frac{nV_s}{2\pi(H_0 - z')} \left[\exp\left(\frac{-(x-x_i)^2}{2i^2}\right) - \exp\left(\frac{-(x-x_f)^2}{2i^2}\right) \right] \exp\left(\frac{-y^2}{2i^2}\right)$$

$$\varepsilon_z = \frac{-nV_s}{i\sqrt{2\pi}(H_0 - z')} \left\{ \frac{-1}{\sqrt{2\pi}} \left[\Gamma\left(\frac{x-x_i}{i}\right) \exp\left(\frac{-(x-x_i)^2}{2i^2}\right) - \left(\frac{x-x_f}{i}\right) \exp\left(\frac{-(x-x_f)^2}{2i^2}\right) \right] + \left(\frac{y^2}{i^2} - 1\right) \left[\Gamma\left(\frac{x-x_i}{i}\right) - \Gamma\left(\frac{x-x_f}{i}\right) \right] \right\} \exp\left(\frac{-y^2}{2i^2}\right)$$

$$\varepsilon_y = \frac{nw}{(H_0 - z')} \left(\frac{y^2}{i^2} - 1\right)$$

$$\varepsilon_x = \frac{-nV_s}{i\sqrt{2\pi}(H_0 - z')} \left[\left(\frac{x-x_i}{i}\right) \exp\left(\frac{-(x-x_i)^2}{2i^2}\right) - \left(\frac{x-x_f}{i}\right) \exp\left(\frac{-(x-x_f)^2}{2i^2}\right) \right] \exp\left(\frac{-y^2}{2i^2}\right)$$

where

$$\Gamma = \frac{1}{2\pi} \int_{-\infty}^{\infty} \exp\left(\frac{-a^2}{2}\right) da$$

Figure 4.2: Displacement and Strain Fields around an Excavation (after Attewell et al. 1986) (continued)

4.2.3.1 Volume Loss at the Tunnel

As excavation proceeds using conventional tunnelling methods, a delay distance is created from the face of excavation to the point where the lining system is mobilized. Volume loss is generated along this distance as the boundaries of the excavation are not supported. As the delay distance and the delay period extend, the soil displacement pattern changes from face movement to radial movement. The amount of volume loss depends on soil deformability, soil strength, and the overcut volume. In the case of soft clayey soils, the variation of the ratio between the shear strength and the modulus of deformation is relatively small, and volume loss may be related to shear strength through the overload factor, OF , (Equation 3.6) and the stability ratio, f' , which is the overload factor at failure.

Based on data collected from Clough and Schmidt (1981) and Attewell et al. (1986), Figure 4.3 shows measured volume losses plotted against the overload factor OF . Simplified elasto-plastic analysis produces a relationship between the relative volume loss, V_t' and OF for an idealized case of isotropic, undrained soft clay material, provided that the excavation is instantaneous and the soil movement follows a radial pattern into the excavation. The following formula is suggested for the case where $OF \geq 1$

$$V_t' = \frac{V_t}{V} = m \cdot \exp(OF - 1) \quad , \quad (4.4)$$

where:

V is the theoretical tunnel volume per unit length (= area of the tunnel cross section), and

$$m = \frac{2c(1 + \nu)}{E_u} \quad ,$$

where:

E_u is the undrained modulus of the clay in elastic zone, and

$\nu = 0.5$

The constant m is suggested to vary between 0.002 and 0.006¹. In the case where $OF < 1$:

¹The suggestion that the value of m varies between 0.002 and 0.006 has been made by a number of authors, among whom are Finno (1983: Figure 2.4) and Lee (1989: Figure 2.1).

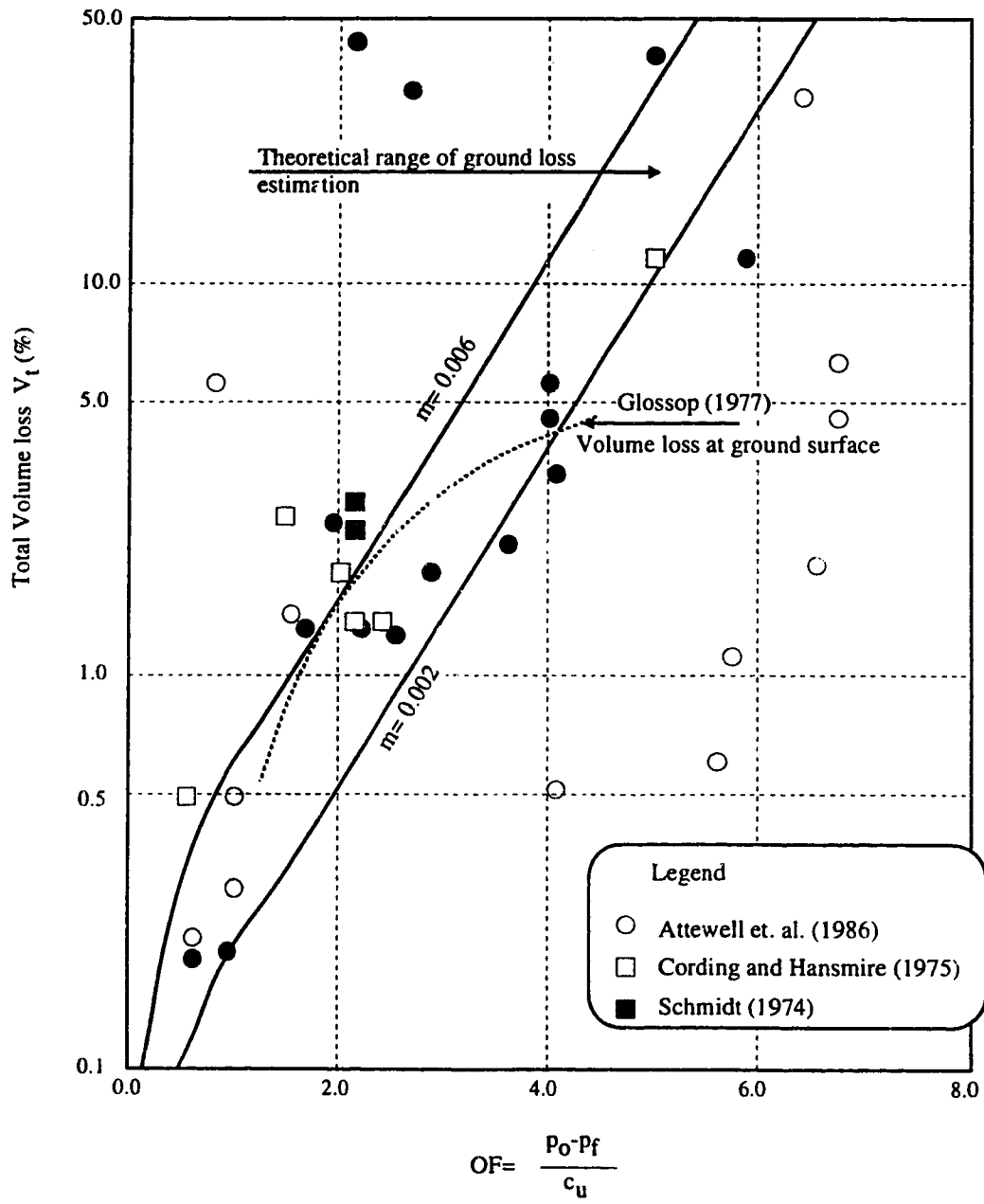


Figure 4.3: Volume Loss versus Overload Factor

$$V'_t = m \frac{P_o}{c} \quad . \quad (4.5)$$

Meanwhile, Mitchell (1983) has suggested the following relationship based on compiled case histories:

$$V'_t = \frac{c_u}{E_u} \cdot \exp\left(\frac{OF}{2}\right) \quad . \quad (4.6)$$

According to this author, poor site conditions may lead to a volume loss as high as three times the proposed estimation. It is, therefore, concluded that methods used to quantify volume losses are only indicative of the order of magnitude of volume losses. It could be believed that more precise estimations have to consider the method of excavation, the mode of deformation, and the relationship between the degree of mobilization of shear strength and the deformability (the flow rule) , as well as, soil stratification.

Volume loss due to tunnelling constructed using shielded excavation is presented by Attewell et al. (1986) as :

$$V_t = V_f + V_b + V_p + V_y + V_u + V_g \quad , \quad (4.7)$$

where:

V_f is the face loss,

V_b is the bead loss,

V_u is the postshield/pregrout loss,

V_g is the postgrout loss,

V_p is the pitch loss, and

V_y is the loss due to distortion at the tail.

Face losses, V_f , are axial losses and are responsible for the spread of soil movement ahead of the face. Losses around the shield are radial losses and are mainly due to overcutting or shield movement. In order to reduce frictional forces around the shield, a certain space is excavated around the shield extrados, and the resulting void is supposed to close as the shield advances creating the bead loss, V_b . If the ground is sufficiently self supported it will be grouted in the subsequent excavation step. Meanwhile, the longitudinal alignment of the shield is affected by the stress changes related to the excavation process.

Therefore, the shield is generally driven with a certain "attitude". In the case of soft clay where the shield tends to plough down, a look-up attitude is necessary to maintain the excavation at its designated grade. As a result, an elliptical hole is created above the shield creating an additional loss to the ground, the pitch loss, V_p . Bracing the shield to increase its rigidity is not practically convenient as this would represent an obstacle to the installation of the machinery inside it. However, the machinery, itself, contributes in an unquantifiable degree to the stiffness of the shield. Ultimately, the shield undergoes a squashing distortion in the horizontal or the vertical directions depending on the initial state of stress leading to the ground loss V_y . Postshield/pregrout losses, V_u , are attributed to the inevitable void created because of the difference between the extrados of the shield and that of the liner. Finally, V_g , postgrout losses refer to the ground-liner interaction, as well as, to losses during the grout curing process.

The effect of the rate of excavation and the sequence of the excavation process has an important impact on the amount of ground loss. This effect can be quantified by the rate of extrusion which is the rate of deformation of the soil surface when exposed to a stress relief process. If a representative constant rate of extrusion can be selected such that it is independent of stress changes and soil anisotropy at the excavation boundary, then ground loss may be linked directly to the rate of excavation. Attewell (1986) proposes a method of estimating the total ground losses by relating tunnel geometry to the extrusion rate and to the rate of excavation. Meanwhile, the sequence of the construction process affects the amount of the volume losses as an important part of the total losses take place behind the shield tail. Ground losses are reduced as the grout and the lining system are activated earlier. This requires a grouting system that fills the annular void simultaneously and as soon as the lining clears out of the shield. For technical and practical reasons this objective is hard to achieve. Simultaneous application of the grout requires complex and cumbersome grout installations. Furthermore, the application of grout after the clearance of each ring may lead to a reduction of the total rate of advance. In some fairly competent ground, it could be more practical to apply grout material after the erection of each two (or more) rings.

4.2.3.2 The Trough Width

Peck (1969: Figure 9) suggests that the relationship between the trough width normalized to the tunnel radius and the depth ratio depends on the soil type. Higher trough width is obtained as soil conditions change from sands below the groundwater table to plastic clays, to nonplastic clay, rocks, or sands above the groundwater table. Attewell and Woodman (1982) discuss this exponential relationship in Equations 4.2 and 4.3, and they

have shown reservations about the value of $n = 0.5$ proposed by Sweet and Bogdanoff (1965) who suggest that $n = 1$ which reduces Equation 4.3 into a linear relationship. O'Reilly and New (1982) endorse the linear relationship assumption by proposing the following expressions:

$$i = 0.43(H_o - z') + 1.1 \quad (3 \leq H_o \leq 34) \quad (4.8.a)$$

for cohesive soils, and

$$i = 0.28(H_o - z') - 0.1 \quad (6 \leq H_o \leq 10) \quad (4.8.b)$$

for granular soils.

Meanwhile, Leach (1985) proposes the following relations:

$$i = 0.45(H_o - z') + 0.57 \pm 1.01 \quad (4.9.a)$$

if the effect of consolidation (negative volumetric strain) is neglected, or

$$i = 0.48(H_o - z') + 0.64 \pm 0.91 \quad (4.9.b)$$

if consolidation is taken into account. In Equations 4.8 and 4.9 the unit length is the metre. Atkinson and Potts (1977) include the influence of the tunnel diameter when suggesting the following expressions based on model tests in kaolin and sandy soils:

$$i = 0.125(2H_o + D) \quad (4.10.a)$$

for sand, and

$$i = 0.125(3H_o + 0.5D) \quad (4.10.b)$$

for clay.

4.2.3.3 Volume of Settlement Trough at The ground surface

The assumption of no volumetric strain generated around the tunnel implies that the volume of the surface settlement trough is equal to the volume loss at the tunnel. It is

believed that this would be a special case as volumetric strains are supposed to take place either positively because of dilation or negatively because of contraction or consolidation. The verification of this assumption requires execution of independent measurement of volume losses both at the tunnel and at the ground surface.

Glossop (1978) has suggested for tunnels constructed in clay where OF varies between 1.5 and 4.0 that the surface movement may be related to the overload factor through the relationship (see Figure 4.3):

$$V_s = 1.33 OF - 1.4 \quad . \quad (4.11)$$

4.3 Idealized Stress Field around an Opening

The idealized stress field related to tunnelling in its simplest form is based on the concept of volume loss. A cavity is created releasing the stresses along the excavation boundary. A closed form elastic solution is proposed by Kirsch (1898) for a uniform stress field conforming to plane strain condition where the stress release is introduced along a circular boundary. Departures from the basic assumptions presented by Kirsch (1898) are numerous, and concern mainly the boundary conditions, the amount and distribution of stress release, the initial conditions of the stress field, and the constitutive models. Unlike strain measurements, stress measurements at tunnelling projects in soft ground are of a limited degree of reliability. Methods used in measuring stresses prove to lack either accuracy or consistency and as a result, the data collected is not sufficient to construct an idealized model of the resultant stress field. The available estimations of the stress field are mainly based on interpretations of strain measurements which involve a certain degree of uncertainty about the actual stress-strain relationship.

4.3.1 The Effect of Tunnel Depth

The effect of tunnel depth is related to the gravitational stress field and the free boundary at the ground surface. The significance of this effect leads to the description of a certain tunnel as "deep" or "shallow". Negro (1988: Table 2.1) has presented a review of elastic analyses which investigated the influence of the free surface boundary and the gravitational stress field on stresses at the tunnel crown and straining actions at the tunnel liner. He concludes that while the presence of the gravitational stress field is significant for depth ratios as high as 50.0, the free surface boundary ceases to affect the stress field at the tunnel boundary when the depth ratio is relatively low. Design recommendations prepared by a German workgroup are presented by Heinz (1984) and they suggest that for the

purposes of lining design, a tunnel may be considered deep if the depth ratio exceeds 3.0, and shallow if the depth ratio is lower than 2.0 . However, German recommendations have to be taken with caution as the depth effect may vary depending on the initial stress field (K_0) and soil stiffness, and it may influence the strain field near the ground surface higher than that near the tunnel boundary.

The departure from the simple basic solution of Kirsch (1898) to include the gravitational stress field leads to a modification of the concept of volume loss, itself. Volume loss at the tunnel is affected by the increase in the initial stresses with depth. Thus, the distribution of radial displacement and consequently that of volume loss are not uniform along the tunnel boundary. It is reasonable, therefore, to describe stresses and displacement at the tunnel boundary by a number of curves corresponding to different points at the tunnel circumference rather than by a single relationship. Volume losses at the ground surface and the shape of the settlement trough is also believed to be affected by the nonuniformity of volume losses at the tunnel. Furthermore, the gravitational stress field produces an overall heave in the tunnel section. Negro (1988) confirms the possibility of such movement although he suggests that the delay of the lining activation reduces the heave action. It could be believed that this is not the case when pressurized shield tunnelling methods are used because in these instances, the presence of the shield between the face and the liner transmits the heave action to the lined section of tunnel.

4.3.2 The Effect of the Delay Distance

The concept of arching is based on the redistribution of induced loads due to the mobilization of shear strength in the transversal plane. The theoretical background of the arching mechanism of a two-dimensional plane strain tunnel is presented by Terzaghi (1943). Three-dimensional aspects of the arching theory are discussed by Eisenstein et al. (1984) who indicate that although the load distribution due to arching is ultimately manifested in the transversal plane, the mechanism leading to it is three-dimensional. As a consequence of delayed lining activation, arching is mobilized near the face in the longitudinal and horizontal planes, as well as, in the transversal plane. The concept of three-dimensional arching is supported by numerical simulation and field measurements at a twin tunnel constructed in Frankfurt, Germany. The results of the investigation indicate that radial stress reduction at the tunnel boundary relative to radial movement (ground reaction curve) depends on the delay distance. Figure 4.4 is modified after Eisenstein et al. (1984) and shows a conceptual description confirmed by numerical application of ground reaction curves at the crown and the effect of the delay distance on it. It could be believed that in the case of a tunnel constructed using pressurized shield technology, the boundary

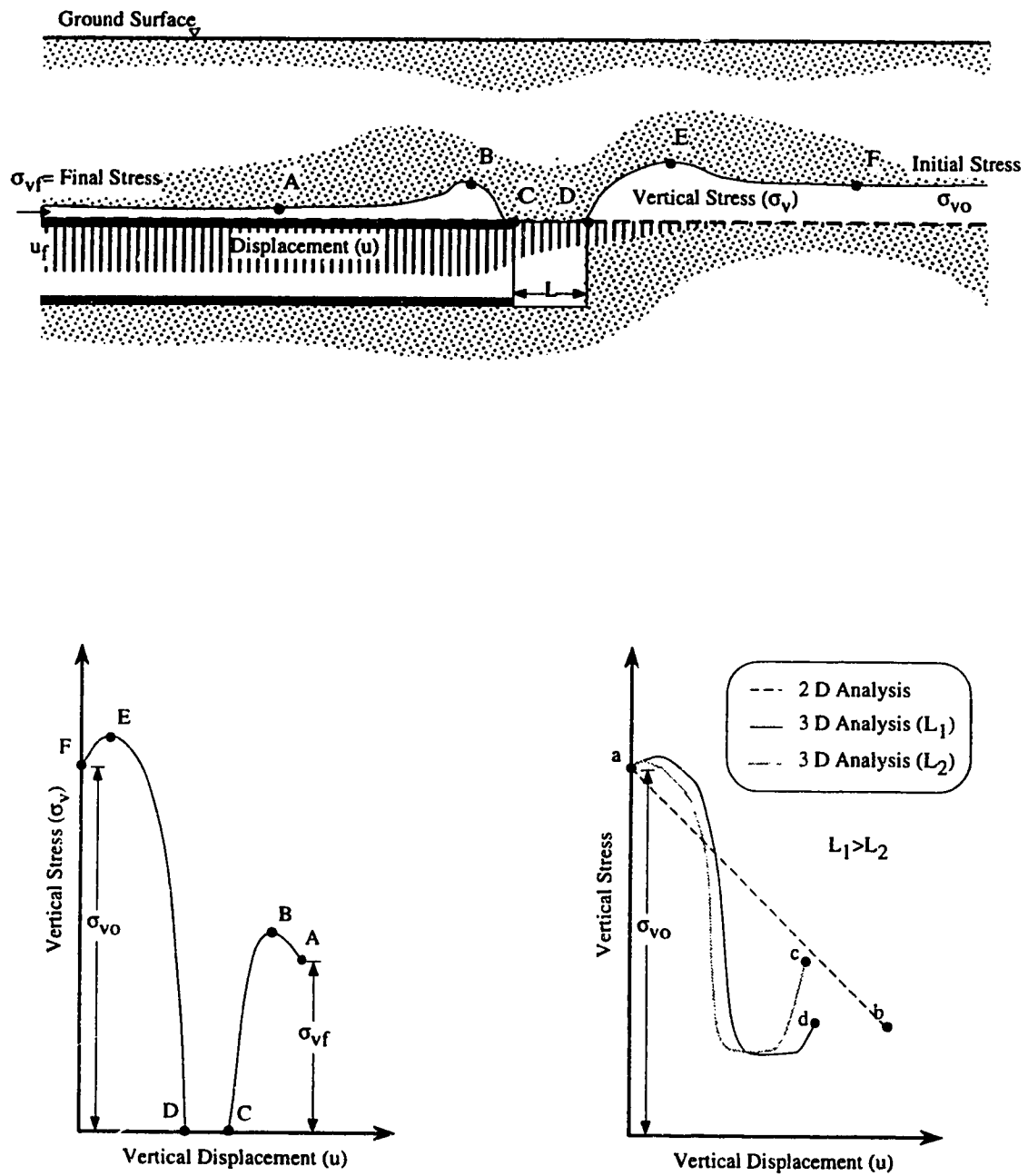


Figure 4.4: Three Dimensional Aspects of Ground Reaction Curves at the Crown Level of the Tunnel (after Eisenstein et. al. 1984)

condition along the delay distance is not a stress free boundary. A more complicated mechanism is expected to develop as the shield is engaged in an interaction process with the ground because of (1) the overall movement of the shield, (2) the mobilization of friction forces between the shield and soil particles, (3) longitudinal forces transmitted from the propelling rams of the shield to the ground, and (4) the improvement of ground properties due to grouting.

4.3.3 Stress Paths related to Tunnel Excavation

It is concluded from the above two sections that during shallow tunnel excavation, different stress changes are expected at different positions at the excavated boundary either along the longitudinal axis or along the tunnel circumference. Consequently, the distribution of the degree of stress release and the degree of mobilized shear strength in the transversal plane do not conform to the radial field of stress release described by Kirsch's solution. Once the yield point is reached, stress distribution departs from the linear elastic constitutive relationship to follow a strain related model. A qualitative study has been carried out by Negro (1988) used the finite element method to identify the stress path related to an idealized case of stress relief. Here a hyperbolic model is used as the constitutive relationship, and stresses at points near the tunnel and at a certain distance from it are recorded. Figure 4.5 shows the stress paths obtained. The effect of the nonlinear model is that at points near the excavation the increase in deviatoric stress, $(\sigma_v - \sigma_h)/2$, results in a decrease in the average normal stress, $(\sigma_v + \sigma_h)/2$, which is a sign of yielding taking place. The reduction in normal pressure is compensated by an increase at points far enough from the excavation.

It is to be expected that if a different constitutive model is used, different stress paths would be obtained. Furthermore, a stress path that describes the whole tunnelling process requires taking into consideration that the ground does not undergo a monotonic constant rate of stress release along the longitudinal axis. The conceptual estimation of stress changes presented in Figure 4.4 is one example of these changes that may take place at the crown.

4.4 Idealized Strain Field around an Opening

A distinctive strain field is expected to develop around tunnels constructed using pressurized methods compared to those constructed using traditional methods. The reason behind this is related to the support system imposed on the ground which affects the traditional mechanism of stress relief particularly in its three-dimensional aspects. Material handling used during pressurized shield tunnelling construction is responsible for further

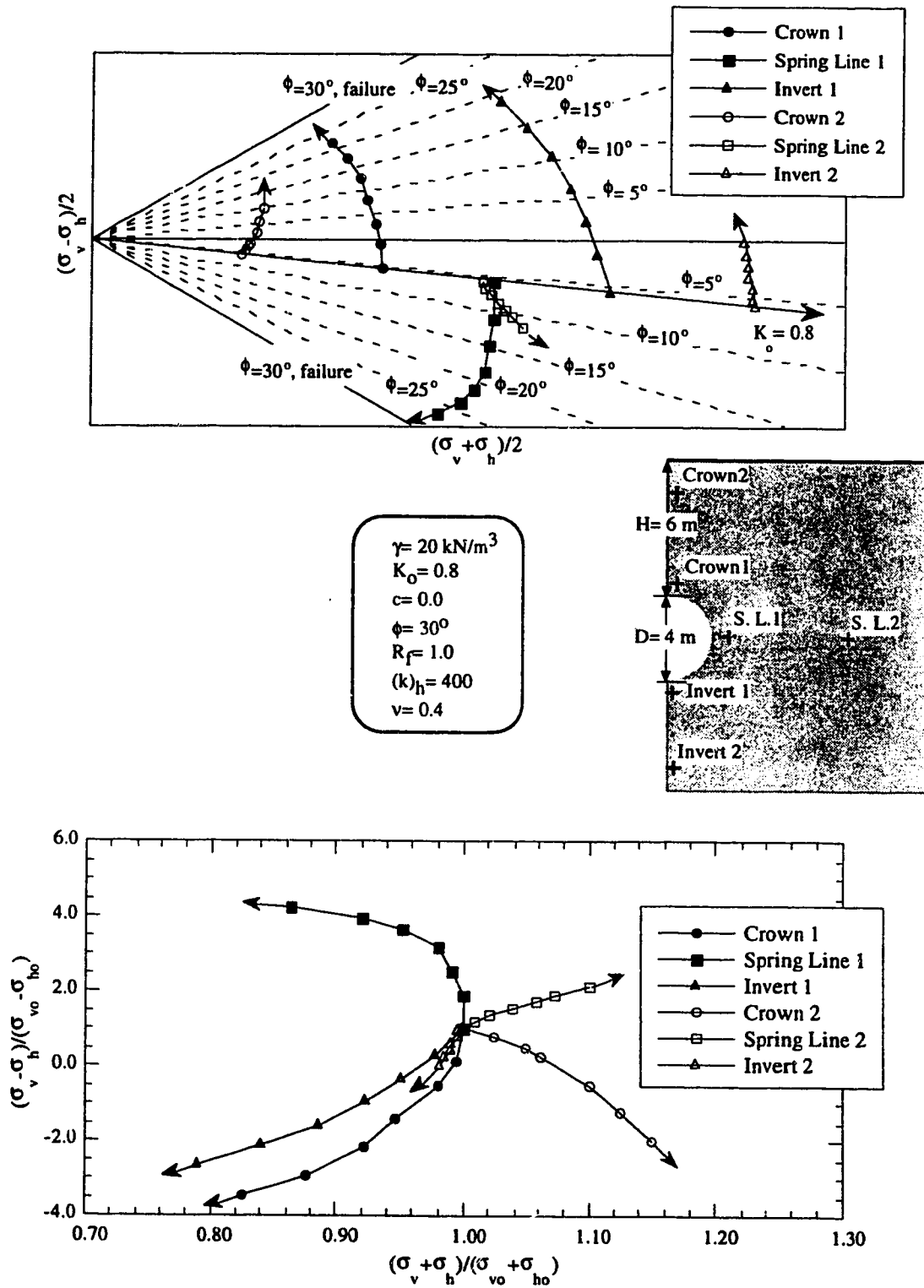


Figure 4.5: Stress Paths Resulting from Numerical Simulation of Conventional Tunnelling (after Negro 1988)

departures from traditional tunnelling strain field. For example application of compressed air results in changes in pore pressure which creates seepage patterns and capillary forces that play, together with the construction sequence, an important role in determining the final strain field. Meanwhile, material handling near the surface of the excavation because of slurry injection at the face, or grout injection, or extruded concrete at the circumference boundary has an effect in stabilizing and restricting soil movement where it is supposed to typically reach its maximum values.

4.4.1 Strain Field near Excavation Boundary

Typical movement near the excavation boundary is related to the stress release principle which is characterized by a consistent trend of radial movement toward the cavity with a rate that is supposed to reach a maximum value at the point of lining activation followed by an interactive process with the liner leading to restricting soil movement. An example of soil movement at the crown may be provided by reexamining the Frankfurt Tunnel mentioned in Section 4.3.2. The tunnel is constructed in fairly stiff, clayey marl known locally as Frankfurt clay. Two tunnels were driven simultaneously using the NATM with an excavated diameter of 7.7 m and a cover depth of 14.65 m. Figure 4.6 shows a representative measured displacement profile of a point near the crown relative to the face advance.

The technicalities of pressurized shield methods is discussed in Chapter 2. An example of soil movement near the crown of a tunnel excavated using a Bentonite Slurry Shield, the Hydroschild, is shown in Figure 4.7 based on data collected from Thurber (1990) during the construction of the Edmonton LRT tunnel. Soil conditions consisted mainly of post-glacial sand and gravel, and silty alluvial deposits overlying the bedrock. From the figure three displacement stages may be identified: the preshield stage where downward soil movement is restricted and in some instances reversed upward, the shield stage where the rate of soil movement increases and reaches a peak near the shield tail, and the post shield stage where grout action combined with the forces exerted on the grout due to shield advance results in a zigzag movement pattern that dampens with the distance from the tail. The larger amount of displacement takes place near the shield tail, thus the effectiveness of the tail sealing is of a paramount importance in case of the Bentonite Slurry Shields. Upward movement in the preshield stage is confirmed in cases of EPBS by Clough et al. (1983) during the construction of the N2 tunnel in San Francisco where ground conditions consisted of soft clay. Similarly, preshield heave is encountered in the case of compressed air shield as described by Shalaby (1990) during the construction of the Cairo sewage project in silty, sandy soil. It could be believed that, except in cases of

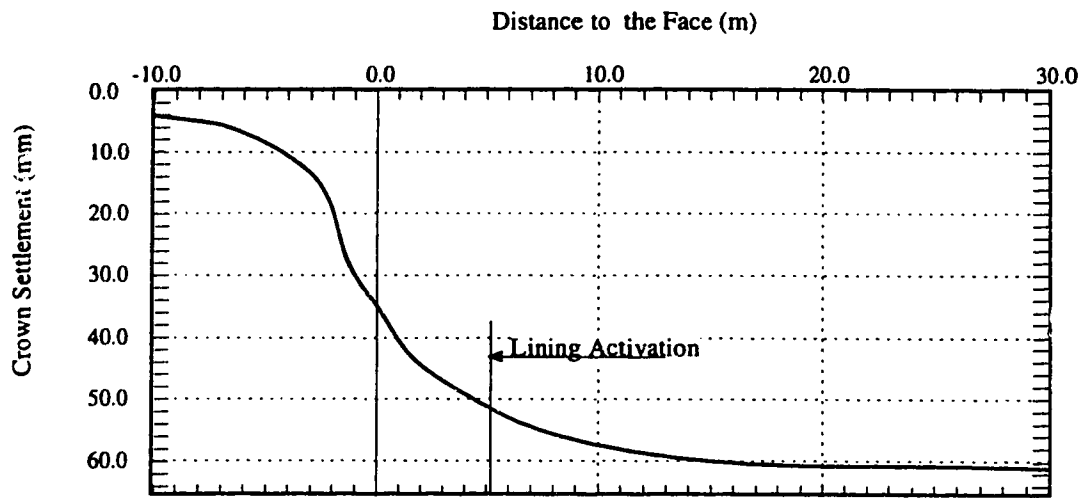


Figure 4.6: Displacement at Crown Level versus Longitudinal Distance at Frankfurt Tunnel (after Eisenstein et. al. 1984)

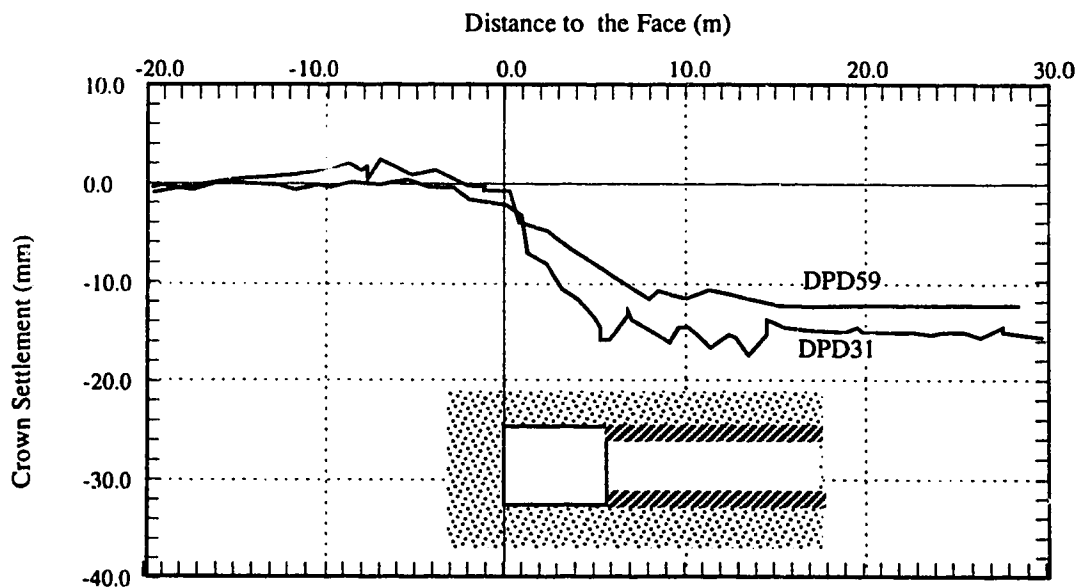


Figure 4.7: Displacement at Crown Level versus Longitudinal Distance at Two Locations at Edmonton LRT Tunnel (after Thurber 1990)

face failure, preshield heave is the general trend for pressurized shield tunnelling. However, it is questionable to generalize the Hydrosshield movement pattern in Figure 4.7 to the other two methods of excavation. As the preshield stage constitutes spending a certain effort to control soil movement, movement patterns at the two subsequent stages depend on how the support effort has been removed. For example in the case of compressed air, final downward movement is accelerated when compressed air is removed which usually takes place far behind the excavated section, and the movement pattern may therefore be described as time dependent. Figure 4.8 is modified after Shalaby (1990: Figure 6.13) and shows the displacement profile near the crown during the construction of the Cairo sewage project using the compressed air shield. In the case of EPBS the main effort of the face stabilization is related to the shield propelling into the ground. The resultant longitudinal action on the ground is reversed behind the shield as the shoving rams transmit shield reaction to the liner which transmit it in turn to the ground. Therefore, shield and postshield stages of crown movement are comparable to those described in Figure 4.7. An interesting case is raised if the longitudinal forces due to shield advance is not reversed which is applicable in case of pipe jacking where the shield forces are transmitted ultimately to a bulkhead at the starting point of the pipe line. De Moor and Taylor (1993) present field measurements around a 2.1 m sewer tunnel constructed using the pipe jacking method in soft peat soil conditions under a cover depth of about 10.0 m. The operating shield is known as "crushingmole" and functions comparably to an EPBS with bentonite as plasticizing agent. Soil movement at the shield and postshield stages do not show downward movement immediately at the tail of the shield and the displacement follows a time dependent pattern similar to that of the compressed air shield due to readjustment of pore pressure (consolidation). Figure 4.9 shows a settlement profile near the crown for two instrumented sections at the project.

4.4.2 Strain Field around the Excavation

Ground movement at the vertical centerline above a tunnel excavated using conventional excavation methods is characterized by two stages that take place before and after lining activation. The first stage is immediate and is initiated by stress release at the tunnel. Consequently, a downward displacement pattern is generated with maximum displacement near the crown. In the case where pore pressure is disturbed because of the excavation, the second stage proceeds as a result of consolidation processes. As the tunnel lining is already placed, the boundary condition is changed from the first stage, and seepage forces are generally directed toward the excavation and the zone of pore pressure reduction created around the tunnel because of stress relief. This results in an additional

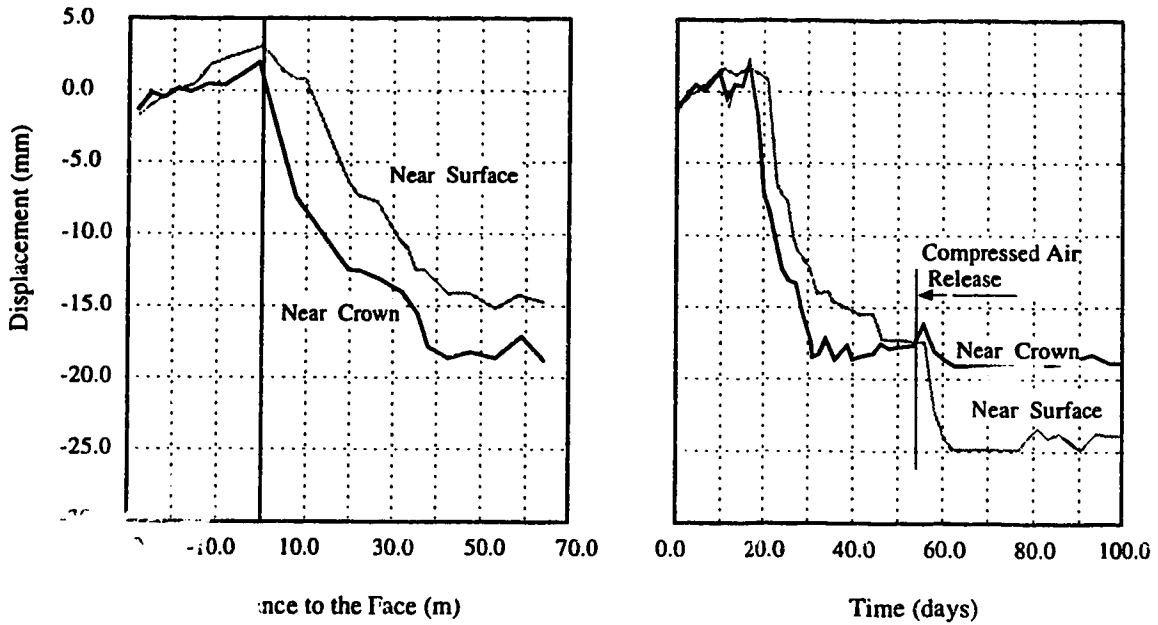


Figure 4 Displacement at Crown Level at Cairo Sewage Tunnel- Location: MPX I (after Shalaby 1990)

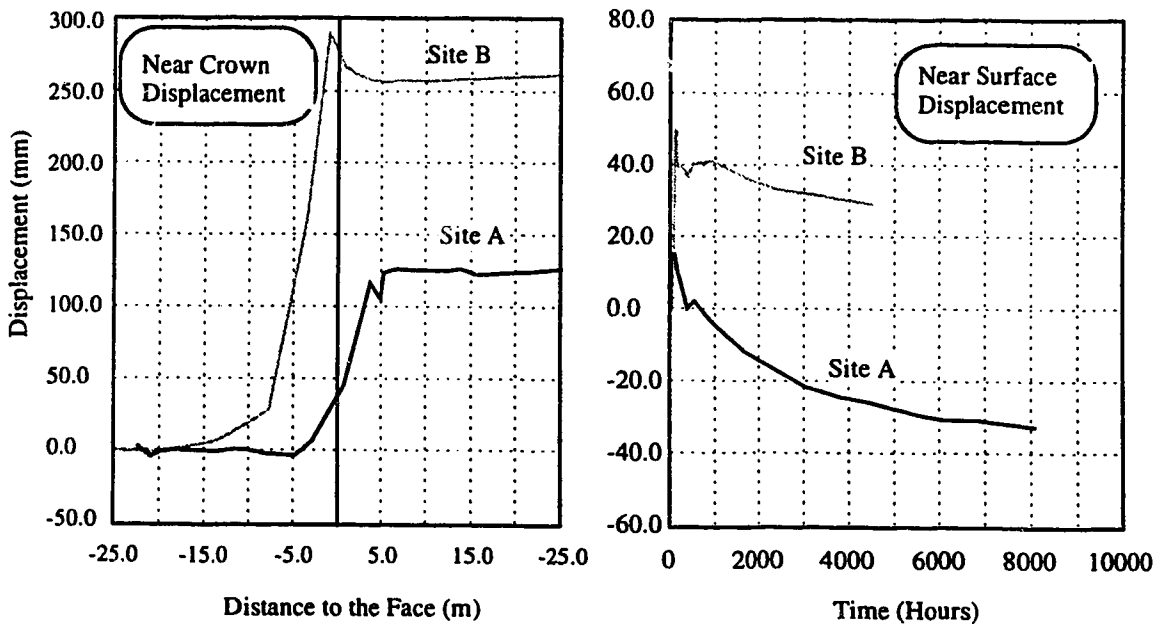
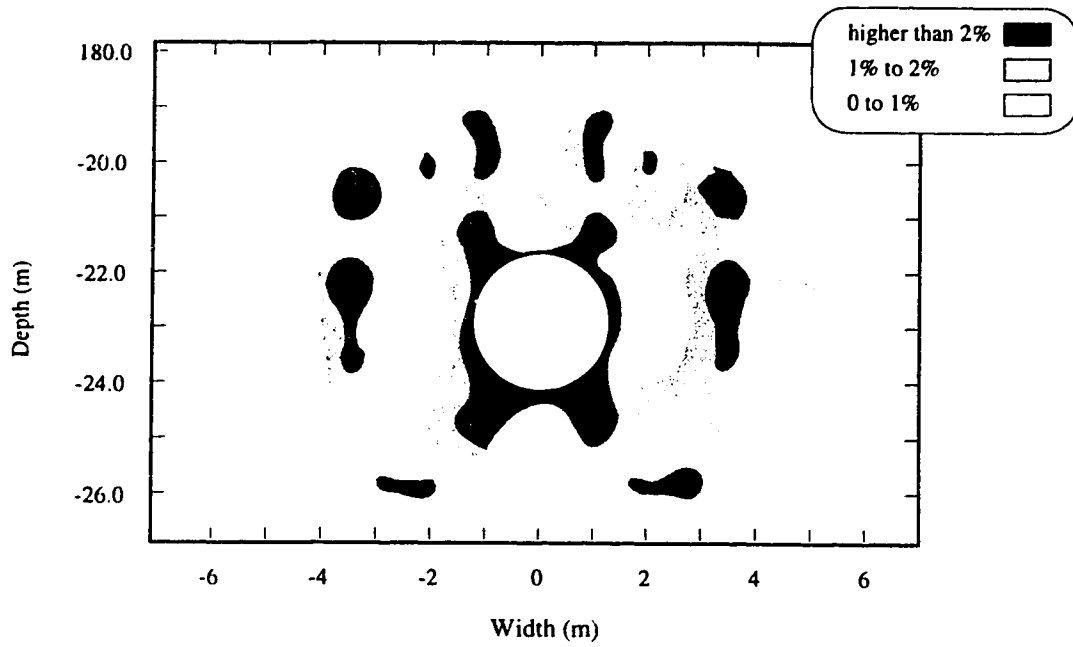


Figure 4.9: Displacement at Crown Level at Tilbury Tunnel at Two Locations (after De Moor and Taylor 1989)

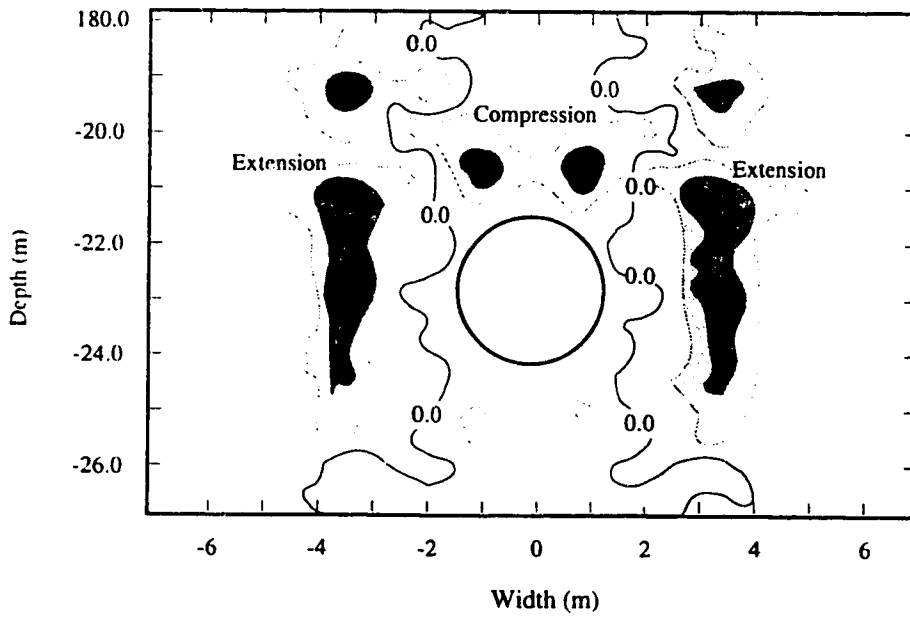
displacement pattern having, contrary to the stress relief pattern, the maximum value far from the excavation. Consolidation settlement then is developed with its minimum value near the crown. This conclusion is verified by Johnston (1981) using numerical analysis. Therefore, in the case where the magnitude of consolidation settlement is comparable to that of immediate settlement the ultimate settlement profile is expected to be, to an extent, uniform with depth. In the longitudinal direction, the profile of the immediate soil movement at the ground surface is generally similar to that at the crown. Negro (1988) has defined the Longitudinal Distortion Index *LDI*, representing the slope of the displacement profile, and he has concluded that *LDI* increases toward the face and reaches a maximum value within the delay distance. At the point of the lining activation the index starts to decrease. Negative values of the *LDI* near the lining is an index of the development of the longitudinal failure mechanism.

In the case where the pressurized shield method is used in the excavation, the resulting displacement field follows three distinctive stages: heave movement at the face, stress release at the tail of the shield, and the post lining activation stage. The compressive air method may show the two stages of the displacement fields in conventional tunnelling. For example, in the case of compressed air tunnelling in the Cairo sewage project (see Figure 4.8) immediate settlement produces crown displacement higher than the near surface displacement. Consolidation settlement is initiated when the compressed air is released. During this stage, the near surface displacement increases remarkably while the crown settlement is not appreciable.

Besides pore pressure equalization, volumetric strain around the excavation is affected by the imposed shear strains. Typical shear strain distribution related to stress release is presented by El-Nahas (1980) and is shown in Figure 4.10. The distribution was obtained as a result of an extensive monitoring program of an experimental tunnel constructed in Edmonton, Canada. The ground condition is mainly a stiff silty clay (glacial ll). The cover depth is about 22.5 m and the tunnel diameter is 2.56 m. Generally the change in the amount of soil movement along the circumference results in placing the region of maximum shear strain between the crown and the spring line as shown in the figure. Accordingly, a certain amount of volumetric strain is generated depending on the soil properties: extensive in case of dilative soil and compressive in case of contracting soil. This strain is added to the initial volumetric strain created because of the stress relief. Figure 4.10 shows the measured volumetric strain at the experimental Edmonton tunnel. From the figure, high initial lateral pressure results in creating a zone of compression above the tunnel and zones of extension at its sides. It may also be noticed that the regions of maximum shear strains produce a reduction in the compressive strains which indicate a



Contours of Shear Strains (%)



Contours of Volumetric Strains (%)

Figure 4.10: Shear and Volumetric Strains around Edmonton Experimental Tunnel (modified after El-Nahhas 1980)

dilation tendency of the till at the tunnel site. An example of the displacement field resulting from pressurized shield tunnelling in soft clay is shown in Figure 4.11 describing the Tilbury tunnel based on De Moor and Taylor (1993: Figures 4.11 and 4.10). Compressive strains are generated because of the application of face pressure by the pressurized crushingmole shield. Then, extensive strains take place because of the tail gap closure. It is noted that the compressive strain region is distant from the excavation while the extensive strain region is confined around the tunnel. It may also be noted that the development of shear strains above the tunnel has an effect in increasing the compressive strains which indicate a contractive tendency of the soft ground. Contour lines of consolidation settlements indicate that the drainage trajectories are initiated generally from the zone of maximum compressive strains above the tunnel crown toward regions of lesser compressive strains.

4.5 Stress Strain Modeling

Predictions of stress-strain fields related to conventional tunnelling are regarded as explicit types of geotechnical problems mainly because they have a common geometrical configuration (circular cavity advancing in the longitudinal direction) and a common loading action: stress release. Therefore, the relationship between the stresses and the strains at a certain point near the excavation can be represented by a simple load-displacement relationship: the ground reaction curve. The use of ground reaction curves in tunnelling design is widely accepted and the ground reaction curves are considered as the basis for the ground confinement method of analysis. In the case of the pressurized shield method, the concept of ground confinement may be extended to include the effect of the three-dimensional aspects, the tunnelling method, and ground-liner interaction.

4.5.1 Ground Reaction Curves for Conventional Tunnelling-Eisenstein Negro Method

The effect of conventional tunnelling on the surrounding ground is characterized by two distinct stages: stress release due to the formation of an unsupported cavity and ground-liner interaction. The Eisenstein-Negro method is formulated in order to predict ground response due to tunnelling in soft ground. As described by Negro (1988), the objective of the method is to determine deformations at the ground surface, and stresses inside the lining, and to evaluate the stability of the unsupported cavity along the delay distance. The applicability of the method, as shown by comparisons with a number of case histories (Negro 1988: Table 7.11) is accepted over a wide range of ground conditions. Conventional tunnelling methods, such as, NATM and non-pressurized shield tunnelling are suitable for the application of the method. Special calculations are not included to

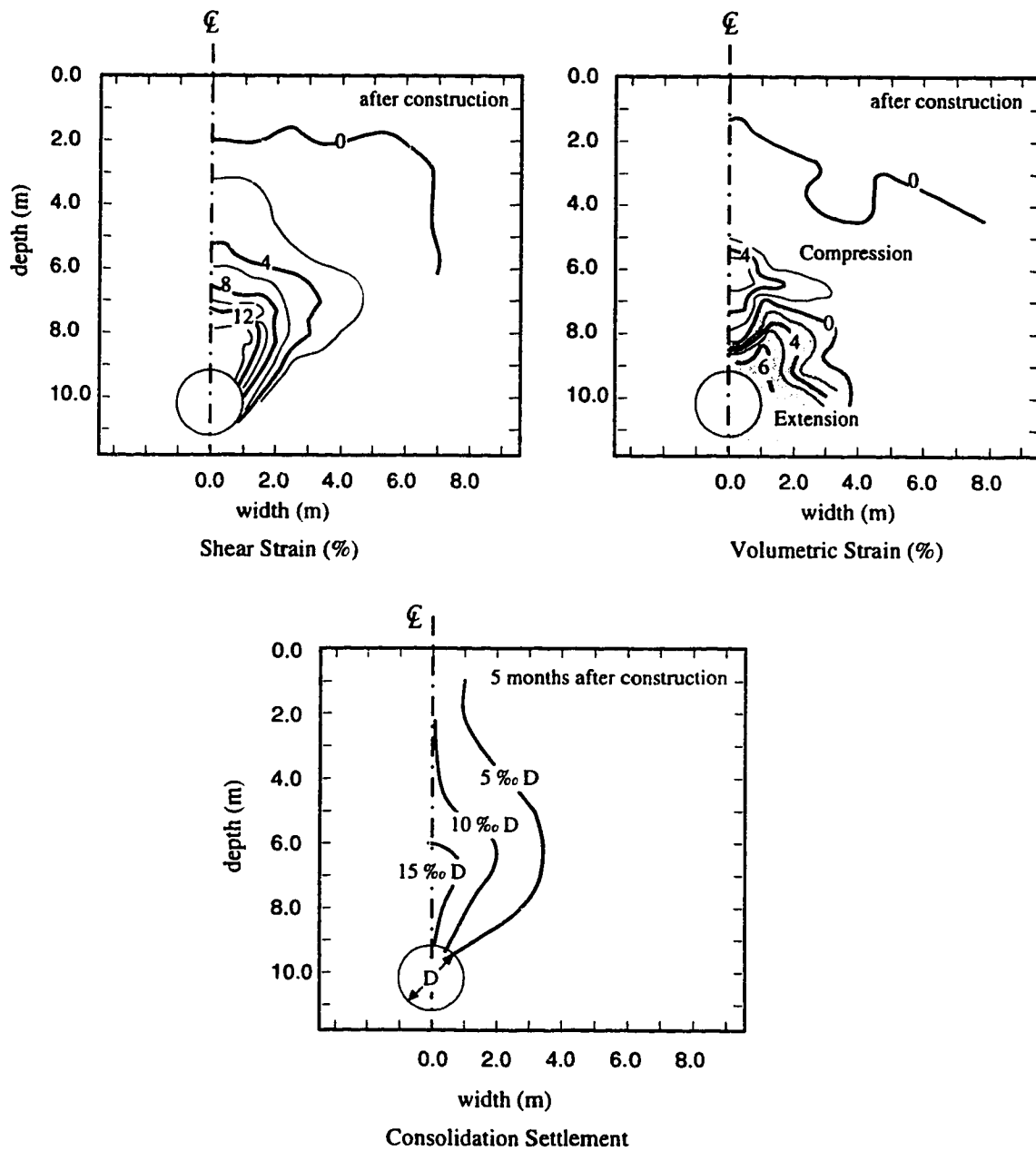


Figure 4.11: Shear and Volumetric Strains around Tilbury Tunnel, Site B (after De Moor and Taylor 1989)

account for the effect of groundwater. Therefore, a reasonable judgment has to be taken into account either by adding the effect of consolidation settlement to the final results or by selecting the drained properties for the parameters used in the method if seepage forces are acting following the same undrained ground patterns. Only a singular circular tunnel is considered, therefore, the effect of twin tunnels may be included by superposition. The calculation method is presented in the form of a calculation sheet and the calculation process includes the following parts:

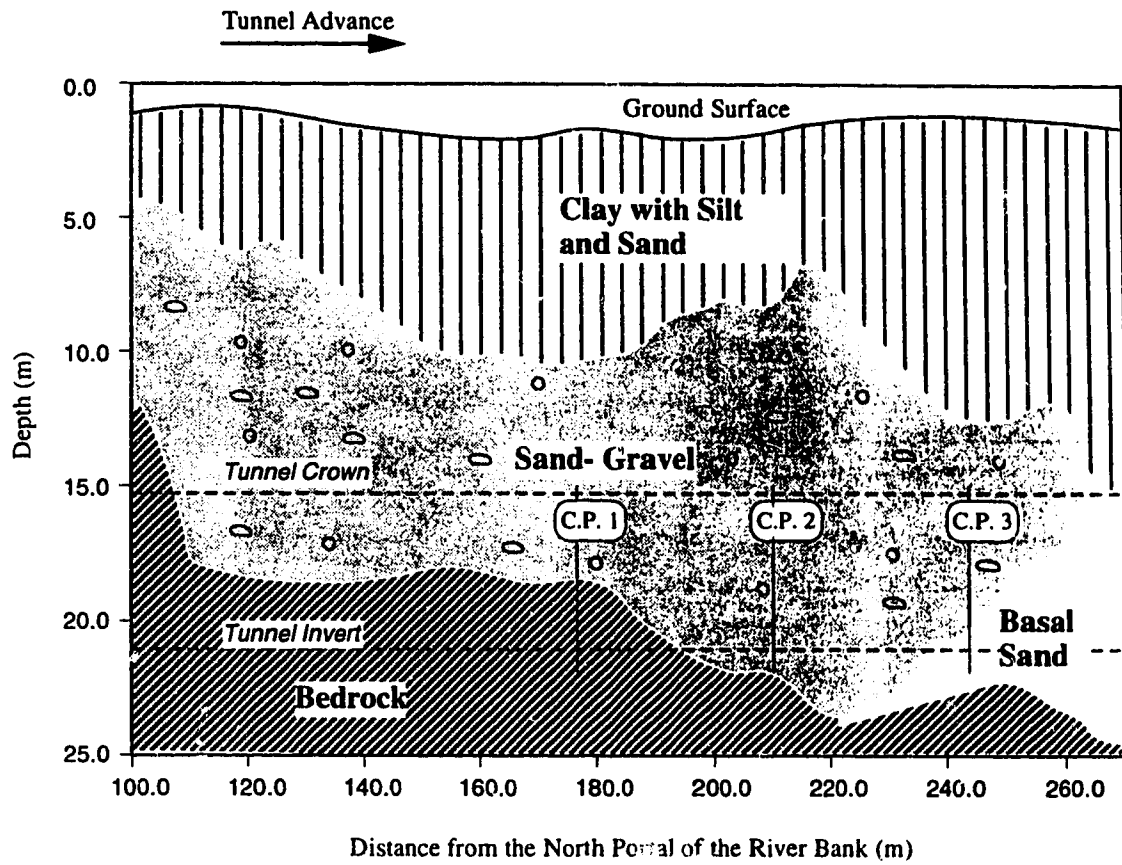
- (1) tunnel closure at lining activation;
- (2) stability Verification;
- (3) amount of stress release;
- (4) lining-ground interaction; and
- (5) subsurface settlements.

The first step considers the three-dimensional effect of carrying out an unsupported excavation along a certain delay distance. For given elastic material properties, and a geometrical configuration a series of charts provide the expected radial displacement at different points of the tunnel circumference associated with the delay distance. Stability verification is based on the d'Escatha and Mandel (1974) solution for shallow tunnels. The above solution uses Coulomb's yield criterion to determine failure conditions of a plane strain tunnel where uniform radial stress is applied at its boundaries and is gradually reduced until failure. The principle of lower bound solution (safe solution) is followed and the obtained failure support pressure are shown to compare well with experimental results. The amount of stress release is calculated based on a number of numerical analyses of plane strain transversal tunnel sections. The analyses use the hyperbolic model (Duncan and Chang, 1970) and the finite element method to calculate the distribution of stress around the tunnel and specifically at a distance $D/2$ away from the circumference at the crown, spring line, and floor position. The homothetic property of the hyperbolic model allows the generalization of the obtained results to cover various values of shear strength and confining pressure. Ground-liner interaction is calculated using Hartmann's solution for soil-lining interaction in elastic media. The solution described by Hartmann (1970 and 1985) includes the effect of lining stiffness, gravitational stress field, and initial stress anisotropy. Based on the average value of stress release a reduced value of ground density and ground stiffness are used in the solution. Normal forces and bending moments inside the lining are evaluated, as well as, the radial and tangential displacements at the lining. The effect of tunnel heave due to excavation may be included in the calculation. An iterative process is used to calculate the additional radial displacement because of tunnel lining interaction. The resultant displacement affects the radial stress around the tunnel and

produces changes to the stiffness of the surrounding soil. These effects are expressed in the calculations by a reduced soil density and a reduced soil deformation modulus. As the converged displacement field is reached, surface movement at the ground surface may be determined from a number of curves relating the normalized soil displacement at the crown to that at the ground surface for various shear strength parameters, geometrical configurations, and initial stress conditions. In some cases interpolation is required between the given shear strength parameters. Ezzeldine (1992) has included the proposed charts and methodology into a computer program to provide the final results based on initial parameters and soil conditions.

4.5.2 Ground Reaction Curves for Tunnels Constructed using Pressurized Shield Methods

In the case of a tunnel constructed using a pressurized shield method, stresses and displacements induced at the boundaries of the excavation from the face and up to the point of the lining activation have an effect on the final state of stresses and displacements around the lining in the transversal plane. An attempt to identify the ground reaction curve of a pressurized shield driven tunnel has been effected by Eisenstein and Ezzeldine (1992: a) during the construction of the LRT Tunnel in Edmonton. Figure 4.12 shows a simplified description of the ground condition at the site. The first 100 metres of the project were constructed in competent Cretaceous bedrock, therefore, no face support was used and the Hydroschild method was not fully implemented. During the following 90 metres, the excavation was conducted in a mixed ground condition of bedrock in the lower half and glacial deposits constituted mainly of sand and gravel in the upper half of the cross section. During the final 70 metres the complete cross section was advanced through the glacial deposits followed by a clean layer of basal sand deposits. Records of the grout and the face pressure are provided by PCL-Hochtief (1990) and the displacement measurements are provided by Thurber (1990) as a result of an extensive monitoring program that included deep and shallow settlement measurement points, multipoint extensometers, slope indicators, and deep bench marks. Convergence measurements were conducted in three locations as indicated in the figure. Measurements from deep settlement points near the crown are compiled with the corresponding face pressure, p_f , grout pressure, p_g , and convergence measurements in the lining to produce an estimation of the most probable ground reaction curve. Figure 4.13 shows the complete set of results along the tunnel. It is to be noted that face pressure and displacement at the face are consistent and they are responsible for a ground surface settlement of about 0.05 % of the tunnel diameter (3 mm). On the other hand, grout pressure and tail displacement show a certain degree of inconsistency, for example, increase in grout pressure does not necessarily produce a



C. P.: Convergence Point

Figure 4.12: Ground Conditions and Locations of Convergence Point Measurements at Edmonton LRT Tunnel

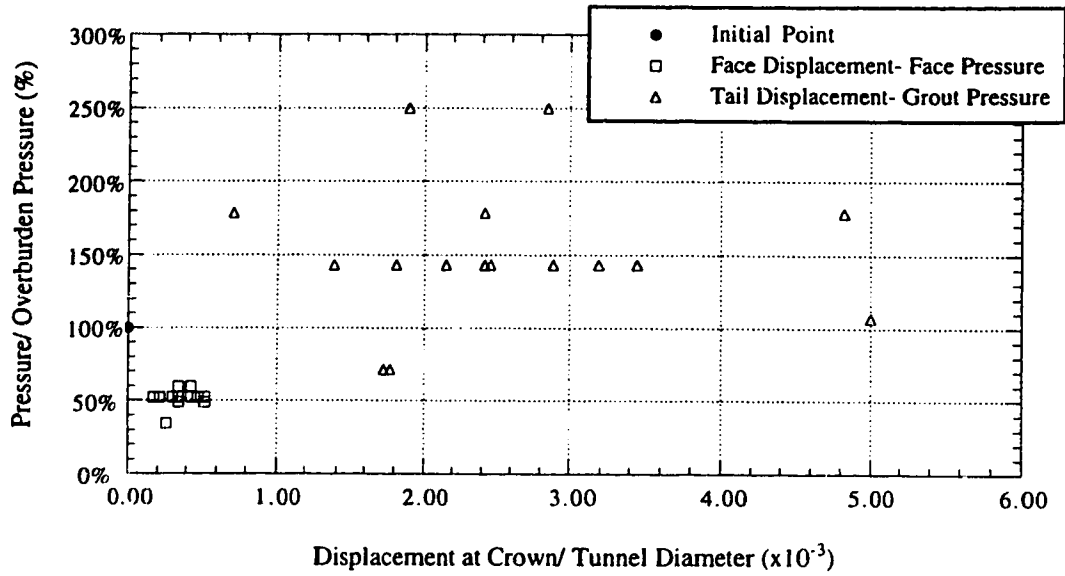


Figure 4.13: Displacement versus Radial Pressure at the Crown of Edmonton LRT Tunnel (after Eisenstein and Ezzeldine (1990)).

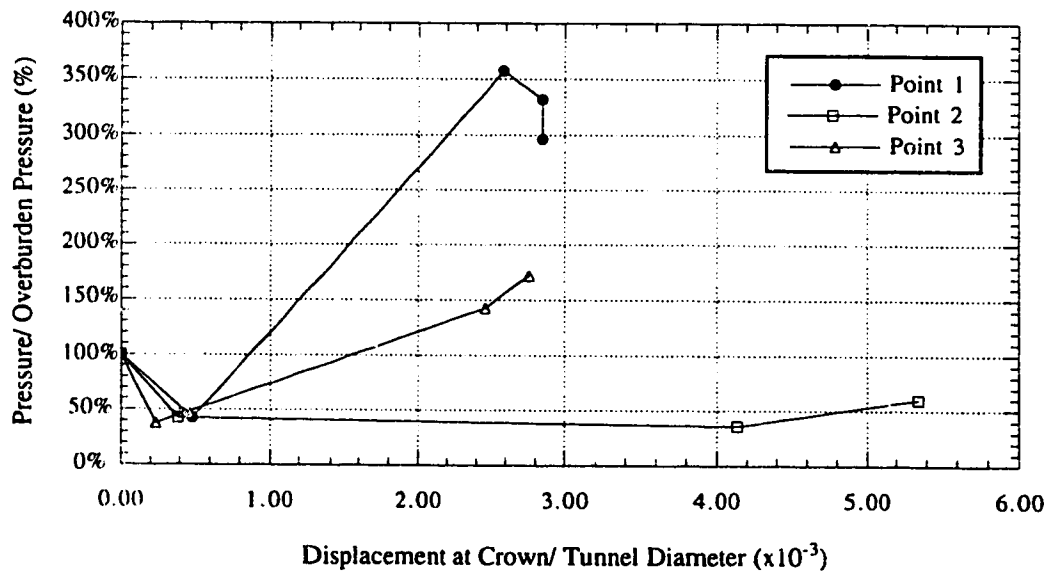


Figure 4.14: Ground Reaction Curves at Edmonton LRT Tunnel (after Eisenstein and Ezzeldine (1990)).

reduction of tail displacement. This may be attributed to a number of factors such as the efficiency in the tail seal, the effect of subsequent excavation steps, and the efficiency of the application of the grout. The highest displacement points are related to special circumstances because of the existence of an abandoned sewer line close to the excavation. Nevertheless, an average total displacement of $0.25 \% D$ (14.5 mm) has taken place due to a grout pressure of about 150 % the overburden pressure at the crown level. Figure 4.14 shows the more complete description of the ground reaction curve where the convergence measurements provide additional points on the curve as the stress in the liner are evaluated. The three convergence points represent three different conditions. The first point is related to an exceptionally high grout pressure. Point 2 represents a case where grout application is not successful which resulted in an excessive displacement at the crown. Point 3 is more likely to represent an average point in the project where a decrease in the radial pressure is noticed at the face followed by an increase to the average grout pressure (150 % of the overburden pressure) and the stress at the lining stabilize at a value close to the grout pressure.

4.6 Concept of Interaction at Construction Phase

The above investigation of the geotechnical characteristics of pressurized shield tunnelling methods shows that the concept of volume loss does not accurately represent the generated stress-and-strain field in the ground for the following reasons:

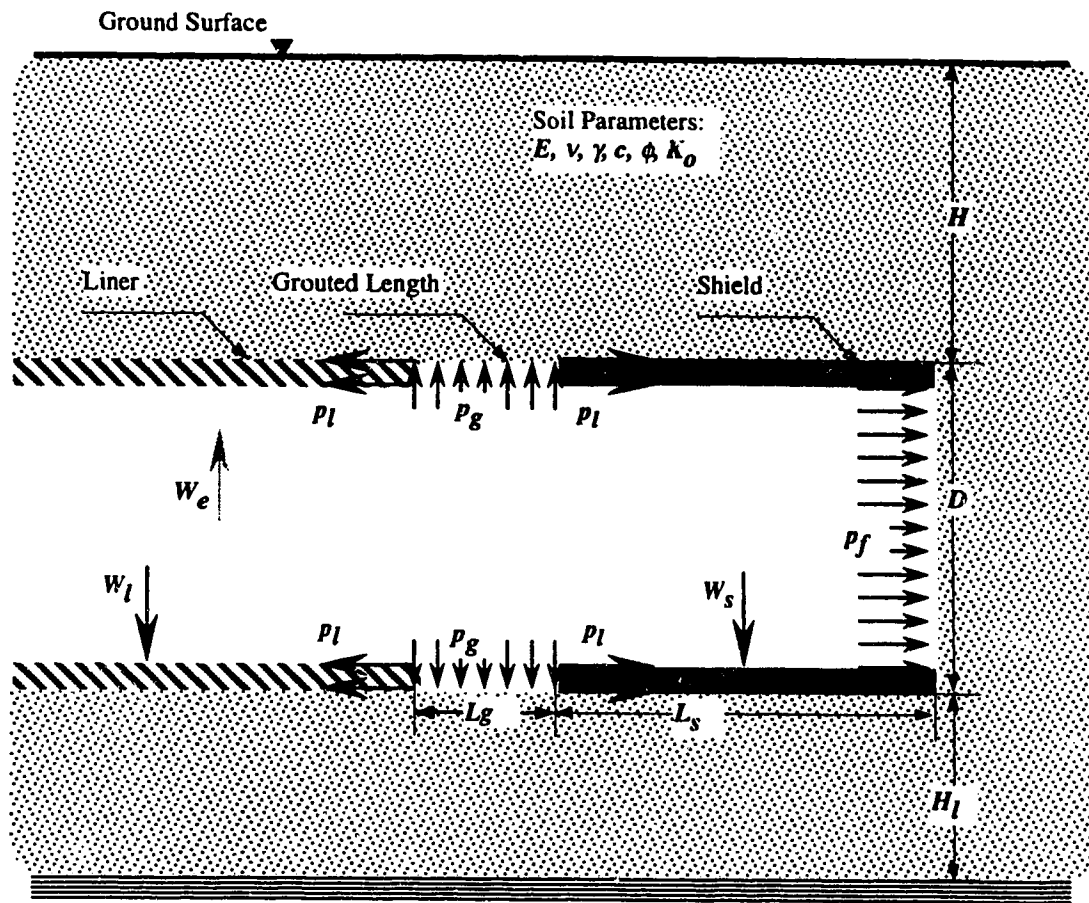
- (1) the two mechanisms of volume loss: material loss due to overcutting or soil movement, are reversible. Material gain takes place at the face in the form of slurry injection and at the tunnel periphery in the form of grout material or extruded liner. Soil movement results in volume gains at the face because of shield propelling forward (especially in case of EPBS) and at the tunnel periphery because of the liner expansion. The assumption that the tail gap consists of the only type of volume loss may be considered as an oversimplification as it overlooks other important aspects of the construction method. It is, therefore, suggested that a structural model that includes the details of the construction scheme and their interaction with the surrounding ground be adopted;
- (2) the entire excavation boundary is always supported at the various steps of the construction. Therefore, the conception of the tunnel as a cavity in which soil moves radially in the transversal plane is subject to discussion. The representation of the tunnel as a structure under different states of support conditions seems more realistic; and

- (3) movement on the horizontal plan, whether in the longitudinal or in the transversal directions has special importance in the case of pressurized shield tunnelling. Longitudinal forces exerted by the shield propelled against the liner are believed to have a substantial contribution to the stress-and-strain fields. Meanwhile, the method of face support affects the characteristics of the settlement trough because of the resultant changes in pore pressure, or the effect of grout pressure, or the effect of the liner pressure.

Therefore, the representation of pressurized shield tunnelling may be considered to resemble soil structure interaction more in this case rather than being a simple case of stress release.

4.6.1 Overall Equilibrium of Forces

Figure 4.15 identifies parameters that are believed to have a significant influence on the stress and strain fields. After the shield advance, the excavation system reaches a state of overall stability through an interactive process with the surrounding ground. Thus results the equilibrium of vertical and horizontal forces. As a result of the soil excavation, a certain amount of weight, W_e , is removed. Meanwhile, downward loads due to the weight of the shield, W_s , and that of the liner, W_l , including the machinery and installations inside them counteract the tunnel tendency to move upward because of W_e . A certain amount of pressure is applied at the face, p_f . The main function of face pressure is to stop soil particle and groundwater intrusion into the gallery. Reaction to the face pressure is ultimately transmitted to the soil depending on soil properties and the method of excavation. Generally, a certain amount of longitudinal forces are transmitted to the ground through the length of shield skin, L_s . The magnitude of these forces depends on the friction and adhesive resistance between the shield skin and the ground. Overcutting due to bead thickness, as well as, the existence of slurry materials influences the transmission of shear stresses between the shield skin and the ground. The reduction of such interaction facilitates shield advance. Therefore, it is normally expected that the major part of the reaction to the face pressure is transmitted to the liner through a system of pistons or hydraulic rams. Along the tunnel length, the longitudinal pressure at the liner, p_l is transmitted to the ground. The distance over which the longitudinal reaction is transmitted to the ground depends on the longitudinal compressibility of the liner, the shearing forces that can be mobilized along the liner skin, and the effect of the grout. Although this action represents a significant additional stress to the lining system, it has the advantage of packing lining rings together. It is to be noted that moment equilibrium induces additional pressure on the surrounding ground. Vertical and transversal rotations are usually



Parameters:

1. Soil Properties

- E : Young's Modulus,
- ν : Poisson's Ratio,
- γ : Soil Density,
- c : Cohesion,
- ϕ : angle of Internal Friction,
- K_0 : coefficient of Lateral Earth Pressure at Rest, and
- W_e : excavated soil weight.

2. Geometry:

- H : depth of the Crown below Ground Surface,
- D : Tunnel Diameter, and
- H_I : depth of Stiff Layer below Tunnel Invert.

3. Construction Method:

- p_f : Face Pressure,
- p_g : Grout Pressure,
- p_l : Longitudinal Reaction on the Liner
- W_s : Shield Weight,
- L_s : Shield Length, and
- L_g : Grouted Length.

4. Liner Properties:

- E_l : Young's Modulus,
- ν_l : Poisson's Ratio, and
- W_l : Weight of the Liner.

Figure 4.15: Parameters affecting the Stress and Strain Fields around a Tunnel Excavated using a Pressurized Shield Method

regulated through a system of pistons between the shield and the liner as part of the alignment control. Longitudinal rotation results from the rotation of the cutting wheel at the face and the required moment to provide the necessary equilibrium is transmitted to the ground through shield skin-ground interaction.

4.6.2 Internal Equilibrium of Forces of the Excavation

As shown above, the overall tunnel stability results in applying a certain amount of forces and movement constraints to the excavation boundary. These actions are the resultant of a number of factors interacting with each other to constitute the internal stability of the excavation. The tail gap is considered the most critical detail affecting the internal stability of the excavation. As a result of the creation of the tail void, soil and water intrude into the cavity creating stress relief and radial strains around the tunnel. The generated stress-strain field depends on a number of factors:

- (1) soil properties: the amount of displacement due to the gap is related to the degree of stress relief produced through soil deformability. Meanwhile, if the stress relief reaches a certain magnitude, post-elastic behaviour is anticipated and although a global failure pattern is not commonly encountered in practice, the magnitude of the resulting strains is expected to increase substantially;
- (2) time effect: soil response to the tail void is of temporary nature as it ceases once the lining system is fully activated. The magnitude of the generated strain field and the associated stress relief depends on a comparison between the rate of advance of the excavation and the rate of soil intrusion. It is expected that this factor is more obvious in running or flowing soil conditions as the void filling generally exceeds the rate of advance. On the other hand, plastic soil conditions have a rate of intrusion comparable to the normal rate of advance and the time factor acquires special importance;
- (3) global stress field: as demonstrated in the preceding section, face pressure is transmitted to the ground through the shield and the lining outer surfaces. As shown in Figure 4.15 the ground region near the gap area undergoes longitudinal forces in opposite directions. This effect is substantial as the face pressure increases. Longitudinal forces transmitted to the ground contribute in increasing the stress release. Thus, soil intrusion into the gap acquires a three-dimensional aspect;
- (4) grouting: in response to the three above factors, grouting is the ground control measure most widely adopted. The effect of the grout is related to the resultant of two actions: grout pressure and improvement of ground properties. Grout

pressure reduces the magnitude to stress relief while the injected material to the grout results in reducing ground deformability and in increasing its shearing resistance; and

- (5) construction sequence: as the excavation proceeds, the above factors act to various extents to affect each other in a repetitive cycle. For example, the application of high grout pressure behind a certain ring may be used to counteract the failure of the tail seal at the preceding ring, and so forth .

4.7 Numerical Analysis

A numerical analysis is carried out to investigate the geotechnical aspects of tunnelling excavation using pressurized shield methods. As presented above, three-dimensional analysis is required as the longitudinal forces imposed on the excavation are of special interest. The finite element method has been proven to be a reliable and effective numerical method to investigate this type of problem as it allows a detailed discretization of the actual site condition. A finite element program SAGE™ was developed at the university of Alberta by Chan (1985).

4.7.1 Statement of the Problem

For different geometrical configurations, and soil parameters a case of pressurized shield tunnel is simulated. The purpose of the analysis is to determine the three-dimensional aspects of the effect of longitudinal pressure at the face and its reaction on the liner, and that of the grout pressure on the stress-and-strain fields around the tunnel. Special emphasis is on the displacement at the ground surface and the ground stresses around the lining system.

4.7.2 Background

From the overview of the stress-and-strain field anticipated around tunnels constructed using pressurized shield methods, it can be concluded that the simulated problem is governed by a number of factors:

- (1) the problem is a moving boundary problem. Therefore, details of the excavation sequence , as well as, the measures undertaken to support the uncovered surfaces are of a substantial importance;
- (2) the possibility of global failure is excluded from the analysis. This is due to the fact that the boundaries of the excavation are controlled either by a certain applied pressure or by a rigid support. Therefore, a failure mechanisms are

supposedly excluded. This does not mean that in actual site conditions the possibility of failure in the transversal plane is non-existent. The nature of incidences involving uncontrolled soil movement into the excavated cavity, as reported by case histories, may be characterized as accidental. Generally the reasons for such failures are related to technical deficiencies in the support system (failure of tail seal for example) or to deficiencies in the operation of the lining system;

- (3) the most critical lining action is settlement at the ground surface as a result of the lack of global failure mechanisms in the transversal plane and as long as the face stability is ensured. This takes place at a position distant from where stress actions have been initiated: tunnel boundaries. Therefore, it can be concluded that except in cases of accidental failure of the support system, the yielded zone is not extended to where the strains are monitored. It is to be noted that "failures" at the ground surface may be related to excessive ground deformation that leads to damages in the foundations of neighbouring structures and this does not necessarily imply that the ground has reached yield state; and
- (4) the importance of yield conditions that are supposed to develop near the tunnel boundaries, is diminished by the effect of three factors. First, material treatment such as grouting and slurry injections are responsible in changing the intrinsic material yield properties. Second, the temporary nature of the excavation process does not allow for the identification of a clear pattern of ground handling. For example, the effect of the application of a certain amount of grout pressure is substantially influenced by whether the grout is injected simultaneously or sequentially around the tunnel. Various details of the grout operation result in different stress paths on the soil particles. Finally, the confinement of the boundary is likely to create a greatly unpredictable flow rule. As the shield and the liner restrain radial displacement of soil particles, movement of the yielded material is likely to be in the longitudinal direction and is induced by a number of factors such as the grout conditions, friction on the lining and shield skins, and the direction of movement of the liner and the shield.

4.7.3 Description of Computational Work

Table 4.1 shows a description of the executed computerized computational runs. The effect of the construction conditions is investigated by adopting various grout and liner pressure ratios, $G.R.$ and $L.R.$, respectively, where

$$G.R. = \frac{p_g}{p_o}, \text{ and} \quad (4.11)$$

$$L.R. = \frac{p_l \cdot \left(\pi \frac{D^2 - D_i^2}{4} \right)}{K_o p_o \cdot \left(\frac{\pi D^2}{4} \right)}, \text{ and} \quad (4.12)$$

where D_i is the internal tunnel diameter as simulated in the model.

4.7.3.1 Choice of Parameters

Various values of $G.R.$, $L.R.$, depth ratio, Poisson's ratio ν , and the initial coefficient of lateral pressure at rest, K_o , are used in the analysis. On the other hand, some parameters are chosen that do not change throughout the analysis as their effect may be normalized in the linear elastic model. The selection of values of these parameters (refer for Figure 4.15 for symbol indications) is done such that they represent an average tunnelling project using the pressurized shield method:

- (1) the tunnel diameters $D = 5.0$ m;
- (2) the shield Length $L_s = D$;
- (3) the grout length $L_g = D/2$;
- (4) the liner and the shield thickness, $(D - D_i) = 0.25$ m;
- (5) the ground density, $\gamma = 19.62$ kN/m³;
- (6) the modulus of deformation of the ground, $E = 10$ MPa;
- (7) the modulus of deformation of the shield and the liner, $E_f = 10$ GPa;
- (8) Poisson's ratio of the shield and the liner, $\nu_f = 0.25$;
- (9) the weight of the shield and weight of the liner, $(W_s + W_l) = W_e$; and
- (10) the depth of the rigid layer below the tunnel floor, $H_f = 7.5$ m.

E=	10.0 MPa
D=	5.0 m
Hl=	7.5 m
γ =	19.6 kN/m ³

#	H/D	G.R.	L.R.	v	Ko
1	1.5	0.0	0.0	0.30	0.80
2	1.5	30.0	0.0	0.30	0.80
3	1.5	75.0	0.0	0.30	0.80
4	1.5	112.5	0.0	0.30	0.80
5	1.5	150.0	0.0	0.30	0.80
6	1.5	225.0	0.0	0.30	0.80
7	1.5	30.0	44.9	0.30	0.80
8	1.5	75.0	44.9	0.30	0.80
9	1.5	112.5	44.9	0.30	0.80
10	1.5	30.0	89.8	0.30	0.80
11	1.5	75.0	89.8	0.30	0.80
12	1.5	112.5	89.8	0.30	0.80
13	1.5	30.0	134.6	0.30	0.80
14	1.5	75.0	134.6	0.30	0.80
15	1.5	112.5	134.6	0.30	0.80
16	1.5	30.0	179.5	0.30	0.80
17	1.5	75.0	179.5	0.30	0.80
18	1.5	112.5	179.5	0.30	0.80
19	1.5	30.0	0.0	0.20	0.80
20	1.5	30.0	0.0	0.45	0.80
21	1.5	30.0	0.0	0.30	0.50
22	1.5	30.0	0.0	0.30	1.00
23	1.5	112.5	0.0	0.20	0.80
24	1.5	112.5	0.0	0.45	0.80
25	1.5	112.5	0.0	0.30	0.50
26	1.5	112.5	0.0	0.30	1.00
27	1.5	30.0	179.5	0.20	0.80
28	1.5	30.0	179.5	0.45	0.80
29	1.5	30.0	287.2	0.30	0.50
30	1.5	30.0	143.6	0.30	1.00
31	1.5	112.5	179.5	0.20	0.80
32	1.5	112.5	179.5	0.45	0.80
33	1.5	112.5	287.2	0.30	0.50
34	1.5	112.5	143.6	0.30	1.00
35	1.5	0.0	0.0	0.20	0.80
36	1.5	0.0	0.0	0.45	0.80
37	1.5	0.0	0.0	0.30	0.50
38	1.5	0.0	0.0	0.30	1.00
39	2.5	0.0	0.0	0.30	0.80
40	2.5	20.0	0.0	0.30	0.80
41	2.5	50.0	0.0	0.30	0.80
42	2.5	75.0	0.0	0.30	0.80
43	2.5	100.0	0.0	0.30	0.80
44	2.5	150.0	0.0	0.30	0.80

#	H/D	G.R.	L.R.	v	Ko
45	2.5	20.0	29.9	0.30	0.80
46	2.5	50.0	29.9	0.30	0.80
47	2.5	75.0	29.9	0.30	0.80
48	2.5	20.0	59.8	0.30	0.80
49	2.5	50.0	59.8	0.30	0.80
50	2.5	75.0	59.8	0.30	0.80
51	2.5	20.0	89.8	0.30	0.80
52	2.5	50.0	89.8	0.30	0.80
53	2.5	75.0	89.8	0.30	0.80
54	2.5	20.0	119.7	0.30	0.80
55	2.5	50.0	119.7	0.30	0.80
56	2.5	75.0	119.7	0.30	0.80
57	2.5	20.0	0.0	0.20	0.80
58	2.5	20.0	0.0	0.45	0.80
59	2.5	20.0	0.0	0.30	0.50
60	2.5	20.0	0.0	0.30	1.00
61	2.5	75.0	0.0	0.20	0.80
62	2.5	75.0	0.0	0.45	0.80
63	2.5	75.0	0.0	0.30	0.50
64	2.5	75.0	0.0	0.30	1.00
65	2.5	20.0	119.7	0.20	0.80
66	2.5	20.0	119.7	0.45	0.80
67	2.5	20.0	191.5	0.30	0.50
68	2.5	20.0	95.7	0.30	1.00
69	2.5	75.0	119.7	0.20	0.80
70	2.5	75.0	119.7	0.45	0.80
71	2.5	75.0	191.5	0.30	0.50
72	2.5	75.0	95.7	0.30	1.00
73	2.5	0.0	0.0	0.20	0.80
74	2.5	0.0	0.0	0.45	0.80
75	2.5	0.0	0.0	0.30	0.50
76	2.5	0.0	0.0	0.30	1.00
77	0.9	0.0	0.0	0.30	0.80
78	0.9	26.8	0.0	0.30	0.80
79	0.9	53.6	0.0	0.30	0.80
80	0.9	80.4	0.0	0.30	0.80
81	0.9	107.1	0.0	0.30	0.80
82	0.9	160.7	0.0	0.30	0.80
83	0.9	26.8	32.2	0.30	0.80
84	0.9	53.6	32.2	0.30	0.80
85	0.9	80.4	32.2	0.30	0.80
86	0.9	26.8	64.5	0.30	0.80
87	0.9	53.6	64.5	0.30	0.80
88	0.9	80.4	64.5	0.30	0.80
89	0.9	26.8	95.0	0.30	0.80
90	0.9	53.6	95.0	0.30	0.80
91	0.9	80.4	95.0	0.30	0.80
92	0.9	26.8	128.6	0.30	0.80
93	0.9	53.6	128.6	0.30	0.80

#	H/D	G.R.	L.R.	v	Ko
94	0.9	80.4	128.6	0.30	0.80
95	0.9	26.8	0.0	0.20	0.80
96	0.9	26.8	0.0	0.45	0.80
97	0.9	26.8	0.0	0.30	0.50
98	0.9	26.8	0.0	0.30	1.00
99	0.9	80.4	0.0	0.20	0.80
100	0.9	80.4	0.0	0.45	0.80
101	0.9	80.4	0.0	0.30	0.50
102	0.9	80.4	0.0	0.30	1.00
103	0.9	26.8	128.6	0.20	0.80
104	0.9	26.8	128.6	0.45	0.80
105	0.9	26.8	205.7	0.30	0.50
106	0.9	26.8	102.9	0.30	1.00
107	0.9	80.4	128.6	0.20	0.80
108	0.9	80.4	128.6	0.45	0.80
109	0.9	80.4	205.7	0.30	0.50
110	0.9	80.4	102.9	0.30	1.00
111	0.9	0.0	0.0	0.20	0.80
112	0.9	0.0	0.0	0.45	0.80
113	0.9	0.0	0.0	0.30	0.50
114	0.9	0.0	0.0	0.30	1.00
115	3.5	20.0	19.9	0.30	0.80
116	3.5	20.0	19.9	0.30	0.80
117	3.5	80.0	19.9	0.30	0.80
118	3.5	20.0	79.8	0.30	0.80
119	3.5	80.0	79.8	0.30	0.80
120	3.5	80.0	19.9	0.20	0.80
121	3.5	20.0	79.8	0.20	0.80
122	3.5	80.0	19.9	0.45	0.80
123	3.5	20.0	79.8	0.45	0.80
124	3.5	80.0	31.9	0.30	0.50
125	3.5	20.0	127.7	0.30	0.50
126	3.5	80.0	16.0	0.30	1.00
127	3.5	20.0	63.8	0.30	1.00
128	3.5	0.0	0.0	0.20	0.80
129	3.5	0.0	0.0	0.45	0.80
130	3.5	0.0	0.0	0.30	0.50
131	3.5	0.0	0.0	0.30	1.00

G.R. and L.R. are in percentage (%)

Table 4.1: Executed Finite Element Runs of Three Dimensional Analysis of a Tunnel Constructed using a Pressurized Shield Method.

4.7.3.2 Finite Element Meshes

Figures 4.16, 4.17, 4.18 and 4.19 show the constructed element meshes. Each mesh consists of eleven transversal slices of variable thicknesses. The smallest thickness is at the middle of the mesh so as to increase the accuracy of the excavation steps. The dimensions of the mesh are 72.5 m long, 47.0 m wide, and 17.0, 20.0, and 25.0 m high. The selected tunnel diameter is 5 m and its axis is 10 m above the bottom of the mesh which is comprised of a rigid base. The thickness of the shield and the liner elements is chosen to be constant at 0.25 m. The selection of the meshes and their dimensions are selected based on a sensitivity analysis taking into account the capacity of the computing system (an IBM RISC/6000™ computer) and the shape ratio of the used elements. Twenty node elements were used for all analyses with a 3x3x3 order of integration. The total number of elements is 846 and the total number of nodal points is 4364. The size of the executed mesh is comparable to recent studies of three-dimensional tunnel modeling such as those of Lee (1989), Heinz (1984), Negro (1988), Kasali and Clough (1983), and Clough (1983).

4.7.3.3 Simulation of Excavation Steps

In order to simulate the excavation steps using different pressurized shield tunnelling methods, the following assumptions are formulated:

- (1) soil material is isotropic homogeneous and elastic;
- (2) shield and liner materials are very stiff compared to the surrounding ground conditions. This assumption is more realistic for the shield than it is for the liner. However, it could be believed that the ground-lining interaction is of a two-dimensional plane strain nature and this effect may be incorporated in the obtained results;
- (3) the weight of the excavated material is equal to the weight of shield. This is closer to a design objective rather than an assumption. The realization of the vertical equilibrium is seen to have a positive effect on the shield alignment as recommended by Schmitter et al. (1988) for the construction of a sewer tunnel in Mexico City using the Bentonite Slurry Shield method. However, the implementation of this objective is not always possible, especially, in excavation above the groundwater table² where the weight of the shield and the

²For example, the Hydrosshield used in the construction of Edmonton LRT project has a weight to volume ratio of about 9.6 kN/m³ which is estimated to be less than the average soil unit weight (PCL-Hochtief, 1988:a).

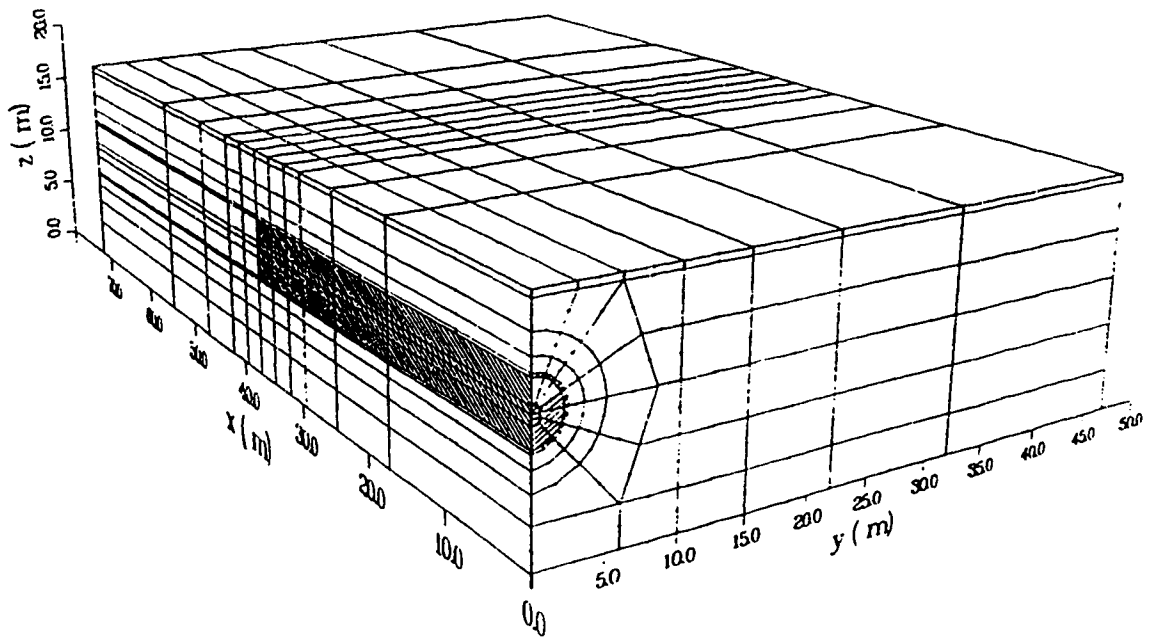


Figure 4.16: Finite Element Mesh for a Tunnel (Depth Ratio= 1.0)

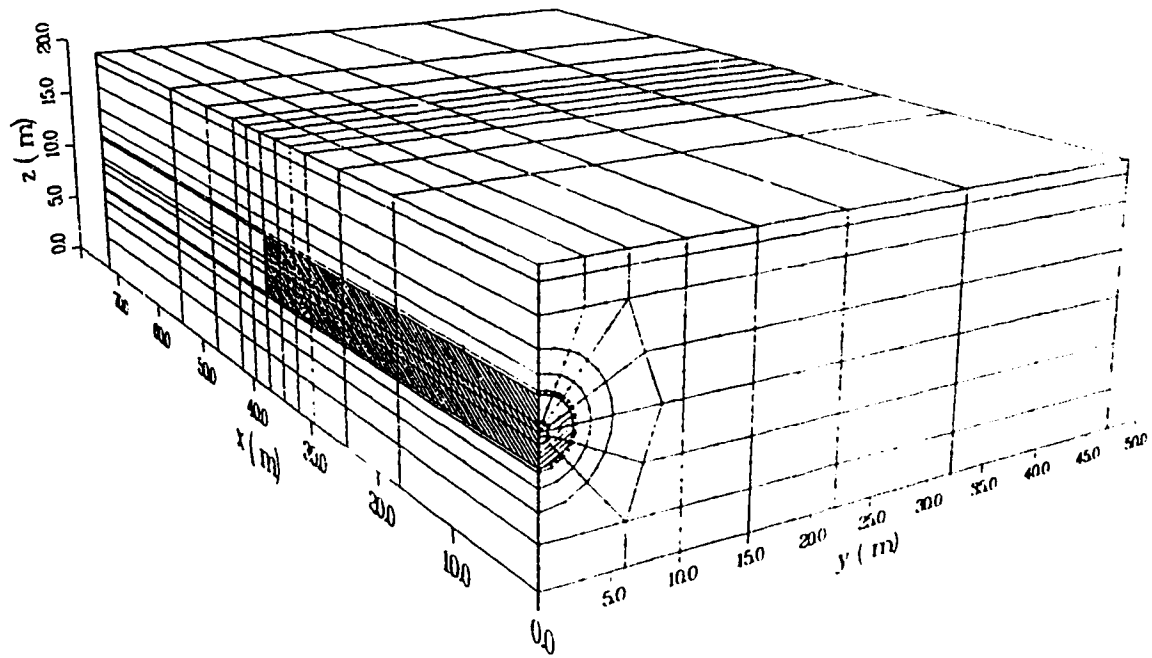


Figure 4.17: Finite Element Mesh for a Tunnel (Depth Ratio= 1.5)

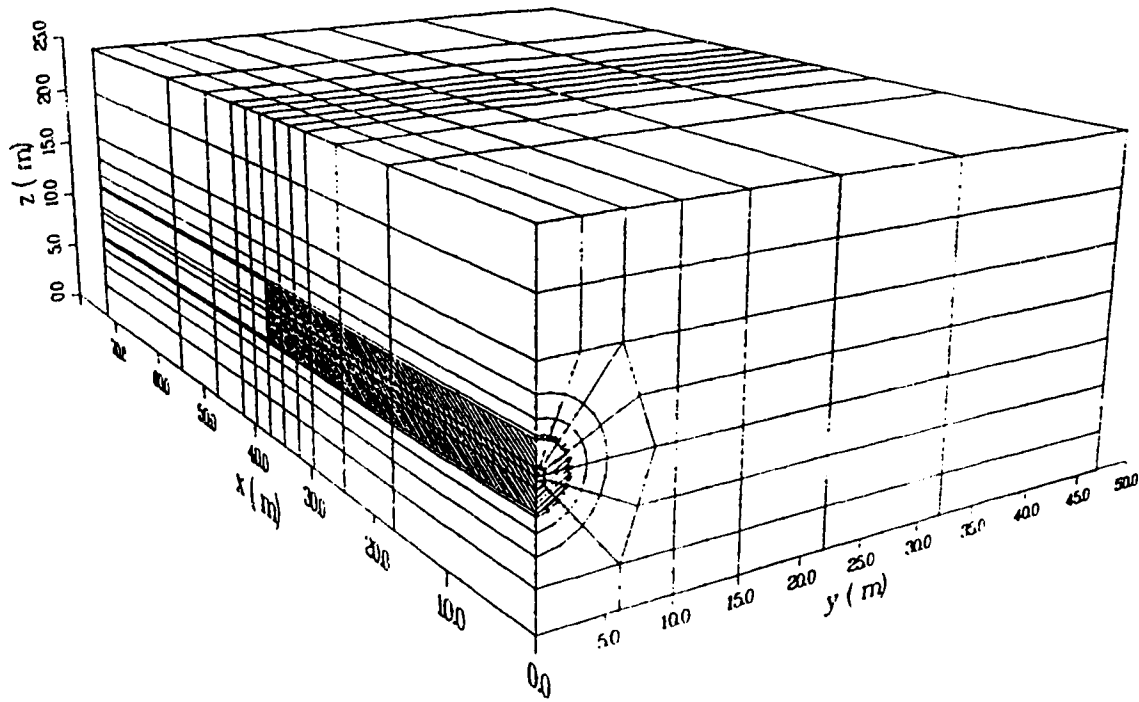


Figure 4.18: Finite Element Mesh for a Tunnel (Depth Ratio= 2.5)

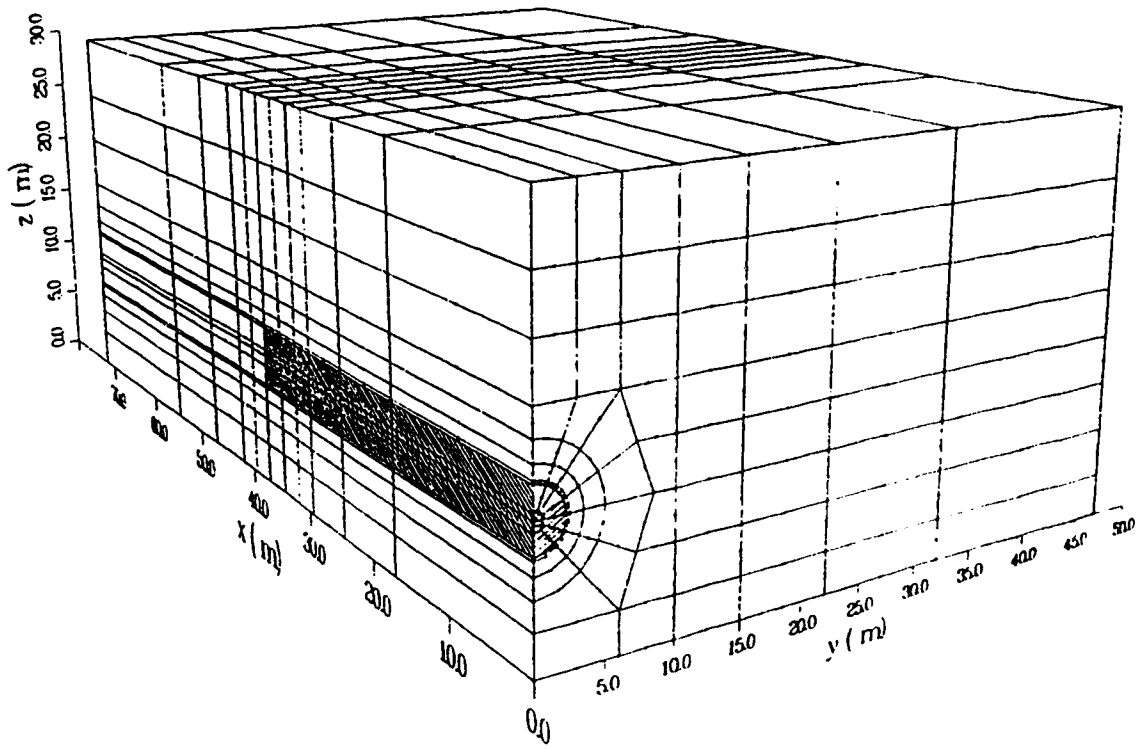


Figure 4.19: Finite Element Mesh for a Tunnel (Depth Ratio= 3.5)

machinery inside it are usually smaller than the weight of the excavated soil mass;

- (4) the grout length is 2.5 m, and the typical ring length is about 1.1 m. It is usually recommended that the grouting be performed after the installation of each ring ("advance one ring-inject one ring" principle). However, the selection of grout length which is roughly equal to two ring lengths is based on the assumption that grouting material is not permanently effective until two rings are installed and grouted. Meanwhile, this assumption has considerable effect in reducing the size of the computational work; and
- (5) ground material is not allowed to move with respect to the shield or the lining skins.

Each computer run consists of five steps as shown in Figure 4.20:

- (1) Step 1 - initial pressure: all elements of the mesh are assigned elastic properties and the assigned unit weight and Poisson's ratio correspond to the soil unit weight with a selected coefficient of lateral pressure at rest;
- (2) Step 2 - tunnel excavation: element strains and displacement from the previous step are automatically reset to zero. Elements within the tunnel boundaries for a length of six slices (37.5 m) are excavated and the liner and the shield elements are installed. The excavation process is achieved by eliminating the excavated element from the global stiffness matrix, and adding surface traction forces calculated based on the global equations of equilibrium, to the boundaries of the elements in contact with the excavated elements. Meanwhile, soil elements at the face are not allowed to move into the shield by assigning high stiffness material parameters at the face of the shield;
- (3) Step 3 - initiation of the gap length: a gap length is created by excavating the fourth slice and applying grout pressure at the exposed ground elements. Meanwhile, a force corresponding to the reaction to the face pressure is applied at the rear end of the shield in the direction of forward movement of the shield;
- (4) Step 4 - tunnel advances of one ring forward: shield elements, as well as, gap elements are shifted one slice forward; and
- (5) Step 5 - Tunnel advances of another ring forward: shield elements, as well as, gap elements are shifted one slice forward.

The simulation of the excavation advance has to deal with two main problems. First, ground forces exerted on the shield are not necessarily in equilibrium with the supporting lining forces which results in a transversal rotation of the whole shield. Second, the reactivation of the lining elements along the grout length may result in a

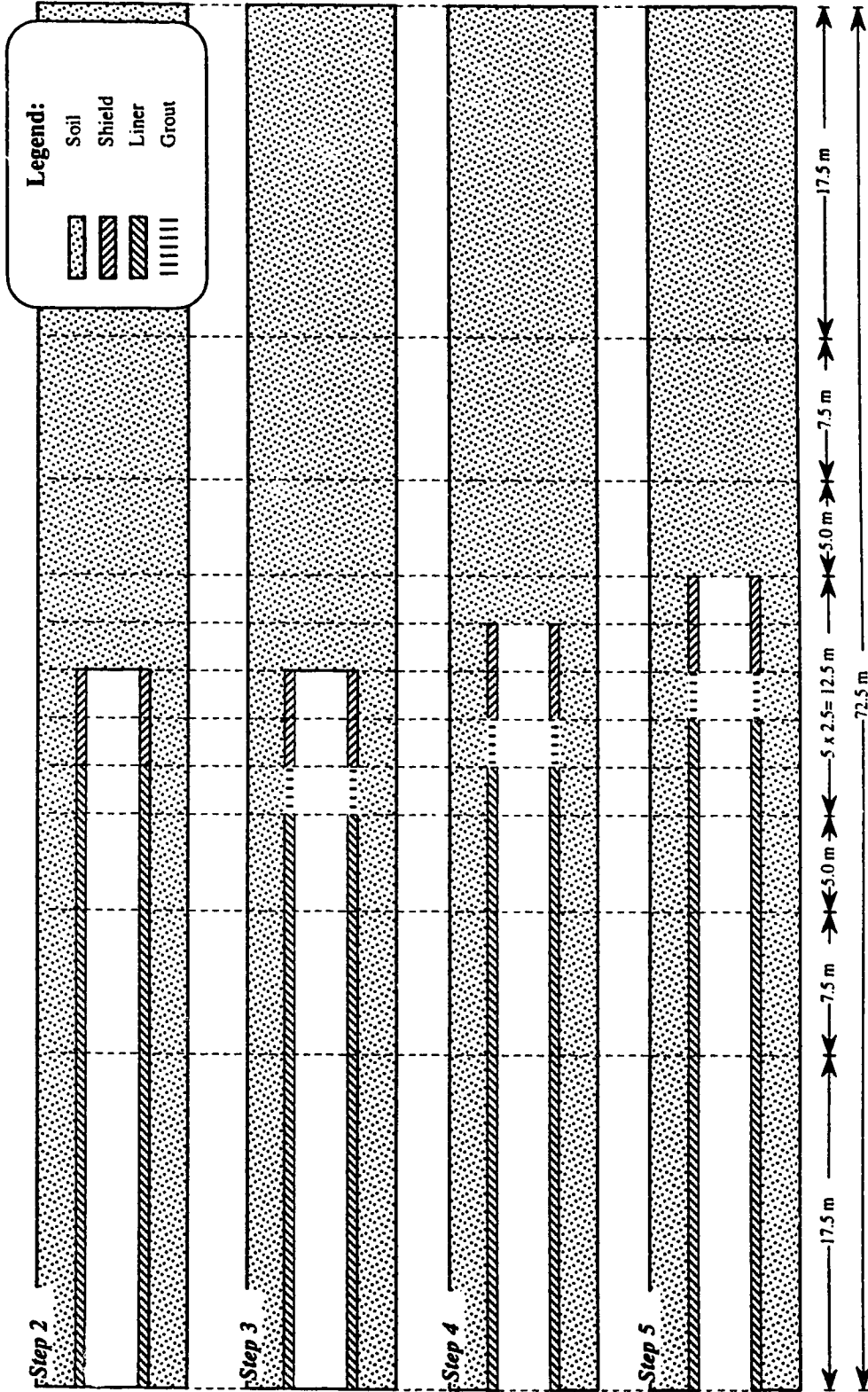


Figure 4.20: Steps used in the Finite Element Simulation of a Tunnel Excavated using a Pressurized Shield Method

distorted lining shape because the new lining element is supposed to share the same degree of freedom as the already displaced ground element. The first problem is solved by using the locking option introduced in the program. Vertical movement of nodal degrees of freedom of the lining elements, as well as, those of the shield elements are locked to that of the corresponding nodal points at the mesh boundary as shown in Figure 4.21. The second problem is dealt with by assigning new elements for the reactivated lining elements with new nodal points having the same coordinates as those of the ground nodes. In this way, the new lining elements interact with the ground elements by locking the two concurrent nodes with each other.

4.7.4 Results

Results related to a depth ratio of 1.5 are only presented, hereafter, as results from other executed runs which show similar patterns of stresses and deformations. Interest on the ground deformation, the magnitude of the stress changes at the tunnel boundary, the mobilized shear strength, and the stress paths is emphasized.

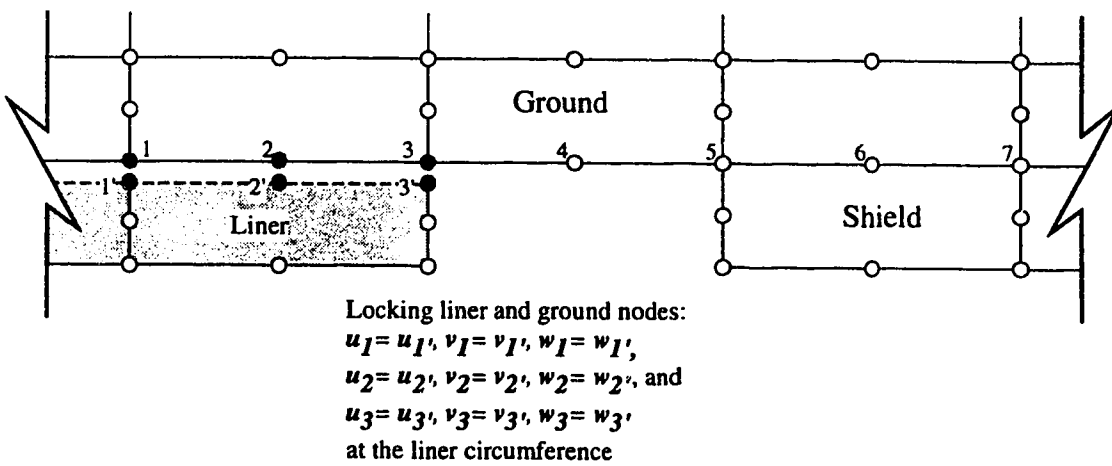
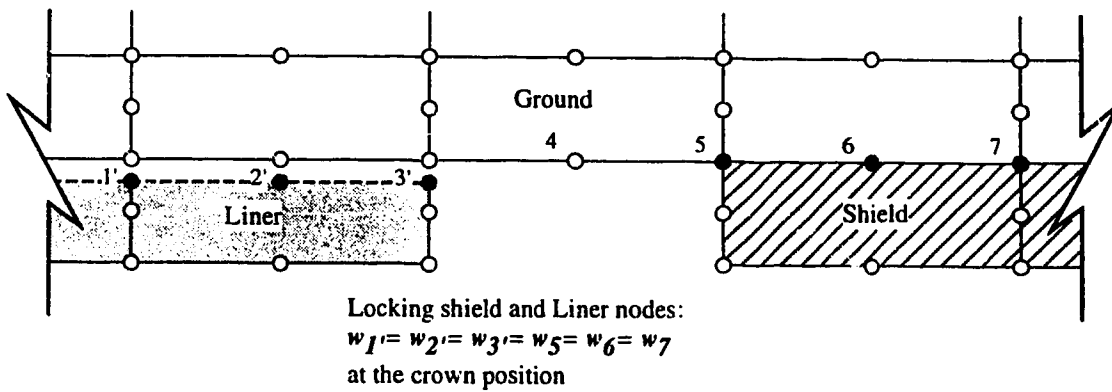
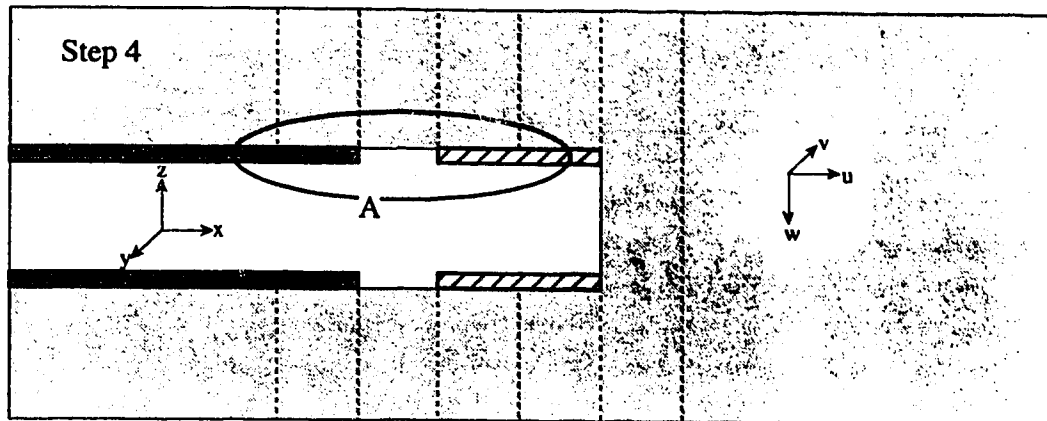
4.7.4.1 Ground Deformation

Figures 4.22 through 4.29 show a three-dimensional view of the vertical settlement around the tunnel. Figures 4.30 through 4.42 show the vertical displacement at the longitudinal axis. As surface movement at the far end of the mesh represents a case of two-dimensional immediate excavation and lining placement, it cannot be representative of the excavation process. Also, surface displacement at the centre line reaches an optimum value behind the point of the lining activation (around 10 m behind the face). Displacement at this point is selected as representative of the final surface displacement and is normalized as:

$$\bar{w}_s = \frac{wE}{Dp_0} \quad (4.13)$$

where w is the downward vertical displacement at the ground surface.

Appendix B shows the obtained normalized transversal profiles at the optimum displacement point in the longitudinal direction. From the figures it can be concluded that the effect of the liner and the grout pressures are in a way self-counteracting. While the liner pressure tends to produce heave at the ground surface ahead of the tunnel face and downward displacement behind the shield tail, grout pressure tends to reduce the ground



Detailing A

Figure 4.21: Nodes Locking used in the Three Dimensional Numerical Simulation of a Tunnel Excavated using Pressurized Shield Method

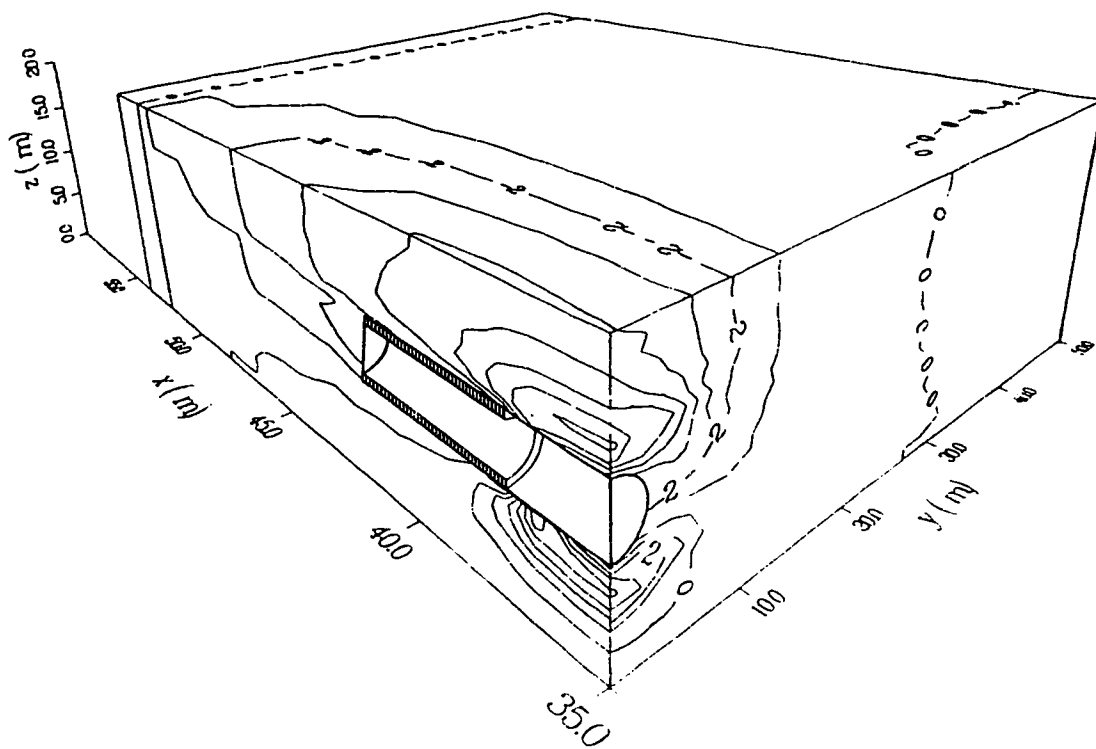


Figure 4.22: Three Dimensional View of Vertical Movement (G.R.= 30.0% and L.R.= 0.0%)

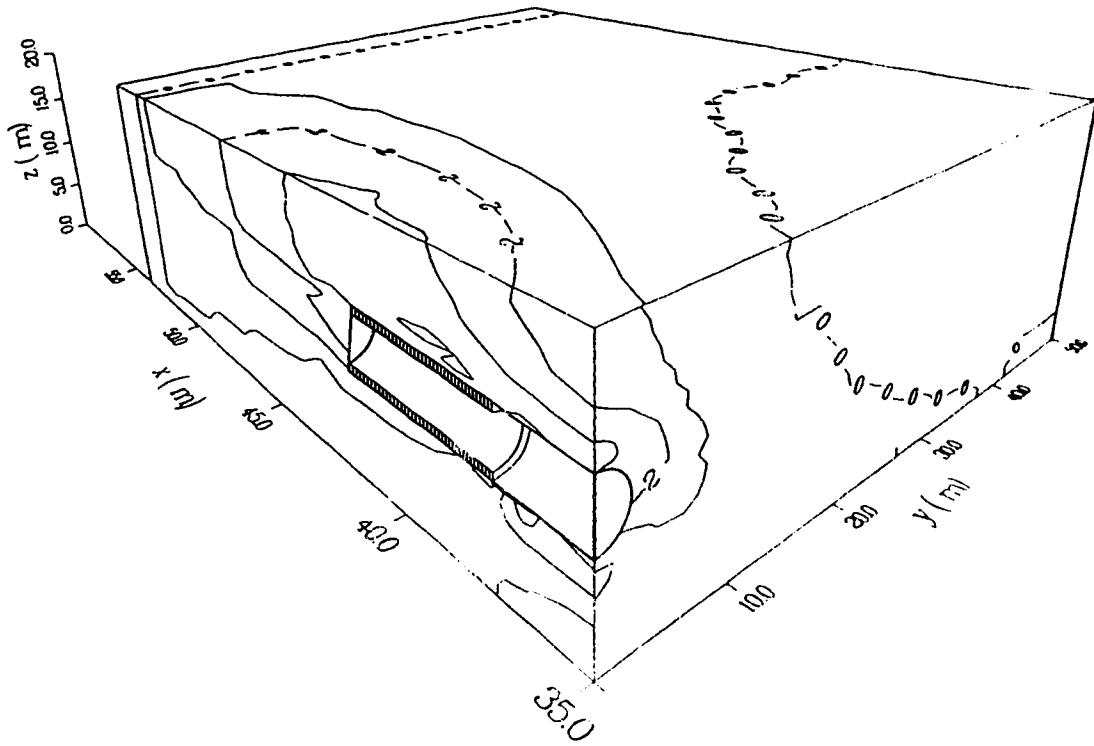


Figure 4.23: Three Dimensional View of Vertical Movement (G.R.= 75.0% and L.R.= 0.0%)

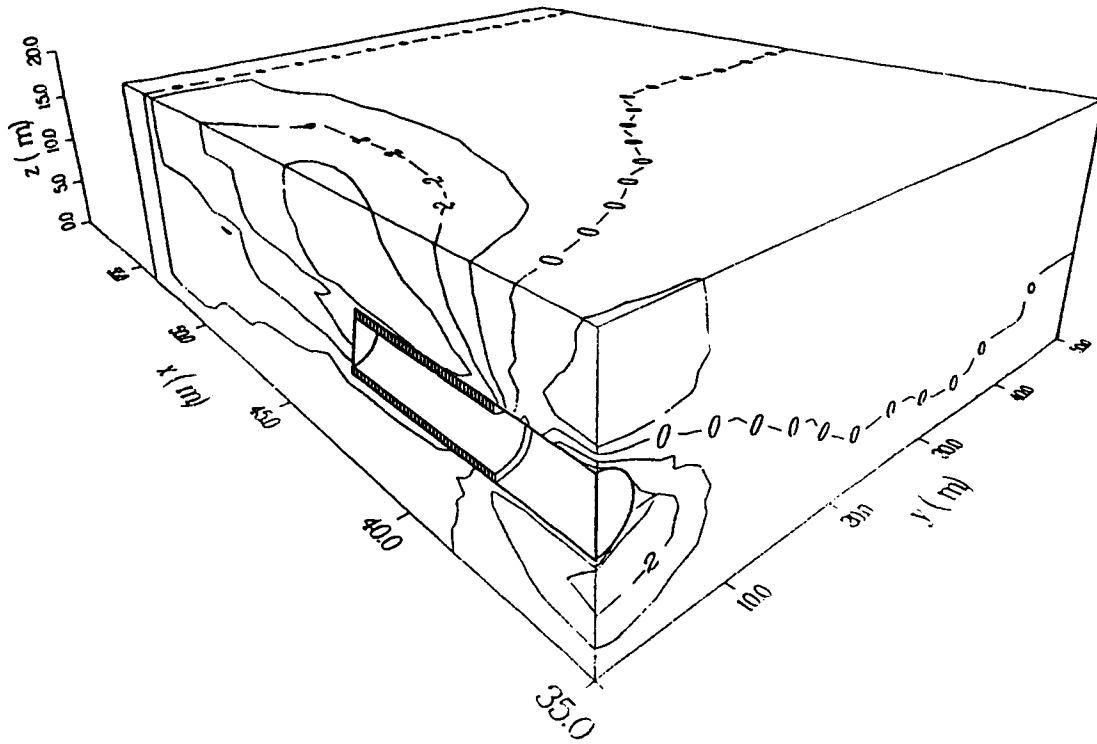


Figure 4.24: Three Dimensional View of Vertical Movement (G.R.= 112.5% and L.R.= 0.0%)

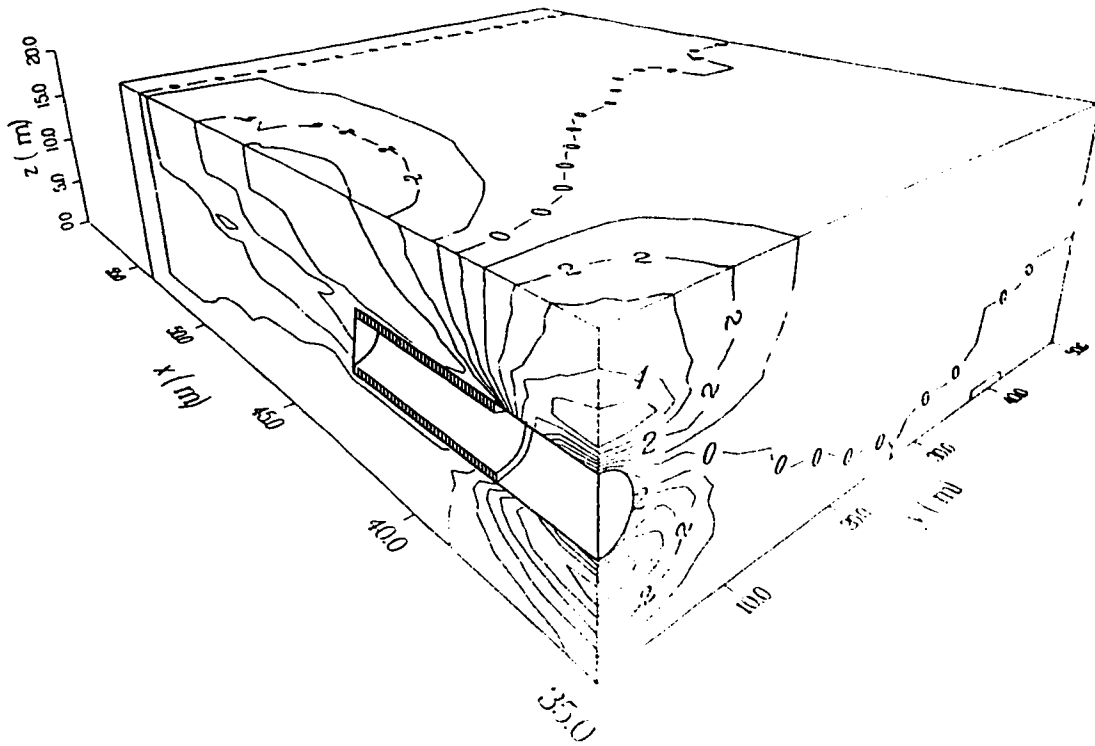


Figure 4.25: Three Dimensional View of Vertical Movement (G.R.= 150.0% and L.R.= 0.0%)

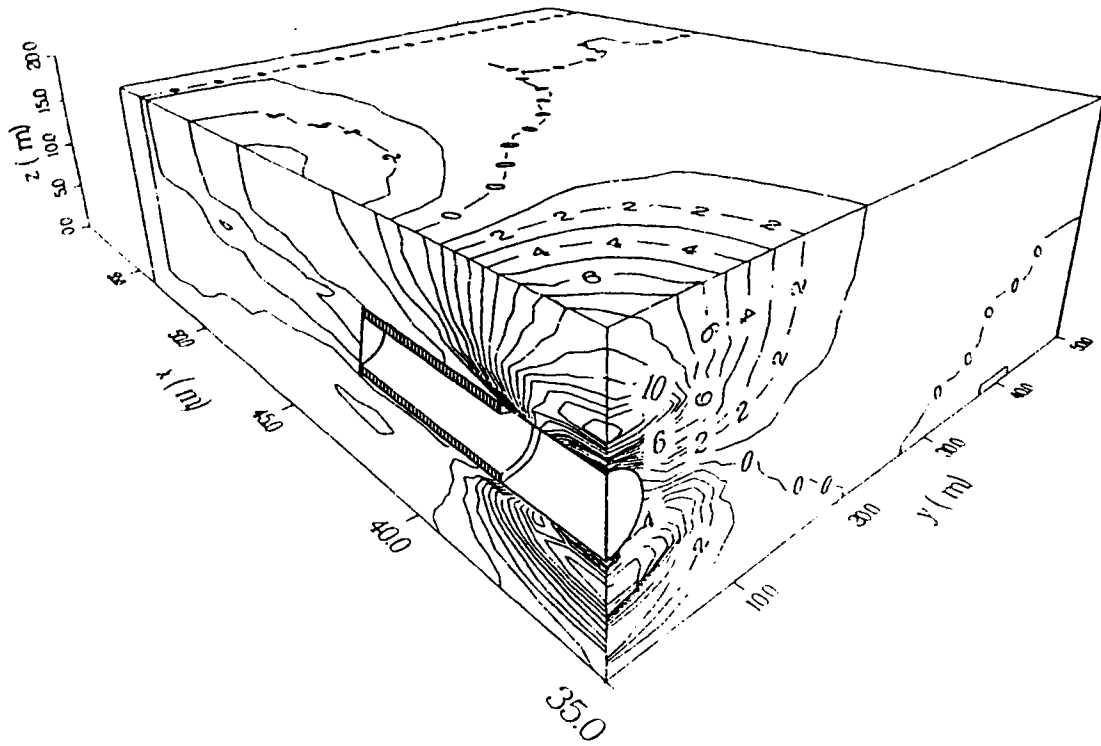


Figure 4.26: Three Dimensional View of Vertical Movement (G.R.= 225.0% and L.R.= 0.0%)

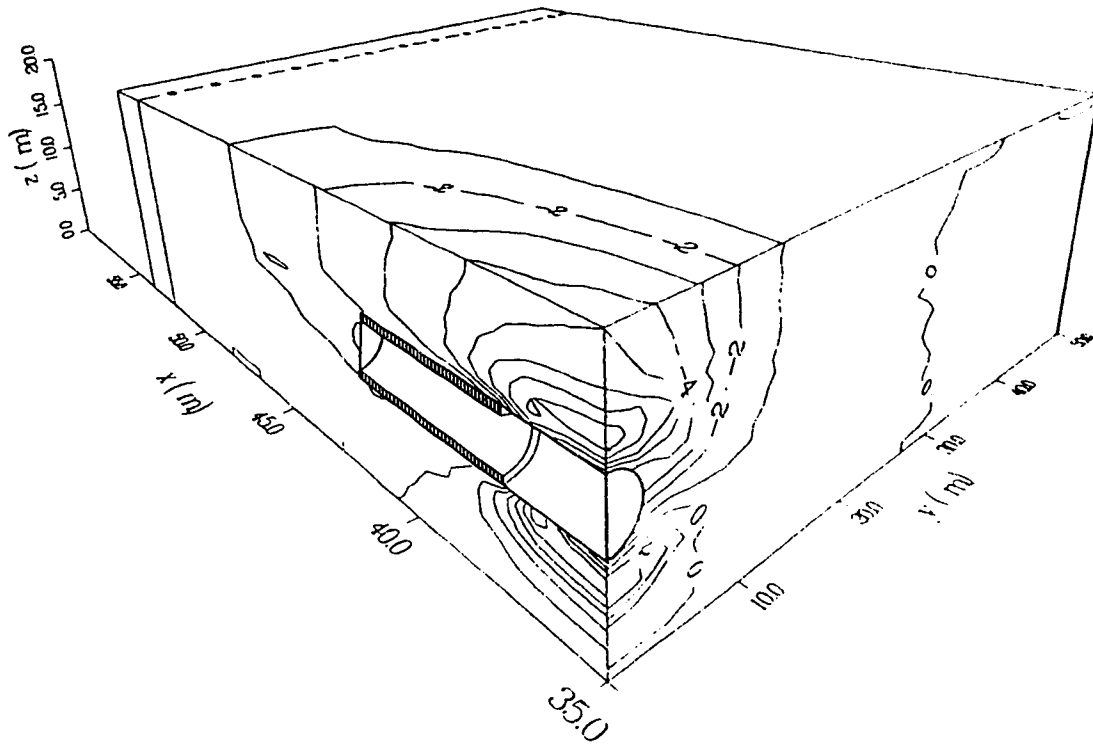


Figure 4.27: Three Dimensional View of Vertical Movement (G.R.= 30.0% and L.R.= 45.0%)

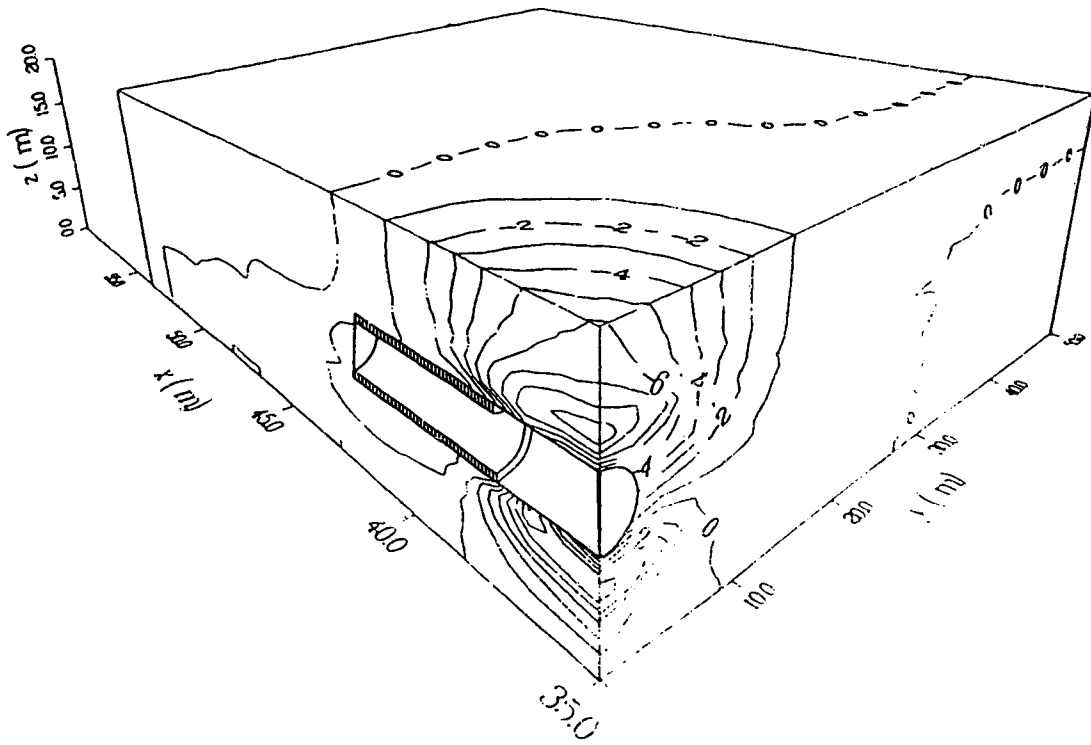


Figure 4.28: Three Dimensional View of Vertical Movement (G.R.= 30.0% and
S.R.= 90.0%)

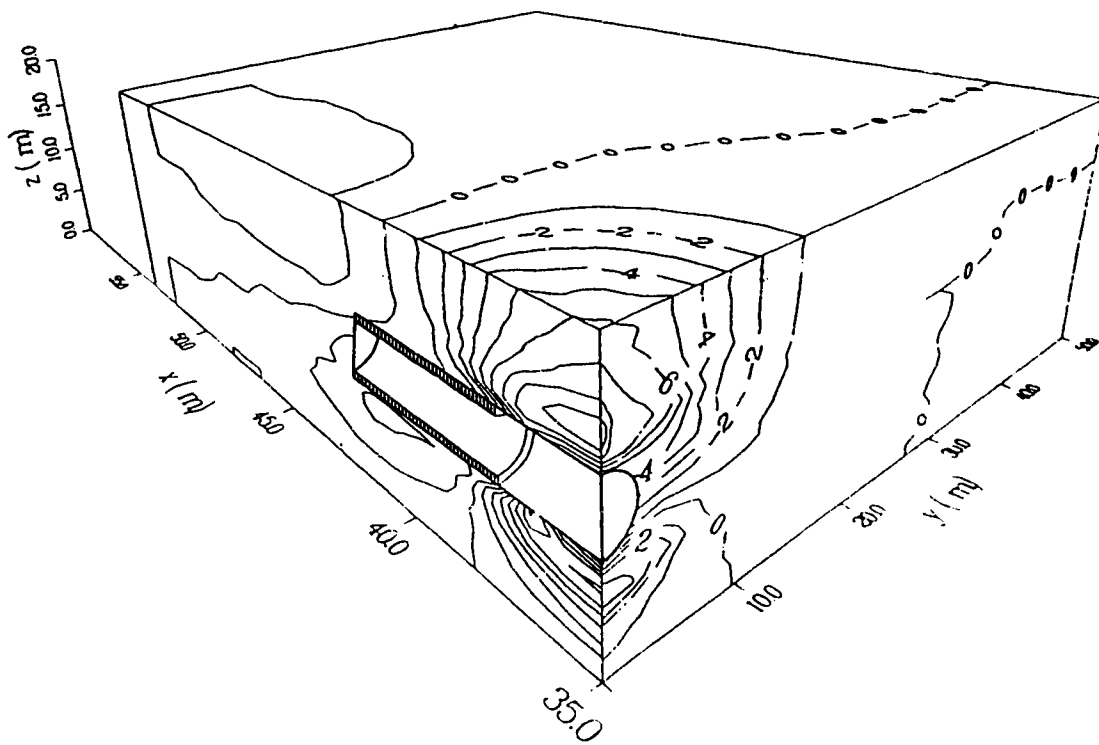


Figure 4.29: Three Dimensional View of Vertical Movement (G.R.= 30.0% and L.R.= 135.0%)

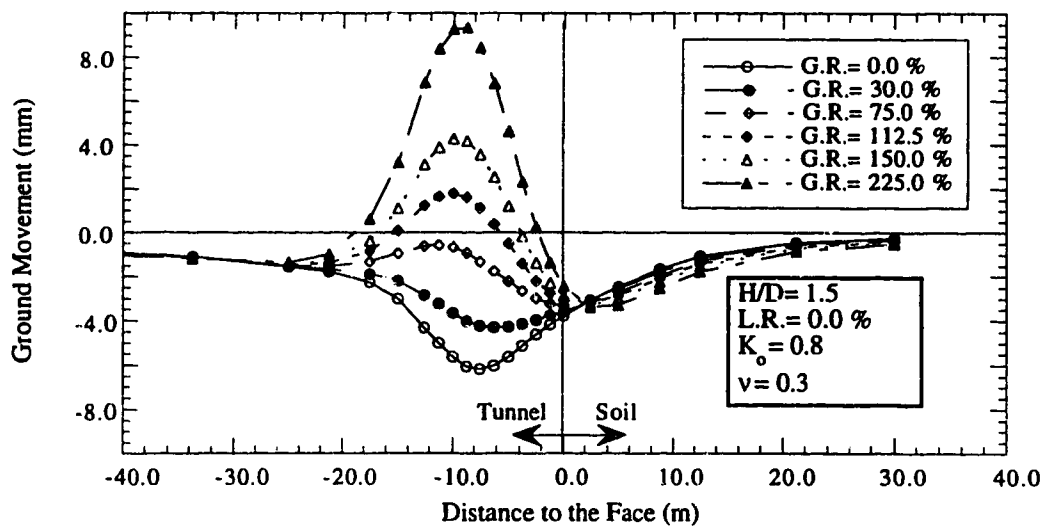


Figure 4.30: Surface Displacement at Longitudinal Axis for various Grout Ratios (L.R.= 0.0%)

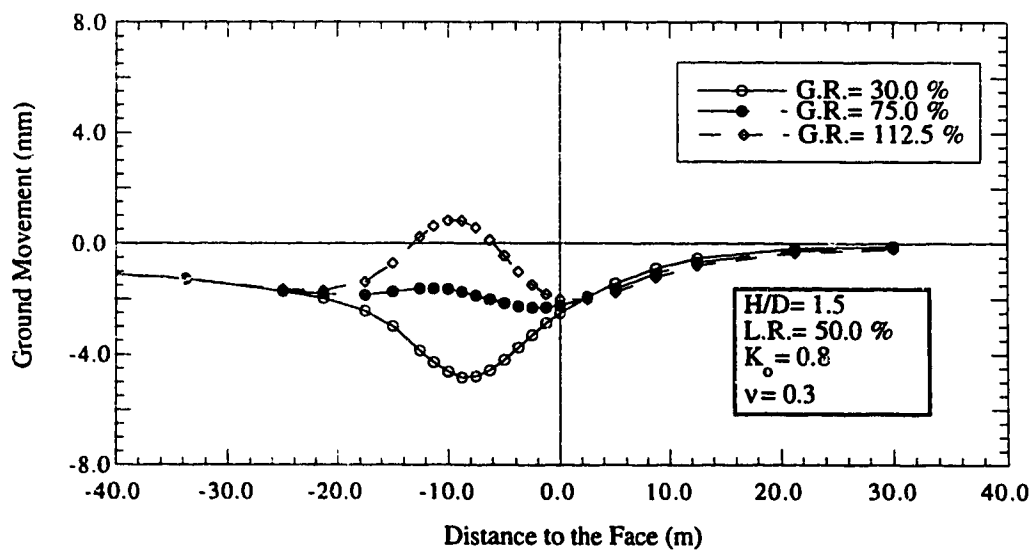


Figure 4.31: Surface Displacement at Longitudinal Axis for various Grout Ratios (L.R.= 45.0%)

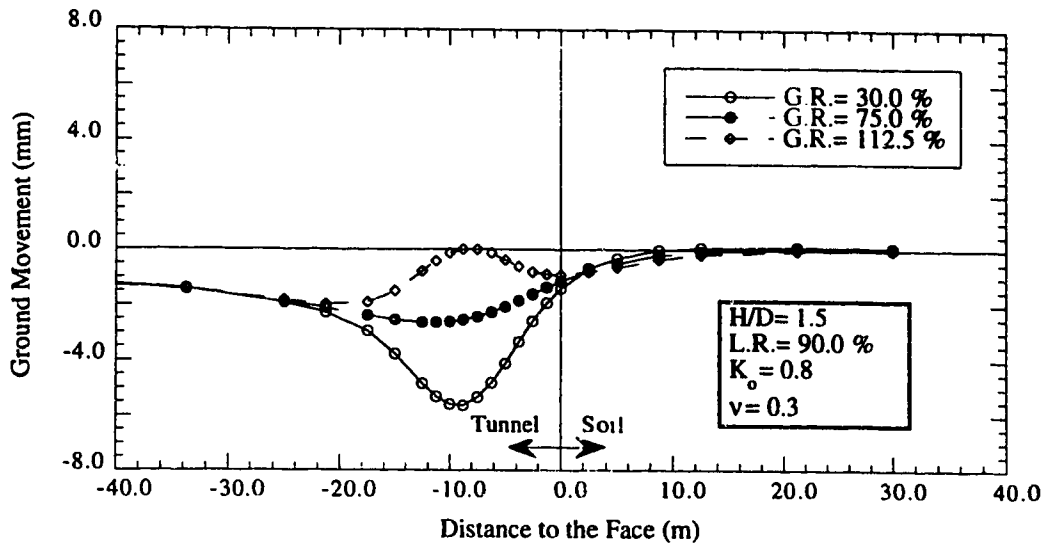


Figure 4.32: Surface Displacement at Longitudinal Axis for various Grout Ratios (L.R.= 90.0%)

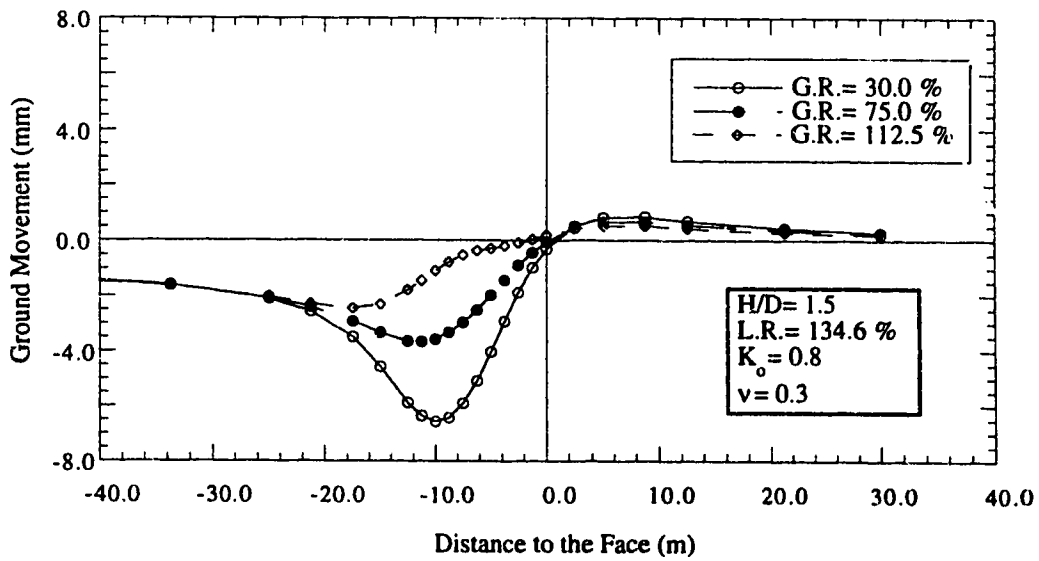


Figure 4.33: Surface Displacement at Longitudinal Axis for various Grout Ratios (L.R.= 135.0%)

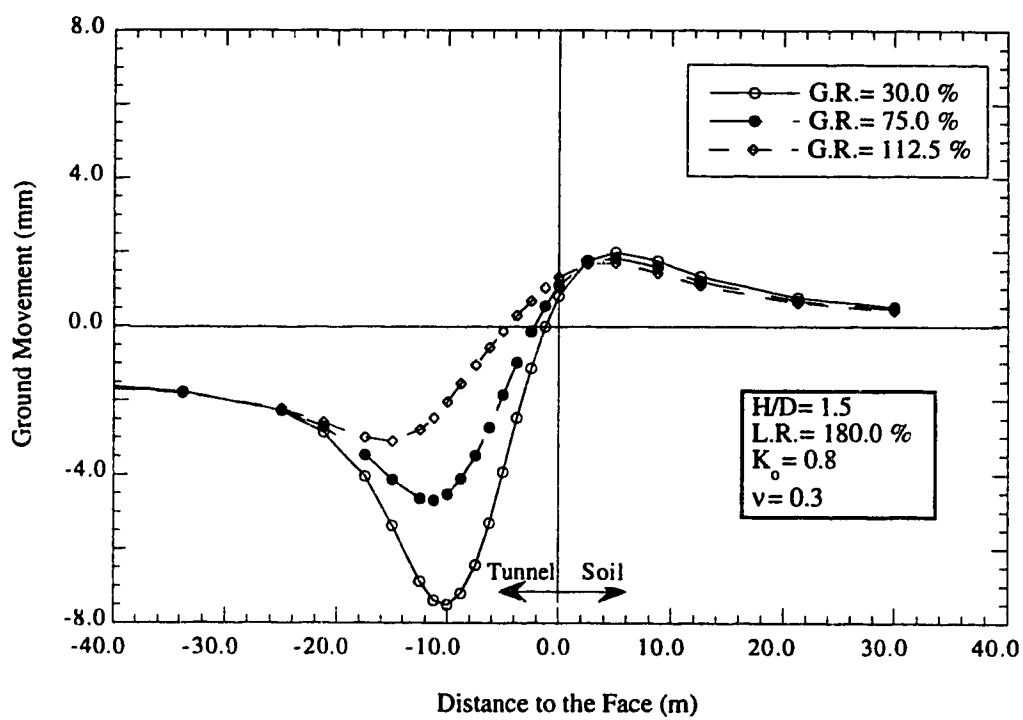


Figure 4.34: Surface Displacement at Longitudinal Axis for various Grout Ratios (L.R.= 180.0%)

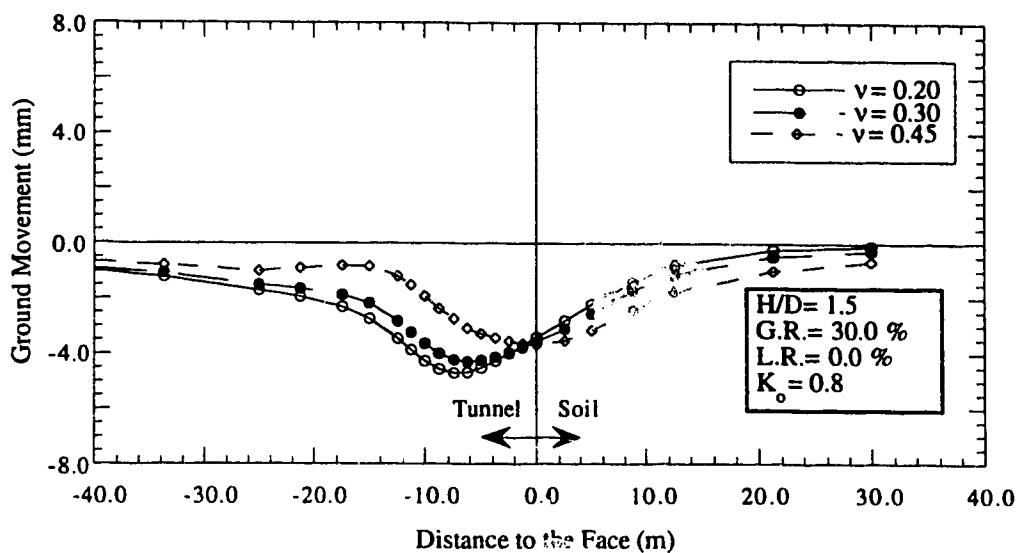


Figure 4.35: Surface Displacement at Longitudinal Axis for various Poisson's Ratios (G.R.= 30.0% and L.R.= 0.0%)

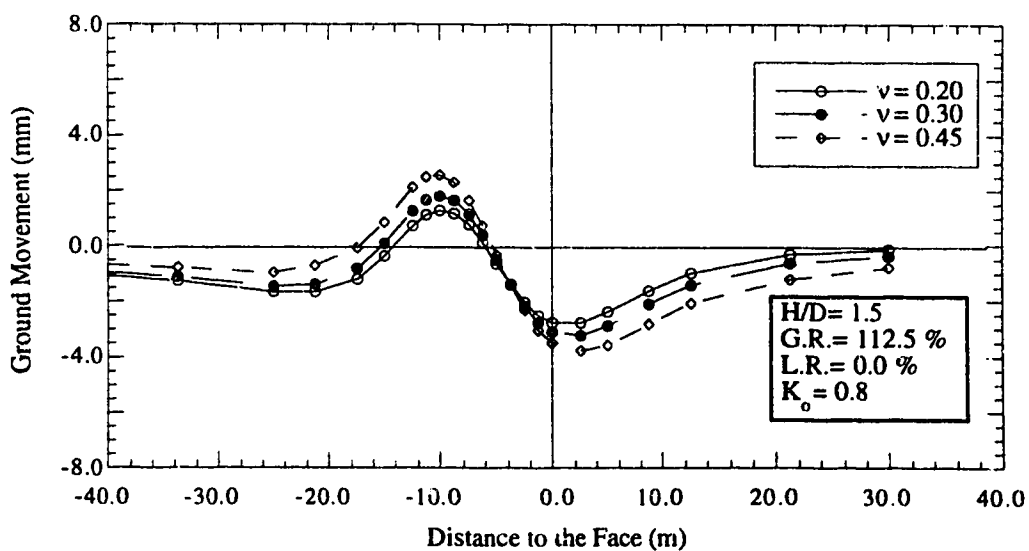


Figure 4.36: Surface Displacement at Longitudinal Axis for various Poisson's Ratios (G.R.= 112.5% and L.R.= 0.0%)

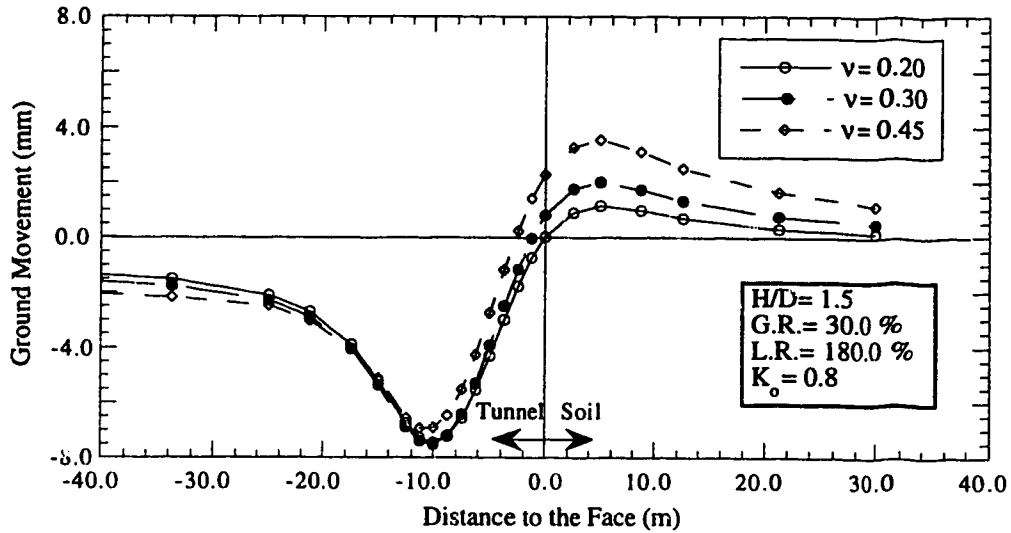


Figure 4.37: Surface Displacement at Longitudinal Axis for various Poisson's Ratios
(G.R.= 30.0% and L.R.= 180.0%)

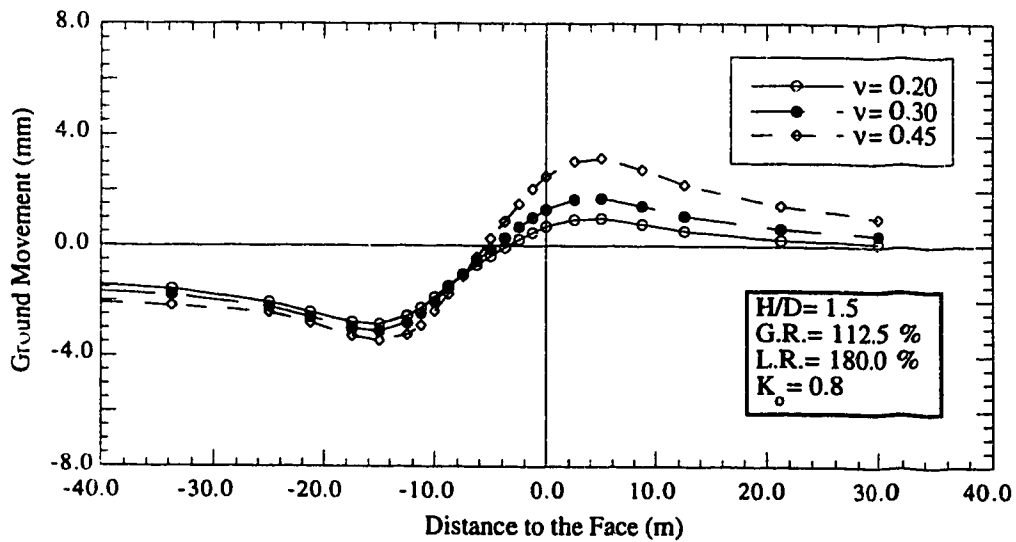


Figure 4.38: Surface Displacement at Longitudinal Axis for various Poisson's Ratios
(G.R.= 112.5% and L.R.= 180.0%)

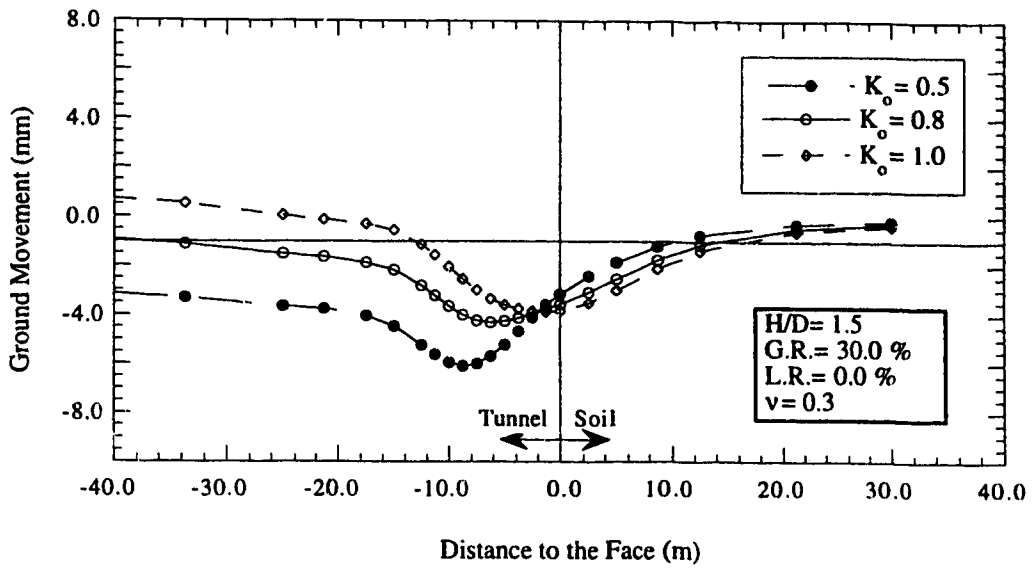


Figure 4.39: Surface Displacement at Longitudinal Axis for various values of K_o (G.R.= 30.0% and L.R.= 0.0%)

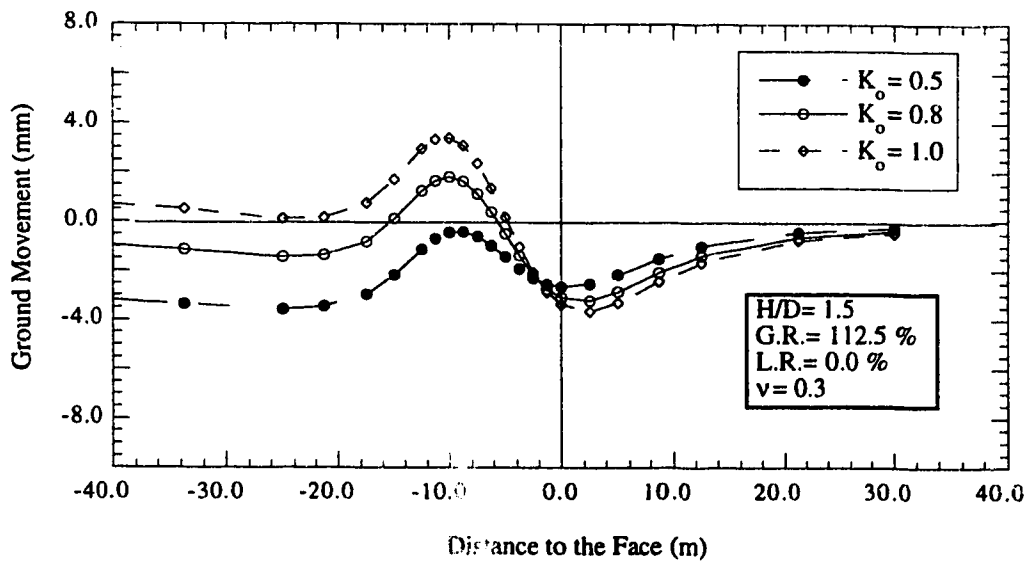


Figure 4.40: Surface Displacement at Longitudinal Axis for various values of K_o (G.R.= 112.5% and L.R.= 0.0%)

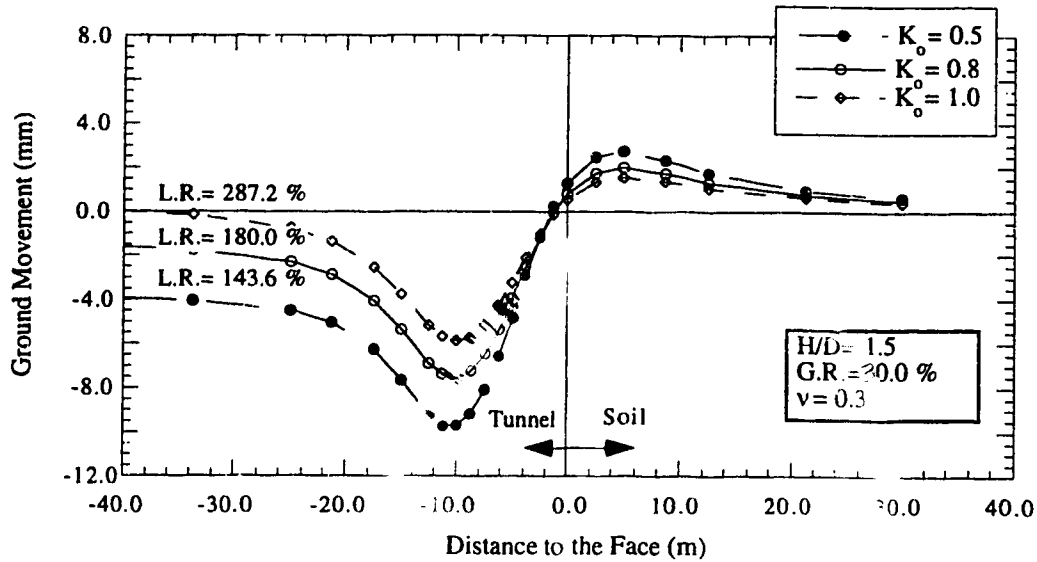


Figure 4.41: Surface Displacement at Longitudinal Axis for various values of K_0 (G.R.= 30.0%)

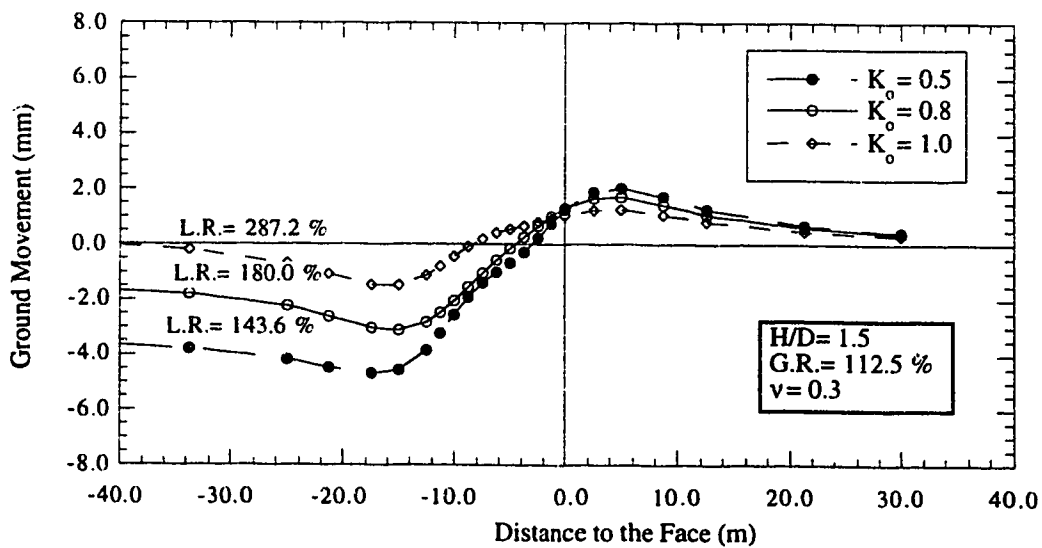


Figure 4.42: Surface Displacement at Longitudinal Axis for various values of K_0 (G.R.= 112.5%)

deformation behind the shield tail. As expected the effect of high values of Poisson's ratio, ν , is to reduce ground deformation because of reduction of material compressibility. At $\nu=0.5$ the material is incompressible. Anisotropy of the initial stress field, expressed by K_0 has the effect of increasing soil deformation.

4.7.4.2 Mean Stress Changes

Changes in the mean stress is expressed in terms of the Stress Ratio $S.R.$:

$$S.R. = \frac{p}{p_i} \quad , \quad (4.14)$$

where:

p is the mean normal stress at a certain point after excavation, and
 p_i is the initial mean stress at the same point.

Figures 4.43 through 4.47 show the effect of the liner pressure on $S.R.$ at the central vertical plane in the tunnel. It can be noticed that the effects of high-liner pressure result in a higher magnitude of stress reduction around the excavation and of stress increase near the ground surface. The maximum stress changes are found to take place near the point of the lining activation. At this specific location, contour lines of $S.R.$ are plotted in the transversal plane of the tunnel for various grout and liner pressures, and they are shown in Figures 4.48 through 4.56. From the figures, grout pressure increases the mean stress around the tunnel while reducing it near the ground surface. The highest amount of stress increase takes place near the crown of the tunnel. The contracting effect of the liner pressures with respect to the grout pressure is further affirmed as stress reduction is noticeable near the excavation while stress increase takes place at near the ground surface.

4.7.4.3 Mobilized Shear Strengths

Mobilized shear strength is expressed in term of the mobilized friction angle. The Mohr-Coulomb expression for the friction angle is adopted for the calculation:

$$\phi = \sin^{-1} \left(\frac{-3 \sin \left(\theta + \frac{\pi}{3} \right)}{\frac{I_1}{\sqrt{J_2}} + \sqrt{3} \cos \left(\theta + \frac{\pi}{3} \right)} \right) \quad . \quad (4.15)$$

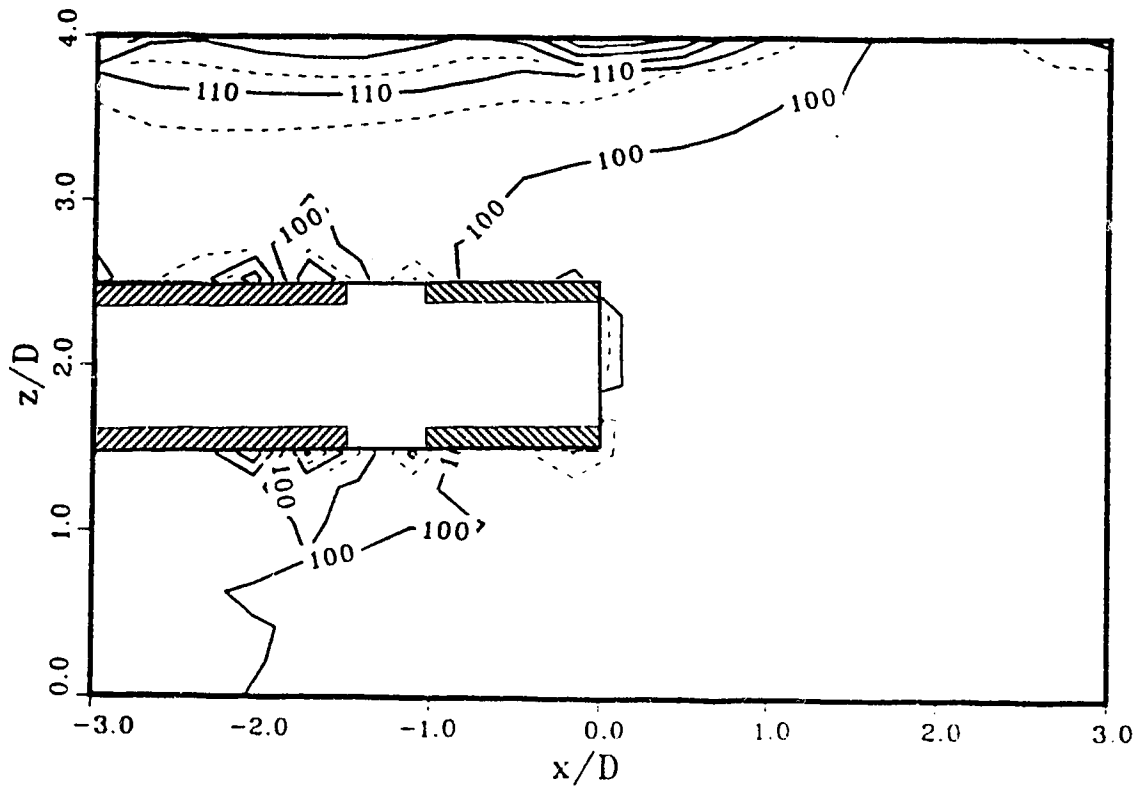


Figure 4.43: Contour Plot of Stress Ratio, S.R., at the Central Longitudinal Plane
(G.R.= 30.0 % and L.R.= 0.0 %)

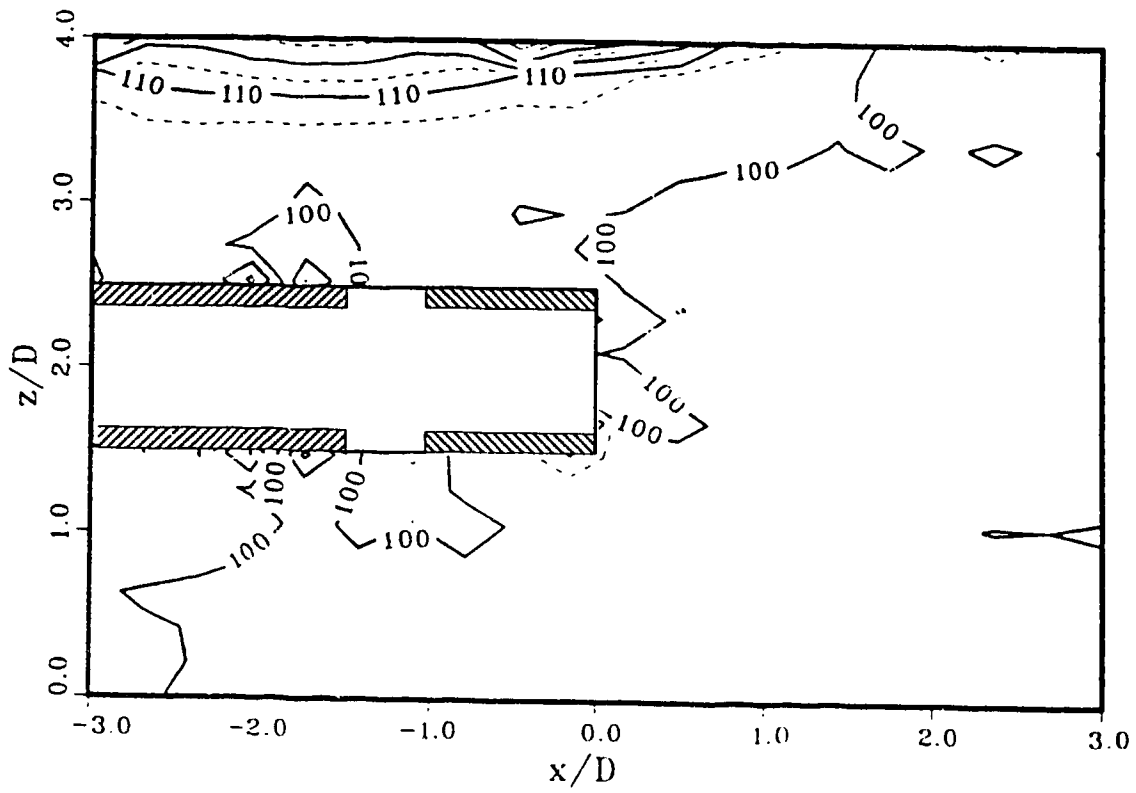


Figure 4.44: Contour Plot of Stress Ratio, S.R., at the Central Longitudinal Plane
(G.R.= 30.0 % and L.R.= 45.0 %)

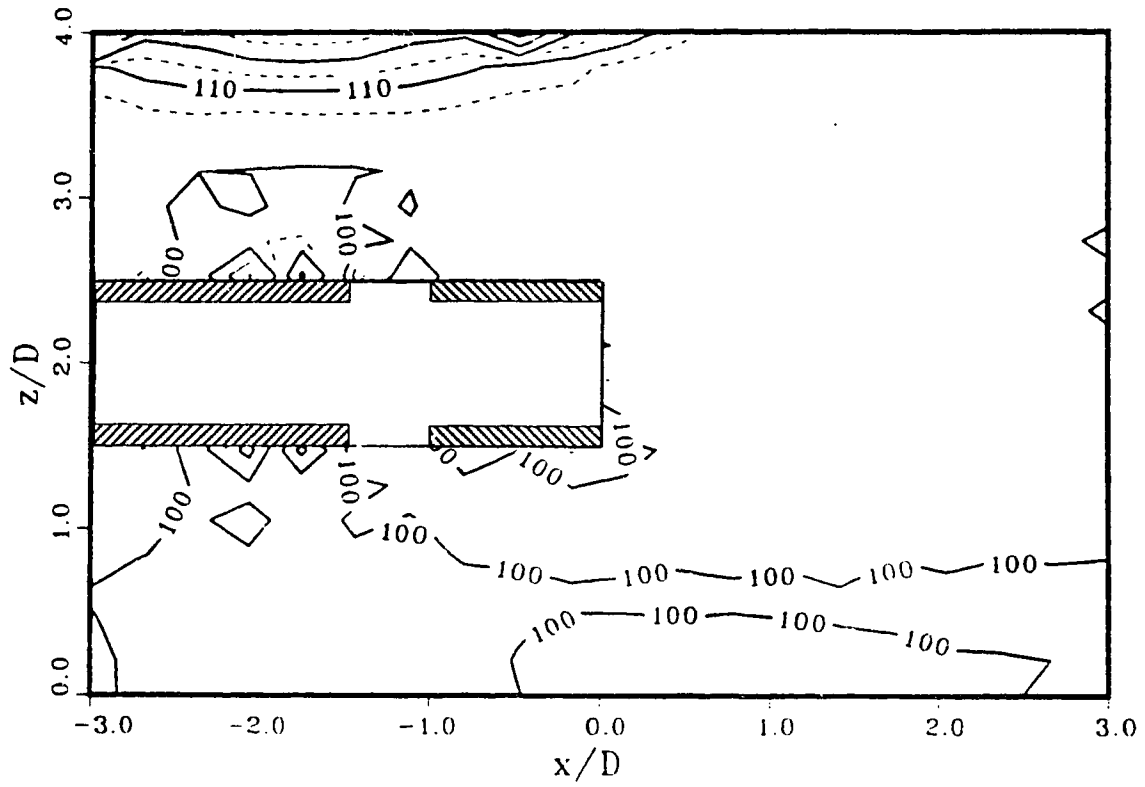


Figure 4.45: Contour Plot of Stress Ratio, S.R., at the Central Longitudinal Plane
(G.R.= 30.0 % and L.R.= 90.0 %)

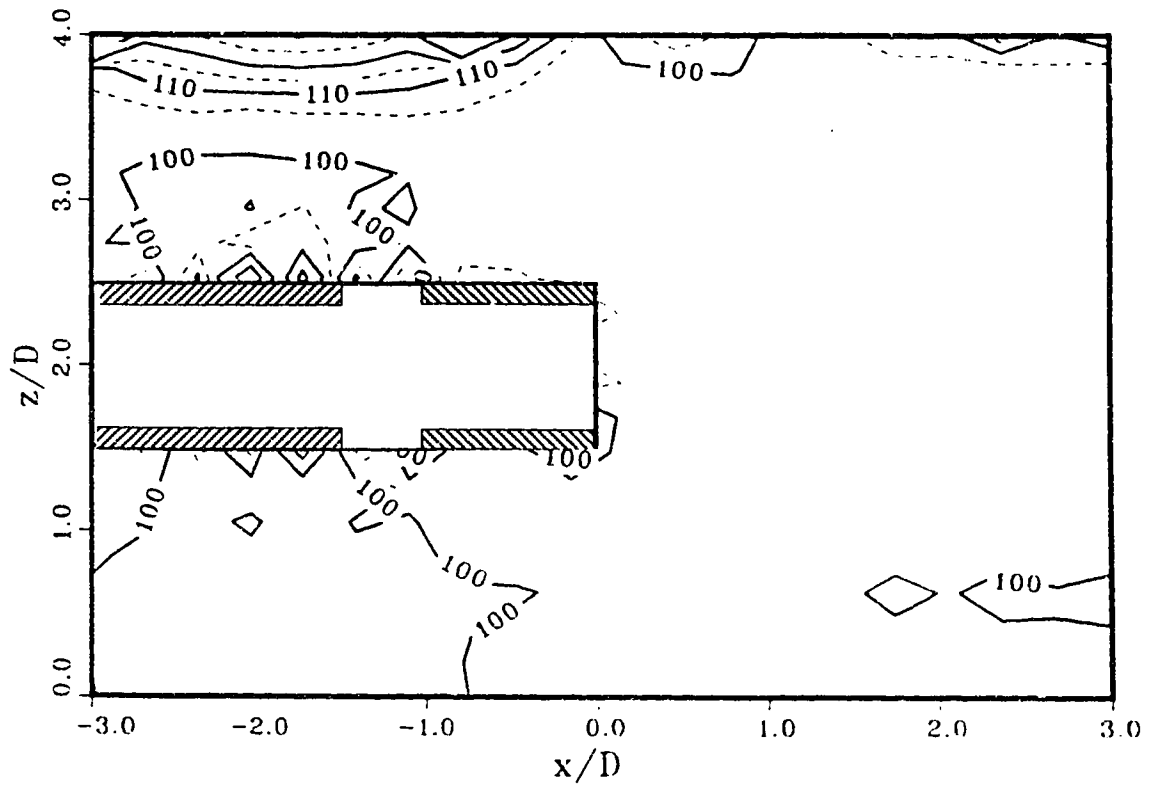


Figure 4.46: Contour Plot of Stress Ratio, S.R., at the Central Longitudinal Plane
(G.R.= 30.0 % and L.R.= 135.0 %)

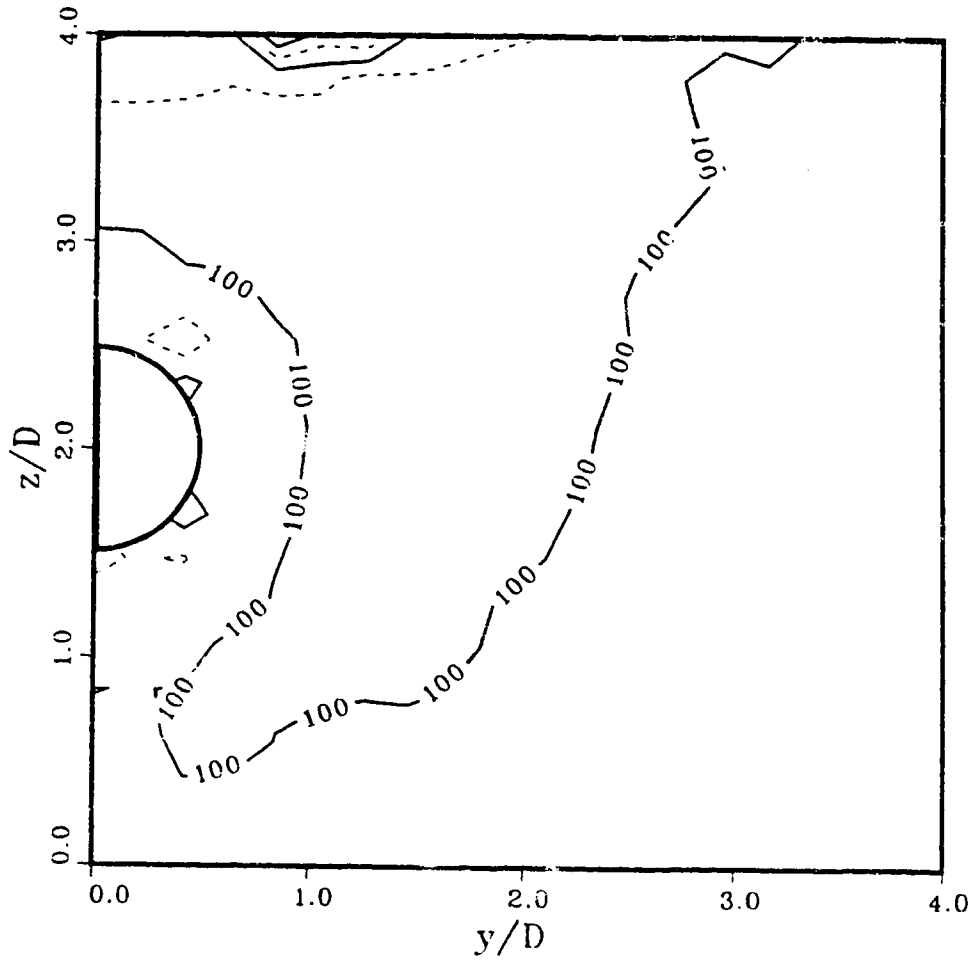


Figure 4.48: Contour Plot of Stress Ratio, S.R., at the Transversal Plane at the Point of Lining Activation (G.R.= 30.0% and L.R.= 0.0%)

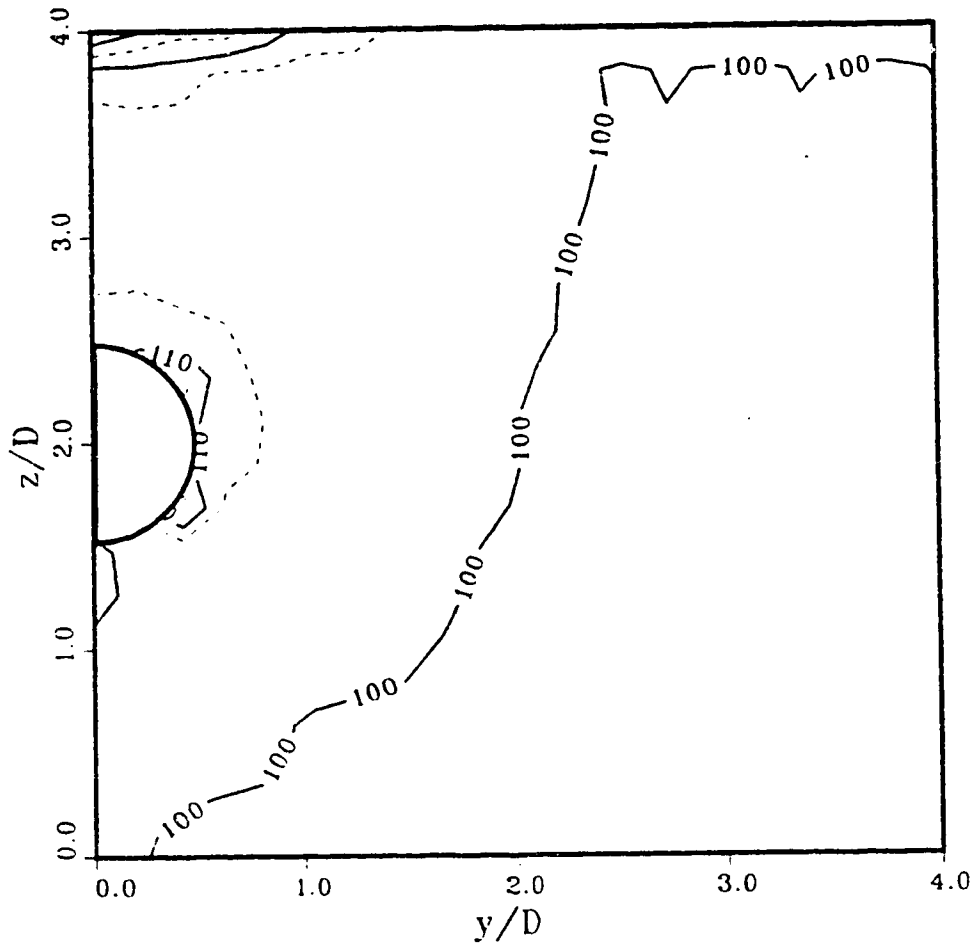


Figure 4.49: Contour Plot of Stress Ratio, S.R., at the Transversal Plane at the Point of Lining Activation (G.R.= 75.0% and L.R.= 0.0%)

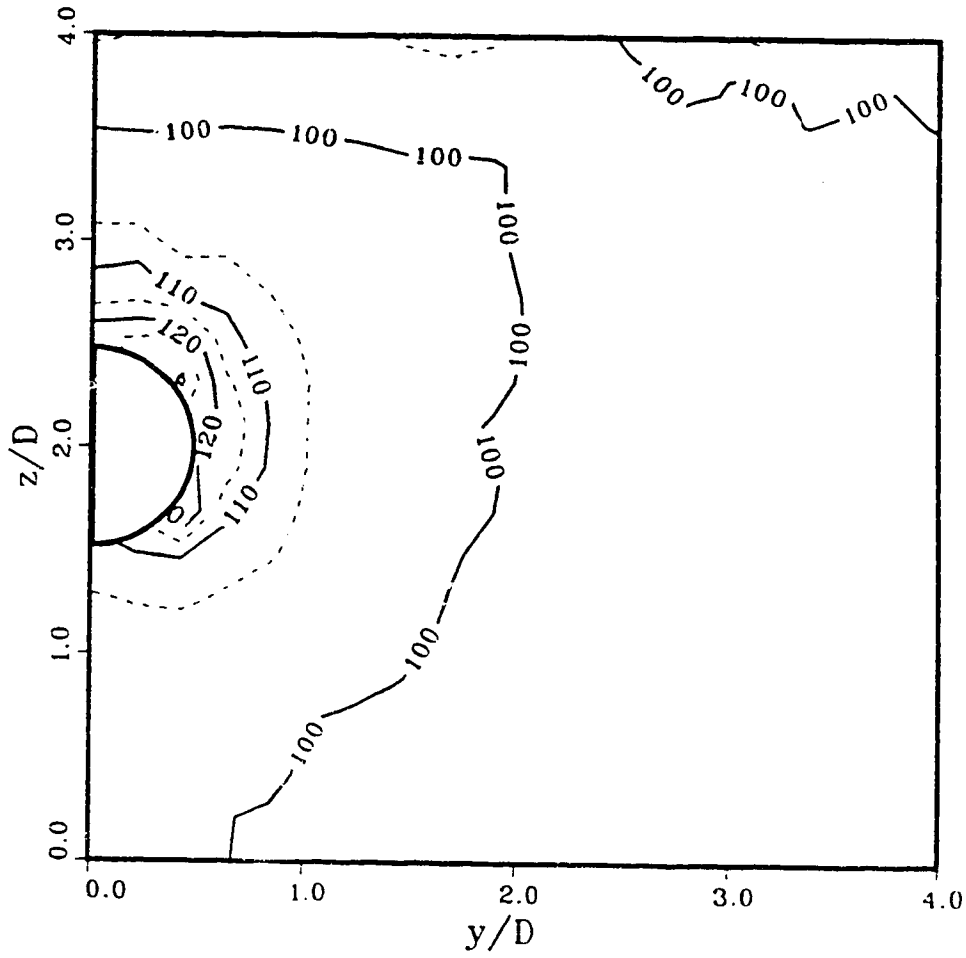


Figure 4.50: Contour Plot of Stress Ratio, S.R., at the Transversal Plane at the Point of Lining Activation (G.R.= 112.5% and L.R.= 0.0%)

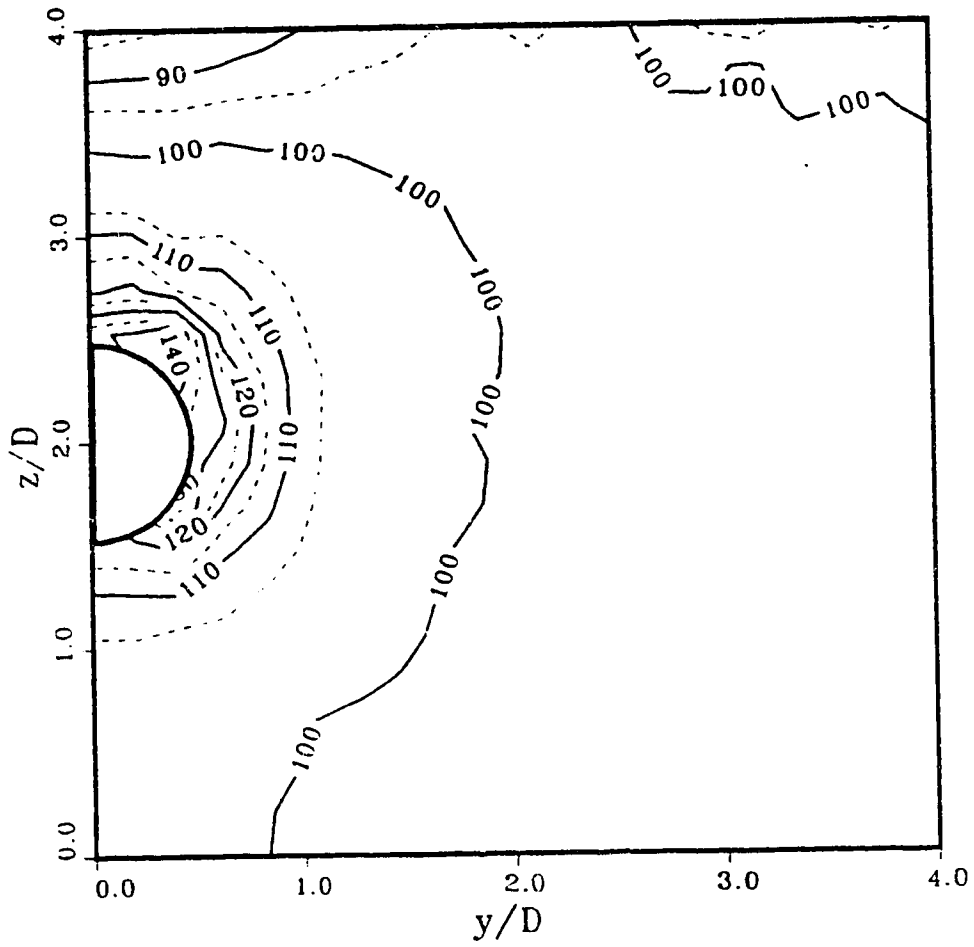


Figure 4.51: Contour Plot of Stress Ratio, S.R., at the Transversal Plane at the Point of Lining Activation (G.R.= 150.0% and L.R.= 0.0%)

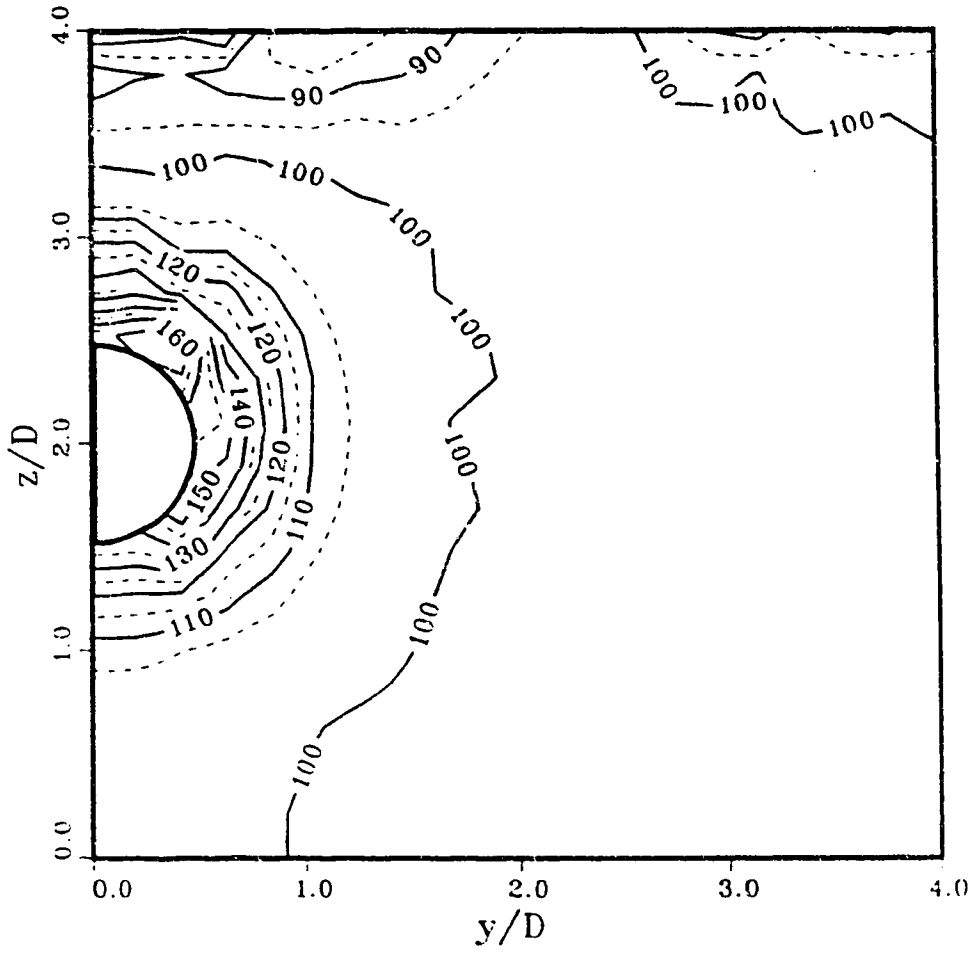


Figure 4.52: Contour Plot of Stress Ratio, S.R., at the Transversal Plane at the Point of Lining Activation (G.R.= 225.5% and L.R.= 0.0%)

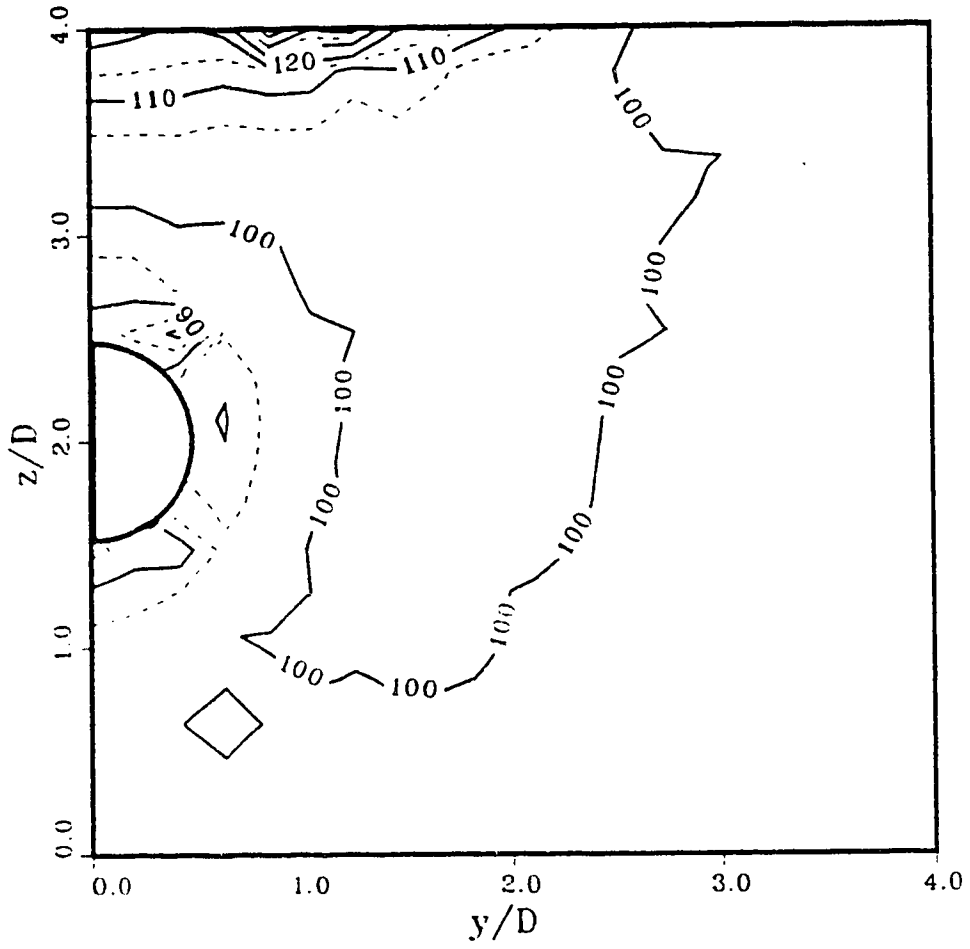


Figure 4.53: Contour Plot of Stress Ratio, S.R., at the Transversal Plane at the Point of Lining Activation (G.R.= 30.0% and L.R.= 45.0%)

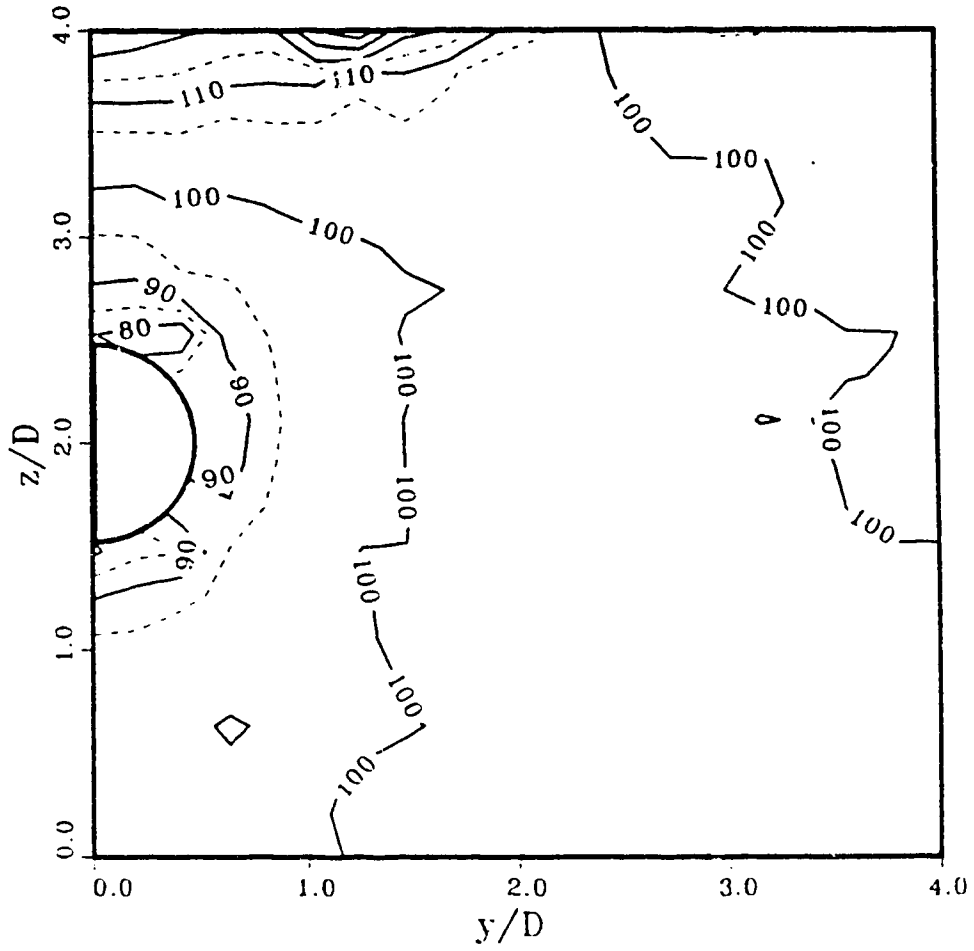


Figure 4.54: Contour Plot of Stress Ratio, S.R., at the Transversal Plane at the Point of Lining Activation (G.R.= 30.0% and L.R.=90.0%)

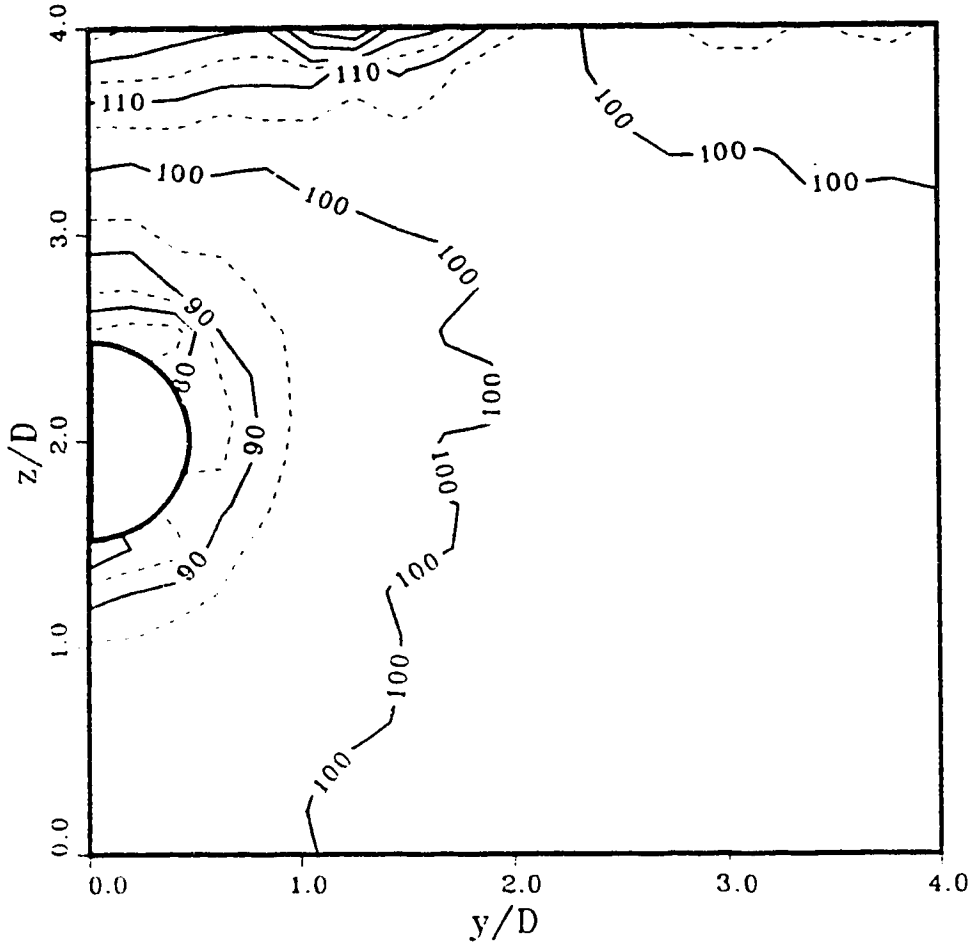


Figure 4.55: Contour Plot of Stress Ratio, S.R., at the Transversal Plane at the Point of Lining Activation (G.R.= 30.0% and L.R.=135.0%)

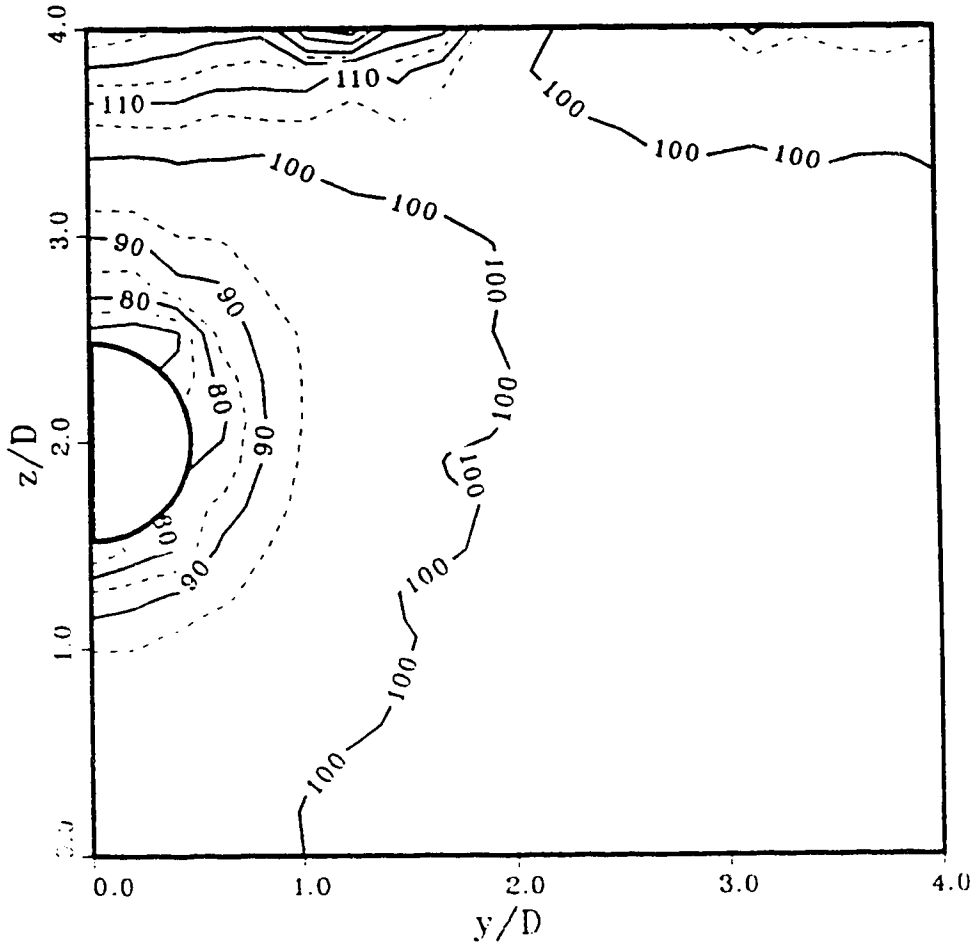


Figure 4.56: Contour Plot of Stress Ratio, S.R., at the Transversal Plane at the Point of Lining Activation (G.R.= 30.0% and L.R.=180.0%)

Figures 4.57 through 4.61 show the mobilized friction angle at the central vertical plane of the tunnel for various liner pressures. It can be concluded that the maximum mobilized friction angle takes place near the tunnel face and that the effect of the lining pressure on the magnitude or the distribution of mobilized shear is not decisively obvious. Contour lines of the mobilized friction angle are plotted in Figures 4.62 through 4.68. From the figures the effect of increasing grout pressure is to reduce the magnitude of mobilized friction. If the grout pressure exceeds the initial pressure, a new pattern for the distribution of mobilized friction angle is created. At low grout pressure the maximum mobilized friction angle takes place near the spring line of the tunnel while at high grout pressure, it is concentrated near the crown and the floor of the tunnel. Meanwhile the effect of the liner pressure is small and is limited in expanding the zone of mobilized friction.

4.7.4.4 Stress Paths

Stress path followed after the excavation is expressed as a function of the mean stress ratio $S.R.$ and the deviatoric stress ρ :

$$\rho = \sqrt{2J_2} \quad . \quad (4.16)$$

Figure 4.69 shows the relationship between $S.R.$ and ρ normalized to the initial mean stress at the crown level for a case of low grout and liner pressures. From the figure, shear stress increases without noticeable changes in the mean stress until the face section is reached (**Path 1-2**), the increase in shear stress is accelerated along the shield length associated with a slight increase in $S.R.$ (**Path 2-3**). **Path 3-4** shows the stress changes at the gap distance (the distance between the shield and the point of the lining activation) which consists of a reduction of $S.R.$ accompanied with a reduction of shear stress. At the point of the lining activation (**Point 4**) $S.R.$ increases due to the supportive action of the lining. The **Path 4-5** related to stress changes behind the acting lining reflects stress changes accumulated during previous excavation steps. **Point 5** represents the point at the beginning of the tunnel which coincides with **Point 1**. Obviously, no stress changes have taken place at this point as the excavation process is not supposed to affect its stress condition. Figure 4.70 shows a case of high grout pressure. A slight decrease of $S.R.$ takes place until the shield tail is reached, (**Point 3**) then it is followed by an increase of $S.R.$ at the gap distance. Figure 4.71 represents a case of high $L.R.$ The resulting stress path is comparable to that of the case of low $L.R.$ (Figure 4.69) except for the reverse of the stress conditions at the two boundary points of the gap (**Points 3 and 4**). Figures 4.72, 4.73, and 4.74 show another expression of the stress path as the shear stress is

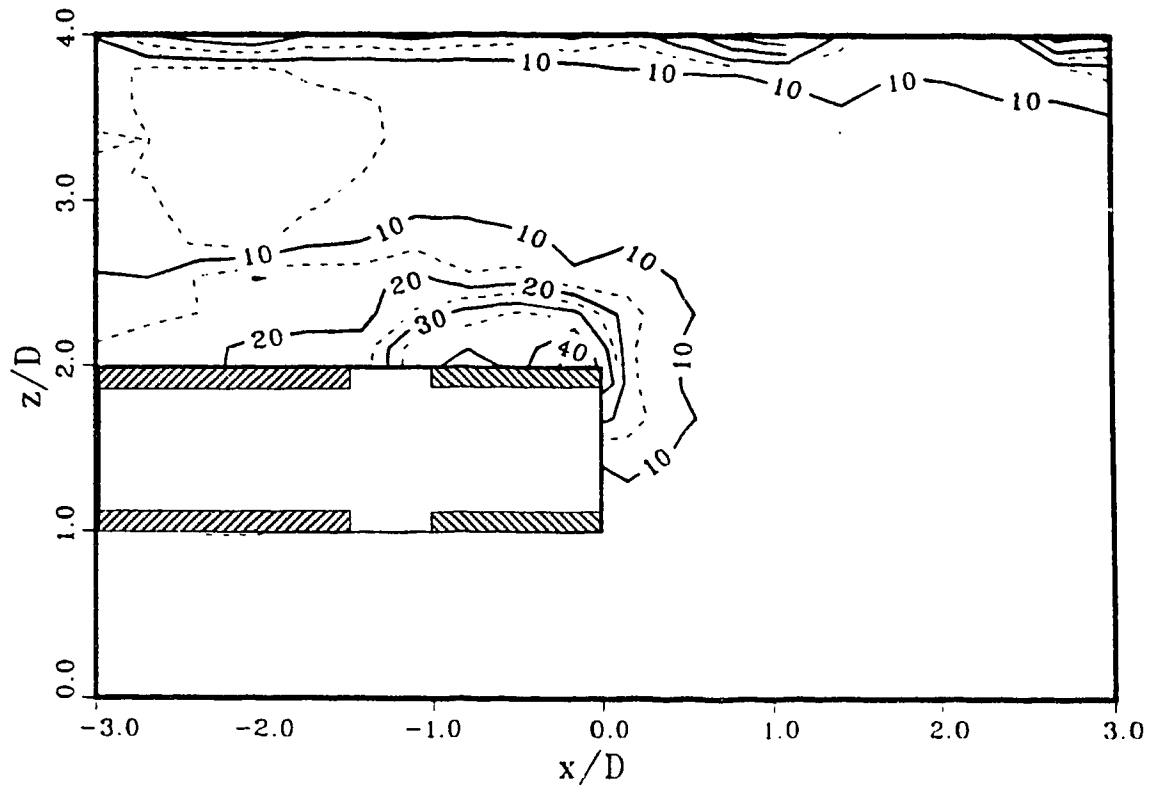


Figure 4.57: Contour Plot of Mobilized Friction Angle, ϕ , at the Central Longitudinal Plane (G.R.= 30.0 % and L.R.= 0.0 %)

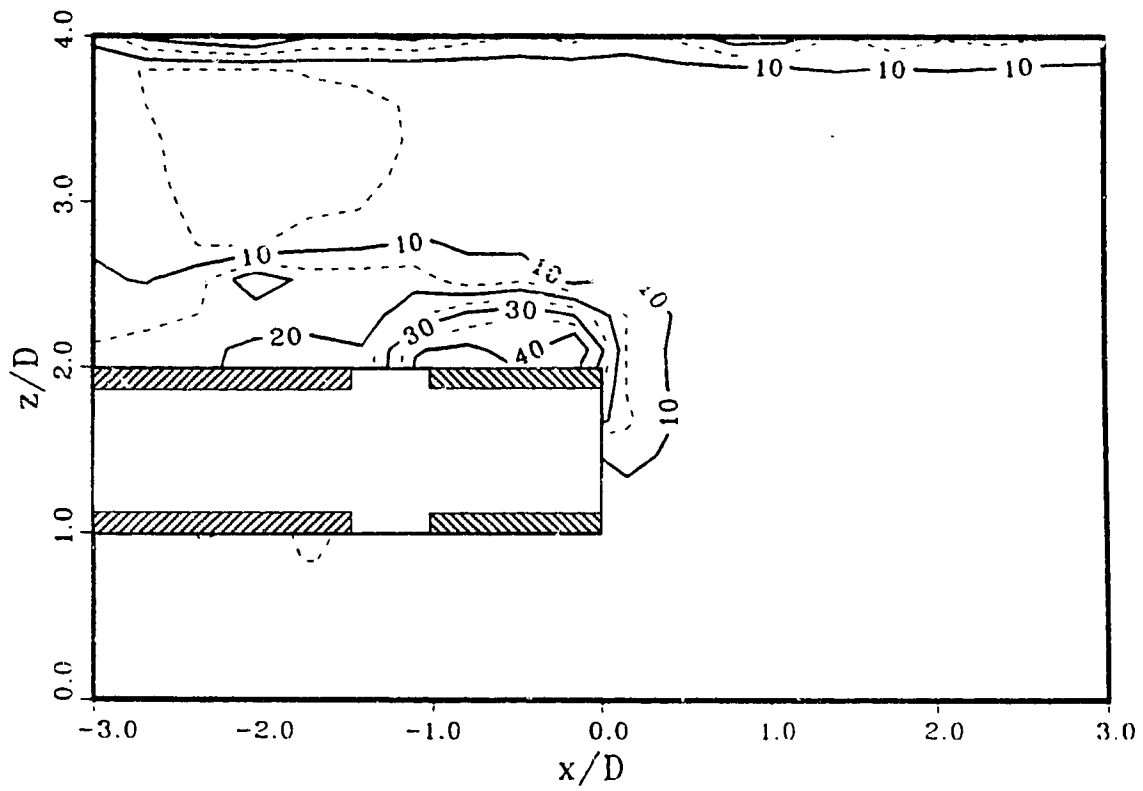


Figure 4.58: Contour Plot of Mobilized Friction Angle, ϕ , at the Central Longitudinal Plane (G.R.= 30.0 % and L.R.= 45.0 %)

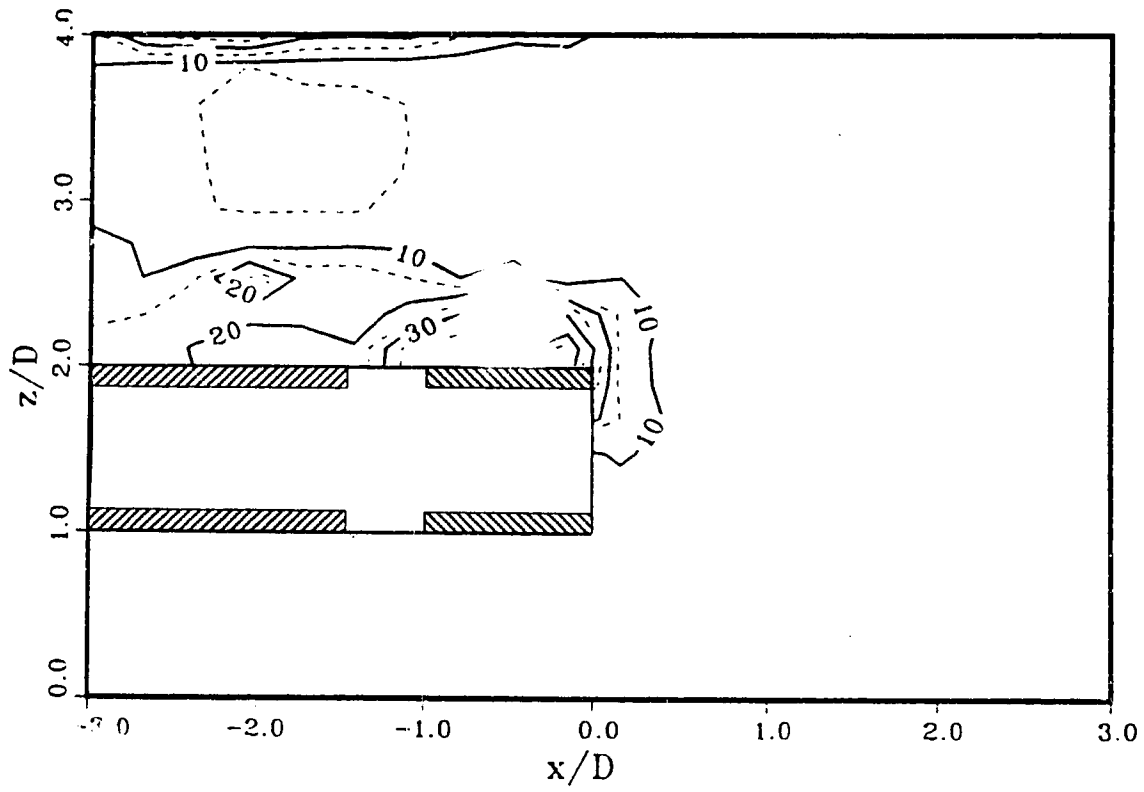


Figure 4.59: Contour Plot of Mobilized Friction Angle, ϕ , at the Central Longitudinal Plane (G.R.= 30.0 % and L.R.= 90.0 %)

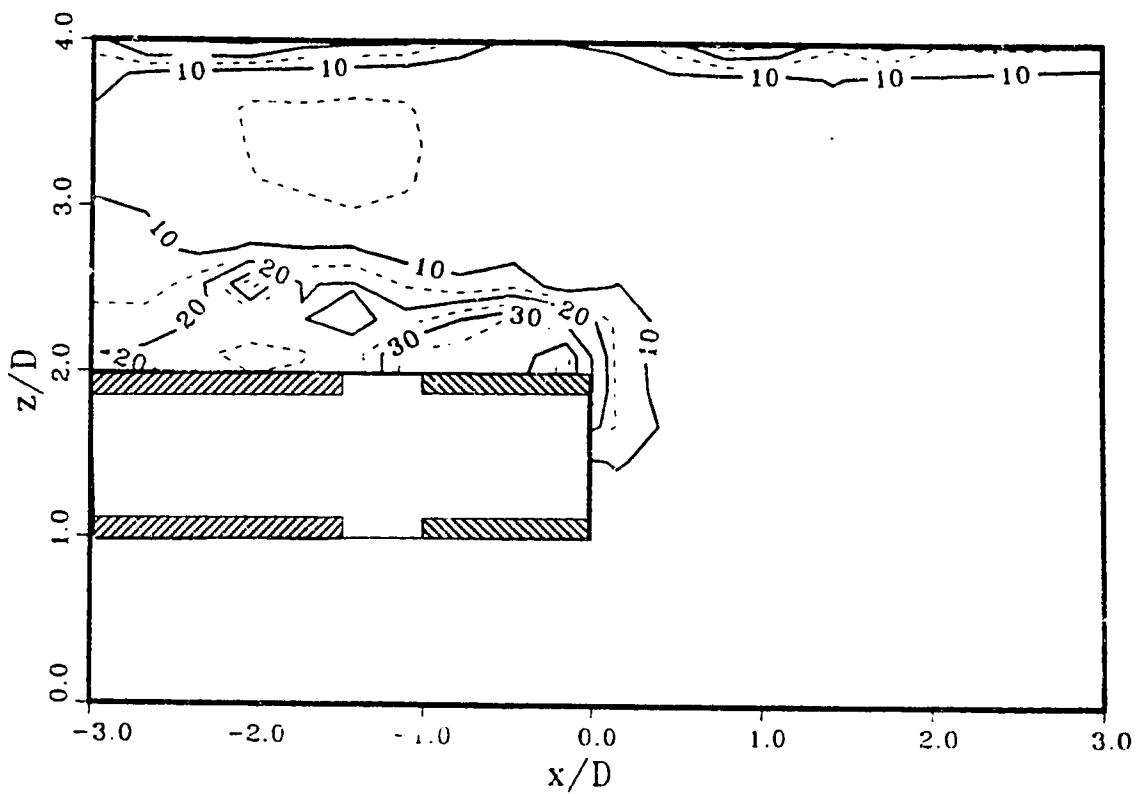


Figure 4.60: Contour Plot of Mobilized Friction Angle, ϕ , at the Central Longitudinal Plane (G.R.= 30.0 % and L.R.= 135.0 %)

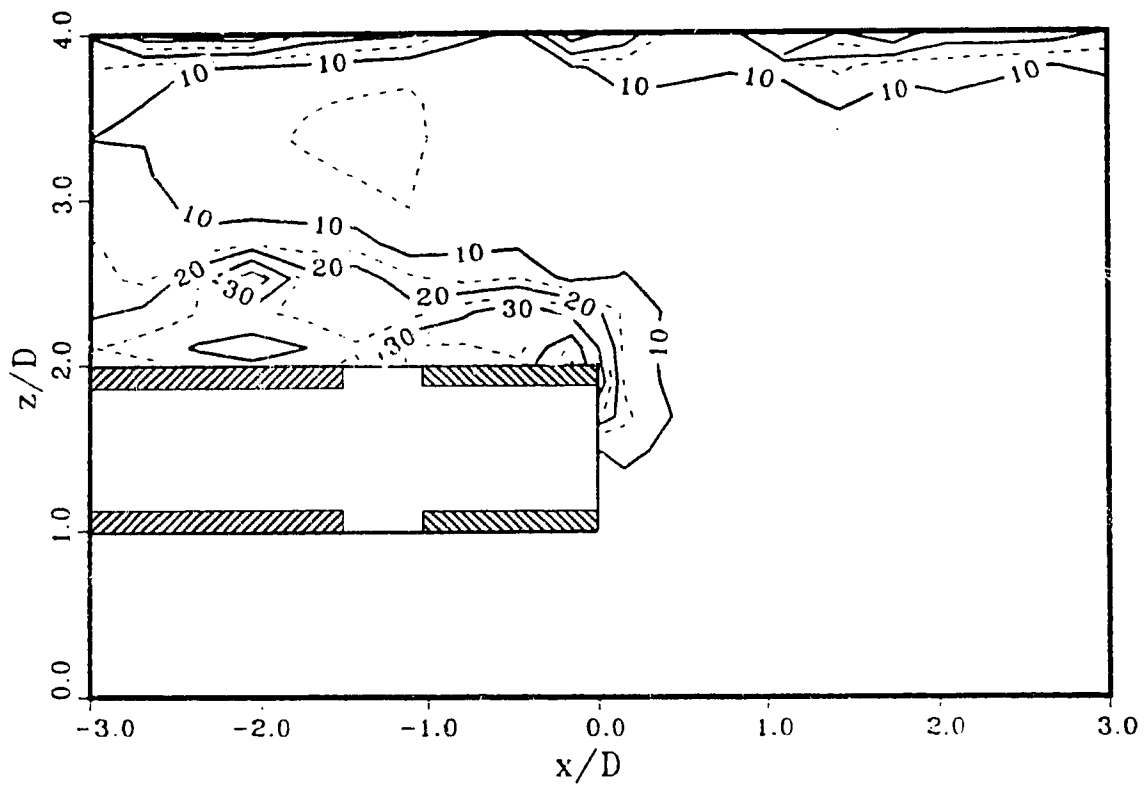


Figure 4.61. Contour Plot of Mobilized Friction Angle, ϕ , at the Central Longitudinal Plane (G.R.= 30.0 % and L.R.= 180.0 %)

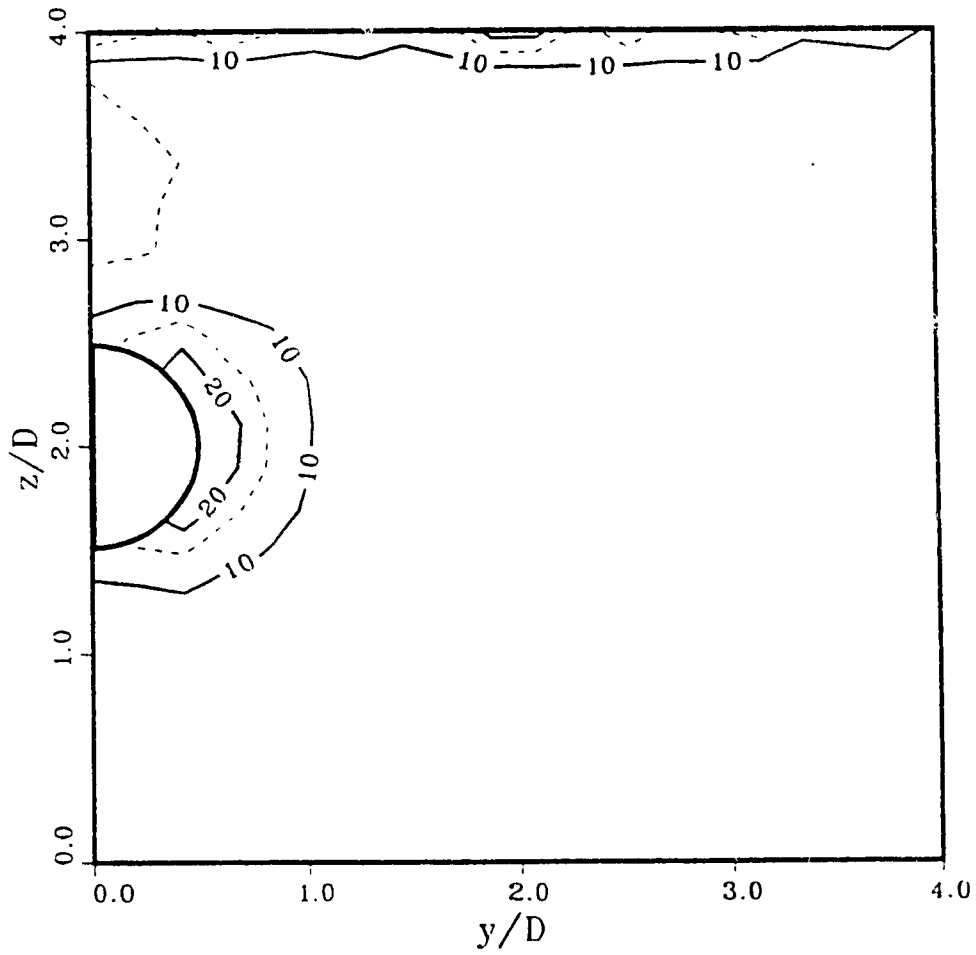


Figure 4.62: Contour Plot of Mobilized Friction Angle, ϕ , at the Transversal Plane at the Point of Lining Activation (G.R.= 30.0% and L.R.=0.0%)

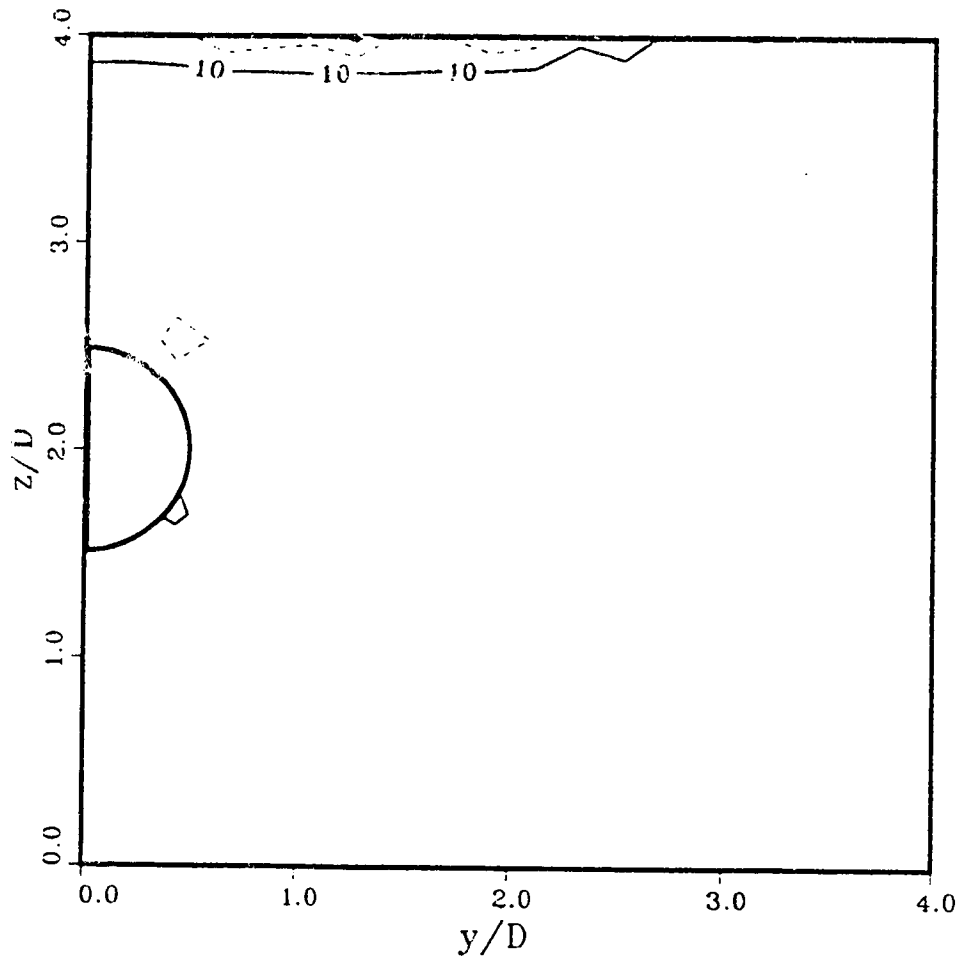


Figure 4.63: Contour Plot of Mobilized Friction Angle, ϕ , at the Transversal Plane at the Point of Lining Activation (G.R.= 75.0% and L.R.=0.0%)

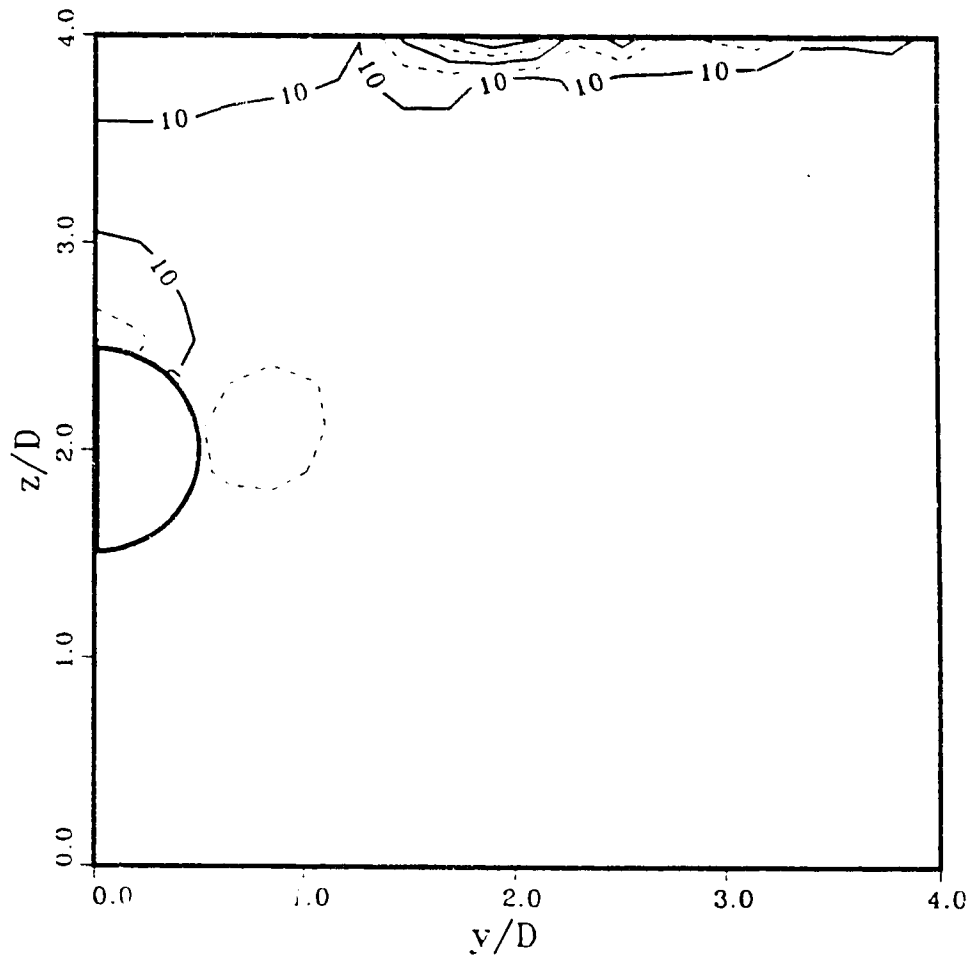


Figure 4.64: Contour Plot of Mobilized Friction Angle, ϕ , at the Transversal Plane at the Point of Lining Activation (G.R.= 112.5% and L.R.=0.0%)

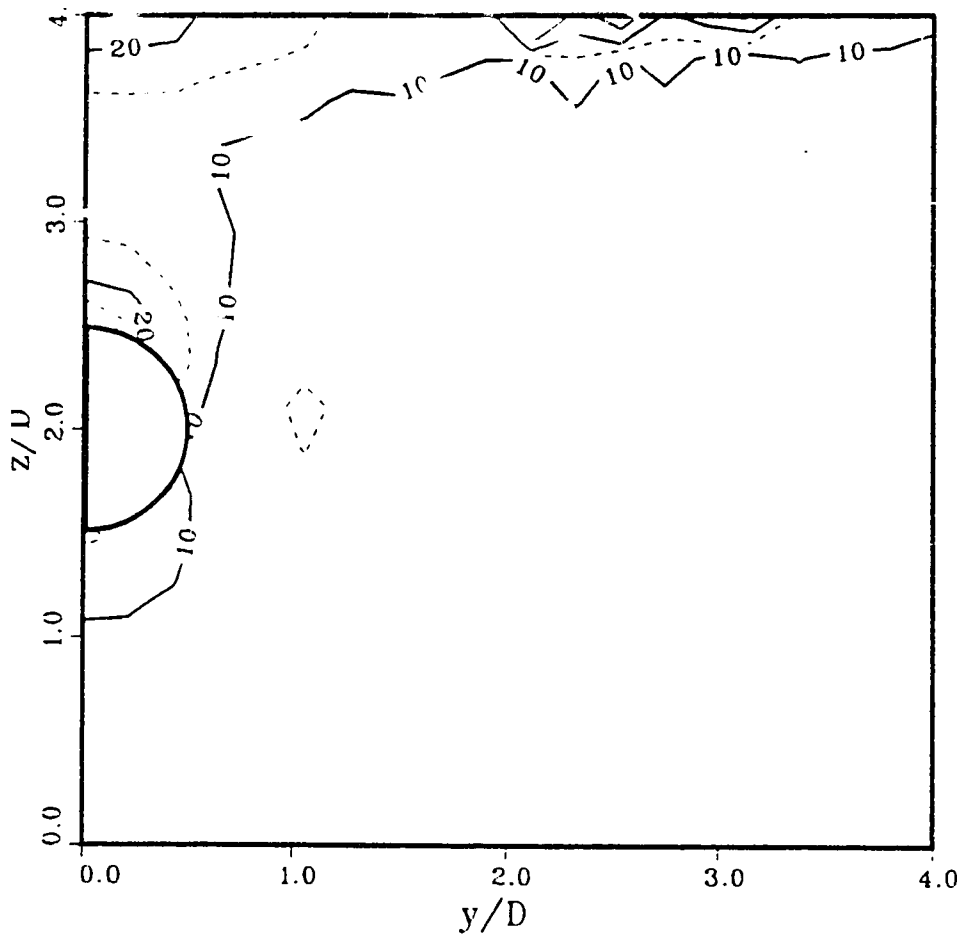


Figure 4.65: Contour Plot of Mobilized Friction Angle, ϕ , at the Transversal Plane at the Point of Lining Activation (G.R.= 150.0% and L.R.=0.0%)

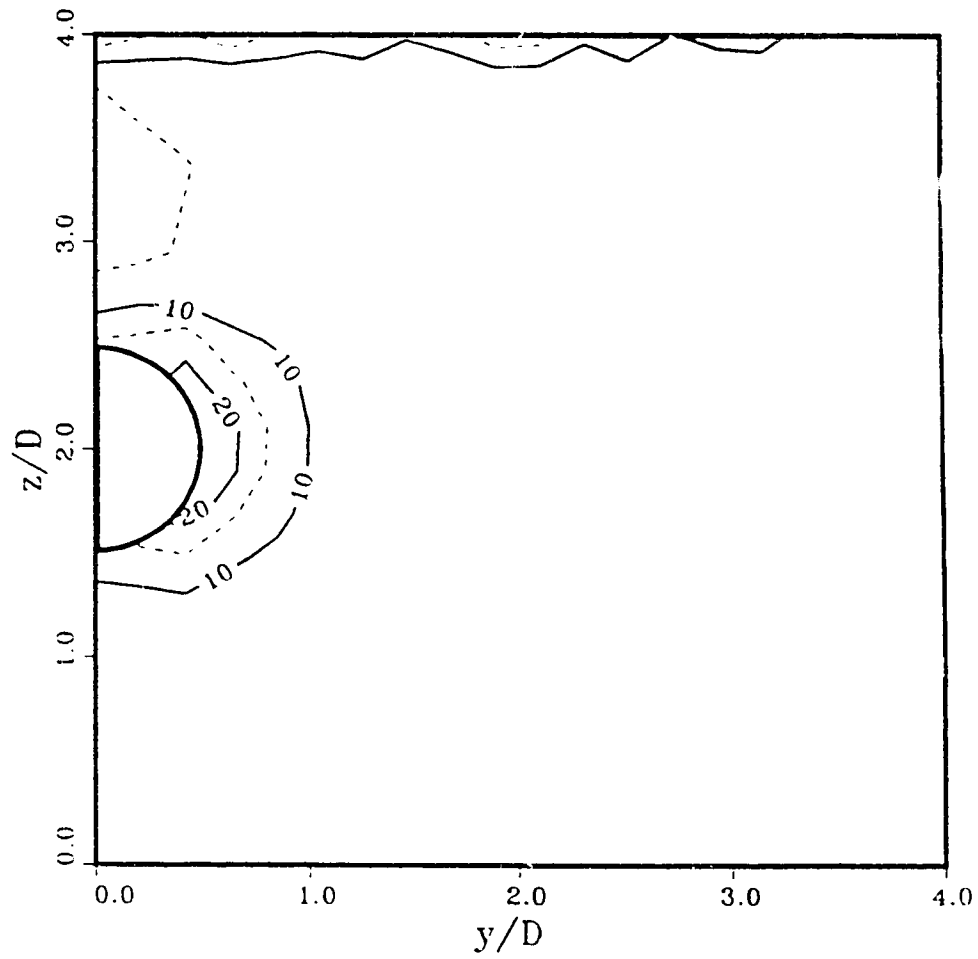


Figure 4.66: Contour Plot of Mobilized Friction Angle, ϕ , at the Transversal Plane at the Point of Lining Activation (G.R.= 30.0% and L.R.=45.0%)

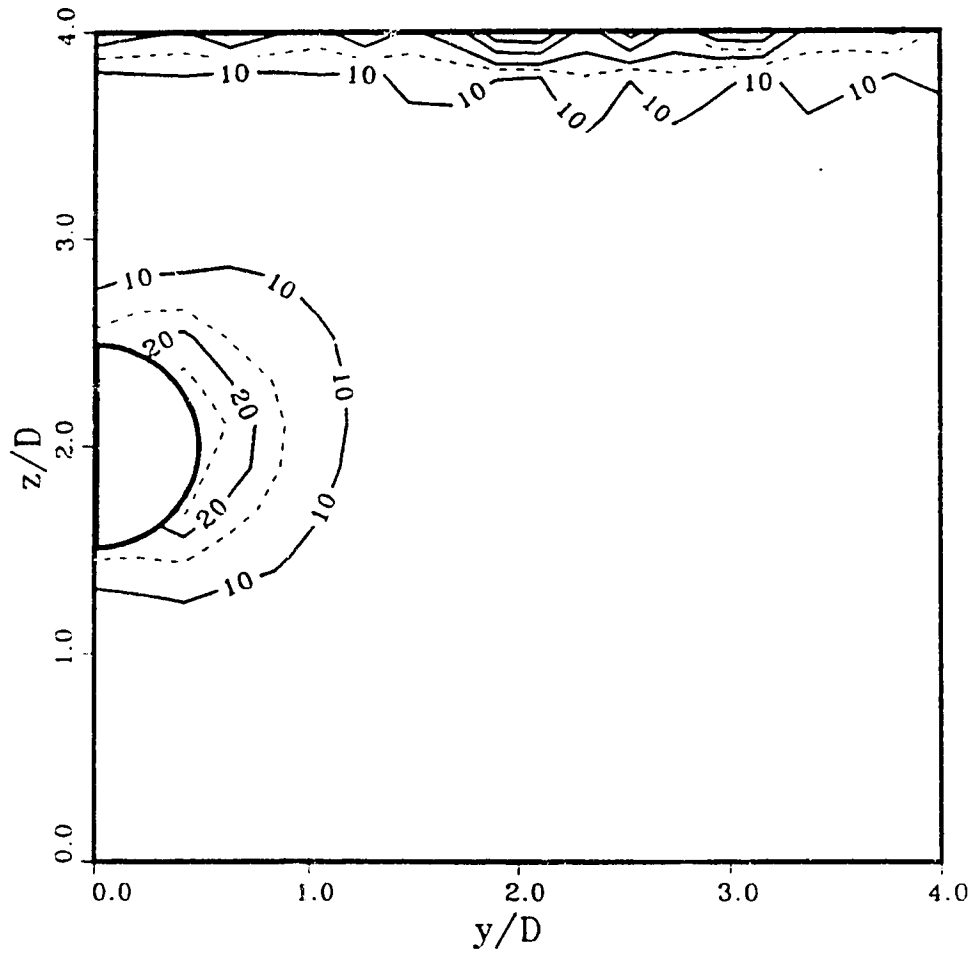


Figure 4.67: Contour Plot of Mobilized Friction Angle, ϕ , at the Transversal Plane at the Point of Lining Activation (G.R.= 30.0% and L.R.=13%)

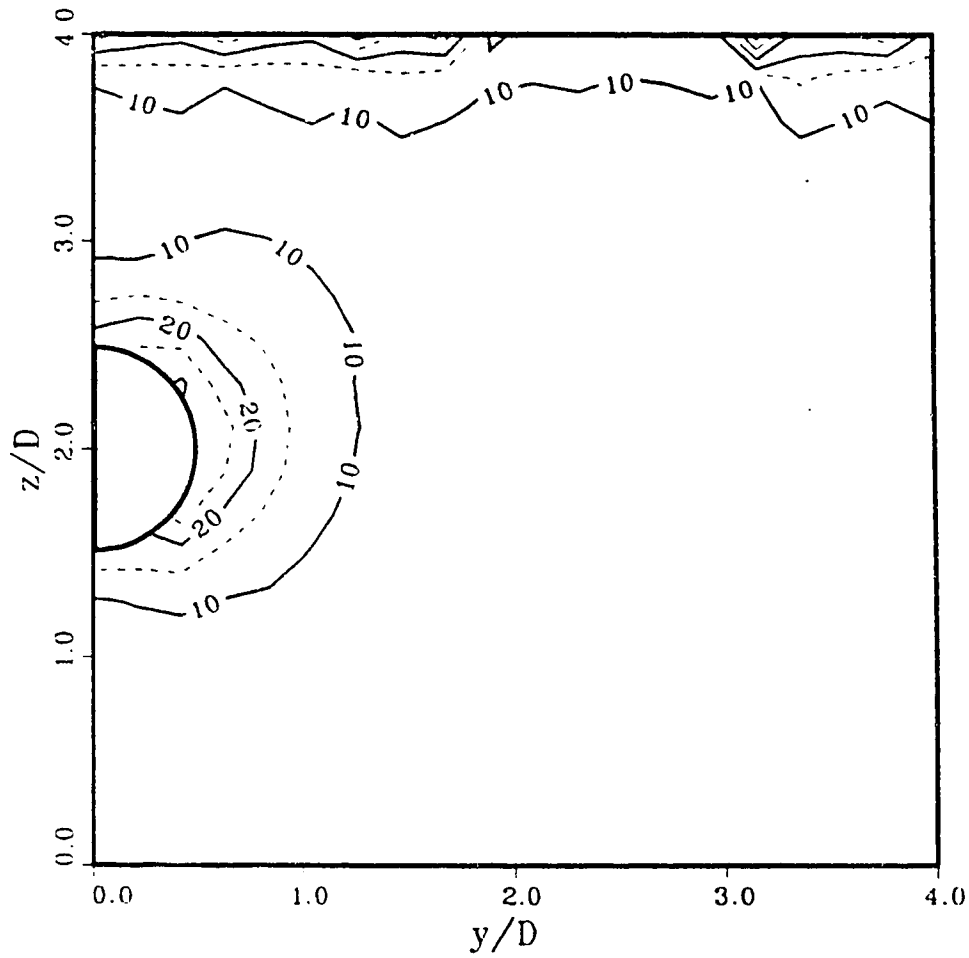


Figure 4.68: Contour Plot of Mobilized Friction Angle, ϕ , at the Transversal Plane at the Point of Lining Activation (G.R.= 30.0% and L.R.=180.0%)

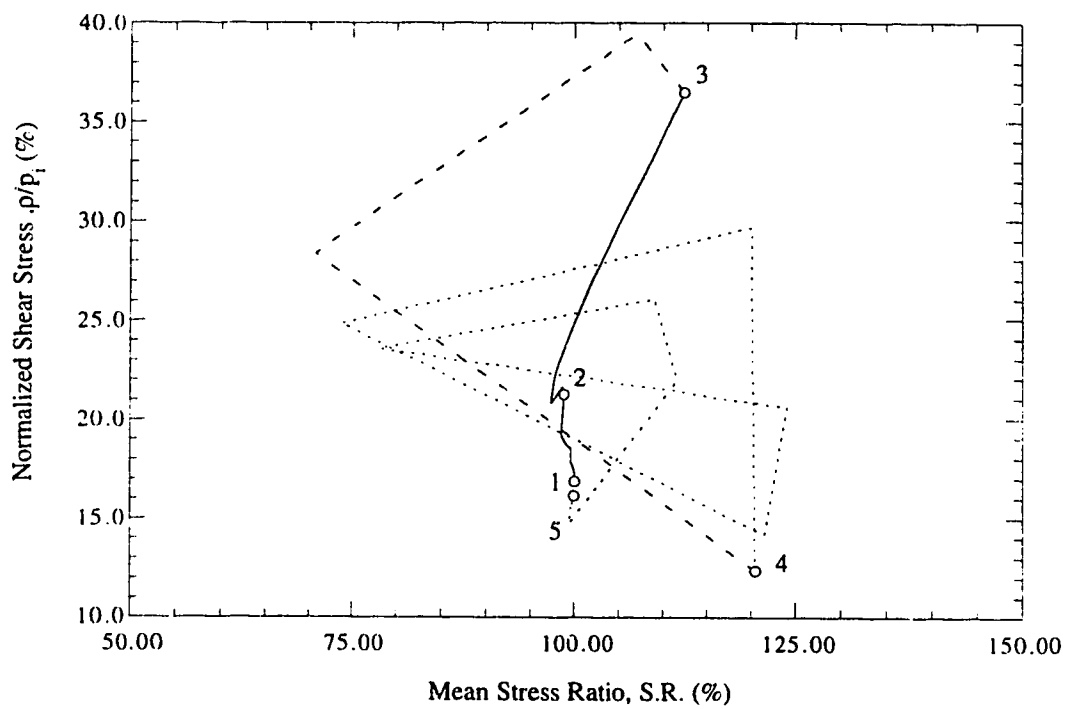
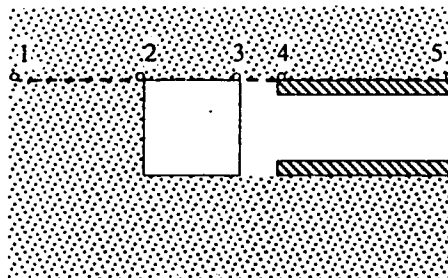


Figure 4.69: Stress Ratio versus the Normalized Shear Stress (G.R.= 30.0% and L.R.= 0.0%)

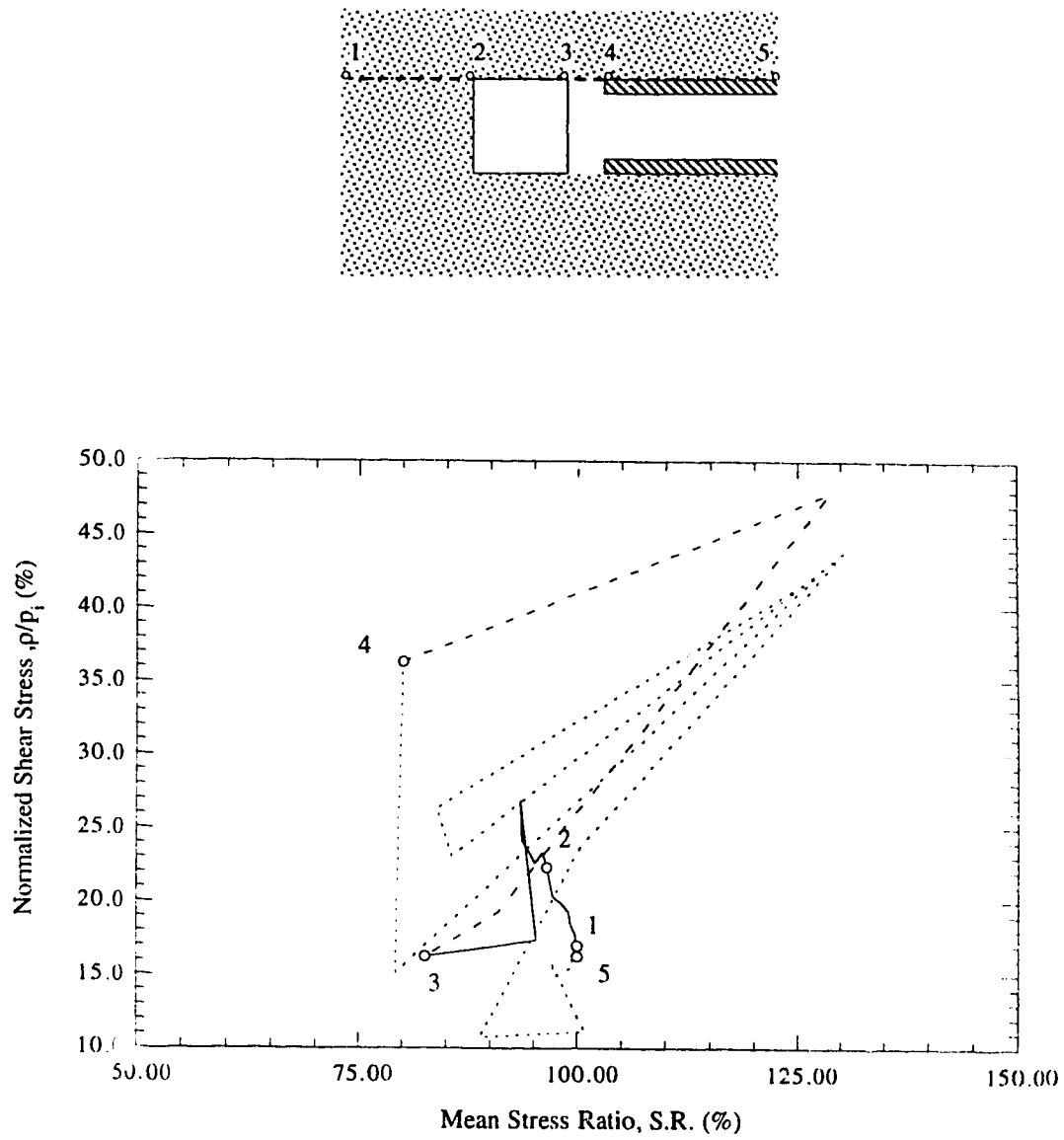


Figure 4.70: Stress Ratio versus the Normalized Shear Stress (G.R.= 112.5% and L.R.= 0.0%)

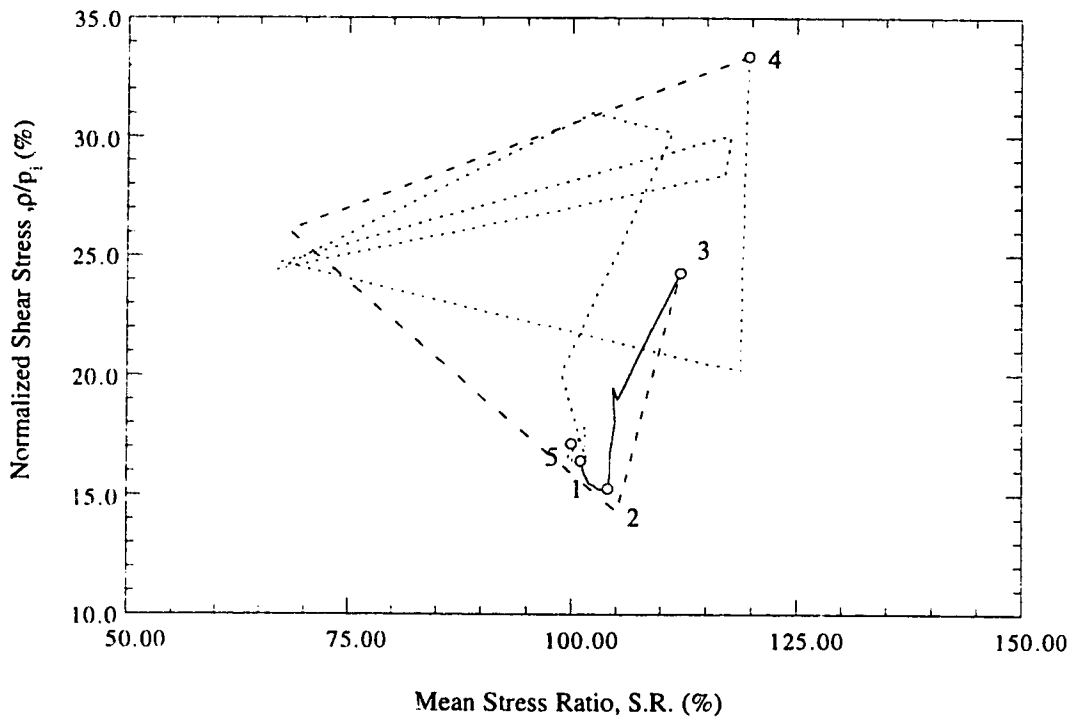
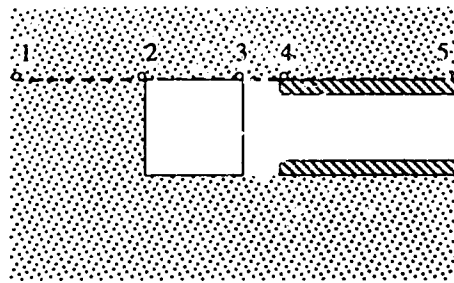


Figure 4.71: Stress Ratio versus the Normalized Shear Stress (G.R.= 30.0% and L.R.= 135.0%)

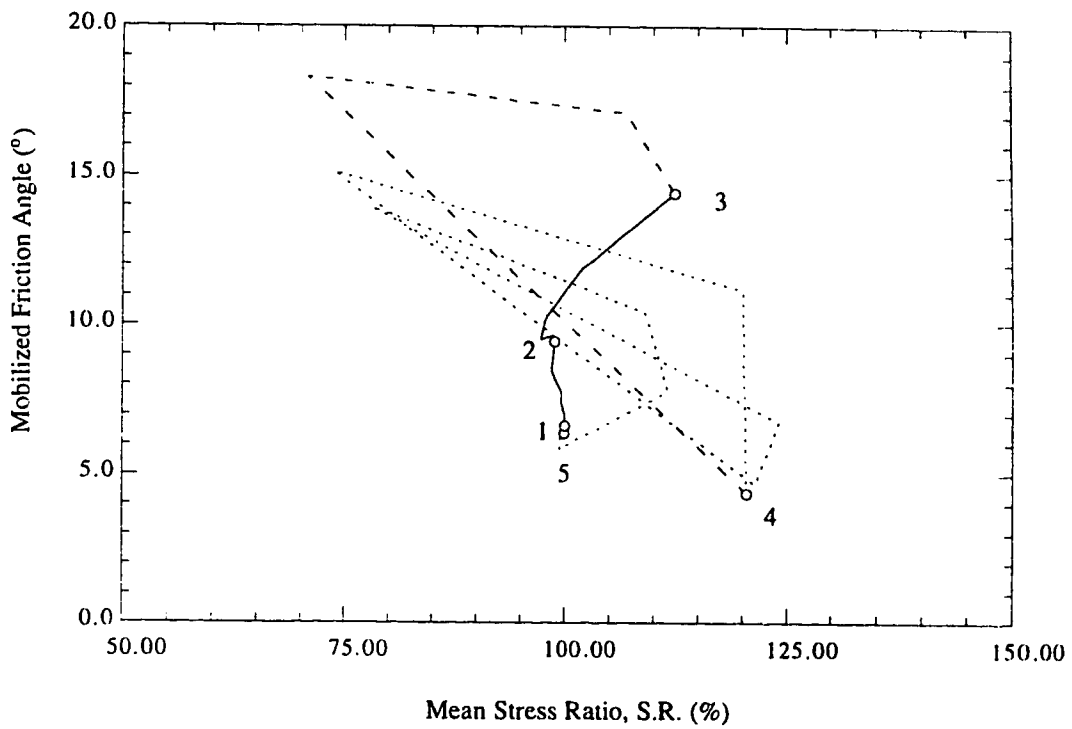
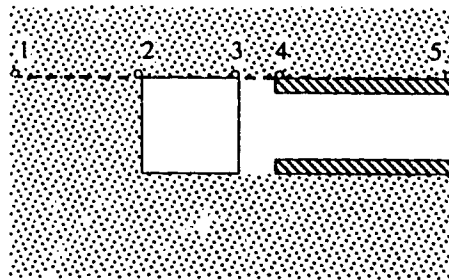


Figure 4.72: Stress Ratio versus the Mobilized Friction Angle, ϕ , (G.R.= 30.0% and L.R.= 0.0%)

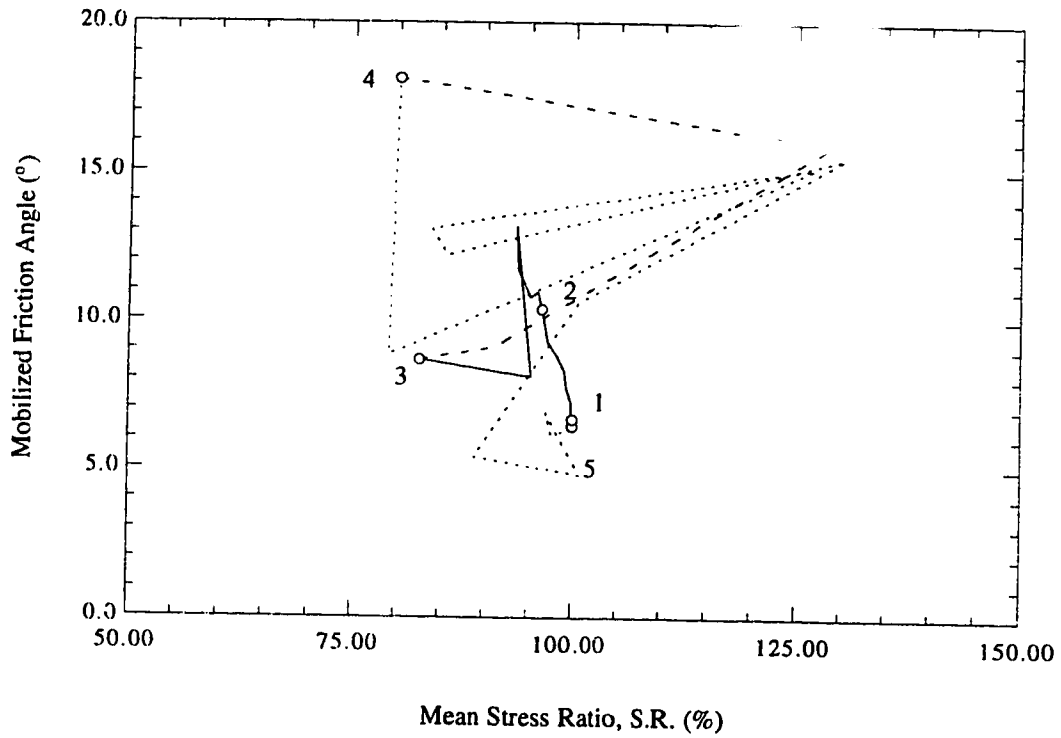
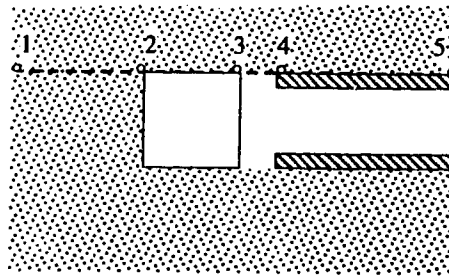


Figure 4.73: Stress Ratio versus the Mobilized Friction Angle, ϕ , (G.R.= 112.5% and L.R.= 0.0%)

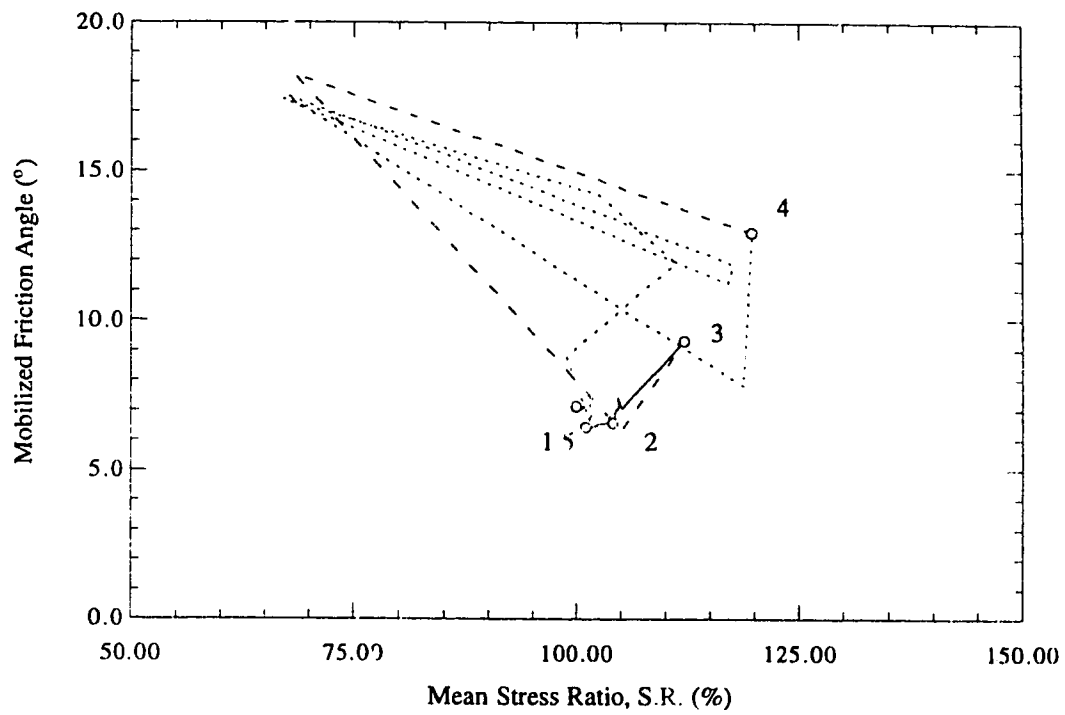
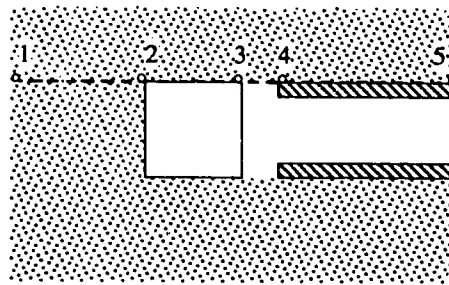


Figure 4.74: Stress Ratio versus the Mobilized Friction Angle, ϕ , (G.R.= 30.0% and L.R.= 135.0%)

represented by the mobilized friction angle.

4.7.5 Analysis

The objective of the analysis of the obtained results is to constitute a generalized model of displacements at the ground surface, displacement at the tunnel crown and of stresses around the liner of a tunnel excavated using pressurized shield methods under various construction and ground conditions. The obtained results are interpolated into simple expressions showing the effects of the most influential parameters.

4.7.5.1 Methodology

The methodology followed during the analysis is to select a number of executed computer runs. Then, normalized results relating to ground displacement, crown displacement, or stress changes around the liner are expressed in the form of a first-order or second-order equations reflecting the effect of a certain parameter. The process is repeated for various parameters, and a generalized form of the investigated result is achieved. Finally, the constant term is calculated by minimizing the average absolute error of all of the results interpolated through the formulated equations.

4.7.5.2 Surface Displacement

As demonstrated above, displacement at the ground surface is expressed in terms of the normalized surface displacement, \bar{w}_s , at the optimum point in the longitudinal direction. The effect of various factors affecting the displacement profile is found to be linear based on a sensitivity analysis of the relatively limited number of the results

$$\bar{w}_s = \left(as_n(v) + \frac{as_k}{K_o} + as_h \right) \left(\frac{H_o}{R_o} \right)^2 + \left(as_g(G.R.) + as_l(L.R.) + as_o \right) \left(\frac{H_o}{R_o} \right) . \quad (4.17)$$

The constants used are self-explanatory. Figure 4.75 shows the selected values for the constants and the influence of the depth of the tunnel on them.

4.7.5.2 Displacement at the Crown

The critical displacement is selected at the middle of the gap distance. Since the nodal displacements at the crown of the liner are locked together and the lining is relatively incompressible, almost the same displacement is calculated at the liner because of previous

$$\omega_s = (as_k/K_o + as_n(v) + as_h)*(Ro/Ho)^2 + (as_g (G.R) + as_i (H.R) + as_o) (Ro/Ho)$$

as_k	1356.00
as_n	-306.46
as_h	-607.02

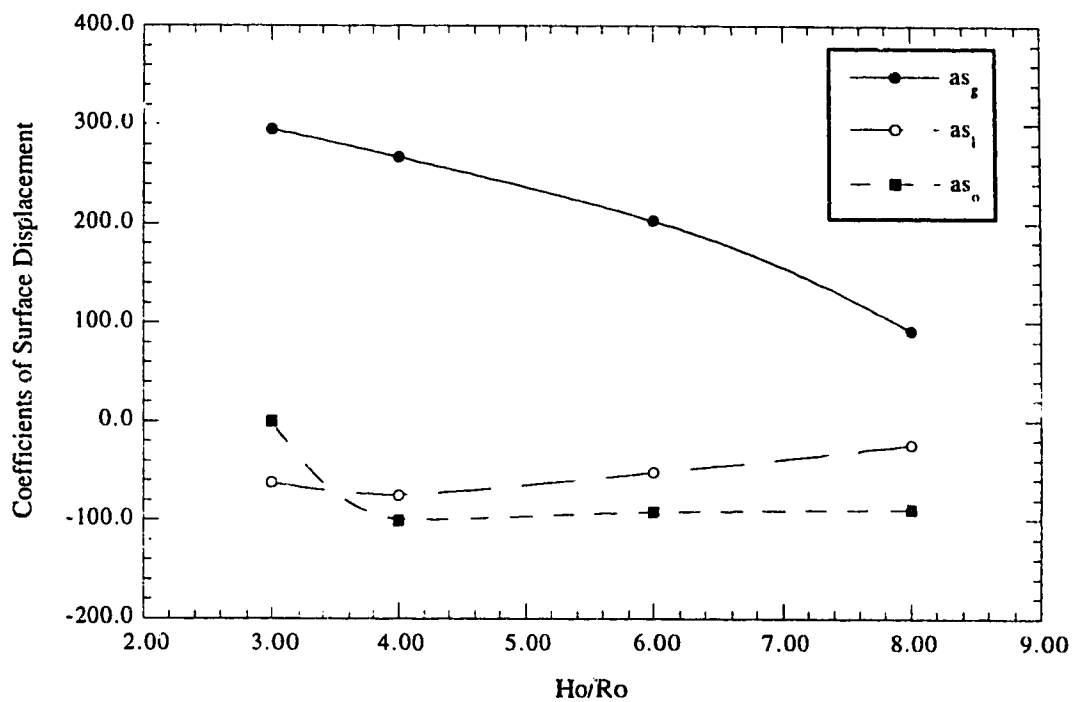


Figure 4.75: Regression Coefficients for Surface Movement ω_s

excavation steps. Similar to surface displacement, crown displacement is normalized through the equation:

$$\bar{w}_c = \frac{wE}{Dp_o} \quad (4.18)$$

Investigation of the results shows that liner pressure has almost no effect on the crown displacement, and *L.R.* is, therefore, excluded from the final generalized form:

$$\bar{w}_c = \left(ac_n(\nu) + \frac{ac_k}{K_o} + ac_h \right) \left(\frac{H_o}{R_o} \right)^2 + \left(ac_g(G.R.) + ac_o \right) \left(\frac{H_o}{R_o} \right) \quad (4.19)$$

Table 4.2 shows the values of the calculated constants.

4.7.5.3 Stress Ratio

The stress ratio is calculated at the crown, spring line, and at the floor of the liner. As shown in Figures 4.69 to 4.74 the optimum change in *S.R.* takes place at the middle of the gap distance and a comparable amount of stress change is recorded behind the point of the lining activation. Results of the analysis show a certain degree of consistency with respect to the effect of the grout pressure, lining pressure, and K_o while the effect of Poisson's ratio does not show the same degree of consistency although it has been regressed to the second degree. The following expression is suggested:

$$S.R. = ar_g(G.R.) + ar_l(L.R.) + ar_{n2}(\nu)^2 + ar_{n1}(\nu) + \frac{ar_k}{K_o} + \frac{ar_h}{H_o/R_o} + ar_o \quad (4.20)$$

Figure 4.76 and Table 4.3 show the results of the analysis and the effect of the depth on different obtained constants.

4.7.5.4 The Deviatoric Stress Ratio

The amount of mobilized shear strength associated with the excavation process in the three-dimensional is related to the deviatoric stress ratio *D.S.R.* defined as:

$$D.S.R. = \frac{\rho}{\gamma H_o} = \frac{\rho}{p_o} \quad (4.21)$$

$$\omega_s = \left(as_n(v) + \frac{as_k}{K_c} + as_h \right) \left(\frac{R_o}{H_o} \right)^2 + (as_g(G.R.) + as_l(L.R.) + as_o) \left(\frac{R_o}{H_o} \right)$$

as_n	-1356.017
as_k	-306.459
as_h	-607.023

i_i/v_h	3.0	4.0	6.0	8.0
as_l	294.948	267.077	202.629	91.485
as_o	-62.470	-75.822	-52.289	-24.186
	-92.777	-98.817	-89.556	-78.191

$$\omega_c = ac_g(G.R.) + ac_n(v) + \frac{ac_k}{K_o} + ac_o + ac_h \left(\frac{R_o}{H_o} \right)$$

ac_g	280.830
ac_n	-27.014
ac_k	97.171
ac_o	-406.630
ac_h	121.968

Table 4.2: Regression Coefficients for Ground Movement Expressions ω_s and ω_c

$$S. R. = ar_g(G. R.) + ar_l(L. R.) + ar_{n2}(v)^2 + ar_{n1}(v) + \frac{ar_k}{K_o} + ar_h \left(\frac{R_o}{H_o} \right) + ar_o$$

	H_o/R_o	3.0	4.0	6.0	8.0
Crown	ar_g	0.703	0.543	0.559	0.524
	ar_l	-0.102	-0.083	-0.072	-0.068
	ar_o	4.575	4.177	5.873	4.866
	ar_{n2}	52.865	46.771	76.938	58.858
	ar_{n1}	-27.826	-24.681	-39.701	-30.736
	ar_k	-0.296	-0.275	-0.258	-0.251
	ar_h	-0.098			
Sp. Lag Line	H_o/R_o	3.0	4.0	6.0	8.0
	ar_g	0.298	0.319	0.318	0.318
	ar_l	-0.147	-0.156	-0.154	-0.152
	ar_o	0.849	0.818	0.866	0.877
	ar_{n2}	2.412	1.916	2.453	2.260
	ar_{n1}	-1.285	-1.041	-1.314	1.213
	ar_k	0.235	0.230	0.224	0.221
ar_h	-0.058				
Floor	H_o/R_o	3.0	4.0	6.0	8.0
	ar_g	0.226	0.262	0.283	0.295
	ar_l	-0.120	-0.128	-0.137	-0.141
	ar_o	1.180	1.200	1.000	1.200
	ar_{n2}	-2.725	-2.836	-6.943	-4.168
	ar_{n1}	0.872	0.896	2.910	1.559
	ar_k	-0.342	-0.358	-0.375	-0.385
ar_h	0.182				

Table 4.3: Regression Coefficients for Stress Ratio, S.R. Expression

$$S.R. = ar_g (G.R.) + ar_l (L.R.) + ar_{n2} (v)^2 + ar_{n1} (v) + ar_h (R_o/H_o) + ar_k / (K_o) + ar_o$$

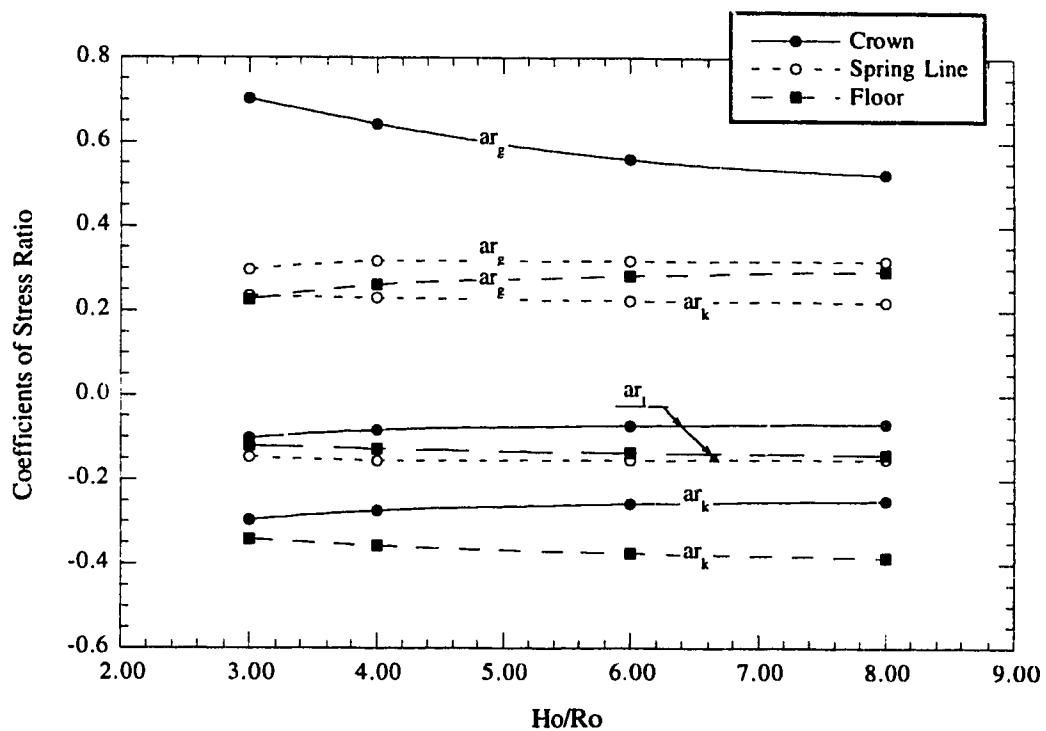
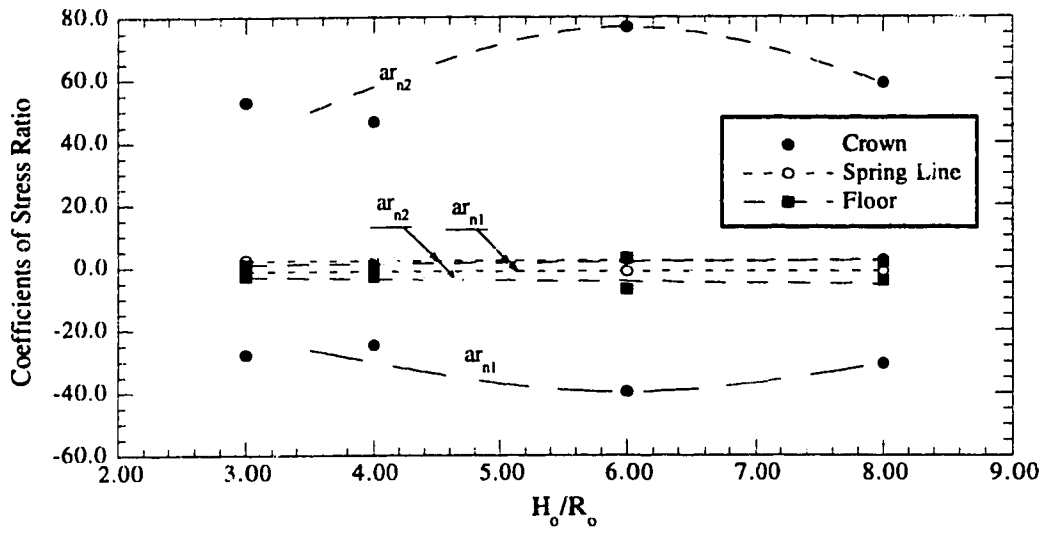


Figure 4.76: Regression Coefficients for Stress Ratio, S.R.



	ar_h
Crown	-0.100
Spring Line	-0.058
Floor	0.182

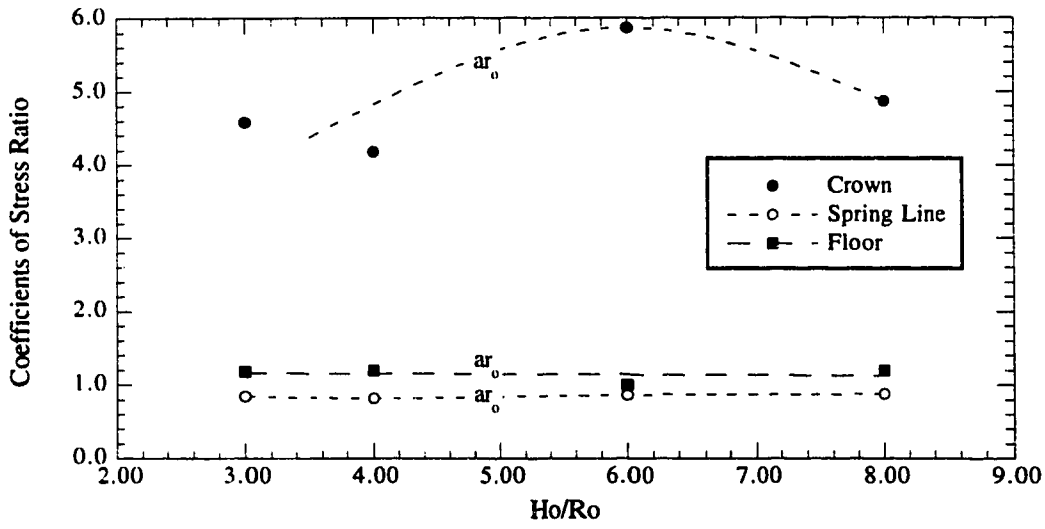


Figure 4.76: Regression Coefficients for Stress Ratio, S.R. (continued)

The evaluation of the *D.S.R.* at the point of the lining activation at the three points of the tunnel circumference (the crown, the spring line, and the floor) shows little effect on the liner pressure ratio *L.R.* . This may be attributed to the assumption that a rigid liner restrains any longitudinal movement at the point of the lining activation. The same process used in establishing the relationship between the stress ratio *S.R.* is used to define the relationship between the deviatoric stress ratio, *D.S.R.* and the various influencing parameters. The following relationship is obtained:

$$D.S.R. = ad_{g2}(G.R.)^2 + ad_{g1}(G.R.) + ad_{n2}(v)^2 + ad_{n1}(v) + \frac{ad_k}{K_o} + \frac{ad_h}{H_o/R_o} + ad_o \quad (4.22)$$

Figure 4.77 and Table 4.4 show the results of the analysis and the effect of the tunnel depth on the different obtained constants.

4.7.6 Verification

Figures 4.78 through 4.85 show the relationship between the obtained and the interpolated values of the different investigated results. A satisfactory degree of consistency is obtained in general. The least degree of consistency is met when Poisson's ratio is varied.

4.8 Conclusions

The conceptual representation of the stress field due to tunnelling is reviewed in the light of recent literature. For the case where a pressurized shield method is used in the construction, a number of adaptations have to be undertaken to readjust the concept of volume loss. The excavation may not be viewed as a cavity that generates a monotonic stress release around it, but rather as a structure that interacts with the surrounding ground by imposing pressures and displacement constraints to the boundary of the excavation. The supportive measures used in the construction system interact with each other to achieve a certain amount of internal equilibrium. The resultant of such interaction is reflected on the ground to produce stress changes around the excavation and displacements that are noticed at the the ground surface as the overall stability of the project is achieved.

Provided that the face stability is achieved, the two major loading actions imposed during the overall stability of the project are the liner pressure imposed on the liner as a

$$D.S.R. = ad_{g2}(G.R.)^2 + ad_{g1}(G.R.) + ad_{n2}(v^2) + ad_{n1}(v) + \frac{ad_k}{K_o} + ad_h \left(\frac{R_o}{H_o} \right) + ad_o$$

		H_o/R_o	3.0	4.0	6.0	8.0
Crown	ad_{g2}		0.609	0.457	0.696	0.522
	ad_{g1}		-0.686	-0.552	-0.837	-0.628
	ad_o		0.702	0.856	1.008	1.034
	ad_{n2}		7.610	8.525	9.424	9.878
	ad_{n1}		-3.992	-4.496	-4.987	-5.236
	ad_k		-0.241	-0.279	-0.318	-0.337
	ad_h		0.375			

		H_o/R_o	3.0	4.0	6.0	8.0
Spring Line	ad_{g2}		0.335	0.499	0.097	0.073
	ad_{g1}		-0.717	-1.102	0.754	-0.565
	ad_o		-0.118	-0.106	-0.151	-0.158
	ad_{n2}		-2.070	-2.074	-2.097	-2.104
	ad_{n1}		0.729	0.754	0.793	0.809
	ad_k		0.108	0.109	0.110	0.110
	ad_h		0.781			

		H_o/R_o	3.0	4.0	6.0	8.0
Floor	ad_{g2}		0.475	0.639	0.601	0.451
	ad_{g1}		-0.869	-0.999	-0.973	-0.730
	ad_o		0.150	0.738	0.672	0.573
	ad_{n2}		-2.608	-2.558	-2.507	-2.482
	ad_{n1}		0.944	0.888	0.831	0.800
	ad_k		-0.589	-0.571	-0.547	-0.533
	ad_h		0.566			

Table 4.4: Regression Coefficients for Deviatoric Stress Ratio, D.S.R. Expression

$$D.S.R. = ad_{g2} (G.R.)^2 + ad_{g1} (G.R.) + ad_{n2} (v)^2 + ad_{n1} (v) + ad_k / Ko + ad_h (R_o / H_o) + ad_o$$

	ad_h
Crown	0.37507
Spring Line	0.78064
Floor	0.56610

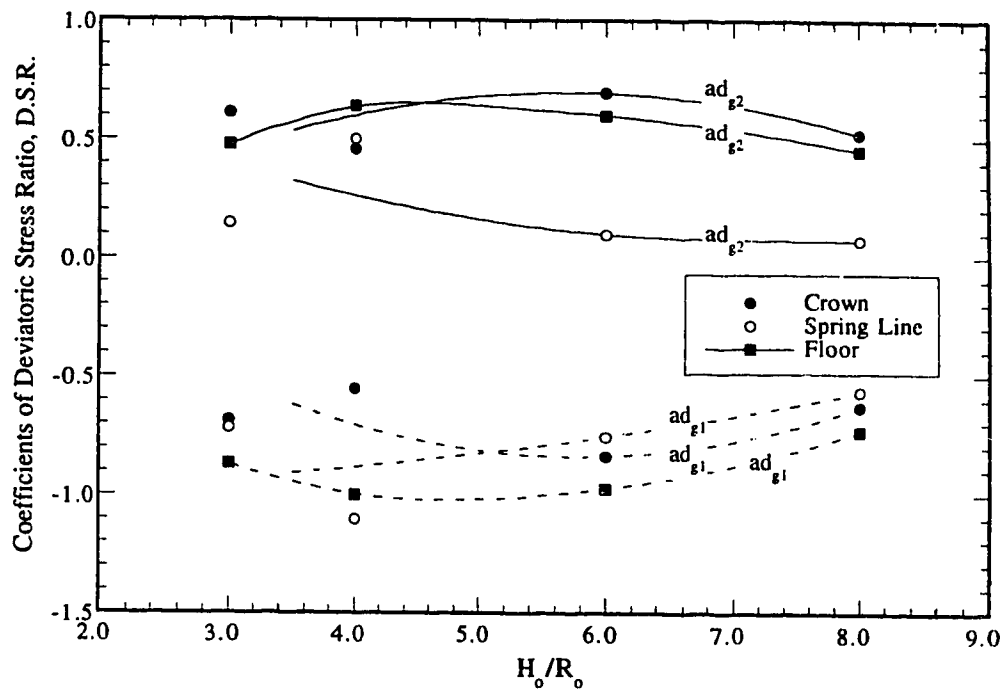


Figure 4.77: Regression Coefficients for Deviatoric Stress Ratio, D.S.R.

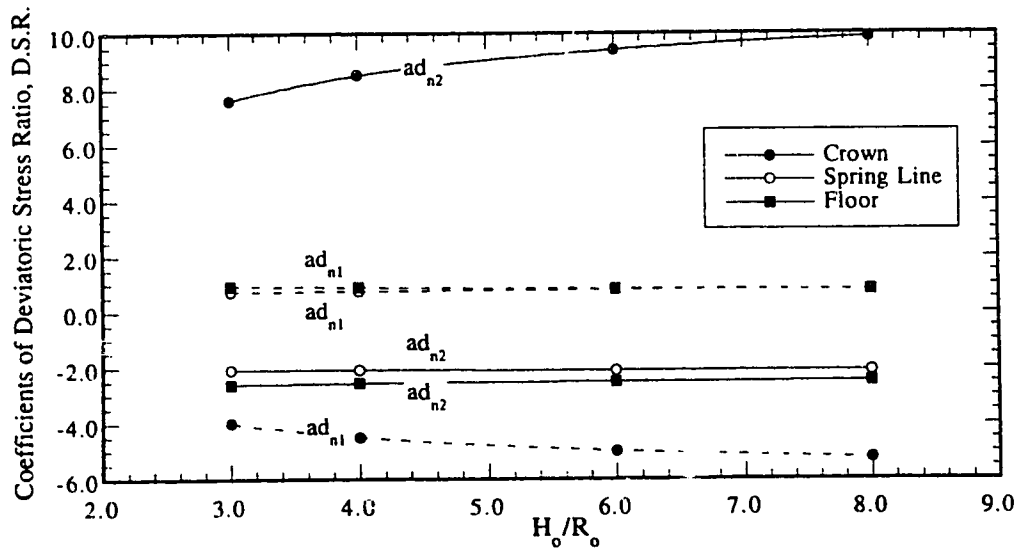
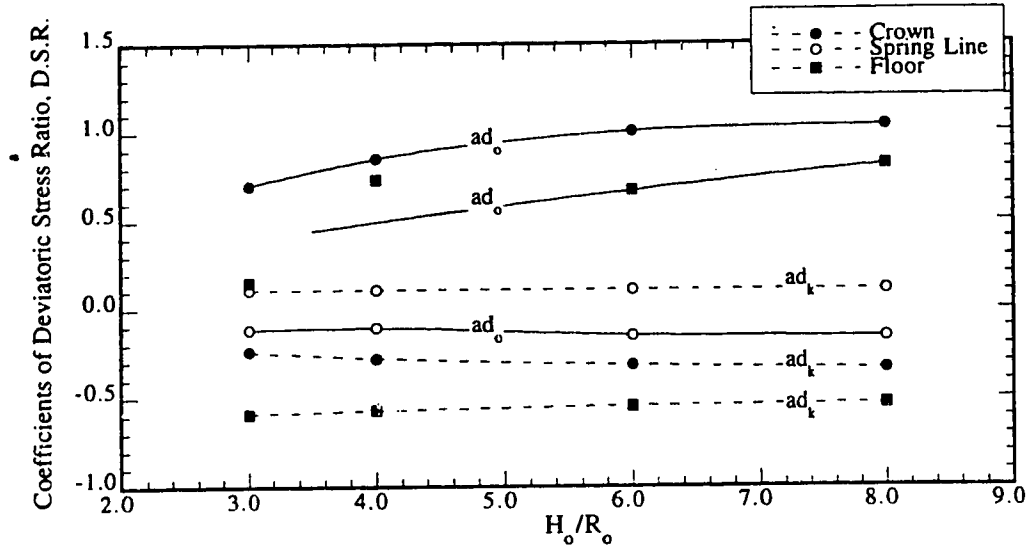


Figure 4.77: Regression Coefficients for Deviatoric Stress Ratio, D.S.R. (continued)

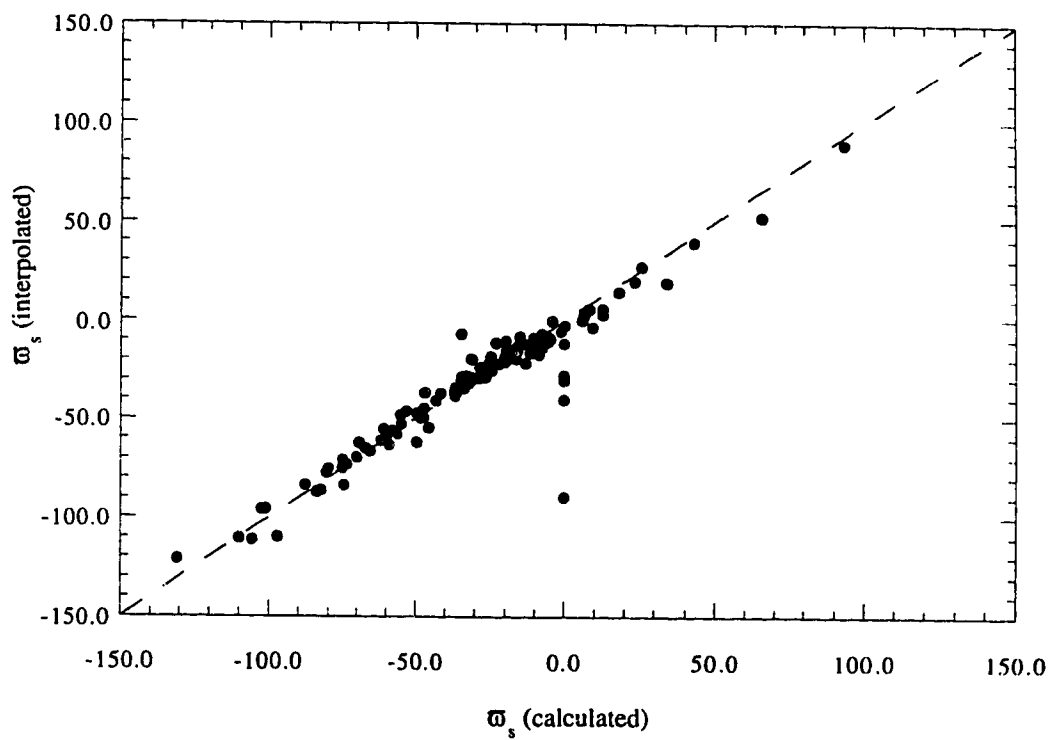


Figure 4.78: Calculated values of Normalized Surface Displacement, ϖ_s , versus Interpolated values.

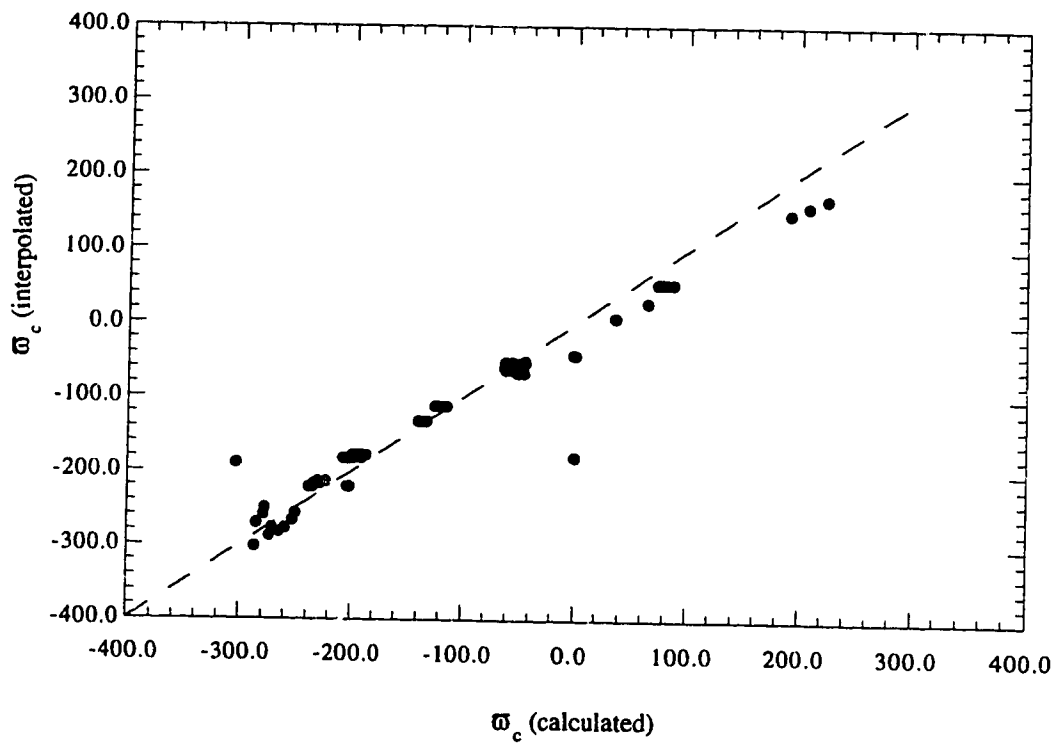


Figure 4.79: Calculated values of Normalized Crown Displacement, \bar{w}_c , versus Interpolated values.

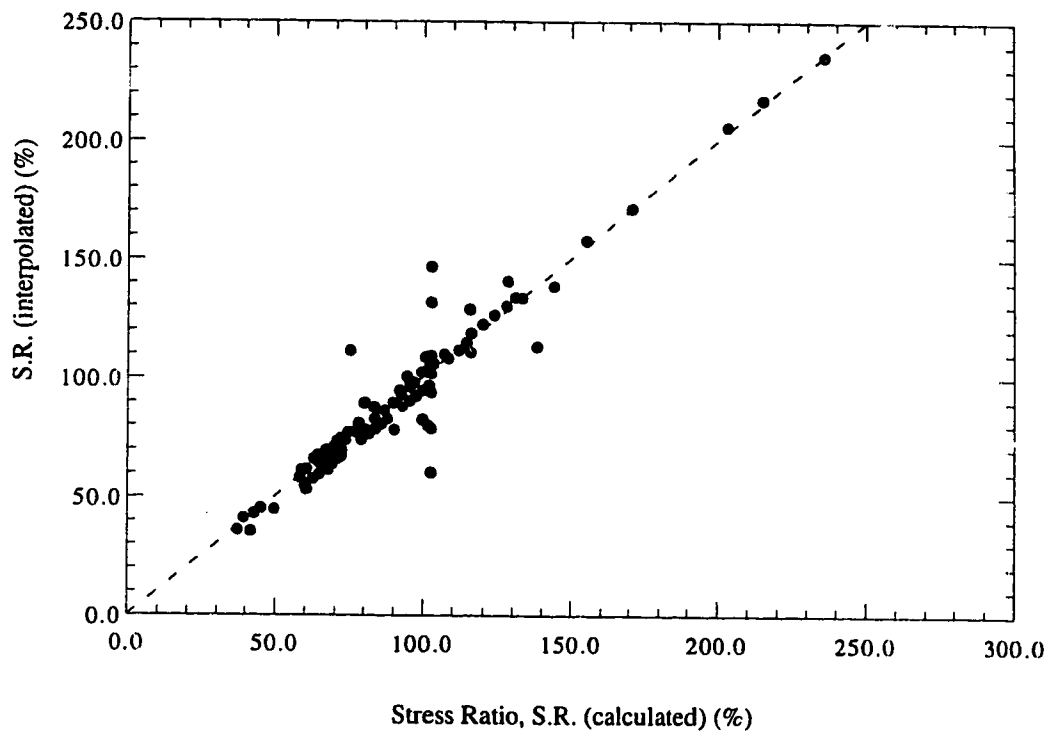


Figure 4.80: Calculated values of Stress Ratio, S.R. at the Crown versus Interpolated values.

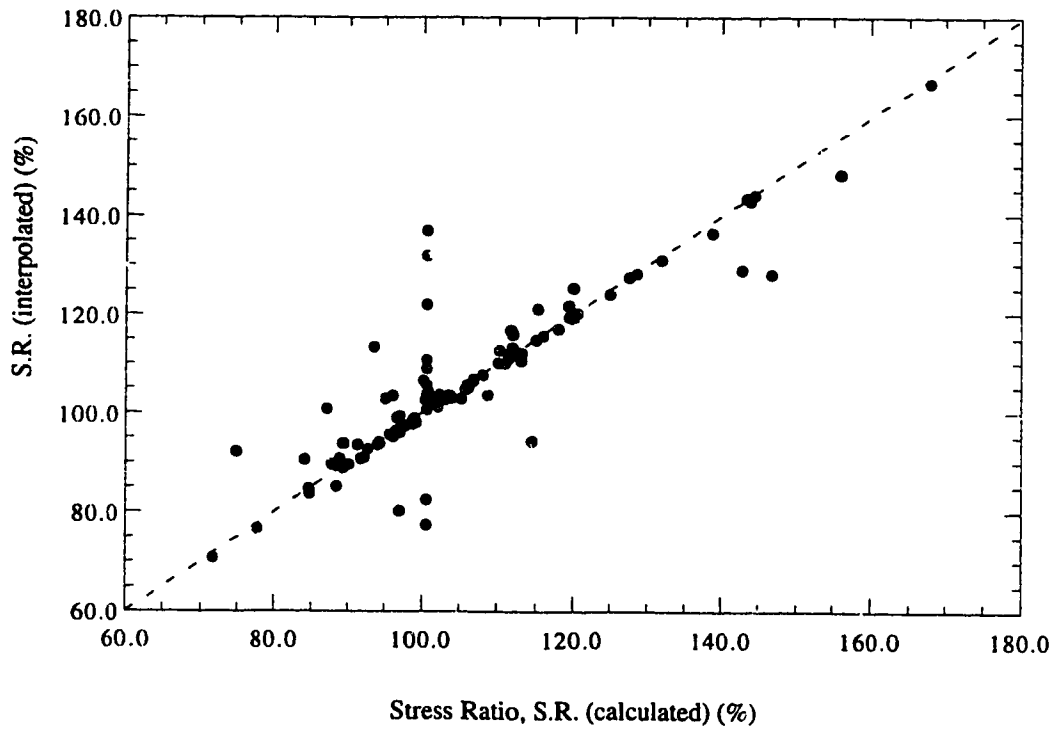


Figure 4.81: Calculated values of Stress Ratio, S.R. at the Spring Line versus Interpolated values.

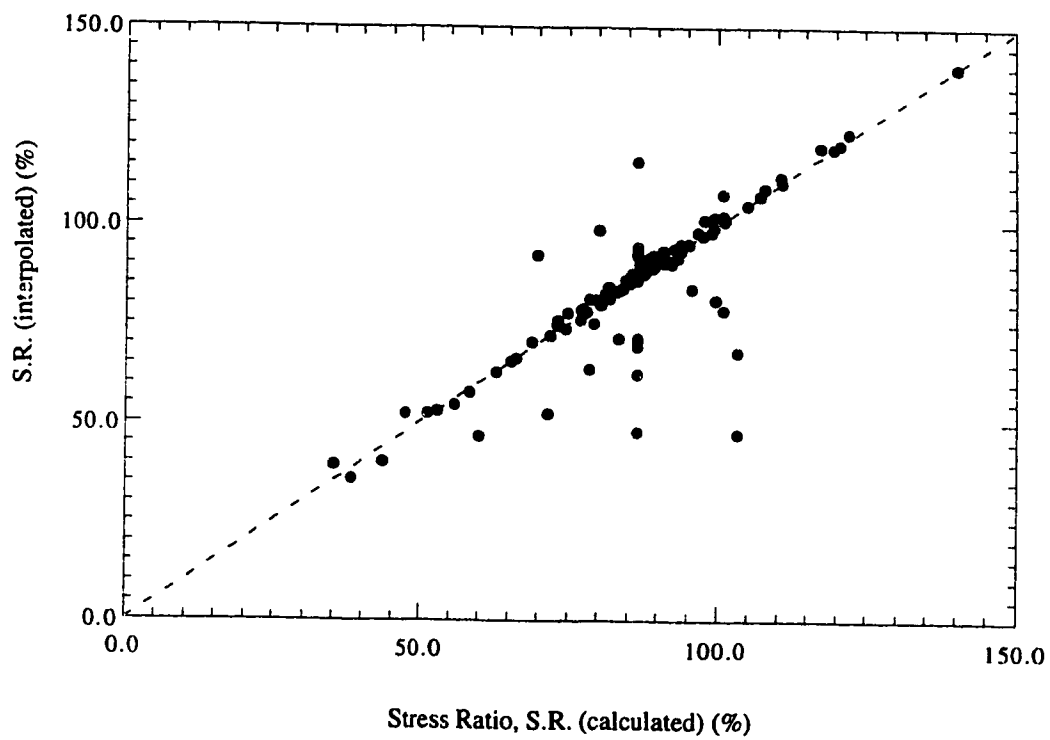


Figure 4.82: Calculated values of Stress Ratio, S.R. at the Floor versus Interpolated values.

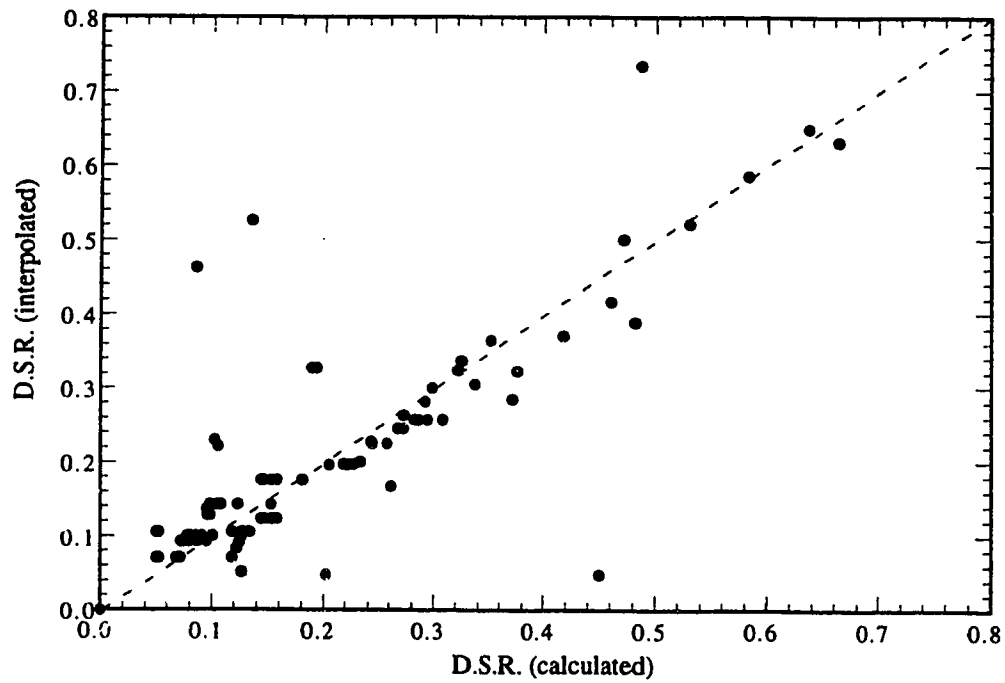


Figure 4.83: Calculated values of Deviatoric Stress Ratio, D.S.R. at the Crown versus Interpolated values.

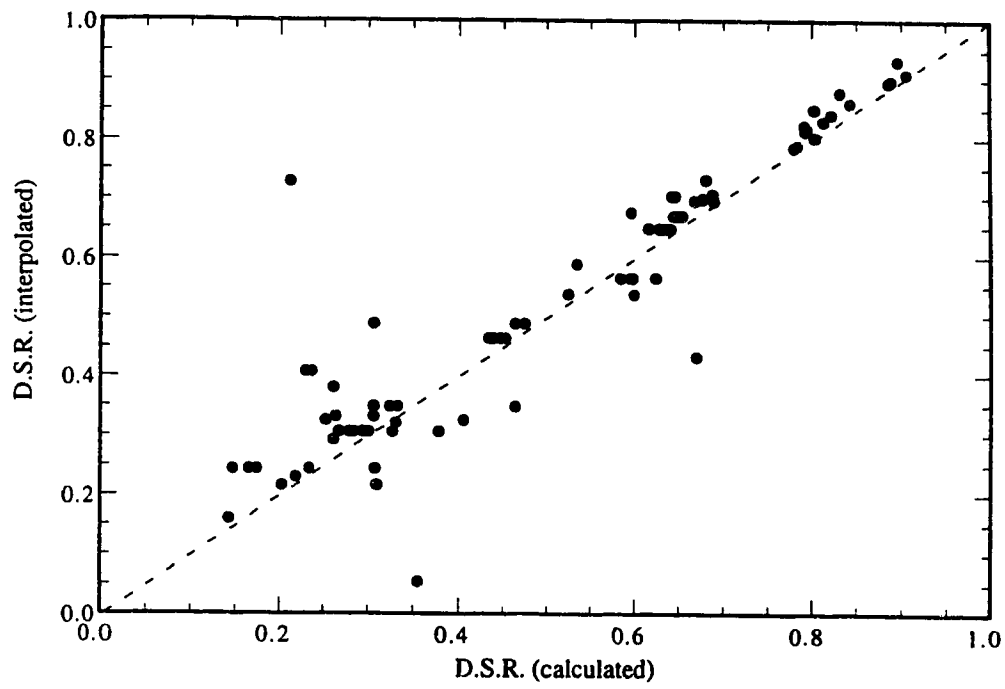


Figure 4.84: Calculated values of Deviatoric Stress Ratio, D.S.R. at the Spring Line versus Interpolated values.

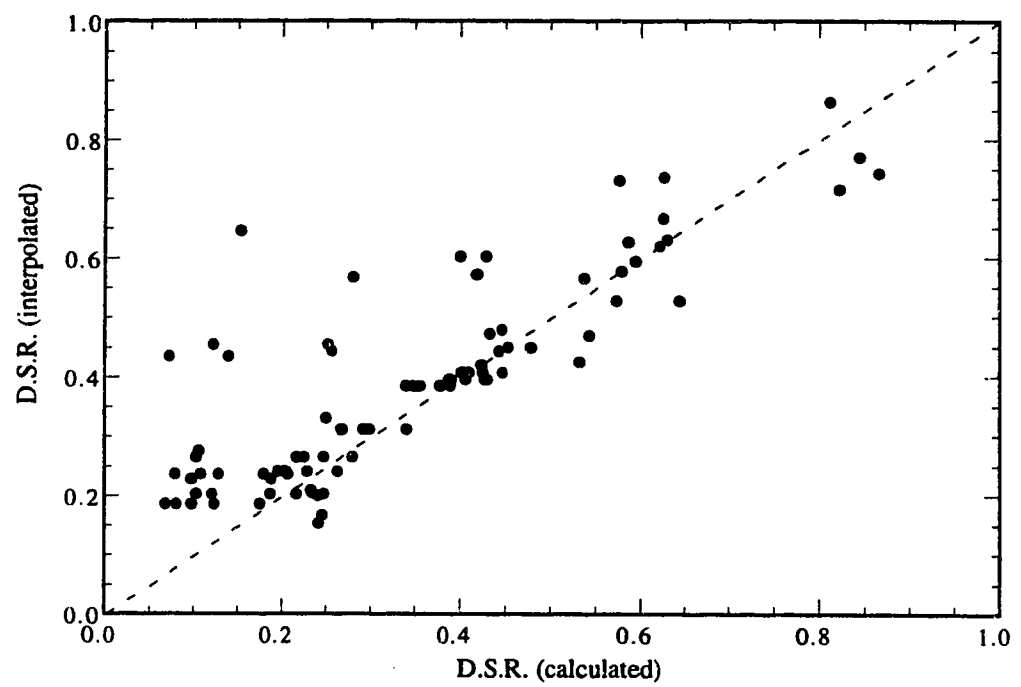


Figure 4.85: Calculated values of Deviatoric Stress Ratio, D.S.R. at the Floor versus Interpolated values.

reaction to the face pressure and the grout pressure applied behind the assembled liner. The effect of these two actions on the stress and strain field around the tunnel are investigated for different site and ground conditions. Three-dimensional finite element schemes are used in the undertaken parametric analysis. The results are presented to show the obtained ground deformation, mobilized shear strengths, and the stress paths related to various site and geological conditions. The results are analyzed such that polynomial expressions of the first or the second degree are suggested to represent the effect of the different parameters on the surface displacement, the displacement at the crown, the stress ratio, and the deviatoric stress ratio. The obtained polynomial expressions are chosen such that they best fit the total obtained results. The accuracy of these expressions depends on the number of effected runs and on the accuracy of the calculations.

The capability of carrying out a parametric analysis using three-dimensional finite element analysis are limited to the computer system's capacity. Therefore, the presented results describe quantitatively a number of relationships that are important to the design of tunnels constructed using pressurized shield methods. On the other hand, some other points are not completely clarified during the investigation, such as, the effect of the lining pressure on the mobilized shear strength near the excavation and the effect of Poisson's ratio on the displacement field. It is believed that higher computer system capabilities are required to completely investigate these points.

A three-dimensional analysis is carried out in order to investigate the effect of the longitudinal liner pressure and the grout pressure on the stress field around the tunnel and on the displacement field near the ground surface.

CHAPTER 5

DESIGN METHOD FOR TUNNELS CONSTRUCTED USING PRESSURIZED SHIELD METHODS

5.1 Introduction

A comprehensive design method of a tunnel constructed using a pressurized shield method is supposed to take into consideration the various engineering aspects of the project, specifically the geotechnical, geometrical, and structural aspects of the site. Geotechnical aspects of the site include the engineering parameters of the ground such as permeability, compressibility and shear strength parameters, as well as, the stress field existing prior to the construction. Geometrical and structural aspects of the project include the size of the excavation, its depth, and the depth of the rigid layer below it. Engineering aspects related to the construction scheme include details of the shield machinery in use, such as (1) the method of face support with respect to the intensity of the supporting pressure and the rigidity of the supporting face; (2) the arrangements of the cutting wheel; (3) the tail gap and the protective measures at the tail of the shield; (4) the material treatment of the ground whether in the form of material injection at the face or grouting behind the liner; (5) the liner properties; and (6) the selected construction sequence and the rate of advance of excavation. Safety requirements are generally concentrated around two aspects: the integrity of the project, and the safety of neighbouring structures. The integrity of the project is accomplished by designing proper support at the face and an effective shield-grout-lining system at the circumference. The acceptable limits of the settlement trough at the ground surface either regarding its magnitude or its gradient are set according to site conditions. The study of the relationship between the engineering aspects of the project including the construction method to the safety requirements is expected to be beneficiary to both the design of the construction method and that of the project. Two aspects are considered to be the main features of the tunnelling construction using pressurized shield methods: the grout pressure, and the longitudinal pressure applied to the shield (the liner pressure). The design method is verified using a well documented case study in Edmonton

during the construction of its subway system.

5.2 Framework

The objective of formulating a new design method is to investigate the effect of tunnelling construction techniques taking into account safety and the economical aspects of the project. Special emphasis is placed on soil deformation around the tunnel and at the ground surface, as well as, the straining actions applied at the liner as the two governing indices of the performance of the construction method. Pressurized shield methods, namely, the BSS method, the EPBS method, and the compressed air method, exert on the ground surrounding the excavation and on the assembled lining system a number of pressurized and supporting actions in order to restrict ground movement toward the excavation. It is, therefore, of interest to identify and evaluate the basic features of the new ground conditions that affect ground deformation and lining stresses. The attempt to adopt a deterministic approach is intended to produce a rational quantification of the effects of the various investigated parameters on the stress and strain fields in the ground. This study relies on results from numerical analyses using the finite element method in conjunction with closed form solutions. The design method is presented in a normalized form to allow the generalization of the results, and thus to enhance usefulness in the design of shallow tunnels. This method is summarized in a systematic scheme and a computer program is provided to facilitate its application with minimal computational effort.

5.3 Tunnel Lining Design

While the initial state of stress is determined according to soil density at the tunnel site, the depth ratio, and the coefficient of lateral pressure at rest, K_0 , the excavation process results in disturbing these initial conditions. Using the concept of volume loss, disturbance of the initial stress conditions is described as a reduction of the radial stresses at the tunnel circumference which is referred to as the stress relief. Factors affecting the stress changes during the construction process are the mechanical properties of the soil (shear strength and compressibility) and the construction method. Once the lining system is assembled to cover the entire tunnel circumference, the lining is in position to start interacting with the surrounding ground: the lining activation point. Stresses inside the lining and around it, in the surrounding soil, undergo readjustments related to the developed strain field in order to reach a state of equilibrium. The process of ground-liner interaction is affected by the lining properties, such as, flexibility and compressibility, in addition to, the factors affecting stress changes during the construction stage.

In general, methods of tunnel lining design emphasized in the stage of the ground-

liner interaction as a solution to the problem could be reached using a simple two dimensional analysis. A realistic assumption has to be taken into account regarding the stress disturbance at the construction stage. Peck (1969) and Peck et al. (1972) give a comprehensive description of the modes of deformation during the ground-liner interaction and stress the fact that the lining loads should not be exclusively calculated according to classical states of active, passive, or lateral earth pressure at rest because the distribution of stresses acting at the lining is affected by the deformation of the liner and that of the ground. They also present records of measurements in a number of constructed tunnels showing that the actual pressure immediately after construction is lower than the overburden pressure. Furthermore, a number of methods are developed to estimate stress and strain during the ground-liner interaction stage such as those described in Bull (1944), Brindley (1983), Muir Wood (1975), Morgan (1961), Ebaid and Hammad (1978), Duong and Erdmann (1982) and Duddeck (1991), Eisenstein et al. (1981), O'Rourke (1985) and (1984), Evison (1988), and El-Nahhas et al. (1992) among others. The various methods of lining design will be addressed separately. Two critical points are to be examined in any lining design method: how much is the actual magnitude of the soil loads on the liner, and how is it distributed along the lining circumference at the starting point of the ground-liner interaction.

5.3.1 Loading Conditions before Ground-liner interaction Stage

One method used in estimating the magnitude of liner pressure is applied in deep tunnelling and is based on the arching theory (Terzaghi, 1943) by relating the imposed pressure on the lining to a ground region extending ηD above the crown where η is an empirical constant defined according to site conditions. The value of η depends on the shear resistance of the soil mass and the characteristics of the fissures in a rock mass. For example, El-Nahhas (1980) and Branco (1981) present an estimation of this constant for two tunnelling projects. For shallow tunnels the problem is more complex as the gravitational stress field, the free boundary at the ground surface, and the three-dimensional effect related to the method of construction play a role in determining the liner pressure at the start of the interaction process. Few design recommendations are available in this domain. Peck (1969) reports that, according to records of measurements in a number of tunnels, the magnitude of the liner pressure after stress relief at the construction stage could be as low as 20%. Since the amount of stress relief is unquantifiable, he suggests that it would be a safe assumption to let the magnitude of the lining load be equal to the full overburden pressure, γH_0 , bearing in mind, at the same time, that lining stresses tend to approach the original overburden pressure in the long term. On the other hand, Muir Wood

1975) suggests that the liner pressure may be taken as one half the overburden pressure and he quotes that Panet (1973) suggests that two thirds of the overburden pressure is acting on the liner as the stress field at the face is not effectively conforming to the assumed plane strain condition. The above two suggestions may be accepted when compared with the case histories shown by Peck (1969). As pointed out by Muir Wood (1975), the conducting of three-dimensional analysis is inevitable if the magnitude of liner pressure is to be reliably determined. Negro (1988) presents a study using the finite element method to estimate the effect of the delay distance on the liner pressure. The results of the analysis are generalized and they are included in Eisenstein-Negro method previously mentioned.

The method of face-support application, if used, has an effect on the magnitude of stresses imposed on the lining. Peck (1969) shows the effect of using compressed air on the tunnel lining. Figure 5.1 shows a sketch of the relationship between the average ring load and the ground deformation around the lining. As the soil moves radially toward the tunnel, the ring load reduces (**Line AD**). A certain amount of displacement takes place before the face, δ_a , and during the delay period, δ_b . At **Point C** the lining interacts with the surrounding soil and reaches equilibrium at **Point C'**. The effect of air pressure is to reduce temporarily the ring load until the air pressure is released. Based on Eisenstein (1993), Figure 5.2 shows the relationship between the radial displacement and the magnitude of pressure at the crown of a tunnel under construction using the EPBS method. As the shield has the effect of pushing the ground in the longitudinal direction at the face, radial pressure increases linearly (**Line ab**) and then nonlinearly (**Line bc**) because of soil yielding. Stress reduction takes place behind the tail of the shield (**Line cd**) until the liner is assembled and interacting with the effect of the grouting and the ground conditions. At **Point d** ground-liner interaction starts as the soil and the liner movements become compatible. The assessment of the actual loading magnitude acting on the liner before the ground-liner interaction process is subject to numerous investigations regarding its relationship with the construction process. Guidelines for the design of tunnels presented by ITA¹ (1988) confirm that liner loading is to be reduced when construction methods are relying on new shield technology.

The distribution of soil pressure around the liner is affected by the change in the magnitude of the liner pressure. A starting point is to assume that the reduction in overburden pressure is evenly distributed around the tunnel and that the same coefficient of lateral pressure at rest, K_0 , is, therefore, still acting. Suggestions regarding this question are even less frequent than those regarding the change in the magnitude of the liner pressure. This is due to the fact that the pressure distribution at the point of lining

¹International Tunnelling Association.

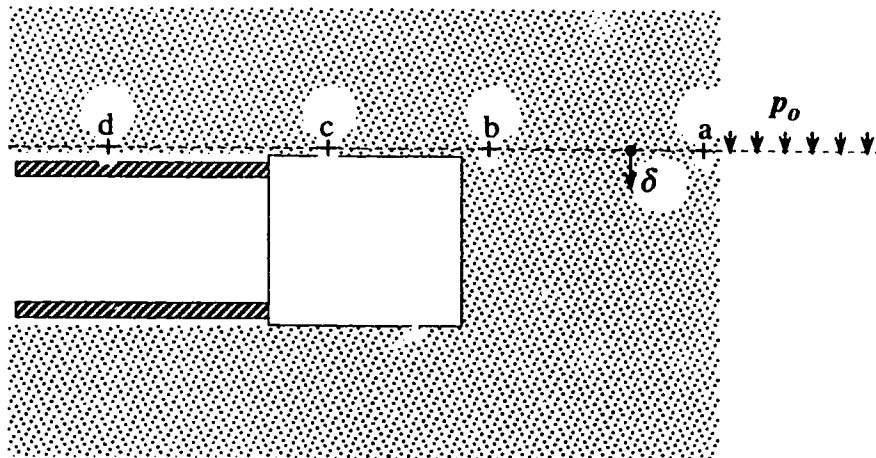
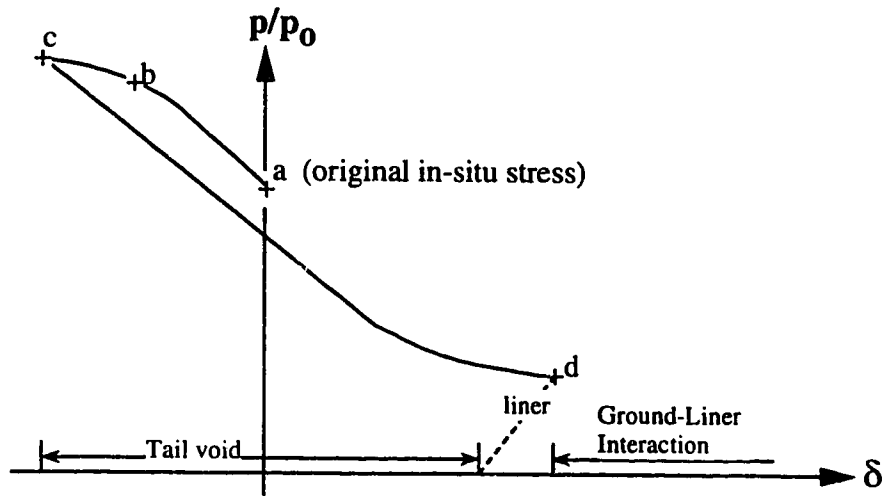
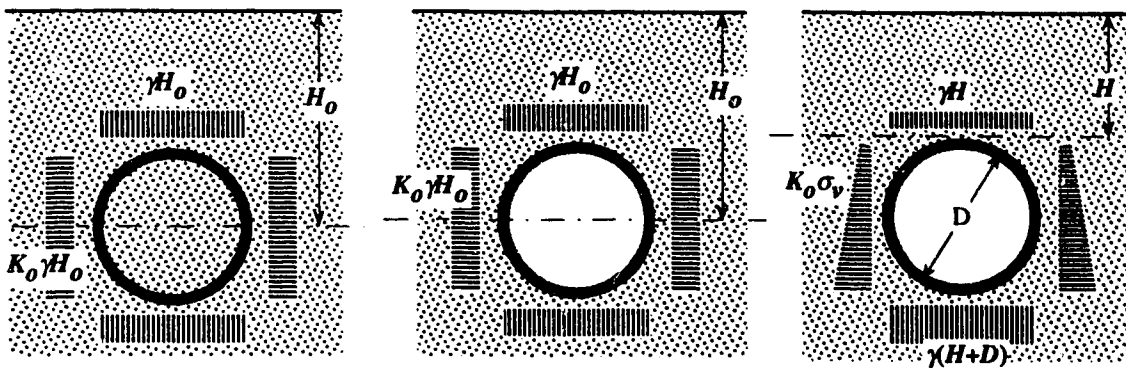


Figure 5.2: the Ground Reaction Curve for the Earth Pressure Balanced Shield (after Eisenstein 1993)

activation is only an intermediate stage between the initial in situ stress distribution and the final distribution after the ground-liner interaction. Site conditions render the problem substantially complex as the distribution is affected by a number of factors that are difficult to quantify such as the distribution of grout pressure and the sequence of applying it, the overall movement of the tunnel, and the friction between the extrados of the shield (if used) and the ground. Some closed form solutions based on the continuum model, such as, those presented by Ranken (1978), Einstein and Schwartz (1979), Matsumoto and Nishioka (1991), and Hartmann (1985) modify this assumption by adopting an initial pressure distribution related to an already excavated elastic space. Such modification is a step forward toward a more realistic representation of the actual stress field. On the other hand, Muir Wood (1975) suggests that the amount of stress relief around the tunnel is evenly distributed, thus the initial stress distribution at the liner is maintained. Figure 5.3 shows a number of loading-condition distributions used by a number of authors. From the figure, Rosza (1963) considers the spring model where the tunnel liner supports vertical load at its upper portion and transfers it to a number of springs distributed along the lower part of the circumference. According to Szechy (1973), Bugayeva (1951) follows an approach similar to that of the Morgan-Muir Wood-Curtis method by predefining a trigonometric function describing radial soil reaction to certain vertical loading conditions. Only the magnitudes of reactions at the floor and at the spring line verify the equilibrium conditions. Windels (1966) and Schulze and Duddeck (1964) consider the influence of gravity at the upper half of the tunnel while maintaining symmetry around the horizontal centre of the tunnel. Similar to Rosza (1963) and Bugayeva (1951), partial embedment at the upper quarter is assumed. Evison (1988) applies a more realistic loading condition by using the closed form solution of Ranken as the loading condition acting on a number of ring-and-spring models including cases of full and partial embedment. The effect of tangential springs is also investigated in the study. Okada et al. (1989) show a loading condition considering partial embedment at the top and at the bottom of the liner while the loading distribution is kept equal to the initial conditions.

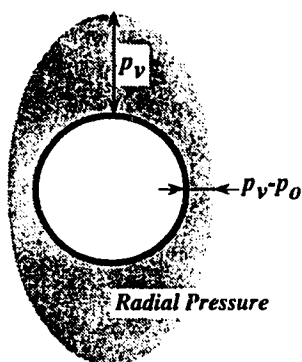
A number of assumptions are made regarding the initial liner pressure distribution but few of them take into account the effect of the construction process. An interesting centrifuge experiment may be considered to demonstrate such effect. Tohda et al. (1988) considers the stress distribution around a rigid pipe during a centrifuge test. While the pipe and the soil properties are the same, two cases of construction conditions are employed. During Case A, a sheet pile is originally inserted and then it is retracted while the centrifuge loading is applied. Case B is performed without disturbing the soil mass. The fact that the pipe is relatively rigid excludes the effect of the ground-liner interaction. As Figure 5.4



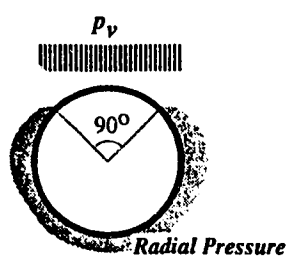
Peck et al. (1972)

Ranken (1978)
Einstein-Schwartz (1979)

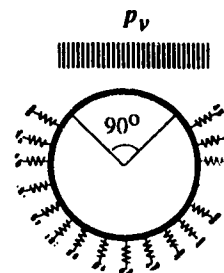
Hartmann (1985)
Matsumoto-Nishioka (1991)



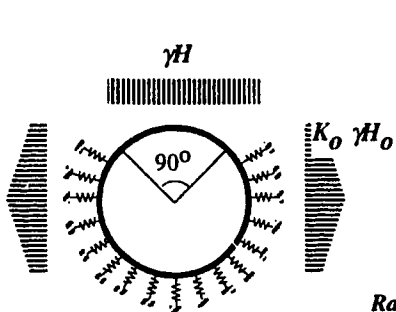
Morgan (1961)
Muir-Wood (1975)
Curtis (1976)



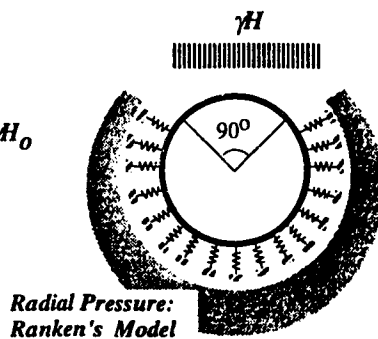
Bogayeva (1951)



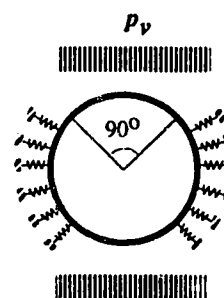
Rosza (1963)



Duddeck and Erdmann (1982)



Evison (1988)



Okada et al. (1989)

Figure 5.3: Loading Conditions for Different Structural Models of Circular Tunnels

shows, the two cases yield a different distribution for the initial pressure. Although the retraction of sheet piles is not a simulation of a usual tunnelling construction process, the results of the experiment show that the method of application of gravity forces on a rigid liner (i.e. without the effect of ground-liner interaction) has an effect on the initial distribution of ground pressure on the liner. The obtained distributions are not necessarily related to the conceptual stress field calculated using K_0 .

In conclusion, loading conditions upon which the tunnel liner is subjected before the stage of the ground-liner interaction are influenced both in their magnitude and distribution by the construction process. While common design practice acknowledges such influence, the evaluation of the design loads relies, in many cases on empiricism, intuition, and on engineering judgment.

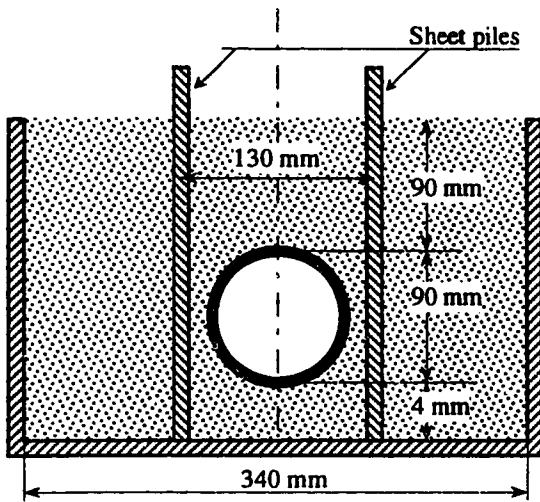
5.3.2 Structural Models for Tunnel Design

Based on the fact that the assessment of straining actions inside the tunnel liner has to consider the mechanical properties of both the soil and the liner materials, a number of structural models are developed to study the resultant interaction process. Duddeck and Erdmann (1982) present a review of a number of design methods. Three structural models are commonly used in tunnel design: the continuum model, the continuum approach with a predefined deformation mode, and the bedding beam model.

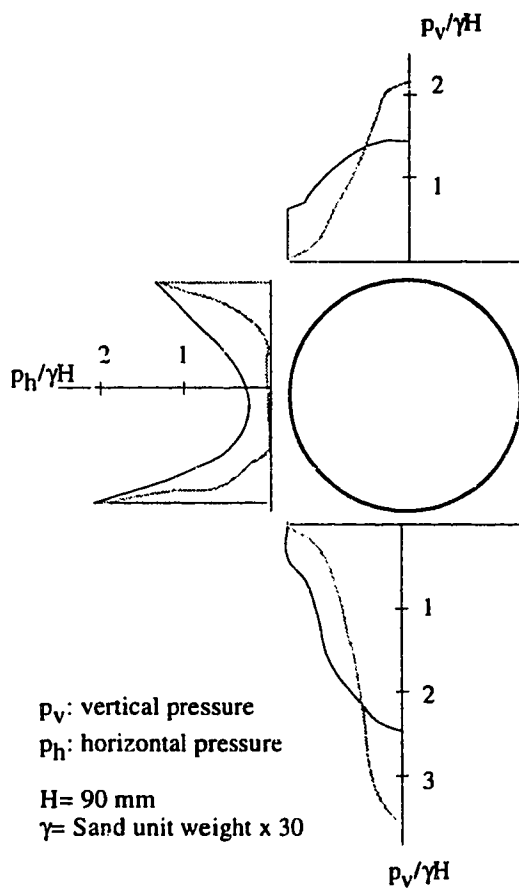
5.3.2.1 Elastic Continuum Model

The continuum model has the advantage of simulating both the soil and the liner in their proper dimensions. However, the mathematical complexity involved in the derivations, results in a number of assumptions that have to be taken. Two basic assumptions are commonly present in the continuum solutions: the soil mass and the liner are linearly elastic and the plane strain condition prevails initially. Peck et al. (1969) modifies the one dimensional form of Burns and Richards (1964) for the case of air blast loading for protective structures to include the effect of the horizontal loading condition which is not necessarily equal to the vertical pressure. The final solution does not include the effect of shear stresses between the extrados of the liner and the ground. Relative properties of the liner, with respect to the ground are expressed in terms of the compressibility and the flexibility ratios, C and F respectively:

$$C = \frac{ER_0(1 - \nu_l^2)}{E_l t(1 + \nu)(1 - 2\nu)} \quad , \quad (5.1)$$



Soil Properties:
 Specific Gravity 2.65
 Grain Size 0.24 to 1.4 mm
 Coefficient of Uniformity 1.75
 Dry Density 15.21 kN/m³
 Cohesion 0
 Angle of Internal Friction 47°



Case A: sheet piles retracted during loading
 Case B: No Disturbance during centrifuge loading

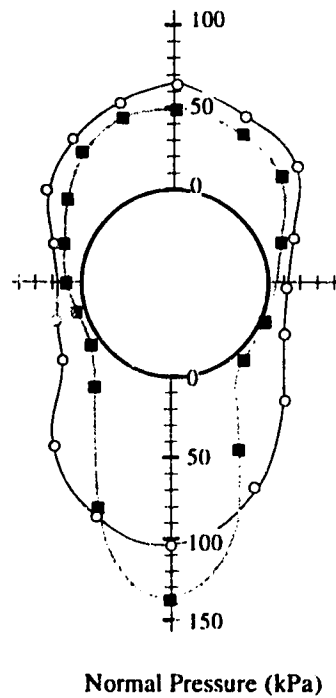


Figure 5.4: Centrifuge test results on Rigid Pipe in Dense Sand (after Tohda et al. 1988)

and

$$F = \frac{ER_o^3(1 - \nu_l^2)}{6E_l I_l(1 + \nu)} \quad , \quad (5.2)$$

where:

t is the liner thickness,

I_l is the moment of inertia of the liner cross section,

E and E_l are the elastic moduli of the ground and the liner respectively, and

ν and ν_l are Poisson's ratios of the ground and the liner, respectively.

Ranken (1978) stresses the loading condition of gravity forces by differentiating between the two methods of simulation: excavation and overpressure. In the case of overpressure, the continuum stress field is applied externally on the liner section which, in a way, represents a case of "switch on gravity". On the other hand, excavation simulation considers the stress field of an unperforated half space, then it annuls the resulting deformations before including the excavation and liner effects. As a result, it gives lower and more realistic values of straining actions in the liner. The final solutions cover a number of cases of practical use, such as, loading conditions (overpressure or excavation), liner thickness, and shear interface (full slippage conditions versus no slippage conditions). Einstein and Schwartz (1979) present, simultaneously, a similar solution and introduce a modification to the compressibility and flexibility ratios to include the effect of the excavation loading condition:

$$C^* = \left(\frac{1 - 2\nu}{1 - \nu} \right) C \quad , \quad (5.3)$$

and

$$F^* = \left(\frac{6}{1 - \nu} \right) F \quad . \quad (5.4)$$

The above mentioned solutions deal with conditions in a deep tunnel. Vertical pressure applied at the crown, as well as, that applied at the floor are equal to the average pressure which is normally the ground pressure at the centerline of the tunnel. Hartmann (1970 and 1985) quoted from Negro (1988:1117) introduces the effect of a gravitational gradient

related to shallow tunnel conditions. Here, only the no slip condition, and the excavation loading condition are considered. Straining actions in the liner are calculated using Flügge's differential equations for cylindrical shells. Relative liner properties are expressed in the form of incompressibility and rigidity ratios, $\dot{\alpha}$ and β .² respectively, which could be related to C^* and F^* defined by Einstein and Schwartz (1979) in Equations 5.3 and 5.4 as:

$$\dot{\alpha} = \frac{I}{C^*(I - \nu)} \quad , \quad (5.5)$$

and

$$\beta = \frac{I}{F^*(I - \nu)} \quad . \quad (5.6)$$

Hartmann's solution is shown in Figure 5.5, and the symbols used in the final derivation are explicitly defined in Figure 5.5 (a). From the figure, as a result of including the effect of gravity stress gradient while the liner is assumed to be weightless, the tunnel is supposed to perform an upward movement due to buoyancy. Engineering judgment is necessary to decide whether to include this heaving action based on the construction method. It is to be noted also that Matsumoto and Nishioka (1991) present a solution for tunnel-liner interaction that includes the effect of stress gradient due to gravity, but a presumed printing error³ does not allow the verification of their solution with that of Hartmann.

As a general remark, continuum models have the advantage of considering a number of practical aspects that affect the ground around the liner and the ground-liner interaction. Excavation type of loading, the gravitational stress field, and shear stresses at the interface between the liner and the ground are modeled. On the other hand, the complexity of the mathematical derivation does not allow the consideration of constitutive models other than the linear elastic model for both the ground and the liner. Also, the free boundary condition at the ground surface is not simulated, therefore, the obtained stress and strain fields, even if the stress gradient due to gravity is considered, cannot be accurately calculated at points relatively distant from the tunnel.

²In Negro's thesis, the ratios $\dot{\alpha}$ and β are named the compressibility and flexibility ratios. It was decided to use different names for them as they are the inverse of the compressibility and flexibility ratios, C and F defined by Peck and by Einstein and Schwartz.

³Constant b_3 is not defined (page 180).

$$\alpha = \frac{E_s(1+\mu)}{E_{r_0}(1-\mu_s^2)} \quad \beta = \frac{E_s J_s(1+\mu)}{E_{r_0}^3(1-\mu_s^2)}$$

$$\sigma_m = \frac{(1+K)(\alpha+\beta)}{2(1+\alpha+\beta)} \gamma_c + \frac{\alpha(1+K)}{4(1+\alpha)} \gamma_c \cos \phi - \frac{(1-K)(3-4\mu)(\alpha-9\beta-12\alpha\beta)}{2(1+\alpha(3-2\mu)+3\beta(5-6\mu+4\alpha(3-4\mu)))} \gamma_c \cos(2\phi) - \frac{(1-K)(3-4\mu)(\alpha-32\beta-72\alpha\beta)}{4(1+\alpha(5-4\mu)+8\beta(7-8\mu+9\alpha(3-4\mu)))} \gamma_c \cos(3\phi)$$

$$\sigma_{\phi_0} = \frac{(1+K)(2+\alpha+\beta)}{2(1+\alpha+\beta)} \gamma_c + \frac{2+\alpha+(K-\mu-\mu K)(4+3\alpha)}{4(1-\mu)(1+\alpha)} \gamma_c \cos \phi - \frac{(1-K)(4+\alpha(3+4\mu)+3\beta(11-12\mu+4\alpha(3-4\mu)))}{2(1+\alpha(3-2\mu)+3\beta(5-6\mu+4\alpha(3-4\mu)))} \gamma_c \cos(2\phi) - \frac{(1-K)(4+\alpha(5+4\mu)+8\beta(16-16\mu+9\alpha(3-4\mu)))}{4(1+\alpha(5-4\mu)+8\beta(7-8\mu+9\alpha(3-4\mu)))} \gamma_c \cos(3\phi)$$

$$\tau_{\phi_0} = \frac{\alpha(1+K)}{4(1+\alpha)} \gamma_c \sin \phi - \frac{\alpha(1-K)(3-4\mu)(1+6\beta)}{1+\alpha(3-2\mu)+3\beta(5-6\mu+4\alpha(3-4\mu))} \gamma_c \sin(2\phi) - \frac{3\alpha(1-K)(3-4\mu)(1+24\beta)}{4(1+\alpha(5-4\mu)+8\beta(7-8\mu+9\alpha(3-4\mu)))} \gamma_c \sin(3\phi)$$

$$v_m = v_m^* + v_{z_0}^* \cos \phi$$

$$v_{\phi_0} = v_{\phi_0}^* + v_{z_0}^* \sin \phi$$

$$v_m^* = \frac{1+\mu}{E} \left(\frac{1+K}{2(1+\alpha+\beta)} \gamma_{c_0}^* + \frac{1+K}{8(1+\alpha)} \gamma_{c_0}^* \cos \phi + \frac{(1-K)(3-4\mu)(1+2\alpha)}{2(1+\alpha(3-2\mu)+3\beta(5-6\mu+4\alpha(3-4\mu)))} \gamma_{c_0}^* \cos(2\phi) - \frac{(1-K)(3-4\mu)(1+3\alpha)}{8(1+\alpha(5-4\mu)+8\beta(7-8\mu+9\alpha(3-4\mu)))} \gamma_{c_0}^* \cos(3\phi) \right)$$

$$v_{z_0}^* = \frac{(1+\mu)(3-4\mu)}{4E(1-\mu)} \gamma_{c_0}^* \ln \left(\frac{r_0}{r_1} \right)$$

$$v_{\phi_0}^* = \frac{1+\mu}{E} \left(\frac{1+K}{8(1+\alpha)} \gamma_{c_0}^* \sin \phi + \frac{(1-K)(3-4\mu)(1+\alpha+3\beta)}{2(1+\alpha(3-2\mu)+3\beta(5-6\mu+4\alpha(3-4\mu)))} \gamma_{c_0}^* \sin(2\phi) + \frac{(1-K)(3-4\mu)(1+\alpha+16\beta)}{8(1+\alpha(5-4\mu)+8\beta(7-8\mu+9\alpha(3-4\mu)))} \gamma_{c_0}^* \sin(3\phi) \right)$$

$$N_{\phi} = \frac{(1+K)(\alpha+\beta)}{2(1+\alpha+\beta)} \gamma_{c_0}^* + \frac{\alpha(1+K)}{4(1+\alpha)} \gamma_{c_0}^* \cos \phi - \frac{(1-K)(3-4\mu)(\alpha+3\beta+12\alpha\beta)}{2(1+\alpha(3-2\mu)+3\beta(5-6\mu+4\alpha(3-4\mu)))} \gamma_{c_0}^* \cos(2\phi) - \frac{(1-K)(3-4\mu)(\alpha+4\beta+36\alpha\beta)}{4(1+\alpha(5-4\mu)+8\beta(7-8\mu+9\alpha(3-4\mu)))} \gamma_{c_0}^* \cos(3\phi)$$

$$M_{\phi} = -\frac{\beta(1+K)}{2(1+\alpha+\beta)} \gamma_{c_0}^* + \frac{3\beta(1-K)(3-4\mu)(1+2\alpha)}{2(1+\alpha(3-2\mu)+3\beta(5-6\mu+4\alpha(3-4\mu)))} \gamma_{c_0}^* \cos(2\phi) + \frac{\beta(1-K)(3-4\mu)(1+3\alpha)}{1+\alpha(5-4\mu)+8\beta(7-8\mu+9\alpha(3-4\mu))} \gamma_{c_0}^* \cos(3\phi)$$

$$Q_{\phi} = -\frac{3\beta(1-K)(3-4\mu)(1+2\alpha)}{1+\alpha(3-2\mu)+3\beta(5-6\mu+4\alpha(3-4\mu))} \gamma_{c_0}^* \sin(2\phi) - \frac{3\beta(1-K)(3-4\mu)(1+3\alpha)}{1+\alpha(5-4\mu)+8\beta(7-8\mu+9\alpha(3-4\mu))} \gamma_{c_0}^* \sin(3\phi)$$

Figure 5.5 b) Hartmann's Solution (after Negro 1988: 7.1)

5.3.2.2 Elastic Continuum Model with Predefined Mode of Deformation (Muir Wood's model)

The mathematical effort in deriving closed form solutions can be reduced if simplifying assumptions are taken regarding the mode of deformation of the liner. Morgan (1961) proposes an elliptical shape for the deformed liner. Consequently, straining actions and displacement of the liner are calculated by solving the equilibrium and compatibility equations between an infinite space representing the ground and a smooth stiff membrane representing the liner. Muir Wood (1975) corrects an error in Morgan's solution regarding the plane-strain assumption and adds to the solution the effect of shear forces between the ground and the liner. Curtis (1976) in his turn, includes in the solution the effect of deformation due to shear stresses at the ground-liner interface. The method, also, described as the intuitive continuum method, has found acceptance because of its simplicity, and this method is applied in tunnel design especially in the United Kingdom (Duddeck and Erdmann, 1982). Ebaid and Hammad (1978) demonstrate that the method gives generally lower estimations of liner-straining actions when compared with other methods.

5.3.2.3 Ring-and-Spring Model

The spring and ring method is widely used in Germany and has the advantage of replacing the ground space by a well-known structural element: the spring. The loading condition, as well as the stiffness and the number of springs has to be carefully chosen to represent actual ground conditions. Partial embedment (refer to Figure 5.3) is a commonly used assumption in order to avoid simulating tensile reaction at the crown region. Basically, there is correspondence between the elastic spring and ring method and the elastic continuum method and if the proper assumptions have been taken, it can be believed that the same results may be reached (Evison (1988). At the same time the absence of ground space from the model does not allow the calculation of stresses or strains within the soil mass. This is true also in the case of the elastic continuum model with a predefined mode of deformation (Muir Wood's model).

5.3.3 Adaptation of Hartmann's Solution to Eisenstein-Negro Method of Tunnel Design

The advantages of Hartmann's solution allow it to be incorporated into the Eisenstein-Negro method of design for shallow tunnels. These advantages may be summarized as follows (Negro, 1988):

- (1) the solution is derived for linearly elastic ground conditions, however, non linear behaviour can be incorporated by using reduced values for the elastic parameters;
- (2) the stress relief due to the construction process can be simulated by using reduced values of gravity, (γ_{red});
- (3) the initial loading condition takes into account the gravitational gradient, lateral pressure at rest, and excavation loading loading method of simulation; and
- (4) the reduction of the lining perimeter will result in an increase of curvature and thus of the development of additional bending moment even in the case of the ideal isotropic conditions. This effect is included as second order terms in the final derivation.

The method is verified by comparison with other closed form solutions in Negro (1988:1126) and shows acceptable agreement with solutions of Windels (1967), Curtis-Muir Wood, Einstein and Schwartz (1979), and Ahrens et al. (1982), and the method reduces to Mindlin's solution (1939 and 1940: 1136) if the liner is neglected ($\alpha = \beta = 0$). Furthermore, finite element results presented by Ranby (1978) compare well with the solution.

5.4 Two Dimensional Stress and Strain Fields due to Tunnelling: Twice Normalized Ground Reaction Curves according to the Eisenstein-Negro Method

Estimation of stress and strain conditions developed because of tunnelling in the plane strain condition is presented in the form of a generalized solution based on a parametric analysis carried out using the finite element method. Figure 5.6 shows a flow chart of the Eisenstein-Negro method. The assumptions which were formulated in this method are cited below (Negro, 1988):

The constitutive model used in the analyses is the hyperbolic model (Duncan and Chang, 1970). The model is described in Figure 5.7. From the figure, the hyperbolic model is based on fitting a hyperbola to the relationship between the axial strain and the deviator stress obtained from the conventional triaxial test. The model is finally presented in form of a relationship between the tangential deformation modulus E_t and the deviator stress ($\sigma_1 - \sigma_3$). The stress-strain relationship includes the effect of shear strength

**Eisenstein- Negro's Method of
Design of Shallow Tunnels**

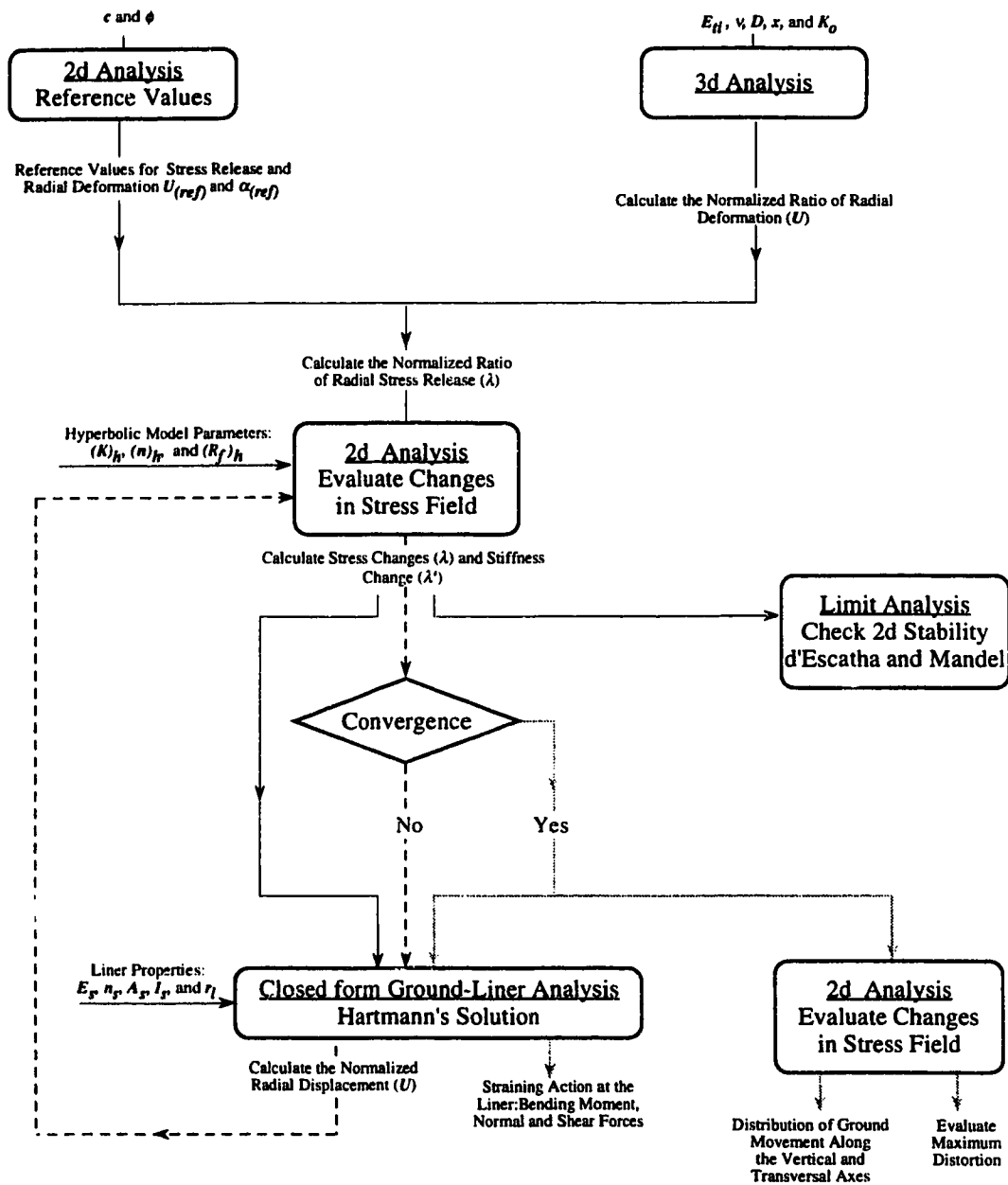
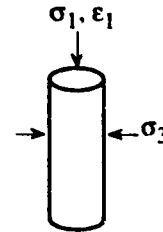
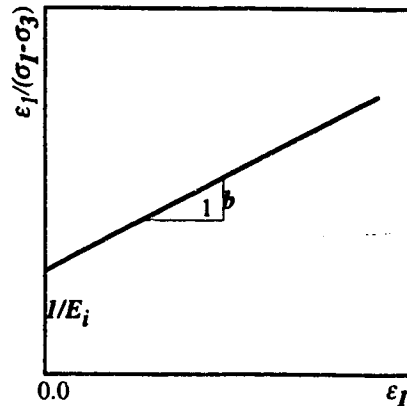
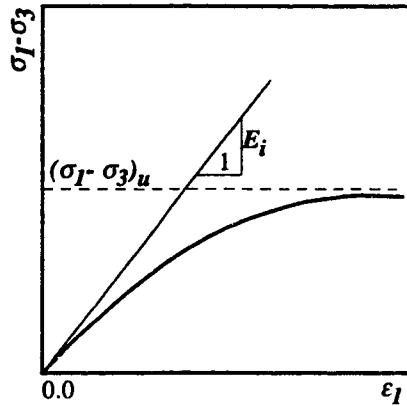


Figure 5.6: Flow Chart of Eisenstein- Negro's Method of Design of Shallow Tunnels

1. Stress Strain Relationship: Hyperbola:

$$\sigma_1 - \sigma_3 = \frac{E_i \varepsilon_1}{a + b \varepsilon_1}$$



$$b = (\sigma_1 - \sigma_3)_u$$

$$a = 1/E_i$$

E_i : initial tangential modulus

$(\sigma_1 - \sigma_3)_u$: ultimate (asymptotic) deviatoric stress

2. Effect of Shear Strength (stress ratio parameter R_f)

$$b = R_f / (\sigma_1 - \sigma_3)_f$$

$(\sigma_1 - \sigma_3)_f$: deviatoric stress at failure

3. Effect of Confining Pressure. Janbu's relationship (Janbu's constants K and n)

$$E_i = K P_a (\sigma_3 / P_a)^n$$

P_a : atmospheric pressure

4. Failure Criterion. Mohr - Coulomb Criterion in the triaxial test

$$(\sigma_1 - \sigma_3)_f = \frac{2c \cos \phi + 2\sigma_3 \sin \phi}{1 - \sin \phi}$$

5. Constitutive Relationship (E_t and ν)

$$E_t = K P_a (\sigma_3 / P_a)^2 \left(1 - R_f \frac{(1 - \sin \phi) (\sigma_1 - \sigma_3)^2}{2c \cos \phi + 2\sigma_3 \sin \phi} \right)^2$$

E_t : tangential modulus

ν : Poisson's ratio

Figure 5.7: the Hyperbolic Model

parameters (c and ϕ) and that of the confining pressure, σ_3 directly and through Janbu's parameters $(n)_h$ and $(K)_h$ and the stress ratio parameter $(R_f)_h^4$.

The method relies on the property of homothety related to the hyperbolic model. Similarities between the characteristics of a group of curves allow these curves to be normalized by constant reference values into a unique relationship representing the entire group. Negro (1988: Figures 6.1 and 6.2) proves that the effect of confining pressure in the hyperbolic model can be normalized for the cases where $(n)_h = c = 0$. Therefore, he proves using a finite element examples that tunnels with different diameters but with the same depth ratio exhibit a unique normalized response with respect to ground reaction curves, as well as, to the displacement field at the ground surface. The restrictive assumptions of $(n)_h = 0$ and of $c = 0$ are dealt with by conducting a sensitivity analysis that reveals that the effect of Janbu's modulus $(n)_h$ on the normalized ground reaction curves at the crown and at the floor can be minimized if the value of the deformation modulus is selected to be equal to the actual tangential deformation modulus at one tunnel radius above the crown and one radius below the floor, respectively. The effect of cohesion is introduced as an increase in the angle of internal friction. The following relationship (Negro (1988): Equation 6.10) is found to yield the closest results to the actual behaviour of the c - ϕ material with a conservative approximation:

$$\phi_a = \arcsin \left(\frac{1 + (\sigma_3/c) \tan \phi}{1 + (\sigma_3/c) \sec \phi} \right), \quad (5.7)$$

where:

ϕ_a is the approximated angle of internal friction to include the effect of cohesion.

For frictionless material ($\phi=0$ and $(n)_h = 0$) the homothety is evident as the tangent modulus is independent for σ_3 . Meanwhile, Janbu's modulus $(K)_h$, being directly related to the initial tangential modulus, E_{ti} , is included into the normalized expression of circumferential displacement U :

$$U = \frac{u_r E_{ti}}{D \sigma_{ro}}, \quad (5.8)$$

where:

⁴Subscript h is added to parameters in the hyperbolic model to avoid confusion with other symbols.

u_r is the radial displacement at the tunnel circumference and
 σ_{ro} is the initial radial pressure at the tunnel circumference.

The effect of Poisson's ratio on the normalized ground reaction curves, as well as, on the surface displacement distribution is shown by finite element analysis to be relatively small, and the displacement shows a general trend to increase as the value of Poisson's ratio increases. An intermediate value of Poisson's ratio is chosen ($\nu=0.4$). The performed finite element analyses investigate the effect of the depth ratio by covering a reasonably wide range of H/D values (between 1.5 and 6). It is shown that, as expected, the ground response becomes stiffer as the tunnel is deeper. Ground reaction curves for frictional material with different values of the angle of internal friction are found to exhibit a homothetic property similar to that of the stress-strain hyperbolic relationship with respect to the confining pressure, σ_3 . Therefore, the normalized ground reaction curve (NGRC), is normalized once more to include the effect of the angle of internal friction, ϕ , and a twice normalized ground reaction curve (NNGRC) is obtained. Figure 5.8 is a sketch of the different constructed ground reaction curves. The same process is found applicable in cases of frictionless material where double normalized ground reaction curves are constructed to produce unique curves independent of the cohesive resistance, c . Details of the statistical analyses involved in the normalization process are found in Negro (1988). As a result of the twice normalized ground reaction curve, the parameter λ is defined as follows:

$$\lambda = \frac{\Sigma - \Sigma_{ref}}{1 - \Sigma_{ref}} \quad , \quad (5.9)$$

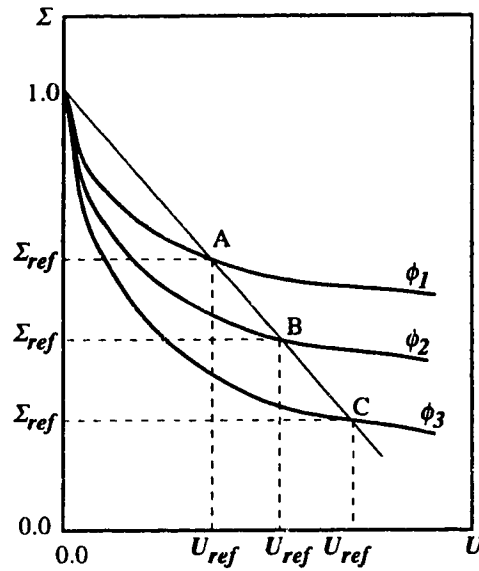
where Σ is the radial stress ratio⁵:

$$\Sigma = \frac{\sigma_r}{\sigma_{ro}} \quad , \quad (5.10)$$

and Σ_{ref} is the reference value of Σ related to the shear strength parameter.

At the end unique relationships are constructed between λ and U/U_{ref} that are independent of the shear strength parameters (c and ϕ), the tunnel size, Janbu's moduli ($(n)_h$ and $(K)_h$), and of the soil unit weight, γ . The formulated relationships are constructed for

⁵In Negro's thesis, the ratio Σ is named the stress ratio. It was decided to use different name for the radial stress ratio to differentiate between it and the stress ratio of the mean normal stress, $S.R.$.



1. Normalized Ground Reaction Curve NGRC

$$\Sigma = \sigma_r / \sigma_{r0}$$

$$U = \frac{u_r E}{\sigma_{r0} D}$$

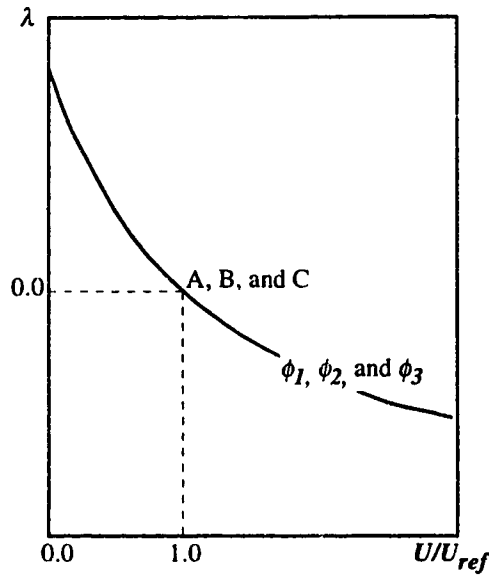
σ_r : radial stress at the liner

σ_{r0} : initial radial stress

u_r : radial deformation

E : tangential modulus

D : tunnel diameter



2. Twice Normalized Ground Reaction Curve NNGRC

$$\lambda = \frac{\Sigma - \Sigma_{ref}}{1 - \Sigma_{ref}}$$

Figure 5.8: Normalization of Shear Strength parameters of the Hyperbolic Model used in Eisenstein- Negro's Method. (Cohesionless Material)

various values of coefficients of lateral pressure at rest K_0 and the depth ratio H/D . The parameters λ and U/U_{ref} are expressions of the stress change and of the deformation at the tunnel circumference due to the process of stress release, respectively. The derivative λ' of λ with respect to U/U_{ref} is an expression of soil stiffness, thus the ratio:

$$\frac{\lambda'}{\lambda'_i} = \frac{E_t}{E_{ti}} \quad , \quad (5.11)$$

where:

$$\lambda' = \frac{\partial \lambda}{\partial (U/U_{ref})} \quad , \quad (5.12)$$

and

λ'_i is the initial value of λ' (at zero stress release).

5.5 Ground-Liner Interaction

From the above two sections, it is shown that the prevailing concept in tunnelling design in general and in the Eisenstein-Negro method in particular is that the ground and the liner are at best accurately simulated into two separate models. This is due to discrepancies in the geometry and in the stiffness between the two adopted structural models. It is, therefore, imperative to relate the two structural models in order to reach a realistic design method. Such a relationship would allow the nonlinearity of the stress-strain curve of the ground to interact with the liner simulated as a cylindrical shell. Thus the two most important features of the two models are accounted for: ground nonlinearity and accuracy in calculating the straining action of the liner. It is, therefore, required to find the proper way to transmit the calculated ground pressure after stress release to the lining system and to transmit the effect of lining deformation on the amount of ground-stress release. Obviously, an interactive process is required to ultimately achieve the required compatibility and equilibrium conditions between the liner and the ground.

Ground-liner interaction according to Eisenstein-Negro Method

The Eisenstein-Negro method uses numerical analyses based on finite element models to represent ground behaviour in the case of an unlined tunnel exposed to a certain amount of stress release. A sequence of normalization allows the generalization of the results such that for a certain radial circumferential displacement at the tunnel boundaries,

the ground surface displacement and the amount of stress release can be assessed. Correspondingly a reduced tangential modulus and a reduced unit weight is estimated for the region surrounding the tunnel. On the other hand, the liner structural model according to Hartmann's solution provides the straining actions (thrust, shear, and bending moment) and the radial deformation corresponding to the reduced modulus and unit weight. An iterative process is effected between the two systems until equal amount of stress release is calculated within an acceptable degree of tolerance.

The above process involves a certain number of assumptions. The surface between the liner and the ground is supposed to develop the required friction by the elastic model (no slip condition). The liner is elastic and its cross-sectional properties are uniform throughout its perimeter which implies that representative values of the actual lining system have to be suggested for the depth, the moment of inertia, and for the elastic parameters. These values must take into account, in the case of the segmented liner, the effect of joints and the shape of the segments. Muir Wood's expression (1975: 47) may be suggested when selecting a reduced value of the lining inertia. The compatibility of deformation is only satisfied at the three points: the crown, the spring line, and the floor. Finally, an engineering decision has to be taken whether to include the effect of tunnel heave into the final analysis. In conclusion, the undertaken assumptions are generally acceptable as they are comparable to those undertaken in other tunnelling design methods.

5.6 Design Method for Tunnels Constructed using Pressurized Shield Methods

A number of requirements have to be incorporated into a design method oriented specifically to tunnels constructed using pressurized shield methods:

- (1) the shield has to impose a certain action in the longitudinal direction in order to provide support at the face and to conduct the cutting operation. Such action is referred to as the three-dimensional effect of the tunnelling process;
- (2) the exposed ground surface behind the face and up to the point where the liner is in a state of stable equilibrium with the surrounding soil mass, is protected by a number of agents such as the rigidity of the shield, the bentonite pressure (if used), the grout pressure, and the rigid liner. Therefore, except for the cases where the tail seal fails, the tunnel circumference is protected in the transversal direction. It follows that there is a lack of failure mechanism in the transversal plane;
- (3) it is appropriate to represent the tunnel as a hollow structure in full interaction with the surrounding ground as the excavation boundaries are supported along the delay distance;

- (4) general requirements for shallow tunnel design methods are valid, such as the importance of the effect of the free boundary at the ground surface, the gravitational gradient, and that of the change of ground stiffness associated with the ground movement on the final stress field around the tunnel; and
- (5) special emphasis is made on the precast concrete segmented liner as it is in the supporting system that is most commonly used in conjunction with the pressurized shield methods. Special attention can be addressed at the same time to other supporting systems in use, such as, the extruded concrete lining system and the precast steel segmented liner.

5.6.1 The Three-dimensional Effects

As has been previously shown, the longitudinal liner pressure is responsible for the three-dimensional effect on the stress field. An attempt is made in Chapter 4 to evaluate, using a parametrical study of a number of finite element analyses, the influence of these two factors on site conditions with different geometrical configurations and different ground conditions. Emphasis is made to the resulting surface deformation and the changes in stress field around the excavation. Thus three normalized parameters are evaluated: the normalized surface displacement, \bar{w}_s , the stress ratio, **S.R.**, and the deviatoric stress ratio, **D.S.R.**. These parameters are defined in Equations 4.13, 4.14, and 4.21, respectively.

5.6.1.1 The Three-dimensional Effect on Stress Changes

It is demonstrated in Equation 4.20 that the changes in the average normal stress **S.R.** can be presented as a polynomial function of the first degree of the **G.R.**, **L.R.**, **K_o**, and **H_o/R_o**, and a polynomial function of the second degree of Poisson's ratio, ν . Meanwhile, the deviatoric stress ratio, **D.S.R.**, presented in Equation 4.22 is expressed as a polynomial function of the first degree of **K_o** and **H_o/R_o**, and a polynomial function of the second degree of Poisson's ratio ν and **G.R.**. The relationship between the various coefficients with the tunnel depth is investigated and it is further fitted to a polynomial function of the second degree. Figures 5.9 through 5.20 show the obtained relationships and the degree of accuracy. From the figures it can be concluded that a very good agreement is achieved between the fitted curves and the calculated coefficients. An exception to that is the case of the coefficients of the second degree polynomials ar_{n2} and ar_{n1} , and ad_{g2} and ad_{g1} . However, it can be believed that the discrepancies in curve fitting of each of the two coefficients of the same polynomial neutralize each other. The final values of **S.R.** and **D.S.R.** coefficients are presented in Tables 5.1 and 5.2, respectively.

$$S.R. = ar_g(G.R.) + ar_l(L.R.) + ar_{n2}(v^2) + ar_{n1}(v) + \frac{ar_k}{K_o} + \frac{ar_h}{(H_o/R_o)} + ar_o$$

where

$$ar_g = (ar_g)_2(H_o/R_o)^2 + (ar_g)_1(H_o/R_o) + (ar_g)_o$$

$$ar_l = (ar_l)_2(H_o/R_o)^2 + (ar_l)_1(H_o/R_o) + (ar_l)_o$$

$$ar_{n2} = (ar_{n2})_2(H_o/R_o)^2 + (ar_{n2})_1(H_o/R_o) + (ar_{n2})_o$$

$$ar_{n1} = (ar_{n1})_2(H_o/R_o)^2 + (ar_{n1})_1(H_o/R_o) + (ar_{n1})_o$$

$$ar_k = (ar_k)_2(H_o/R_o)^2 + (ar_k)_1(H_o/R_o) + (ar_k)_o$$

$$ar_o = (ar_o)_2(H_o/R_o)^2 + (ar_o)_1(H_o/R_o) + (ar_o)_o$$

		Crown	Spring Line	Floor
<i>arg</i>	(<i>arg</i>) ₂	0.00616	-0.00201	-0.00318
	(<i>arg</i>) ₁	-0.10359	0.02515	0.04770
	(<i>arg</i>) _o	0.95832	0.24377	0.11534
<i>arl</i>	(<i>arl</i>) ₂	-0.00181	0.00092	0.00067
	(<i>arl</i>) ₁	0.02320	-0.01076	-0.01162
	(<i>arl</i>) _o	-0.16238	-0.12438	-0.09141
<i>arn2</i>	(<i>arn2</i>) ₂	-2.28144	0.00799	0.42832
	(<i>arn2</i>) ₁	28.03099	-0.07240	-5.20009
	(<i>arn2</i>) _o	-17.00942	2.39077	9.74742
<i>arn1</i>	(<i>arn1</i>) ₂	1.12211	-0.00300	-0.20628
	(<i>arn1</i>) ₁	-13.79419	0.02428	2.50583
	(<i>arn1</i>) _o	6.61744	-1.24705	-5.15029
<i>ark</i>	(<i>ark</i>) ₂	-0.00212	0.00045	0.00137
	(<i>ark</i>) ₁	0.03186	-0.00777	-0.02357
	(<i>ark</i>) _o	-0.37099	0.25403	-0.28405
<i>aro</i>	(<i>aro</i>) ₂	-0.12194	0.03209	0.02422
	(<i>aro</i>) ₁	1.49905	-3.01449	-0.37037
	(<i>aro</i>) _o	0.81395	0.86308	1.82854
<i>arh</i>	(<i>arh</i>)	-0.09751	-0.05836	0.18202

Table 5.1: Curve Fitting Coefficients *ar* of the Stress Ratio, S.R.

$$D.S.R. = ad_{g2}(G.R.)^2 + ad_{g1}(G.R.) + ad_{n2}(v^2) + ad_{n1}(v) + \frac{ad_k}{K_o} + \frac{ad_h}{(H_o/R_o)} + ad_o$$

where

$$ad_{g2} = (ad_{g2})_2(H_o/R_o)^2 + (ad_{g2})_1(H_o/R_o) + (ad_{g2})_o$$

$$ad_{g1} = (ad_{g1})_2(H_o/R_o)^2 + (ad_{g1})_1(H_o/R_o) + (ad_{g1})_o$$

$$ad_{n2} = (ad_{n2})_2(H_o/R_o)^2 + (ad_{n2})_1(H_o/R_o) + (ad_{n2})_o$$

$$ad_{n1} = (ad_{n1})_2(H_o/R_o)^2 + (ad_{n1})_1(H_o/R_o) + (ad_{n1})_o$$

$$ad_k = (ad_k)_2(H_o/R_o)^2 + (ad_k)_1(H_o/R_o) + (ad_k)_o$$

$$ad_o = (ad_o)_2(H_o/R_o)^2 + (ad_o)_1(H_o/R_o) + (ad_o)_o$$

		Crown	Spring Line	Floor
<i>adg</i>	(<i>adg</i>) ₂	-0.01091	-0.01927	-0.02747
	(<i>adg</i>) ₁	0.12149	0.16655	0.29106
	(<i>adg</i>) _o	0.27407	-0.06886	-0.12815
<i>adl</i>	(<i>adl</i>) ₂	0.01772	0.03915	0.03307
	(<i>adl</i>) ₁	-0.20369	-0.37289	-0.33326
	(<i>adl</i>) _o	-0.15983	-0.05009	-0.17694
<i>adn2</i>	(<i>adn2</i>) ₂	-0.08418	0.00076	-0.00464
	(<i>adn2</i>) ₁	1.36650	-0.01565	0.07563
	(<i>adn2</i>) _o	4.31583	-2.02813	-2.79076
<i>adn1</i>	(<i>adn1</i>) ₂	0.04630	-0.00257	0.00520
	(<i>adn1</i>) ₁	-0.75088	0.04439	-0.08470
	(<i>adn1</i>) _o	-2.18276	0.61858	1.14892
<i>adk</i>	(<i>adk</i>) ₂	0.00356	-0.00016	-0.00151
	(<i>adk</i>) ₁	-0.05798	0.00207	0.02772
	(<i>adk</i>) _o	-0.10053	0.10331	-0.65811
<i>ado</i>	(<i>ado</i>) ₂	-0.01867	0.00010	-0.04069
	(<i>ado</i>) ₁	0.27039	-0.01117	0.54930
	(<i>ado</i>) _o	0.06359	-0.07736	-1.01871
<i>adh</i>	(<i>adh</i>)	0.37507	0.78064	0.56610

Table 5.2: Curve Fitting Coefficients *ad* of the Deviatoric Stress Ratio, D.S.R.

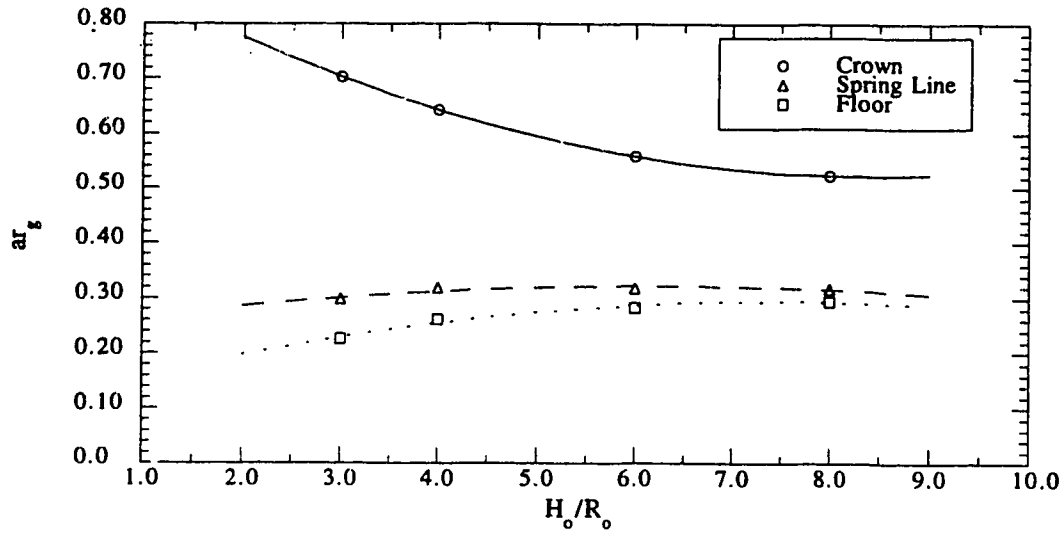


Figure 5.9: Calculated and Curve Fitted values of ar_g versus the Normalized Tunnel Depth

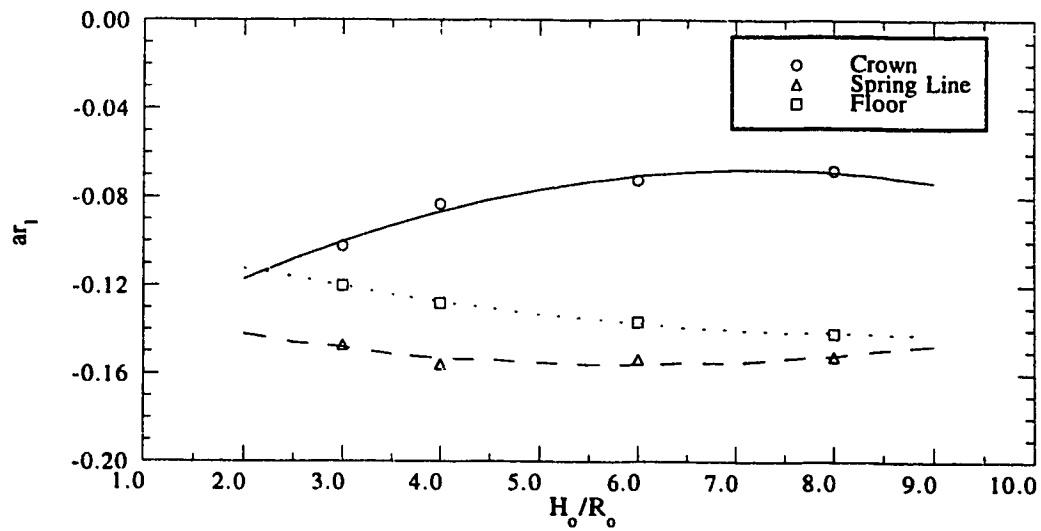


Figure 5.10: Calculated and Curve Fitted values of ar_l versus the Normalized Tunnel Depth

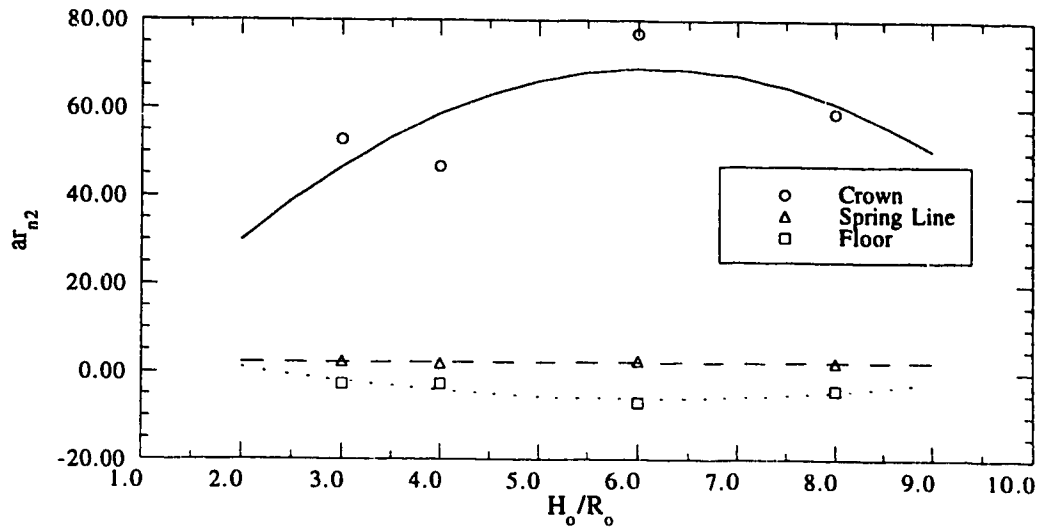


Figure 5.11: Calculated and Curve Fitted values of ar_{n2} versus the Normalized Tunnel Depth

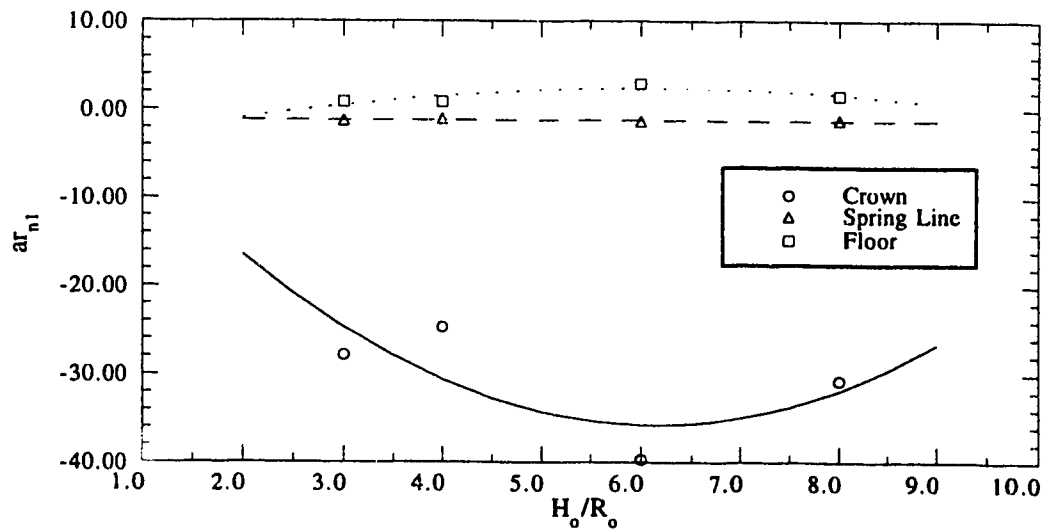


Figure 5.12: Calculated and Curve Fitted values of ar_{n1} versus the Normalized Tunnel Depth

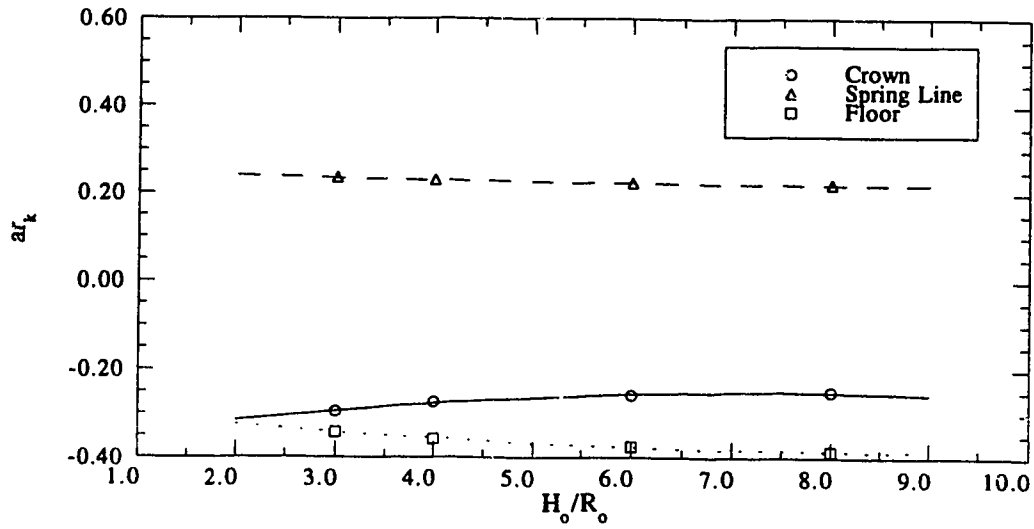


Figure 5.13: Calculated and Curve Fitted values of ar_k versus the Normalized Tunnel Depth

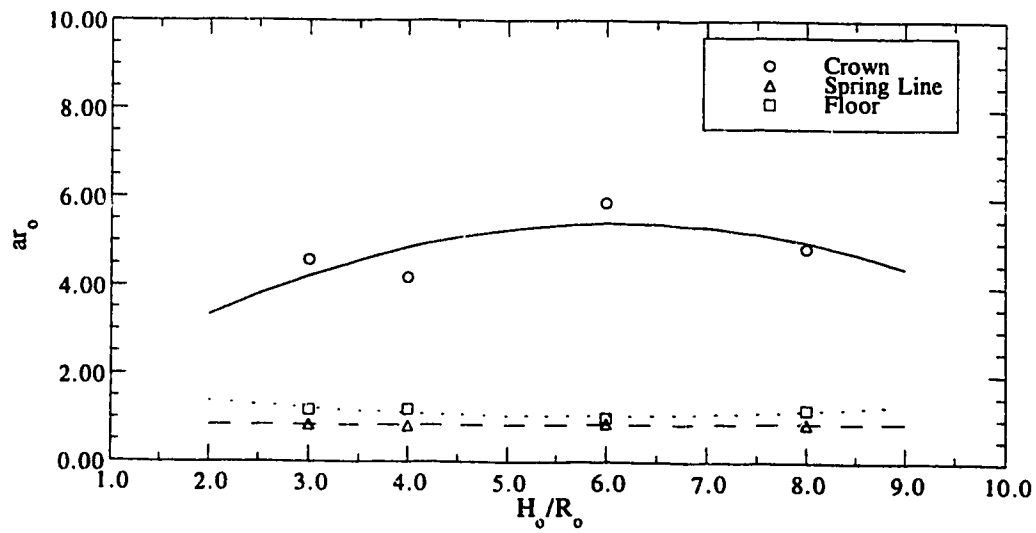


Figure 5.14: Calculated and Curve Fitted values of ar_0 versus the Normalized Tunnel Depth

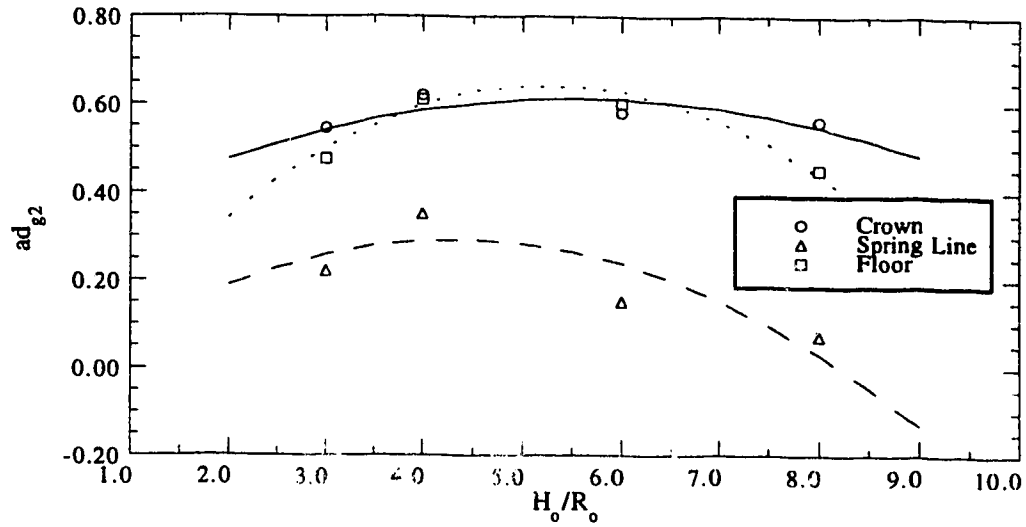


Figure 5.15: Calculated and Curve Fitted values of ad_{g2} versus the Normalized Tunnel Depth

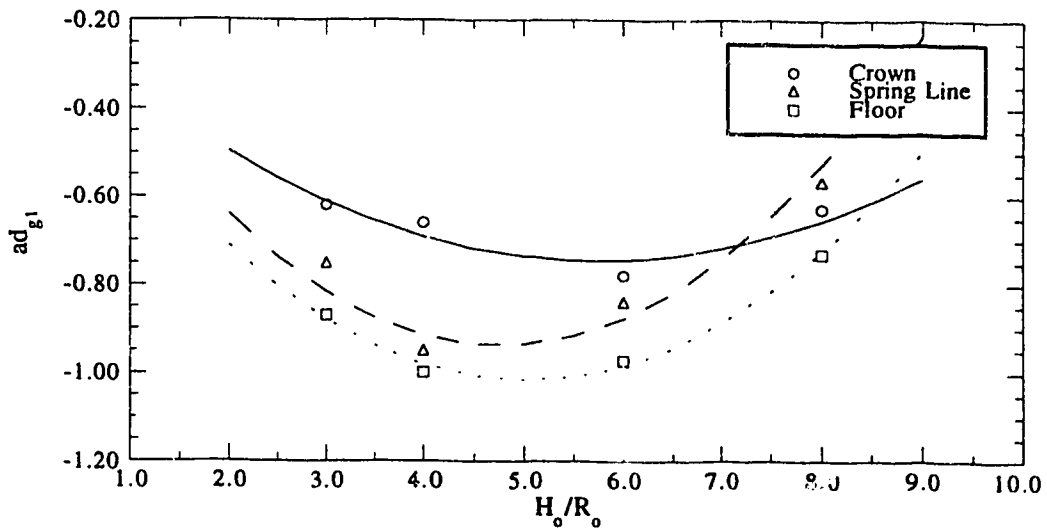


Figure 5.16: Calculated and Curve Fitted values of ad_{g1} versus the Normalized Tunnel Depth

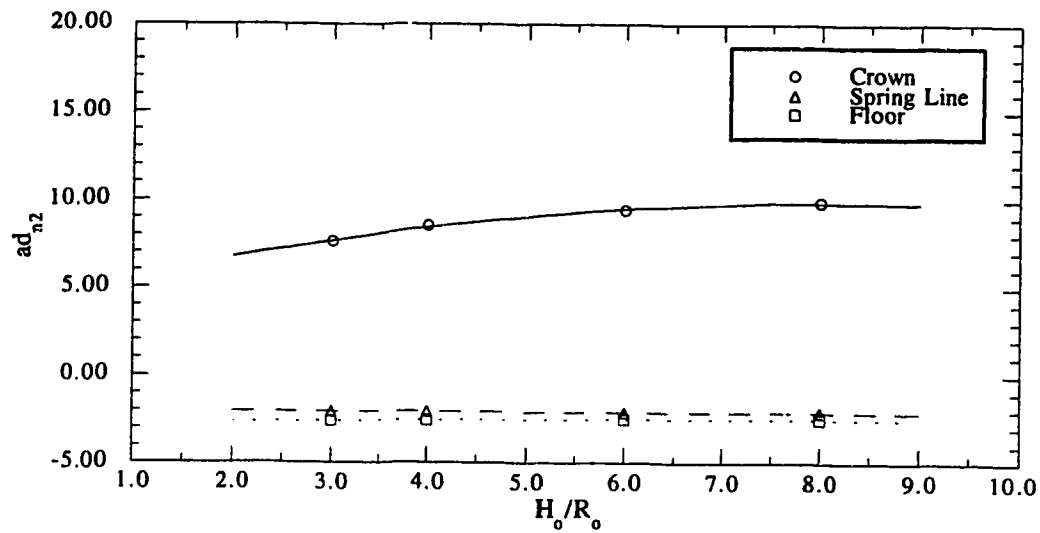


Figure 5.17: Calculated and Curve Fitted values of ad_{n2} versus the Normalized Tunnel Depth

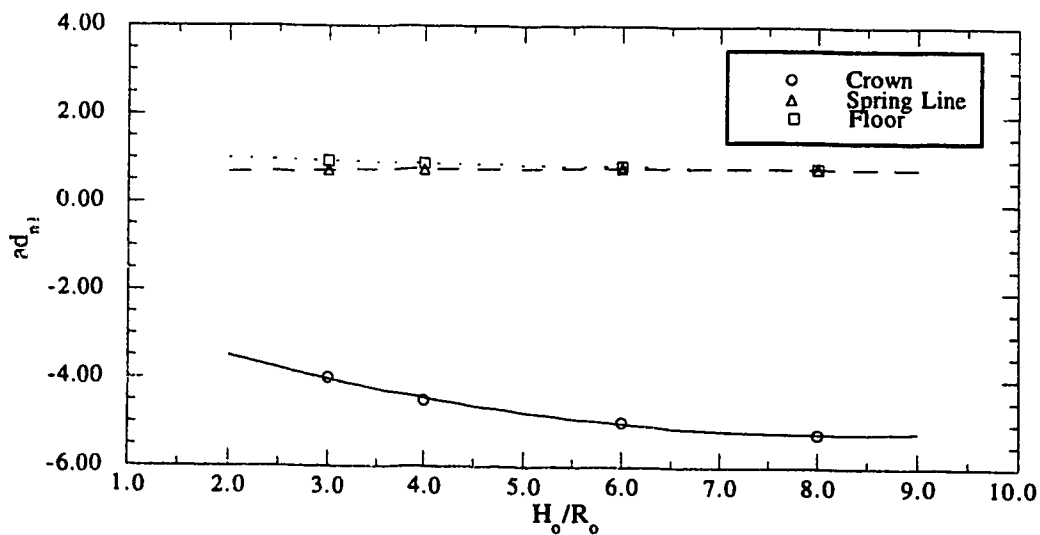


Figure 5.18: Calculated and Curve Fitted values of ad_{n1} versus the Normalized Tunnel Depth

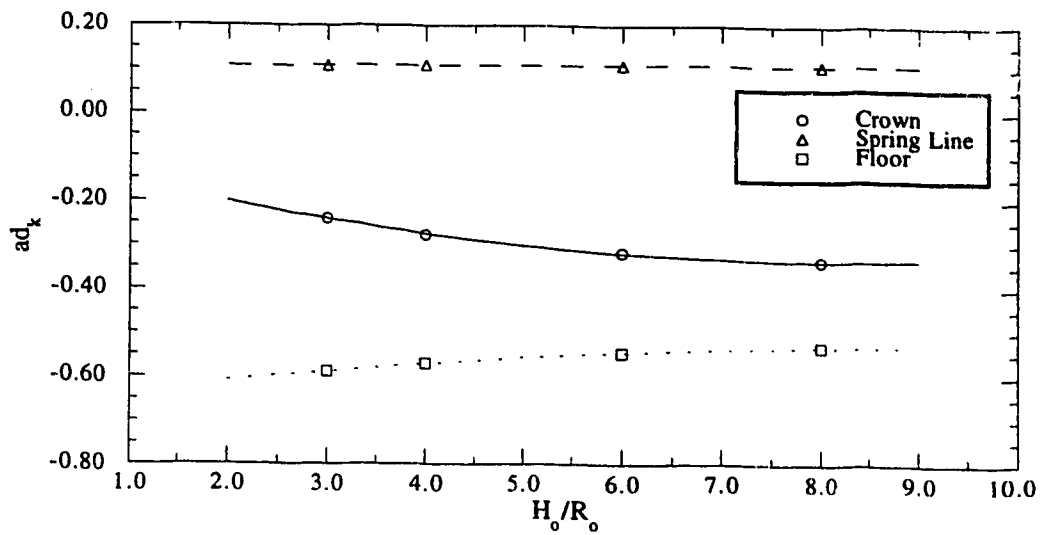


Figure 5.19: Calculated and Curve Fitted values of ad_k versus the Normalized Tunnel Depth

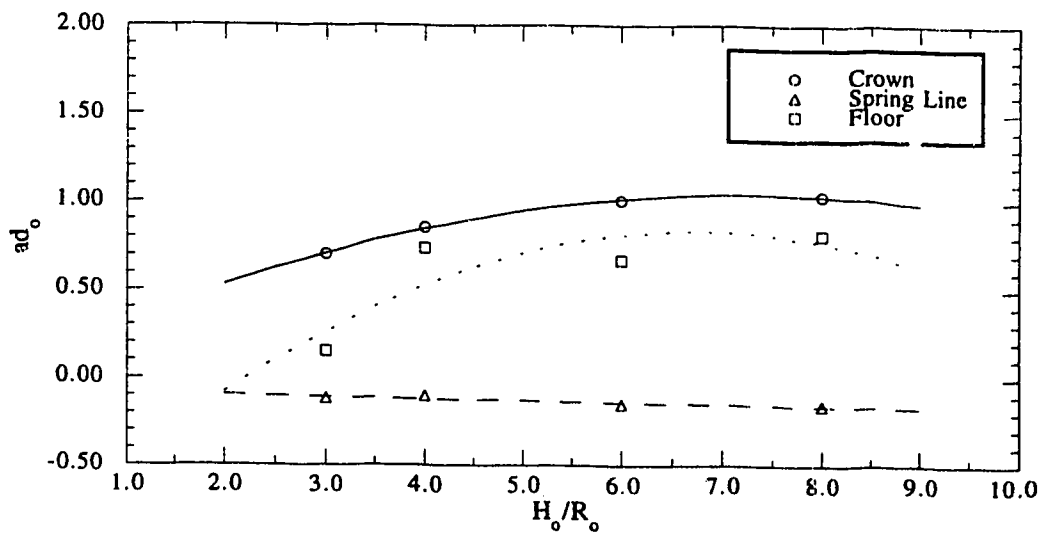


Figure 5.20: Calculated and Curve Fitted values of ad_o versus the Normalized Tunnel Depth

5.6.1.2 The Three-dimensional Effect on Surface Movements

Equation 4.13 shows the definition of the normalized surface movement, and Equation 4.17 shows calculated coefficients of first and second degree polynomials that describe the influence of $G.R.$, $L.R.$, K_o , H_o/R_o , and ν . Figure 5.21 shows a curve fitted polynomial of the second degree for the coefficients as_g , as_l , and as_c . From the figure good agreement is achieved in the three relationships. The final values of $\bar{\omega}_s$ coefficients are presented in Table 5.3.

5.6.1.3 Limitations of the Evaluations of the Three-dimensional Effects

It has to be noted that the evaluations of the three-dimensional effect on the changes in the stress field and on surface movements involves a number of approximations:

- (1) the accuracy of the parametric analysis, as suggested in Chapter 4, is affected by the computer system limitations, and it is not able to clearly identify a number of relationships, such as, the effect of $L.R.$ on the $D.S.R.$ and the effect of Poisson's ratio on the surface displacement. Further analyses may be required to investigate these details. Meanwhile, the size of the mesh and the accuracy of the simulating process are limited by the capacity of the computing system. It has to be noted in that regard that the calculations directed toward a parametric analysis required a substantial effort in storing and handling the output data. The improvement in the capacity and efficiency of the computing system, as well as, the improvement of data handling facilities will have an important effect on the improvement of the quality of the obtained results;
- (2) one important limitation is the degree of accuracy of stress computation at the point of lining activation. Although a high order of stress integration is used ($3 \times 3 \times 3$), the representation of the excavation step as a one element slice has an effect on reducing the accuracy of computations at that point. It should be noted also that at this specific point, especially in the case of high $L.R.$ and low $G.R.$, a condition of stress concentration is developed near the rigid liner which has an effect on the numerical accuracy of the results; and
- (3) it is difficult to pre-estimate the influence of the different parameters included in the analysis on each others because of the complexity of the problem and that of the excavation process. Therefore the assumption that each parameter is acting independently and affects the stress changes and the surface displacement in the form of a polynomial function of first or second order may be considered as a first approximation and is only justified by the obtained data output field.

$$\bar{\omega}_s = (as_g(G.R.) + as_l(L.R.) + as_o)(H_o/R_o)^{-1} + \left(as_n(v) + \frac{ask}{K_o} + ash \right) (H_o/R_o)^{-2}$$

where

$$as_g = (as_g)_2 (H_o/R_o)^2 + (as_g)_1 (H_o/R_o) + (as_g)_o$$

$$as_l = (as_l)_2 (H_o/R_o)^2 + (as_l)_1 (H_o/R_o) + (as_l)_o$$

$$as_o = (as_o)_2 (H_o/R_o)^2 + (as_o)_1 (H_o/R_o) + (as_o)_o$$

<i>asg</i>	(<i>asg</i>) ₂	-4.58077
	(<i>asg</i>) ₁	10.27782
	(<i>asg</i>) _o	303.22511
<i>asl</i>	(<i>asl</i>) ₂	2.80582
	(<i>asl</i>) ₁	-22.17239
	(<i>asl</i>) _o	-24.96859
<i>aso</i>	(<i>aso</i>) ₂	1.20644
	(<i>aso</i>) ₁	-9.91671
	(<i>aso</i>) _o	-75.47406
<i>asn</i>	(<i>ash</i>)	1356.01683
<i>ask</i>	(<i>ash</i>)	-306.45943
<i>ash</i>	(<i>ash</i>)	-607.02338

Table 5.3: Curve Fitting Coefficients $\bar{\omega}_s$ of Ground Surface Displacement

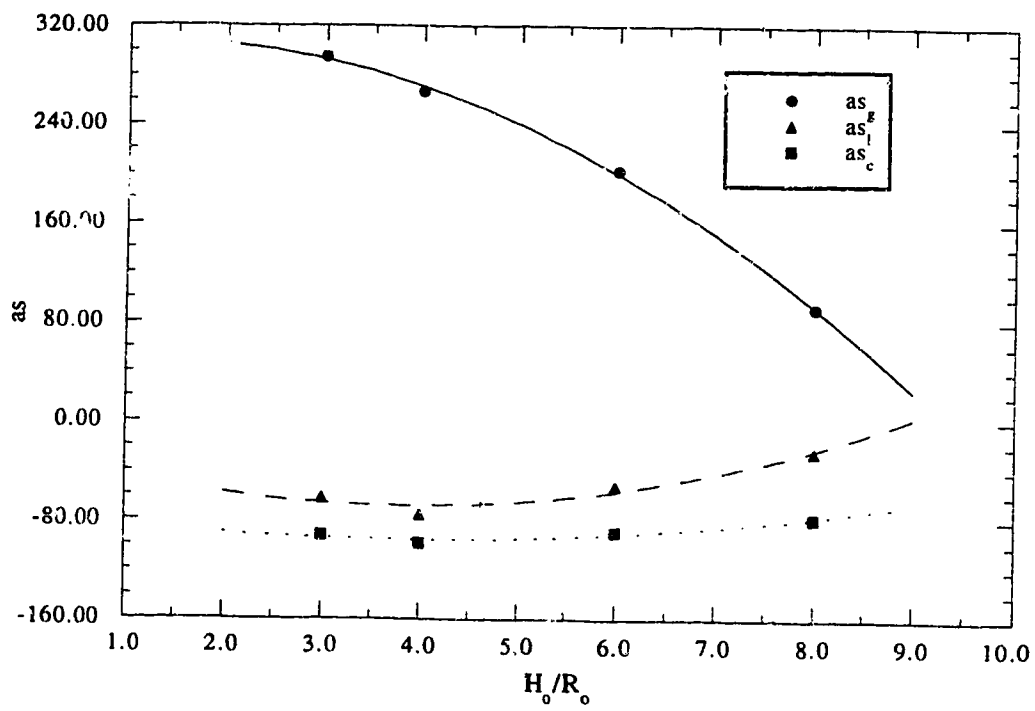


Figure 5.21: Calculated and Curve Fitted values of as versus the Normalized Tunnel Depth

5.6.2 Evaluation of Stress Changes and Surface Displacement at Plane Strain Condition

It is to be expected that the final stress field after the tunnel construction will follow the plane-strain condition. Therefore, the plane-strain condition prevails only at a certain distance behind the point of lining activation although the initial in situ condition is idealized as an other plane strain condition. Long term action resulting from tunnelling can be considered as an indication of the differences between the two stress fields: the near tunnel conditions and the initial site conditions that are still existing at the remote boundaries of the tunnel. Shield action in the longitudinal direction is expected to substantially influence the new plane strain conditions that will govern the final stress field.

Reviewing the limitations of the performed three-dimensional analysis, it is to be noted that the assessment of the final plane strain condition around a tunnel constructed with rigid liner is affected by a number of factors. In the numerical simulation the stress field at the far end of the liner represents a state of stress that does not include the construction process but is rather representative of the initial stress field in which the tunnel is excavated and supported instantaneously. Such a condition does not conform to the actual state of stress in the field where the new state of plane strain condition prevails. In addition, the degree of approximation involved in the simulation of the construction process contributes in increasing the unsteady pattern of stress values in the longitudinal direction at the proximity of the liner. A certain number of assumptions have to be taken in account in order to evaluate loading conditions on the liner:

- (1) the mean normal pressure at the final state of stress is equal to that at the point of lining activation. Referring to Figures 4.69 through 4.73 the *S.R.*, which is a normalized expression of the mean normal pressure, undergoes a substantial degree of variation behind the point of lining activation (*Point 4* in the Figures). The changes may be attributed to stress concentration that takes place near the liner corners. The stress concentration is expected to be exaggerated due to the adopted finite element mesh that is relatively coarse. It could be believed that in actual conditions, the existence of grout material with sufficient degree of fluidity and homogeneity is capable of reducing such effects;
- (2) the deviatoric pressure at the final state of stress is equal to that at the same point: the point of lining activation. As in the case of the mean normal pressure, the variation of the values of *D.S.R.*, which is a normalized expression of the deviatoric pressure behind the point of lining activation is attributed to stress concentration near the liner;
- (3) the directions of principal stresses are in the radial and tangential directions with

respect to the tunnel circumference. This is an inevitable approximation that has to be undertaken. This assumption could be justified as the presence of the grout material in a fluid state eliminates any friction between the ground and the liner before the stage of ground-liner interaction;

- (4) the longitudinal principal stress is equal to the minor principal stress. This assumption, results in a simplification of the calculations as a state of compressive triaxial stresses is considered around the liner. This assumption enables the hyperbolic model to be implemented into the calculations; and
- (5) the assumed deviatoric stress does not violate the failure criterion. Otherwise, for the predefined principal stresses, deviatoric stress is reassessed based on the shear strength parameters.

On the other hand the amount of displacement at the ground surface of the plane strain condition is calculated to be equal to the three-dimensional surface movement. This amount of displacement can be considered as the best estimation of the surface movement that can be obtained using three-dimensional finite element analysis.

5.6.3 The use of Eisenstein-Negro Method in the Design Method

In Sections 5.3 through 5.5 emphasis is made to the Eisenstein-Negro method as it has numerous advantages for tunnel design. The method is used and verified with success with a number of case histories (refer to Negro (1988): Chapter 7). The advantages of the method may be summarized as follows:

- (1) the ground surface nonlinearity is included as the hyperbolic model is adopted;
- (2) a rational method for evaluating the effect of delayed liner activation using three-dimensional finite element analyses is proposed;
- (3) the straining actions of the liner are calculated using the theory of cylindrical shell which provides a relatively higher accuracy over finite element methods where the aspect ratio of the elements affects the final results;
- (4) the gravitational stress field including the gravitational gradient is adequately considered which allows the method to be applied for the design of shallow tunnels;
- (5) the method is simple and practical and can be applied with minimum computational effort provided the proposed assumptions and restrictions are properly considered; and
- (6) the method is applicable for a large number of cases that render it useful for the use of tunnelling designers in urban areas.

The above advantages render the adoption of the method attractive for the design of shallow

tunnels constructed using pressurized shield methods. It is to be remembered that the use of the pressurized shield induces a stress field that departs from the conventional concept of volume loss (as shown in Chapter 4). However, as the stress disturbance in the longitudinal direction due to the excavation ceases at some distance behind the point of lining activation, the liner interacts with the ground following a rather plane strain condition and conventional design methods become fully applicable. The choice is therefore made to use the Eisenstein-Negro method for the proposed method of shallow tunnel design with a number of adaptations as will be shown in the following sections.

5.6.4 The Plane Strain Model

The plane strain condition at the end of tunnel construction is conceived to be a resultant of three processes: the three-dimensional effect, the ground-liner interaction and soil deformation above the tunnel due to the new conditions. Considering the assumptions formulated in Section 5.6.2 the mean and deviatoric stresses are evaluated around the liner. Thus, the principal stresses are calculated based on the identities:

$$\sigma_3 = p - \frac{\rho}{\sqrt{6}} \quad , \text{ and} \quad (5.13)$$

$$\sigma_1 = \sigma_3 + \sqrt{1.5}\rho \quad . \quad (5.14)$$

These stresses correspond to a certain continuum stress field condition. Using Hartmann's solution, the final stress field condition may be described in terms of the ground unit weight, γ , and the coefficient of lateral earth pressure at rest, K_0 . For certain values of ν , α , β , and R_0/H_0 , normal and tangential stresses around the liner are evaluated at the crown, the spring line, and at the floor as follows:

$$SUM = (A_1 + A_2 K_0) \gamma H_0 \quad , \quad (5.15)$$

and

$$DIF = (A_3 + A_4 K_0) \gamma H_0 \quad , \quad (5.16)$$

where:

$$SUM = \sigma_r + \sigma_\theta \quad , \quad (5.17)$$

and

$$DIF = \sigma_r - \sigma_\theta \quad . \quad (5.18)$$

The stresses σ_r and σ_θ are, respectively, the radial and tangential stresses at the liner, and A_1, A_2, A_3 , and A_4 are constants defined in Figure 5.22 based on Hartmann's solution. The assumption that the principal stresses are in the radial and tangential directions result in providing the values of *SUM* and *DIF* according to Equations 5.17 and 5.18 by substituting σ_r and σ_θ by σ_1 and σ_3 . Solving Equations 5.15 and 5.16 simultaneously gives the new γ and K_o related to the new stress field. An assumption has to be made in order to define the sign *DIF*. A number of preliminary calculations shows that acceptable results can be achieved if the sign of *DIF* is chosen such that the value of the calculated K_o is closer to the initial value of K_o . This choice is compatible with the conception that for the new normal and deviatoric stress conditions around the liner, the orientation of principal stresses is as much as possible closer to the initial state of stress that is believed to be still prevailing at the remote boundaries of the excavation.

For the new field conditions related to the construction process, ground-liner interaction is supposed to take place as described in the Eisenstein-Negro method. The twice normalized ground reaction curve along with the iterative process with Hartmann's solutions result in defining the final state of surface movement and the straining actions in the liner.

5.6.5 The Design Method

A flow chart of the design method is shown in Figure 5.23. Results of three-dimensional analyses is presented in normalized forms of movement, \bar{w}_s , at the ground surface and of the mean and deviatoric stresses *S.R.* and *D.S.R.* at three points of the tunnel circumference: the crown, the spring line and the floor. Mean normal stress and deviatoric stresses are, respectively, calculated through Equations 4.20 and 4.22 at the specified points. The triaxial principal stresses are calculated through Equations 5.13 and 5.14. Based on the values of the principal stresses, and on the proposed hyperbolic parameter, the modulus of deformation, E_{ti} , is calculated from Figure 5.6. The average deformation modulus of the four points of the tunnel circumference (the crown, two spring lines, and the floor) is considered to be representative of the stiffness condition around the excavation at the point of lining activation before the process of ground-liner interaction. The new calculated value is used in Equations 4.13 and 4.17 to calculate the deformation at

$$\begin{aligned} \text{SUM} &= A_1 + A_2 K_0 \\ \text{DIF} &= A_3 + A_4 K_0 \end{aligned}$$

At the crown:

$$\begin{aligned} (A_1)_c &= \left(\frac{-1+2v}{2-2v} + \frac{1+2\alpha+8\beta}{1+5\alpha+56\beta+216\alpha\beta-4\dot{\alpha}v-64\beta v-288\dot{\alpha}\beta v} \right) \left(\frac{R_0}{H_0} \right) + \frac{-1+12\beta+36\dot{\alpha}\beta-2\dot{\alpha}v-18\beta v-48\dot{\alpha}\beta v}{1+3\alpha+15\beta+36\dot{\alpha}\beta-2\dot{\alpha}v-18\beta v-48\dot{\alpha}\beta v} \\ (A_2)_c &= \left(\frac{-2-7\dot{\alpha}-64\beta-216\alpha\beta+4\dot{\alpha}v+64\beta v+288\dot{\alpha}\beta v}{1+5\alpha+56\beta+216\alpha\beta-4\dot{\alpha}v-64\beta v-288\dot{\alpha}\beta v} \right) \left(\frac{R_0}{H_0} \right) + \frac{3+6\dot{\alpha}+18\beta+36\dot{\alpha}\beta-2\dot{\alpha}v-18\beta v-48\dot{\alpha}\beta v}{1+3\alpha+15\beta+36\dot{\alpha}\beta-2\dot{\alpha}v-18\beta v-48\dot{\alpha}\beta v} \\ (A_3)_c &= \left(\frac{1-2v-\dot{\alpha}v}{2+2\dot{\alpha}-2v-2\dot{\alpha}v} + \frac{-2-\dot{\alpha}-112\beta-216\alpha\beta-4\dot{\alpha}v+128\beta v+288\dot{\alpha}\beta v}{2(1+5\alpha+56\beta+216\alpha\beta-4\dot{\alpha}v-64\beta v-288\dot{\alpha}\beta v)} \right) \left(\frac{R_0}{H_0} \right) + \frac{-1}{1+\alpha+\beta} + \frac{2+30\beta+36\dot{\alpha}\beta+4\dot{\alpha}v-36\beta v-48\dot{\alpha}\beta v}{1+3\alpha+15\beta+36\dot{\alpha}\beta-2\dot{\alpha}v-18\beta v-48\dot{\alpha}\beta v} \\ (A_4)_c &= \left(\frac{2+\dot{\alpha}}{2+2\dot{\alpha}} + \frac{2+\dot{\alpha}+112\beta+216\alpha\beta+4\dot{\alpha}v-128\beta v-288\dot{\alpha}\beta v}{2(1+5\alpha+56\beta+216\alpha\beta-4\dot{\alpha}v-64\beta v-288\dot{\alpha}\beta v)} \right) \left(\frac{R_0}{H_0} \right) + \frac{-1}{1+\alpha+\beta} + \frac{-2-30\beta-36\dot{\alpha}\beta-4\dot{\alpha}v+36\beta v+48\dot{\alpha}\beta v}{1+3\alpha+15\beta+36\dot{\alpha}\beta-2\dot{\alpha}v-18\beta v-48\dot{\alpha}\beta v} \end{aligned}$$

At the spring line:

$$\begin{aligned} (A_1)_s &= \frac{3+3\dot{\alpha}+45\beta+72\dot{\alpha}\beta+2\dot{\alpha}v-54\beta v-96\dot{\alpha}\beta v}{1+3\alpha+15\beta+36\dot{\alpha}\beta-2\dot{\alpha}v-18\beta v-48\dot{\alpha}\beta v} \\ (A_2)_s &= \frac{-1+3\dot{\alpha}-15\beta-6\dot{\alpha}v+18\beta v}{1+3\alpha+15\beta+36\dot{\alpha}\beta-2\dot{\alpha}v-18\beta v-48\dot{\alpha}\beta v} \\ (A_3)_s &= \frac{-1}{1+\alpha+\beta} + \frac{-2-30\beta-36\dot{\alpha}\beta-4\dot{\alpha}v+36\beta v+48\dot{\alpha}\beta v}{1+3\alpha+15\beta+36\dot{\alpha}\beta-2\dot{\alpha}v-18\beta v-48\dot{\alpha}\beta v} \\ (A_4)_s &= \frac{-1}{1+\alpha+\beta} + \frac{2+30\beta+36\dot{\alpha}\beta+4\dot{\alpha}v-36\beta v-48\dot{\alpha}\beta v}{1+3\alpha+15\beta+36\dot{\alpha}\beta-2\dot{\alpha}v-18\beta v-48\dot{\alpha}\beta v} \end{aligned}$$

At the floor:

$$\begin{aligned} (A_1)_f &= \left(\frac{1-2v}{2-2v} + \frac{-1-2\dot{\alpha}-8\beta}{1+5\alpha+56\beta+216\alpha\beta-4\dot{\alpha}v-64\beta v-288\dot{\alpha}\beta v} \right) \left(\frac{R_0}{H_0} \right) + \frac{-1+12\beta+36\dot{\alpha}\beta-2\dot{\alpha}v-18\beta v-48\dot{\alpha}\beta v}{1+3\alpha+15\beta+36\dot{\alpha}\beta-2\dot{\alpha}v-18\beta v-48\dot{\alpha}\beta v} \\ (A_2)_f &= \left(\frac{2+7\dot{\alpha}+64\beta+216\alpha\beta-4\dot{\alpha}v-64\beta v-288\dot{\alpha}\beta v}{1+5\alpha+56\beta+216\alpha\beta-4\dot{\alpha}v-64\beta v-288\dot{\alpha}\beta v} \right) \left(\frac{R_0}{H_0} \right) + \frac{3+6\dot{\alpha}+18\beta+36\dot{\alpha}\beta-2\dot{\alpha}v-18\beta v-48\dot{\alpha}\beta v}{1+3\alpha+15\beta+36\dot{\alpha}\beta-2\dot{\alpha}v-18\beta v-48\dot{\alpha}\beta v} \\ (A_3)_f &= \left(\frac{-1+2v+\dot{\alpha}v}{2+2\dot{\alpha}-2v-2\dot{\alpha}v} + \frac{2+\dot{\alpha}+112\beta+216\alpha\beta+4\dot{\alpha}v-128\beta v+288\dot{\alpha}\beta v}{2(1+5\alpha+56\beta+216\alpha\beta-4\dot{\alpha}v-64\beta v-288\dot{\alpha}\beta v)} \right) \left(\frac{R_0}{H_0} \right) + \frac{-1}{1+\alpha+\beta} + \frac{2+30\beta+36\dot{\alpha}\beta+4\dot{\alpha}v-36\beta v-48\dot{\alpha}\beta v}{1+3\alpha+15\beta+36\dot{\alpha}\beta-2\dot{\alpha}v-18\beta v-48\dot{\alpha}\beta v} \\ (A_4)_f &= \left(\frac{-2-\dot{\alpha}}{2+2\dot{\alpha}} + \frac{-2-\dot{\alpha}-112\beta-216\alpha\beta-4\dot{\alpha}v+128\beta v+288\dot{\alpha}\beta v}{2(1+5\alpha+56\beta+216\alpha\beta-4\dot{\alpha}v-64\beta v-288\dot{\alpha}\beta v)} \right) \left(\frac{R_0}{H_0} \right) + \frac{-1}{1+\alpha+\beta} + \frac{-2-30\beta-36\dot{\alpha}\beta-4\dot{\alpha}v+36\beta v+48\dot{\alpha}\beta v}{1+3\alpha+15\beta+36\dot{\alpha}\beta-2\dot{\alpha}v-18\beta v-48\dot{\alpha}\beta v} \end{aligned}$$

Figure 5.22: Coefficients A1, A2, A3, and A4 Calculated Based on Hartmann's Solution

Design Method for Shallow Tunnels
Constructed using Pressurized
Shield Methods

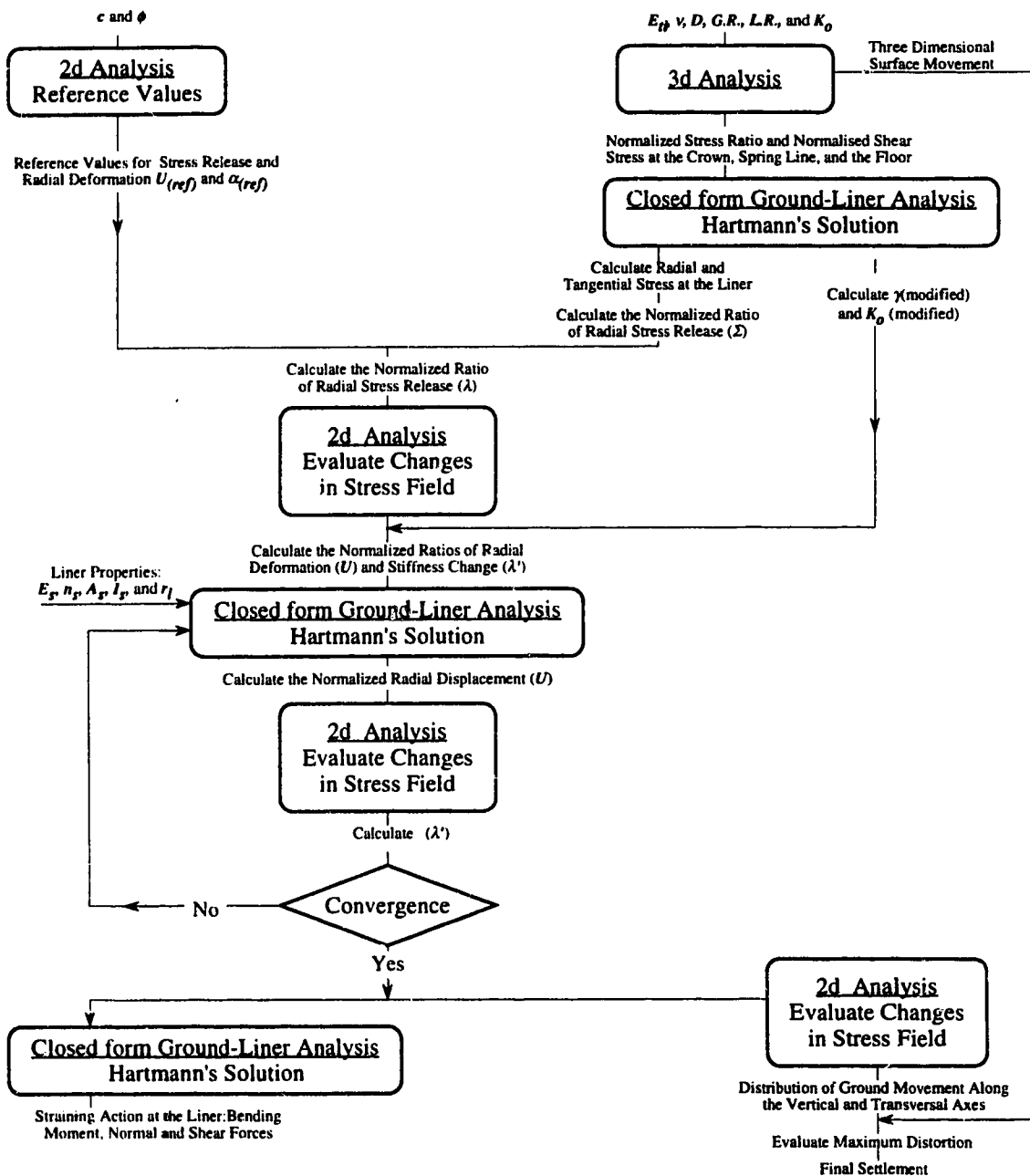


Figure 5.23: Flow Chart of a Design Method of Tunnels constructed using Pressurized Shield Methods

the ground surface. Charts in Appendix B are used to determine the transversal profile of the surface deformation due to three-dimensional effect. As mentioned in the preceding section, an assumption is made by considering the sum and the difference of the principal stresses as the sum and the difference of the radial and tangential stresses at the three points on the tunnel circumference. Equations 5.15 and 5.16 are solved for the given values of SUM and $\pm DIF$ and A_1, A_2, A_3 , and A_4 to get the modified values of γ and K_o for two signs of DIF . The chosen sign of DIF is selected such that at each point the calculated values of γ and K_o are closer to their values at the initial condition. Representative values of the new stress field are calculated as the average values of γ and K_o at the four points of the tunnel circumference. Meanwhile reference values of stress and deformation α_{ref} (or Σ_{ref}) and U_{ref} related to shear strength parameters c and ϕ are calculated from (Negro 1988: Figures 6.92, 6.93, 6.100, 6.101, 6.109, and 6.108).

The ground-liner interaction process starts at the liner. Using Hartmann's solution (Figure 5.5) and the modified ground condition parameters, radial and tangential stresses at the tunnel circumference are calculated. The twice normalized parameter of stress release λ is, therefore, calculated through Equation 5.9. Back substitution into the twice normalized ground reaction curve (Negro 1988: Figures 6.94, 6.95, 6.96, 6.102, 6.103, 6.104, 6.110, 6.111, and 6.112) produces the corresponding twice normalized radial deformation at the three points of the lining circumference U/U_{ref} . The obtained radial displacement u_{ro} through Equation 5.8 is related to the radial deformation that would have taken place if the new stress field were developed in plane strain conditions and should be, therefore, subtracted from the final results. Using U/U_{ref} , the normalized parameter of stiffness, λ , is obtained at the three points of the tunnel circumference (Negro 1988: Figures 6.97, 6.98, 6.99, 6.105, 6.106, 6.113, 6.114, and 6.115). Based on Equation 5.11 new values of the deformation modulus, E_{ii} , are calculated and an average value is calculated. If the value of the new modulus is close, within acceptable tolerance, to the preceding value the solution is considered to be convergent. Otherwise, the new value of E_{ii} is introduced into Hartmann's solution for a new round of iteration. General application of the method shows that a number of iterations, around three or four, is enough to reach acceptable convergence.

As convergence is achieved, final results can be calculated. For the new stress field, straining actions inside the liner are assessed using Hartmann's solution (Figure 5.5). Radial deformation is assessed by subtracting u_{ro} from the final value of radial displacement. For the calculated radial stress release, Σ , the relation between the crown and the ground surface displacement are determined through a number of charts (Negro 1988: Appendix C). These charts provide the deformation profiles at the ground surface

and at the vertical axis of the tunnel because of ground-liner interaction. Final ground deformation is determined by adding the three-dimensional deformation previously obtained to the ground lining deformation.

5.7 Application: Edmonton LRT Tunnel

The expansion of the LRT system in the city of Edmonton requires the construction of a twin tunnel of about 6 m diameter through a complicated geological profile. Figures 5.24 and 5.25 show a general alignment and a simplified ground section. The main difficulty encountered was during the construction of the southbound tunnel from Grandin Station to the North Portal on the Saskatchewan River because the excavation had to go through a layer of post-glacial deposits consisting mainly of medium dense sand with a low amount of cementation. Here a conventional shield without a face support was chosen as the method of excavation in conjunction with jet grouting around the cross section in order to improve the ground properties. Excessive settlement took place. The nature of the ground movement was characterized as being local and funnel shaped starting at the tunnel crown and extending upward to the ground surface. Therefore, during the construction of the northbound tunnel, using the pressurized shield method, the Hydroshield, was selected to accommodate the difficult ground conditions. As described by Eisenstein and Ezzeldine (1992:a), the total length of the project is about 305 m and the tunnel's crown is about 13 m deep. The most critical part of the project is between 100.0 to 260.0 m from the river bank portal.

5.7.1 Ground Conditions

A simplified profile of ground conditions at the project is shown Figure 4.12. Four main geological patterns are distinguished: glacial till, post-glacial deposits consisting of sand and gravel, basal sand, and bedrock. The geology of the area is investigated and presented by Thomson and Townsend (1979) and the engineering properties of the site were carried out and presented by Hardy BBT Ltd. (1988). Preglacial channels are formed due to a subaerial erosion with its thawleg running close to the existing North Saskatchewan River. A number of factors such as erosion and valley rebound after the glacial ice retreat are responsible for the irregular surface of the bedrock at the project site. The material is described as an Upper Cretaceous sedimentary sequence of poorly indurated clay shales, coal, and siltstone with bentonite as an admixture between the seams. The till layer is encountered at the first part of the project usually as part of a mixed face condition with the bedrock. Since both materials are highly competent, construction conditions are easier than at the following parts of the project. The till is a medium plastic clay soil in a

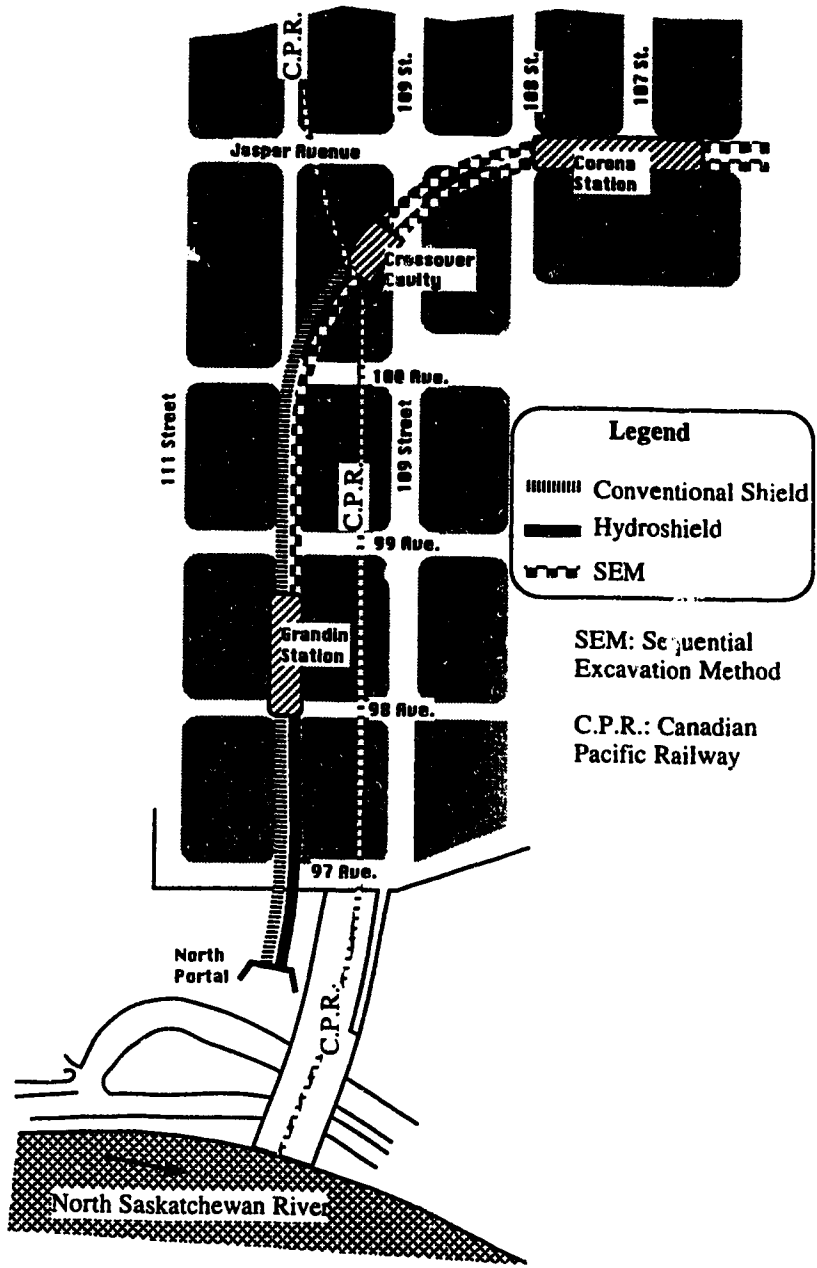


Figure 5.2 : Site Plan of the Edmonton LRT Project

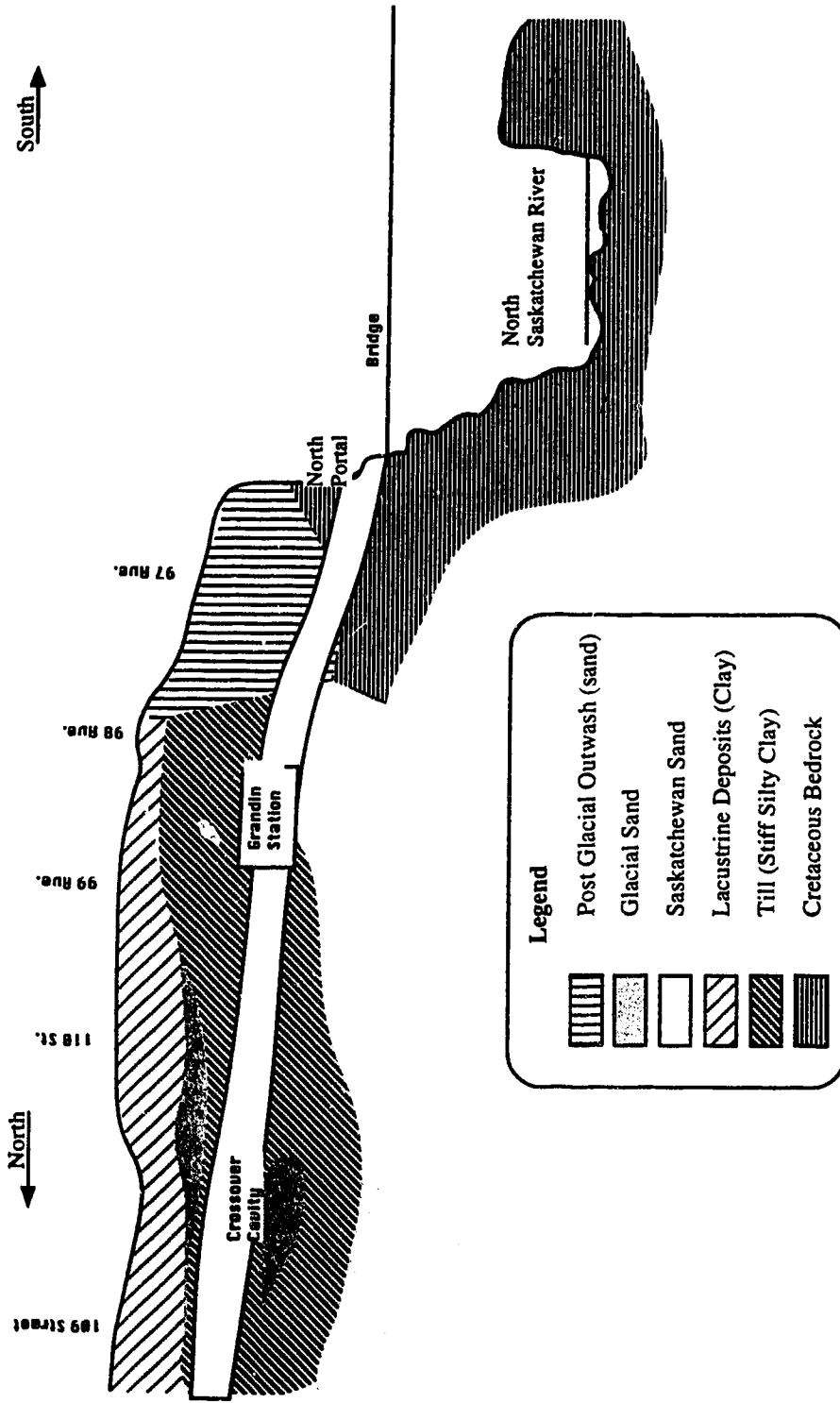


Figure 5.25: Simplified Geological Profile for the Edmonton LRT Project

hard state of consistency, and it is interspersed with numerous sand lenses and partings, small pebbles, bedrock fragments and occasional cobbles. The till along the project has been heavily overconsolidated and, as a result, it is cracked and fissured. Results from this investigation show the Standard Penetration Test (SPT) number ranging from 33 to 100. Post-glacial deposits are mainly sand and gravel at the tunnel section. Alluvial debris sediments are found in the form of isolated layers of silt. Clay layers with sand and silt predominate at the upper 5 to 10 m. Investigation of the sand and gravel layers has given SPT numbers ranging between 12 and 86 blows indicating a variation of density between medium and very dense deposits. Triaxial tests on Shelby tube samples of sand shows an effective friction angle, ϕ , of about 33.5° . The presence of silt results in a higher value of ϕ . Pressuremeter tests were conducted in the sand deposits and yielded unrealistically high values of E (around 400 MPa) and of K_o (from 1.1 to 1.8). Basal sand is known locally as Saskatchewan sand and gravel and it was deposited by preglacial streams and rivers. Sand particles are comprised of a closely even mixture of quartz, chert, and metamorphic and volcanic fragments. Performed Standard Penetration tests have shown that the formation is in a very dense state as the SPT number ranges between 117 and 200. Triaxial tests performed on remoulded and "undisturbed" block samples show that the angle of internal friction, ϕ , is about 37.5° . The planned alignment of the tunnel trajectory was selected to avoid the basal sand as much as possible because of its lack of cohesion. The water table is mainly below the tunnel invert and occasional water seepage is encountered because of an existing abandoned sewage line, and because of surface water flow.

The preliminary settlement analysis was carried out by W. Wittke (PCL-Hochtief, 1988:b). Calculations were carried out on the basis of the geotechnical parameters provided by the City of Edmonton (UMA, 1988). These parameters are derived from back analyses of data from projects constructed in the area. Typical values of the proposed parameters for the four formations in the project are presented in Table 5.4 .

5.7.2 Construction Details

As demonstrated in Chapter 2, the Hydroschild method exerts on the face using the bentonite slurry regulated by an air cushion. As excavation proceeds, the shield is pushed forward against the erected liner using hydraulic jacks (fourteen main jacks) at the same time, the newly exposed lining ring is grouted. Then, a new ring of segmented lining is assembled inside the shield. The lining system (refer to Figure 2.3) consists of seven segments and a key. In order to maintain the face stability during the lining assembly, the shield is pushed against only six segments using twelve main jacks until the entire ring is completed and the shield becomes ready for a new drive using the full jacking forces.

Type of Soil	Unit Weight kN/m ³	Shear Strength		Elastic Modulus E MPa	Earth Pressure Coefficient Ko
		ϕ (°)	c kPa		
Till	20.0	35	25.0	25.0	0.7-1.0
Basal Sand	20.0	35	0.0	50.0	0.7-1.0
Post Glacial Channel Deposits	19.0	30	0.0	10.0	0.7-1.0
Bedrock	23.0	40	50.0	50.0	0.7-1.0

Figure 5.4: Soil Properties at Edmonton LRT Site (after PCL- Hochtief 1988)

Applied grout pressure along the tunnel trajectory is presented in Figures 5.26 based on installation records (PCL-Hochtief, 1990). From the figure it is noticed that a grout ratio **G.R.** is selected for the entire project to be around 150% . At the first stage of the project where the tunnel cross section is excavated completely in relatively competent bedrock, the grout pressure can be easily regulated. In the mixed face zone (bedrock-sand and gravel) the grout pressure was frequently reduced to about 75% in order to avoid excessive losses of grout material. In the post-glacial sand and gravel zone, better control of grout losses allowed the increase of grout pressure from the average value. In the final stage of the tunnel governed by basal sand deposits grout pressure reduction has found to be reduced again to about 75% . Grout volume losses are demonstrated in Figure 5.27. According to the shield machine specifications PCL-Hochtief (1988:a) the distance between the extrados of the shield and that of the liner, which is called the physical gap, is 89.5 mm around the circumference which results in a gap volume of 1.82 m³ per metre length. Excess grout volume is calculated as:

$$\text{Excess Grout Volume} = \frac{\text{Grout Volume} - \text{Gap Volume}}{\text{Gap Volume}} \times 100 \quad (5.19)$$

From the figure, it can be shown that the loss of grout material has been totally avoided in many occasions in the bedrock zone. In the mixed face and in the post-glacial deposit zones substantial loss of grout material took place. This may be attributed to a number of factors such as the high permeability of the sand material, the non-homogeneity of the surrounding ground, and to the high grout pressure applied. The final zone of basal sand exhibits relatively more restrained grout losses mostly due to grout pressure reduction and to the relatively more homogeneous ground profile. It is to be noted that on a number of occasions, failure of the tail seal has occurred. This is characterized by a sharp and sudden drop in grout pressure and a sudden increase in excess grout volume. From the figures infiltration of grout material into the surrounding ground takes place and results in loss of grout material and loss of effectiveness in the application of grout pressure. Back analysis of the case history requires, therefore, a certain assumption regarding the amount of reduction of grout pressure. Liner pressure ratio, **L.R.**, is presented in Figure 5.28 based on installation records (PCL-Hochtief, 1990) and on the assumption of an average K_c of 0.8 for the whole project. From the figure, a certain amount of discrepancy is noticed between the push pressure (during ring assembly) and the drive pressure (during excavation). Nevertheless, the general pattern is that **L.R.** is related to the ground stiffness. Therefore, the least liner pressure is recorded at the zone of post-glacial deposits

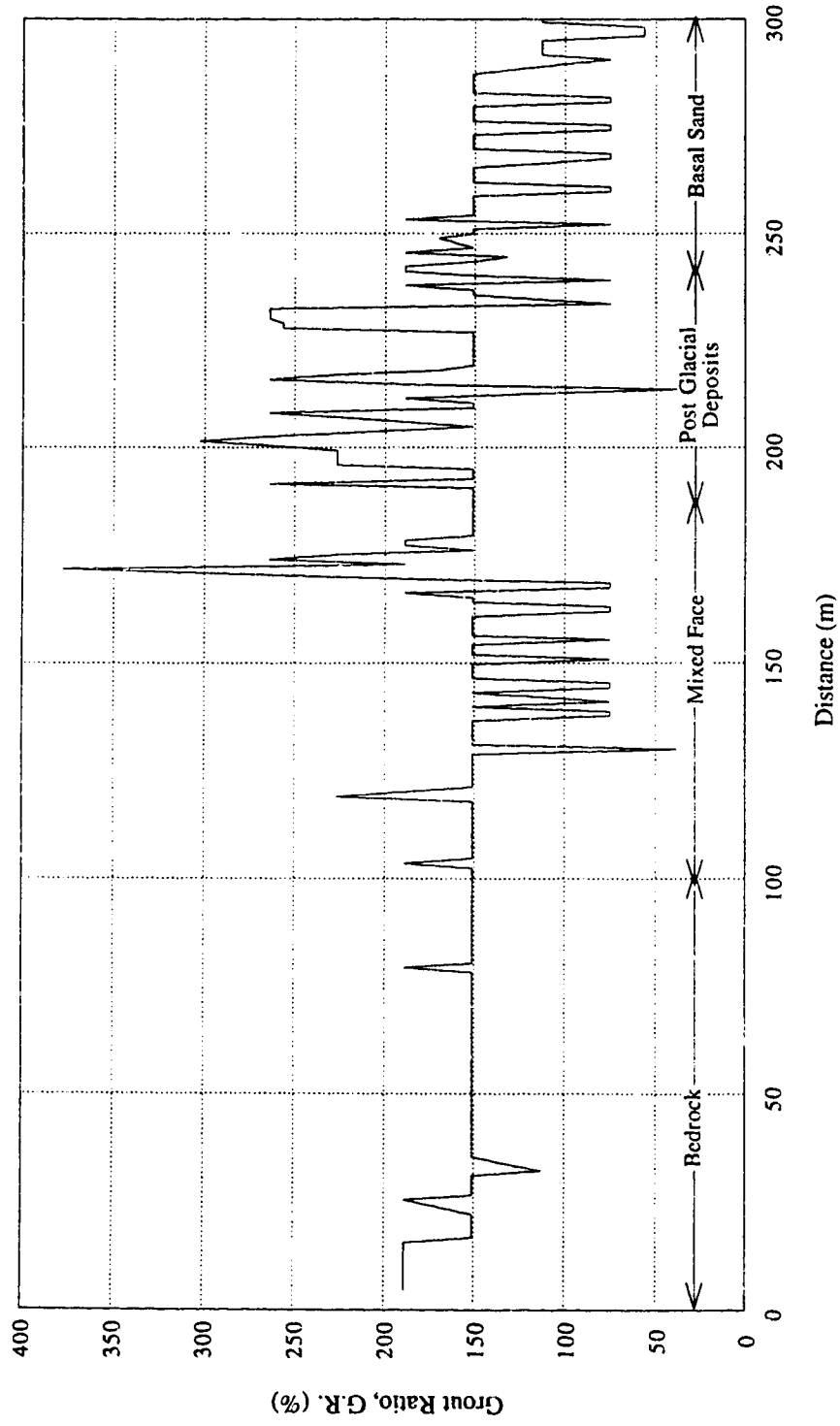


Figure 5.26: Grout Pressure Ratio used at the Edmonton LRT Project

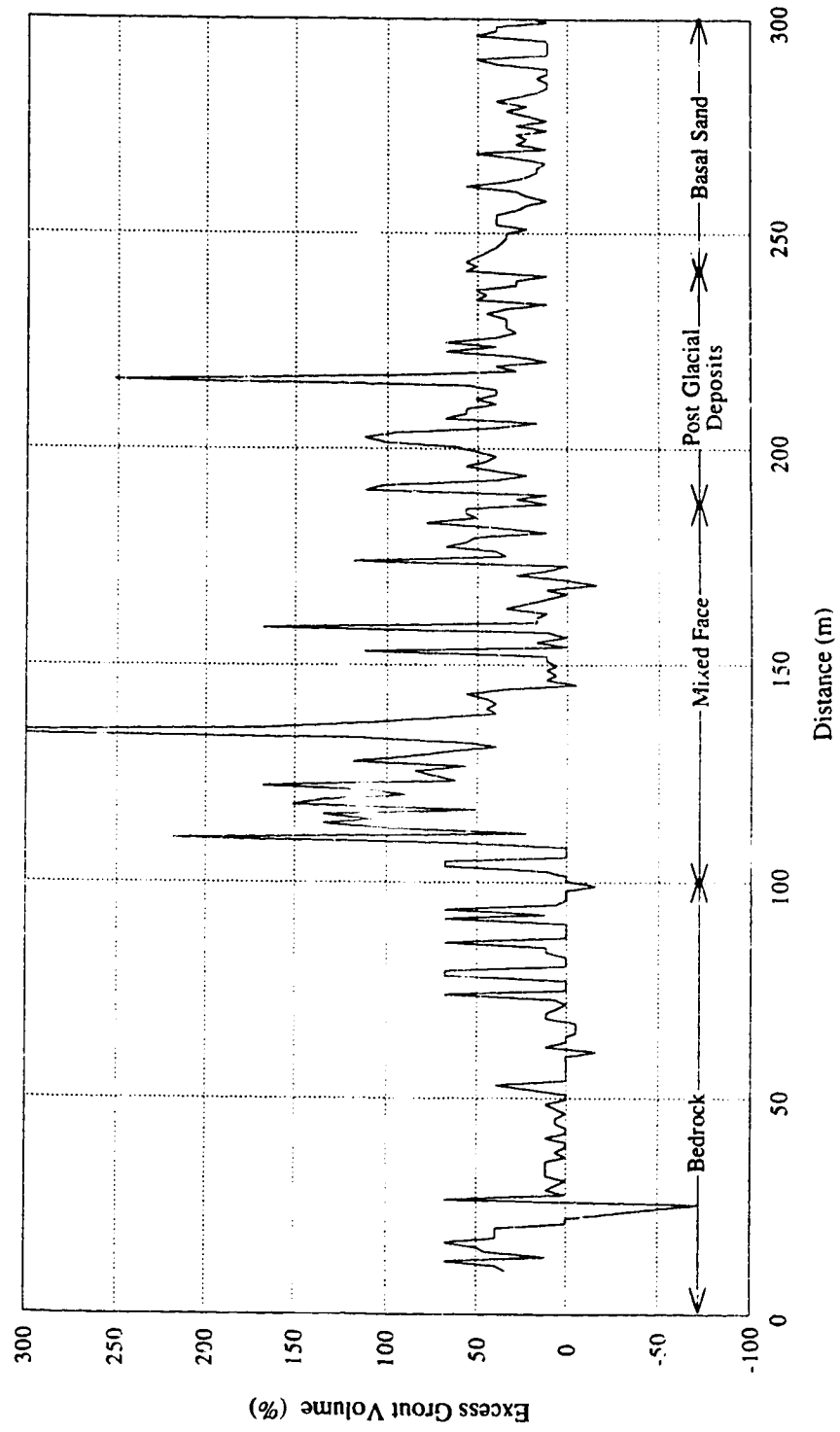


Figure 5.27: Excess Grout Volume used at the Edmonton LRT Project

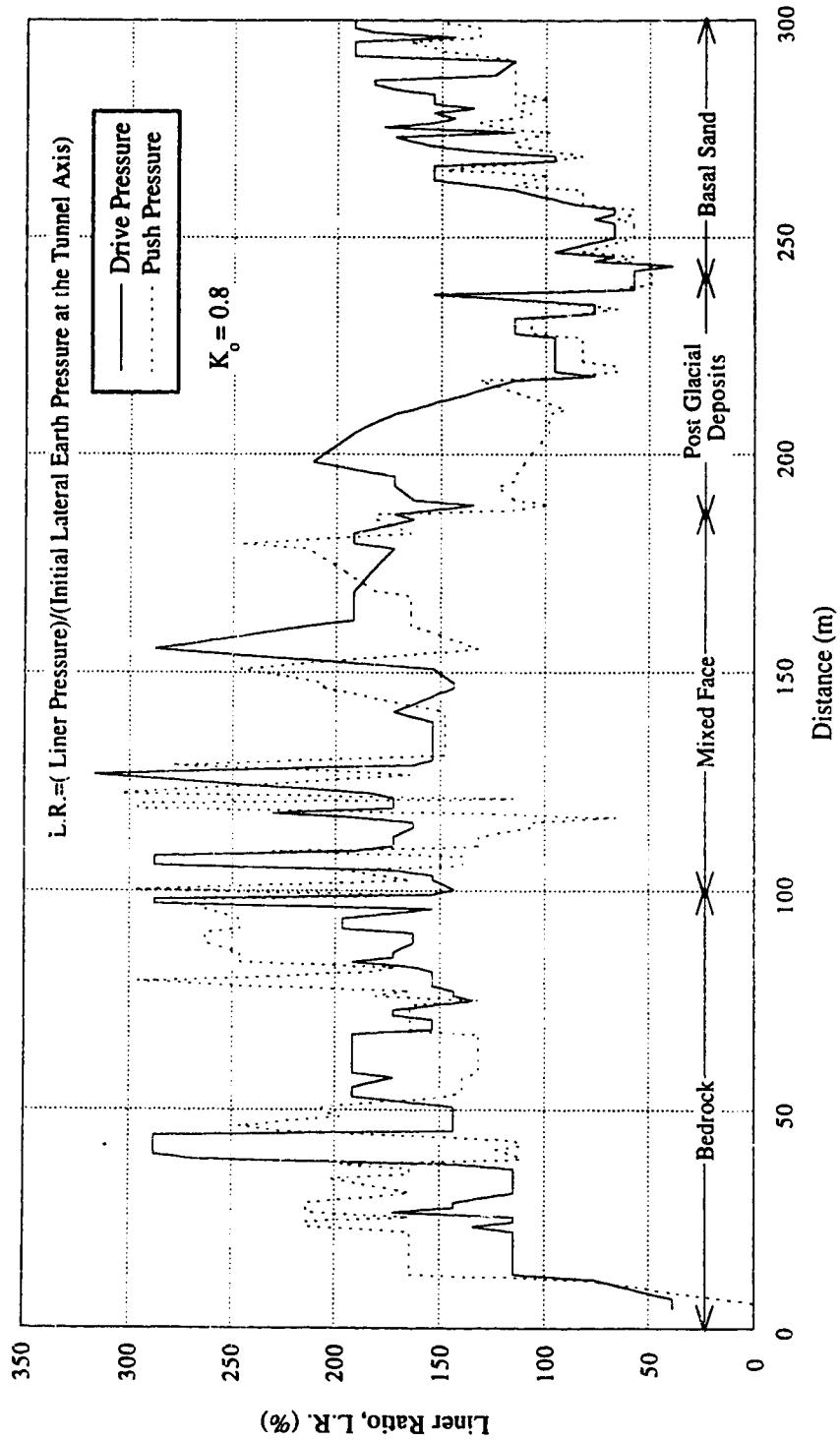


Figure 5.28: Liner Pressure Ratio, L.R. used at the Edmonton LRT Project

where 50% may be considered an extreme minimum and the highest pressure is recorded at the mixed face zone due to the existence of bedrock at the lower portion of the tunnel cross section. A value of 250% may be considered as an extreme maximum value.

5.7.3 Algorithm of the Design Method

As an example of the implementation of the design method to the LRT project, two soil profiles are selected to simulate a typical ground condition in the post-glacial deposit zone. The values of the proposed parameters are shown in Figure 5.29. A detailed numerical example is provided for the case where an *L.R.* of 100% and a *G.R.* of 75% are assumed for Profile 2. The selected values are intended to be representative of the actually applied liner pressure, and the effective grout pressure is considered to be one half of the applied pressure because of losses in grout pressure and grout material (see Babendererde (1985)). A FORTRAN program was formulated to produce the final results directly. The program is presented in Appendix C. Appendix D shows the input file for the detailed example and Appendix D shows the output file. The units of all input and output data are specified at the end of the output file. The input file consists of eight lines. The first line of the input file contains the title of the project. The second line contains the ground properties: H , D , γ , K_o , c , ϕ , $(R_f)_h$, $(K)_h$, $(n)_h$, P_a , ν where P_a is the atmospheric pressure. The fourth line contains the construction details: *G.R.* and *L.R.* . The fifth line is disregarded. Liner properties are entered at the sixth line: E_l , ν_l , A_l , and I_l . The modulus E_l is chosen to be 37 GPa which is an average value for reinforced concrete used in the precast segmental liner. It is to be observed that the original Eisenstein-Negro method suggests the use of a reduced liner modulus as the new casted concrete mix is not completely cured at the time of lining activation. It is considered that this is not applicable for the case of the precast segmented liner. Values of ν_l are chosen within average values for reinforced concrete: A_l is the cross sectional area of the liner per unit length and I_l is the moment of inertial of the liner. A reduced value is chosen to take into account the effect of joints between segments. Then, the depth of the firm ground level below the tunnel axis (R_l) is entered at the seventh line. In this case R_l is chosen to be equal to the tunnel radius, thus, no ground heave is included in the calculations. This assumption is taken based on the geological profile where the bedrock formation is either close to the tunnel floor or above it in the case of the mixed face condition. Then the number of iterations required during the ground-liner interaction calculations is entered at the eighth and last line. From the output file it can be shown that convergence has occurred after the second iteration. The last input parameter is an indicator of whether a special detailed output file is required.

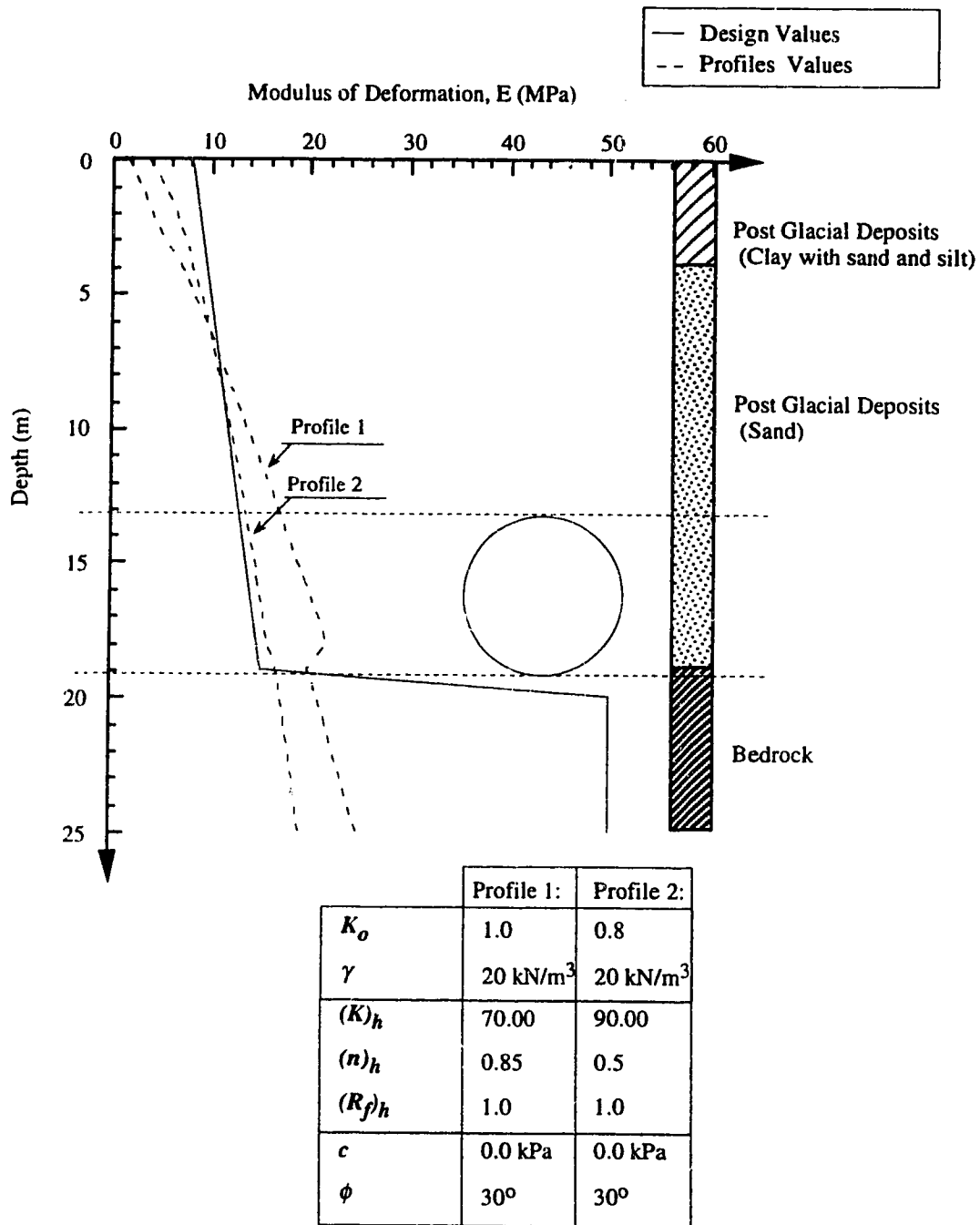


Figure 5.29: Profiles of Ground Parameters at the LRT Project versus the actual Design Parameters

5.7.4 Detailed Numerical Example

The first step is to evaluate the three-dimensional effect using the equations and coefficients given in Tables 5.1, 5.2, and 5.3 . The input parameters are ν , K_o , and H_o/R_o . The parameters $S.R.$ and $D.S.R.$ are evaluated, respectively, as 91.69% and 11.85% at the crown, 100.165% and 28.85% at the spring line, and 84.69% and 22.49% at the floor. The surface movement parameter \bar{w}_s is calculated to be 22.07 . Based on the definitions of $S.R.$ and $D.S.R.$ the mean normal stress p and the deviatoric stress ρ are calculated, respectively, as 203.84 and 37.78 kPa at the crown, 276.75 and 91.98 kPa at the spring line, and 279.74 and 71.70 kPa at the floor. The stress conditions are not allowed to violate a failure criterion related to the shear strength parameters. The developed program is formulated such that the Mohr-Coulomb criterion is selected for frictional material and the Von Mises criterion is selected for cohesive material. Thus the two conditions:

$$\sin \phi \geq \frac{3\rho}{\rho + 2\sqrt{6}p} \quad (5.20)$$

for purely frictional material, and

$$c \geq \sqrt{2}\rho \quad (5.21)$$

for purely cohesive material.

In the case of c - ϕ material, the approximation proposed by Negro (1988) indicated in Equation 5.7 for ϕ_a is used. For this specific case, the failure criterion for the angle of friction ϕ of 30° is not violated. According to Equations 5.13 and 5.14 the major and minor principal stresses in the triaxial configuration σ_1 and σ_3 are, respectively, 234.69 and 188.41 kPa at the crown, 351.87 and 239.22 kPa at the spring line, and 338.28 and 250.47 kPa at the floor. Hyperbolic parameters $(R_f)_h$, $(n)_h$, and $(K)_h$ are implemented into the hyperbolic model (Figure 5.6) to yield the tangent modulus of deformation E_t as 9.57 MPa at the crown, 8.19 MPa at the spring line, and 9.75 at the floor. A mean value of E_t of 8.93 MPa is calculated based on the average of four points. This value is used in estimating surface movement due to the three-dimensional effect according to Equation 4.15 which gives 5.17 mm. Then, the relative values of the liner α and β are calculated based on lining parameters A_l , I_l , E_l , and ν_l , as well as, on the ν and the average E_t of the ground (Equations 5.5 and 5.6) and are found to be, respectively, 379.25 and 0.0127

at the crown, 443.07 and 0.0148 at the spring line, and 372.13 and 0.0124 at the floor. Constants $A_1, A_2, A_3,$ and A_4 are calculated from Figure 5.22, respectively, as 0.107, 1.856, 0.440, and 0.390 at the crown, 1.56, 0.43991, 0.56, and 0.558 at the spring line, and 0.142, 2.40, 0.660, and 0.72 at the floor. Modified values of γ and K_o are calculated and are, respectively, 19.27 kN/m³ and 0.763 at the crown, 20.22 kN/m³ and 0.413 at the spring line, and 25.62 kN/m³ and 0.63 at the floor. A restrictive condition has to be implemented regarding the value of K_o . As interpolation through the given chart using the Eisenstein-Negro method has to be performed within the investigated range, the value of K_o is not allowed to be lower than 0.55 or higher than 1.1. Therefore, K_o at the spring line is corrected to 0.55. Average values on the four point basis are 21.33 kN/m³ for γ and 0.624 for K_o . According to the rational given in Section 5.6.4 about the choice of the direction of the principal stresses and the sign of DIF , radial stresses are given the same values as the principal stresses at the crown and at the floor. In the case of the spring line, σ_r and σ_θ have to be recalculated according to the new value of K_o . Therefore, σ_r is 351.87 and σ_θ is 239.217 kPa at the spring line. The determination of σ_r on three points of the circumference allow the determination of the radial stress release Σ that will be 91.45%, 120.0% at the spring line, and 88.76% at the floor.

At this point, the problem is reduced to an equivalent plane strain problem where the stress field is determined according to the new modified average values of γ and K_o . The amount of stress release is determined according to the radial stress ratios Σ on the three points of the circumference. The Eisenstein-Negro method can, therefore, be applicable for the new conditions. Reference values are determined according to the shear strength parameter ϕ . Thus, α_{ref} , and U_{ref} are calculated. Accordingly, λ is evaluated from Equation 5.9. By substituting back into Negro's charts (Negro 1988: Figures 6.97, 6.98, 6.99, 6.105, 6.106, 6.113, 6.114, and 6.115), the nondimensional circumferential displacement U/U_{ref} , and accordingly the radial displacement u_r are calculated. These displacements are considered the equivalent displacement that would have taken place had the stress and strain fields been plane strain during the excavation process. For the new stress field, a process of ground-liner interaction is calculated according to the Eisenstein-Negro method, and convergence is reached giving the straining actions at the tunnel lining and the displacement at the circumference. Displacement at the crown because of ground-liner interaction is found to be 15.09 mm which corresponds to 5.9 mm at the ground surface. Adding surface movement due to ground-liner interaction to the movement due to the three-dimensional effect (5.17 mm) gives the final movement at the ground surface (= 11.06 mm).

5.7.5 Validation of the Results

The design method is used a number of times in order to provide a scan of the estimated values of the ground surface movement for various values of **G.R.** and **L.R.** . Figures 5.30 and 5.31 show the estimated maximum ground displacement for the two profiles of the ground conditions suggested in Figure 5.29. A reduction factor of 2.5 is used to calculate the effective grout pressure with respect to the actual applied grout pressure. Therefore, the measured displacements at the ground surface are plotted in the figure using the effective grout pressure related to the average grout pressure at the location of the measurement. From Figures 5.30 and 5.31, **L.R.** corresponding to the measured displacements ranges between 50% and 150% as extreme values which corresponds to the actual **L.R.** applied at the ground. In general then, as grout pressure increases and the lining pressure decreases, surface movement decreases. Grout pressure provides support to the ground after excavation and tends to restrict and reverse ground intrusion into the tunnel. Meanwhile, lining pressure although it provides support at the face, results in increasing the stress relief behind the shield, and thus leads to an increasing surface displacement although its effect is not obvious at the crown level. The settlement profile is estimated by adding the magnitude of the settlement profile calculated from the Eisenstein-Negro method for the plane strain analysis (Negro (1988): Appendix C) to that calculated from the three-dimensional effect (Appendix B). Interpolation between a number of charts is necessary to obtain the settlement trough corresponding to the actual ground conditions. Figure 5.32 shows that the measured surface displacement in the transversal plane as compared with the estimated surface trough for **L.R.** equals 100 % considering ground properties at Profile 2 (Figure 5.29). It is found that the method overestimates the trough width and a correction factor of 0.8 is multiplied by the estimated width length (**y**) to emulate the measured surface trough. Straining actions in the liner are calculated for the same parameters. Lining thickness is calculated as the equivalent uniform thickness of the actual cross-sectional area of the segment which is equal to 232 mm. A reduced moment of inertia is calculated for the liner to take into consideration the effect of the segmental joints. The selected value is $8.33 \times 10^{-5} \text{ m}^4$ which is equivalent to a segment of 100 mm thickness. The calculated normal forces, shearing forces, and bending moments are shown in Figures 5.33 and 5.34 . The figures show that as the objective of the construction method is to minimize ground disturbance around the tunnel, normal forces are close to the initial soil pressure while shear and bending moments within the liner have relatively low values.

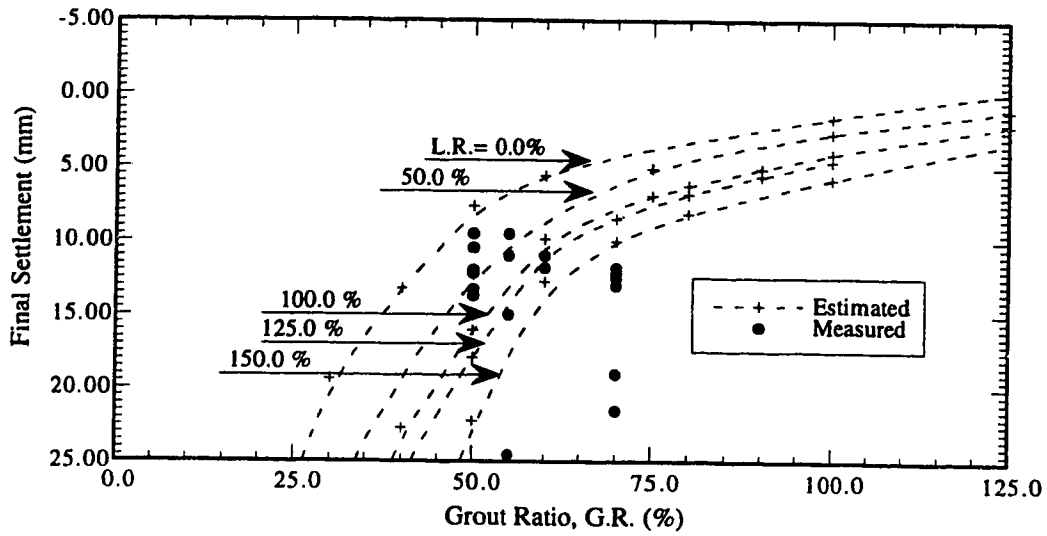


Figure 5.30: Measured and Estimated Maximum Ground Surface Settlement versus the Grout Ratio at the Edmonton LRT Project, Material Parameters of Profile 1

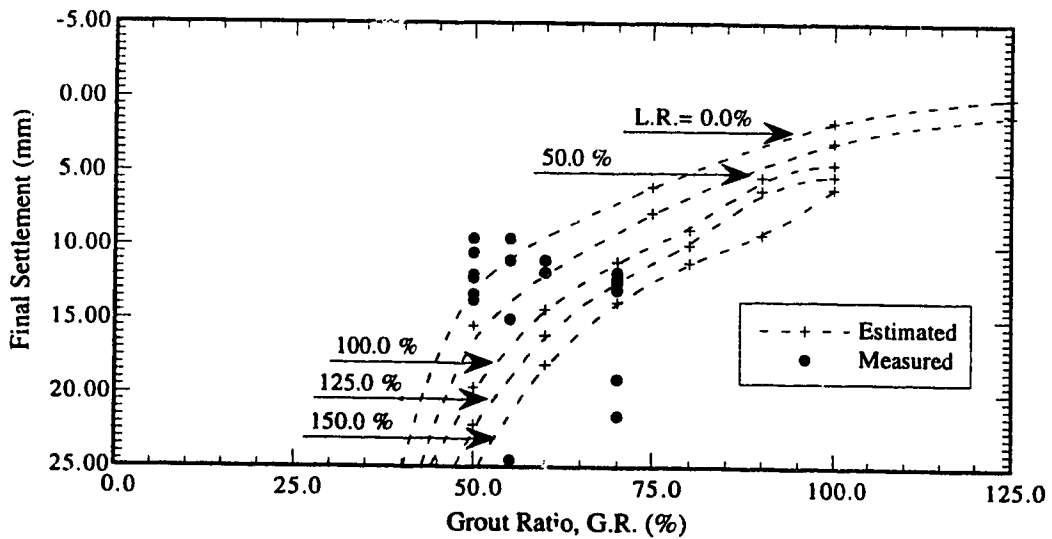


Figure 5.31: Measured and Estimated Maximum Ground Surface Settlement versus the Grout Ratio at the Edmonton LRT Project, Material Parameters of Profile 2

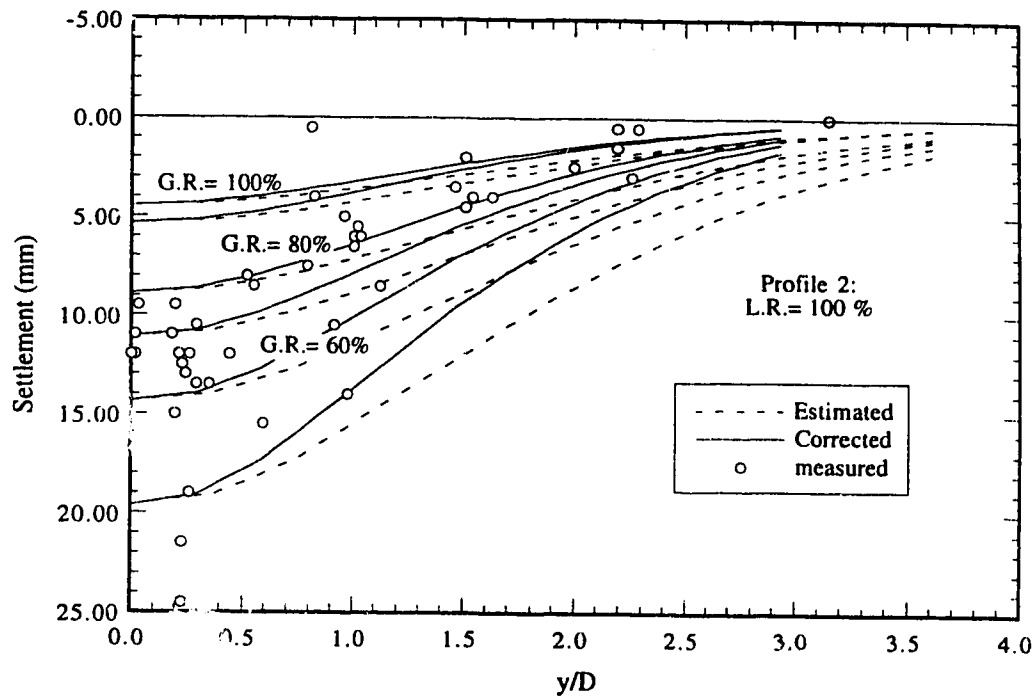


Figure 5.32: Measured and Estimated Settlement Trough at Ground Surface at the Edmonton LRT Project, Material Parameters of Profile 2

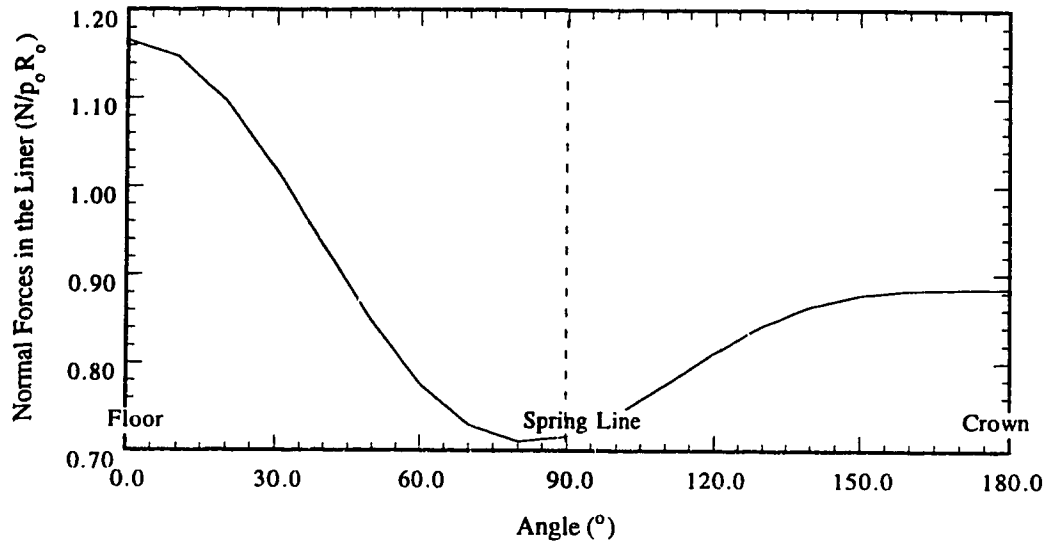


Figure 5.33: Calculated Normal Forces at the Liner Edmonton LRT Project, Material Parameters of Profile 2

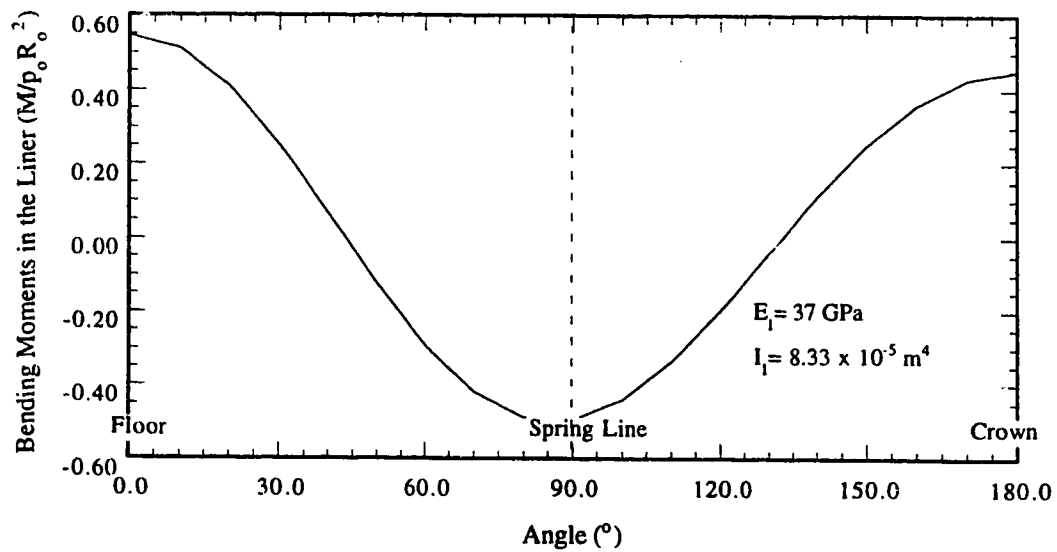


Figure 5.34: Calculated Bending Moment at the Liner Edmonton LRT Project, Material Parameters of Profile 2

5.8 Conclusions

Tunnelling design methods are required to produce estimations of the final stress field around the excavation and the straining actions inside the lining system. A review of a number design methods and of their estimations compared to field measurements is given. Special emphasis is made on the Eisenstein-Negro method for shallow tunnel as it provides a number of realistic assumptions concerning the ground deformation model and the initial stress conditions.

A certain number of adaptations to the Eisenstein-Negro method are effected in order to apply the method to cases of tunnels constructed using pressurized shield methods. The three-dimensional effect is based on the three-dimensional analysis presented in Chapter 4. The concept of the tunnel-ground interaction is suggested instead of the concept of volume loss to evaluate of the stress field around the tunnel at the tail of the shield. The resultant stress field at the tail is introduced into the original method to calculate the stress changes around the liner using the twice normalized ground reaction curve NNGRC. According to the original method Hartmann's solution is used to evaluate the straining actions inside the liner, as well as, the lining displacement. The final movement at the ground surface is calculated as the resultant of the displacement due to the three-dimensional effect and that due to the ground-liner interaction.

The proposed design method is applied in the case of the LRT tunnel constructed in Edmonton using the Bentonite Slurry Shield, the Hydroshield. Input parameters are selected according to actual design parameters and according to the field lining installation records. Estimations of the ground movement are shown to compare well with the measured ground movement at the site.

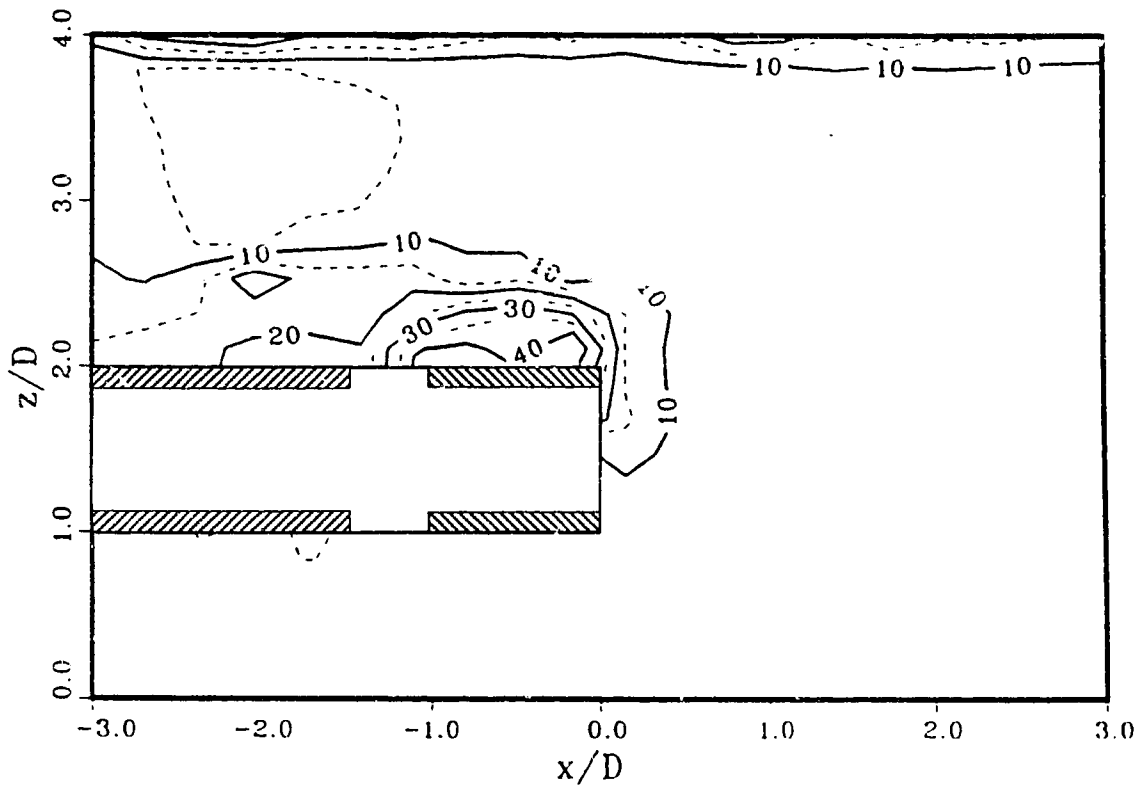


Figure 4.58: Contour Plot of Mobilized Friction Angle, ϕ , at the Central Longitudinal Plane (G.R.= 30.0 % and L.R.= 45.0 %)

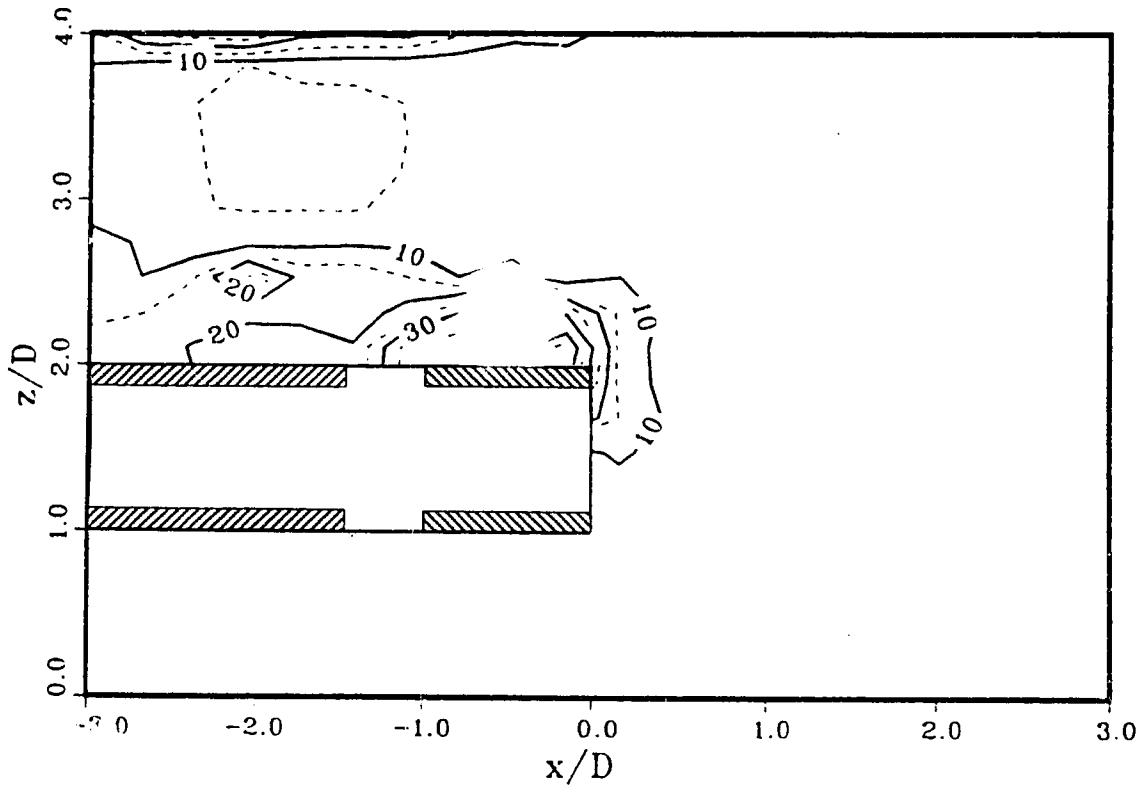


Figure 4.59: Contour Plot of Mobilized Friction Angle, ϕ , at the Central Longitudinal Plane (G.R.= 30.0 % and L.R.= 90.0 %)

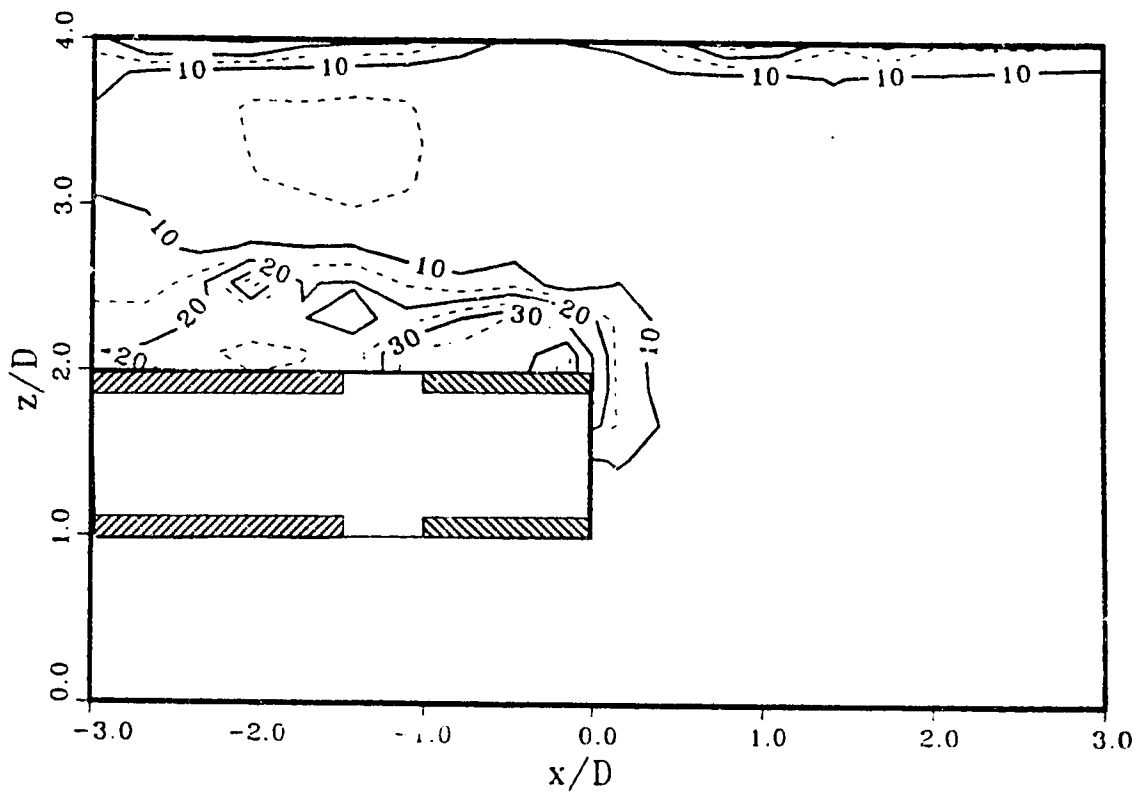


Figure 4.60: Contour Plot of Mobilized Friction Angle, ϕ , at the Central Longitudinal Plane (G.R.= 30.0 % and L.R.= 135.0 %)

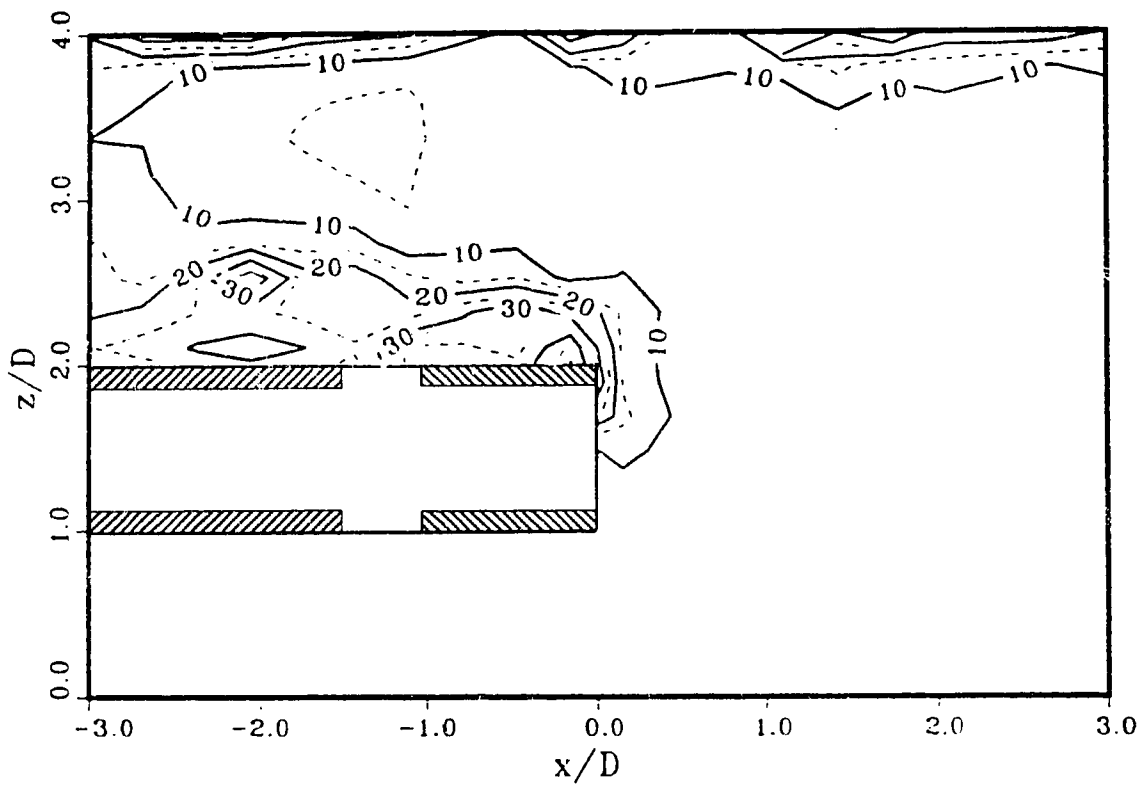


Figure 4.61. Contour Plot of Mobilized Friction Angle, ϕ , at the Central Longitudinal Plane (G.R.= 30.0 % and L.R.= 180.0 %)

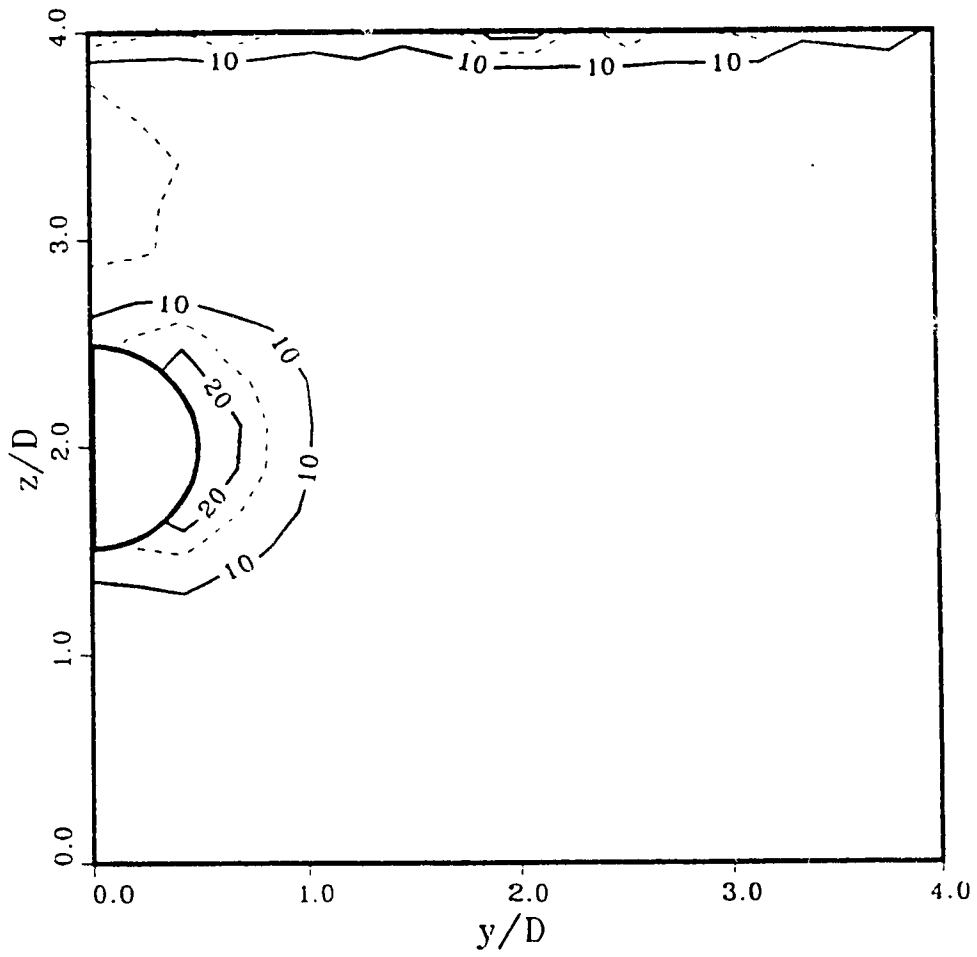


Figure 4.62: Contour Plot of Mobilized Friction Angle, ϕ , at the Transversal Plane at the Point of Lining Activation (G.R.= 30.0% and L.R.=0.0%)

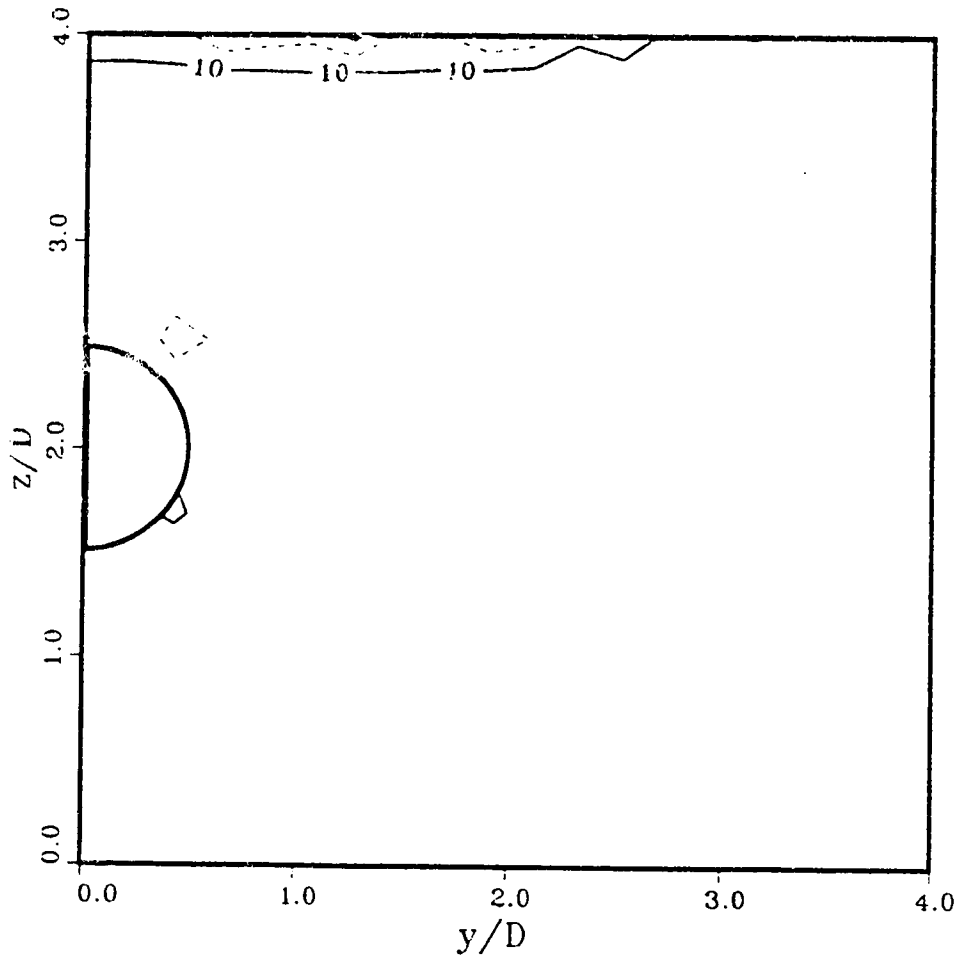


Figure 4.63: Contour Plot of Mobilized Friction Angle, ϕ , at the Transversal Plane at the Point of Lining Activation (G.R.= 75.0% and L.R.=0.0%)

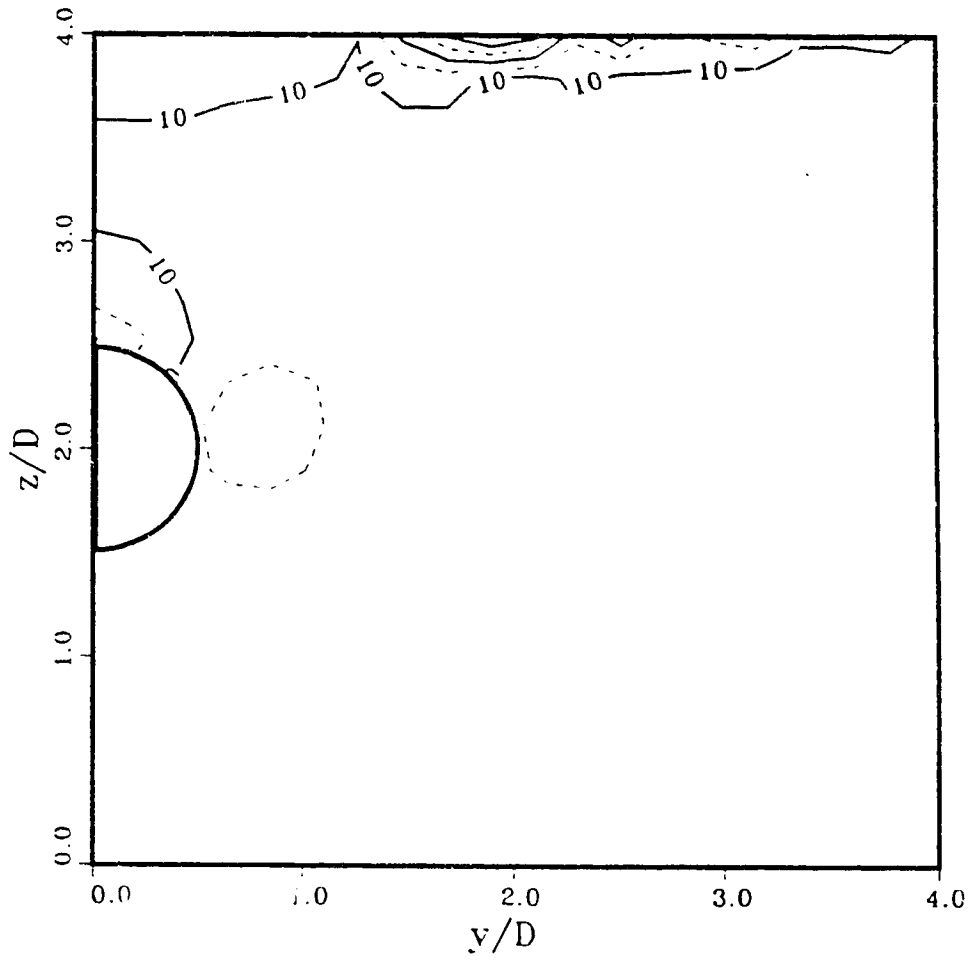


Figure 4.64: Contour Plot of Mobilized Friction Angle, ϕ , at the Transversal Plane at the Point of Lining Activation (G.R.= 112.5% and L.R.=0.0%)

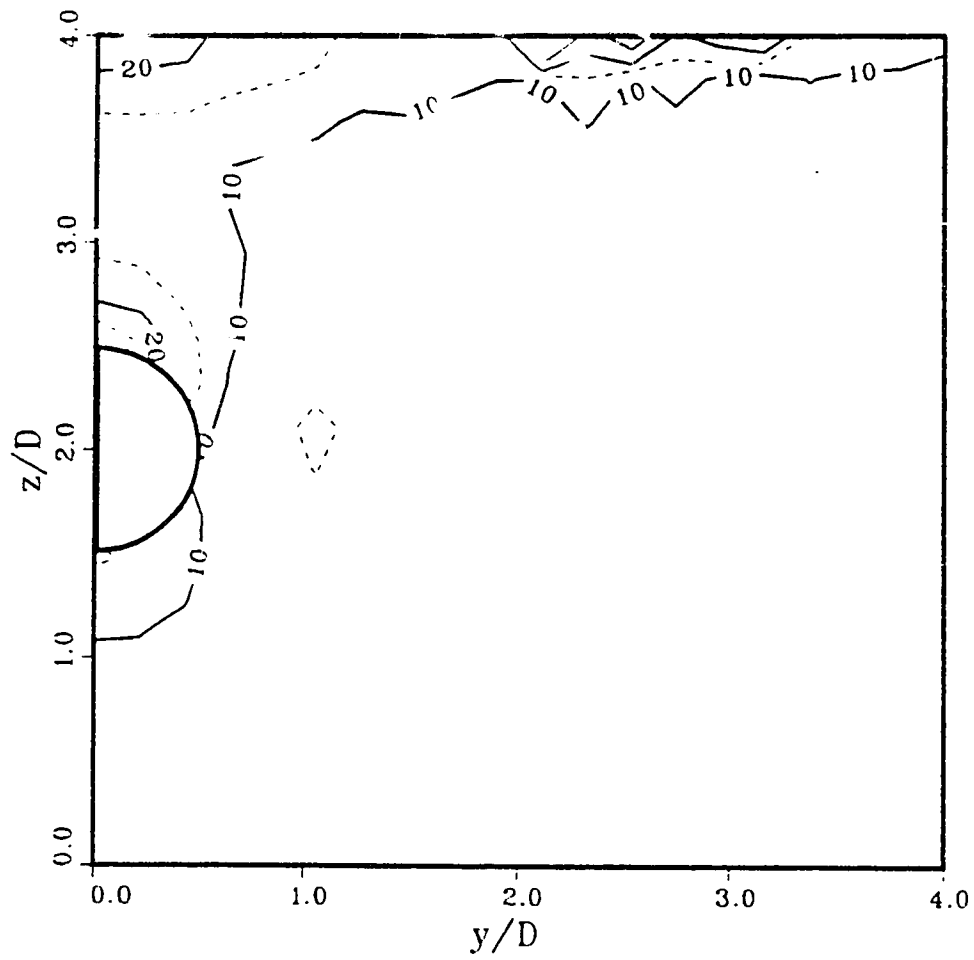


Figure 4.65: Contour Plot of Mobilized Friction Angle, ϕ , at the Transversal Plane at the Point of Lining Activation (G.R.= 150.0% and L.R.=0.0%)

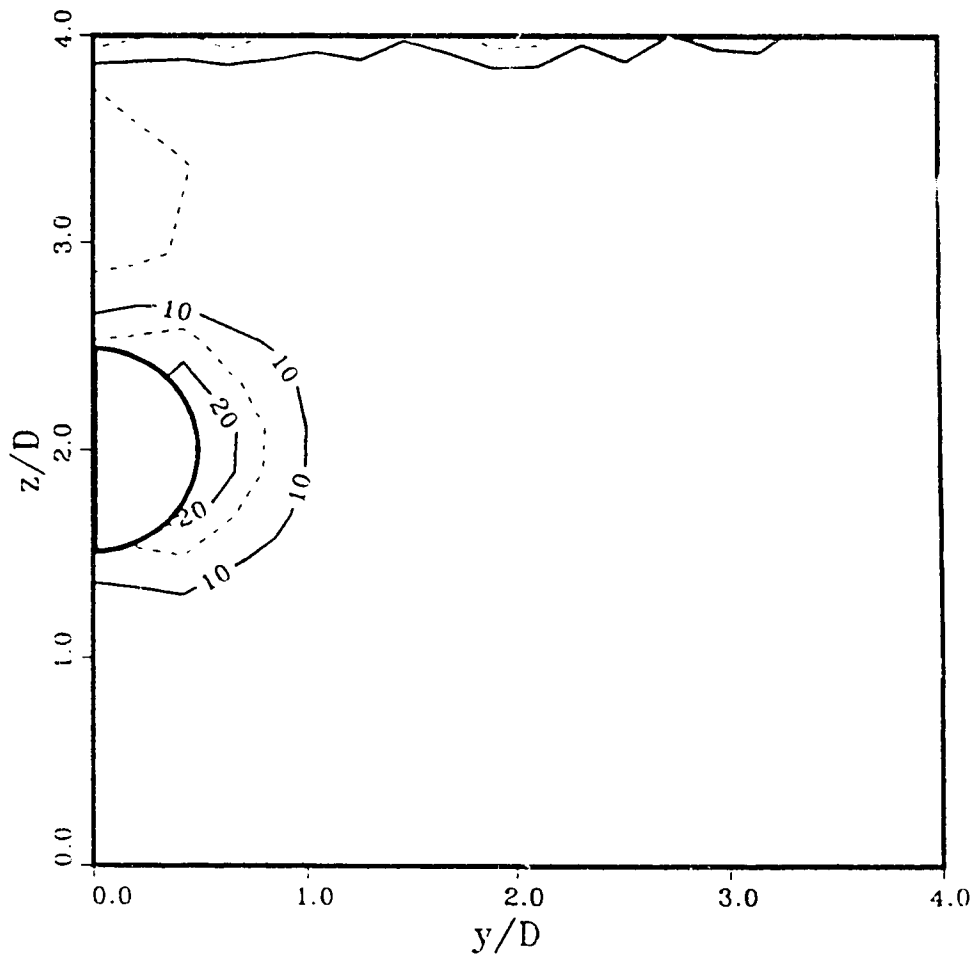


Figure 4.66: Contour Plot of Mobilized Friction Angle, ϕ , at the Transversal Plane at the Point of Lining Activation (G.R.= 30.0% and L.R.=45.0%)

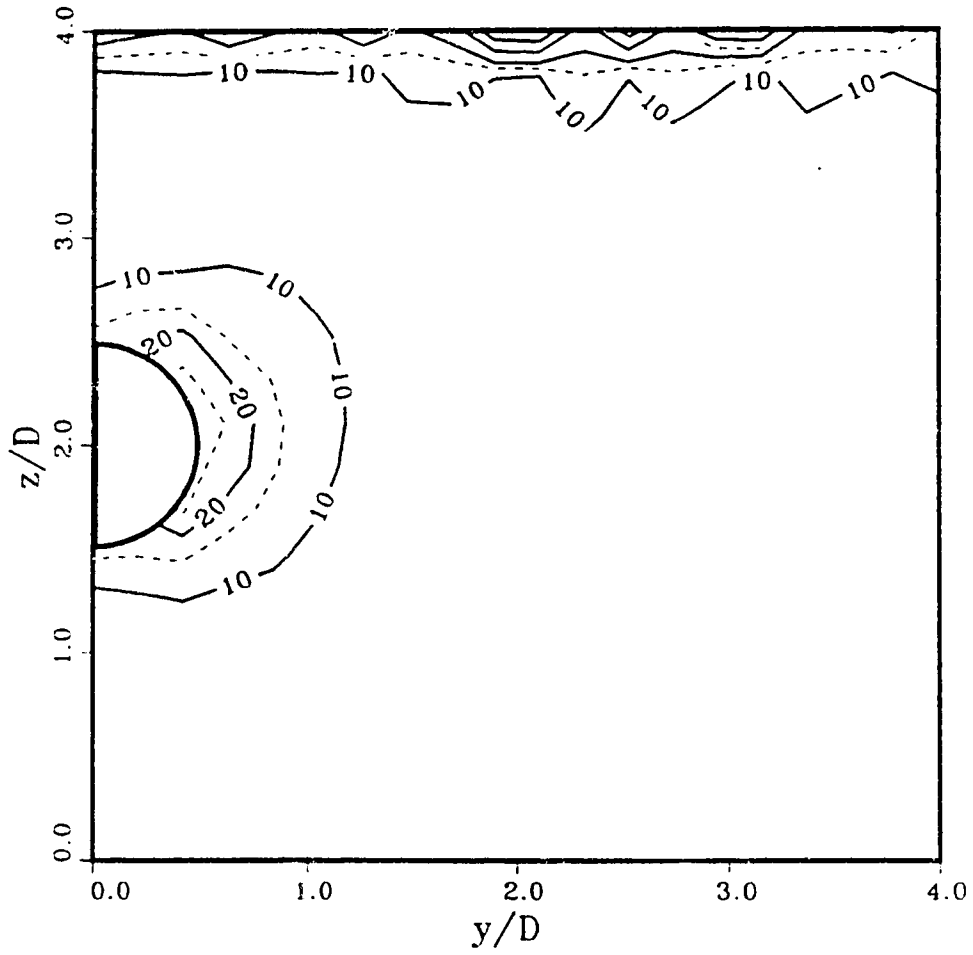


Figure 4.67: Contour Plot of Mobilized Friction Angle, ϕ , at the Transversal Plane at the Point of Lining Activation (G.R.= 30.0% and L.R.=13%)

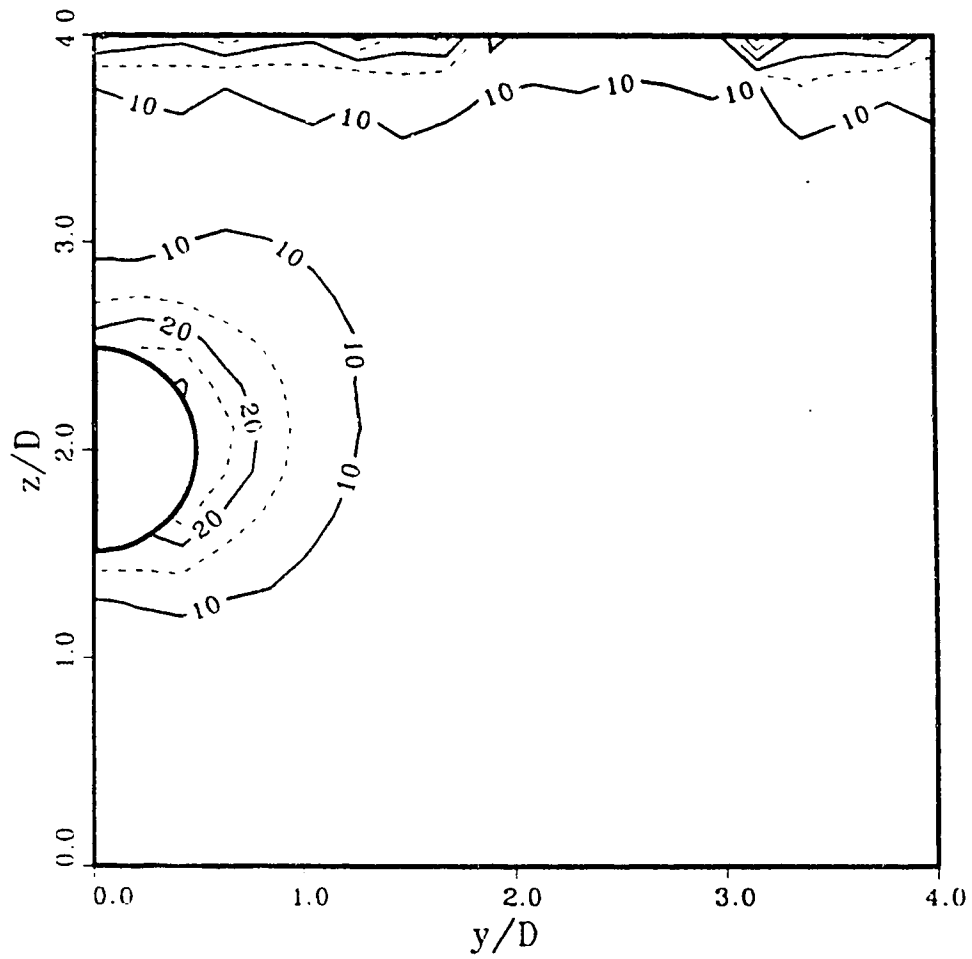


Figure 4.68: Contour Plot of Mobilized Friction Angle, ϕ , at the Transversal Plane at the Point of Lining Activation (G.R.= 30.0% and L.R.=180.0%)

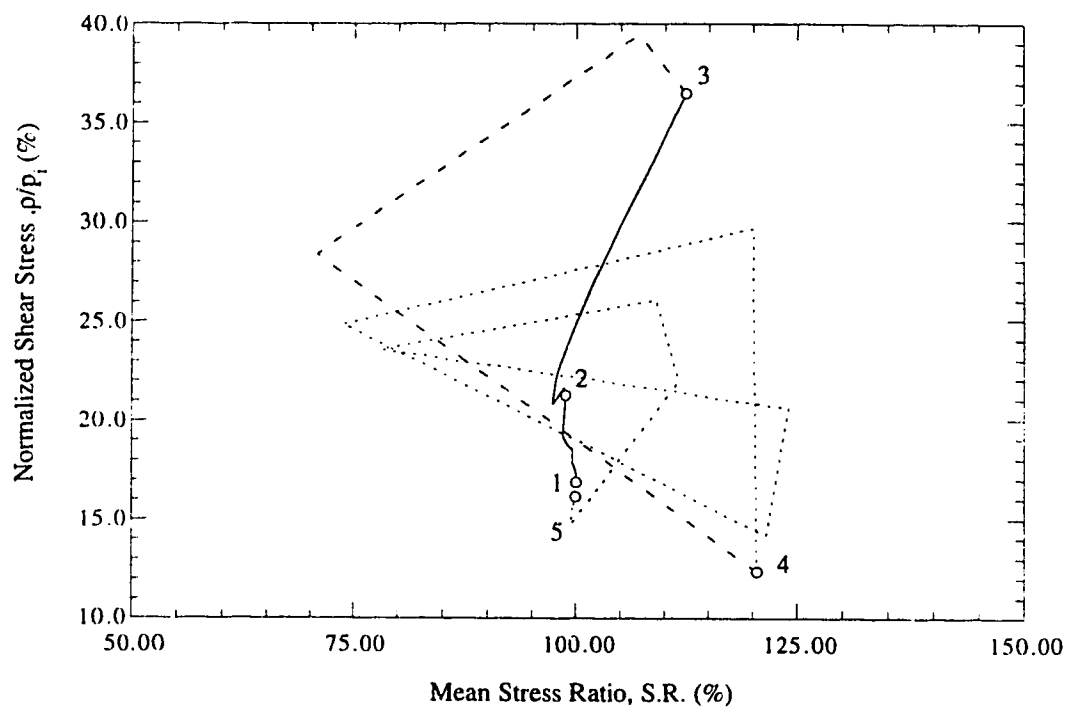
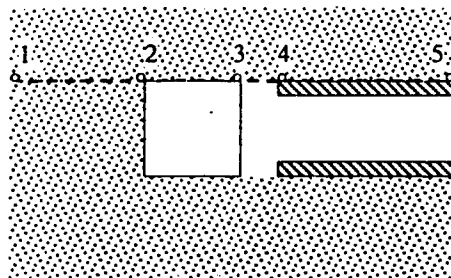


Figure 4.69: Stress Ratio versus the Normalized Shear Stress (G.R.= 30.0% and L.R.= 0.0%)

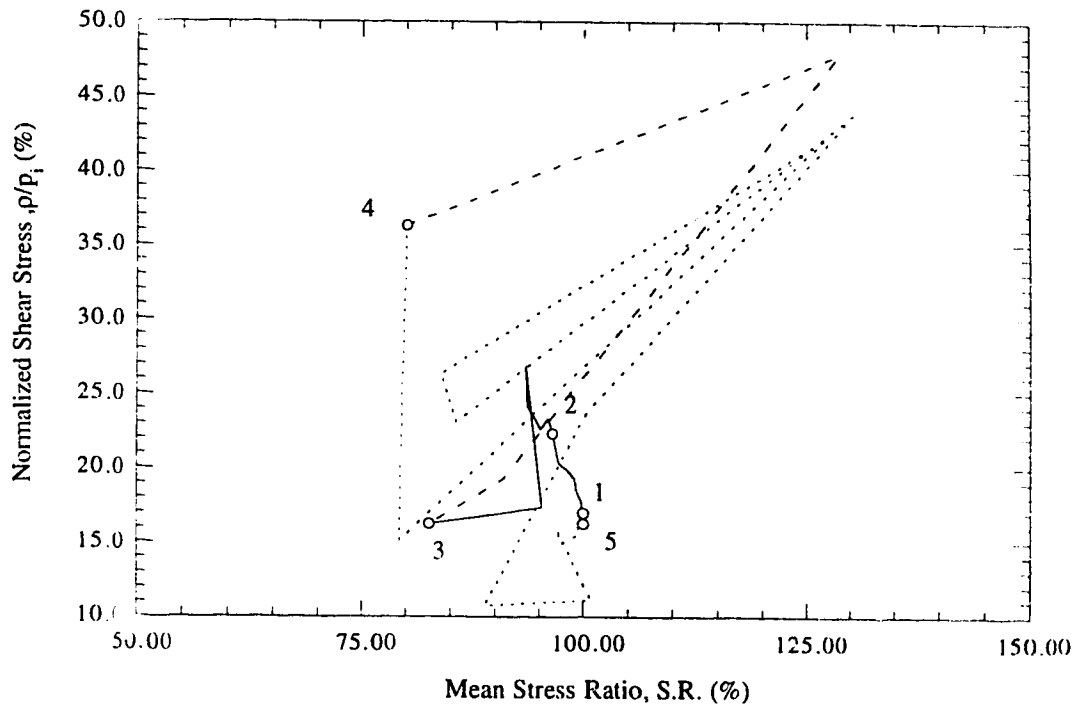
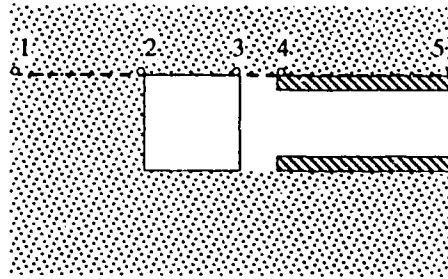


Figure 4.70: Stress Ratio versus the Normalized Shear Stress (G.R.= 112.5% and L.R.= 0.0%)

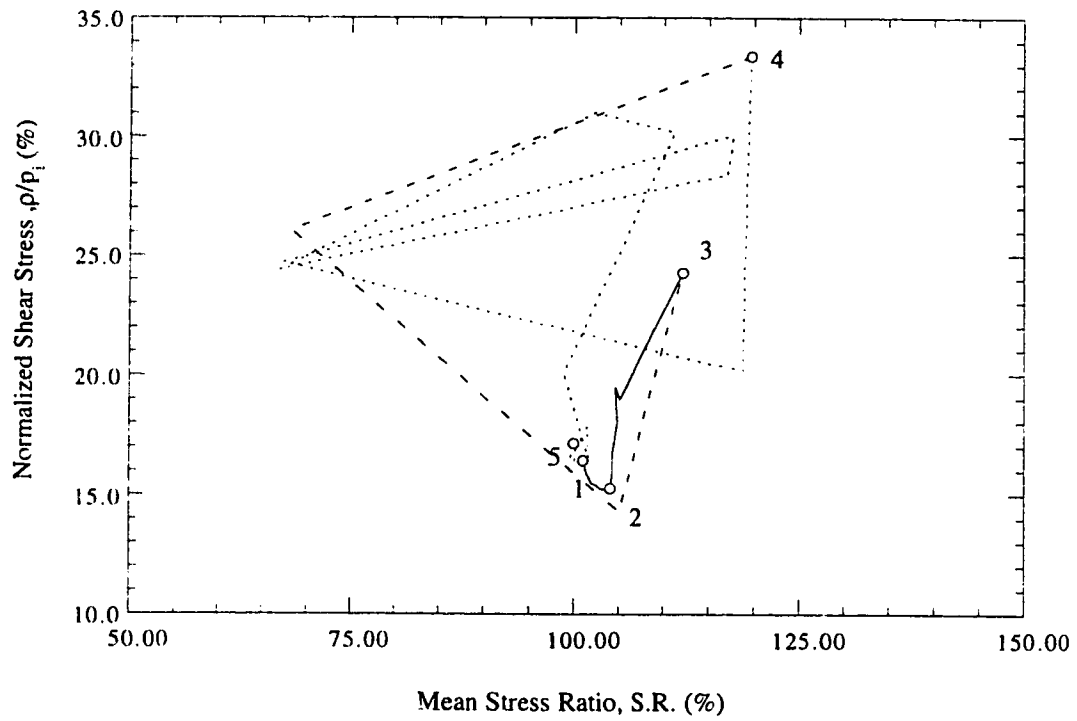
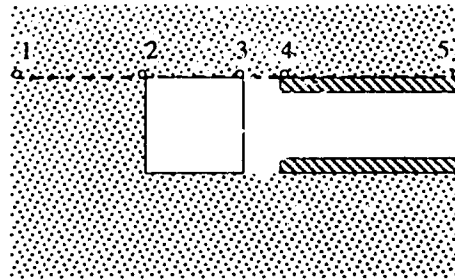


Figure 4.71: Stress Ratio versus the Normalized Shear Stress (G.R.= 30.0% and L.R.= 135.0%)

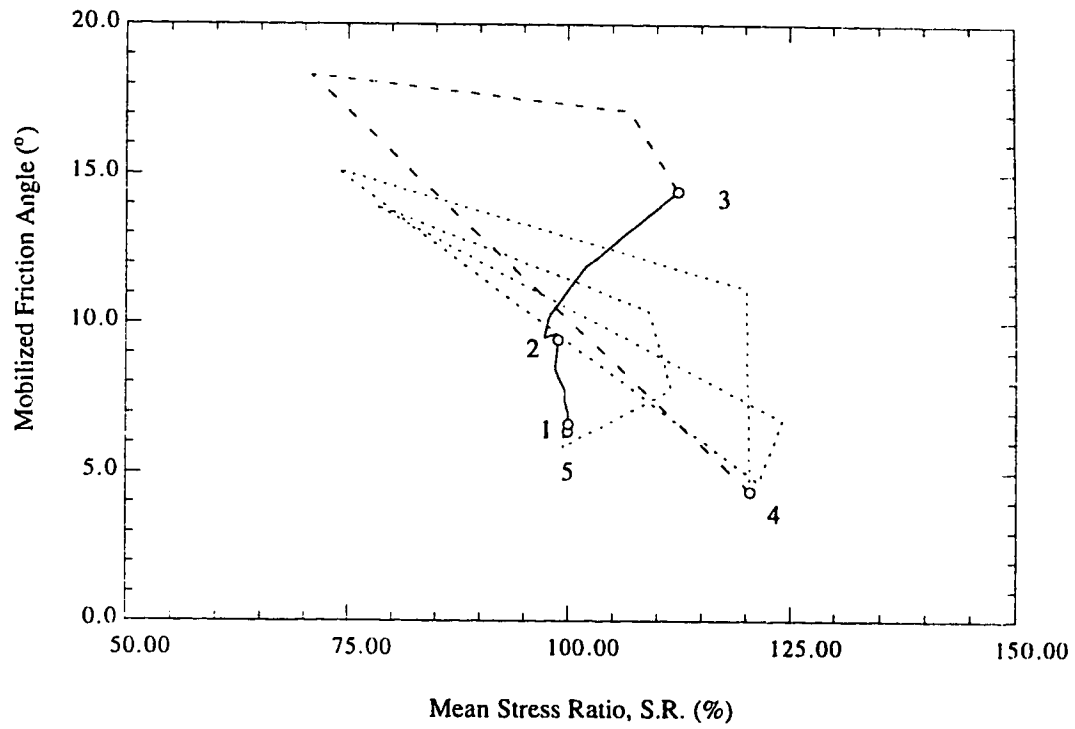
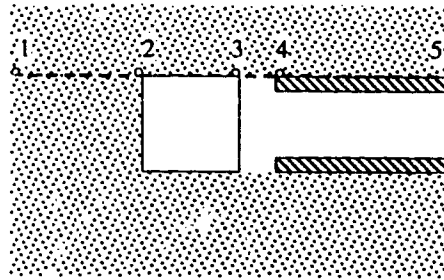


Figure 4.72: Stress Ratio versus the Mobilized Friction Angle, ϕ , (G.R.= 30.0% and L.R.= 0.0%)

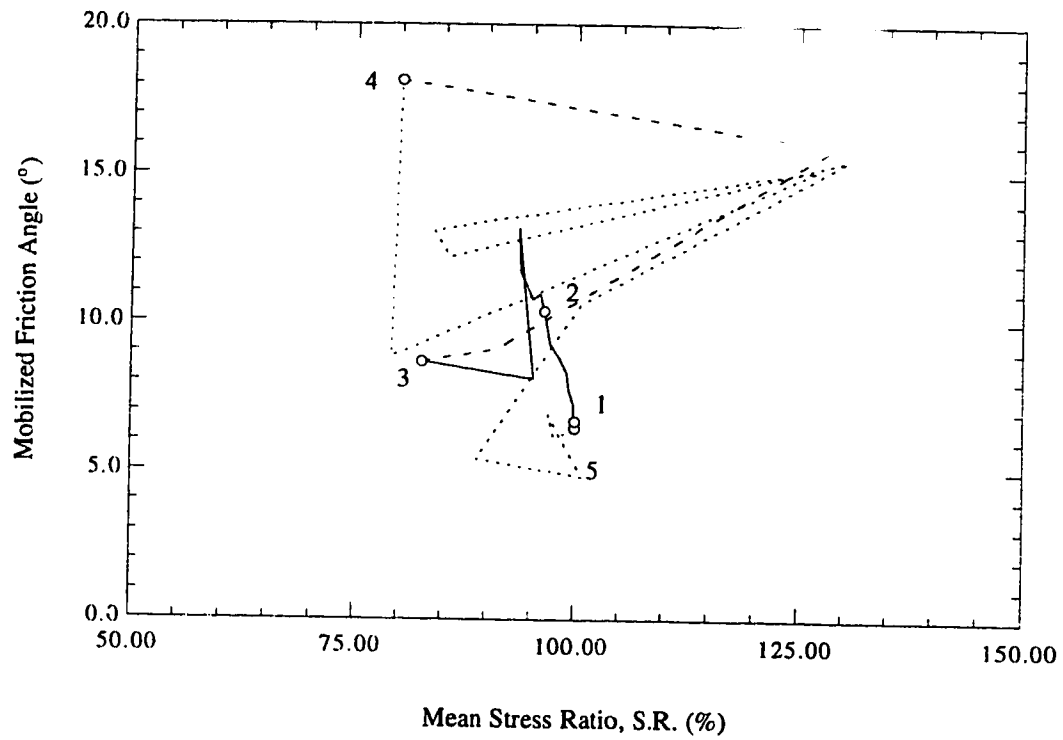
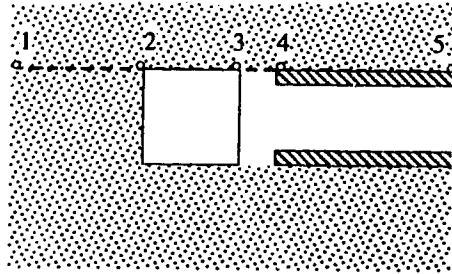


Figure 4.73: Stress Ratio versus the Mobilized Friction Angle, ϕ , (G.R.= 112.5% and L.R.= 0.0%)

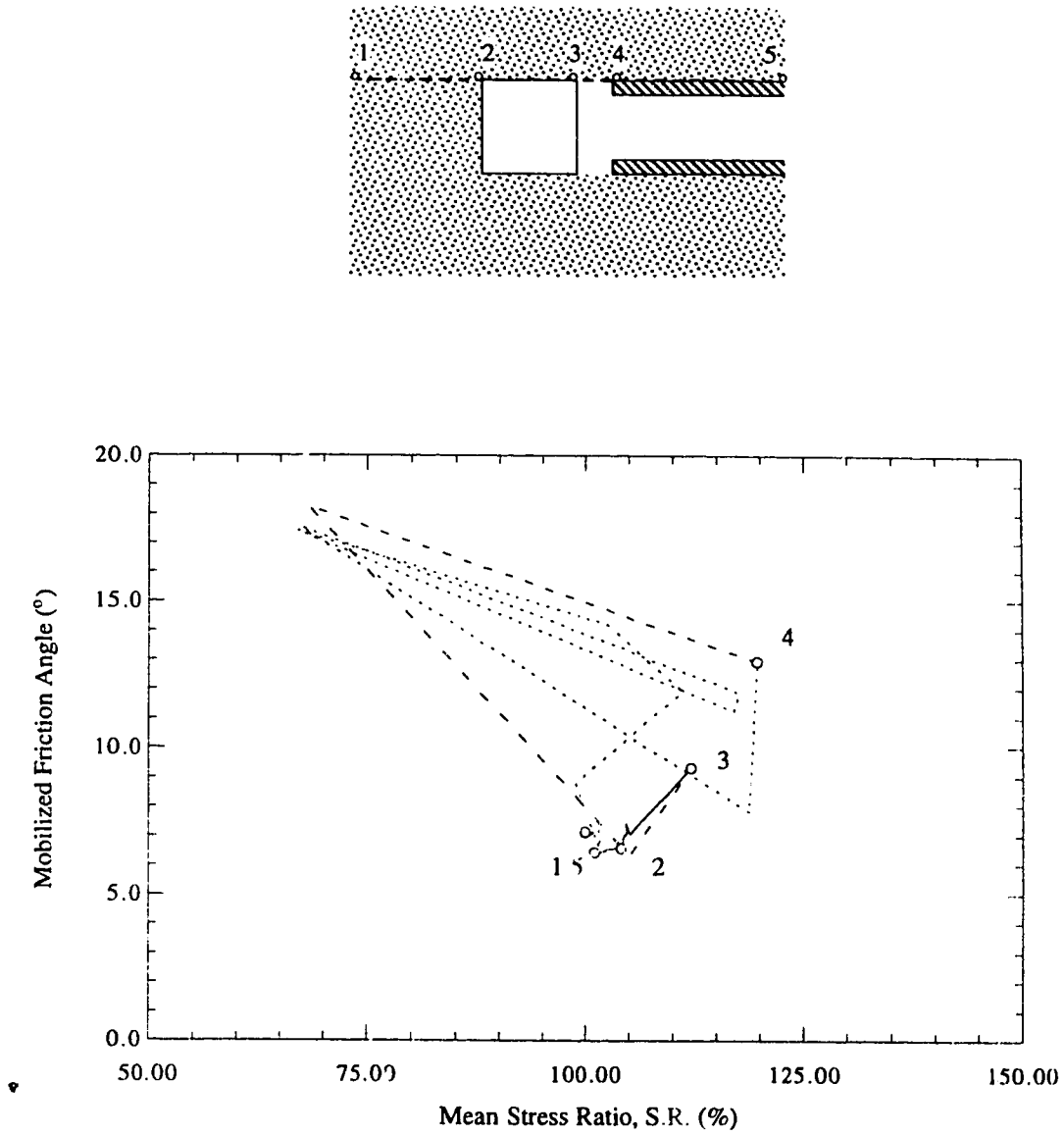


Figure 4.74: Stress Ratio versus the Mobilized Friction Angle, ϕ , (G.R.= 30.0% and L.R.= 135.0%)

represented by the mobilized friction angle.

4.7.5 Analysis

The objective of the analysis of the obtained results is to constitute a generalized model of displacements at the ground surface, displacement at the tunnel crown and of stresses around the liner of a tunnel excavated using pressurized shield methods under various construction and ground conditions. The obtained results are interpolated into simple expressions showing the effects of the most influential parameters.

4.7.5.1 Methodology

The methodology followed during the analysis is to select a number of executed computer runs. Then, normalized results relating to ground displacement, crown displacement, or stress changes around the liner are expressed in the form of a first-order or second-order equations reflecting the effect of a certain parameter. The process is repeated for various parameters, and a generalized form of the investigated result is achieved. Finally, the constant term is calculated by minimizing the average absolute error of all of the results interpolated through the formulated equations.

4.7.5.2 Surface Displacement

As demonstrated above, displacement at the ground surface is expressed in terms of the normalized surface displacement, \bar{w}_s , at the optimum point in the longitudinal direction. The effect of various factors affecting the displacement profile is found to be linear based on a sensitivity analysis of the relatively limited number of the results

$$\bar{w}_s = \left(as_n(\nu) + \frac{as_k}{K_o} + as_h \right) \left(\frac{H_o}{R_o} \right)^2 + \left(as_g(G.R.) + as_l(L.R.) + as_o \right) \left(\frac{H_o}{R_o} \right) . \quad (4.17)$$

The constants used are self-explanatory. Figure 4.75 shows the selected values for the constants and the influence of the depth of the tunnel on them.

4.7.5.2 Displacement at the Crown

The critical displacement is selected at the middle of the gap distance. Since the nodal displacements at the crown of the liner are locked together and the lining is relatively incompressible, almost the same displacement is calculated at the liner because of previous

$$\omega_s = (as_k/K_o + as_n(v) + as_h) * (Ro/Ho)^2 + (as_g (G.R) + as_l (L.R) + as_o) (Ro/Ho)$$

as_k	1356.00
as_n	-306.46
as_h	-607.02

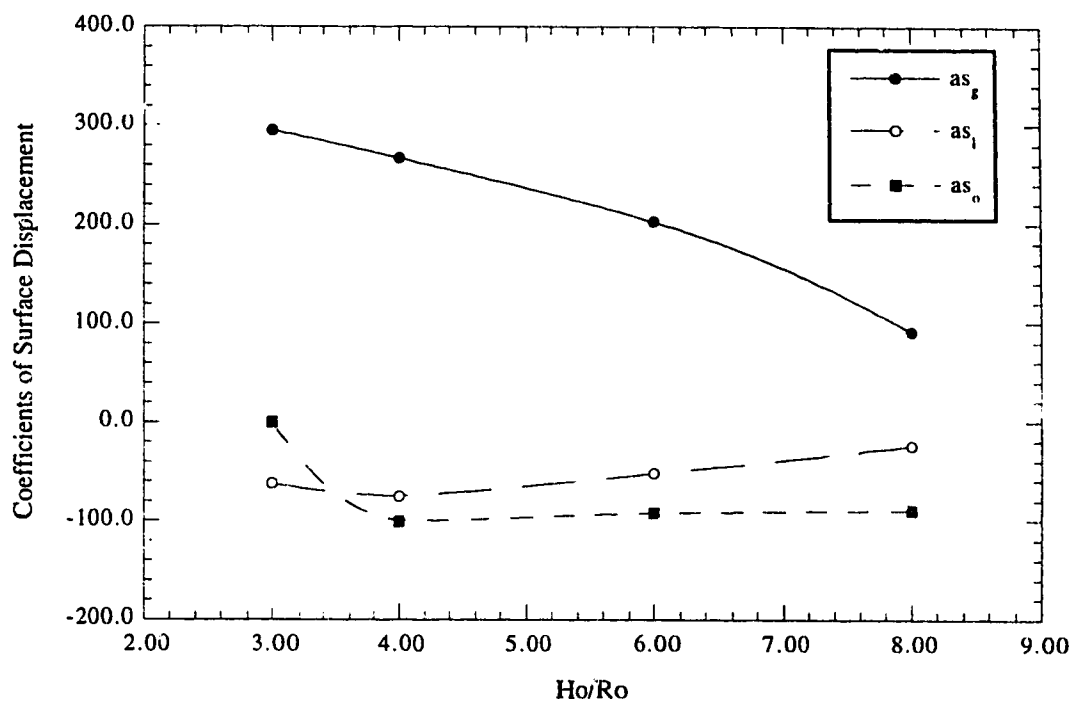


Figure 4.75: Regression Coefficients for Surface Movement ω_s

excavation steps. Similar to surface displacement, crown displacement is normalized through the equation:

$$\bar{w}_c = \frac{wE}{Dp_o} \quad (4.18)$$

Investigation of the results shows that liner pressure has almost no effect on the crown displacement, and *L.R.* is, therefore, excluded from the final generalized form:

$$\bar{w}_c = \left(ac_n(v) + \frac{ac_k}{K_o} + ac_h \right) \left(\frac{H_o}{R_o} \right)^2 + \left(ac_g(G.R.) + ac_o \right) \left(\frac{H_o}{R_o} \right) \quad (4.19)$$

Table 4.2 shows the values of the calculated constants.

4.7.5.3 Stress Ratio

The stress ratio is calculated at the crown, spring line, and at the floor of the liner. As shown in Figures 4.69 to 4.74 the optimum change in *S.R.* takes place at the middle of the gap distance and a comparable amount of stress change is recorded behind the point of the lining activation. Results of the analysis show a certain degree of consistency with respect to the effect of the grout pressure, lining pressure, and K_o while the effect of Poisson's ratio does not show the same degree of consistency although it has been regressed to the second degree. The following expression is suggested:

$$S.R. = ar_g(G.R.) + ar_l(L.R.) + ar_{n2}(v)^2 + ar_{n1}(v) + \frac{ar_k}{K_o} + \frac{ar_h}{H_o/R_o} + ar_o \quad (4.20)$$

Figure 4.76 and Table 4.3 show the results of the analysis and the effect of the depth on different obtained constants.

4.7.5.4 The Deviatoric Stress Ratio

The amount of mobilized shear strength associated with the excavation process in the three-dimensional is related to the deviatoric stress ratio *D.S.R.* defined as:

$$D.S.R. = \frac{\rho}{\gamma H_o} = \frac{\rho}{p_o} \quad (4.21)$$

$$\bar{\omega}_s = \left(as_n(v) + \frac{as_k}{K_c} + as_h \right) \left(\frac{R_o}{H_o} \right)^2 + (as_g(G.R.) + as_l(L.R.) + as_o) \left(\frac{R_o}{H_o} \right)$$

as_n	-1356.017
as_k	-306.459
as_h	-607.023

H_o/h	3.0	4.0	6.0	8.0
	294.948	267.077	202.629	91.485
as_l	-62.470	-75.822	-52.289	-24.186
as_o	-92.777	-98.817	-89.556	-78.191

$$\bar{\omega}_c = ac_g(G.R.) + ac_n(v) + \frac{ac_k}{K_o} + ac_o + ac_h \left(\frac{R_o}{H_o} \right)$$

ac_g	280.830
ac_n	-27.014
ac_k	97.171
ac_o	-406.630
ac_h	121.968

Table 4.2: Regression Coefficients for Ground Movement Expressions $\bar{\omega}_s$ and $\bar{\omega}_c$

$$S.R. = ar_g(G.R.) + ar_l(L.R.) + ar_{n2}(v)^2 + ar_{n1}(v) + \frac{ar_k}{K_o} + ar_h\left(\frac{R_o}{H_o}\right) + ar_o$$

	H_o/R_o	3.0	4.0	6.0	8.0
Crown	ar_g	0.703	0.543	0.559	0.524
	ar_l	-0.102	-0.083	-0.072	-0.068
	ar_o	4.575	4.177	5.873	4.866
	ar_{n2}	52.865	46.771	76.938	58.858
	ar_{n1}	-27.826	-24.681	-39.701	-30.736
	ar_k	-0.296	-0.275	-0.258	-0.251
	ar_h	-0.098			

	H_o/R_o	3.0	4.0	6.0	8.0
Spring Line	ar_g	0.298	0.319	0.318	0.318
	ar_l	-0.147	-0.156	-0.154	-0.152
	ar_o	0.849	0.818	0.866	0.877
	ar_{n2}	2.412	1.916	2.453	2.260
	ar_{n1}	-1.285	-1.041	-1.314	1.213
	ar_k	0.235	0.230	0.224	0.221
	ar_h	-0.058			

	H_o/R_o	3.0	4.0	6.0	8.0
Floor	ar_g	0.226	0.262	0.283	0.295
	ar_l	-0.120	-0.128	-0.137	-0.141
	ar_o	1.180	1.200	1.000	1.200
	ar_{n2}	-2.725	-2.836	-6.943	-4.168
	ar_{n1}	0.872	0.896	2.910	1.559
	ar_k	-0.342	-0.358	-0.375	-0.385
	ar_h	0.182			

Table 4.3: Regression Coefficients for Stress Ratio, S.R. Expression

$$S.R. = ar_g (G.R.) + ar_l (L.R.) + ar_{n2} (v)^2 + ar_{n1} (v) + ar_h (R_o/H_o) + ar_k / (K_o) + ar_o$$

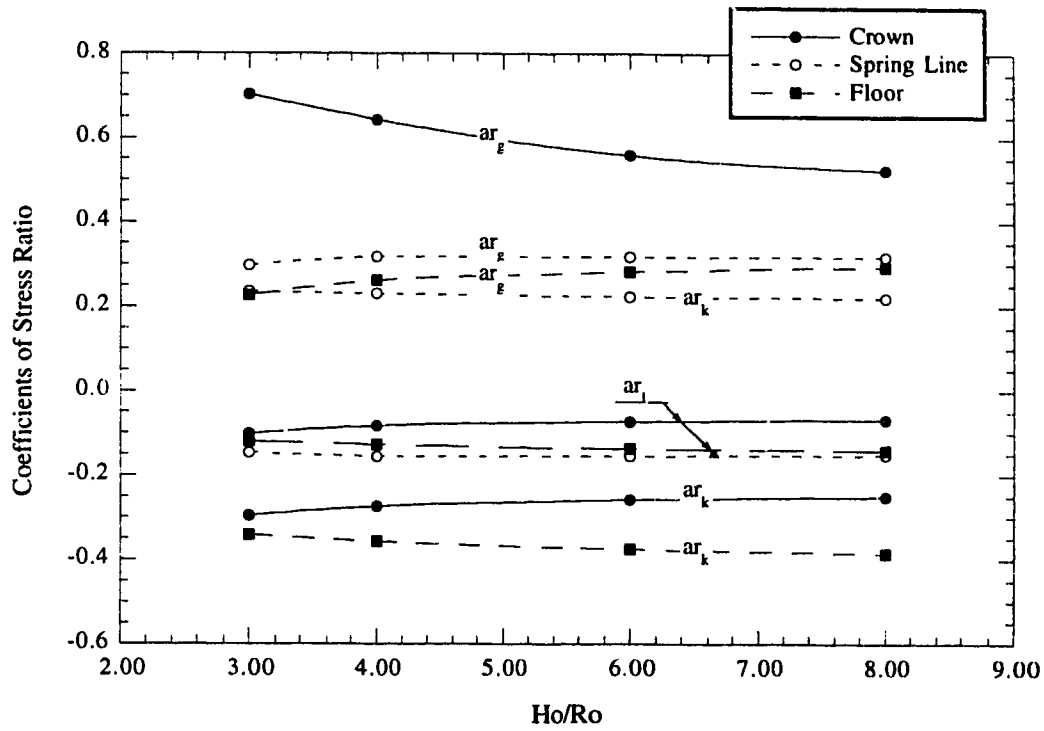
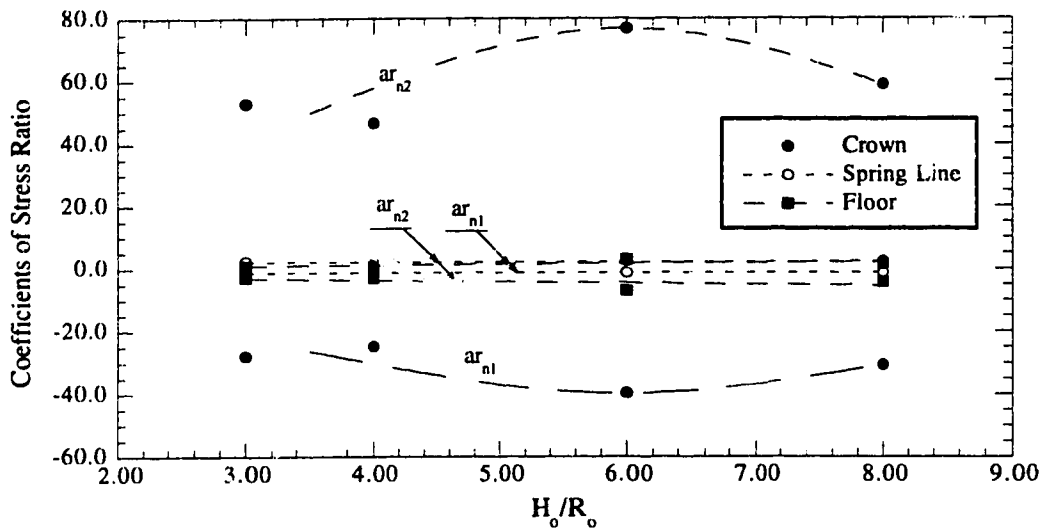


Figure 4.76: Regression Coefficients for Stress Ratio, S.R.



	ar_b
Crown	-0.100
Spring Line	-0.058
Floor	0.182

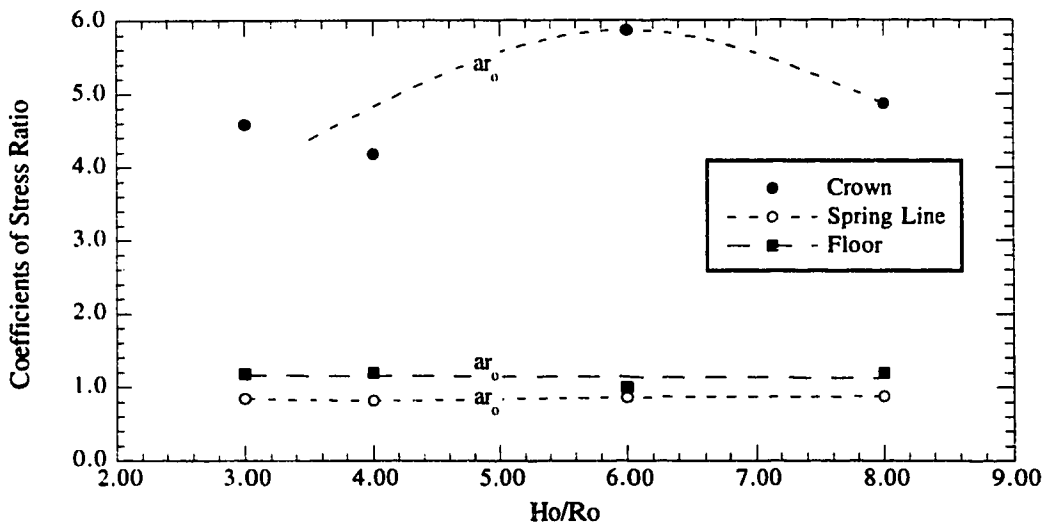


Figure 4.76: Regression Coefficients for Stress Ratio, S.R. (continued)

The evaluation of the *D.S.R.* at the point of the lining activation at the three points of the tunnel circumference (the crown, the spring line, and the floor) shows little effect on the liner pressure ratio *L.R.* . This may be attributed to the assumption that a rigid liner restrains any longitudinal movement at the point of the lining activation. The same process used in establishing the relationship between the stress ratio *S.R.* is used to define the relationship between the deviatoric stress ratio, *D.S.R.* and the various influencing parameters. The following relationship is obtained:

$$D.S.R. = ad_{g2}(G.R.)^2 + ad_{g1}(G.R.) + ad_{n2}(\nu)^2 + ad_{n1}(\nu) + \frac{ad_k}{K_o} + \frac{ad_h}{H_o/R_o} + ad_o \quad (4.22)$$

Figure 4.77 and Table 4.4 show the results of the analysis and the effect of the tunnel depth on the different obtained constants.

4.7.6 Verification

Figures 4.78 through 4.85 show the relationship between the obtained and the interpolated values of the different investigated results. A satisfactory degree of consistency is obtained in general. The least degree of consistency is met when Poisson's ratio is varied.

4.8 Conclusions

The conceptual representation of the stress field due to tunnelling is reviewed in the light of recent literature. For the case where a pressurized shield method is used in the construction, a number of adaptations have to be undertaken to readjust the concept of volume loss. The excavation may not be viewed as a cavity that generates a monotonic stress release around it, but rather as a structure that interacts with the surrounding ground by imposing pressures and displacement constraints to the boundary of the excavation. The supportive measures used in the construction system interact with each other to achieve a certain amount of internal equilibrium. The resultant of such interaction is reflected on the ground to produce stress changes around the excavation and displacements that are noticed at the the ground surface as the overall stability of the project is achieved.

Provided that the face stability is achieved, the two major loading actions imposed during the overall stability of the project are the liner pressure imposed on the liner as a

$$D.S.R. = ad_{g2}(G.R.)^2 + ad_{g1}(G.R.) + ad_{n2}(v^2) + ad_{n1}(v) + \frac{ad_k}{K_o} + ad_h \left(\frac{R_o}{H_o} \right) + ad_o$$

	H_o/R_o	3.0	4.0	6.0	8.0
Crown	ad_{g2}	0.609	0.457	0.696	0.522
	ad_{g1}	-0.686	-0.552	-0.837	-0.628
	ad_o	0.702	0.856	1.008	1.034
	ad_{n2}	7.610	8.525	9.424	9.878
	ad_{n1}	-3.992	-4.496	-4.987	-5.236
	ad_k	-0.241	-0.279	-0.318	-0.337
	ad_h	0.375			
Spring Line	H_o/R_o	3.0	4.0	6.0	8.0
	ad_{g2}	0.515	0.499	0.097	0.073
	ad_{g1}	-0.717	-1.102	0.754	-0.565
	ad_o	-0.118	-0.106	-0.151	-0.158
	ad_{n2}	-2.070	-2.074	-2.097	-2.104
	ad_{n1}	0.729	0.754	0.793	0.809
	ad_k	0.108	0.109	0.110	0.110
ad_h	0.781				
Floor	H_o/R_o	3.0	4.0	6.0	8.0
	ad_{g2}	0.475	0.639	0.601	0.451
	ad_{g1}	-0.869	-0.999	-0.973	-0.730
	ad_o	0.150	0.738	0.672	0.593
	ad_{n2}	-2.608	-2.558	-2.507	-2.482
	ad_{n1}	0.944	0.888	0.831	0.803
	ad_k	-0.589	-0.571	-0.547	-0.533
ad_h	0.566				

Table 4.4: Regression Coefficients for Deviatoric Stress Ratio, D.S.R. Expression

$$D.S.R. = ad_{g2} (G.R.)^2 + ad_{g1} (G.R.) + ad_{n2} (v)^2 + ad_{n1} (v) + ad_k/Ko + ad_h (R_o/H_o) + ad_o$$

	ad_h
Crown	0.37507
Spring Line	0.78064
Floor	0.56610

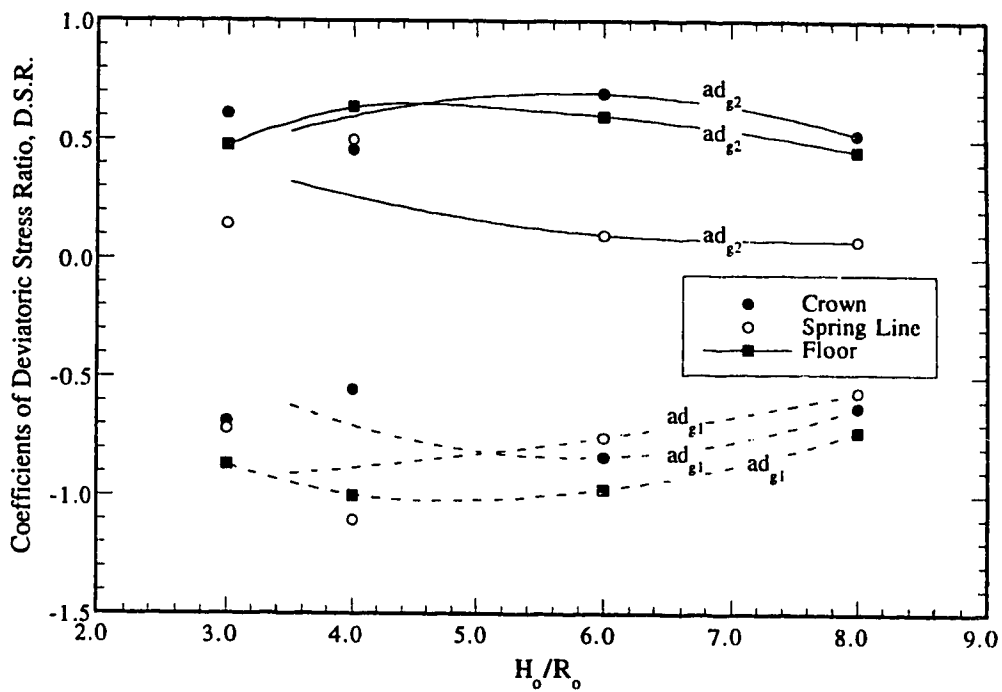


Figure 4.77: Regression Coefficients for Deviatoric Stress Ratio, D.S.R.

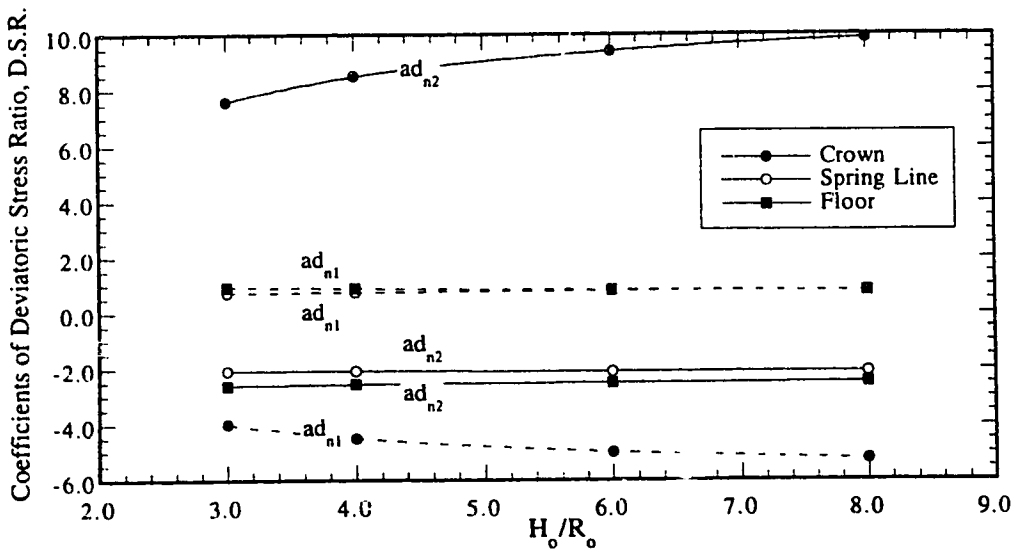
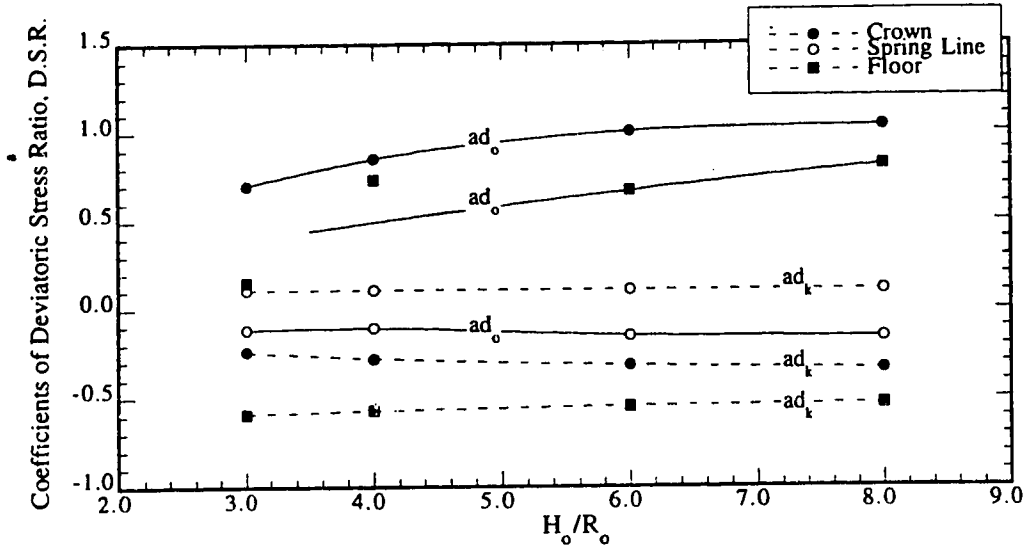


Figure 4.77: Regression Coefficients for Deviatoric Stress Ratio, D.S.R. (continued)

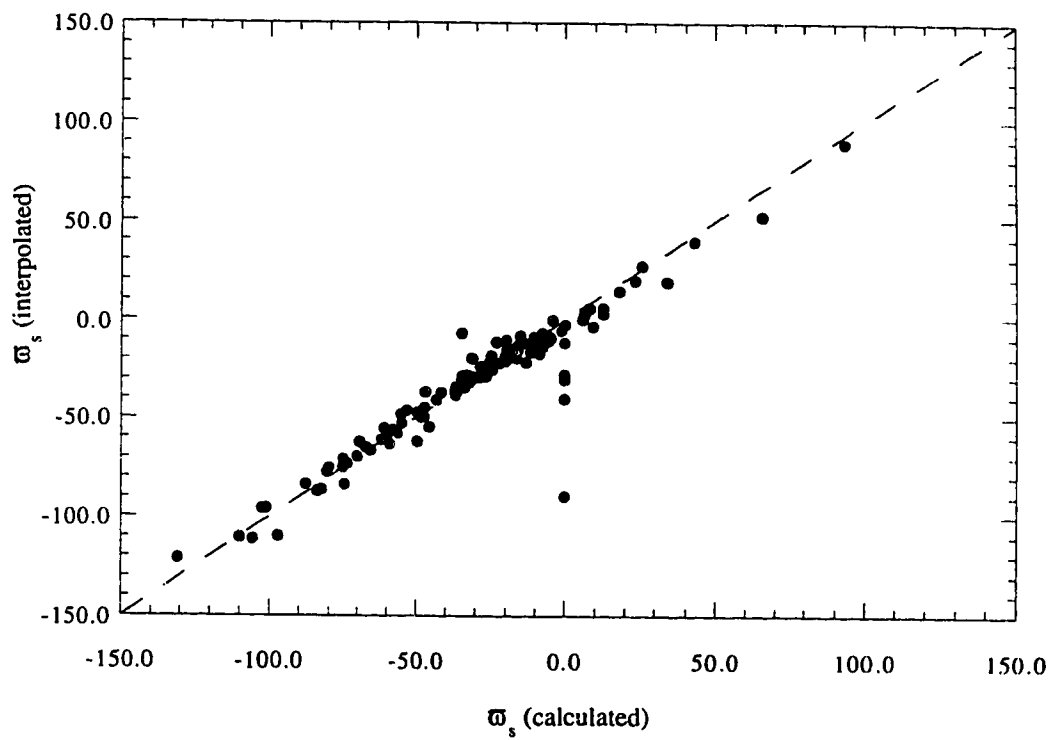


Figure 4.78: Calculated values of Normalized Surface Displacement, ϖ_s , versus Interpolated values.

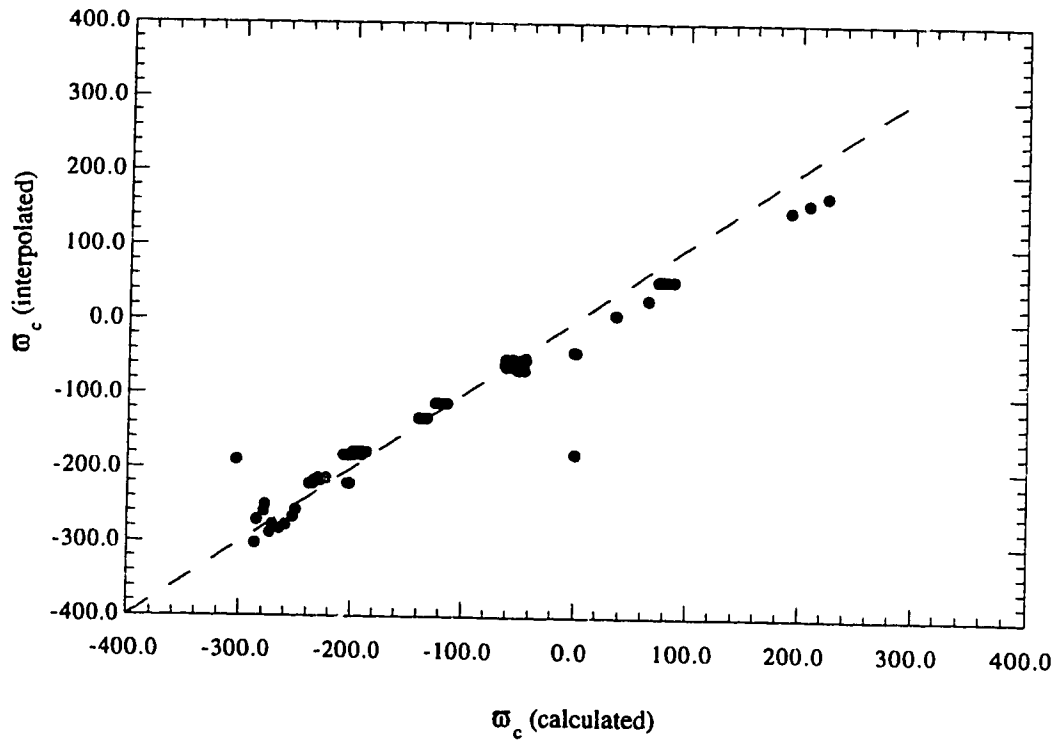


Figure 4.79: Calculated values of Normalized Crown Displacement, ϖ_c , versus Interpolated values.

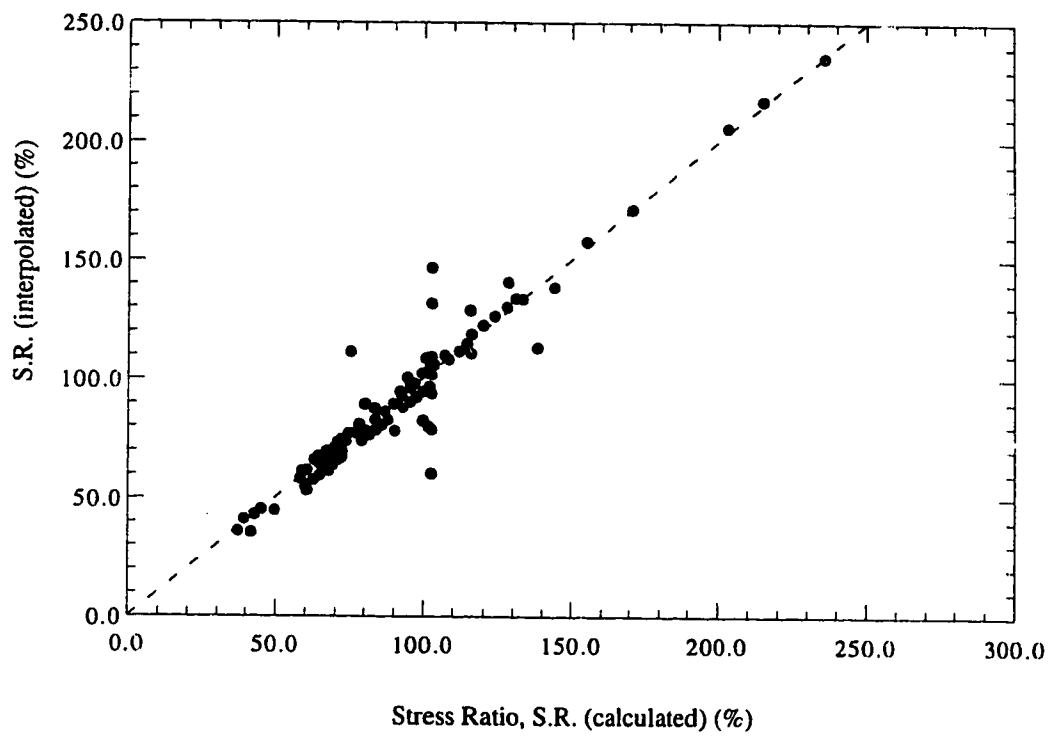


Figure 4.80: Calculated values of Stress Ratio, S.R. at the Crown versus Interpolated values.

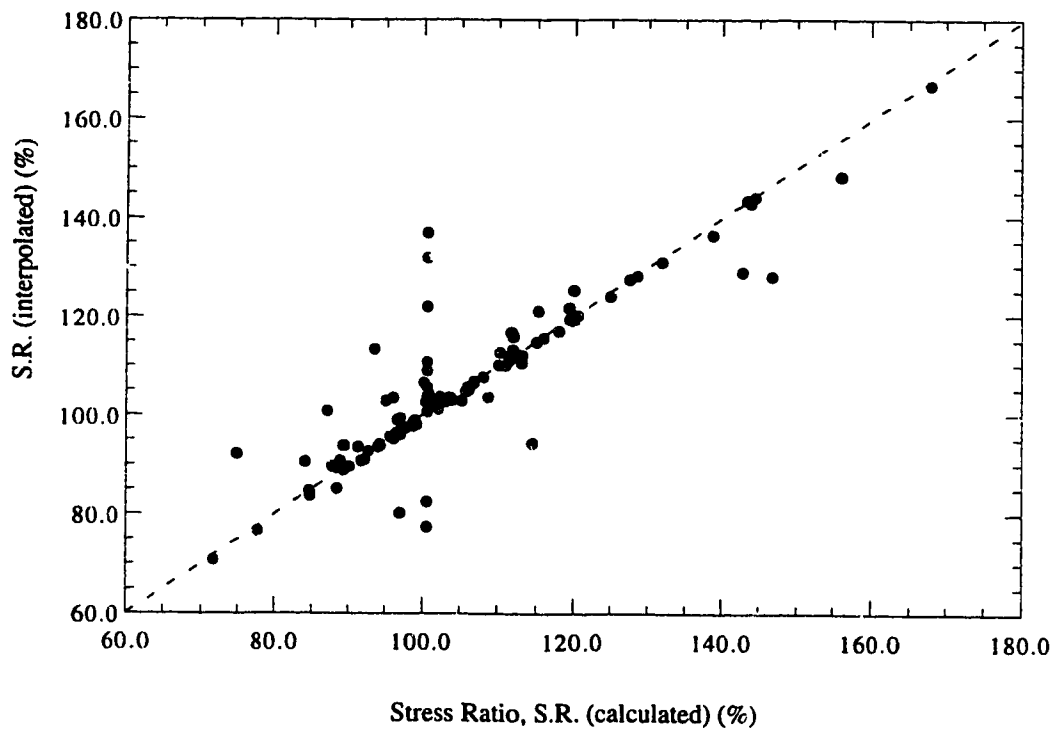


Figure 4.81: Calculated values of Stress Ratio, S.R. at the Spring Line versus Interpolated values.

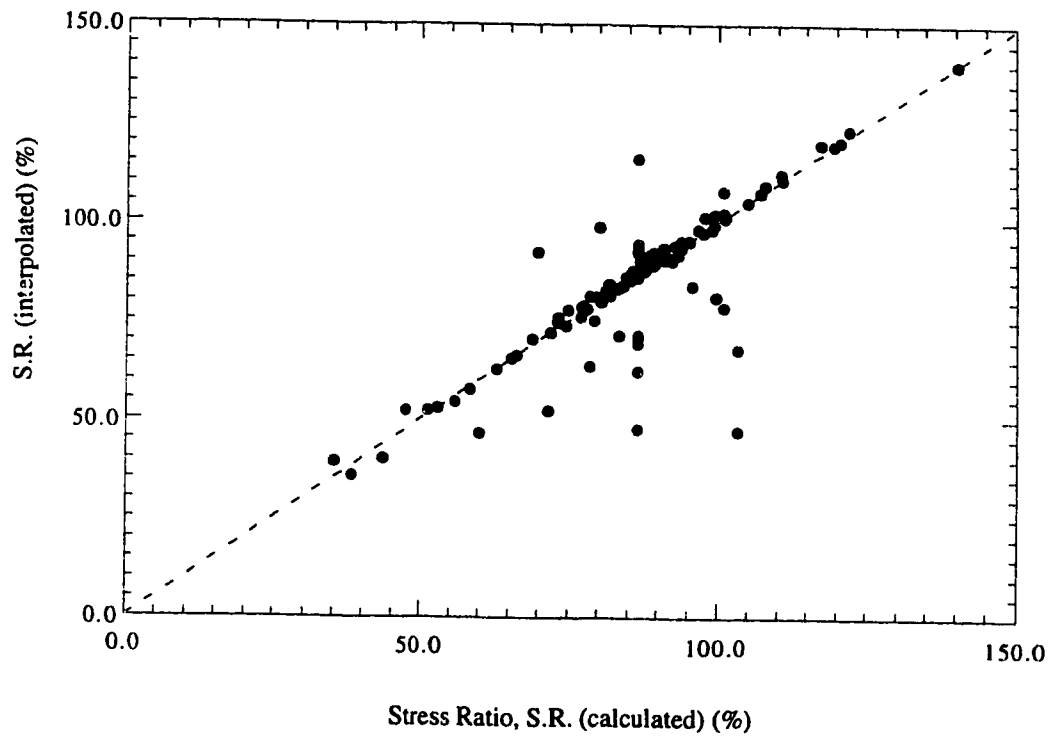


Figure 4.82: Calculated values of Stress Ratio, S.R. at the Floor versus Interpolated values.

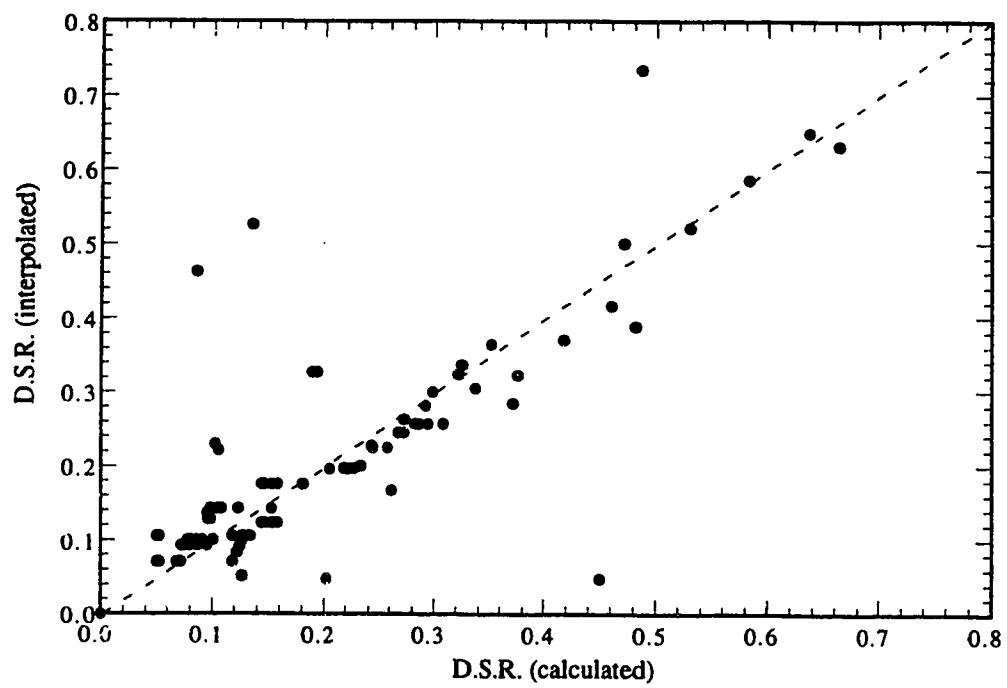


Figure 4.83: Calculated values of Deviatoric Stress Ratio, D.S.R. at the Crown versus Interpolated values.

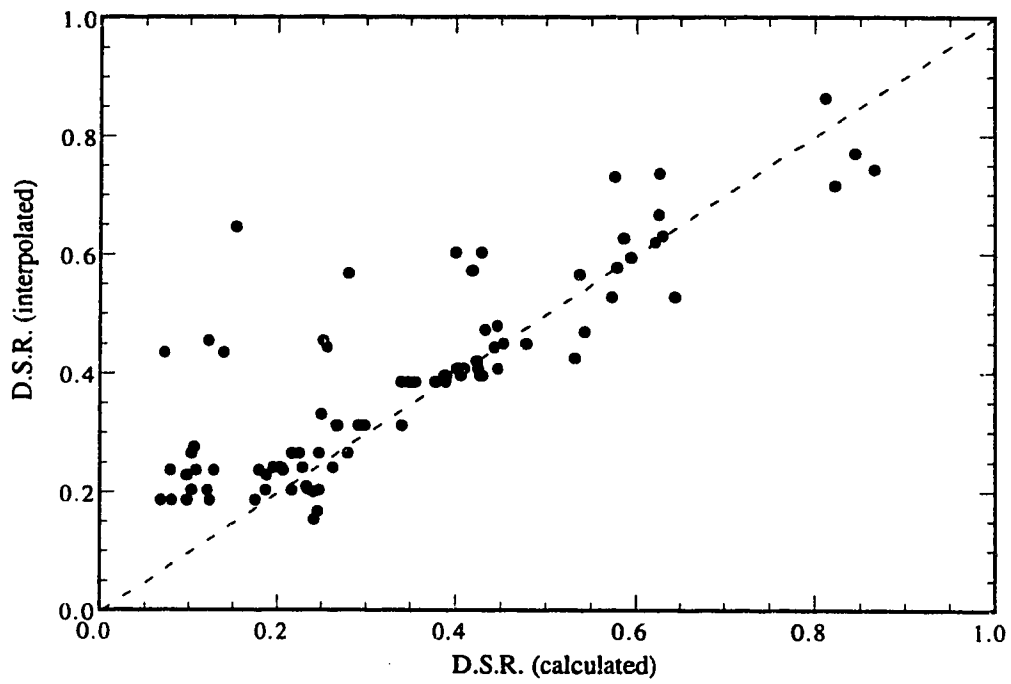


Figure 4.85: Calculated values of Deviatoric Stress Ratio, D.S.R. at the Floor versus Interpolated values.

reaction to the face pressure and the grout pressure applied behind the assembled liner. The effect of these two actions on the stress and strain field around the tunnel are investigated for different site and ground conditions. Three-dimensional finite element schemes are used in the undertaken parametric analysis. The results are presented to show the obtained ground deformation, mobilized shear strengths, and the stress paths related to various site and geological conditions. The results are analyzed such that polynomial expressions of the first or the second degree are suggested to represent the effect of the different parameters on the surface displacement, the displacement at the crown, the stress ratio, and the deviatoric stress ratio. The obtained polynomial expressions are chosen such that they best fit the total obtained results. The accuracy of these expressions depends on the number of effected runs and on the accuracy of the calculations.

The capability of carrying out a parametric analysis using three-dimensional finite element analysis are limited to the computer system's capacity. Therefore, the presented results describe quantitatively a number of relationships that are important to the design of tunnels constructed using pressurized shield methods. On the other hand, some other points are not completely clarified during the investigation, such as, the effect of the lining pressure on the mobilized shear strength near the excavation and the effect of Poisson's ratio on the displacement field. It is believed that higher computer system capabilities are required to completely investigate these points.

A three-dimensional analysis is carried out in order to investigate the effect of the longitudinal liner pressure and the grout pressure on the stress field around the tunnel and on the displacement field near the ground surface.

CHAPTER 5

DESIGN METHOD FOR TUNNELS CONSTRUCTED USING PRESSURIZED SHIELD METHODS

5.1 Introduction

A comprehensive design method of a tunnel constructed using a pressurized shield method is supposed to take into consideration the various engineering aspects of the project, specifically the geotechnical, geometrical, and structural aspects of the site. Geotechnical aspects of the site include the engineering parameters of the ground such as permeability, compressibility and shear strength parameters, as well as, the stress field existing prior to the construction. Geometrical and structural aspects of the project include the size of the excavation, its depth, and the depth of the rigid layer below it. Engineering aspects related to the construction scheme include details of the shield machinery in use, such as (1) the method of face support with respect to the intensity of the supporting pressure and the rigidity of the supporting face; (2) the arrangements of the cutting wheel; (3) the tail gap and the protective measures at the tail of the shield; (4) the material treatment of the ground whether in the form of material injection at the face or grouting behind the liner; (5) the liner properties; and (6) the selected construction sequence and the rate of advance of excavation. Safety requirements are generally concentrated around two aspects: the integrity of the project, and the safety of neighbouring structures. The integrity of the project is accomplished by designing proper support at the face and an effective shield-grout-lining system at the circumference. The acceptable limits of the settlement trough at the ground surface either regarding its magnitude or its gradient are set according to site conditions. The study of the relationship between the engineering aspects of the project including the construction method to the safety requirements is expected to be beneficiary to both the design of the construction method and that of the project. Two aspects are considered to be the main features of the tunnelling construction using pressurized shield methods: the grout pressure, and the longitudinal pressure applied to the shield (the liner pressure). The design method is verified using a well documented case study in Edmonton

during the construction of its subway system.

5.2 Framework

The objective of formulating a new design method is to investigate the effect of tunnelling construction techniques taking into account safety and the economical aspects of the project. Special emphasis is placed on soil deformation around the tunnel and at the ground surface, as well as, the straining actions applied at the liner as the two governing indices of the performance of the construction method. Pressurized shield methods, namely, the BSS method, the EPBS method, and the compressed air method, exert on the ground surrounding the excavation and on the assembled lining system a number of pressurized and supporting actions in order to restrict ground movement toward the excavation. It is, therefore, of interest to identify and evaluate the basic features of the new ground conditions that affect ground deformation and lining stresses. The attempt to adopt a deterministic approach is intended to produce a rational quantification of the effects of the various investigated parameters on the stress and strain fields in the ground. This study relies on results from numerical analyses using the finite element method in conjunction with closed form solutions. The design method is presented in a normalized form to allow the generalization of the results, and thus to enhance usefulness in the design of shallow tunnels. This method is summarized in a systematic scheme and a computer program is provided to facilitate its application with minimal computational effort.

5.3 Tunnel Lining Design

While the initial state of stress is determined according to soil density at the tunnel site, the depth ratio, and the coefficient of lateral pressure at rest, K_0 , the excavation process results in disturbing these initial conditions. Using the concept of volume loss, disturbance of the initial stress conditions is described as a reduction of the radial stresses at the tunnel circumference which is referred to as the stress relief. Factors affecting the stress changes during the construction process are the mechanical properties of the soil (shear strength and compressibility) and the construction method. Once the lining system is assembled to cover the entire tunnel circumference, the lining is in position to start interacting with the surrounding ground: the lining activation point. Stresses inside the lining and around it, in the surrounding soil, undergo readjustments related to the developed strain field in order to reach a state of equilibrium. The process of ground-liner interaction is affected by the lining properties, such as, flexibility and compressibility, in addition to, the factors affecting stress changes during the construction stage.

In general, methods of tunnel lining design emphasized in the stage of the ground-

liner interaction as a solution to the problem could be reached using a simple two dimensional analysis. A realistic assumption has to be taken into account regarding the stress disturbance at the construction stage. Peck (1969) and Peck et al. (1972) give a comprehensive description of the modes of deformation during the ground-liner interaction and stress the fact that the lining loads should not be exclusively calculated according to classical states of active, passive, or lateral earth pressure at rest because the distribution of stresses acting at the lining is affected by the deformation of the liner and that of the ground. They also present records of measurements in a number of constructed tunnels showing that the actual pressure immediately after construction is lower than the overburden pressure. Furthermore, a number of methods are developed to estimate stress and strain during the ground-liner interaction stage such as those described in Bull (1944), Eason (1983), Muir Wood (1975), Morgan (1961), Ebaid and Hammad (1978), Duong and Erdmann (1982) and Duddeck (1991), Eisenstein et al. (1981), O'Rourke (1985) and (1984), Evison (1988), and El-Nahas et al. (1992) among others. The various methods of lining design will be addressed separately. Two critical points are to be examined in any lining design method: how much is the actual magnitude of the soil loads on the liner, and how is it distributed along the lining circumference at the starting point of the ground-liner interaction.

5.3.1 Loading Conditions before Ground-liner interaction Stage

One method used in estimating the magnitude of liner pressure is applied in deep tunnelling and is based on the arching theory (Terzaghi, 1943) by relating the imposed pressure on the lining to a ground region extending ηD above the crown where η is an empirical constant defined according to site conditions. The value of η depends on the shear resistance of the soil mass and the characteristics of the fissures in a rock mass. For example, El-Nahas (1980) and Branco (1981) present an estimation of this constant for two tunnelling projects. For shallow tunnels the problem is more complex as the gravitational stress field, the free boundary at the ground surface, and the three-dimensional effect related to the method of construction play a role in determining the liner pressure at the start of the interaction process. Few design recommendations are available in this domain. Peck (1969) reports that, according to records of measurements in a number of tunnels, the magnitude of the liner pressure after stress relief at the construction stage could be as low as 20%. Since the amount of stress relief is unquantifiable, he suggests that it would be a safe assumption to let the magnitude of the lining load be equal to the full overburden pressure, γH_0 , bearing in mind, at the same time, that lining stresses tend to approach the original overburden pressure in the long term. On the other hand, Muir Wood

1975) suggests that the liner pressure may be taken as one half the overburden pressure and he quotes that Panet (1973) suggests that two thirds of the overburden pressure is acting on the liner as the stress field at the face is not effectively conforming to the assumed plane strain condition. The above two suggestions may be accepted when compared with the case histories shown by Peck (1969). As pointed out by Muir Wood (1975), the conducting of three-dimensional analysis is inevitable if the magnitude of liner pressure is to be reliably determined. Negro (1988) presents a study using the finite element method to estimate the effect of the delay distance on the liner pressure. The results of the analysis are generalized and they are included in Eisenstein-Negro method previously mentioned.

The method of face-support application, if used, has an effect on the magnitude of stresses imposed on the lining. Peck (1969) shows the effect of using compressed air on the tunnel lining. Figure 5.1 shows a sketch of the relationship between the average ring load and the ground deformation around the lining. As the soil moves radially toward the tunnel, the ring load reduces (**Line AD**). A certain amount of displacement takes place before the face, δ_a , and during the delay period, δ_b . At **Point C** the lining interacts with the surrounding soil and reaches equilibrium at **Point C'**. The effect of air pressure is to reduce temporarily the ring load until the air pressure is released. Based on Eisenstein (1993), Figure 5.2 shows the relationship between the radial displacement and the magnitude of pressure at the crown of a tunnel under construction using the EPBS method. As the shield has the effect of pushing the ground in the longitudinal direction at the face, radial pressure increases linearly (**Line ab**) and then nonlinearly (**Line bc**) because of soil yielding. Stress reduction takes place behind the tail of the shield (**Line cd**) until the liner is assembled and interacting with the effect of the grouting and the ground conditions. At **Point d** ground-liner interaction starts as the soil and the liner movements become compatible. The assessment of the actual loading magnitude acting on the liner before the ground-liner interaction process is subject to numerous investigations regarding its relationship with the construction process. Guidelines for the design of tunnels presented by ITA¹ (1988) confirm that liner loading is to be reduced when construction methods are relying on new shield technology.

The distribution of soil pressure around the liner is affected by the change in the magnitude of the liner pressure. A starting point is to assume that the reduction in overburden pressure is evenly distributed around the tunnel and that the same coefficient of lateral pressure at rest, K_0 , is, therefore, still acting. Suggestions regarding this question are even less frequent than those regarding the change in the magnitude of the liner pressure. This is due to the fact that the pressure distribution at the point of lining

¹International Tunnelling Association.

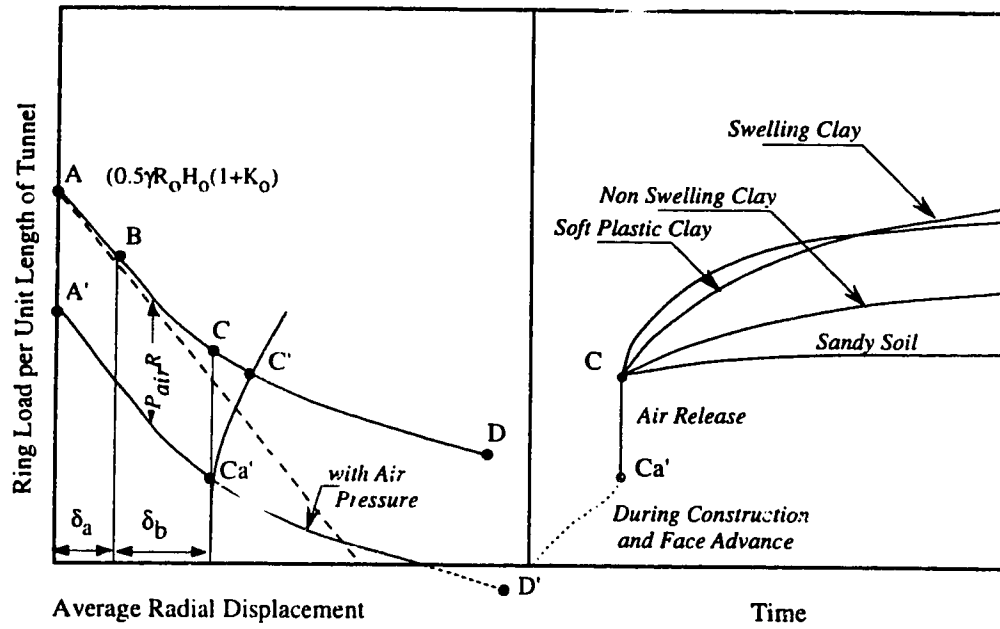


Figure 5.1: Influence of Compressed Air Pressure on the Ground Reaction Curve (after Peck (1969))

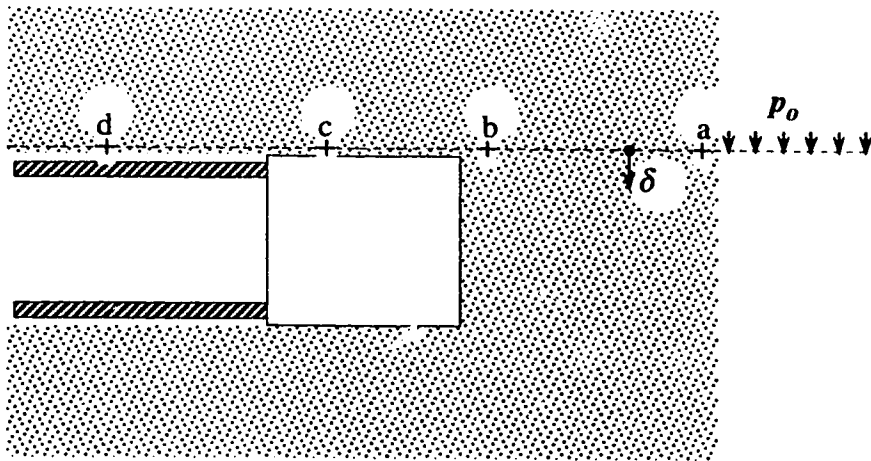
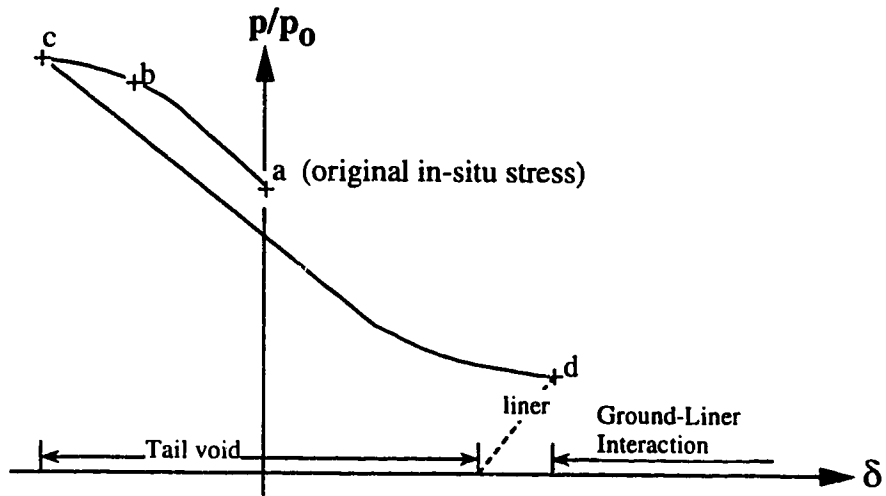


Figure 5.2: the Ground Reaction Curve for the Earth Pressure Balanced Shield (after Eisenstein 1993)

activation is only an intermediate stage between the initial in situ stress distribution and the final distribution after the ground-liner interaction. Site conditions render the problem substantially complex as the distribution is affected by a number of factors that are difficult to quantify such as the distribution of grout pressure and the sequence of applying it, the overall movement of the tunnel, and the friction between the extrados of the shield (if used) and the ground. Some closed form solutions based on the continuum model, such as, those presented by Ranken (1978), Einstein and Schwartz (1979), Matsumoto and Nishioka (1991), and Hartmann (1985) modify this assumption by adopting an initial pressure distribution related to an already excavated elastic space. Such modification is a step forward toward a more realistic representation of the actual stress field. On the other hand, Muir Wood (1975) suggests that the amount of stress relief around the tunnel is evenly distributed, thus the initial stress distribution at the liner is maintained. Figure 5.3 shows a number of loading-condition distributions used by a number of authors. From the figure, Rosza (1963) considers the spring model where the tunnel liner supports vertical load at its the upper portion and transfers it to a number of springs distributed along the lower part of the circumference. According to Szechy (1973), Bugayeva (1951) follows an approach similar to that of the Morgan-Muir Wood-Curtis method by predefining a trigonometric function describing radial soil reaction to certain vertical loading conditions. Only the magnitudes of reactions at the floor and at the spring line verify the equilibrium conditions. Windels (1966) and Schulze and Duddeck (1964) consider the influence of gravity at the upper half of the tunnel while maintaining symmetry around the horizontal centre of the tunnel. Similar to Rosza (1963) and Bugayeva (1951), partial embedment at the upper quarter is assumed. Evison (1988) applies a more realistic loading condition by using the closed form solution of Ranken as the loading condition acting on a number of ring-and-spring models including cases of full and partial embedment. The effect of tangential springs is also investigated in the study. Okada et al. (1989) show a loading condition considering partial embedment at the top and at the bottom of the liner while the loading distribution is kept equal to the initial conditions.

A number of assumptions are made regarding the initial liner pressure distribution but few of them take into account the effect of the construction process. An interesting centrifuge experiment may be considered to demonstrate such effect. Tohda et al. (1988) considers the stress distribution around a rigid pipe during a centrifuge test. While the pipe and the soil properties are the same, two cases of construction conditions are employed. During Case A, a sheet pile is originally inserted and then it is retracted while the centrifuge loading is applied. Case B is performed without disturbing the soil mass. The fact that the pipe is relatively rigid excludes the effect of the ground-liner interaction. As Figure 5.4

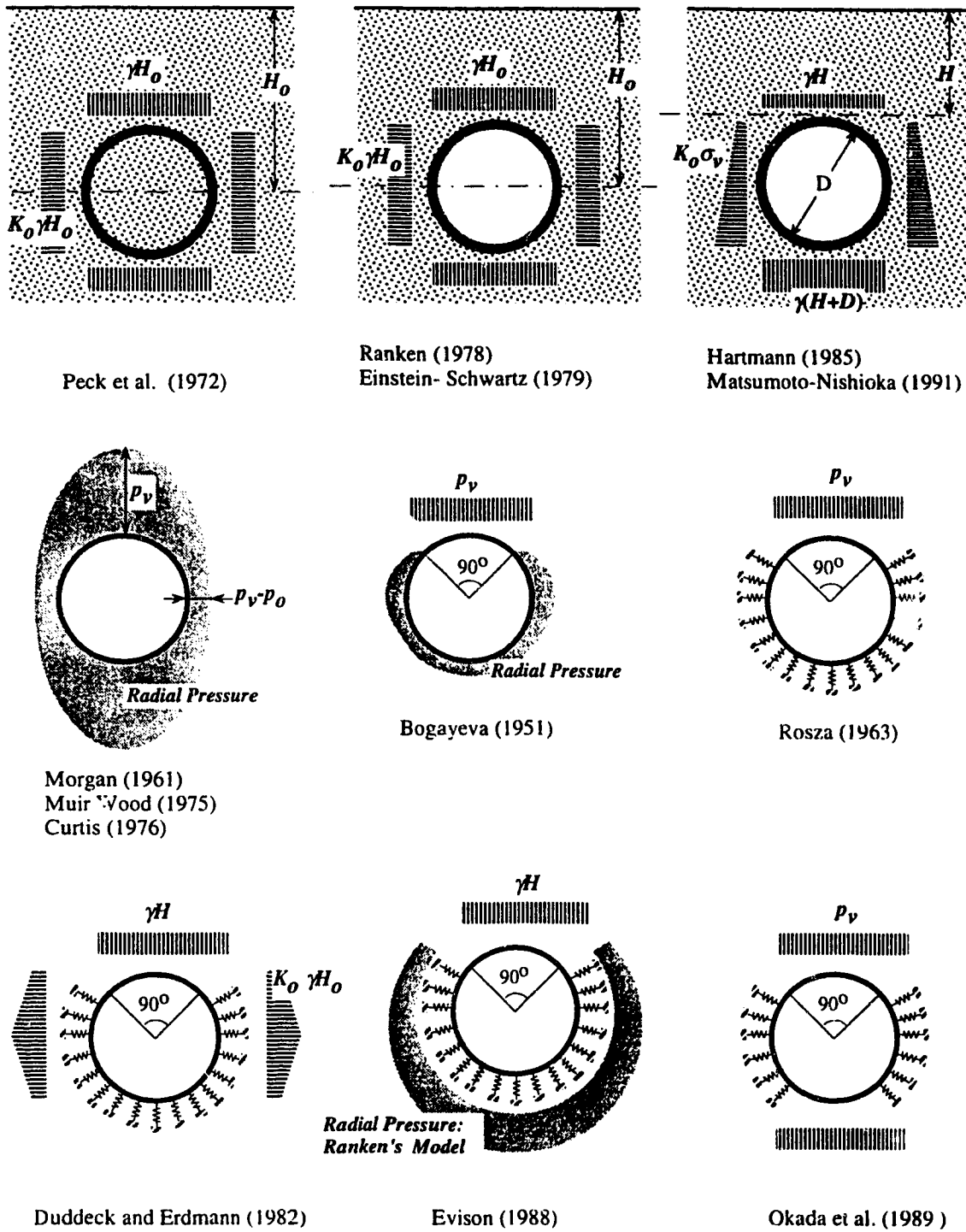


Figure 5.3: Loading Conditions for Different Structural Models of Circular Tunnels

shows, the two cases yield a different distribution for the initial pressure. Although the retraction of sheet piles is not a simulation of a usual tunnelling construction process, the results of the experiment show that the method of application of gravity forces on a rigid liner (i.e. without the effect of ground-liner interaction) has an effect on the initial distribution of ground pressure on the liner. The obtained distributions are not necessarily related to the conceptual stress field calculated using K_0 .

In conclusion, loading conditions upon which the tunnel liner is subjected before the stage of the ground-liner interaction are influenced both in their magnitude and distribution by the construction process. While common design practice acknowledges such influence, the evaluation of the design loads relies, in many cases on empiricism, intuition, and on engineering judgment.

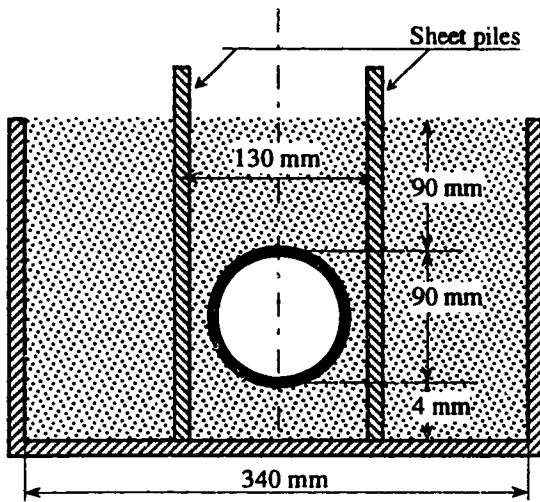
5.3.2 Structural Models for Tunnel Design

Based on the fact that the assessment of straining actions inside the tunnel liner has to consider the mechanical properties of both the soil and the liner materials, a number of structural models are developed to study the resultant interaction process. Duddeck and Erdmann (1982) present a review of a number of design methods. Three structural models are commonly used in tunnel design: the continuum model, the continuum approach with a predefined deformation mode, and the bedding beam model.

5.3.2.1 Elastic Continuum Model

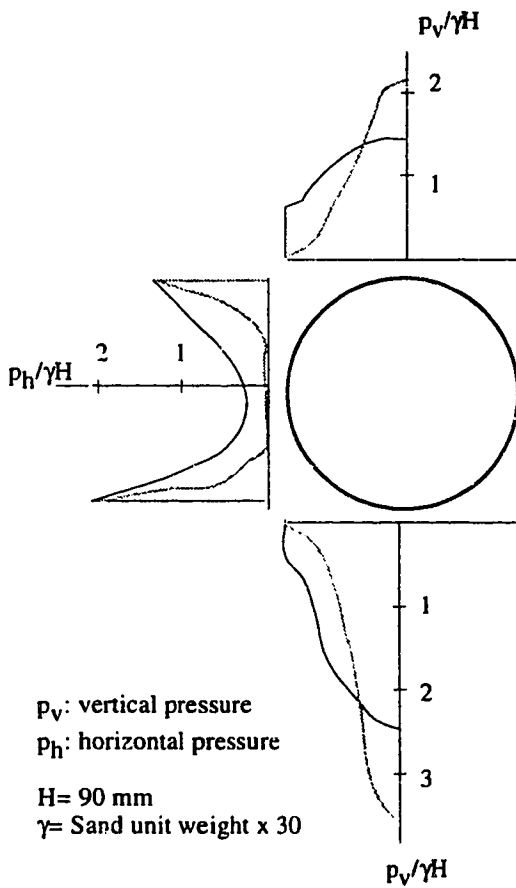
The continuum model has the advantage of simulating both the soil and the liner in their proper dimensions. However, the mathematical complexity involved in the derivations, results in a number of assumptions that have to be taken. Two basic assumptions are commonly present in the continuum solutions: the soil mass and the liner are linearly elastic and the plane strain condition prevails initially. Peck et al. (1969) modifies the one dimensional form of Burns and Richards (1964) for the case of air blast loading for protective structures to include the effect of the horizontal loading condition which is not necessarily equal to the vertical pressure. The final solution does not include the effect of shear stresses between the extrados of the liner and the ground. Relative properties of the liner, with respect to the ground are expressed in terms of the compressibility and the flexibility ratios, C and F respectively:

$$C = \frac{ER_o(1 - \nu_l^2)}{E_l t(1 + \nu)(1 - 2\nu)} \quad , \quad (5.1)$$



Soil Properties:

Specific Gravity	2.65
Grain Size	0.24 to 1.4 mm
Coefficient of Uniformity	1.75
Dry Density	15.21 kN/m ³
Cohesion	0
Angle of Internal Friction	47°



Case A: sheet piles retracted during loading
 Case B: No Disturbance during centrifuge loading

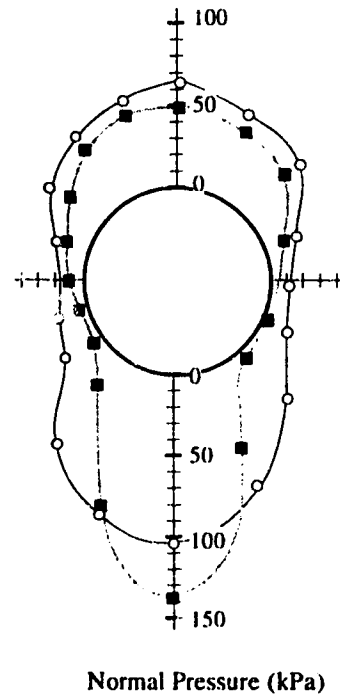


Figure 5.4: Centrifuge test results on Rigid Pipe in Dense Sand (after Tohda et al. 1988)

and

$$F = \frac{ER_o^3(1 - \nu_l^2)}{6E_l I_l(1 + \nu)} \quad , \quad (5.2)$$

where:

t is the liner thickness,

I_l is the moment of inertia of the liner cross section,

E and E_l are the elastic moduli of the ground and the liner respectively, and

ν and ν_l are Poisson's ratios of the ground and the liner, respectively.

Ranken (1978) stresses the loading condition of gravity forces by differentiating between the two methods of simulation: excavation and overpressure. In the case of overpressure, the continuum stress field is applied externally on the liner section which, in a way, represents a case of "switch on gravity". On the other hand, excavation simulation considers the stress field of an unperforated half space, then it annuls the resulting deformations before including the excavation and liner effects. As a result, it gives lower and more realistic values of straining actions in the liner. The final solutions cover a number of cases of practical use, such as, loading conditions (overpressure or excavation), liner thickness, and shear interface (full slippage conditions versus no slippage conditions). Einstein and Schwartz (1979) present, simultaneously, a similar solution and introduce a modification to the compressibility and flexibility ratios to include the effect of the excavation loading condition:

$$C^* = \left(\frac{1 - 2\nu}{1 - \nu} \right) C \quad , \quad (5.3)$$

and

$$F^* = \left(\frac{6}{1 - \nu} \right) F \quad . \quad (5.4)$$

The above mentioned solutions deal with conditions in a deep tunnel. Vertical pressure applied at the crown, as well as, that applied at the floor are equal to the average pressure which is normally the ground pressure at the centerline of the tunnel. Hartmann (1970 and 1985) quoted from Negro (1988:1117) introduces the effect of a gravitational gradient

related to shallow tunnel conditions. Here, only the no slip condition, and the excavation loading condition are considered. Straining actions in the liner are calculated using Flügge's differential equations for cylindrical shells. Relative liner properties are expressed in the form of incompressibility and rigidity ratios, $\dot{\alpha}$ and β .² respectively, which could be related to C^* and F^* defined by Einstein and Schwartz (1979) in Equations 5.3 and 5.4 as:

$$\dot{\alpha} = \frac{I}{C^*(1-\nu)} \quad , \quad (5.5)$$

and

$$\beta = \frac{I}{F^*(1-\nu)} \quad . \quad (5.6)$$

Hartmann's solution is shown in Figure 5.5, and the symbols used in the final derivation are explicitly defined in Figure 5.5 (a). From the figure, as a result of including the effect of gravity stress gradient while the liner is assumed to be weightless, the tunnel is supposed to perform an upward movement due to buoyancy. Engineering judgment is necessary to decide whether to include this heaving action based on the construction method. It is to be noted also that Matsumoto and Nishioka (1991) present a solution for tunnel-liner interaction that includes the effect of stress gradient due to gravity, but a presumed printing error³ does not allow the verification of their solution with that of Hartmann.

As a general remark, continuum models have the advantage of considering a number of practical aspects that affect the ground around the liner and the ground-liner interaction. Excavation type of loading, the gravitational stress field, and shear stresses at the interface between the liner and the ground are modeled. On the other hand, the complexity of the mathematical derivation does not allow the consideration of constitutive models other than the linear elastic model for both the ground and the liner. Also, the free boundary condition at the ground surface is not simulated, therefore, the obtained stress and strain fields, even if the stress gradient due to gravity is considered, cannot be accurately calculated at points relatively distant from the tunnel.

²In Negro's thesis, the ratios $\dot{\alpha}$ and β are named the compressibility and flexibility ratios. It was decided to use different names for them as they are the inverse of the compressibility and flexibility ratios, C and F defined by Peck and by Einstein and Schwartz.

³Constant b_3 is not defined (page 180).

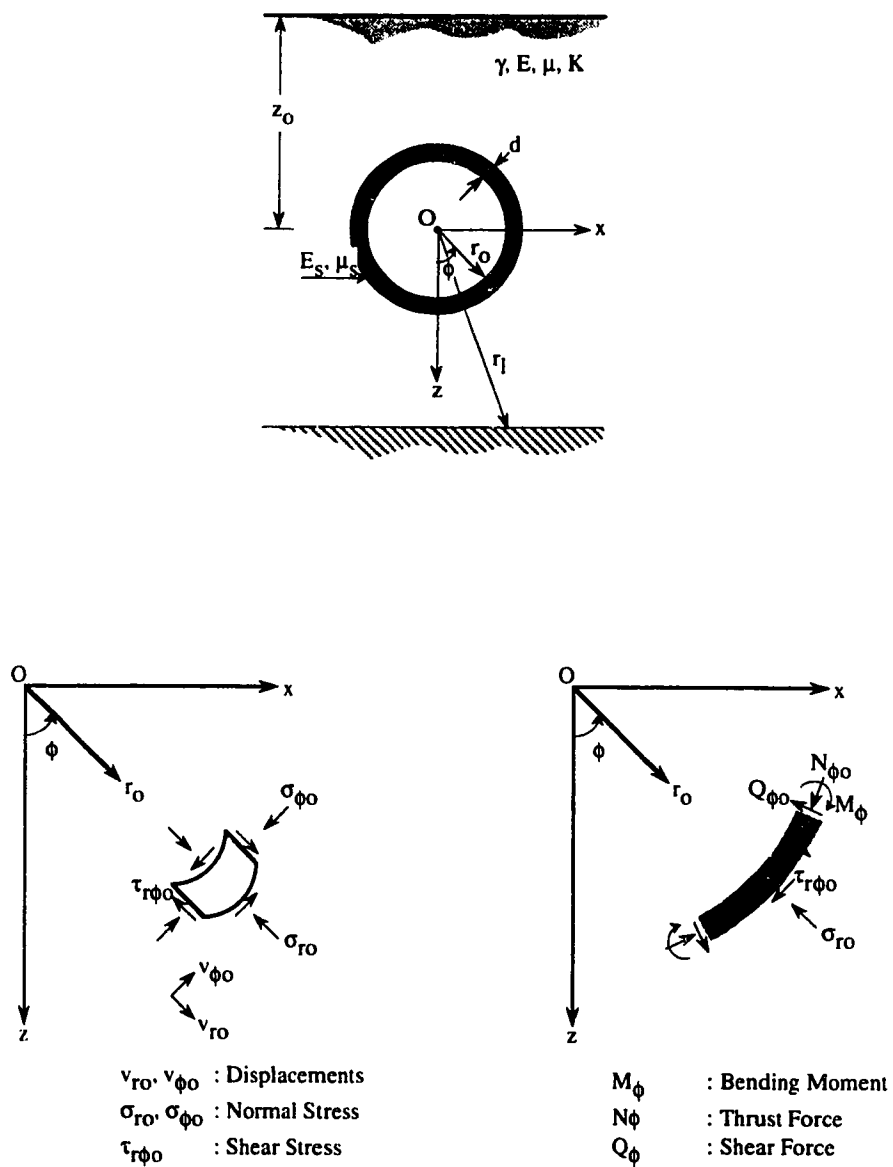


Figure 5.5 a) Notations and Conventions used in Hartmann's Solutions (after Negro 1988: 7.1)

$$\alpha = \frac{E_s(1+\mu)}{E_r\alpha(1-\mu_s^2)} \quad \beta = \frac{E_s I_s(1+\mu)}{E_r r_s^3(1-\mu_s^2)}$$

$$\sigma_m = \frac{(1+K)(\alpha+\beta)}{2(1+\alpha+\beta)} \gamma_{r_0} + \frac{\alpha(1+K)}{4(1+\alpha)} \gamma_{r_0} \cos\phi - \frac{(1-K)(3-4\mu)(\alpha-9\beta-12\alpha\beta)}{2(1+\alpha(3-2\mu)+3\beta(5-6\mu+4\alpha(3-4\mu)))} \gamma_{r_0} \cos(2\phi) - \frac{(1-K)(3-4\mu)(\alpha-32\beta-72\alpha\beta)}{4(1+\alpha(5-4\mu)+8\beta(7-8\mu+9\alpha(3-4\mu)))} \gamma_{r_0} \cos(3\phi)$$

$$\sigma_{\phi_0} = \frac{(1+K)(2+\alpha+\beta)}{2(1+\alpha+\beta)} \gamma_{r_0} + \frac{2+\alpha+(K-\mu-\mu K)(4+3\alpha)}{4(1-\mu)(1+\alpha)} \gamma_{r_0} \cos\phi - \frac{(1-K)(4+\alpha(3+4\mu)+3\beta(11-12\mu+4\alpha(3-4\mu)))}{2(1+\alpha(3-2\mu)+3\beta(5-6\mu+4\alpha(3-4\mu)))} \gamma_{r_0} \cos(2\phi) - \frac{(1-K)(4+\alpha(5+4\mu)+8\beta(16-16\mu+9\alpha(3-4\mu)))}{4(1+\alpha(5-4\mu)+8\beta(7-8\mu+9\alpha(3-4\mu)))} \gamma_{r_0} \cos(3\phi)$$

$$\tau_{\phi_0} = \frac{\alpha(1+K)}{4(1+\alpha)} \gamma_{r_0} \sin\phi - \frac{\alpha(1-K)(3-4\mu)(1+6\beta)}{1+\alpha(3-2\mu)+3\beta(5-6\mu+4\alpha(3-4\mu))} \gamma_{r_0} \sin(2\phi) - \frac{3\alpha(1-K)(3-4\mu)(1+24\beta)}{4(1+\alpha(5-4\mu)+8\beta(7-8\mu+9\alpha(3-4\mu)))} \gamma_{r_0} \sin(3\phi)$$

$$v_m = v_m^* + v_{z_0}^* \cos\phi$$

$$v_{\phi_0} = v_{\phi_0}^* + v_{z_0}^* \sin\phi$$

$$v_m^* = -\frac{1+\mu}{E} \left(\frac{1+K}{2(1+\alpha+\beta)} \gamma_{r_0}^2 \cos\phi + \frac{1+K}{8(1+\alpha)} \gamma_{r_0}^2 \cos^2\phi + \frac{(1-K)(3-4\mu)(1+2\alpha)}{2(1+\alpha(3-2\mu)+3\beta(5-6\mu+4\alpha(3-4\mu)))} \gamma_{r_0} r_0 \cos(2\phi) - \frac{(1-K)(3-4\mu)(1+3\alpha)}{8(1+\alpha(5-4\mu)+8\beta(7-8\mu+9\alpha(3-4\mu)))} \gamma_{r_0}^2 \cos(3\phi) \right)$$

$$v_{z_0}^* = \frac{(1+\mu)(3-4\mu)}{4E(1-\mu)} \gamma_{r_0}^2 \ln\left(\frac{r_0}{r_1}\right)$$

$$v_{\phi_0}^* = \frac{1+\mu}{E} \left(-\frac{1+K}{8(1+\alpha)} \gamma_{r_0}^2 \sin\phi + \frac{(1-K)(3-4\mu)(1+\alpha+3\beta)}{2(1+\alpha(3-2\mu)+3\beta(5-6\mu+4\alpha(3-4\mu)))} \gamma_{r_0} r_0 \sin(2\phi) + \frac{(1-K)(3-4\mu)(1+\alpha+16\beta)}{8(1+\alpha(5-4\mu)+8\beta(7-8\mu+9\alpha(3-4\mu)))} \gamma_{r_0}^2 \sin(3\phi) \right)$$

$$N_{\phi} = \frac{(1+K)(\alpha+\beta)}{2(1+\alpha+\beta)} \gamma_{r_0} r_0 + \frac{\alpha(1+K)}{4(1+\alpha)} \gamma_{r_0}^2 \cos\phi - \frac{(1-K)(3-4\mu)(\alpha+3\beta+12\alpha\beta)}{2(1+\alpha(3-2\mu)+3\beta(5-6\mu+4\alpha(3-4\mu)))} \gamma_{r_0} r_0 \cos(2\phi) - \frac{(1-K)(3-4\mu)(\alpha+4\beta+36\alpha\beta)}{4(1+\alpha(5-4\mu)+8\beta(7-8\mu+9\alpha(3-4\mu)))} \gamma_{r_0}^2 \cos(3\phi)$$

$$M_{\phi} = -\frac{\beta(1+K)}{2(1+\alpha+\beta)} \gamma_{r_0}^2 + \frac{3\beta(1-K)(3-4\mu)(1+2\alpha)}{2(1+\alpha(3-2\mu)+3\beta(5-6\mu+4\alpha(3-4\mu)))} \gamma_{r_0}^2 \cos(2\phi) + \frac{\beta(1-K)(3-4\mu)(1+3\alpha)}{1+\alpha(5-4\mu)+8\beta(7-8\mu+9\alpha(3-4\mu))} \gamma_{r_0}^3 \cos(3\phi)$$

$$Q_{\phi} = -\frac{3\beta(1-K)(3-4\mu)(1+2\alpha)}{1+\alpha(3-2\mu)+3\beta(5-6\mu+4\alpha(3-4\mu))} \gamma_{r_0} r_0 \sin(2\phi) - \frac{3\beta(1-K)(3-4\mu)(1+3\alpha)}{1+\alpha(5-4\mu)+8\beta(7-8\mu+9\alpha(3-4\mu))} \gamma_{r_0}^2 \sin(3\phi)$$

Figure 5.5 b) Hartmann's Solution (after Negro 1988: 7.1)

5.3.2.2 Elastic Continuum Model with Predefined Mode of Deformation (Muir Wood's model)

The mathematical effort in deriving closed form solutions can be reduced if simplifying assumptions are taken regarding the mode of deformation of the liner. Morgan (1961) proposes an elliptical shape for the deformed liner. Consequently, straining actions and displacement of the liner are calculated by solving the equilibrium and compatibility equations between an infinite space representing the ground and a smooth stiff membrane representing the liner. Muir Wood (1975) corrects an error in Morgan's solution regarding the plane-strain assumption and adds to the solution the effect of shear forces between the ground and the liner. Curtis (1976) in his turn, includes in the solution the effect of deformation due to shear stresses at the ground-liner interface. The method, also, described as the intuitive continuum method, has found acceptance because of its simplicity, and this method is applied in tunnel design especially in the United Kingdom (Duddeck and Erdmann, 1982). Ebaid and Hammad (1978) demonstrate that the method gives generally lower estimations of liner-straining actions when compared with other methods.

5.3.2.3 Ring-and-Spring Model

The spring and ring method is widely used in Germany and has the advantage of replacing the ground space by a well-known structural element: the spring. The loading condition, as well as the stiffness and the number of springs has to be carefully chosen to represent actual ground conditions. Partial embedment (refer to Figure 5.3) is a commonly used assumption in order to avoid simulating tensile reaction at the crown region. Basically, there is correspondence between the elastic spring and ring method and the elastic continuum method and if the proper assumptions have been taken, it can be believed that the same results may be reached (Evison (1988). At the same time the absence of ground space from the model does not allow the calculation of stresses or strains within the soil mass. This is true also in the case of the elastic continuum model with a predefined mode of deformation (Muir Wood's model).

5.3.3 Adaptation of Hartmann's Solution to Eisenstein-Negro Method of Tunnel Design

The advantages of Hartmann's solution allow it to be incorporated into the Eisenstein-Negro method of design for shallow tunnels. These advantages may be summarized as follows (Negro, 1988):

- (1) the solution is derived for linearly elastic ground conditions, however, non linear behaviour can be incorporated by using reduced values for the elastic parameters;
- (2) the stress relief due to the construction process can be simulated by using reduced values of gravity, (γ_{red});
- (3) the initial loading condition takes into account the gravitational gradient, lateral pressure at rest, and excavation loading method of simulation; and
- (4) the reduction of the lining perimeter will result in an increase of curvature and thus of the development of additional bending moment even in the case of the ideal isotropic conditions. This effect is included as second order terms in the final derivation.

The method is verified by comparison with other closed form solutions in Negro (1988:1126) and shows acceptable agreement with solutions of Windels (1967), Curtis-Muir Wood, Einstein and Schwartz (1979), and Ahrens et al. (1982), and the method reduces to Mindlin's solution (1939 and 1940: 1136) if the liner is neglected ($\alpha = \beta = 0$). Furthermore, finite element results presented by Rabinen (1978) compare well with the solution.

5.4 Two Dimensional Stress and Strain Fields due to Tunnelling: Twice Normalized Ground Reaction Curves according to the Eisenstein-Negro Method

Estimation of stress and strain conditions developed because of tunnelling in the plane strain condition is presented in the form of a generalized solution based on a parametric analysis carried out using the finite element method. Figure 5.6 shows a flow chart of the Eisenstein-Negro method. The assumptions which were formulated in this method are cited below (Negro, 1988):

The constitutive model used in the analyses is the hyperbolic model (Duncan and Chang, 1970). The model is described in Figure 5.7. From the figure, the hyperbolic model is based on fitting a hyperbola to the relationship between the axial strain and the deviator stress obtained from the conventional triaxial test. The model is finally presented in form of a relationship between the tangential deformation modulus E_t and the deviator stress ($\sigma_1 - \sigma_3$). The stress-strain relationship includes the effect of shear strength

Eisenstein- Negro's Method of Design of Shallow Tunnels

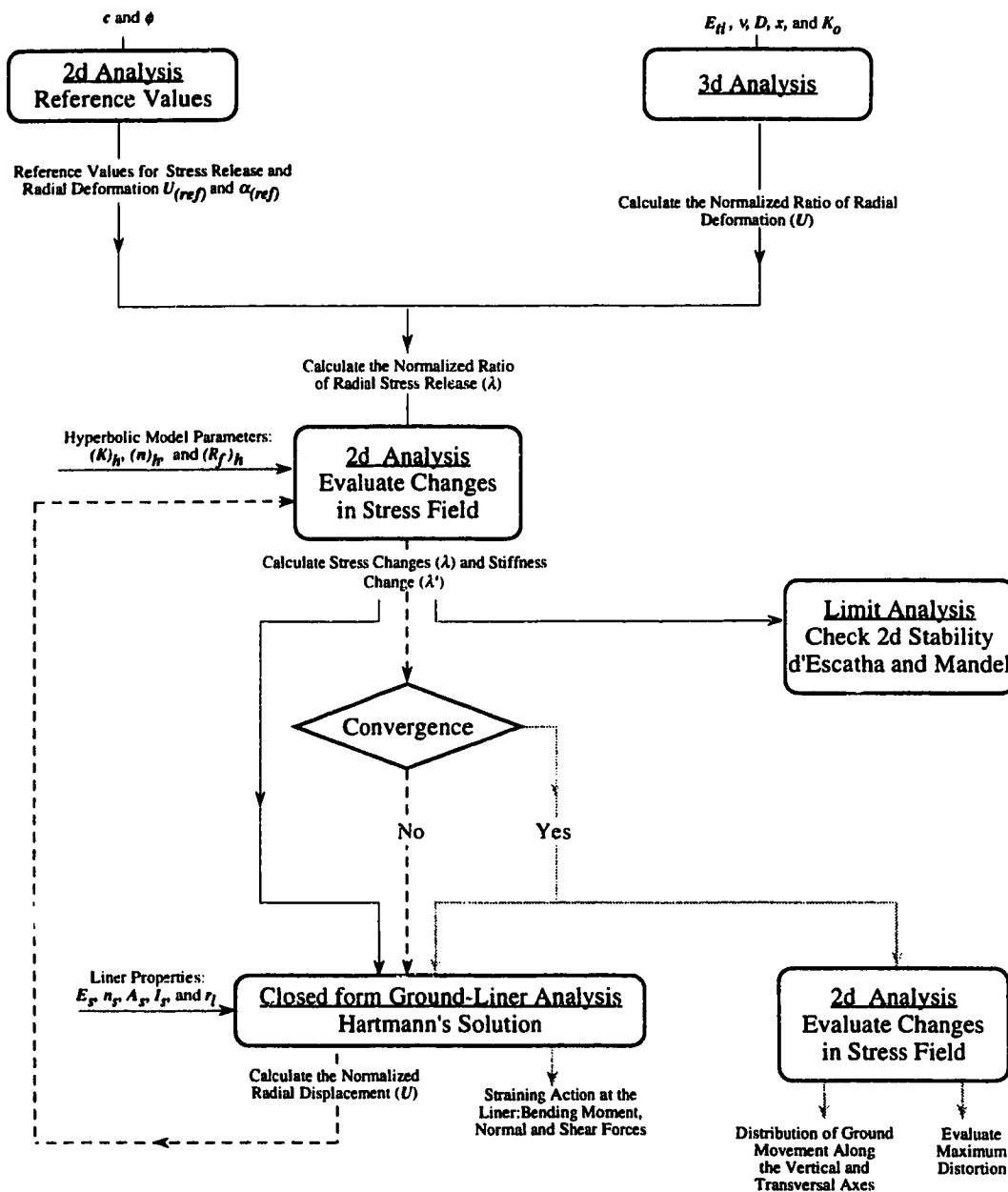
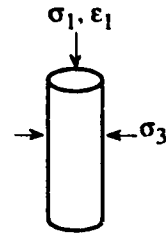
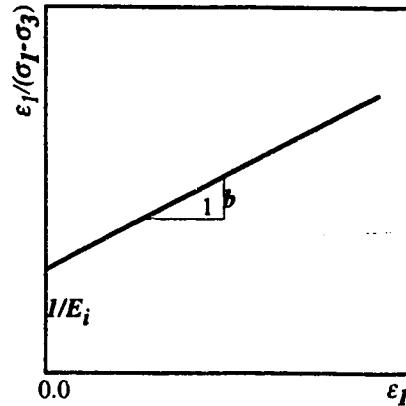
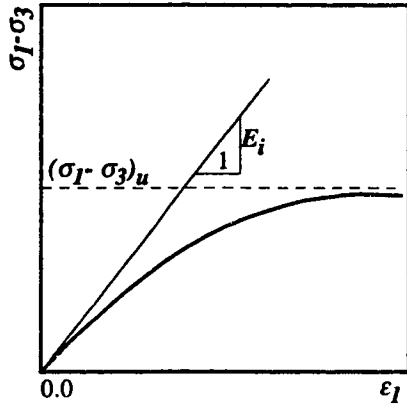


Figure 5.6: Flow Chart of Eisenstein- Negro's Method of Design of Shallow Tunnels

1. Stress Strain Relationship: Hyperbola:

$$\sigma_1 - \sigma_3 = \frac{\epsilon_1 E_i}{a + b \epsilon_1}$$



$$b = (\sigma_1 - \sigma_3)_u$$

$$a = 1/E_i$$

E_i : initial tangential modulus

$(\sigma_1 - \sigma_3)_u$: ultimate (asymptotic) deviatoric stress

2. Effect of Shear Strength (stress ratio parameter R_f)

$$b = R_f / (\sigma_1 - \sigma_3)_f$$

$(\sigma_1 - \sigma_3)_f$: deviatoric stress at failure

3. Effect of Confining Pressure. Janbu's relationship (Janbu's constants K and n)

$$E_i = K P_a (\sigma_3 / P_a)^n$$

P_a : atmospheric pressure

4. Failure Criterion. Mohr - Coulomb Criterion in the triaxial test

$$(\sigma_1 - \sigma_3)_f = \frac{2c \cos \phi + 2\sigma_3 \sin \phi}{1 - \sin \phi}$$

5. Constitutive Relationship (E_t and ν)

$$E_t = K P_a (\sigma_3 / P_a)^2 \left(1 - R_f \frac{(1 - \sin \phi) (\sigma_1 - \sigma_3)^2}{2c \cos \phi + 2\sigma_3 \sin \phi} \right)^2$$

E_t : tangential modulus

ν : Poisson's ratio

Figure 5.7: the Hyperbolic Model

parameters (c and ϕ) and that of the confining pressure, σ_3 directly and through Janbu's parameters $(n)_h$ and $(K)_h$ and the stress ratio parameter $(R_f)_h^4$.

The method relies on the property of homothety related to the hyperbolic model. Similarities between the characteristics of a group of curves allow these curves to be normalized by constant reference values into a unique relationship representing the entire group. Negro (1988: Figures 6.1 and 6.2) proves that the effect of confining pressure in the hyperbolic model can be normalized for the cases where $(n)_h = c = 0$. Therefore, he proves using a finite element examples that tunnels with different diameters but with the same depth ratio exhibit a unique normalized response with respect to ground reaction curves, as well as, to the displacement field at the ground surface. The restrictive assumptions of $(n)_h = 0$ and of $c = 0$ are dealt with by conducting a sensitivity analysis that reveals that the effect of Janbu's modulus $(n)_h$ on the normalized ground reaction curves at the crown and at the floor can be minimized if the value of the deformation modulus is selected to be equal to the actual tangential deformation modulus at one tunnel radius above the crown and one radius below the floor, respectively. The effect of cohesion is introduced as an increase in the angle of internal friction. The following relationship (Negro (1988): Equation 6.10) is found to yield the closest results to the actual behaviour of the c - ϕ material with a conservative approximation:

$$\phi_a = \arcsin\left(\frac{1 + (\sigma_3/c)\tan\phi}{1 + (\sigma_3/c)\sec\phi}\right), \quad (5.7)$$

where:

ϕ_a is the approximated angle of internal friction to include the effect of cohesion.

For frictionless material ($\phi=0$ and $(n)_h = 0$) the homothety is evident as the tangent modulus is independent for σ_3 . Meanwhile, Janbu's modulus $(K)_h$, being directly related to the initial tangential modulus, E_{ti} , is included into the normalized expression of circumferential displacement U :

$$U = \frac{u_r E_{ti}}{D\sigma_{r0}}, \quad (5.8)$$

where:

⁴Subscript h is added to parameters in the hyperbolic model to avoid confusion with other symbols.

u_r is the radial displacement at the tunnel circumference and
 σ_{r0} is the initial radial pressure at the tunnel circumference.

The effect of Poisson's ratio on the normalized ground reaction curves, as well as, on the surface displacement distribution is shown by finite element analysis to be relatively small, and the displacement shows a general trend to increase as the value of Poisson's ratio increases. An intermediate value of Poisson's ratio is chosen ($\nu=0.4$). The performed finite element analyses investigate the effect of the depth ratio by covering a reasonably wide range of H/D values (between 1.5 and 6). It is shown that, as expected, the ground response becomes stiffer as the tunnel is deeper. Ground reaction curves for frictional material with different values of the angle of internal friction are found to exhibit a homothetic property similar to that of the stress-strain hyperbolic relationship with respect to the confining pressure, σ_3 . Therefore, the normalized ground reaction curve (NGRC), is normalized once more to include the effect of the angle of internal friction, ϕ , and a twice normalized ground reaction curve (NNGRC) is obtained. Figure 5.8 is a sketch of the different constructed ground reaction curves. The same process is found applicable in cases of frictionless material where double normalized ground reaction curves are constructed to produce unique curves independent of the cohesive resistance, c . Details of the statistical analyses involved in the normalization process are found in Negro (1988). As a result of the twice normalized ground reaction curve, the parameter λ is defined as follows:

$$\lambda = \frac{\Sigma - \Sigma_{ref}}{1 - \Sigma_{ref}} \quad , \quad (5.9)$$

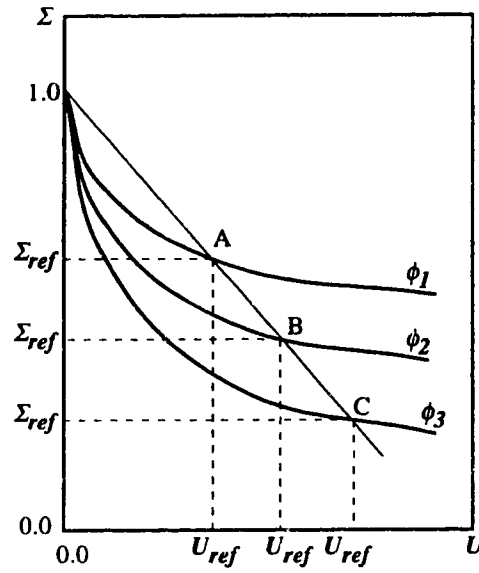
where Σ is the radial stress ratio⁵:

$$\Sigma = \frac{\sigma_r}{\sigma_{r0}} \quad , \quad (5.10)$$

and Σ_{ref} is the reference value of Σ related to the shear strength parameter.

At the end unique relationships are constructed between λ and U/U_{ref} that are independent of the shear strength parameters (c and ϕ), the tunnel size, Janbu's moduli ($(n)_h$ and $(K)_h$), and of the soil unit weight, γ . The formulated relationships are constructed for

⁵In Negro's thesis, the ratio Σ is named the stress ratio. It was decided to use different name for the radial stress ratio to differentiate between it and the stress ratio of the the mean normal stress, $S.R.$.

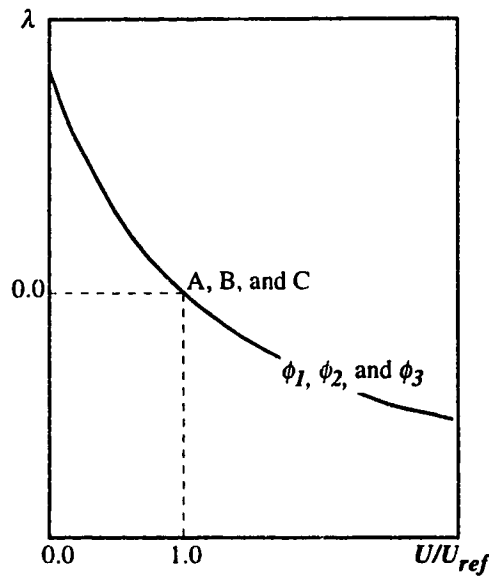


1. Normalized Ground Reaction Curve NGRC

$$\Sigma = \sigma_r / \sigma_{r0}$$

$$U = \frac{u_r E}{\sigma_{r0} D}$$

σ_r : radial stress at the liner
 σ_{r0} : initial radial stress
 u_r : radial deformation
 E : tangential modulus
 D : tunnel diameter



2. Twice Normalized Ground Reaction Curve NNGRC

$$\lambda = \frac{\Sigma - \Sigma_{ref}}{1 - \Sigma_{ref}}$$

Figure 5.8: Normalization of Shear Strength parameters of the Hyperbolic Model used in Eisenstein- Negro's Method. (Cohesionless Material)

various values of coefficients of lateral pressure at rest K_0 and the depth ratio H/D . The parameters λ and U/U_{ref} are expressions of the stress change and of the deformation at the tunnel circumference due to the process of stress release, respectively. The derivative λ' of λ with respect to U/U_{ref} is an expression of soil stiffness, thus the ratio:

$$\frac{\lambda'}{\lambda'_i} = \frac{E_t}{E_{ii}} \quad , \quad (5.11)$$

where:

$$\lambda' = \frac{\partial \lambda}{\partial (U/U_{ref})} \quad , \quad (5.12)$$

and

λ'_i is the initial value of λ' (at zero stress release).

5.5 Ground-Liner Interaction

From the above two sections, it is shown that the prevailing concept in tunnelling design in general and in the Eisenstein-Negro method in particular is that the ground and the liner are at best accurately simulated into two separate models. This is due to discrepancies in the geometry and in the stiffness between the two adopted structural models. It is, therefore, imperative to relate the two structural models in order to reach a realistic design method. Such a relationship would allow the nonlinearity of the stress-strain curve of the ground to interact with the liner simulated as a cylindrical shell. Thus the two most important features of the two models are accounted for: ground nonlinearity and accuracy in calculating the straining action of the liner. It is, therefore, required to find the proper way to transmit the calculated ground pressure after stress release to the lining system and to transmit the effect of lining deformation on the amount of ground-stress release. Obviously, an interactive process is required to ultimately achieve the required compatibility and equilibrium conditions between the liner and the ground.

Ground-liner interaction according to Eisenstein-Negro Method

The Eisenstein-Negro method uses numerical analyses based on finite element models to represent ground behaviour in the case of an unlined tunnel exposed to a certain amount of stress release. A sequence of normalization allows the generalization of the results such that for a certain radial circumferential displacement at the tunnel boundaries,

the ground surface displacement and the amount of stress release can be assessed. Correspondingly a reduced tangential modulus and a reduced unit weight is estimated for the region surrounding the tunnel. On the other hand, the liner structural model according to Hartmann's solution provides the straining actions (thrust, shear, and bending moment) and the radial deformation corresponding to the reduced modulus and unit weight. An iterative process is effected between the two systems until equal amount of stress release is calculated within an acceptable degree of tolerance.

The above process involves a certain number of assumptions. The surface between the liner and the ground is supposed to develop the required friction by the elastic model (no slip condition). The liner is elastic and its cross-sectional properties are uniform throughout its perimeter which implies that representative values of the actual lining system have to be suggested for the depth, the moment of inertia, and for the elastic parameters. These values must take into account, in the case of the segmented liner, the effect of joints and the shape of the segments. Muir Wood's expression (1975: 47) may be suggested when selecting a reduced value of the lining inertia. The compatibility of deformation is only satisfied at the three points: the crown, the spring line, and the floor. Finally, an engineering decision has to be taken whether to include the effect of tunnel heave into the final analysis. In conclusion, the undertaken assumptions are generally acceptable as they are comparable to those undertaken in other tunnelling design methods.

5.6 Design Method for Tunnels Constructed using Pressurized Shield Methods

A number of requirements have to be incorporated into a design method oriented specifically to tunnels constructed using pressurized shield methods:

- (1) the shield has to impose a certain action in the longitudinal direction in order to provide support at the face and to conduct the cutting operation. Such action is referred to as the three-dimensional effect of the tunnelling process;
- (2) the exposed ground surface behind the face and up to the point where the liner is in a state of stable equilibrium with the surrounding soil mass, is protected by a number of agents such as the rigidity of the shield, the bentonite pressure (if used), the grout pressure, and the rigid liner. Therefore, except for the cases where the tail seal fails, the tunnel circumference is protected in the transversal direction. It follows that there is a lack of failure mechanism in the transversal plane;
- (3) it is appropriate to represent the tunnel as a hollow structure in full interaction with the surrounding ground as the excavation boundaries are supported along the delay distance;

- (4) general requirements for shallow tunnel design methods are valid, such as the importance of the effect of the free boundary at the ground surface, the gravitational gradient, and that of the change of ground stiffness associated with the ground movement on the final stress field around the tunnel; and
- (5) special emphasis is made on the precast concrete segmented liner as it is in the supporting system that is most commonly used in conjunction with the pressurized shield methods. Special attention can be addressed at the same time to other supporting systems in use, such as, the extruded concrete lining system and the precast steel segmented liner.

5.6.1 The Three-dimensional Effects

As has been previously shown, the longitudinal liner pressure is responsible for the three-dimensional effect on the stress field. An attempt is made in Chapter 4 to evaluate, using a parametrical study of a number of finite element analyses, the influence of these two factors on site conditions with different geometrical configurations and different ground conditions. Emphasis is made to the resulting surface deformation and the changes in stress field around the excavation. Thus three normalized parameters are evaluated: the normalized surface displacement, \bar{w}_s , the stress ratio, $S.R.$, and the deviatoric stress ratio, $D.S.R.$. These parameters are defined in Equations 4.13, 4.14, and 4.21, respectively.

5.6.1.1 The Three-dimensional Effect on Stress Changes

It is demonstrated in Equation 4.20 that the changes in the average normal stress $S.R.$ can be presented as a polynomial function of the first degree of the $G.R.$, $L.R.$, K_o , and H_o/R_o , and a polynomial function of the second degree of Poisson's ratio, ν . Meanwhile, the deviatoric stress ratio, $D.S.R.$, presented in Equation 4.22 is expressed as a polynomial function of the first degree of K_o and H_o/R_o , and a polynomial function of the second degree of Poisson's ratio ν and $G.R.$. The relationship between the various coefficients with the tunnel depth is investigated and it is further fitted to a polynomial function of the second degree. Figures 5.9 through 5.20 show the obtained relationships and the degree of accuracy. From the figures it can be concluded that a very good agreement is achieved between the fitted curves and the calculated coefficients. An exception to that is the case of the coefficients of the second degree polynomials ar_{n2} and ar_{n1} , and ad_{g2} and ad_{g1} . However, it can be believed that the discrepancies in curve fitting of each of the two coefficients of the same polynomial neutralize each other. The final values of $S.R.$ and $D.S.R.$ coefficients are presented in Tables 5.1 and 5.2, respectively.

$$S.R. = ar_g(G.R.) + ar_l(L.R.) + ar_{n2}(v^2) + ar_{n1}(v) + \frac{ar_k}{K_o} + \frac{ar_h}{(H_o/R_o)} + ar_o$$

where

$$ar_g = (ar_g)_2(H_o/R_o)^2 + (ar_g)_1(H_o/R_o) + (ar_g)_o$$

$$ar_l = (ar_l)_2(H_o/R_o)^2 + (ar_l)_1(H_o/R_o) + (ar_l)_o$$

$$ar_{n2} = (ar_{n2})_2(H_o/R_o)^2 + (ar_{n2})_1(H_o/R_o) + (ar_{n2})_o$$

$$ar_{n1} = (ar_{n1})_2(H_o/R_o)^2 + (ar_{n1})_1(H_o/R_o) + (ar_{n1})_o$$

$$ar_k = (ar_k)_2(H_o/R_o)^2 + (ar_k)_1(H_o/R_o) + (ar_k)_o$$

$$ar_o = (ar_o)_2(H_o/R_o)^2 + (ar_o)_1(H_o/R_o) + (ar_o)_o$$

		Crown	Spring Line	Floor
<i>arg</i>	(<i>arg</i>) ₂	0.00616	-0.00201	-0.00318
	(<i>arg</i>) ₁	-0.10359	0.02515	0.04770
	(<i>arg</i>) _o	0.95832	0.24377	0.11534
<i>arl</i>	(<i>arl</i>) ₂	-0.00181	0.00092	0.00067
	(<i>arl</i>) ₁	0.02120	-0.01076	-0.01162
	(<i>arl</i>) _o	-0.16238	-0.12438	-0.09141
<i>arn2</i>	(<i>arn2</i>) ₂	-2.28144	0.00799	0.42832
	(<i>arn2</i>) ₁	28.03099	-0.07240	-5.20009
	(<i>arn2</i>) _o	-17.00942	2.39077	9.74742
<i>arn1</i>	(<i>arn1</i>) ₂	1.12211	-0.00300	-0.20628
	(<i>arn1</i>) ₁	-13.79419	0.02428	2.50583
	(<i>arn1</i>) _o	6.61744	-1.24705	-5.15029
<i>ark</i>	(<i>ark</i>) ₂	-0.00212	0.00045	0.00137
	(<i>ark</i>) ₁	0.03186	-0.00777	-0.02357
	(<i>ark</i>) _o	-0.37099	0.25403	-0.28405
<i>aro</i>	(<i>aro</i>) ₂	-0.12194	0.00209	0.02422
	(<i>aro</i>) ₁	1.49905	-0.01449	-0.27437
	(<i>aro</i>) _o	0.81395	0.86308	1.82854
<i>arh</i>	(<i>arh</i>)	-0.09751	-0.05836	0.18202

Table 5.1: Curve Fitting Coefficients *ar* of the Stress Ratio, S.R.

$$D.S.R. = ad_{g2}(G.R.)^2 + ad_{g1}(G.R.) + ad_{n2}(v^2) + ad_{n1}(v) + \frac{ad_k}{K_o} + \frac{ad_h}{(H_o/R_o)} + ad_o$$

where

$$ad_{g2} = (ad_{g2})_2(H_o/R_o)^2 + (ad_{g2})_1(H_o/R_o) + (ad_{g2})_o$$

$$ad_{g1} = (ad_{g1})_2(H_o/R_o)^2 + (ad_{g1})_1(H_o/R_o) + (ad_{g1})_o$$

$$ad_{n2} = (ad_{n2})_2(H_o/R_o)^2 + (ad_{n2})_1(H_o/R_o) + (ad_{n2})_o$$

$$ad_{n1} = (ad_{n1})_2(H_o/R_o)^2 + (ad_{n1})_1(H_o/R_o) + (ad_{n1})_o$$

$$ad_k = (ad_k)_2(H_o/R_o)^2 + (ad_k)_1(H_o/R_o) + (ad_k)_o$$

$$ad_o = (ad_o)_2(H_o/R_o)^2 + (ad_o)_1(H_o/R_o) + (ad_o)_o$$

		Crown	Spring Line	Floor
<i>adg</i>	(<i>adg</i>) ₂	-0.01091	-0.01927	-0.02747
	(<i>adg</i>) ₁	0.12149	0.16655	0.29106
	(<i>adg</i>) _o	0.27407	-0.06886	-0.12815
<i>adl</i>	(<i>adl</i>) ₂	0.01772	0.03915	0.03307
	(<i>adl</i>) ₁	-0.20369	-0.37289	-0.33326
	(<i>adl</i>) _o	-0.15983	-0.05009	-0.17694
<i>adn2</i>	(<i>adn2</i>) ₂	-0.08418	0.00076	-0.00464
	(<i>adn2</i>) ₁	1.36650	-0.01565	0.07563
	(<i>adn2</i>) _o	4.31583	-2.02813	-2.79076
<i>adn1</i>	(<i>adn1</i>) ₂	0.04630	-0.00257	0.00520
	(<i>adn1</i>) ₁	-0.75088	0.04439	-0.08470
	(<i>adn1</i>) _o	-2.18276	0.61858	1.14892
<i>adk</i>	(<i>adk</i>) ₂	0.00356	-0.00016	-0.00151
	(<i>adk</i>) ₁	-0.05798	0.00207	0.02772
	(<i>adk</i>) _o	-0.10053	0.10331	-0.65811
<i>ado</i>	(<i>ado</i>) ₂	-0.01867	0.00010	-0.04069
	(<i>ado</i>) ₁	0.27039	-0.01117	0.54930
	(<i>ado</i>) _o	0.06359	-0.07736	-1.01871
<i>adh</i>	(<i>adh</i>)	0.37507	0.78064	0.56610

Table 5.2: Curve Fitting Coefficients *ad* of the Deviatoric Stress Ratio, D.S.R.

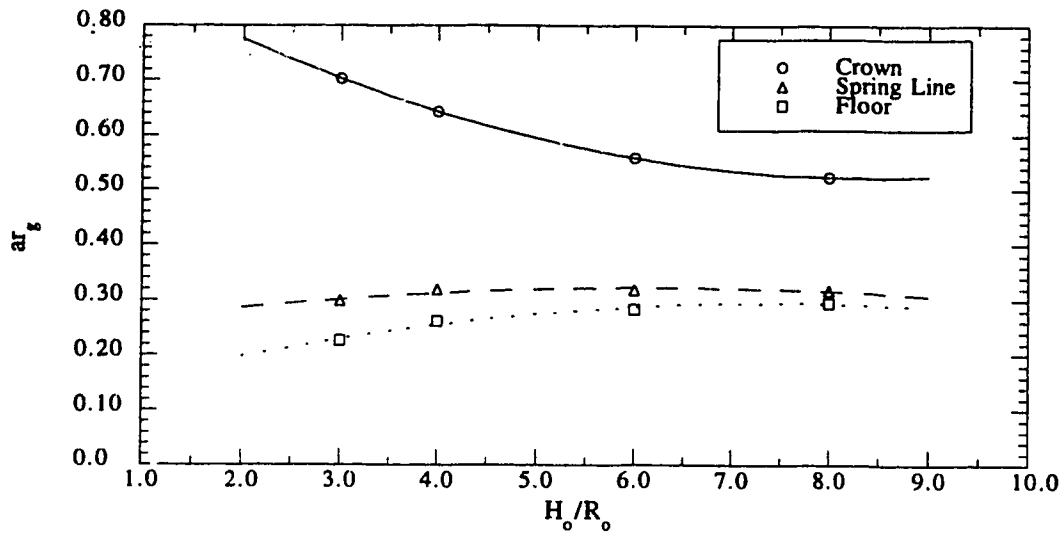


Figure 5.9: Calculated and Curve Fitted values of ar_g versus the Normalized Tunnel Depth

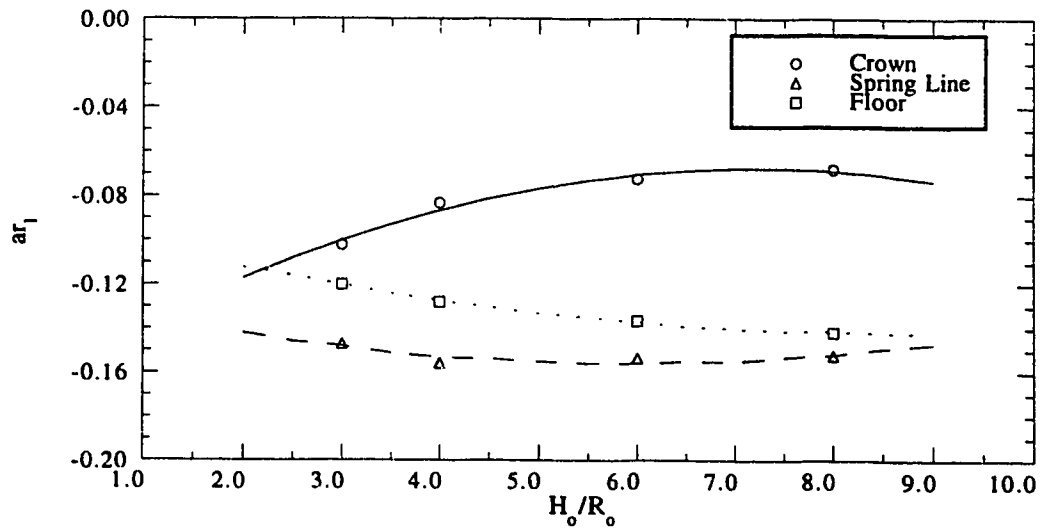


Figure 5.10: Calculated and Curve Fitted values of ar_l versus the Normalized Tunnel Depth

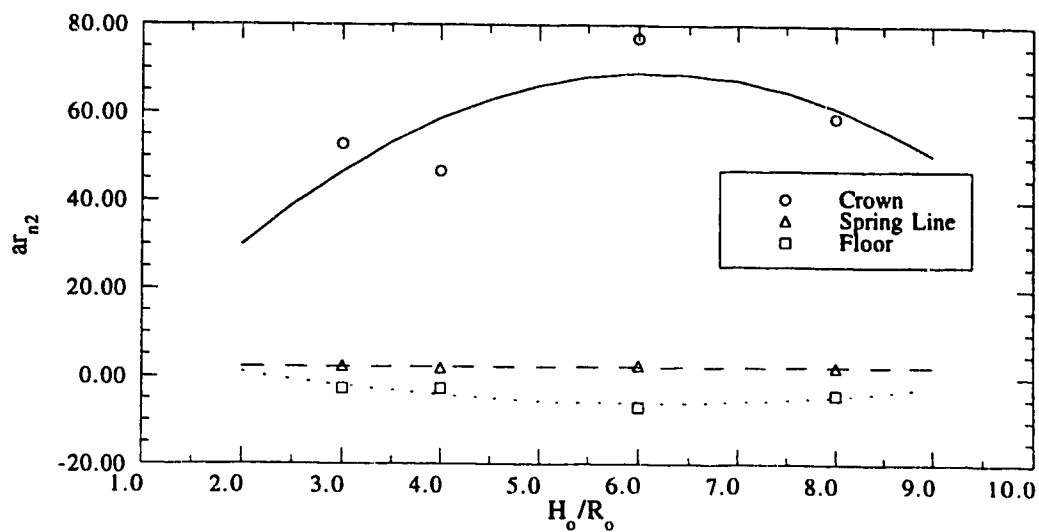


Figure 5.11: Calculated and Curve Fitted values of ar_{n2} versus the Normalized Tunnel Depth

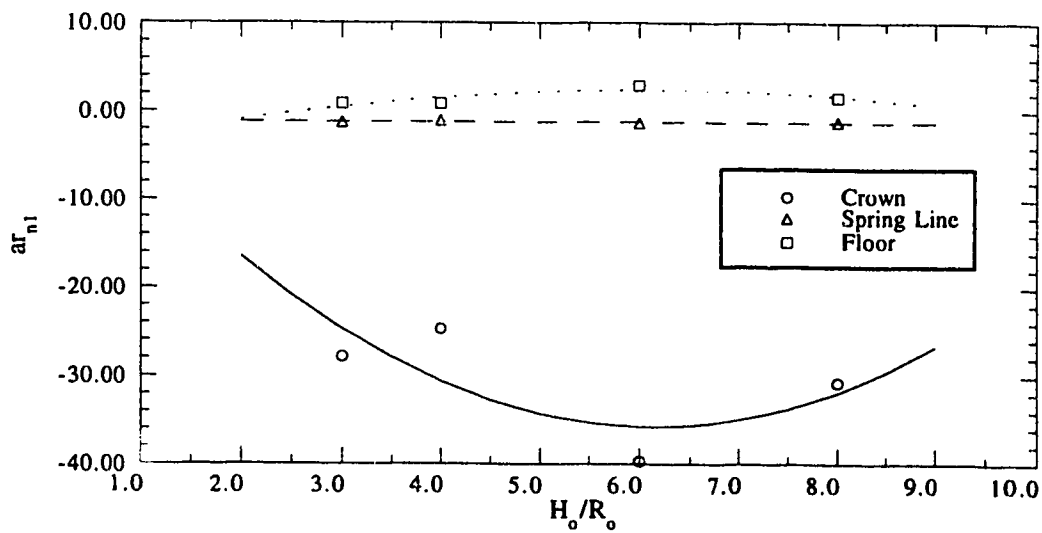


Figure 5.12: Calculated and Curve Fitted values of ar_{n1} versus the Normalized Tunnel Depth

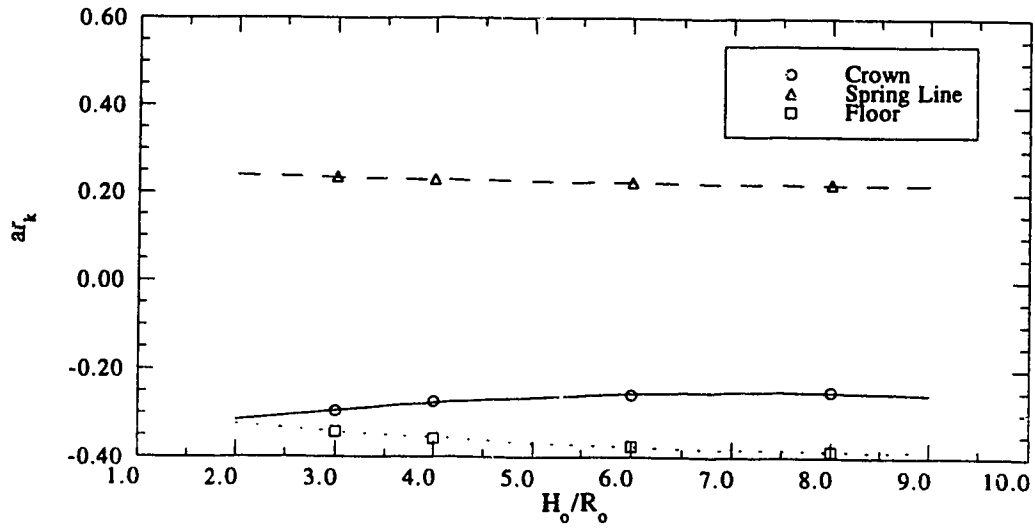


Figure 5.13: Calculated and Curve Fitted values of ar_k versus the Normalized Tunnel Depth

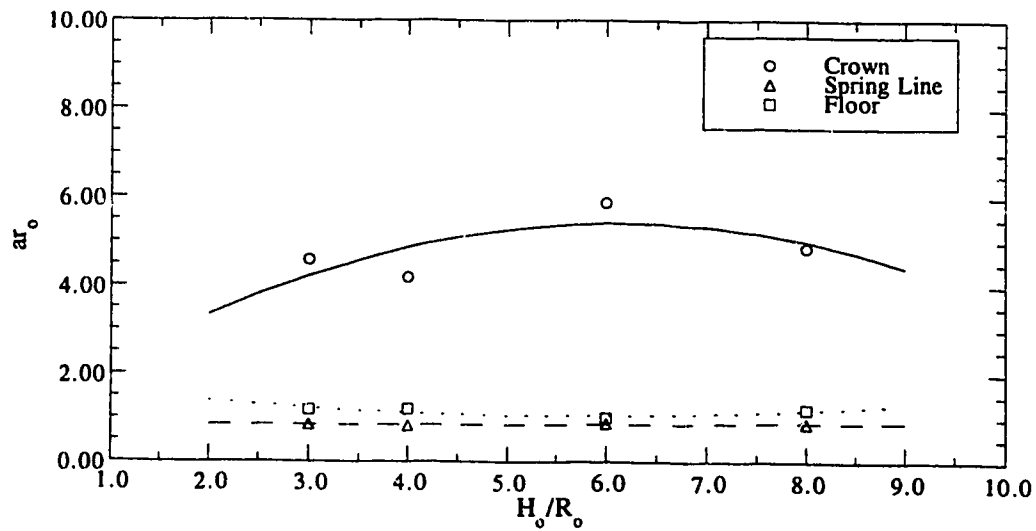


Figure 5.14: Calculated and Curve Fitted values of ar_0 versus the Normalized Tunnel Depth

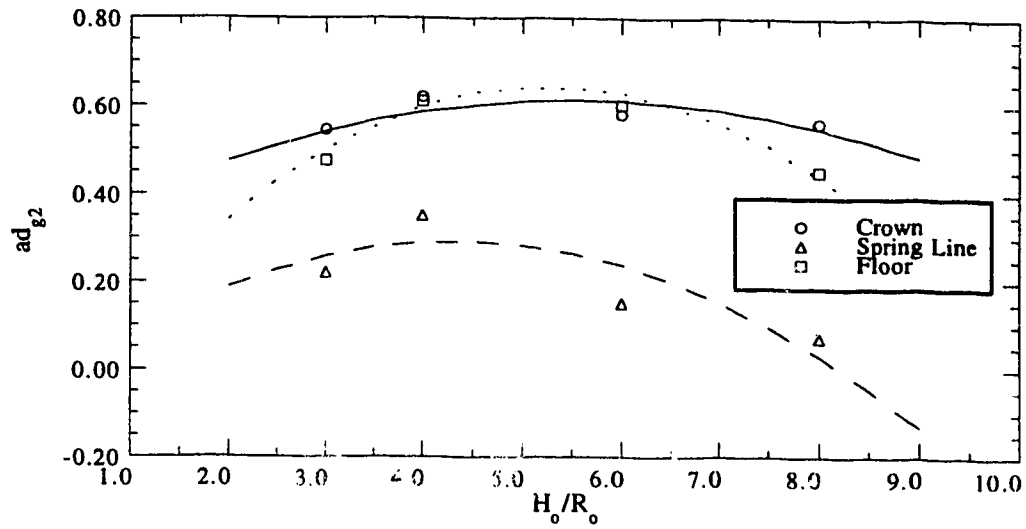


Figure 5.15: Calculated and Curve Fitted values of ad_{g2} versus the Normalized Tunnel Depth

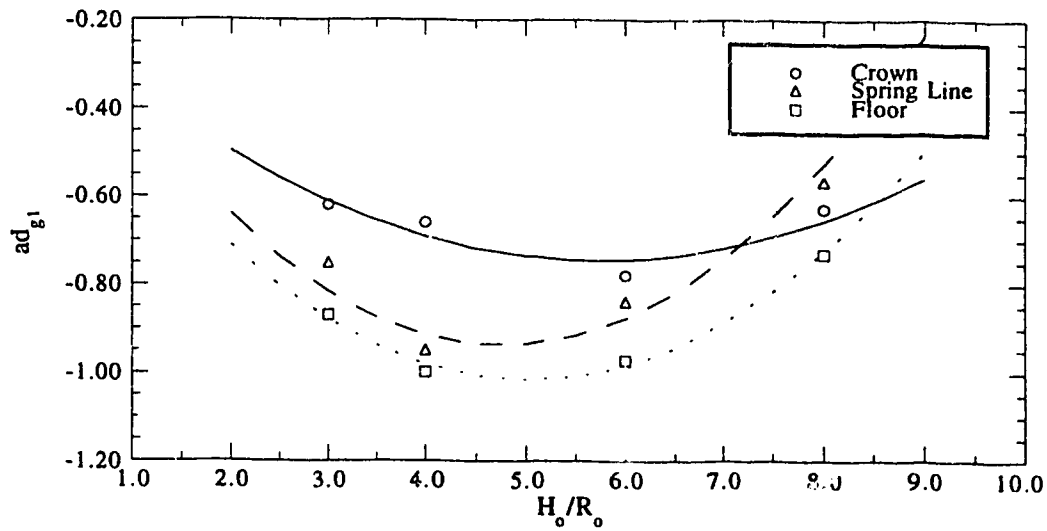


Figure 5.16: Calculated and Curve Fitted values of ad_{g1} versus the Normalized Tunnel Depth

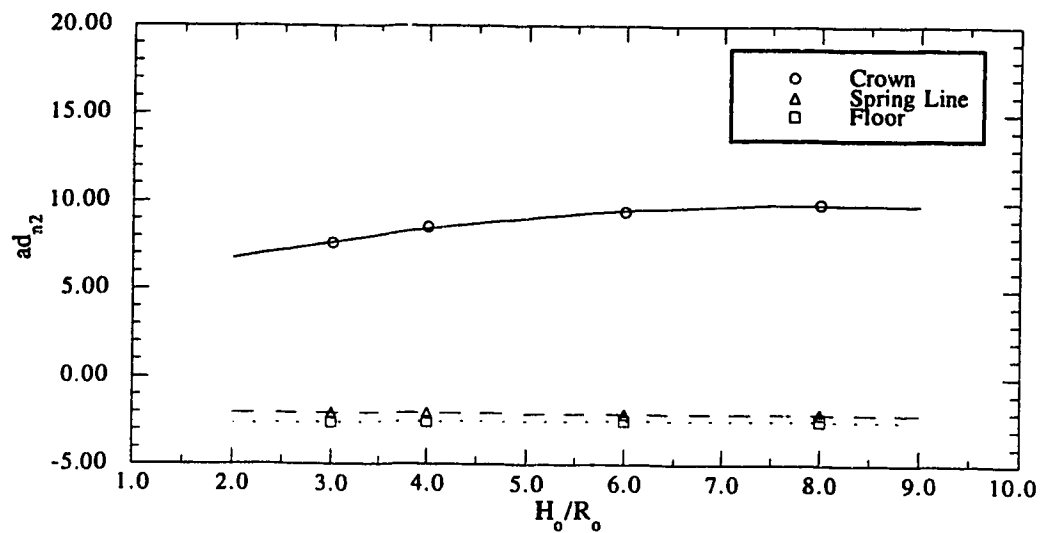


Figure 5.17: Calculated and Curve Fitted values of ad_{n2} versus the Normalized Tunnel Depth

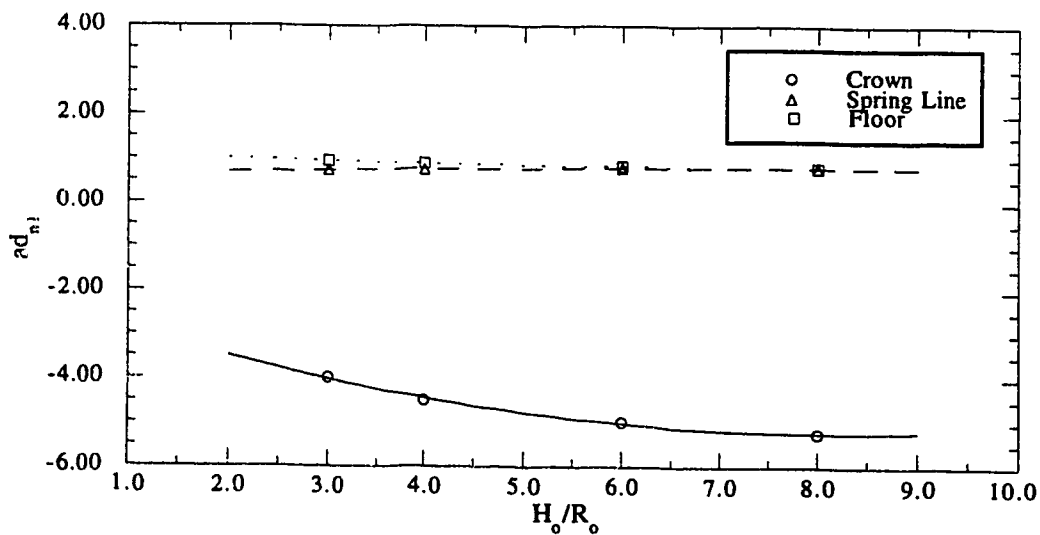


Figure 5.18: Calculated and Curve Fitted values of ad_{n1} versus the Normalized Tunnel Depth

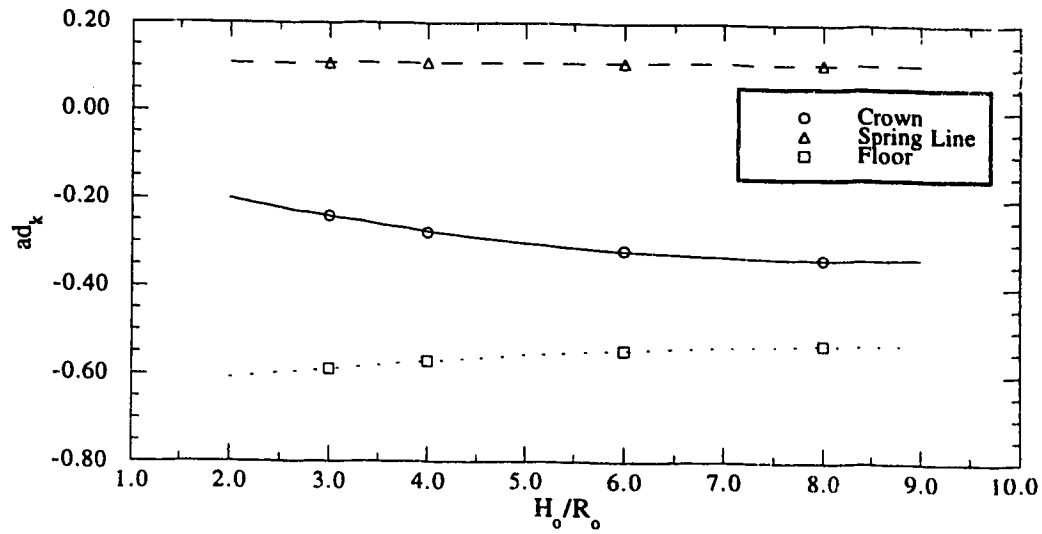


Figure 5.19: Calculated and Curve Fitted values of ad_k versus the Normalized Tunnel Depth

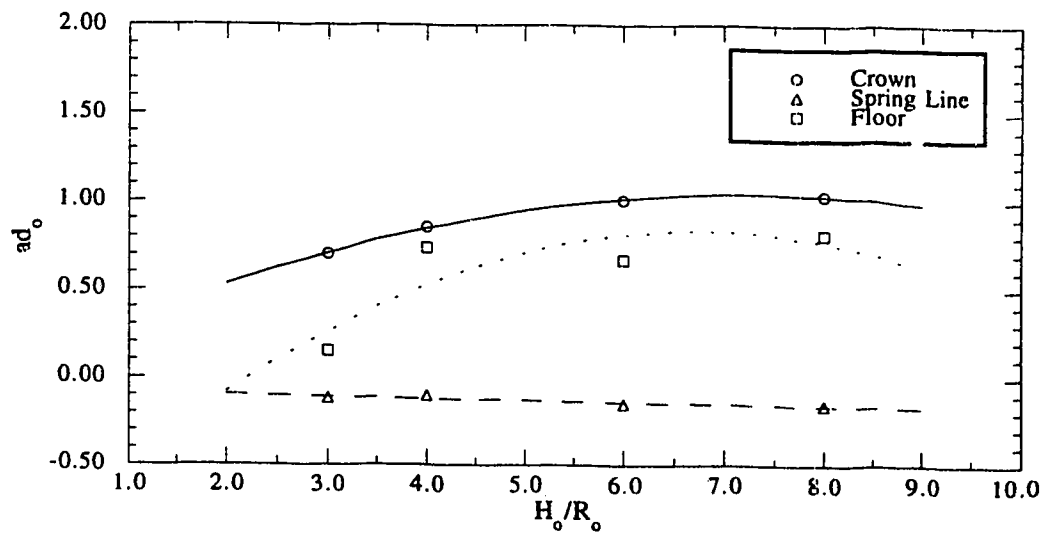


Figure 5.20: Calculated and Curve Fitted values of ad_o versus the Normalized Tunnel Depth

5.6.1.2 The Three-dimensional Effect on Surface Movements

Equation 4.13 shows the definition of the normalized surface movement, and Equation 4.17 shows calculated coefficients of first and second degree polynomials that describe the influence of $G.R.$, $L.R.$, K_o , H_o/R_o , and v . Figure 5.21 shows a curve fitted polynomial of the second degree for the coefficients as_g , as_l , and as_c . From the figure good agreement is achieved in the three relationships. The final values of $\bar{\omega}_g$ coefficients are presented in Table 5.3.

5.6.1.3 Limitations of the Evaluations of the Three-dimensional Effects

It has to be noted that the evaluations of the three-dimensional effect on the changes in the stress field and on surface movements involves a number of approximations:

- (1) the accuracy of the parametric analysis, as suggested in Chapter 4, is affected by the computer system limitations, and it is not able to clearly identify a number of relationships, such as, the effect of $L.R.$ on the $D.S.R.$ and the effect of Poisson's ratio on the surface displacement. Further analyses may be required to investigate these details. Meanwhile, the size of the mesh and the accuracy of the simulating process are limited by the capacity of the computing system. It has to be noted in that regard that the calculations directed toward a parametric analysis required a substantial effort in storing and handling the output data. The improvement in the capacity and efficiency of the computing system, as well as, the improvement of data handling facilities will have an important effect on the improvement of the quality of the obtained results;
- (2) one important limitation is the degree of accuracy of stress computation at the point of lining activation. Although a high order of stress integration is used ($3 \times 3 \times 3$), the representation of the excavation step as a one element slice has an effect on reducing the accuracy of computations at that point. It should be noted also that at this specific point, especially in the case of high $L.R.$ and low $G.R.$, a condition of stress concentration is developed near the rigid liner which has an effect on the numerical accuracy of the results; and
- (3) it is difficult to pre-estimate the influence of the different parameters included in the analysis on each others because of the complexity of the problem and that of the excavation process. Therefore the assumption that each parameter is acting independently and affects the stress changes and the surface displacement in the form of a polynomial function of first or second order may be considered as a first approximation and is only justified by the obtained data output field.

$$\bar{\omega}_s = (as_g(G.R.) + as_l(L.R.) + as_o)(H_o/R_o)^{-1} + \left(as_n(v) + \frac{ask}{K_o} + ash \right) (H_o/R_o)^{-2}$$

where

$$as_g = (as_g)_2 (H_o/R_o)^2 + (as_g)_1 (H_o/R_o) + (as_g)_o$$

$$as_l = (as_l)_2 (H_o/R_o)^2 + (as_l)_1 (H_o/R_o) + (as_l)_o$$

$$as_o = (as_o)_2 (H_o/R_o)^2 + (as_o)_1 (H_o/R_o) + (as_o)_o$$

<i>asg</i>	(<i>asg</i>) ₂	-4.58077
	(<i>asg</i>) ₁	10.27782
	(<i>asg</i>) _o	303.22511
<i>asl</i>	(<i>asl</i>) ₂	2.80582
	(<i>asl</i>) ₁	-22.17239
	(<i>asl</i>) _o	-24.96859
<i>aso</i>	(<i>aso</i>) ₂	1.20644
	(<i>aso</i>) ₁	-9.91671
	(<i>aso</i>) _o	-75.47406
<i>asn</i>	(<i>ash</i>)	1356.01683
<i>ask</i>	(<i>ash</i>)	-306.45943
<i>ash</i>	(<i>ash</i>)	-607.02338

Table 5.3: Curve Fitting Coefficients $\bar{\omega}_s$ of Ground Surface Displacement

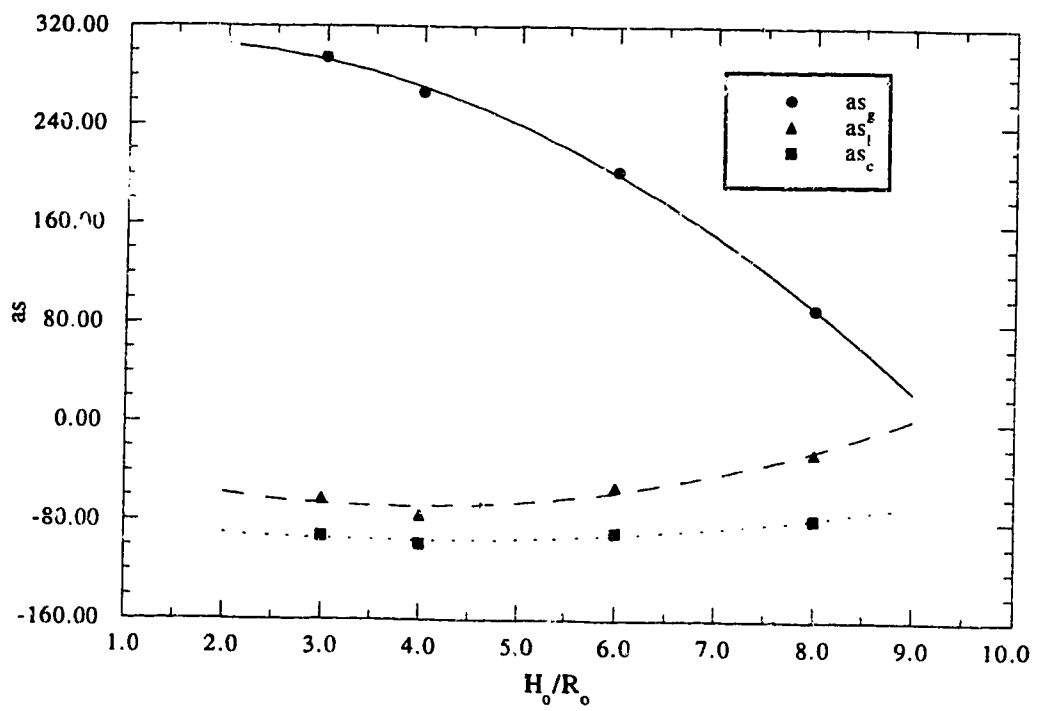


Figure 5.21: Calculated and Curve Fitted values of as versus the Normalized Tunnel Depth

5.6.2 Evaluation of Stress Changes and Surface Displacement at Plane Strain Condition

It is to be expected that the final stress field after the tunnel construction will follow the plane-strain condition. Therefore, the plane-strain condition prevails only at a certain distance behind the point of lining activation although the initial in situ condition is idealized as an other plane strain condition. Long term action resulting from tunnelling can be considered as an indication of the differences between the two stress fields: the near tunnel conditions and the initial site conditions that are still existing at the remote boundaries of the tunnel. Shield action in the longitudinal direction is expected to substantially influence the new plane strain conditions that will govern the final stress field.

Reviewing the limitations of the performed three-dimensional analysis, it is to be noted that the assessment of the final plane strain condition around a tunnel constructed with rigid liner is affected by a number of factors. In the numerical simulation the stress field at the far end of the liner represents a state of stress that does not include the construction process but is rather representative of the initial stress field in which the tunnel is excavated and supported instantaneously. Such a condition does not conform to the actual state of stress in the field where the new state of plane strain condition prevails. In addition, the degree of approximation involved in the simulation of the construction process contributes in increasing the unsteady pattern of stress values in the longitudinal direction at the proximity of the liner. A certain number of assumptions have to be taken in account in order to evaluate loading conditions on the liner:

- (1) the mean normal pressure at the final state of stress is equal to that at the point of lining activation. Referring to Figures 4.69 through 4.73 the *S.R.*, which is a normalized expression of the mean normal pressure, undergoes a substantial degree of variation behind the point of lining activation (*Point 4* in the Figures). The changes may be attributed to stress concentration that takes place near the liner corners. The stress concentration is expected to be exaggerated due to the adopted finite element mesh that is relatively coarse. It could be believed that in actual conditions, the existence of grout material with sufficient degree of fluidity and homogeneity is capable of reducing such effects;
- (2) the deviatoric pressure at the final state of stress is equal to that at the same point: the point of lining activation. As in the case of the mean normal pressure, the variation of the values of *D.S.R.*, which is a normalized expression of the deviatoric pressure behind the point of lining activation is attributed to stress concentration near the liner;
- (3) the directions of principal stresses are in the radial and tangential directions with

respect to the tunnel circumference. This is an inevitable approximation that has to be undertaken. This assumption could be justified as the presence of the grout material in a fluid state eliminates any friction between the ground and the liner before the stage of ground-liner interaction;

- (4) the longitudinal principal stress is equal to the minor principal stress. This assumption, results in a simplification of the calculations as a state of compressive triaxial stresses is considered around the liner. This assumption enables the hyperbolic model to be implemented into the calculations; and
- (5) the assumed deviatoric stress does not violate the failure criterion. Otherwise, for the predefined principal stresses, deviatoric stress is reassessed based on the shear strength parameters.

On the other hand the amount of displacement at the ground surface of the plane strain condition is calculated to be equal to the three-dimensional surface movement. This amount of displacement can be considered as the best estimation of the surface movement that can be obtained using three-dimensional finite element analysis.

5.6.3 The use of Eisenstein-Negro Method in the Design Method

In Sections 5.3 through 5.5 emphasis is made to the Eisenstein-Negro method as it has numerous advantages for tunnel design. The method is used and verified with success with a number of case histories (refer to Negro (1988): Chapter 7). The advantages of the method may be summarized as follows:

- (1) the ground surface nonlinearity is included as the hyperbolic model is adopted;
- (2) a rational method for evaluating the effect of delayed liner activation using three-dimensional finite element analyses is proposed;
- (3) the straining actions of the liner are calculated using the theory of cylindrical shell which provides a relatively higher accuracy over finite element methods where the aspect ratio of the elements affects the final results;
- (4) the gravitational stress field including the gravitational gradient is adequately considered which allows the method to be applied for the design of shallow tunnels;
- (5) the method is simple and practical and can be applied with minimum computational effort provided the proposed assumptions and restrictions are properly considered; and
- (6) the method is applicable for a large number of cases that render it useful for the use of tunnelling designers in urban areas.

The above advantages render the adoption of the method attractive for the design of shallow

tunnels constructed using pressurized shield methods. It is to be remembered that the use of the pressurized shield induces a stress field that departs from the conventional concept of volume loss (as shown in Chapter 4). However, as the stress disturbance in the longitudinal direction due to the excavation ceases at some distance behind the point of lining activation, the liner interacts with the ground following a rather plane strain condition and conventional design methods become fully applicable. The choice is therefore made to use the Eisenstein-Negro method for the proposed method of shallow tunnel design with a number of adaptations as will be shown in the following sections.

5.6.4 The Plane Strain Model

The plane strain condition at the end of tunnel construction is conceived to be a resultant of three processes: the three-dimensional effect, the ground-liner interaction and soil deformation above the tunnel due to the new conditions. Considering the assumptions formulated in Section 5.6.2 the mean and deviatoric stresses are evaluated around the liner. Thus, the principal stresses are calculated based on the identities:

$$\sigma_3 = p - \frac{\rho}{\sqrt{6}} \quad , \text{ and} \quad (5.13)$$

$$\sigma_1 = \sigma_3 + \sqrt{1.5}\rho \quad . \quad (5.14)$$

These stresses correspond to a certain continuum stress field condition. Using Hartmann's solution, the final stress field condition may be described in terms of the ground unit weight, γ , and the coefficient of lateral earth pressure at rest, K_0 . For certain values of ν , α , β , and R_0/H_0 , normal and tangential stresses around the liner are evaluated at the crown, the spring line, and at the floor as follows:

$$SUM = (A_1 + A_2 K_0) \gamma H_0 \quad , \quad (5.15)$$

and

$$DIF = (A_3 + A_4 K_0) \gamma H_0 \quad , \quad (5.16)$$

where:

$$SUM = \sigma_r + \sigma_\theta \quad , \quad (5.17)$$

and

$$DIF = \sigma_r - \sigma_\theta \quad . \quad (5.18)$$

The stresses σ_r and σ_θ are, respectively, the radial and tangential stresses at the liner, and A_1, A_2, A_3 , and A_4 are constants defined in Figure 5.22 based on Hartmann's solution. The assumption that the principal stresses are in the radial and tangential directions result in providing the values of *SUM* and *DIF* according to Equations 5.17 and 5.18 by substituting σ_r and σ_θ by σ_1 and σ_3 . Solving Equations 5.15 and 5.16 simultaneously gives the new γ and K_o related to the new stress field. An assumption has to be made in order to define the sign *DIF*. A number of preliminary calculations shows that acceptable results can be achieved if the sign of *DIF* is chosen such that the value of the calculated K_o is closer to the initial value of K_o . This choice is compatible with the conception that for the new normal and deviatoric stress conditions around the liner, the orientation of principal stresses is as much as possible closer to the initial state of stress that is believed to be still prevailing at the remote boundaries of the excavation.

For the new field conditions related to the construction process, ground-liner interaction is supposed to take place as described in the Eisenstein-Negro method. The twice normalized ground reaction curve along with the iterative process with Hartmann's solutions result in defining the final state of surface movement and the straining actions in the liner.

5.6.5 The Design Method

A flow chart of the design method is shown in Figure 5.23. Results of three-dimensional analyses is presented in normalized forms of movement, ω_s , at the ground surface and of the mean and deviatoric stresses *S.R.* and *D.S.R.* at three points of the tunnel circumference: the crown, the spring line and the floor. Mean normal stress and deviatoric stresses are, respectively, calculated through Equations 4.20 and 4.22 at the specified points. The triaxial principal stresses are calculated through Equations 5.13 and 5.14. Based on the values of the principal stresses, and on the proposed hyperbolic parameter, the modulus of deformation, E_{ij} , is calculated from Figure 5.6. The average deformation modulus of the four points of the tunnel circumference (the crown, two spring lines, and the floor) is considered to be representative of the stiffness condition around the excavation at the point of lining activation before the process of ground-liner interaction. The new calculated value is used in Equations 4.13 and 4.17 to calculate the deformation at

$$\begin{aligned} \text{SUM} &= A_1 + A_2 K_0 \\ \text{DIF} &= A_3 + A_4 K_0 \end{aligned}$$

At the crown:

$$\begin{aligned} (A_1)_c &= \left(\frac{-I+2v}{2-2v} + \frac{I+2\alpha+8\beta}{I+5\alpha+56\beta+216\alpha\beta-4\dot{\alpha}v-64\beta v-288\dot{\alpha}\beta v} \right) \left(\frac{R_0}{H_0} \right) + \frac{-I+12\beta+36\dot{\alpha}\beta-2\dot{\alpha}v-18\beta v-48\dot{\alpha}\beta v}{I+3\dot{\alpha}+15\beta+36\dot{\alpha}\beta-2\dot{\alpha}v-18\beta v-48\dot{\alpha}\beta v} \\ (A_2)_c &= \left(\frac{-2-7\dot{\alpha}-64\beta-216\dot{\alpha}\beta+4\dot{\alpha}v+64\beta v+288\dot{\alpha}\beta v}{I+5\alpha+56\beta+216\alpha\beta-4\dot{\alpha}v-64\beta v-288\dot{\alpha}\beta v} \right) \left(\frac{R_0}{H_0} \right) + \frac{3+6\dot{\alpha}+18\beta+36\dot{\alpha}\beta-2\dot{\alpha}v-18\beta v-48\dot{\alpha}\beta v}{I+3\dot{\alpha}+15\beta+36\dot{\alpha}\beta-2\dot{\alpha}v-18\beta v-48\dot{\alpha}\beta v} \\ (A_3)_c &= \left(\frac{I-2v-\dot{\alpha}v}{2+2\dot{\alpha}-2v-2\dot{\alpha}v} + \frac{-2-\dot{\alpha}-112\beta-216\dot{\alpha}\beta-4\dot{\alpha}v+128\beta v+288\dot{\alpha}\beta v}{2(I+5\alpha+56\beta+216\alpha\beta-4\dot{\alpha}v-64\beta v-288\dot{\alpha}\beta v)} \right) \left(\frac{R_0}{H_0} \right) + \frac{-I}{I+\dot{\alpha}+\beta} + \frac{2+30\beta+36\dot{\alpha}\beta+4\dot{\alpha}v-36\beta v-48\dot{\alpha}\beta v}{I+3\dot{\alpha}+15\beta+36\dot{\alpha}\beta-2\dot{\alpha}v-18\beta v-48\dot{\alpha}\beta v} \\ (A_4)_c &= \left(\frac{2+\dot{\alpha}}{2+2\dot{\alpha}} + \frac{2+\dot{\alpha}+112\beta+216\dot{\alpha}\beta+4\dot{\alpha}v-128\beta v-288\dot{\alpha}\beta v}{2(I+5\alpha+56\beta+216\alpha\beta-4\dot{\alpha}v-64\beta v-288\dot{\alpha}\beta v)} \right) \left(\frac{R_0}{H_0} \right) + \frac{-I}{I+\dot{\alpha}+\beta} + \frac{-2-30\beta-36\dot{\alpha}\beta-4\dot{\alpha}v+36\beta v+48\dot{\alpha}\beta v}{I+3\dot{\alpha}+15\beta+36\dot{\alpha}\beta-2\dot{\alpha}v-18\beta v-48\dot{\alpha}\beta v} \end{aligned}$$

At the spring line:

$$\begin{aligned} (A_1)_s &= \frac{3+3\dot{\alpha}+45\beta+72\dot{\alpha}\beta+2\dot{\alpha}v-54\beta v-96\dot{\alpha}\beta v}{I+3\dot{\alpha}+15\beta+36\dot{\alpha}\beta-2\dot{\alpha}v-18\beta v-48\dot{\alpha}\beta v} \\ (A_2)_s &= \frac{-I+3\dot{\alpha}-15\beta-6\dot{\alpha}v+18\beta v}{I+3\dot{\alpha}+15\beta+36\dot{\alpha}\beta-2\dot{\alpha}v-18\beta v-48\dot{\alpha}\beta v} \\ (A_3)_s &= \frac{-I}{I+\dot{\alpha}+\beta} + \frac{-2-30\beta-36\dot{\alpha}\beta-4\dot{\alpha}v+36\beta v+48\dot{\alpha}\beta v}{I+3\dot{\alpha}+15\beta+36\dot{\alpha}\beta-2\dot{\alpha}v-18\beta v-48\dot{\alpha}\beta v} \\ (A_4)_s &= \frac{-I}{I+\dot{\alpha}+\beta} + \frac{2+30\beta+36\dot{\alpha}\beta+4\dot{\alpha}v-36\beta v-48\dot{\alpha}\beta v}{I+3\dot{\alpha}+15\beta+36\dot{\alpha}\beta-2\dot{\alpha}v-18\beta v-48\dot{\alpha}\beta v} \end{aligned}$$

At the floor:

$$\begin{aligned} (A_1)_f &= \left(\frac{I-2v}{2-2v} + \frac{-I-2\dot{\alpha}-8\beta}{I+5\alpha+56\beta+216\alpha\beta-4\dot{\alpha}v-64\beta v-288\dot{\alpha}\beta v} \right) \left(\frac{R_0}{H_0} \right) + \frac{-I+12\beta+36\dot{\alpha}\beta-2\dot{\alpha}v-18\beta v-48\dot{\alpha}\beta v}{I+3\dot{\alpha}+15\beta+36\dot{\alpha}\beta-2\dot{\alpha}v-18\beta v-48\dot{\alpha}\beta v} \\ (A_2)_f &= \left(\frac{2+7\dot{\alpha}+64\beta+216\dot{\alpha}\beta-4\dot{\alpha}v-64\beta v-288\dot{\alpha}\beta v}{I+5\alpha+56\beta+216\alpha\beta-4\dot{\alpha}v-64\beta v-288\dot{\alpha}\beta v} \right) \left(\frac{R_0}{H_0} \right) + \frac{3+6\dot{\alpha}+18\beta+36\dot{\alpha}\beta-2\dot{\alpha}v-18\beta v-48\dot{\alpha}\beta v}{I+3\dot{\alpha}+15\beta+36\dot{\alpha}\beta-2\dot{\alpha}v-18\beta v-48\dot{\alpha}\beta v} \\ (A_3)_f &= \left(\frac{-I+2v+\dot{\alpha}v}{2+2\dot{\alpha}-2v-2\dot{\alpha}v} + \frac{2+\dot{\alpha}+112\beta+216\dot{\alpha}\beta+4\dot{\alpha}v-128\beta v+288\dot{\alpha}\beta v}{2(I+5\alpha+56\beta+216\alpha\beta-4\dot{\alpha}v-64\beta v-288\dot{\alpha}\beta v)} \right) \left(\frac{R_0}{H_0} \right) + \frac{-I}{I+\dot{\alpha}+\beta} + \frac{2+30\beta+36\dot{\alpha}\beta+4\dot{\alpha}v-36\beta v-48\dot{\alpha}\beta v}{I+3\dot{\alpha}+15\beta+36\dot{\alpha}\beta-2\dot{\alpha}v-18\beta v-48\dot{\alpha}\beta v} \\ (A_4)_f &= \left(\frac{-2-\dot{\alpha}}{2+2\dot{\alpha}} + \frac{-2-\dot{\alpha}-112\beta-216\dot{\alpha}\beta-4\dot{\alpha}v+128\beta v+288\dot{\alpha}\beta v}{2(I+5\alpha+56\beta+216\alpha\beta-4\dot{\alpha}v-64\beta v-288\dot{\alpha}\beta v)} \right) \left(\frac{R_0}{H_0} \right) + \frac{-I}{I+\dot{\alpha}+\beta} + \frac{-2-30\beta-36\dot{\alpha}\beta-4\dot{\alpha}v+36\beta v+48\dot{\alpha}\beta v}{I+3\dot{\alpha}+15\beta+36\dot{\alpha}\beta-2\dot{\alpha}v-18\beta v-48\dot{\alpha}\beta v} \end{aligned}$$

Figure 5.22: Coefficients A1, A2, A3, and A4 Calculated Based on Hartmann's Solution

Design Method for Shallow Tunnels
Constructed using Pressurized
Shield Methods

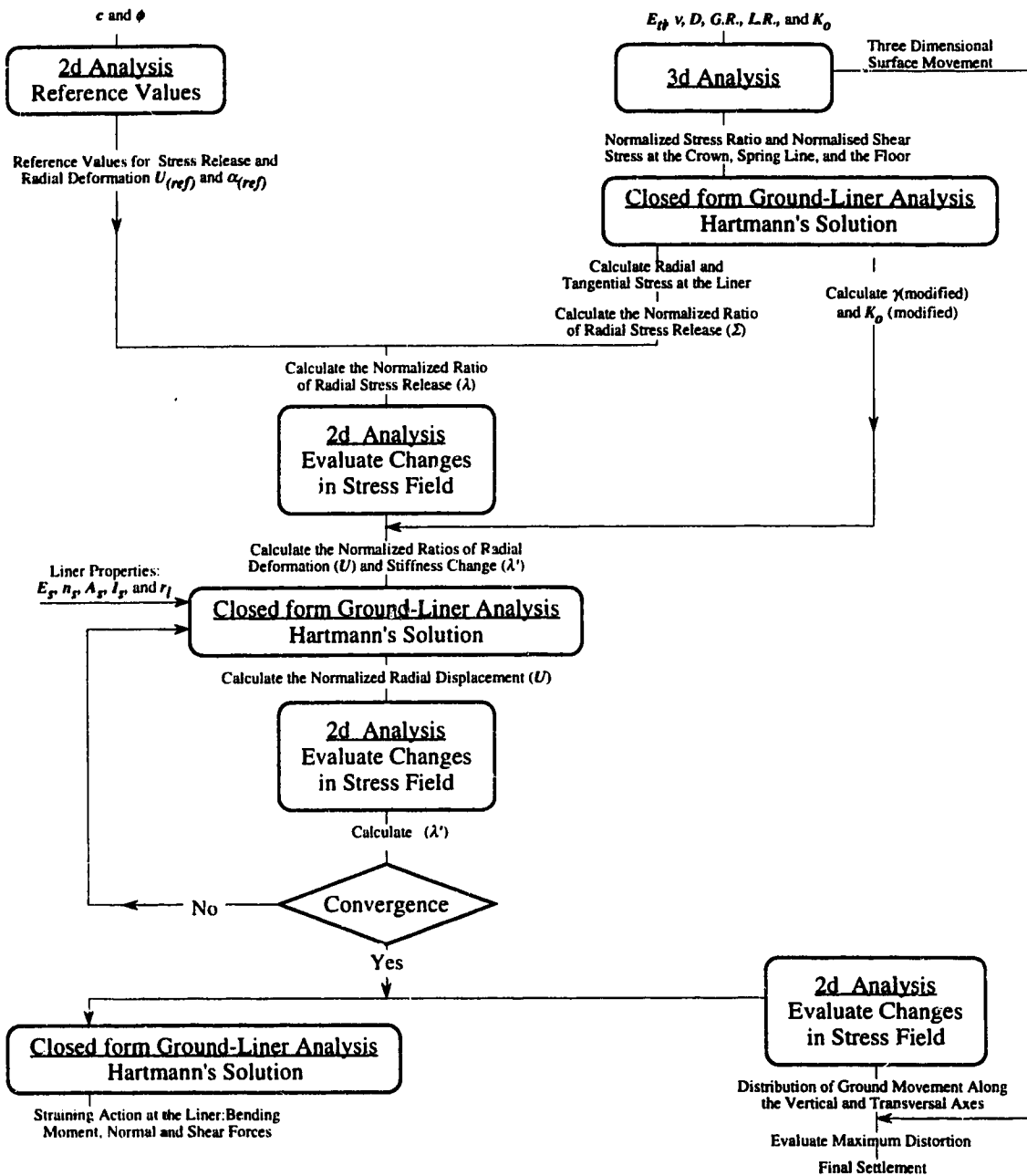


Figure 5.23: Flow Chart of a Design Method of Tunnels constructed using Pressurized Shield Methods

the ground surface. Charts in Appendix B are used to determine the transversal profile of the surface deformation due to three-dimensional effect. As mentioned in the preceding section, an assumption is made by considering the sum and the difference of the principal stresses as the sum and the difference of the radial and tangential stresses at the three points on the tunnel circumference. Equations 5.15 and 5.16 are solved for the given values of SUM and $\pm DIF$ and A_1, A_2, A_3 , and A_4 to get the modified values of γ and K_o for two signs of DIF . The chosen sign of DIF is selected such that at each point the calculated values of γ and K_o are closer to their values at the initial condition. Representative values of the new stress field are calculated as the average values of γ and K_o at the four points of the tunnel circumference. Meanwhile reference values of stress and deformation α_{ref} (or Σ_{ref}) and U_{ref} related to shear strength parameters c and ϕ are calculated from (Negro 1988: Figures 6.92, 6.93, 6.100, 6.101, 6.109, and 6.108).

The ground-liner interaction process starts at the liner. Using Hartmann's solution (Figure 5.5) and the modified ground condition parameters, radial and tangential stresses at the tunnel circumference are calculated. The twice normalized parameter of stress release λ is, therefore, calculated through Equation 5.9. Back substitution into the twice normalized ground reaction curve (Negro 1988: Figures 6.94, 6.95, 6.96, 6.102, 6.103, 6.104, 6.110, 6.111, and 6.112) produces the corresponding twice normalized radial deformation at the three points of the lining circumference U/U_{ref} . The obtained radial displacement u_{r0} through Equation 5.8 is related to the radial deformation that would have taken place if the new stress field were developed in plane strain conditions and should be, therefore, subtracted from the final results. Using U/U_{ref} , the normalized parameter of stiffness, λ , is obtained at the three points of the tunnel circumference (Negro 1988: Figures 6.97, 6.98, 6.99, 6.105, 6.106, 6.113, 6.114, and 6.115). Based on Equation 5.11 new values of the deformation modulus, E_{ti} , are calculated and an average value is calculated. If the value of the new modulus is close, within acceptable tolerance, to the preceding value the solution is considered to be convergent. Otherwise, the new value of E_{ti} is introduced into Hartmann's solution for a new round of iteration. General application of the method shows that a number of iterations, around three or four, is enough to reach acceptable convergence.

As convergence is achieved, final results can be calculated. For the new stress field, straining actions inside the liner are assessed using Hartmann's solution (Figure 5.5). Radial deformation is assessed by subtracting u_{r0} from the final value of radial displacement. For the calculated radial stress release, Σ , the relation between the crown and the ground surface displacement are determined through a number of charts (Negro 1988: Appendix C). These charts provide the deformation profiles at the ground surface

and at the vertical axis of the tunnel because of ground-liner interaction. Final ground deformation is determined by adding the three-dimensional deformation previously obtained to the ground lining deformation.

5.7 Application: Edmonton LRT Tunnel

The expansion of the LRT system in the city of Edmonton requires the construction of a twin tunnel of about 6 m diameter through a complicated geological profile. Figures 5.24 and 5.25 show a general alignment and a simplified ground section. The main difficulty encountered was during the construction of the southbound tunnel from Grandin Station to the North Portal on the Saskatchewan River because the excavation had to go through a layer of post-glacial deposits consisting mainly of medium dense sand with a low amount of cementation. Here a conventional shield without a face support was chosen as the method of excavation in conjunction with jet grouting around the cross section in order to improve the ground properties. Excessive settlement took place. The nature of the ground movement was characterized as being local and funnel shaped starting at the tunnel crown and extending upward to the ground surface. Therefore, during the construction of the northbound tunnel, using the pressurized shield method, the Hydrosield, was selected to accommodate the difficult ground conditions. As described by Eisenstein and Ezzeldine (1992:a), the total length of the project is about 305 m and the tunnel's crown is about 13 m deep. The most critical part of the project is between 100.0 to 260.0 m from the river bank portal.

5.7.1 Ground Conditions

A simplified profile of ground conditions at the project is shown Figure 4.12. Four main geological patterns are distinguished: glacial till, post-glacial deposits consisting of sand and gravel, basal sand, and bedrock. The geology of the area is investigated and presented by Thomson and Townsend (1979) and the engineering properties of the site were carried out and presented by Hardy BBT Ltd. (1988). Preglacial channels are formed due to a subaerial erosion with its thawleg running close to the existing North Saskatchewan River. A number of factors such as erosion and valley rebound after the glacial ice retreat are responsible for the irregular surface of the bedrock at the project site. The material is described as an Upper Cretaceous sedimentary sequence of poorly indurated clay shales, coal, and siltstone with bentonite as an admixture between the seams. The till layer is encountered at the first part of the project usually as part of a mixed face condition with the bedrock. Since both materials are highly competent, construction conditions are easier than at the following parts of the project. The till is a medium plastic clay soil in a

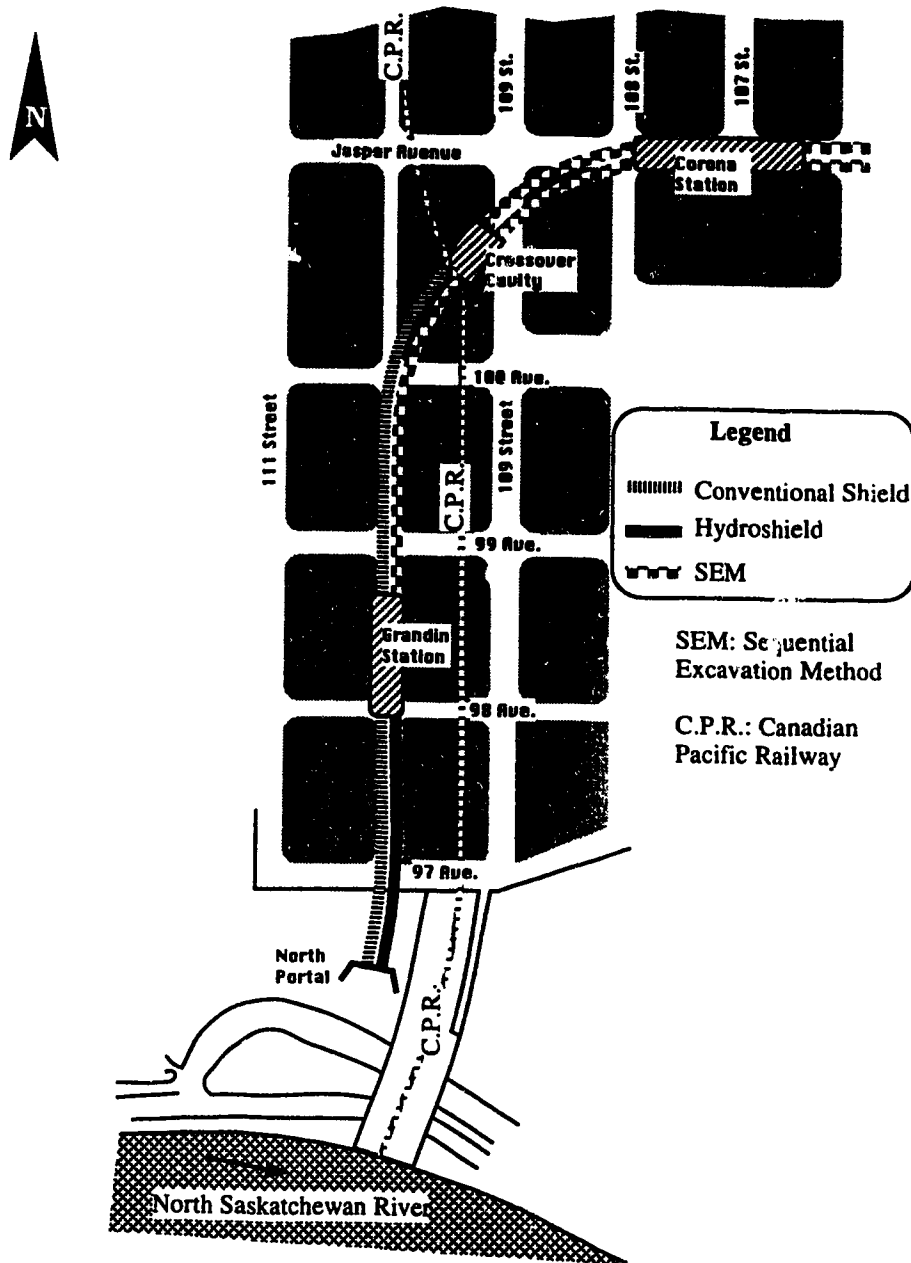


Figure 5.2 : Site Plan of the Edmonton LRT Project

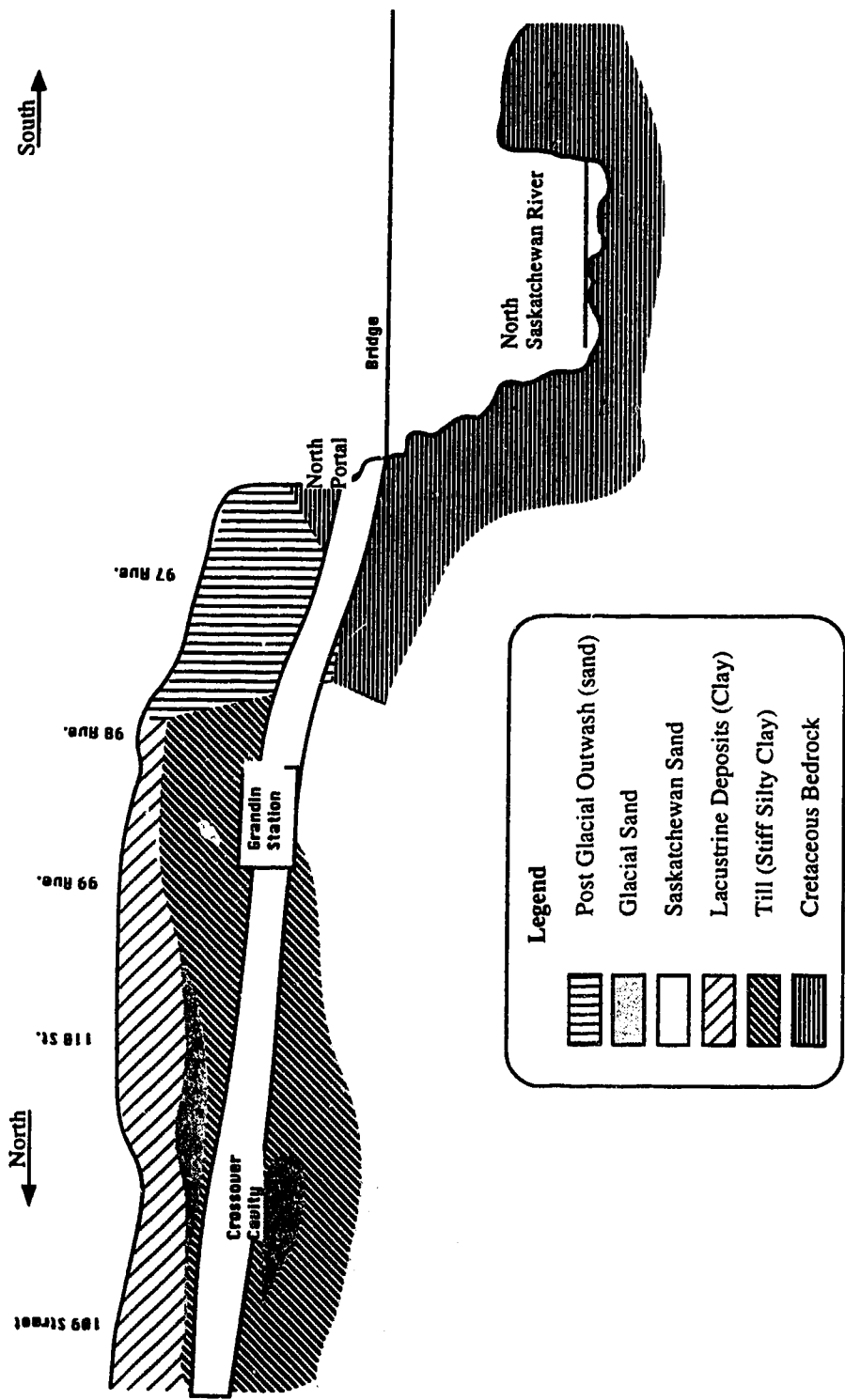


Figure 5.25: Simplified Geological Profile for the Edmonton LRT Project

hard state of consistency, and it is interspersed with numerous sand lenses and partings, small pebbles, bedrock fragments and occasional cobbles. The till along the project has been heavily overconsolidated and, as a result, it is cracked and fissured. Results from this investigation show the Standard Penetration Test (SPT) number ranging from 33 to 100. Post-glacial deposits are mainly sand and gravel at the tunnel section. Alluvial debris sediments are found in the form of isolated layers of silt. Clay layers with sand and silt predominate at the upper 5 to 10 m. Investigation of the sand and gravel layers has given SPT numbers ranging between 12 and 86 blows indicating a variation of density between medium and very dense deposits. Triaxial tests on Shelby tube samples of sand shows an effective friction angle, ϕ , of about 33.5° . The presence of silt results in a higher value of ϕ . Pressuremeter tests were conducted in the sand deposits and yielded unrealistically high values of E (around 400 MPa) and of K_o (from 1.1 to 1.8). Basal sand is known locally as Saskatchewan sand and gravel and it was deposited by preglacial streams and rivers. Sand particles are comprised of a closely even mixture of quartz, chert, and metamorphic and volcanic fragments. Performed Standard Penetration tests have shown that the formation is in a very dense state as the SPT number ranges between 117 and 200. Triaxial tests performed on remoulded and "undisturbed" block samples show that the angle of internal friction, ϕ , is about 37.5° . The planned alignment of the tunnel trajectory was selected to avoid the basal sand as much as possible because of its lack of cohesion. The water table is mainly below the tunnel invert and occasional water seepage is encountered because of an existing abandoned sewage line, and because of surface water flow.

The preliminary settlement analysis was carried out by W. Wittke (PCL-Hochtief, 1988:b). Calculations were carried out on the basis of the geotechnical parameters provided by the City of Edmonton (UMA, 1988). These parameters are derived from back analyses of data from projects constructed in the area. Typical values of the proposed parameters for the four formations in the project are presented in Table 5.4 .

5.7.2 Construction Details

As demonstrated in Chapter 2, the Hydroshield method exerts on the face using the bentonite slurry regulated by an air cushion. As excavation proceeds, the shield is pushed forward against the erected liner using hydraulic jacks (fourteen main jacks) at the same time, the newly exposed lining ring is grouted. Then, a new ring of segmented lining is assembled inside the shield. The lining system (refer to Figure 2.3) consists of seven segments and a key. In order to maintain the face stability during the lining assembly, the shield is pushed against only six segments using twelve main jacks until the entire ring is completed and the shield becomes ready for a new drive using the full jacking forces.

Type of Soil	Unit Weight kN/m ³	Shear Strength		Elastic Modulus E MPa	Earth Pressure Coefficient Ko
		ϕ (°)	c kPa		
Till	20.0	35	25.0	25.0	0.7-1.0
Basal Sand	20.0	35	0.0	50.0	0.7-1.0
Post Glacial Channel Deposits	19.0	30	0.0	10.0	0.7-1.0
Bedrock	23.0	40	50.0	50.0	0.7-1.0

Table 5.4: Soil Properties at Edmonton LRT Site (after PCL- Hochtief 1988)

Applied grout pressure along the tunnel trajectory is presented in Figures 5.26 based on installation records (PCL-Hochtief, 1990). From the figure it is noticed that a grout ratio **G.R.** is selected for the entire project to be around 150% . At the first stage of the project where the tunnel cross section is excavated completely in relatively competent bedrock, the grout pressure can be easily regulated. In the mixed face zone (bedrock-sand and gravel) the grout pressure was frequently reduced to about 75% in order to avoid excessive losses of grout material. In the post-glacial sand and gravel zone, better control of grout losses allowed the increase of grout pressure from the average value. In the final stage of the tunnel governed by basal sand deposits grout pressure reduction has found to be reduced again to about 75% . Grout volume losses are demonstrated in Figure 5.27. According to the shield machine specifications PCL-Hochtief (1988:a) the distance between the extrados of the shield and that of the liner, which is called the physical gap, is 89.5 mm around the circumference which results in a gap volume of 1.82 m³ per metre length. Excess grout volume is calculated as:

$$\text{Excess Grout Volume} = \frac{\text{Grout Volume} - \text{Gap Volume}}{\text{Gap Volume}} \times 100 \quad (5.19)$$

From the figure, it can be shown that the loss of grout material has been totally avoided in many occasions in the bedrock zone. In the mixed face and in the post-glacial deposit zones substantial loss of grout material took place. This may be attributed to a number of factors such as the high permeability of the sand material, the non-homogeneity of the surrounding ground, and to the high grout pressure applied. The final zone of basal sand exhibits relatively more restrained grout losses mostly due to grout pressure reduction and to the relatively more homogeneous ground profile. It is to be noted that on a number of occasions, failure of the tail seal has occurred. This is characterized by a sharp and sudden drop in grout pressure and a sudden increase in excess grout volume. From the figures infiltration of grout material into the surrounding ground takes place and results in loss of grout material and loss of effectiveness in the application of grout pressure. Back analysis of the case history requires, therefore, a certain assumption regarding the amount of reduction of grout pressure. Liner pressure ratio, **L.R.**, is presented in Figure 5.28 based on installation records (PCL-Hochtief, 1990) and on the assumption of an average K_c of 0.8 for the whole project. From the figure, a certain amount of discrepancy is noticed between the push pressure (during ring assembly) and the drive pressure (during excavation). Nevertheless, the general pattern is that **L.R.** is related to the ground stiffness. Therefore, the least liner pressure is recorded at the zone of post-glacial deposits

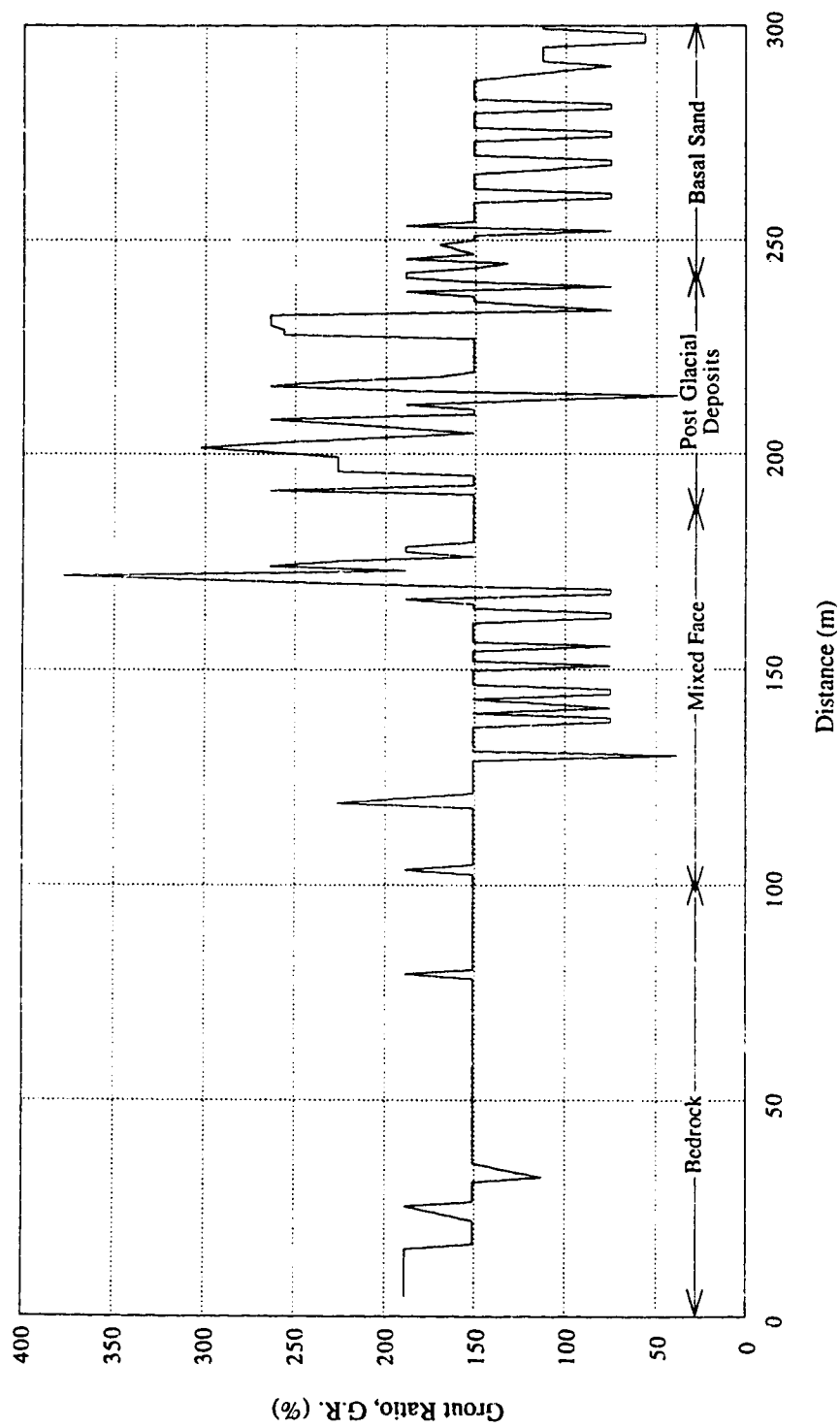


Figure 5.26: Grout Pressure Ratio used at the Edmonton LRT Project

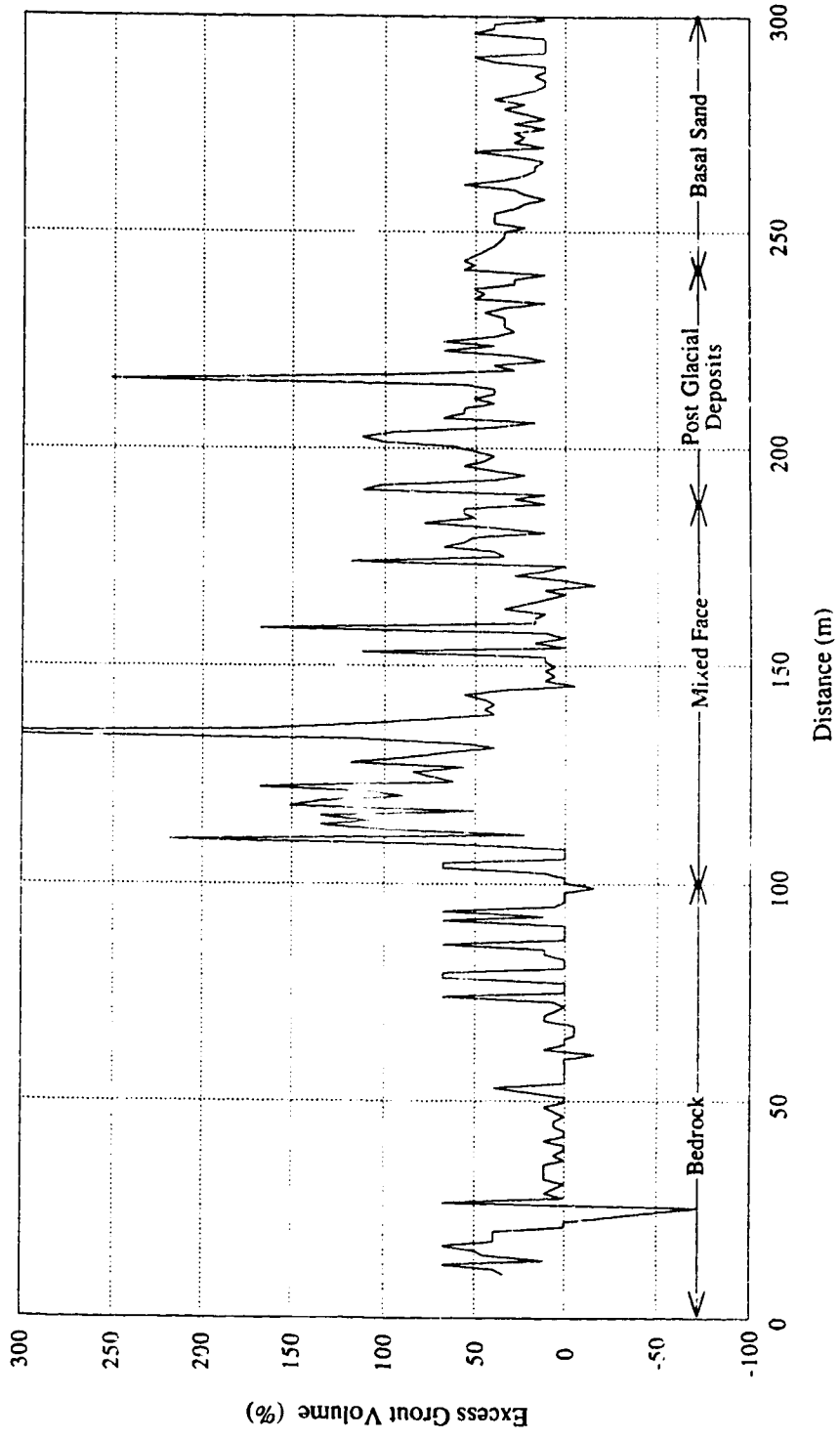


Figure 5.27: Excess Grout Volume used at the Edmonton LRT Project

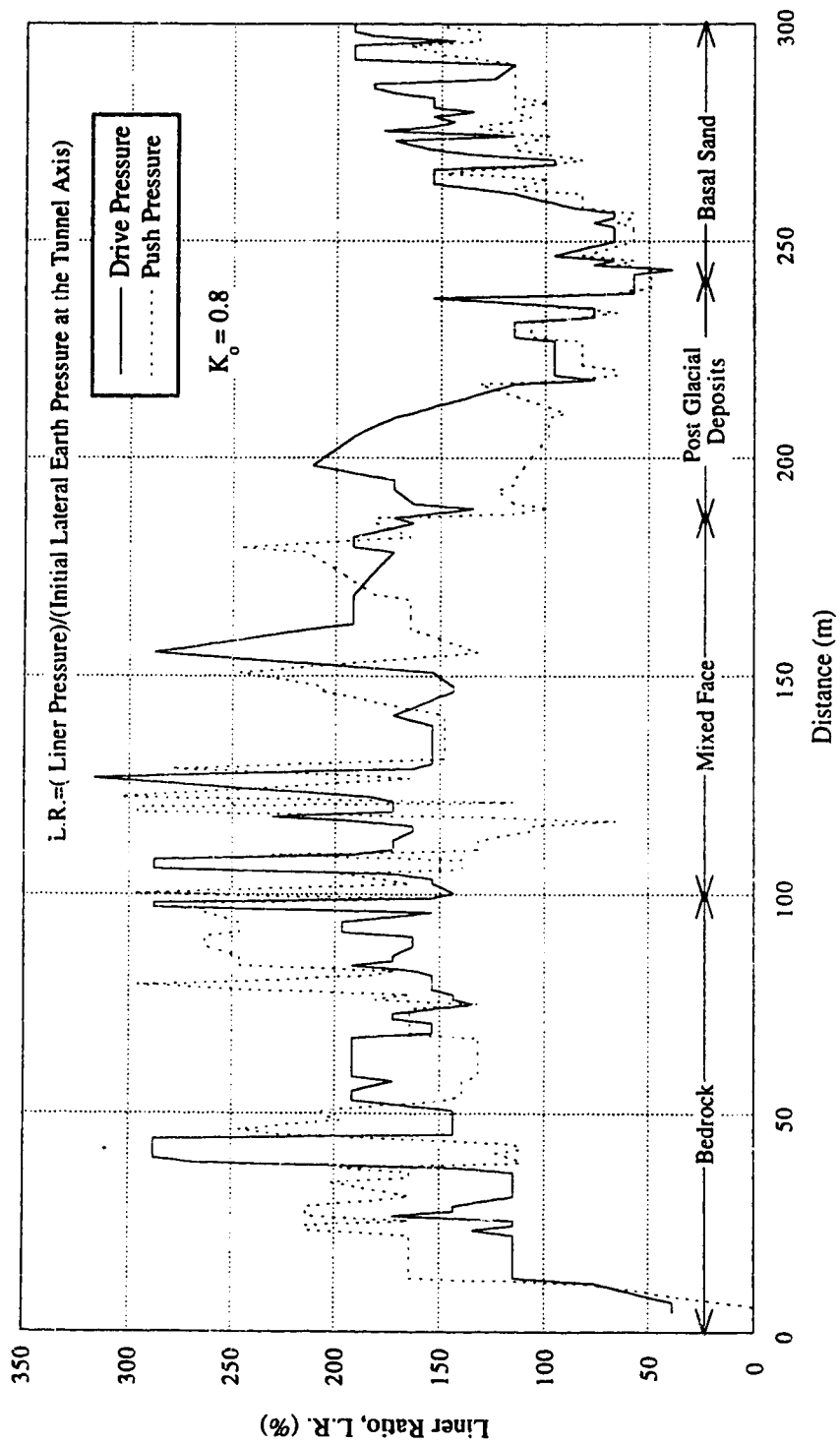
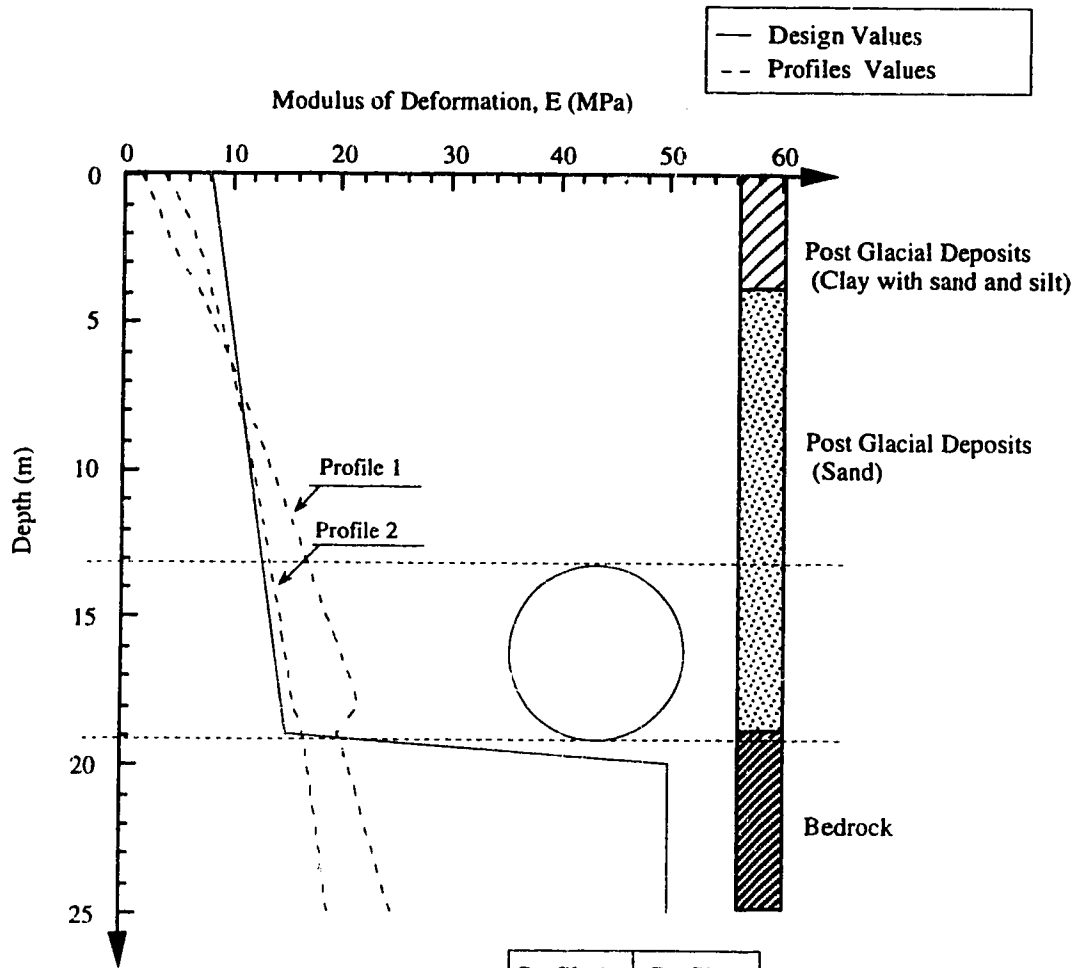


Figure 5.28: Liner Pressure Ratio, L.R. used at the Edmonton LRT Project

where 50% may be considered an extreme minimum and the highest pressure is recorded at the mixed face zone due to the existence of bedrock at the lower portion of the tunnel cross section. A value of 250% may be considered as an extreme maximum value.

5.7.3 Algorithm of the Design Method

As an example of the implementation of the design method to the LRT project, two soil profiles are selected to simulate a typical ground condition in the post-glacial deposit zone. The values of the proposed parameters are shown in Figure 5.29. A detailed numerical example is provided for the case where an *L.R.* of 100% and a *G.R.* of 75% are assumed for Profile 2. The selected values are intended to be representative of the actually applied liner pressure, and the effective grout pressure is considered to be one half of the applied pressure because of losses in grout pressure and grout material (see Babendererde (1985)). A FORTRAN program was formulated to produce the final results directly. The program is presented in Appendix C. Appendix D shows the input file for the detailed example and Appendix D shows the output file. The units of all input and output data are specified at the end of the output file. The input file consists of eight lines. The first line of the input file contains the title of the project. The second line contains the ground properties: H , D , γ , K_o , c , ϕ , $(R_f)_h$, $(K)_h$, $(n)_h$, P_a , ν where P_a is the atmospheric pressure. The fourth line contains the construction details: *G.R.* and *L.R.* . The fifth line is disregarded. Liner properties are entered at the sixth line: E_l , ν_l , A_l , and I_l . The modulus E_l is chosen to be 37 GPa which is an average value for reinforced concrete used in the precast segmental liner. It is to be observed that the original Eisenstein-Negro method suggests the use of a reduced liner modulus as the new casted concrete mix is not completely cured at the time of lining activation. It is considered that this is not applicable for the case of the precast segmented liner. Values of ν_l are chosen within average values for reinforced concrete: A_l is the cross sectional area of the liner per unit length and I_l is the moment of inertial of the liner. A reduced value is chosen to take into account the effect of joints between segments. Then, the depth of the firm ground level below the tunnel axis (R_l) is entered at the seventh line. In this case R_l is chosen to be equal to the tunnel radius, thus, no ground heave is included in the calculations. This assumption is taken based on the geological profile where the bedrock formation is either close to the tunnel floor or above it in the case of the mixed face condition. Then the number of iterations required during the ground-liner interaction calculations is entered at the eighth and last line. From the output file it can be shown that convergence has occurred after the second iteration. The last input parameter is an indicator of whether a special detailed output file is required.



	Profile 1:	Profile 2:
K_o	1.0	0.8
γ	20 kN/m ³	20 kN/m ³
$(K)_h$	70.00	90.00
$(n)_h$	0.85	0.5
$(R_f)_h$	1.0	1.0
c	0.0 kPa	0.0 kPa
ϕ	30°	30°

Figure 5.29: Profiles of Ground Parameters at the LRT Project versus the actual Design Parameters

5.7.4 Detailed Numerical Example

The first step is to evaluate the three-dimensional effect using the equations and coefficients given in Tables 5.1, 5.2, and 5.3 . The input parameters are ν , K_o , and H_o/R_o . The parameters $S.R.$ and $D.S.R.$ are evaluated, respectively, as 91.69% and 11.85% at the crown, 100.165% and 28.85% at the spring line, and 84.69% and 22.49% at the floor. The surface movement parameter ω_s is calculated to be 22.07 . Based on the definitions of $S.R.$ and $D.S.R.$ the mean normal stress p and the deviatoric stress ρ are calculated, respectively, as 203.84 and 37.78 kPa at the crown, 276.75 and 91.98 kPa at the spring line, and 279.74 and 71.70 kPa at the floor. The stress conditions are not allowed to violate a failure criterion related to the shear strength parameters. The developed program is formulated such that the Mohr-Coulomb criterion is selected for frictional material and the Von Mises criterion is selected for cohesive material. Thus the two conditions:

$$\sin \phi \geq \frac{3\rho}{\rho + 2\sqrt{6}p} \quad (5.20)$$

for purely frictional material, and

$$c \geq \sqrt{2}\rho \quad (5.21)$$

for purely cohesive material.

In the case of c - ϕ material, the approximation proposed by Negro (1988) indicated in Equation 5.7 for ϕ_a is used. For this specific case, the failure criterion for the angle of friction ϕ of 30° is not violated. According to Equations 5.13 and 5.14 the major and minor principal stresses in the triaxial configuration σ_1 and σ_3 are, respectively, 234.69 and 188.41 kPa at the crown, 351.87 and 239.22 kPa at the spring line, and 338.28 and 250.47 kPa at the floor. Hyperbolic parameters $(R_f)_h$, $(n)_h$, and $(K)_h$ are implemented into the hyperbolic model (Figure 5.6) to yield the tangent modulus of deformation E_t as 9.57 MPa at the crown, 8.19 MPa at the spring line, and 9.75 at the floor. A mean value of E_t of 8.93 MPa is calculated based on the average of four points. This value is used in estimating surface movement due to the three-dimensional effect according to Equation 4.15 which gives 5.17 mm. Then, the relative values of the liner α and β are calculated based on lining parameters A_l , I_l , E_l , and ν_l , as well as, on the ν and the average E_t of the ground (Equations 5.5 and 5.6) and are found to be, respectively, 379.25 and 0.0127

at the crown, 443.07 and 0.0148 at the spring line, and 372.13 and 0.0124 at the floor. Constants A_1 , A_2 , A_3 , and A_4 are calculated from Figure 5.22, respectively, as 0.107, 1.856, 0.440, and 0.390 at the crown, 1.56, 0.43991, 0.56, and 0.558 at the spring line, and 0.142, 2.40, 0.660, and 0.72 at the floor. Modified values of γ and K_o are calculated and are, respectively, 19.27 kN/m³ and 0.763 at the crown, 20.22 kN/m³ and 0.413 at the spring line, and 25.62 kN/m³ and 0.63 at the floor. A restrictive condition has to be implemented regarding the value of K_o . As interpolation through the given chart using the Eisenstein-Negro method has to be performed within the investigated range, the value of K_o is not allowed to be lower than 0.55 or higher than 1.1. Therefore, K_o at the spring line is corrected to 0.55. Average values on the four point basis are 21.33 kN/m³ for γ and 0.624 for K_o . According to the rational given in Section 5.6.4 about the choice of the direction of the principal stresses and the sign of DIF , radial stresses are given the same values as the principal stresses at the crown and at the floor. In the case of the spring line, σ_r and σ_θ have to be recalculated according to the new value of K_o . Therefore, σ_r is 351.87 and σ_θ is 239.217 kPa at the spring line. The determination of σ_r on three points of the circumference allow the determination of the radial stress release Σ that will be 91.45%, 120.0% at the spring line, and 88.76% at the floor.

At this point, the problem is reduced to an equivalent plane strain problem where the stress field is determined according to the new modified average values of γ and K_o . The amount of stress release is determined according to the radial stress ratios Σ on the three points of the circumference. The Eisenstein-Negro method can, therefore, be applicable for the new conditions. Reference values are determined according to the shear strength parameter ϕ . Thus, α_{ref} , and U_{ref} are calculated. Accordingly, λ is evaluated from Equation 5.9. By substituting back into Negro's charts (Negro 1988: Figures 6.97, 6.98, 6.99, 6.105, 6.106, 6.113, 6.114, and 6.115), the nondimensional circumferential displacement U/U_{ref} , and accordingly the radial displacement u_r are calculated. These displacements are considered the equivalent displacement that would have taken place had the stress and strain fields been plane strain during the excavation process. For the new stress field, a process of ground-liner interaction is calculated according to the Eisenstein-Negro method, and convergence is reached giving the straining actions at the tunnel lining and the displacement at the circumference. Displacement at the crown because of ground-liner interaction is found to be 15.09 mm which corresponds to 5.9 mm at the ground surface. Adding surface movement due to ground-liner interaction to the movement due to the three-dimensional effect (5.17 mm) gives the final movement at the ground surface (= 11.06 mm).

5.7.5 Validation of the Results

The design method is used a number of times in order to provide a scan of the estimated values of the ground surface movement for various values of $G.R.$ and $L.R.$. Figures 5.30 and 5.31 show the estimated maximum ground displacement for the two profiles of the ground conditions suggested in Figure 5.29. A reduction factor of 2.5 is used to calculate the effective grout pressure with respect to the actual applied grout pressure. Therefore, the measured displacements at the ground surface are plotted in the figure using the effective grout pressure related to the average grout pressure at the location of the measurement. From Figures 5.30 and 5.31, $L.R.$ corresponding to the measured displacements ranges between 50% and 150% as extreme values which corresponds to the actual $L.R.$ applied at the ground. In general then, as grout pressure increases and the lining pressure decreases, surface movement decreases. Grout pressure provides support to the ground after excavation and tends to restrict and reverse ground intrusion into the tunnel. Meanwhile, lining pressure although it provides support at the face, results in increasing the stress relief behind the shield, and thus leads to an increasing surface displacement although its effect is not obvious at the crown level. The settlement profile is estimated by adding the magnitude of the settlement profile calculated from the Eisenstein-Negro method for the plane strain analysis (Negro (1988): Appendix C) to that calculated from the three-dimensional effect (Appendix B). Interpolation between a number of charts is necessary to obtain the settlement trough corresponding to the actual ground conditions. Figure 5.32 shows that the measured surface displacement in the transversal plane as compared with the estimated surface trough for $L.R.$ equals 100 % considering ground properties at Profile 2 (Figure 5.29). It is found that the method overestimates the trough width and a correction factor of 0.8 is multiplied by the estimated width length (y) to emulate the measured surface trough. Straining actions in the liner are calculated for the same parameters. Lining thickness is calculated as the equivalent uniform thickness of the actual cross-sectional area of the segment which is equal to 232 mm. A reduced moment of inertia is calculated for the liner to take into consideration the effect of the segmental joints. The selected value is $8.33 \times 10^{-5} \text{ m}^4$ which is equivalent to a segment of 100 mm thickness. The calculated normal forces, shearing forces, and bending moments are shown in Figures 5.33 and 5.34 . The figures show that as the objective of the construction method is to minimize ground disturbance around the tunnel, normal forces are close to the initial soil pressure while shear and bending moments within the liner have relatively low values.

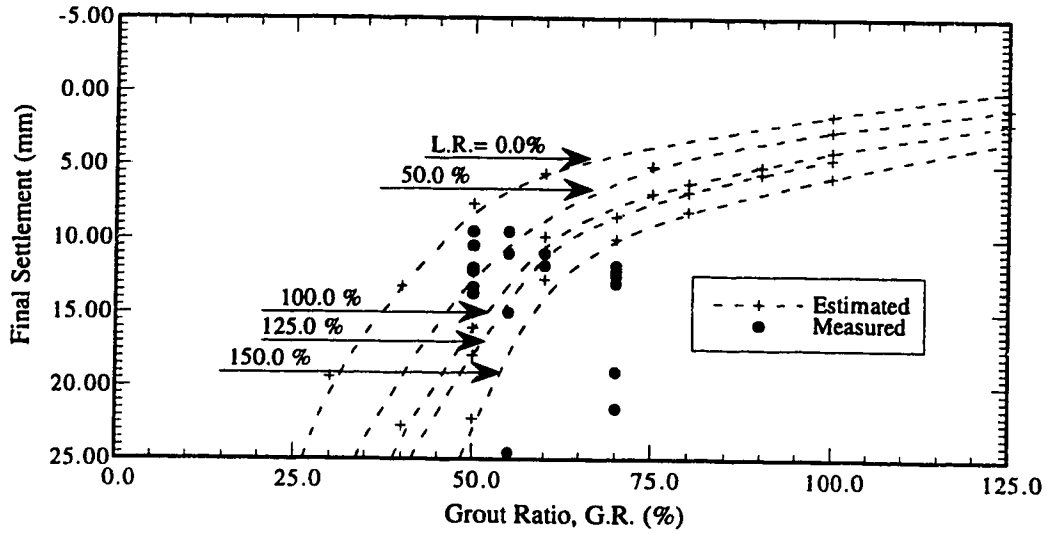


Figure 5.30: Measured and Estimated Maximum Ground Surface Settlement versus the Grout Ratio at the Edmonton LRT Project, Material Parameters of Profile 1

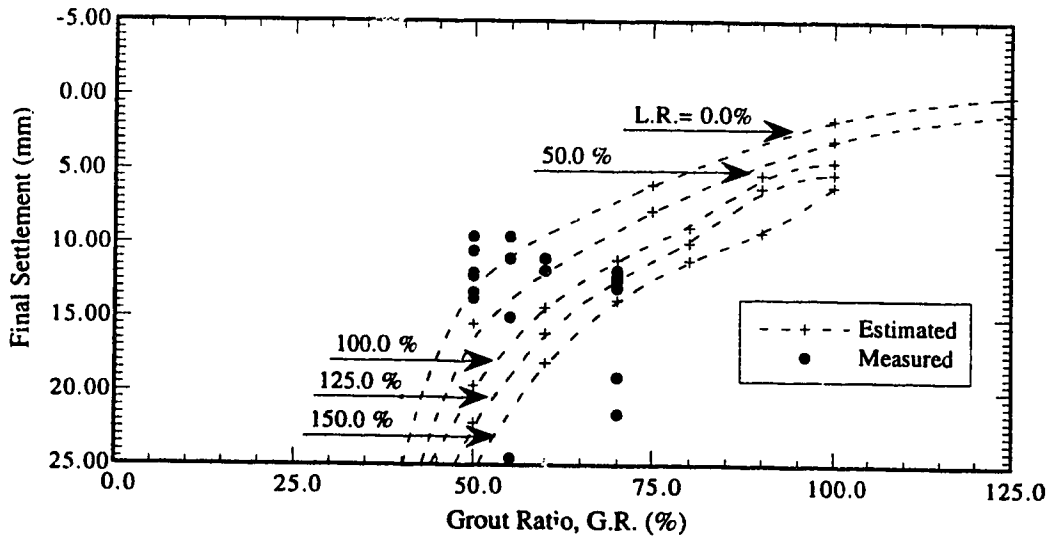


Figure 5.31: Measured and Estimated Maximum Ground Surface Settlement versus the Grout Ratio at the Edmonton LRT Project, Material Parameters of Profile 2

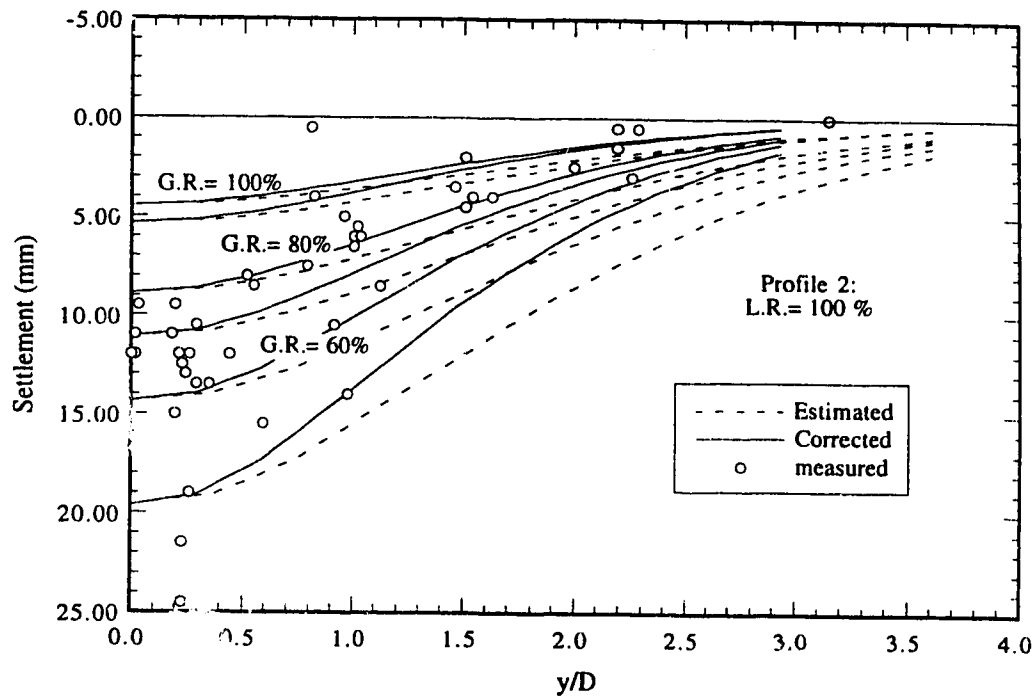


Figure 5.32: Measured and Estimated Settlement Trough at Ground Surface at the Edmonton LRT Project, Material Parameters of Profile 2

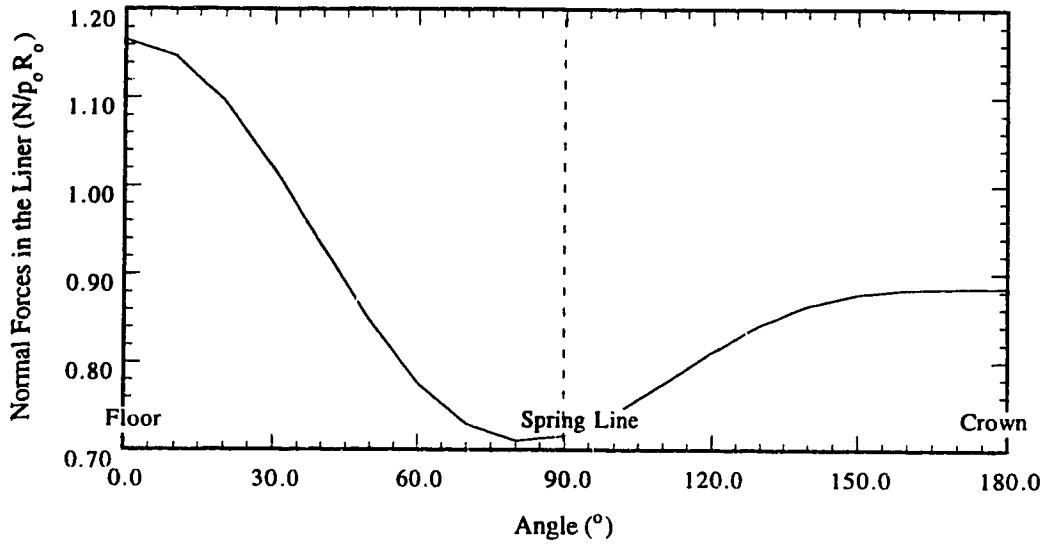


Figure 5.33: Calculated Normal Forces at the Liner Edmonton LRT Project, Material Parameters of Profile 2

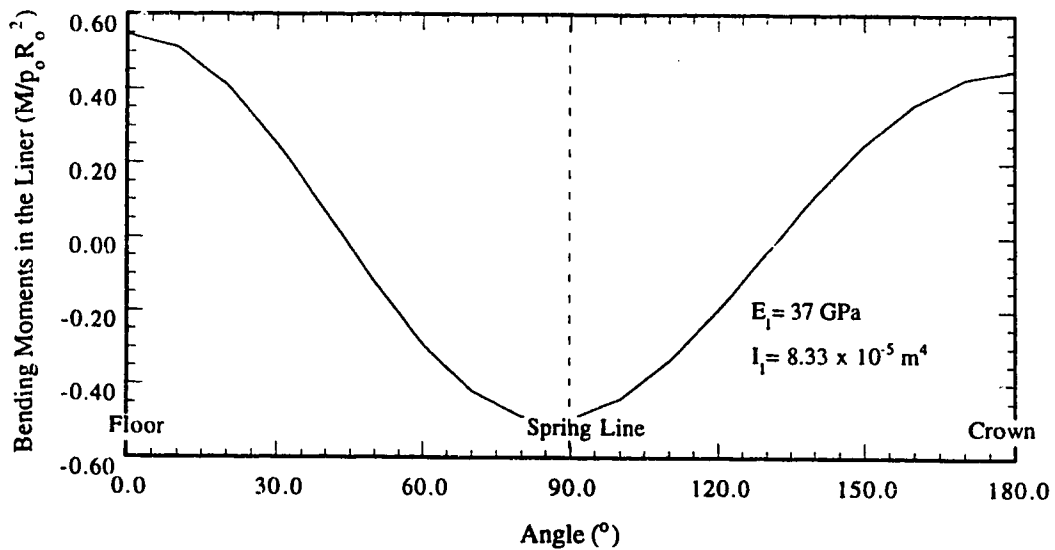


Figure 5.34: Calculated Bending Moment at the Liner Edmonton LRT Project, Material Parameters of Profile 2

5.8 Conclusions

Tunnelling design methods are required to produce estimations of the final stress field around the excavation and the straining actions inside the lining system. A review of a number design methods and of their estimations compared to field measurements is given. Special emphasis is made on the Eisenstein-Negro method for shallow tunnel as it provides a number of realistic assumptions concerning the ground deformation model and the initial stress conditions.

A certain number of adaptations to the Eisenstein-Negro method are effected in order to apply the method to cases of tunnels constructed using pressurized shield methods. The three-dimensional effect is based on the three-dimensional analysis presented in Chapter 4. The concept of the tunnel-ground interaction is suggested instead of the concept of volume loss to evaluate of the stress field around the tunnel at the tail of the shield. The resultant stress field at the tail is introduced into the original method to calculate the stress changes around the liner using the twice normalized ground reaction curve NNGRC. According to the original method Hartmann's solution is used to evaluate the straining actions inside the liner, as well as, the lining displacement. The final movement at the ground surface is calculated as the resultant of the displacement due to the three-dimensional effect and that due to the ground-liner interaction.

The proposed design method is applied in the case of the LRT tunnel constructed in Edmonton using the Bentonite Slurry Shield, the Hydroshield. Input parameters are selected according to actual design parameters and according to the field lining installation records. Estimations of the ground movement are shown to compare well with the measured ground movement at the site.

CHAPTER 5

CONCLUSIONS

The present research work deals with the geotechnical implications of the use of pressurized shields in tunnel construction. As presented in Chapter 1, the aims of the study are:

- (1) to provide a better understanding of the pressurized shield methods by identifying their different methods, the specific constructional and mechanical characteristics involved in each method, and the actual field performance of each method with respect to the economy and the safety requirements of the project;
- (2) to investigate the stress-and-strain fields related to tunnel construction using pressurized shield methods in light of current state-of-the-art of shallow tunnel analyses, and thus to estimate the specific features of the developed stress field related to these methods. Special emphasis is directed toward the expected mechanisms of failure, displacement at the ground surface, and straining actions on the liner;
- (3) to identify soil parameters that affect the ground response to tunnelling activity and the stress paths that are expected to take place at different construction stages;
- (4) to develop a design method that takes into account the new construction techniques and that enables the evaluation of the resulting ground deformation and the straining actions in the liner;
- (5) to validate the proposed design method by comparing it with actual case histories;
- (6) to put the results of the analysis within the perspective of current developments in constructions methods and of the prospected developments in the near future and, at the same time, to take into account the emerging requirements of successful tunnelling practices in modern urban areas; and

(7) to present the formulated design method in a comprehensive manner and in a way that enables it to be used by practitioners.

A classification of pressurized shield methods is presented in Chapter 2. Three main methods are identified: the BSS, the EPBS, and the compressed air shield method. The investigation of the case histories throughout the available literature shows that, in general, pressurized shield tunnelling, specifically, the BSS and the EPBS methods are most commonly used in recent years and they have been implemented in various projects around the world. Tunnel sizes vary between 3 to 11 m in diameter and the construction includes transportation, sewage, and storm-water galleries. Improvements in the technical details allow tunnelling activity through difficult conditions such as construction under river beds, through highly permeable soils, through noncompressible soils, through very heterogeneous ground, and near deformation sensitive structures and so forth. The most commonly adopted lining system is the precast-concrete-segmental liner. Recently, the use of extruded concrete lining in some projects has proven to be a promising alternative, with respect to, the control of the ground surface settlement.

The main advantage of pressurized shield tunnelling methods is that they allow for the protection of the circumference of the excavation from the location of the face to the point of the lining activation. Therefore, the only conceivable mechanism of failure is at the face. A theoretical idealization of stress changes at the face is suggested based on the principle of passive stress relief. Accordingly, the coefficient of confinement is defined and an idealized stress path is proposed to simulate the actual stress changes at the face of the excavation. Experimental models and centrifuge tests of face collapse are compared with analytical solutions estimating the limit pressure at the face. A finite element analysis was carried out to estimate the limit face at the face required to achieve stability for various ground conditions. The results of the analysis are presented in a simplified form and they are compared to actual field conditions. The comparison shows that the level of face pressure used in successful projects is equal to or higher than proposed expression results.

A review of the concept of volume losses and the principle of ground confinement derived from that concept is undertaken. The above concept established for cases of conventional methods of tunnelling is re-examined for cases of pressurized shield tunnelling. At the same time, an approach is proposed for shield tunnelling at shallow depths that relies on considering ground structure interaction around the tunnel circumference. According to the proposed concept, the tunnel is considered as a hollow structure with the reference point below it at the depth of the rigid layer instead of considering the tunnel as a cylindrical void in a soil mass with its reference point at the centre of the circle. A finite element analysis is carried out to establish relationships

between the main parameters associated to ground conditions and to the construction method with the stress state around the tunnel and the displacement field at the ground surface. The analysis is based on a three-dimensional simulation of a tunnel of dimensions corresponding to average values of actually existing tunnels. The study takes into consideration the sequence of the construction process for various values of face and grout pressure. As the adopted constitutive model is a simple linear elastic model, the obtained results related to the state of stress around the tunnel and to the displacement at the ground surface are curve fitted into linear relationship.

The Eisenstein-Negro method is chosen in order to put the obtained results into a frame-work that allows them to be generalized for tunnel designers. Adaptations are made to the method to include the effect of longitudinal liner pressure and grout pressure on the stress field. Meanwhile, the basic concept of the Eisenstein-Negro method is maintained so that a state of stress change is imposed around the tunnel based on the hyperbolic model. Then, conditions of equilibrium and compatibility are met at the boundary between the soil and the lining system at three principal points: the crown, the spring line, and the floor. Stresses inside the lining are calculated using a closed form elastic solution: Hartmann's solution. The design method is provided in a computer program that facilitates its use.

As an example of the application of the proposed design algorithm, the Edmonton LRT extension project is considered. Data from installation records data and back-calculated ground parameters are used as input data and the results are compared with the recorded ground surface displacement at the site. Close agreement is noticed between the ranges of values of maximum settlement while a reduction factor may be suggested for the width of the settlement trough.

The advantages of the proposed design method are that it takes into account the gravitational stress field and the effect of strain softening through the hyperbolic model while an accurate ground-liner interaction allows the estimation of the straining action inside the lining system. Details of the construction process are represented through a step-wise simulation that takes into account the magnitudes of the longitudinal liner pressure and that of the grout pressure at each excavation step. As such, the design method can accommodate cases of pressurized shield methods that uses extruded concrete lining systems by assigning an appropriate grout ratio related to the effective pressure of the injected concrete. In addition, the method is applicable to cases of high-face pressure which is expected in the cases of EPBS. The analysis shows that the positive effect of high face pressure is restrictive to displacement at the ground surface only if appropriate measures of ground control are provided at the tail of the shield. These measures include a sufficient grout pressure and an efficient system of tail seals at the end of the shield.

In conclusion, the aims of the research are fulfilled with respect to the literature available and the computer system at hand. Interest in studying the effects of pressurized shields methods is expected to grow in the subsequent years, along with the rising need for more efficient tunnelling methods. Experimental models, especially centrifuge models can provide useful tools for better understanding the mechanism of face failure in different ground conditions. Also, the performance of injection materials whether at the face or behind the lining system are of crucial importance for the success of the construction method. For example, there is a need to determine the best composition of bentonite that will allow the slurry to effect its complicated role as a face supporting material, and an impediment to groundwater intrusion, and at the same time acts as a muck transporting agent. It is expected that a certain amount of grout material and grout pressure is lost during the interaction between the grout material and the surrounding soil due to the effect of a number of factors such as bleeding, aggregate segregation, and the effect of the physical gap. The determination of the best composition of grout material for different ground conditions and at different grout pressure levels is expected to be beneficiary to both to the economy and the safety of the project. Numerical analyses using finite element methods are extensively employed to study the various aspects of tunnelling methods. It is expected that their role will further increase in the near future, especially as computer systems reach higher degrees of sophistication. As this study shows, parametrical analysis using three dimensional models is presently affordable. Nevertheless, the accuracy of the results have to be improved as the finite element mesh is refined. Furthermore, there is a need to establish relationships between various influencing parameters affecting the stress and strain fields around the tunnel. The assessment of time effects and changes in pore pressure due to tunnelling is of major importance, especially, for the design of tunnels constructed using the compressed air method. Instrumentation techniques are of a particular importance in allowing the quantifying the effects of pressurized tunnelling. Besides, conventional displacement monitoring at the ground surface and within the ground mass, there is a need to improve methods of measuring stress conditions around the tunnel and inside the liner. Similarly, measurement of the changes in the ground stiffness because of the excavation process is highly important as it will provide a better understanding of the ground material behaviour, as well as, permitting verification the efficiency of the grout operation.

In conclusion, pressurized shield methods of tunnelling have great potential in successfully executing tunnelling projects in urban areas under the most difficult conditions. The performance of these methods is directly related to the construction process and the levels of face and grout pressures. A design method is supplied to

determine the safety of the face of the excavation and to estimate the displacement field at the ground surface and the straining actions inside the liner. The design method is successfully demonstrated in the case of the Edmonton LRT project. Provided that there is availability of construction records, further applications of this design method to other tunnelling projects should have positive results on tunnelling design practice and on the development of construction techniques.

REFERENCES

- AFTES, Association Française des Travaux en Souterrain, 1991. Recommendations on Grouting for Underground Works. *Tunnelling and Underground Space Technology*, Vol. 6, No. 4, pp. 383-461.
- Ahmed, A.A.A., 1997. Interaction of Tunnel Lining and Ground. Ph. D. Thesis, Ain Shams University, Cairo, Egypt.
- Ahrens, H., Lindner, E., and Lux, K.H., 1982. Zur Dimensionierung von Tunnelblausbauten nach den Empfehlungen zur Berechnung von Tunneln im Lockergestein (1980). *Die Bautechnik*, 59, pp. 260-273; 303-311.
- Anderson, J.M. and Lamont, D.R., 1991. A Comparison of International Legislation Concerned with Tunnelling in Compressed Air. 'Tunnelling 91', 6th Int. Symposium the Institution of Mining and Metallurgy, London, England, pp. 55-64.
- Anheuser, L., 1982. Gemessene Setzungen über mit dem Hydroschild Aufgefahrene Tunneln. In *Forschung+ Praxis, Construction underground-Present and Future*, STUVA, pp.120-128.
- Anheuser, L., 1985. Technologie et Application récentes des Boucliers à Boue Allemands. *Tunnelling in Soft and Water-Bearing Grounds*, M. Legrand, Editor, pp. 15-20.
- Atkinson, J.H. and Potts, D.M., 1977. Stability of a Shallow Circular Tunnel in Cohesionless Soil. *Geotechnique*, Vol. 27, No. 2, pp. 203-215.
- Attewell, P.B. and Woodman, J. P., 1982. Predicting the Dynamics of Ground Settlement and its Derivatives caused by Tunnelling in Soil. *Ground Engineering*, 15, (8), 13-22, 36.
- Attewell, P.B., Yeates, J., and Selby, A.R., 1986. *Soil Movement Induced by Tunnelling and their Effects on Pipelines and Structures*. Publisher: Blackie and Son Ltd., 7 Leicester Place, London, WC2H 7BP, London, 326 pages.
- Babendererde, S., 1985. Tunnel-Auskleidungen. *Tunnel*, Vol. 2, pp. 61-71.
- Babendererde, S., 1987. Underpassing the Rhône in Lyon, France with a Hydroshield and Extruded Steel Fiber Concrete Lining. *Rapid Excavation Tunnelling Conference, Proceedings*, Vol. 1, pp. 611-623.

- Babendererde, S., 1989. Extruded Concrete Lining. Proceedings of the International Congress on Progress in Tunnelling, Toronto, Canada, pp. 607-611.
- Babendererde, S., 1991. Tunnelling Machines in Soft Ground: a Comparison of Slurry and EPB Shield Systems. Tunnelling and Underground Space Technology, Vol. 6, No. 2, pp. 169-175.
- Balthaus, H., 1989. Tunnel Face Stability in Slurry Shield Tunneling. Proceedings of the twelfth International Conference on Soil Mechanics and Foundation Engineering, Rio de Janeiro, pp. 775-778.
- Bartlett, J.V., Biggart, A.R., and Triggs, R. L., 1973. The Bentonite Tunneling Machine. Proceeding of the Institution of Civil Engineers, Part I, 54, Paper No. 7670, pp. 605-624.
- Becker, C., 1985. Galleria Aurelia Roma-Europe's Largest Hydrosield. Tunnelling in Soft and Water-Bearing Grounds, M. Legrand, Editor, pp. 69-72.
- Bishop, A.W. and Wesley, L.D., 1975. A Hydraulic Triaxial Apparatus for Controlled Stress Path Testing. Geotechnique, Vol. 25, No., pp. 657-670.
- Borttscheller, M., 1990. Die Prozeßgesteuerte Ringspalt-Verfüllung. Tunnel/2, pp. 90-96.
- Bouyat, C., Mohkam, M., and Morcrette J.P., 1985. Le Soutainement Liquide, une Recherche Appliquée pour le Bouclier à Pression de Boue du Metro de Lyon. Revue Française de Géotechnique, N. 32, pp. 59-69.
- Branco, P., 1981. Behaviour of a Shallow Tunnel in Till. M.Sc. Thesis, Department of Civil Engineering, University of Alberta. 351 pages.
- Briglia, P., Bove, Y., and Saradin, J., 1988. Presentation des Dispositifs de mesures de Deplacement du Sol pour les Chantiers de la Ligne 1 bis du Metro de Lille (lot 3) et des Tunnels SNCF de Villejust-Quelques Observations Preliminaires. Collectivites territoriales et utilization du sous-sol, Bordeaux, M. Legrand, editor, pp. 185-190.
- Broms, B.B and Bennermark, H., 1967. Stability of Clay at Vertical Openings. Journal of Soil Mechanics and Foundation Engineering Division, American Society of Civil Engineers, Vol. 93, pp. 71-94.
- Brown E.T., Bray, J.W., Ladanyi, B., and Hoek, E., 1983. Ground Response Curves for Rock Tunnels. Journal of Soil Mechanics and Foundation Engineering Division, American Society of Civil Engineers, Vol. 109, pp. 15-39.
- Bull, A., 1944. Stresses in the Linings of Shield-Driven Tunnels. Journal of Soil Mechanics and Foundation Engineering Division, American Society of Civil Engineers, pp. 1363-1395.
- Burland J. B. and Fourie, A., 1985. The Testing of Soils under Conditions of Passive Stress Relief. Geotechnique, 35, N. 2, 193-198.
- Burns, J. Q. and Richard, R. M., 1964. Attenuation of Stresses for Buried Cylindres. Proceedings, Symposium on Soil-Structure Interaction, Tuscon, pp. 378-392.

5. **Bridge, J.R., Shirlaw, N., Feberweek, J.J., and Ruel, M., 1993.** A Review of the Problems experienced during the construction of the 1890 St. Clair Tunnel using Recent Geotechnical Data. *Canadian Tunnelling, 1993* ed. by K.Y. Lo, pp. 155-164.
- Cappellari G. and Ottaviani, M., 1982.** Predicted Surface Settlements due to Shield Tunneling with Compressed Air. *Proceedings of the 4th International Conference on Numerical Methods in Geomechanics, Edmonton, Vol. 2, pp. 531-536.*
- Casarin, C. and Mair, R.J., 1981.** The Assessment of Tunnel Stability in Clay by Model Tests. In: *Soft-Ground Tunnelling, Failures and Displacements* (edited by D. Resendiz and M. P. Romo), Balkema, Rotterdam, pp. 3rd -4.
- Cassinis, C., Nisio, P., and Capata, V., 1985.** Settlement and Face Stability Boring a Large Tunnel. *Eleventh International Conference on Soil Mechanics and Foundation Engineering, San Francisco, pp. 2057-2062*
- Chaffois, S. Lareal, P., Monnet, J., and Chapeau, C., 1988.** Study of Tunnel Face in Gravel Site. *Numerical Methods in Geomechanics, Innsbruck, pp. 1493-1498.*
- Chambon, P., Corté, J-F., 1989.** Stabilité du Front de Taille d'un Tunnel Faiblement Enterré: Modelisation en Centrifuge. In: *International Conference on Tunnelling and Microtunnelling in Soft Ground, Paris.*
- Chambon, P. and Corté, J.-F., 1990.** Stabilité du Front de Taille d'un Tunnel dans un Milieu Frottant Approche Cinématique en Calcul à la Rupture. *Revue Française de Géotechnique, N. 51, pp. 51-59.*
- Chambon, P., Corté, J-F., Garnier, J., and König, D., 1991.** Face Stability of Shallow Tunnels in Granular Soils. In: *Centrifuge 91, University of Colorado, Boulder, (edited by Ko H-Y. and Mclean, F. G.), Balkema, Rotterdam, pp. 99-105.*
- Chan, D., 1985.** Finite Element Analysis of Strain Softening Materials. Ph.D. Thesis. Department of Civil Engineering, University of Alberta, Edmonton, Alberta. 355p.
- Charalambu, H., Finch, A.P., and MacLennan, D.G., 1993.** The New St. Clair River Tunnel - an Overview. *Canadian Tunnelling, 1993* ed. by K.Y. Lo, pp. 137-154.
- Chi, P.C., Lu, K. and Lu, H., 1985.** Application of the Shield Method on Soft Ground Tunneling in Taiwan. *Tunnelling in Soft and Water-Bearing Grounds, M. Legrand, Editor, pp. 79-84.*
- Cloquet, V, 1985.** Aspects Pratiques des Entrées et Sorties du Bouclier à la Bentonite au Droit des Puits d'accès et Gares. *Protection des ouvrages le long du Tracé. Tunnelling in Soft and Water-Bearing Grounds, M. Legrand, Editor, pp. 29-36.*
- Clough, G.W., Finno, R.J., Sweeney, B.P., and Kavazanjian, E., 1983.** Development of a Design Technology for Ground Support for Tunnels in Soil- Volume III-Observed Behavior of an Earth Pressure Balanced Shield in San Francisco Bay Mud. Report No UNTA-MA_06-0100-82-3 submitted to the U.S. Department of Transportation, Washington, D.C., 20590, 196 pages.

- Clough, G.W. and Schmidt, B., 1981. Design and Performance of Excavation and Tunnels in Soft Clay. In: *Soft Clay Engineering* (edited by E.W. Brand and R.P. Brenner), Elsevier, pp. 569-634.
- Clough, G.W., Shirasuna, T., and Finno, R.J., 1985. Finite Element Analysis of Advanced Shield Tunneling in Soils. *Proceeding of the 5th International Conference on Numerical Methods in Geomechanics*, Nagoya, pp. 1167-1174.
- Clough, G. W., Sweeney, B.P. and Finno, R.J, 1983. Measured Soil Response to EPB Shield Tunneling. *Journal of Soil Mechanics and Foundation Engineering Division, American Society of Civil Engineers*, Vol. 109, pp. 131-149.
- Cording, E.J. and Hansmire, W.H., 1975. Displacements around Soft Ground Tunnel. *General Report: Session IV, Tunnels in Soil, 5th Pan-American Congress on Soil Mechanics and Foundation Engineering*, Buenos Aires, November, 1975.
- Curtis, D.J., 1976. The Circular Tunnel in Elastic Ground. *Discussion, Geotechnique*, Vol. 26, pp. 231-237.
- Darling, P., 1991. Tunnelling alongside Egypt's Heart-beat. *Tunnels & Tunnelling*, July, 1991, pp. 17 -18.
- Darling, P., 1992. Steep Tunnelling for EPBM under the Avon Estuary. *Tunnels and Tunnelling*, January, 1992, pp. 45-50.
- Davis, E.H., Gunn, M.J., Mair, R.J., and Seneviratne, H.N., 1980. The Stability of Shallow tunnels and Underground Openings in Cohesive Material. *Geotechnique*, Vol. 30, No. 4, pp. 397-416.
- De Moor, E. K. and Taylor, R.N., 1991. Ground Response to Construction of a Sewer Tunnel in Very Soft Ground. 'Tunnelling 91', 6th International Symposium organized by the Institution of Mining and Metallurgy, London, England, pp. 43-54.
- De Moor, E.K. and Taylor, R.N., 1993. Field Studies of a Shallow Tunnel in Very Soft Ground at Tilbury. *Geotechnical Engineering Research Centre, Report GE/89/22*.
- Duddeck, H., 1991. Application of Numerical Analyses for Tunnelling. *International Journal for Numerical Methods in Geomechanics*, Vol. 15, pp. 223-239.
- Duddeck, H., and Erdmann, J., 1982. Structural Design models for Tunnels. *Proceedings, Tunnelling '82* (edited by M.J. Jones), 'The Institution of Mining and Metallurgy, London, pp. 83-91.
- Duncan J.M., and Chang, C.V., 1970. Nonlinear Analysis of Stress and Strain in Soils. *Journal of the Soil Mechanics and Foundation Engineering Division. American Society of Civil Engineers*, Vol. 96, pp. 1629-1653.
- Ebaid, G.S. and Hammad, M.E., 1978. Aspects of Circular Tunnel Design., *Tunnels and Tunnelling.*, 10, July, pp. 59-63.
- Einstein, H.H. and Schwartz, C.W., 1979. Simplified Analysis for Tunnel Supports. *Journal of the Geotechnical Engineering Division, American Society of Civil Engineers*, V. 106, pp. 499-518.

- Eisenstein, Z., 1993. Large Undersea Tunnels and the Progress of Tunnelling Technology. In: Technology of Bored Tunnels under Deep Waters, International Symposium organized by the Danish Society for Tunnels and Underground Works and the International Tunnelling Society, Forlag, T. editor, Copenhagen, pp. 9-23.
- Eisenstein, Z., El Nahhas, F., and Thomson, S., 1981. Pressure-Displacement Relations in Two Systems of Tunnel Lining. Soft Ground Tunnelling, Failures and Displacements (Editor, D. Resendiz and M.P. Romo) A.A. Balkema (Rotterdam), pp. 85-94.
- Eisenstein, Z. and Ezzeldine, O., 1992(a). The Effect of Tunnelling Technology on Ground Control. Tunnelling and Underground Space Technology, Vol. 7, No. 3, pp. 273-279
- Eisenstein, Z. and Ezzeldine, O., 1992(b). Ground Control by Shields with Positive Soil Support. Cairo second International Symposium on Tunnelling; Current Experiences in Tunnelling, January 27-28, pp. 75-88.
- Eisenstein, Z., Heinz, H., and Negro, A., 1984. On Three-Dimensional Ground Response to Tunnelling. Proceedings, Geotech' 84, American Society of Civil Engineers (edited by K.Y. Lo), pp. 107-127.
- Eisenstein, Z. and Medeiros, L. V., 1983. A Deep Retaining Structure in Till and Sand. Part II: Performance and Analysis. Canadian Geotechnical Journal, Vol. 20, pp. 131-140.
- El-Nahhas, F., 1980. The behaviour of Tunnels in Stiff Soils. Ph. D. Thesis, Department of Civil Engineering, University of Alberta. 305 pages.
- El-Nahhas F., El-Kadi F. and Shalaby, A., 1991. Field Measurements During Construction of a Compressed Air Tunnel in Cairo. Tunnelling and Underground Space Technology, Vol. 6, No. 1, pp. 123-127.
- El-Nahhas, F., El-Kadi, F., and Ahmed, A., 1992. Interaction of Tunnel Linings and Soft Ground. Tunnelling and Underground Space Technology, Vol. 7, No. 1, pp. 33-43.
- El-Nahhas, F., El-Kadi, F., and Shalaby, A., 1992. Subsidence Contour Maps for a Compressed Air Tunnel. Proceedings of the First Geotechnical Engineering Conference, Cairo University, pp. 161-170.
- d'Escatha Y. and Mandel J., 1974. Stabilité d'une Galerie Peu Profonde en Terrain Meuble. Revue de l'Industrie Minière (Special Issue), April, pp. 45-53.
- Evison, S. E., 1988. A Ring and Spring Model for Tunnel Liner Design. M.Sc. Thesis, University of Alberta.
- Ezzeldine, O.Y., 1992. Tunnel User Manual. Cole, Sherman & Ass. Ltd.
- Ferrand, J. and Bouyat, C., 1985. Le Métro de Lyon et son Bouclier à Pression de Boue. Tunnelling in Soft and Water-Bearing Grounds, Proceedings of an International Symposium organized by AFTES (Association française des Travaux Souterrains), Lyon, France, pp. 21-28.

- Ferrand, J. and Morcrette, J.P., 1988. Metro Ligne D: Premiers Resultats et Bilan des Chantiers de Genie Civil. Tunnels and Water (J. Manuel Serrano, editor), Balkema Rotterdam, pp. 869-876.
- Finno, R.J., 1983. Response of Cohesive Soil to Advanced Shield Tunneling. Ph. D. Thesis, Stanford University.
- Flint, G.R., 1992. Tunnelling using Earth Pressure Balance Machines for the Boulac Spine Sewer of the Greater Cairo Wastewater Project. Tunnelling and Underground Space Technology, Vol. 7, No. 4, pp. 415-424.
- Flint, G.R., 1993. Personal Communication.
- Flint, G.R. and Foreman, W., 1992. Bentonite Tunnelling for the Greater Cairo Wastewater Project. Tunnelling and Underground Space Technology, Vol. 7, No. 1, pp. 45-53.
- Galle, E. and Wilhoit, J., 1962. Stresses around a Wellbore due to Internal Pressure and Unequal Principal Geostatic Stresses. Society of Petroleum Engineers Journal, 2(2), pp. 145-155.
- Gebauer, B. and Frohlich, H., 1985. Die Weiterentwicklung des Slurry-Shildes aus der Sicht der Baupraxis. Tunnel/1, pp. 30-33.
- Glossop, N. H., 1978. Ground Movements caused by Tunnelling in Soft Soils. Ph.D. Thesis, University of Durham.
- Glossop, N. H., and Farmer, I. W., 1979. Settlement Associated with Removal of Compressed Air Pressure during Tunnelling in Alluvial Clay. Geotechnique, Vol. 29, No. 1, pp. 67-72.
- Golder Associates, 1992. Geotechnical Design Summary Report for CN - St. Clair River Tunnel. Report to Hatch and Mott Macdonald.
- Guillaume, J., 1989. The Villejust Tunnels for the New very High Speed Train Link to the Atlantic. Proceedings of the International Congress on Progress and Innovation in Tunnelling, Toronto, Canada, pp. 679-685.
- Hagimoto, H. and Kashima, Y., 1985. D.K. Shield Method. Tunnelling in Soft and Water-Bearing Grounds, M. Legrand, Editor, pp. 53-60.
- Hardy BBT Limited, 1988. South LRT Extension-Northbound Tunnel Grandin Station to the North Bank of North Saskatchewan River, Edmonton, Alberta. Geotechnical Engineering Report. EG-06431, July 4, 1988, 23 pages.
- Hartmann, F., 1970. Elastizitätstheorie des ausgekleideten Tunnelhohlraumes und des eingebohrten kreisförmigen Rohres. Strasse Brücke Tunnel 22 (1970), Heft 8, 209-215, Heft 9, 241-246, und Jg. 24 (1972), Heft 1, 13-20, Heft 2, 39-45.
- Hartmann, F., 1985. Einfache Berechnung überschütteter, kreisförmiger Rohre von beliebiger Steifigkeit Elastizitätstheorie des überschütteten Rohres. Bautechnik, 62, Heft 7, pp. 224-235.

- Hashimoto, K., Kato, T., Watanabe, Y., Matsuda, M., Tamiya, Y., Shima, M., Fujihara, Y., and Tadao, Y., 1988. Underground Stormwater Reservoir Constructed by Full Scale Slurry Shields. *Tunnels and Water* (J. Manuel Serrano, editor), Balkema Rotterdam, pp. 473-488.
- Hashimoto, K., Takeyama, T. and Kurosawa, S., 1985. Tunnel Excavation with the World Largest Slurry Shield. *Tunnelling in Soft and Water-Bearing Grounds*, M. Legrand. Editor, pp. 45-52.
- Heinz, H. K. Jr., 1984. Applications of the New Austrian Tunnelling Method in Urban Areas. M. Sc. Thesis, University of Alberta.
- Heinz, H. K. Jr., 1988. Large Cross Section Tunnels in Soft Ground. Ph. D. Thesis, University of Alberta.
- Hirokawa, H. and Nishitake, S., 1985. Slurry Shield Machine (Automatic Operation and Control). *Tunnelling in Soft and Water-Bearing Grounds*, M. Legrand, Editor, pp. 37-44.
- Hollstegge, W. and Meseck, H., 1989. Thixshield-Tunnelling with Steel Lining in a Mining Subsidence Region. 12th International Conference on Soil Mechanics and Foundation Engineering, Rio de Janeiro, pp. 1493-1496.
- Hubbard, H.W., Potts, D.M., Miller, D., and Burland, J.B., 1984. Design of the Retaining Walls for the M25 Cut and Cover Tunnel at Bell Common. *Geotechnique*, 34, N. 4, 495-512.
- Hurpin, L. and Boussert, P., 1988. Metro de Lille: Execution du Lot 8 de la Ligne 1 bis. *Collectivités territoriales et utilisation du sous-sol*, Bordeaux, M. Legrand, editor, pp. 327-334.
- ITA, International Tunnelling Association's Working Group on Research, 1981. Development and Future Trends of Shield Tunnelling. *Advances in Tunnelling and Subsurface Use*, 1, (3), pp. 199-365.
- ITA, International Tunnelling Association's Working Group on General Approaches to the Design of Tunnels, 1988. Guidelines for the Design of Tunnels. *Tunnelling and Underground Space Technology*, Vol. 3, No. 3, pp. 237-249.
- Jacob, E., 1976. The Bentonite Shield Technology and Initial Application in Germany. 'Tunnelling 76', International Symposium organized by the Institution of Mining and Metallurgy, London, England, pp. 201-208.
- Jardine, F.M., Evans, A., and McCaig, R.H., 1991. Studies of the Incidence of Decompression Sickness on United Kingdom Compressed-Air Projects. 'Tunnelling 91', Sixth International Symposium organized by the Institution of Mining and Metallurgy, London, England, pp. 29-40.
- Johnston, P.R., 1981. Finite Element Consolidation Analyses of Tunnel Behavior in Clay. Ph. D. Thesis, Stanford University, 224 pages.
- Jones, I., 1990. SLRT Tunnel Construction-Hydroshield Method. Unpublished Report.

- Kasali, G. and Clough, G.W., 1983. Development of a Design Technology for Ground Support for Tunnels in Soil-Volume III-Three Dimensional Finite Element Analysis of Advanced and Conventional Shield Tunneling. Report No UNTA-MA_06-0100-82-2 submitted to the U.S. Department of Transportation, Washington, D.C., 20590, 232 pages.
- Kimura, T. and Mair, R. J., 1981. Centrifugal Testing of Model Tunnels in Soft Clay. 10th International Conference on Soil Mechanics and Foundation Engineering, Stockholm, pp. 319-322.
- Kirkland, C.J., 1984. Design and Construction of Urban Tunnels-Compressed Air. Advances in Tunnelling Technology and Subsurface Use, Volume 4, No. 4, pp. 191-194.
- Kirsch, G., 1898. Die Theorie der Elasticitat und Die Bedurfnisse der Festigkeitslehre. Zeitschrift des Vereines Deutscher Ingenieure, 42:49.
- Kongrad, Y. and Anheuser, L., 1988. Le Lot 3 de la Ligne 1 bis du Metro de Lille. Collectivites territoriales et utilization du sous-sol, Bordeaux, M. Legrand, editor, pp. 319-325.
- Kramer, G.J.E., Kerrigan, R.E., Tattersall, C.J., and Forbes, J.A., 1993. Tunnel Enabling Works for the New St. Clair Tunnel. Canadian Tunnelling, 1993, ed. by K.Y. Lo, pp. 165-182.
- Krause, T., 1991. Der Mischwasser-Sammler "Burgerpark " in Bremen Erstanwendung eines Erddruckschildes in Deutschland. Tunnel, April, 1991.
- Krywiak, G.J. and Morison, R.M., 1990. Analysis and Design Aspects of the Precast Concrete Tunnel Installed by the Hydroshield Method. Unpublished Report.
- Kuesel, T. R., 1972. Soft Ground Tunnels for the BART Project. First Rapid Excavation Tunnelling Conference, Chicago, Vol. I, pp. 287-313.
- Kurosawa, S., 1985. Up-to-date of the Art of Japanese Shield. The Selection Criteria of Slurry Shield and Earth Pressure Balanced Shield. Tunnelling in Soft and Water-Bearing Grounds, Proceedings of an International Symposium organized by AFTES (Association française des Travaux en Souterrain), Lyon, France (M. Legrand, editor), pp. 9-13.
- Leach, G., 1985. Pipeline Response to Tunnelling, Unpublished Paper Presented to the North of England Gaz Association, January 1985.
- Leblais, Y. and Bochon, A., 1991. Villejust Tunnel: Slurry Shield Effects on Soil and Lining Behaviour and Comments on Monitoring Requirement. 'Tunnelling 91', 6th International Symposium organized by the Institution of Mining and Metallurgy, London, England. pp. 65-78.
- Leca, E. and Dormieux, L., 1990. Upper and Lower Bound Solutions for the face Stability of Shallow Circular Tunnels in Frictional Material. Geotechnique, Vol. 40, No. 4, pp. 581-606.
- Leca, E. and Panet M., 1988. Application du Calcul à la Rupture à la Stabilité du Front de Taille d'un Tunnel. Revue Française de Géotechnique, N. 43, pp. 5-19.

- Lee, K.M., 1989. Prediction of Ground Deformations Resulting from Shield Tunnelling in Soft Clays." Ph. D. Thesis, The University of Western Ontario.
- Magata, H., Nakauchi, S., and Sogabe, H., 1982. Subsidence Measurements associated with Shield Tunneling in Soft Ground. 'Tunnelling 82', Third International Symposium organized by the Institution of Mining and Metallurgy, London, England, pp. 231-240.
- Maidl, B., 1988. Erfahrungen mit Schildvortrieben beim Tunnelbau in Shanghai. Tunnel 1/88, pp. 3-7.
- Maidl, B., Hou, X., and Yi, X., 1990. Field Measurement of Ground Movements and Variations of Pore Pressure caused by EBP Shield Construction. Tunnel and Underground Works Today and Future. Proceedings of the International Congress, The International Tunnelling Association Annual Meeting Chengdu, China, 1990, pp. 335-349.
- Mair, R., J., 1979. Centrifugal Modelling of Tunnel Construction in Soft Clay. Ph. D. Thesis, Cambridge University, England.
- Mair, R.J. and Taylor, R.N., 1993. Prediction of Clay Behaviour around Tunnels using Plasticity Solutions. Under Publication, Personal communication.
- Matsumoto, Y., Arai, T., Ohta, H., and Ooishi, Y., 1991. An Experimental Study on the Multi-Circular Face Shield. Rapid Excavation Tunnelling Conference, Proceedings, pp. 815-828.
- Matsumoto, Y., Iida, H., and Nagashima, Y., 1986. The Extruded and Prestressed Concrete Lining in shield Tunnel. International Congress on Large Underground Openings, Firenze, Italy, pp. 788-793.
- Matsumoto, Y. and Nishioka, T., 1991. Theoretical Tunnel Mechanics. University of Tokyo Press, 223 pages.
- Matsuzaki, S., Yamada, K., and Tanaka, H., 1986. An Example of Observation for Risk Reduction against Existing Underground Structures in Shield Tunnelling. International Congress on Large Underground Openings, Firenze, Italy, pp. 630-639.
- Matsumoto, H., Takamatu, Y., Kawada, H., and Arai, T., 1989. Results and Future Prospect of MF Shield Tunnelling. Proceedings of the International Congress on Progress and Innovation in Tunnelling, Toronto, Canada, pp. 1011-1016.
- Medeiros, L. V. and Eisenstein, Z., 1983. A Deep Retaining Structure in Till and Sand. Part I: Stress Path Effects. Canadian Geotechnical Journal, Vol. 20, pp. 120-130.
- Megaw, T.M. and Bartlett, J.V., 1981. Tunnels: Planning, Design, Construction. Ellis Horwood Ltd., publisher, 280 pages.
- Miki, G., Saito, T. and Yamazaki, H., 1977. Theory and Praxice of Soft Ground Tunneling by the Slurry Mole Method. 9th International Conference on Soil Mechanics and Foundation Engineering.

- Mindlin, R.D., 1939. Stress Distribution around a Tunnel. *Proceedings of the American Society of Civil Engineers*, Vol. 65, pp. 619-642. Also in 1940, *Trans. ASCE*, Vol. 105, pp. 1117-1153.
- Mitchell, R.J., 1983. *Earth Structures Engineering*. Publisher: Allen and Unwin Inc., Boston.
- Mohkam, M., 1989. 'Injectoshield' an Innovation in Tunnelling Techniques. *Proceedings of the International Congress on Progress and Innovation in Tunnelling*, Toronto, Canada, pp. 1023-1028.
- Mohkam, M. and Bouyat, C., 1985. Research Studies for Slurry Shield Tunneling. 'Tunnelling 85', 4th International Symposium organized by the Institution of Mining and Metallurgy, London, England, pp. 235-242.
- Mohkam, M. and Bouyat, C., 1989. Simulation en Laboratoire du creusement de Tunnel avec des Conditions Hydrogeologiques Differentes. *Tunnels and Water* (J. Manuel Serrano, editor), Balkema Rotterdam, pp. 1239-1246.
- Mohkam, M. and Wong, Y.W., 1989. Three Dimensional Stability Analysis of the Tunnel Face under Fluid Pressure. *Numerical Methods in Geomechanics* (Innsbruck, 1988), Swoboda, editor, pp. 2271-2278.
- Morcrette, J.P., 1988. La Traversée sous Fluviale de la Ligne D du Metro de Lyon. *Collectivités territoriales et utilisation du sous-sol*, Bordeaux, M. Legrand, editor, pp. 335-339.
- Morcrette, J.P. and Bouyat, C., 1986. Metro de Lyon. Les Difficultés du Creusement sous le Rhône avec le Bouclier à Pression de Boue. *International Congress on Large Underground Openings*, Firenze, Italy, pp. 822-827.
- Morgan, H.D., 1961. A Contribution to the Analysis of Stress in a Circular Tunnel. *Geotechnique*, 11, pp. 37-46.
- Moromoto, Y., Tokushige, H., and Hirayama T., 1985. Construction of Sewer Tunnel Main Crossing under a River Bed with Shallow Overburden-Using Pressurized Slurry-Faced Shield. *Tunnelling in Soft and Water-Bearing Grounds*, M. Legrand, Editor, pp. 61-67.
- Muir Wood, A.M., 1975. The Circular Tunnel in Elastic Ground. *Geotechnique*, 25, N.1, pp. 115-127.
- Mülhaus, H. B., 1985. Lower Bound Solutions for Circular Tunnels in Two and Three dimensions. *Rock Mechanics and Rock Engineering*, Vol. 18, pp. 37-52.
- Murakami, K., Nakano, M., and Suzuki, S., 1990. Measurements and Analysis of Ground Deformation for Shield Tunneling undercrossing a Class A River. *Tunnel and Underground Works Today and Future. Proceedings of the International Congress, The International Tunnelling Association Annual Meeting 1990*, Chengdu, China, pp. 357-365.

- Murata, T., Mitsuhsa, H., and Sotani, T., 1990. Launching a Shield Machine from an Enlarged Space in a Tunnel. *Tunnels and Underground Works Today and Future. Proceedings of the International Congress, The International Tunnelling Association Annual Meeting Chengdu, China, 1990*, pp. 301-309.
- Negro, A.Jr., 198^o. Design of Shallow Tunnel in Soft Ground. Ph.D. Thesis, University of Alberta, 1453 pages.
- Nishitake, S., 1987. Earth Pressure Balanced Shield Machines to Cope with Boulders. *Rapid Excavation Tunnelling Conference, Vol. 1*, pp. 552-572.
- Nishitake, S., 1990. Advanced Technology Realize High-Performance Earth Pressure Balanced Shield. *Franchissement Souterrains pour l'Europe*, M. Legrand editor, pp. 291-302.
- O'Reilly, M.P., Mair, R.J., and Algerman, G.H., 1991. Long-Term Settlement over Tunnels: an Eleven-Year Study at Grimsby. 'Tunnelling 91', 6th International Symposium organized by the Institution of Mining and Metallurgy, London, England, pp. 55-64.
- O'Reilly, M.P. and New, B.M., 1982. Settlement above Tunnels in the United Kingdom-Their Magnitude and Prediction. 'Tunnelling 82', Third International Symposium organized by the Institution of Mining and Metallurgy, London, England, pp. 173-182.
- O'Rourke, T.D., 1984. Guidelines for Tunnel Lining Design. Prepared by the Technical Committee on Tunnel Lining Design of the Underground Technology Research Council of the ASCE Technical Council on Research, edited by O'Rourke, ASCE publications, 82 pages.
- O'Rourke, T.D., 1985. Design of Tunnel Linings, UTRC Study: Underground Space, Vol. 9, pp. 102-108.
- Ohta, Y., Matsui, T., Matsubara, H., Akiyama, M., and Baba, T., 1978. Slurry Shield Method in Complex Formation under Sea-Construction of Water Supply Tunnel under Nagoya Harbor. *Tunnelling under Difficult Conditions, Proceedings of the International Tunnel Symposium, Tokyo*, (I. Kitamura, editor), pp. 203-208.
- Okada, H., Yamamoto, S., and Kita, K., 1989. Development of New Type Extruded Concrete Lining System. *Proceedings of the International Congress on Progress and Innovation in Tunnelling, Toronto, Canada*, pp. 545-552.
- Ono, K., Shimamura, S. and Yoshida, K., 1989. The rigidity of a Shield Tunnel under the Sea and the Soil and Water Pressure acting on the Tunnel. *Proceedings of the International Congress on Progress and Innovation in Tunnelling, Toronto, Canada*, pp. 431-438.
- Ostenfeld, K.H. and Curtis, J., 1992. The Great Belt Link: The East Railway Tunnels. *Symposium on Large Tunnels, Madrid, Spain, October, 1992*.
- Pandolfo, A., 1986. Il Sottoattraversamento Ferroviario di Centri Urbani con Scarsa Copertura ed in Ambienti Idrogeologici Particolarmente Difficili. *International Congress on Large Underground Openings, Firenze, Italy*, pp. 252-263.

- Panet, H., 1973. *La Stabilité des Ouvrages Souterrains-Soutènement et Revêtement*. Rapport de Recherche No. 28. Paris: Laboratoire des Ponts et Chaussées.
- Paulus, J.F., Avesque, A., and Pascual, P., 1988. *L'Utilisation de deux Tunneliers LOVAT en Terrains Alluvionnaires et Schisteux (Metro de Caracas)*. Collectivités territoriales et utilisation du sous-sol, Bordeaux, M. Legrand, editor, pp. 351-355.
- PCL-Hochtief, 1988(a). *SLRT-Phase II - Northbound Tunnel*. Contract No. 8884, Section 12-Technical Submission. Volume I. The City of Edmonton, Transportation Department. 18 pages.
- PCL-Hochtief, 1988(b). *SLRT-Phase II - Northbound Tunnel, Supplementary Information*. Contract No. 8884. The City of Edmonton, Transportation Department. 73 pages.
- PCL-Hochtief, 1990. *SLRT-Phase II - Northbound Tunnel. Ring Installation Records*.
- Peck, R., 1969. *Deep Excavation and Tunneling in Soft Ground*. Proceedings, 7th International Conference on Soil Mechanics and Foundation Engineering, Mexico, State-of-Art Vol., pp. 225-290.
- Peck, R., Hendron Jr., A.J., and Mohraz, B., 1972. *State of the Art of Soft Ground Tunneling*. State-of-the-Art of Soft Ground Tunnelling. Proceedings, 1st North American Rapid Excavation and Tunnelling Conference, Vol. 1, pp. 259-286.
- Piquand, J.L. and Gesta, P., 1986. *Les Tunnels de Villebon-Villejust du TGV Atlantique*. International Congress on Large Underground Openings, Firenze, Italy, pp. 264-268.
- Ranken, R.E., 1978. *Analysis of Ground-Liner Interaction for Tunnels*. Ph.D. Thesis, University of Illinois at Urbana-Champaign. 425 pages.
- Romo, M.P. and Diaz, M.C., 1981. *Face Stability and Ground Settlement in Shield Tunneling*. Proceedings, 10th International Conference on Soil Mechanics and Foundation Engineering, Vol. 1, Stockholm, pp. 357-360.
- Rowe, R. K. and Kack, G.J., 1983. *A Theoretical Examination of the Settlements induced by Tunnelling: Four Case Histories*. Canadian Geotechnical Journal, Vol. 20, pp. 299-314.
- Rozsa, L., 1963. *Die Bemessung Kreisformiger Tunnelwundungen aus Prefabrizierten Stahlbetonelementen nach dem Verfahren der Grenzbelastungen*. Bauingenieur 38, Heft 11, pp. 434-441.
- Safwat, A., 1983. *The Greater Cairo Wastewater Project*. World Water '83, the World Problem, pp. 163-171.
- Saito, T. and Kobayashi, T., 1979. *Driving an 8.48 m Diameter Sewer Tunnel by use of an Earth-Pressure Balancing Shield*. 'Tunnelling 79', Second International Symposium organized by the Institution of Mining and Metallurgy, London, England, pp. 295-304.

- Sasanabe, M. and Matsubara, H., 1986. Planing and Results of Large Diameter Tunnel Driven by Soil Plasticizing Shield. Chichibu Section of Nagoya Municipal Subway. International Congress on Large Underground Openings, Firenze, Italy, pp. 925-932.
- Sato, Y. and Takamatsu, N., 1989. A New ECL Construction Method Effectively using Rings and Tie Rods. Proceedings of the International Congress on Progress and Innovation in Tunnelling, Toronto, Canada, pp. 1037-1043.
- Schmitter, J.M., Lopez Postillo, M.V., and Orozco, J.C., 1988. Slurry Shield Tunneling for Mexico City. 'Tunnelling 88', 5th International Symposium organized by the Institution of Mining and Metallurgy, London, England, pp. 289-294.
- Schofield, A.N., 1980. Cambridge Geotechnical Centrifuge Operations. Geotechnique, Vol. 30, No. 3, pp. 227-268.
- Schulze, H. and Duddeck, H., 1964. Spannungen in Schildvorgetriebenen Tunneln. Beton Stahlbetonb, 59, 1964, pp. 169-175.
- Shalaby, A., 1990. Behaviour of Tunnels in some Egyptian Soils. Ph. D. Thesis, Ain Shams University, Cairo, Egypt.
- Shimizu, R. and Maeda, M., 1989. Design and Construction of the Shinkawa Tunnel using the Mudwater-Type Shield Method. Proceedings of the International Congress on Progress and Innovation in Tunnelling, Toronto, Canada, pp. 431-438.
- Shirlaw, J.N. and Doran, S., 1991. Ground Movements and Settlements caused by Tunnelling for the Singapore Mass Rapid Transit System. 'Tunnelling 88', 5th International Symposium organized by the Institution of Mining and Metallurgy, London, England, pp. 295-314.
- Sinha, R.S. (editor), 1989. Underground Structures, Design and Instrumentation, Elsevier, 529 pages.
- Sonoda, T. Hagiwara, H., Osaki, H., Noguchi, T., and Nakamura, M., 1992. Construction of Underground Space by a New Shield Tunnelling Method: Spiral Tunnelling and Ramification of Multi-circular Face Shield. Tunnelling and Underground Space Technology, Vol. 7, No. 4, pp. 355-361.
- Steiner, W., 1989. Grauholz Tunnel, Tunneling with a Slurry Shield. Tunnels and Water (J. Manuel Serrano, editor), Balkema Rotterdam, pp. 1381-1385.
- Steiner, W. and Becker, C., 1991. Grauholz Tunnel in Switzerland: Large Mixed Face Slurry Shield. Rapid Excavation Tunnelling Conference, Proceedings, pp. 329-347.
- Steiner, W., 1992. Dual-mode Machine for the Grauholz Tunnel. Tunnels and Tunnelling, January, 1992, pp. 58-60.
- Sweet, A. L. and Bogdanoff, J. L., 1965. Stochastic Model for Predicting Subsidence. Journal of the Mechanics Division, Proceedings of the American Society of Civil Engineers, Vol. 9, No. EM2, April, 1965.

- Szechy, K., 1973. *The Art of tunnelling*. Akademiai Kiado, Budapest, 1097 pages.
- Tamai, T., Chiba, Y., and Yoshimura, M., 1989. The Soil Plasticizing ~~Shield~~ Driving Method using a Super-Absorbent Polymer. *Proceedings of the International Congress on Progress and Innovation in Tunnelling*, Toronto, Canada, pp. 431-438.
- Terzaghi, K., 1943. *Theoretical Soil Mechanics*. John Wiley, New York.
- Thomson, S. and Townsend, D.L., 1979. River Erosion and Bank Stabilization-North Saskatchewan River, Edmonton, Alberta. *Canadian Geotechnical Journal*, Vol. 16, pp. 567-576.
- Thurber Consultants Ltd., 1990. Instrumentation Report No. 5. South Light Rail Transit Extension, Phase II, North Tunnel Instrumentation and Monitoring, North Portal to Grandin Station (Northbound, Sta. 401+070 to 400+764).
- Tohda, J., Mikasa, M. and Hachiya, M., 1988. Earth Pressure on Underground Rigid Pipes: Centrifuge Model Tests and FEM Analysis. *Centrifuge 88*, Corté (editor) pp. 395-402.
- UMA Engineering Ltd., 1988. North Tunnel-Grandin Station to North Portal, Northbound Twin Tunnel. Preliminary Engineering Report-South Light Rail Transit-Phase II, 58 pages
- Vinnel, C. and Herman, A., 1969. Tunnel dans le Sable de Bruxelles, par la Methode du Bouclier. *7th International Conference on Soil Mechanics and Foundation Engineering*, Mexico City, Session IV, Vol. 3, pp.487-494.
- Wallis, S., 1984. Hydroschild Alleviates the Pressure on Rome's Urban Railway Drives. *Tunnels & Tunnelling*, October, 1984, pp. 11-16.
- Wallis, S., 1986. TGV Bores its Way through France to the Atlantic Coast. *Tunnels & Tunnelling*, June, 1986, pp. 19-22.
- Wallis, S., 1987. Deciphering Cairo's Mysteries. *Tunnels & Tunnelling*, June, 1987, pp. 18-24.
- Wallis, S., 1990(b). Redesigned Hydroschild Gives Boulders Short Drift. *Tunnels and Tunnelling*, June, 1990, pp. 41-42.
- Wallis, S., 1991. Mixshield Masters the Ruhr in Mulheim. *Tunnels & Tunnelling*, January, 1991, pp. 29-31.
- Wallis, S., 1992(a). Der Eisenbahntunnel unter Großen Belt Tunnel 1/92, pp. 30-34.
- Wallis, S., 1992(b). Edmonton, a Tunnelling Laboratory for North America. *Tunnels and Tunnelling*, March, 1992, pp. 33-37.
- Walsh, T. and Biggart, A.R., 1976. The Bentonite Tunnelling Machine at Warrington. 'Tunnelling 76', International Symposium organized by the Institution of Mining and Metallurgy, London, England, pp. 209-218.

- West, G., 1988. *Innovation and the Rise of the Tunnelling Industry*. Cambridge University Press, publisher, 355 pages.
- Windels, R., 1966. Spannungstheorie Zweiter Ordnung für den Teilweise Gebetteten Kreisring. *Bautechnik* 43, Heft 8, pp. 265-274.
- Windels, R., 1967. Kreisring im Elastischen Kontinuum. *Bauingenieur* 42. Jahrgang, Heft 12, pp. 429-439.
- Wittemans, A. and Bonvoisin, J., 1988. Tunnel Pre-Metro sous l'Escaut à Anvers. *Collectivités territoriales et utilisation du sous-sol*, Bordeaux, M. Legrand, editor, pp. 341-349.
- Xi, Z., 1990. Control Measures Employed in Earth Pressure Balanced Shield. *Tunnel and Underground Works Today and Future. Proceedings of the International Congress, The International Tunnelling Association Annual Meeting, Chengdu, China, 1990*, pp. 445-451.
- Yamashita, O., Ono, K., Wasano, S., and Kobayashi, I., 1988. Construction of a Shield Tunnel under the Sea. *Tunnels and Water* (J. Manuel Serrano, editor), Balkema Rotterdam, pp. 959-964.

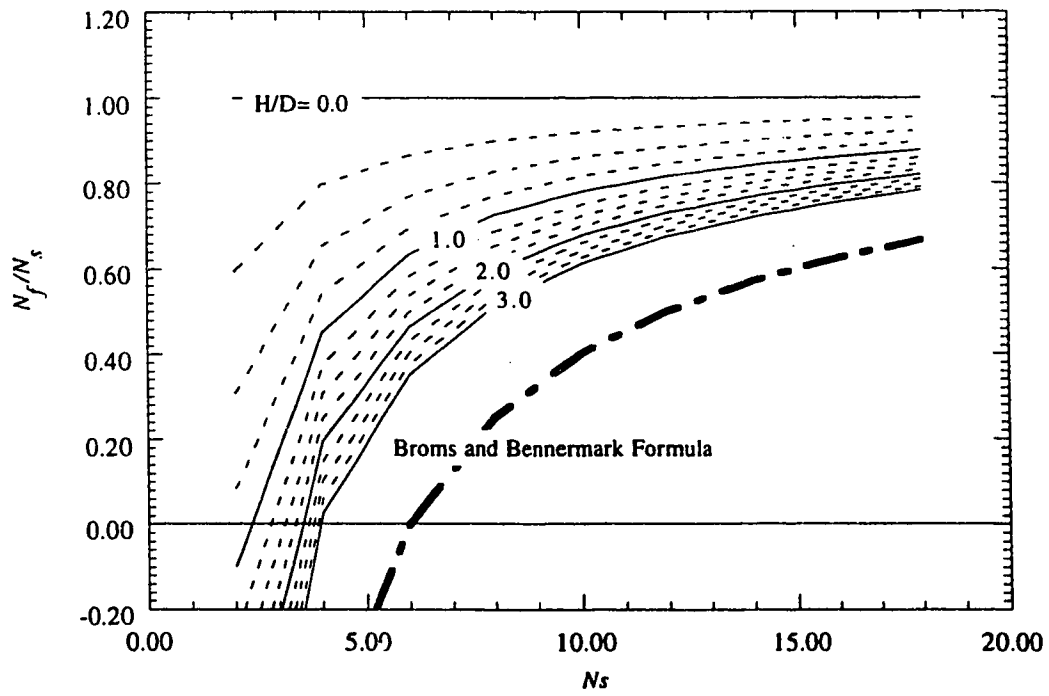
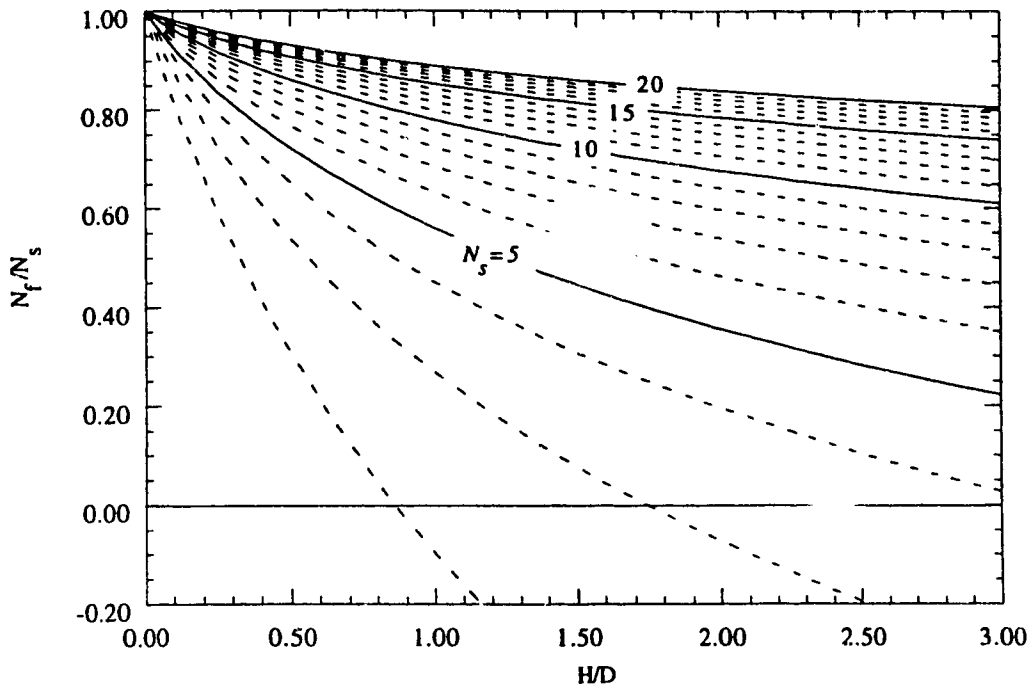


Figure A1: Lower Bound Solution of Spherical Configuration for Face Stability in Cohesive Soil (Extended Mülhaus Solution)

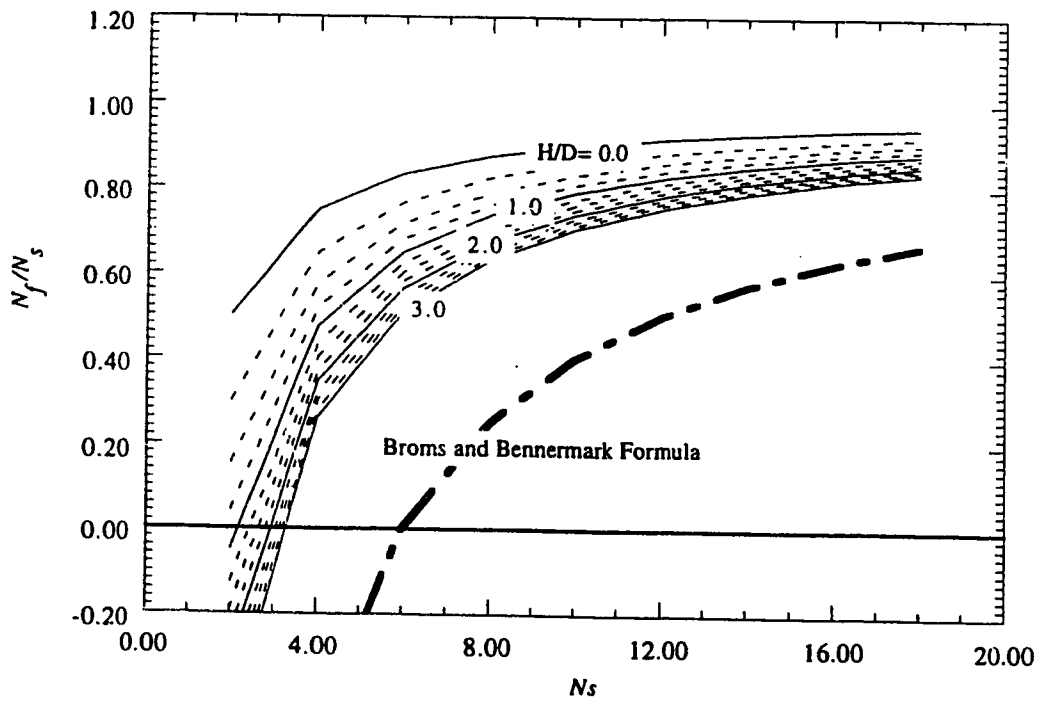
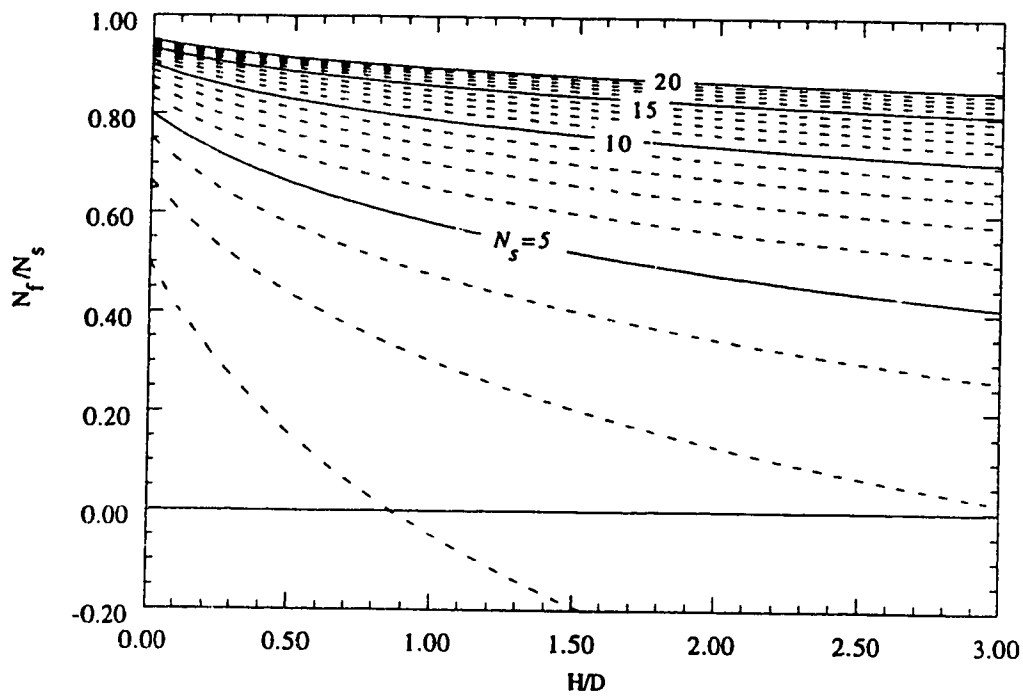


Figure A2: Lower Bound Solution of Cylindrical Configuration for Face Stability in Cohesive Soil (Davis Solution)

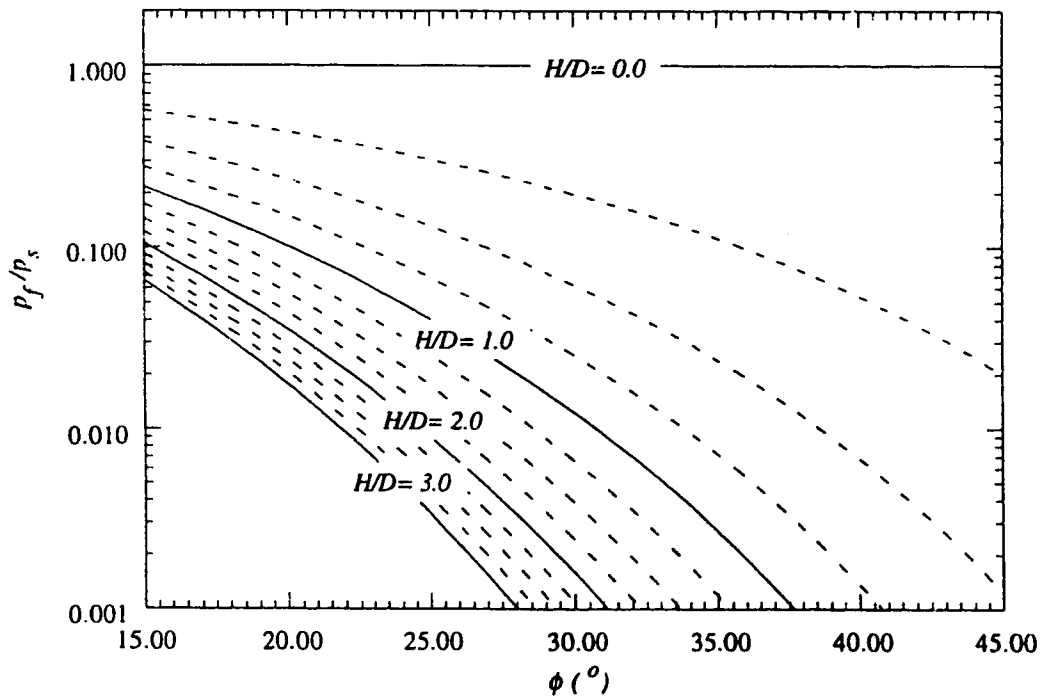
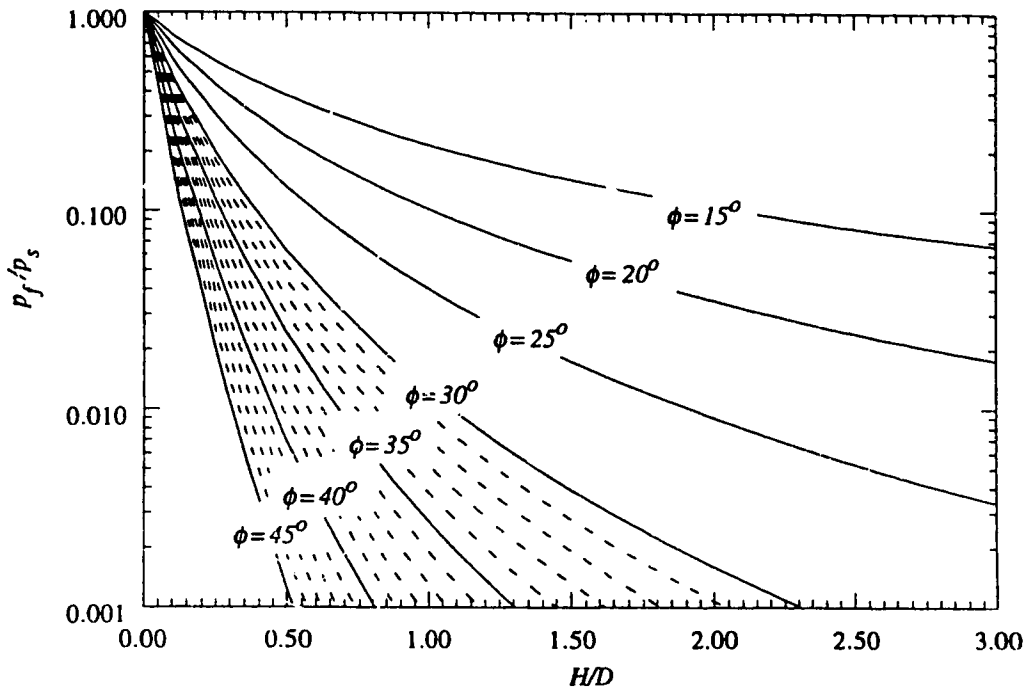


Figure A3: Lower Bound Solution of Spherical Configuration for Face Stability in Frictional Soil (Extended Mülhaus Solution)

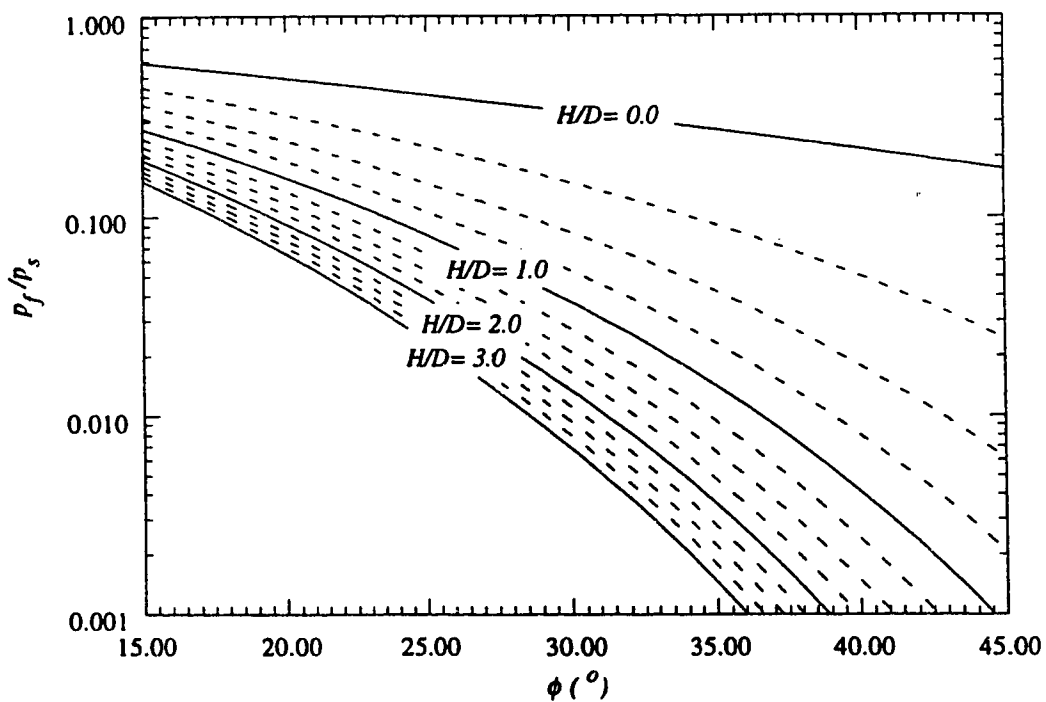
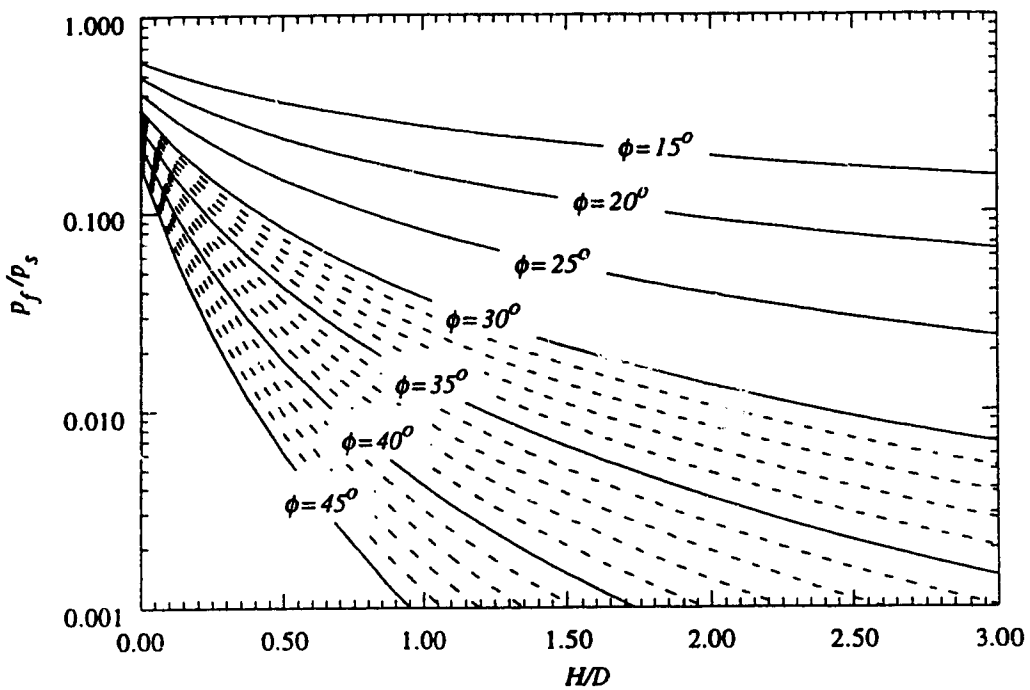


Figure A4: Lower Bound Solution of Cylindrical Configuration for Face Stability in Frictional Soil (Leca and Panet Solution)

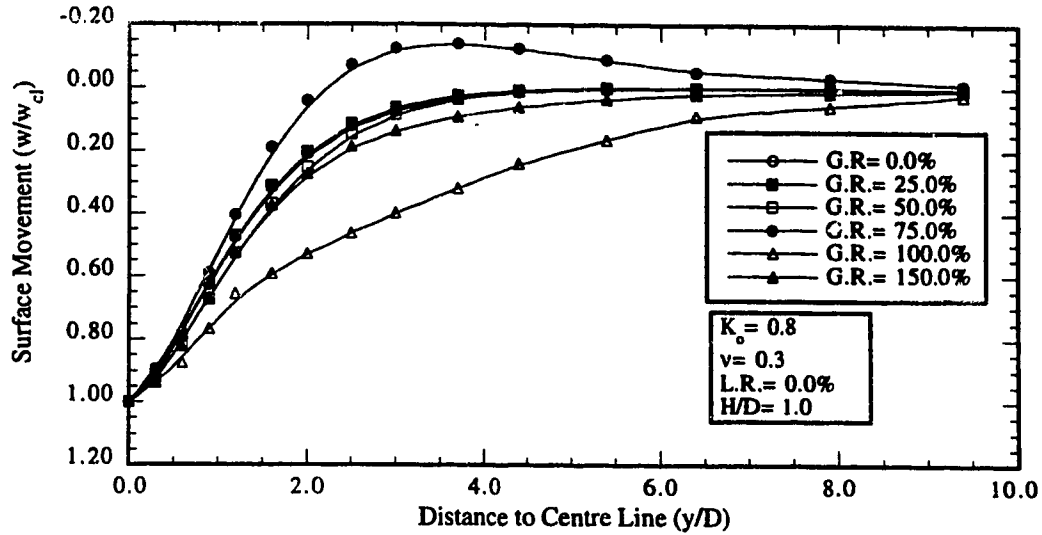


Figure B1: Distribution of Normalized Surface Movement due to 3-D Action in the Transversal Plane for various values of G.R. ($H/D = 1.0$, L.R. = 0.0 %)

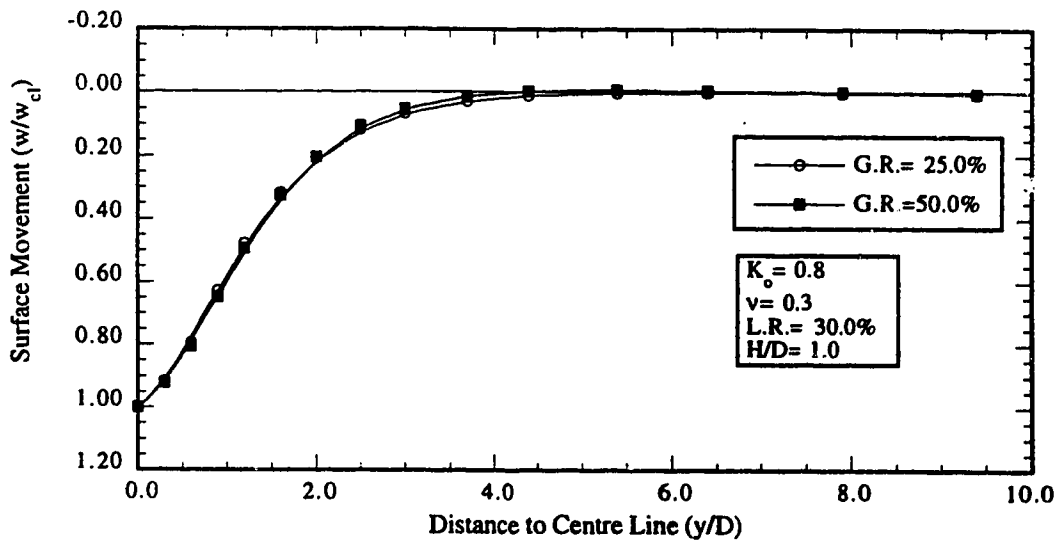


Figure B2: Distribution of Normalized Surface Movement due to 3-D Action in the Transversal Plane for various values of G.R. ($H/D = 1.0$, L.R. = 30.0 %)

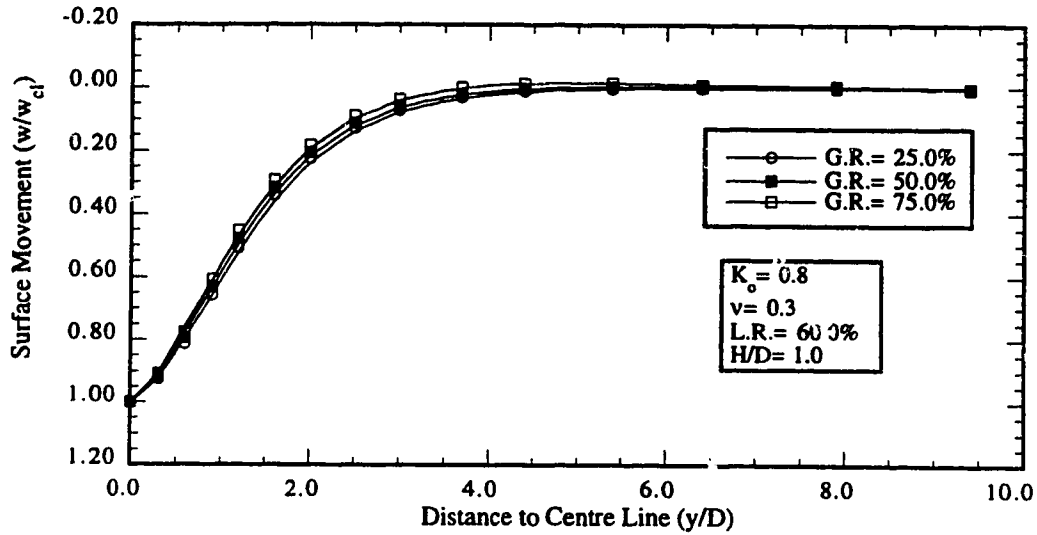


Figure B3: Distribution of Normalized Surface Movement due to 3-D Action in the Transversal Plane for various values of G.R. (H/D= 1.0, L.R.= 60.0 %)

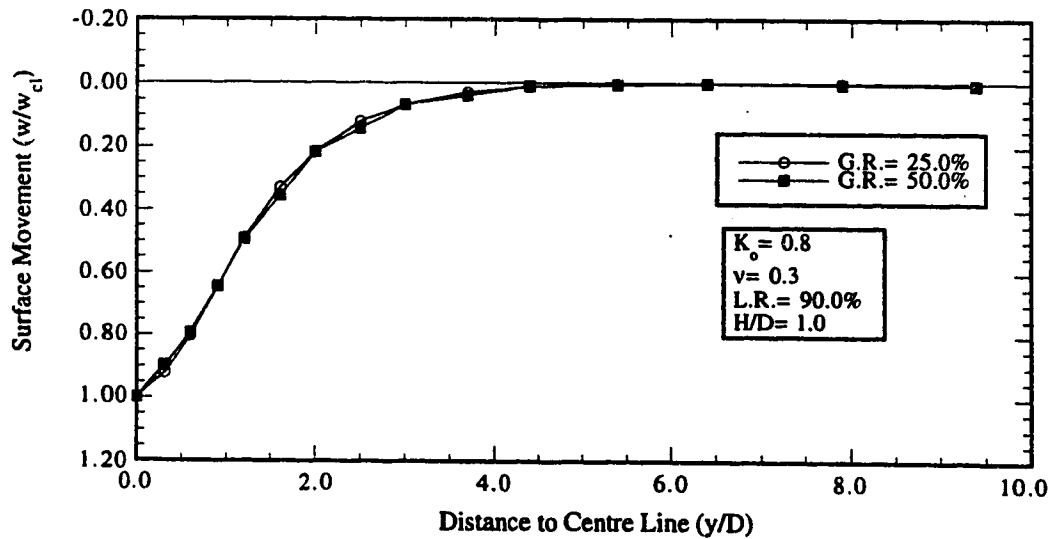


Figure B4: Distribution of Normalized Surface Movement due to 3-D Action in the Transversal Plane for various values of G.R. (H/D= 1.0, L.R.= 90.0 %)

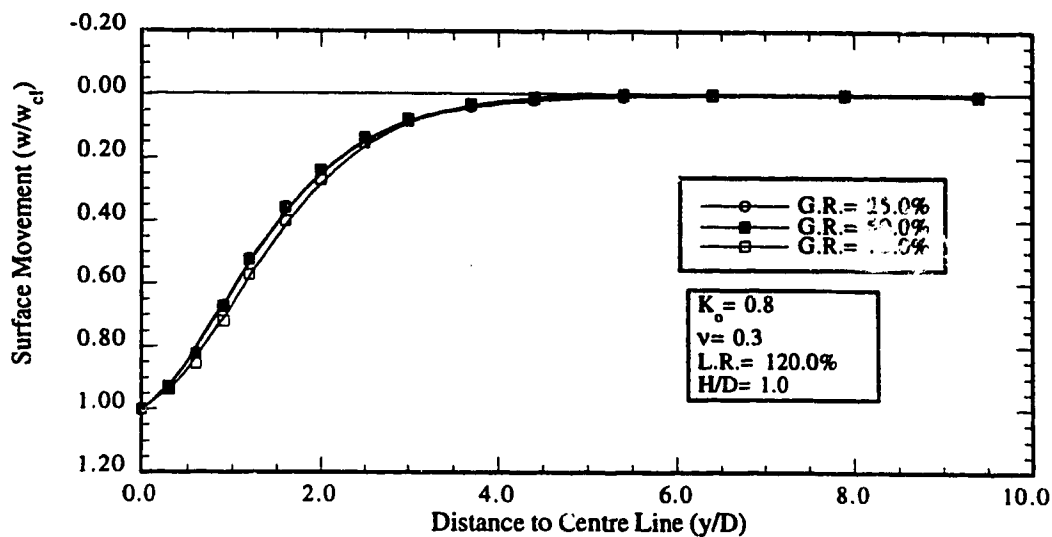


Figure B5: Distribution of Normalized Surface Movement due to 3-D Action in the Transversal Plane for various values of G.R. ($H/D= 1.0$, $L.R.= 120.0\%$)

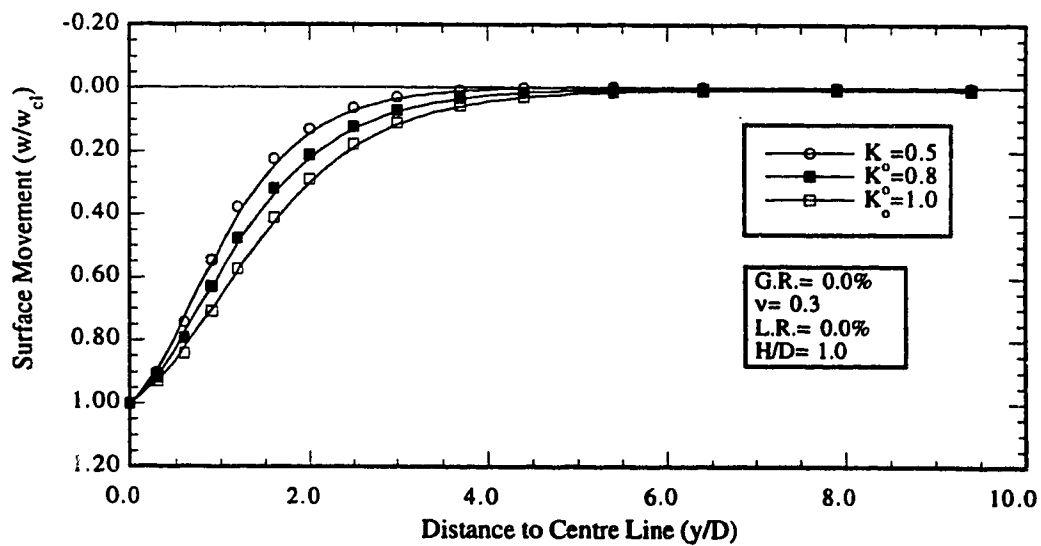


Figure B6: Distribution of Normalized Surface Movement due to 3-D Action in the Transversal Plane for various values of K_o ($H/D= 1.0$)

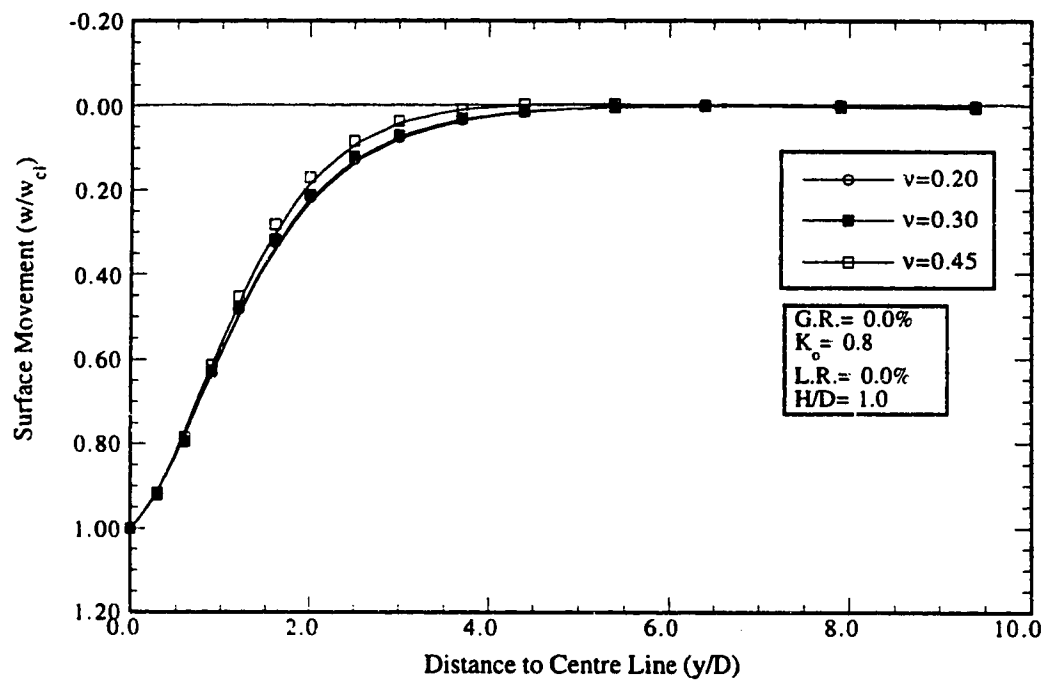


Figure B7: Distribution of Normalized Surface Movement due to 3-D Action in the Transversal Plane for various values of v ($H/D= 1.0$)

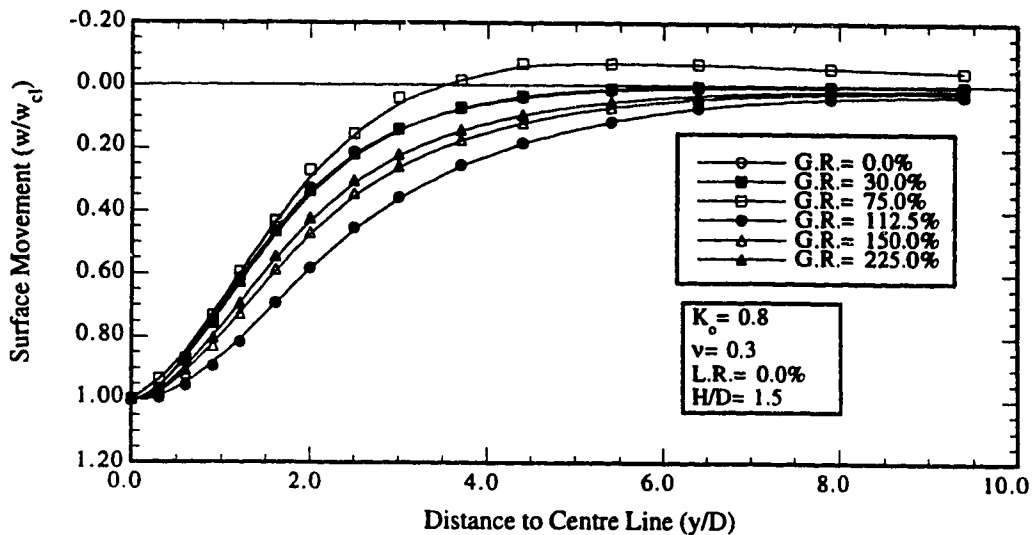


Figure B8: Distribution of Normalized Surface Movement due to 3-D Action in the Transversal Plane for various values of G.R. ($H/D = 1.5$, L.R. = 0.0 %)

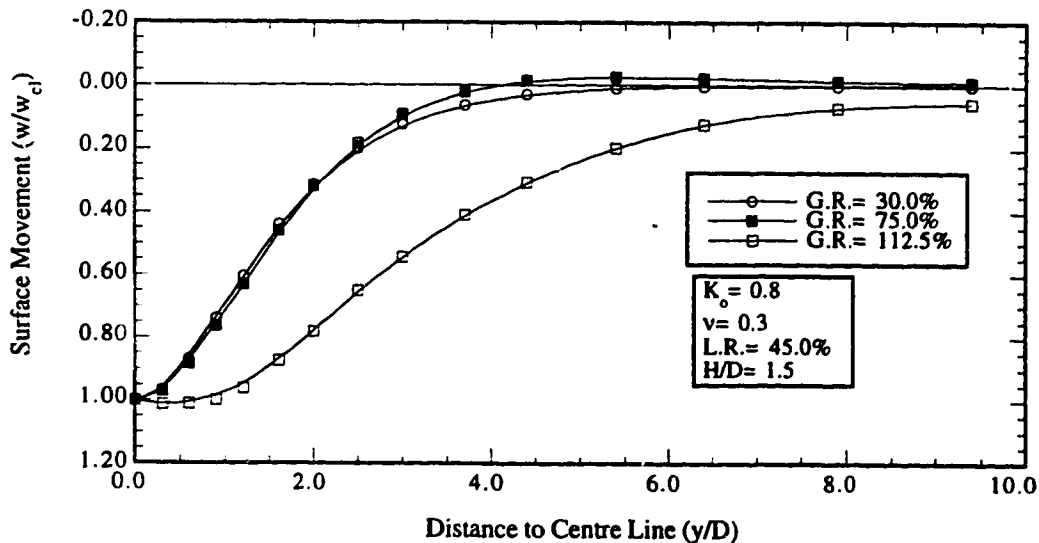


Figure B9: Distribution of Normalized Surface Movement due to 3-D Action in the Transversal Plane for various values of G.R. ($H/D = 1.5$, L.R. = 45.0 %)

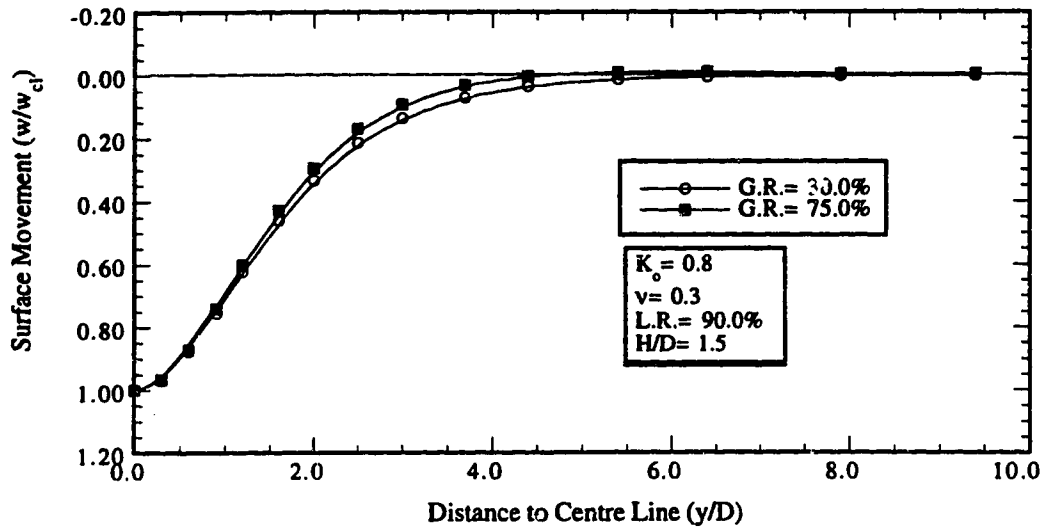


Figure B10: Distribution of Normalized Surface Movement due to 3-D Action in the Transversal Plane for various values of G.R. ($H/D = 1.5$, L.R. = 90.0 %)

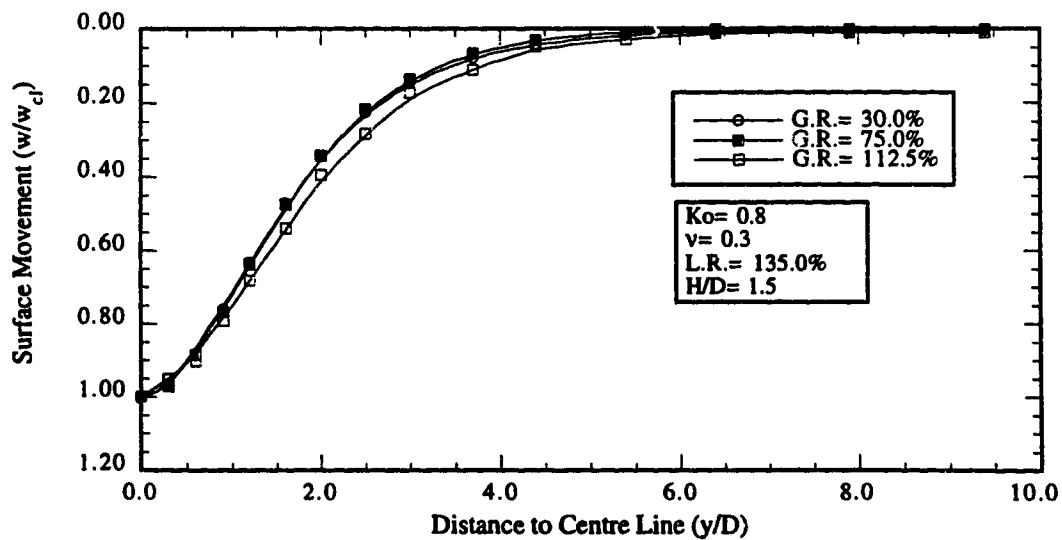


Figure B11: Distribution of Normalized Surface Movement due to 3-D Action in the Transversal Plane for various values of G.R. ($H/D = 1.5$, L.R. = 135.0 %)

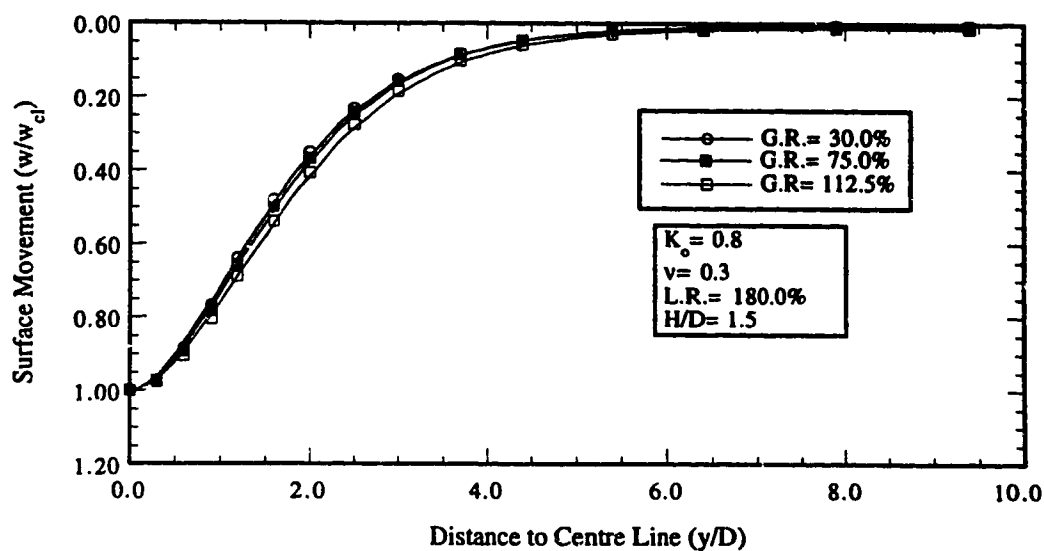


Figure B12: Distribution of Normalized Surface Movement due to 3-D Action in the Transversal Plane for various values of G.R. ($H/D= 1.5$, L.R.= 180.0 %)

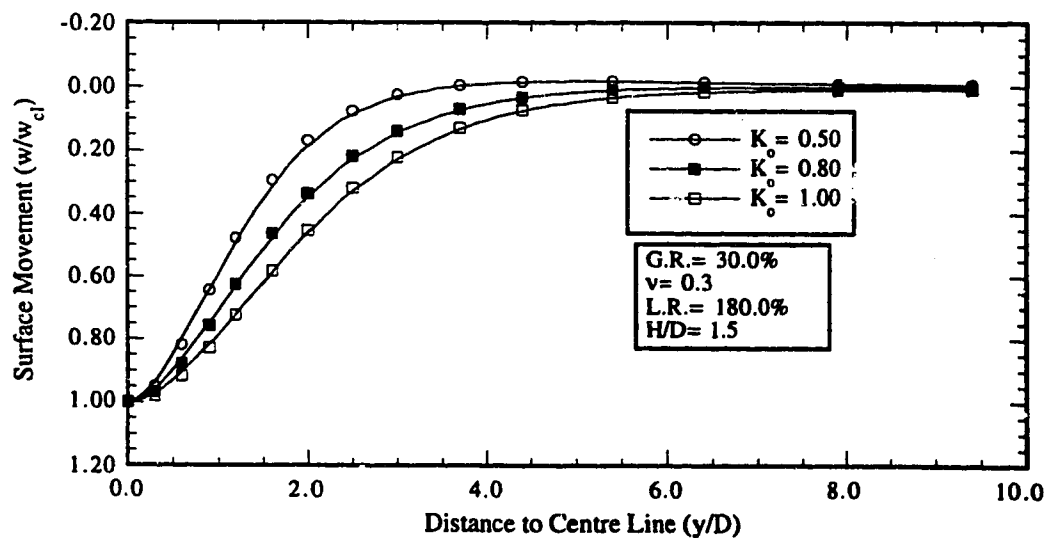


Figure B13: Distribution of Normalized Surface Movement due to 3-D Action in the Transversal Plane for various values of K_o ($H/D= 1.5$)

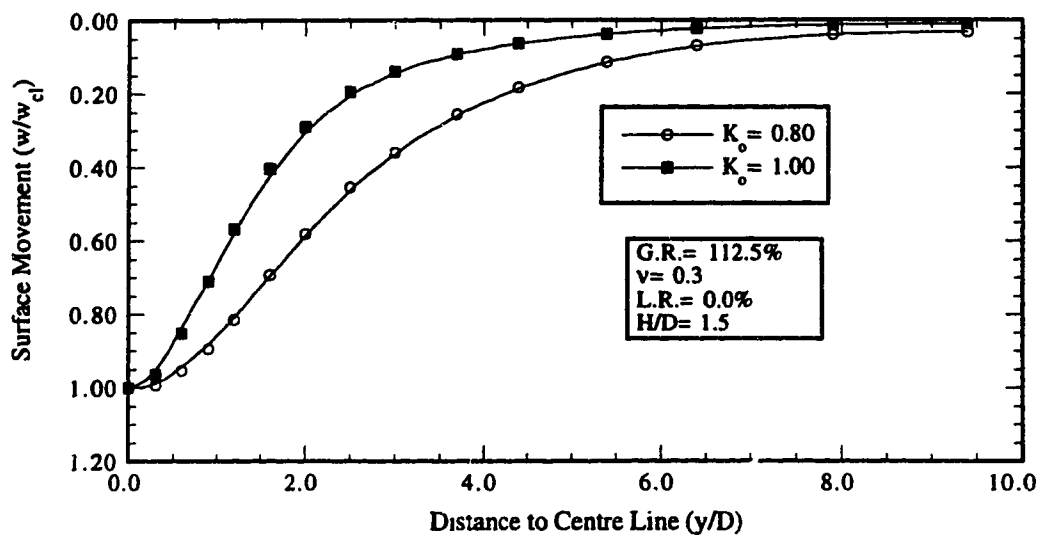


Figure B14: Distribution of Normalized Surface Movement due to 3-D Action in the Transversal Plane for various values of K_o ($H/D = 1.5$)

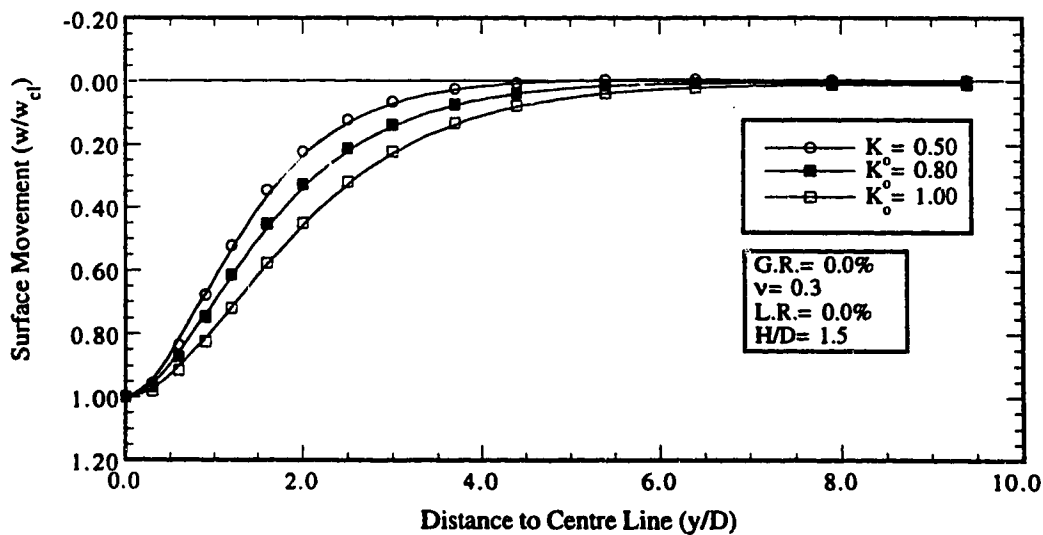


Figure B15: Distribution of Normalized Surface Movement due to 3-D Action in the Transversal Plane for various values of K_o ($H/D = 1.5$)

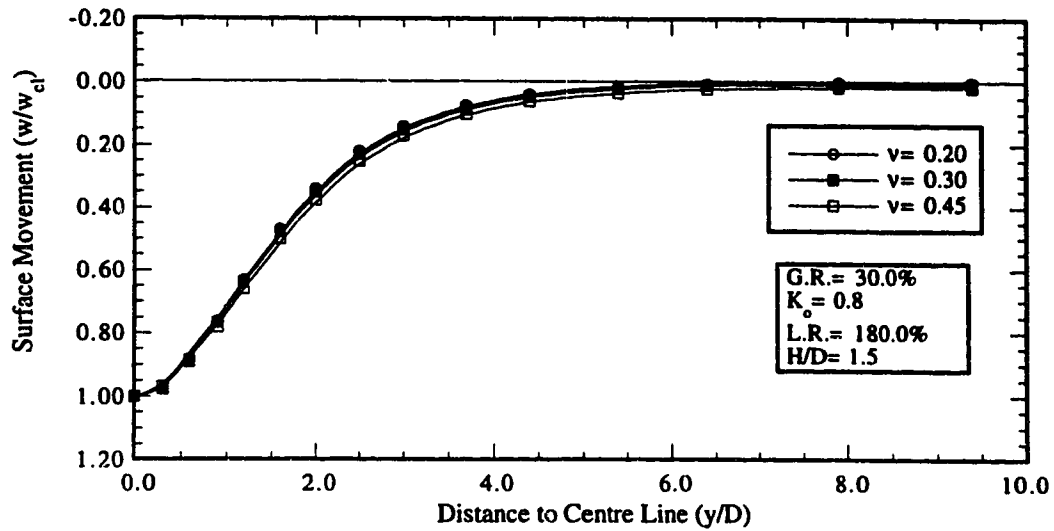


Figure B16: Distribution of Normalized Surface Movement due to 3-D Action in the Transversal Plane for various values of ν ($H/D= 1.5$)

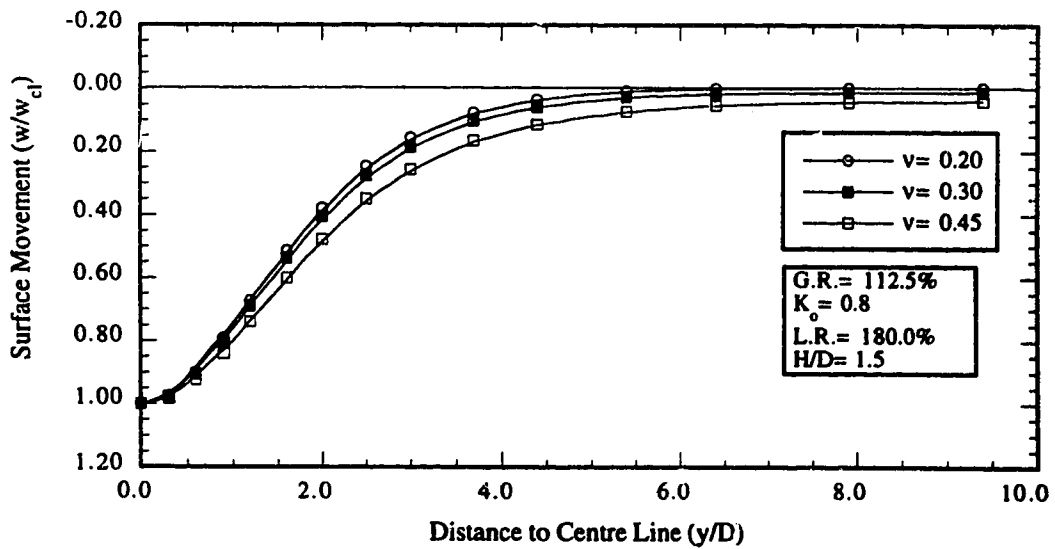


Figure B17: Distribution of Normalized Surface Movement due to 3-D Action in the Transversal Plane for various values of ν ($H/D= 1.5$)

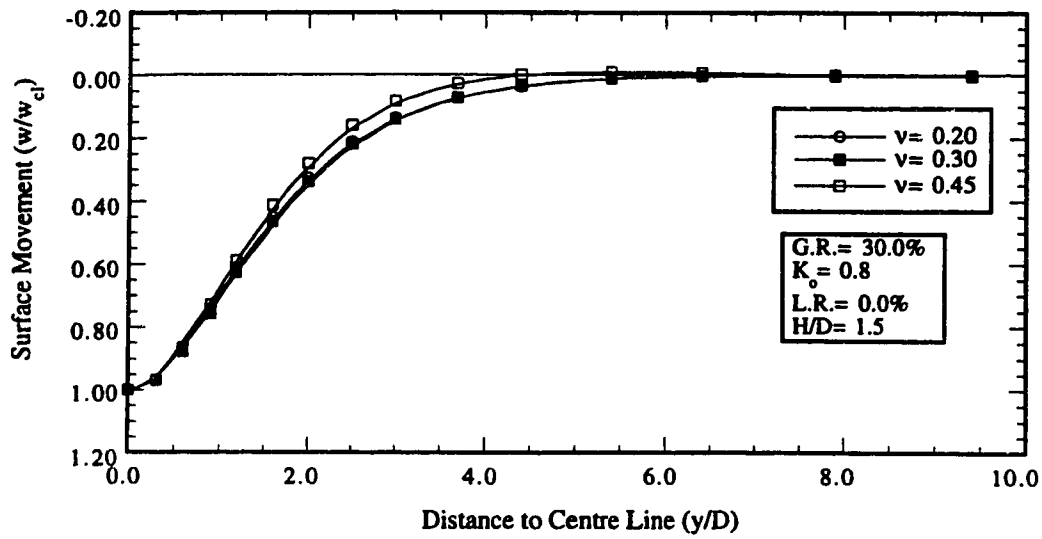


Figure B18: Distribution of Normalized Surface Movement due to 3-D Action in the Transversal Plane for various values of v ($H/D= 1.5$)

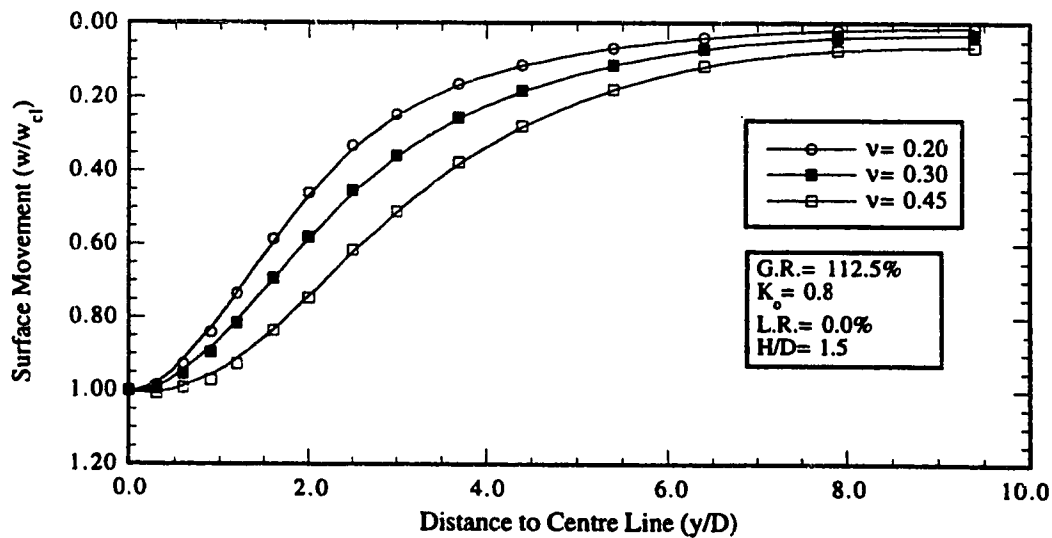


Figure B19: Distribution of Normalized Surface Movement due to 3-D Action in the Transversal Plane for various values of v ($H/D= 1.5$)

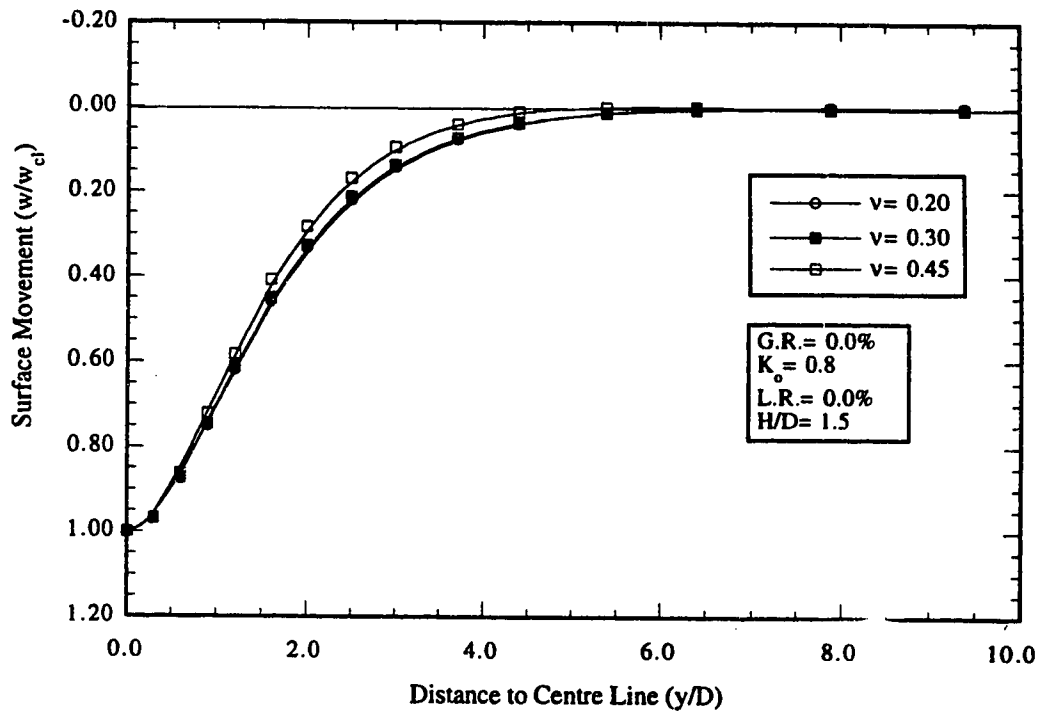


Figure B20: Distribution of Normalized Surface Movement due to 3-D Action in the Transversal Plane for various values of ν ($H/D = 1.5$)

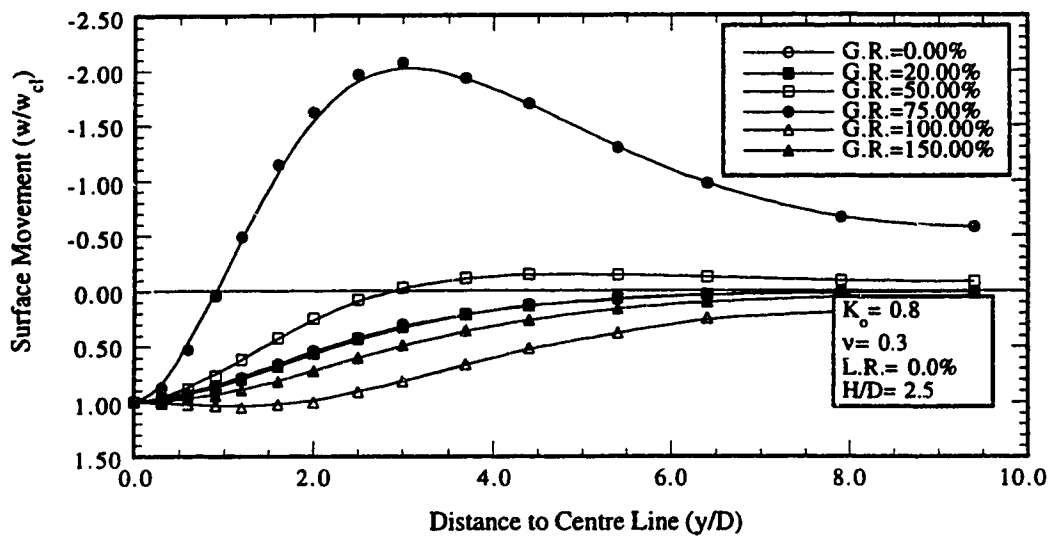


Figure B21: Distribution of Normalized Surface Movement due to 3-D Action in the Transversal Plane for various values of G.R. ($H/D= 2.5$, $L.R.= 0.0\%$)

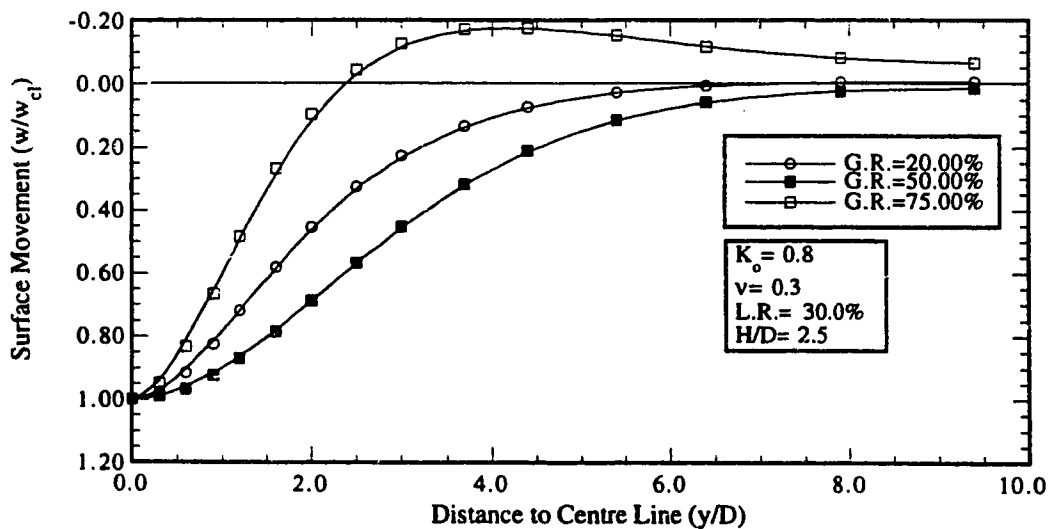


Figure B22: Distribution of Normalized Surface Movement due to 3-D Action in the Transversal Plane for various values of G.R. ($H/D= 2.5$, $L.R.= 30.0\%$)

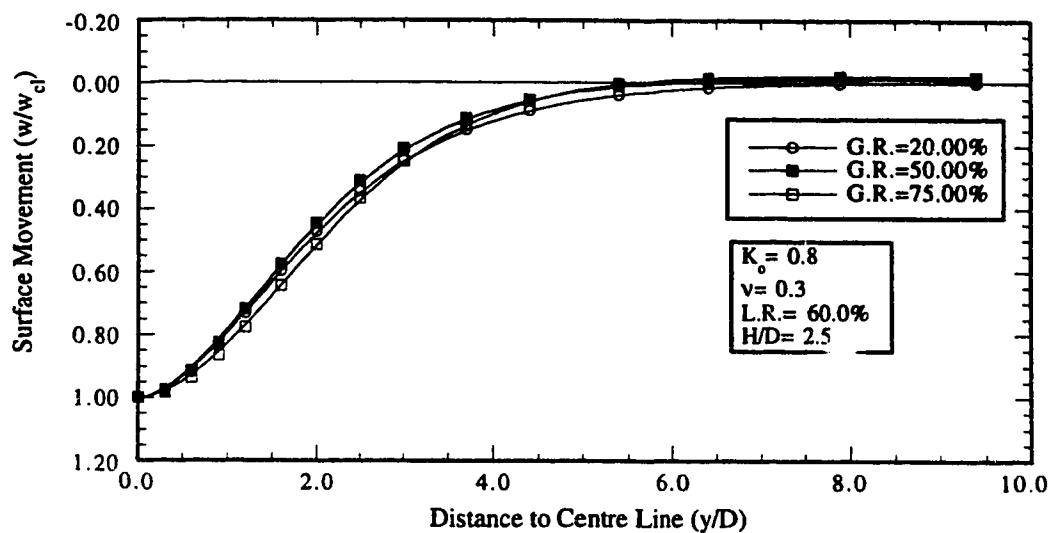


Figure B23: Distribution of Normalized Surface Movement due to 3-D Action in the Transversal Plane for various values of G.R. ($H/D = 2.5$, $L.R. = 60.0\%$)

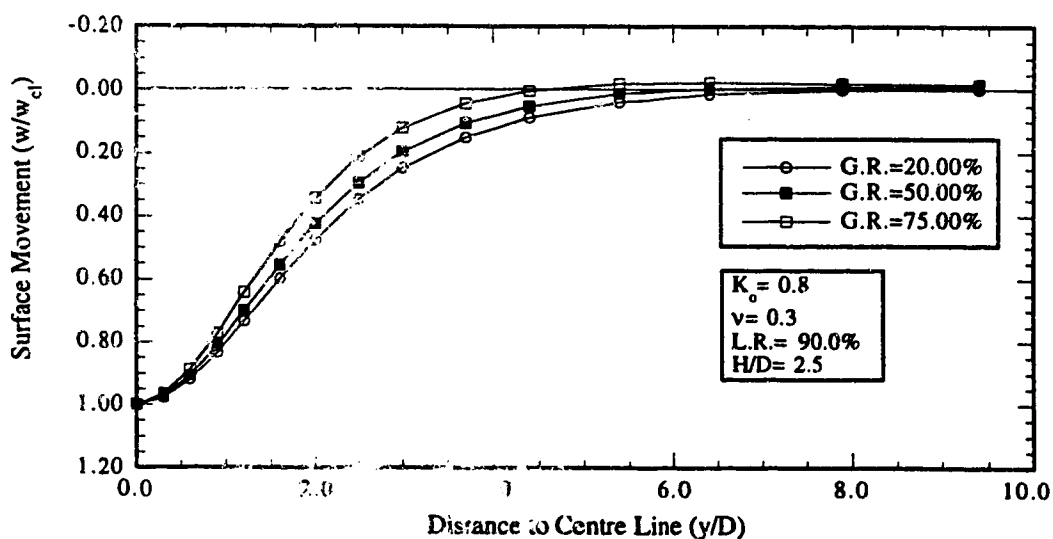


Figure B24: Distribution of Normalized Surface Movement due to 3-D Action in the Transversal Plane for various values of G.R. ($H/D = 2.5$, $L.R. = 90.0\%$)

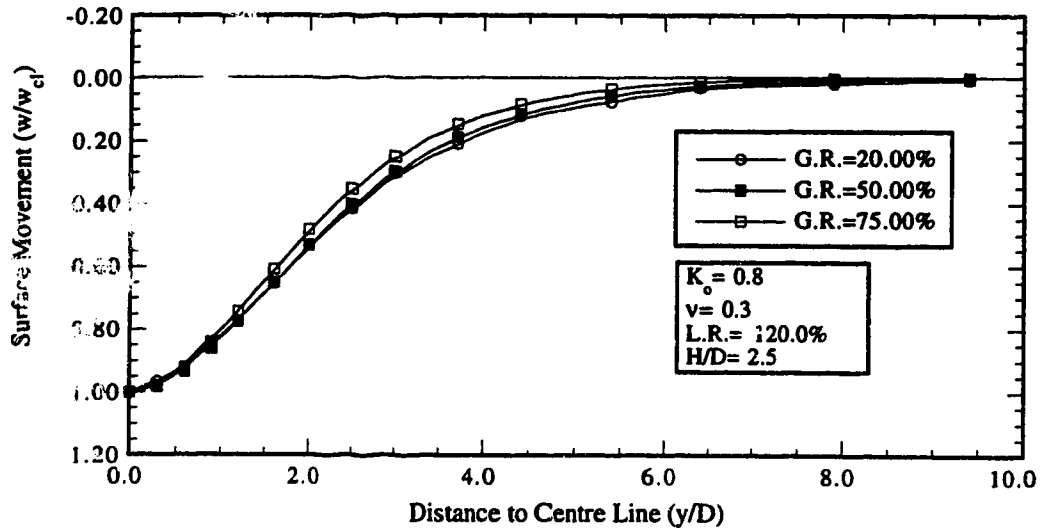


Figure B25: Distribution of Normalized Surface Movement due to 3-D Action in the Transversal Plane for various values of G.R. ($H/D = 2.5$, L.R. = 120.0 %)

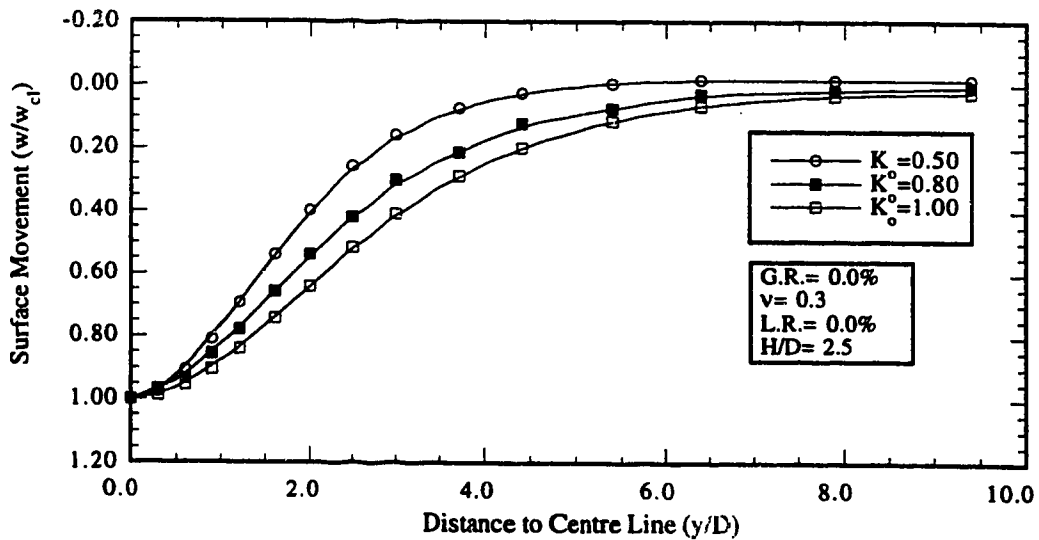


Figure B26: Distribution of Normalized Surface Movement due to 3-D Action in the Transversal Plane for various values of K_o ($H/D = 2.5$)

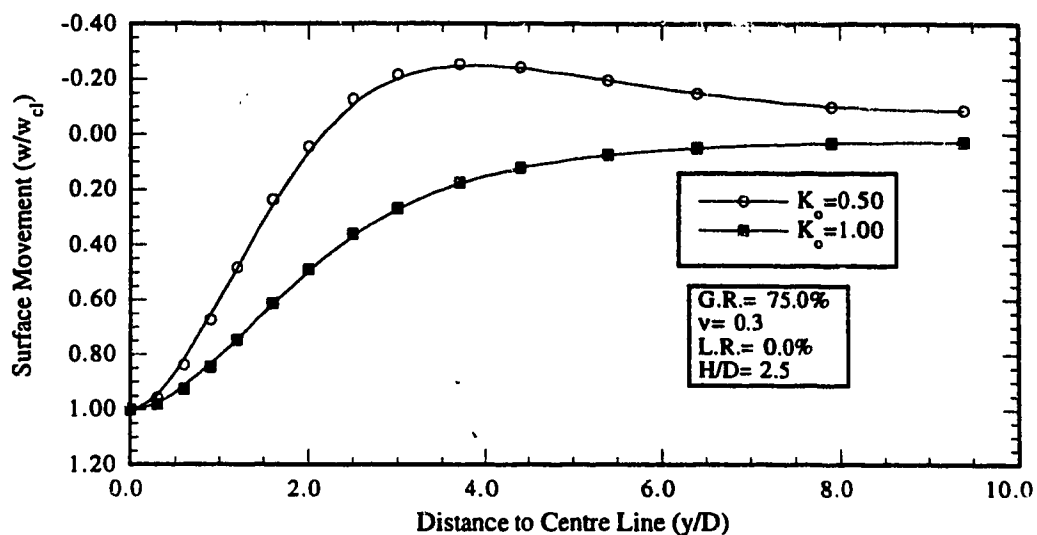


Figure B27: Distribution of Normalized Surface Movement due to 3-D Action in the Transversal Plane for various values of K_o ($H/D= 2.5$)

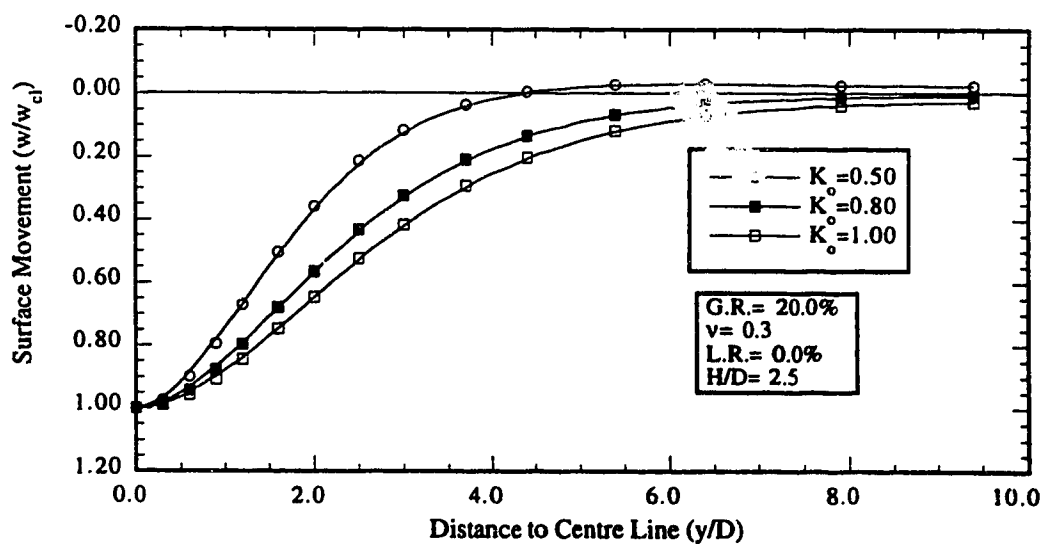


Figure B28: Distribution of Normalized Surface Movement due to 3-D Action in the Transversal Plane for various values of K_o ($H/D= 2.5$)

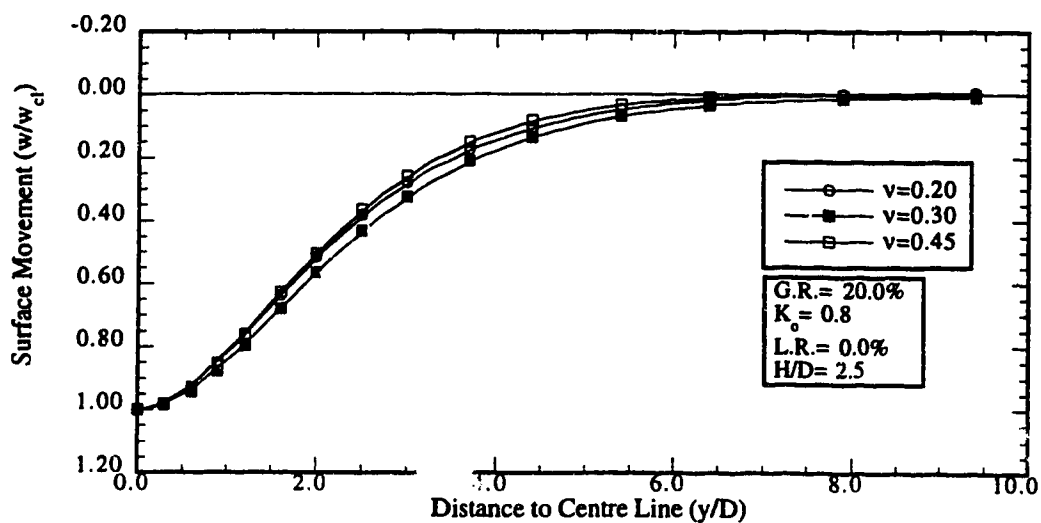


Figure B29: Distribution of Normalized Surface Movement due to 3-D Action in the Transversal Plane for various values of v ($H/D= 2.5$)

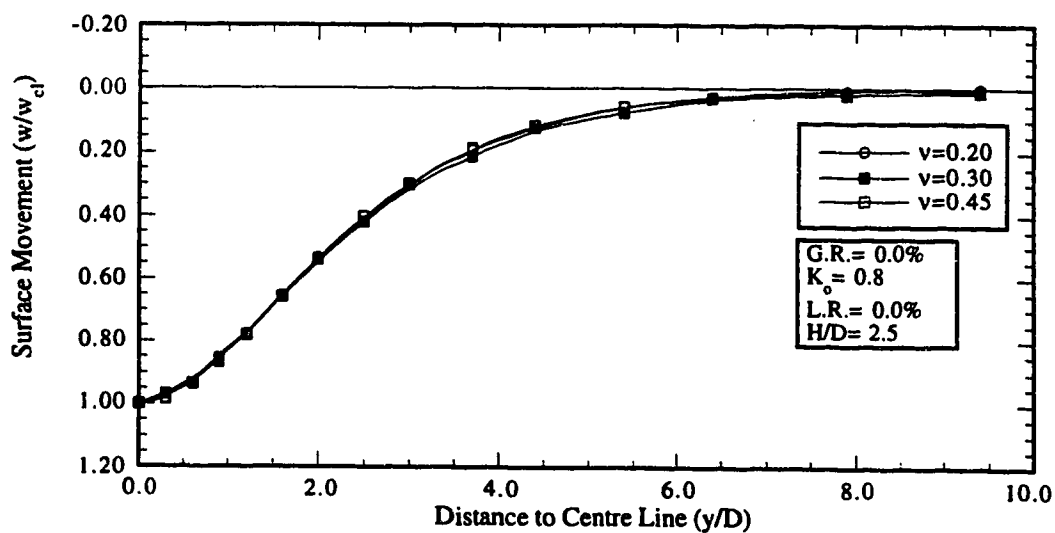


Figure B30: Distribution of Normalized Surface Movement due to 3-D Action in the Transversal Plane for various values of v ($H/D= 2.5$)

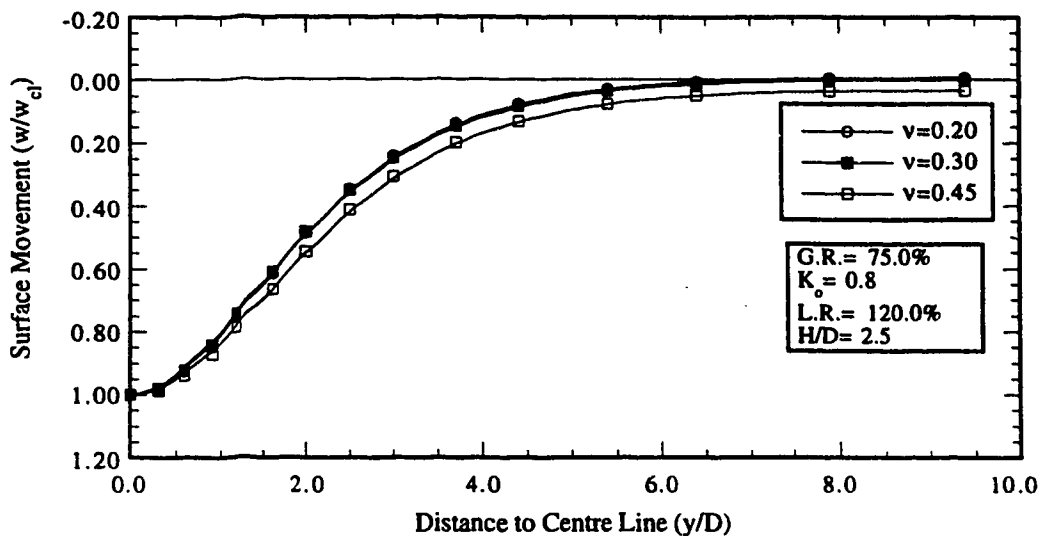


Figure B31: Distribution of Normalized Surface Movement due to 3-D Action in the Transversal Plane for various values of ν ($H/D= 2.5$)

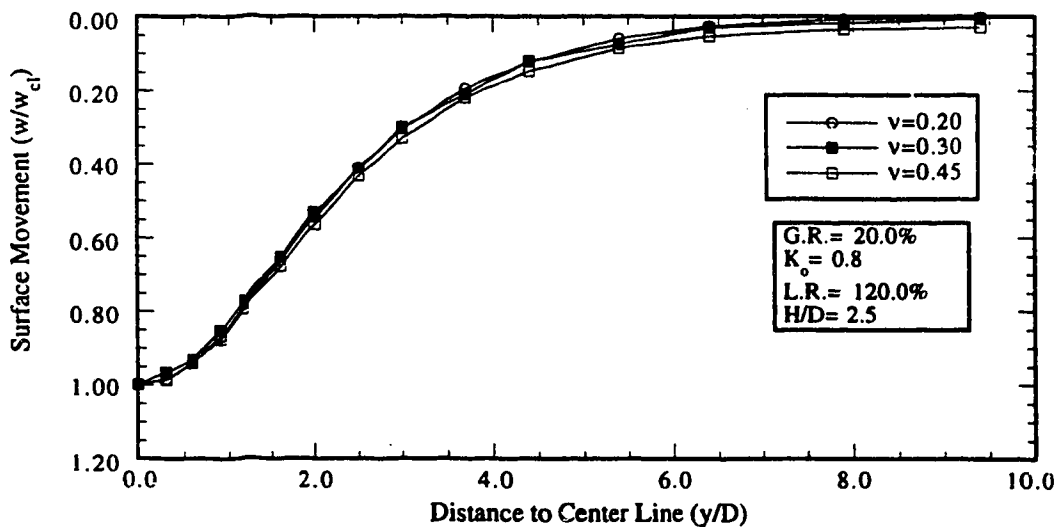


Figure B32: Distribution of Normalized Surface Movement due to 3-D Action in the Transversal Plane for various values of ν ($H/D= 2.5$)

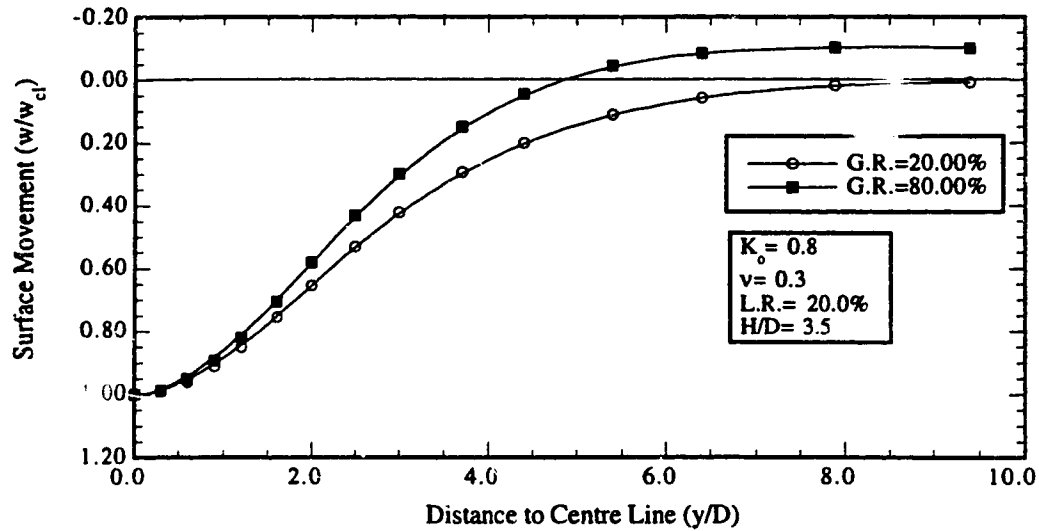


Figure B33: Distribution of Normalized Surface Movement due to 3-D Action in the Transversal Plane for various values of G.R. (H/D= 3.5, L.R.= 20.0%)

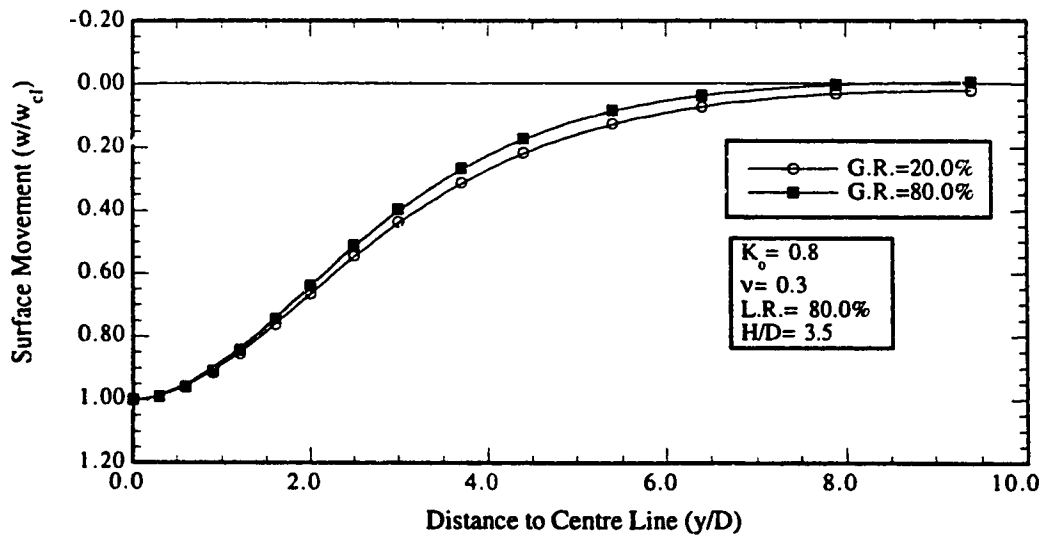


Figure B34: Distribution of Normalized Surface Movement due to 3-D Action in the Transversal Plane for various values of G.R. (H/D= 3.5, L.R.= 80.0%)

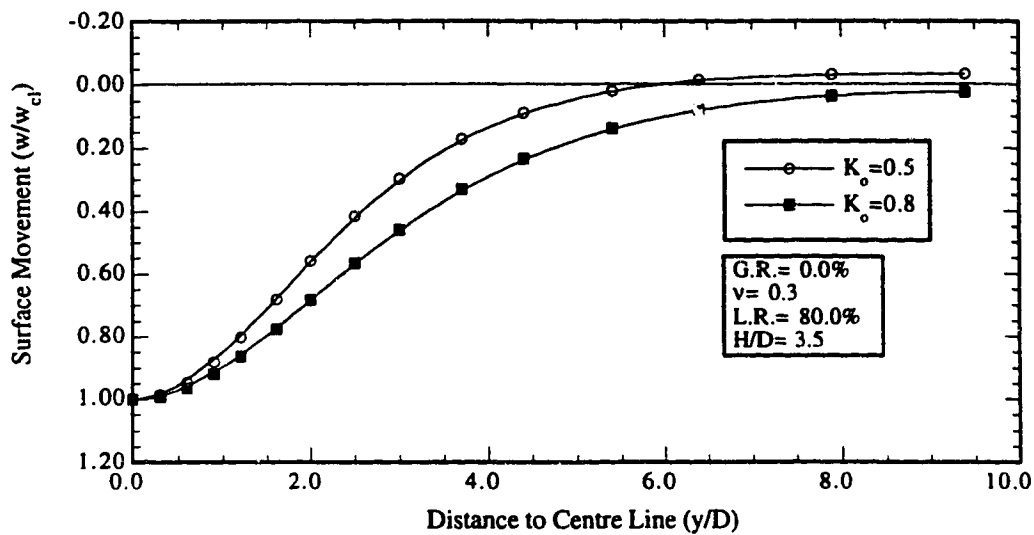


Figure B35: Distribution of Normalized Surface Movement due to 3-D Action in the Transversal Plane for various values of K_o ($H/D= 3.5$)

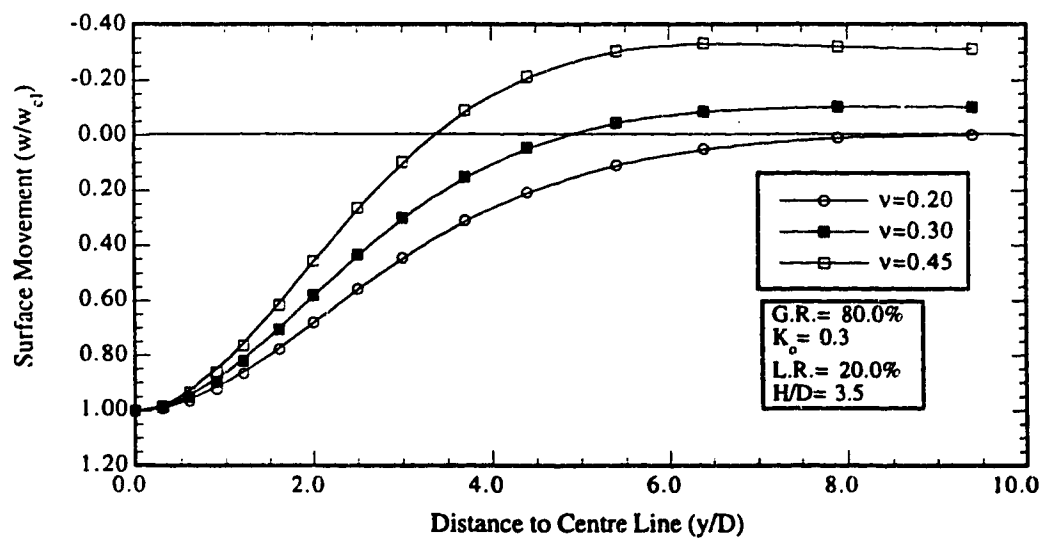


Figure B36: Distribution of Normalized Surface Movement due to 3-D Action in the Transversal Plane for various values of v ($H/D= 3.5$)

```
1  LRT Example
2  13.5 6.56
3  19 0.8 0 30 1
4  90 0.5 101.33 0.3
5  0.75 1.25
6  0
7  37 0.25 0.232 8.33
8  3.28
9  9
10 1
```

1
2
3
4
5
6
7
8
9
10
11
12
13
14
15
16
17
18
19
20
21
22
23
24
25
26
27
28
29
30
31
32
33
34
35
36
37
38
39
40
41
42
43
44
45
46
47
48
49
50

Design Method
for Tunnels Constructed
using Pressurized Shields

A. Input Data

1. Title: LRT- Example
2. Geometry:
H= 13.500 D= 6.560 R1= 3.280
3. Ground Properties
Gama= 19.000 Ko= .800
c= .000 Phi= 30.000
Hyperbolic Parameters:
K= 90.000 n= .500
nu= .300
Pa= 101.330 Rf= 1.000
4. Construction Method:
G.R. (%) = 75.000 L.R. (%) =125.000
5. Liner Properties:
E= 37.000 nu= .250
t= .232 I= 8.330
6. Modified Shear Strength Parameters:
Phi (a)= 30.000 Phi (e)= 30.000
m-1 = 2.000

B. Stress Changes due to Three Dimensional Effect:

1. Stress Changes:

	S.R. (%)	D.S.R. (%)
C	91.6947	11.8508
S	100.1649	28.8492
F	84.6882	22.4880
2. Modified Stress Field:

	Gama (mod)	Ko (mod)
C	19.2650	.7630
S	20.2238	.5500
F	25.6244	.6314
Average	21.3343	.6236

51 3. Modified Stiffness:

	Sigma 1	Sigma 3	Et/1000
52 C	234.6869	188.4126	9.5689
53 S	351.8653	239.2168	8.1906
54 F	338.2829	250.4733	9.7521
55			
56			
57			
58 Average			8.9256

59

60 4. Surface Displacement:

61 S3D= 5.172

62

63

64 C. Stress Changes in Plane Stain Condition:

65

66 1. Reference Values:

	Alfa ref	Alfa/U ref	Uref
67 C	.4195	1.0346	.4055
68 S	.3225	1.2731	.2533
69 F	.2444	1.9879	.1229

70

71

72 2. Twice Normalized Ground Reaction Curve:

	Lambda	Deriv. Lambda
73 C	.7963	1.2315
74 S	1.1000	1.4171
75 F	.5398	1.0082

76

77

78

79 3. Equivalent Deformations at the Tunnel:

	U/Uref	U	Sigma	D(Sigma)/E	ur
80 C	.2134	.0865	234.5806	.1608	13.9170
81 S	-.0943	-.0239	306.0632	.2451	-5.8547
82 F	.4717	.0580	338.2829	.2276	13.1936

83

84

85

86

87 Remark: Units

88 Dimensions:.....m

89 Soil Density:.....kN/m³

90 c:.....kPa

91 Phi:.....degree

92 P(atmospheric):.....kPa (=101.325)

93 Soil movements:.....mm

94 Soil Modulus(Et):.....MPa

95 Liner Modulus(Es):.....GPa

96 Liner Thickness(As):.....m²/m

97 Liner Inertia(Is):.....1E-05 m⁴/m

98 Stresses:.....kPa

99 Forces:.....kN/m

100 Moments:.....kN.m/m

101

102

103

104 EISENSTEIN- NEGRO METHOD FOR GROUND
105 REACTION PREDICTION OF SHALLOW TUNNELLING
106
107
108 LRT- Example
109 1. GEOMETRY
110 H= 13.5000 D= 6.5600 H/D= 2.0579
111
112 2. GROUND PROPERTIES
113 GAMA= 19.0000 KO= .6236
114 SIGMA3=198.812 C= .0000 PHI= 30.0000 RF= 1.0000
115 PHI A= 30.0000 PHI E= 30.0000
116 M-1= 2.0000
117 K= 90.000 N= .5000 PA= 101.330 NU= .3000
118
119 LOCATION SIGMA3 SIGMA1 ETI
120 1/2 D ABOVE C 121.088 194.180 9.5689
121 AT S 198.812 318.820 8.1906
122 1/2 D BELOW F 276.535 443.460 9.7521
123 5. STRESS RELEASE AND STIFFNESS CHANGE
124 AT LINING ACTIVATION
125
126 U U/U(REF) LAMBDA LAMBDA`
127 C .0865 .213 .7720 1.0730
128 S -.0239 -.094 1.1323 1.5056
129 F .0580 .472 .5508 .9784
130 STRESSES: SIGMA= 1-(1-LAMBDA)*ALFA REF.
131 1-LAMBDA SIGMA
132 C .2280 .904
133 S -.1323 1.043
134 F .4492 .890
135 SIGMA AV.= (SIGMA(C)+2 SIGMA(S)+SIGMA(F))/4= .9700
136 ALFA AV. = 1- SIGMA AV.= .0300
137 GAMA REDUCED=GAMA* SIGMA AV. = 18.4294
138
139 STIFFNESS: ET= (LAMBDA`/LAMBDA` (I)) *ETI
140 LAMBDA` (I) ETI/LAMBDA` (I) ET
141 C 1.0753 8.8988 9.5489
142 S 1.3249 6.1820 9.3077
143 F .9953 9.7986 9.5867
144 ET(AV.)= (ET(C)+2 ET(S)+ET(F))/4= 9.4378
145 7. LINING GROUND INTERACTION
146 ZO= 16.7800 RO= 3.1640 RL= 3.2800
147 ET AV.= 9.4378 NU= .3000 GAMA RED.= 18.4294
148 KO= .6236
149 ES= 37.0000 NU,S= .2500 AS= .2320
150 IS= 8.3300
151
152

```

153      ITERATION N.  1
154
155      WITHOUT HEAVE
156      ET AV.=      9.4378      ALFA=      398.6173      BETA=      .0143
157
158      UR      D(UR)      URF      U      U/U REF      LAMBDA`      ET      SIGMA R
159      C      13.917      30.666      44.583      .2535      .6253      .9931      8.837      194.759
160      S      -5.855      -33.444      -39.299      -.2468      -.5000      6.5388      40.423      282.409
161      F      13.194      37.317      50.511      .1970      1.6027      1.0071      9.868      242.084
162      NEW ET AV.=      24.8877
163
164      WITH HEAVE
165      ET AV.=      9.4378      ALFA=      398.6173      BETA=      .0143
166
167      UR      D(UR)      URF      U      U/U REF      LAMBDA`      ET      SIGMA R
168      C      13.917      30.666      43.995      .2502      .6170      .9967      8.869      194.759
169      S      -5.855      -33.444      -39.299      -.2468      -.5000      6.5388      40.423      282.409
170      F      13.194      37.317      51.099      .1993      1.6214      1.0040      9.838      242.084
171      NEW ET AV.=      24.8883
172      UPWARD HEAVE=      .588
173
174
175      ITERATION N.  2
176
177      WITHOUT HEAVE
178      ET AV.=      24.8877      ALFA=      151.1577      BETA=      .0054
179
180      UR      D(UR)      URF      U      U/U REF      LAMBDA`      ET      SIGMA R
181      C      13.917      14.381      28.298      .1609      .3969      1.0667      9.493      204.750
182      S      -5.855      -14.661      -20.516      -.1288      -.5000      6.5388      40.423      313.160
183      F      13.194      16.126      29.320      .1144      .9303      1.0747      10.530      252.954
184      NEW ET AV.=      25.2172
185
186      WITH HEAVE
187      ET AV.=      24.8883      ALFA=      151.1577      BETA=      .0054
188
189      UR      D(UR)      URF      U      U/U REF      LAMBDA`      ET      SIGMA R
190      C      13.917      14.381      28.056      .1595      .3935      1.0673      9.498      204.750
191      S      -5.855      -14.661      -20.516      -.1288      -.5000      6.5388      40.423      313.160
192      F      13.194      16.126      29.562      .1153      .9380      1.0750      10.534      252.954
193      NEW ET AV.=      25.2194
194      UPWARD HEAVE=      .242
195
196
197      ITERATION N.  3
198
199      WITHOUT HEAVE
200      ET AV.=      25.2172      ALFA=      149.1734      BETA=      .0054
201
202      UR      D(UR)      URF      U      U/U REF      LAMBDA`      ET      SIGMA R
203      C      13.917      15.126      29.043      .1652      .4073      1.0649      9.476      217.919
204      S      -5.855      -15.410      -21.265      -.1335      -.5000      6.5388      40.423      333.456
205      F      13.194      16.955      30.149      .1176      .9566      1.0757      10.540      269.204
206      NEW ET AV.=      25.2156
207
208      WITH HEAVE
209      ET AV.=      25.2194      ALFA=      149.1734      BETA=      .0054
210
211      UR      D(UR)      URF      U      U/U REF      LAMBDA`      ET      SIGMA R
212      C      13.917      15.126      28.789      .1637      .4037      1.0655      9.482      217.919
213      S      -5.855      -15.410      -21.265      -.1335      -.5000      6.5388      40.423      333.456

```

Appendix D: Output File for the Edmonton LRT Example (continued)

```

214      F      13.194 16.955 30.404 .1186 .9647 1.0759 10.542 269.204
215      NEW ET AV.= 25.2176
216      UPWARD HEAVE= .255
217
218
219 *****Omitted from Output File *****
220
221      ITERATION N. 9
222
223      WITHOUT HEAVE
224      ET AV.= 25.2157      ALFA= 149.1832      BETA= .0054
225
226      UR      D(UR)      URF      U      U/U REF      LAMBDA`      ET      SIGMA R
227      C      13.917 15.090 29.007 .1650 .4068 1.0650 9.477 217.383
228      S      -5.855 -15.373 -21.228 -.1333 -.5000 6.5388 40.423 332.635
229      F      13.194 16.915 30.108 .1174 .9553 1.0757 10.540 268.542
230      NEW ET AV.= 25.2157
231
232      WITH HEAVE
233      ET AV.= 25.2177      ALFA= 149.1949      BETA= .0054
234
235      UR      D(UR)      URF      U      U/U REF      LAMBDA`      ET      SIGMA R
236      C      13.917 15.090 28.753 .1635 .4032 1.0656 9.483 217.383
237      S      -5.855 -15.373 -21.228 -.1333 -.5000 6.5388 40.423 332.635
238      F      13.194 16.915 30.362 .1184 .9634 1.0759 10.542 268.542
239      NEW ET AV.= 25.2177
240      UPWARD HEAVE= .254
241
242      STRAINING ACTIONS
243
244      WITHOUT HEAVE
245      ANGLE      NORMAL F.      SHEAR FORCE      MOMENT
246      F      .00 .12193152E+04 .00000000E+00 .18752917E+02
247      10.00 .12000592E+04 -.41155718E+01 .17508012E+02
248      20.00 .11457065E+04 -.76207773E+01 .13955659E+02
249      30.00 .10657709E+04 -.10009407E+02 .86123140E+01
250      40.00 .97384110E+03 -.10962819E+02 .22426616E+01
251      50.00 .88474871E+03 -.10396557E+02 -.42648265E+01
252      60.00 .81159214E+03 -.84623478E+01 -.16037260E+02
253      70.00 .76329957E+03 -.55074551E+01 -.14346192E+02
254      80.00 .74326128E+03 -.20022494E+01 -.16704108E+02
255      S      90.00 .74928233E+03 .15470595E+01 -.16914599E+02
256      100.00 .77477314E+03 .46818352E+01 -.15072476E+02
257      110.00 .81079579E+03 .70545149E+01 -.11520122E+02
258      120.00 .84839356E+03 .84623485E+01 -.67739952E+01
259      130.00 .88059709E+03 .88494980E+01 -.14387555E+01
260      140.00 .90362657E+03 .82832349E+01 .38742955E+01
261      150.00 .91705687E+03 .69152889E+01 .86123163E+01
262      160.00 .92301159E+03 .49411919E+01 .12324029E+02
263      170.00 .92471986E+03 .25685118E+01 .14681945E+02
264      C      180.00 .92493357E+03 -.13027550E-05 .15489655E+02
265
266      WITH HEAVE
267      ANGLE      NORMAL F.      SHEAR FORCE      MOMENT
268      F      .00 .12191750E+04 .00000000E+00 .18749203E+02
269      10.00 .11999207E+04 -.41147867E+01 .17504543E+02
270      20.00 .11455730E+04 -.76193228E+01 .13952891E+02
271      30.00 .10656449E+04 -.10007495E+02 .86106008E+01
272      40.00 .97372404E+03 -.10960722E+02 .22422086E+01
273      50.00 .88464077E+03 -.10394563E+02 -.42639881E+01
274      60.00 .81149236E+03 -.84607201E+01 -.10035271E+02

```

Appendix D: Output File for the Edmonton LRT Example (continued)

```

275          70.00 .76320606E+03 -.55063891E+01 -.14343338E+02
276          80.00 .74317161E+03 -.20018529E+01 -.16700773E+02
277          90.00 .74919394E+03 .15467751E+01 -.16911209E+02
278          100.00 .77468371E+03 .46809460E+01 -.15069441E+02
279          110.00 .81070353E+03 .70531646E+01 -.11517788E+02
280          120.00 .84829735E+03 .84607208E+01 -.67726064E+01
281          130.00 .88049650E+03 .88477892E+01 -.14384368E+01
282          140.00 .90352176E+03 .82816302E+01 .38735425E+01
283          150.00 .91694845E+03 .69139456E+01 .86106031E+01
284          160.00 .92290045E+03 .49402302E+01 .12321561E+02
285          170.00 .92460705E+03 .25680112E+01 .14678996E+02
286          C 180.00 .92482019E+03 -.13025010E-05 .15486540E+02
287
288      8. SUBSURFACE SETTLEMENTS
289
290      WITHOUT HEAVE
291      CROWN SETTLM.= 29.00712      U/Uref= .40681
292      LAMBDA(crown)= .56439      % STRESS RELEASE= 18.27444
293
294      DEPTH  SETTLEMENT
295      .00000  11.33222
296      2.70000  12.46503
297      5.40000  13.90696
298      8.10000  15.89317
299      10.80000 19.10732
300
301      WITH HEAVE
302      CROWN SETTLM.= 28.75305      U/Uref= .40325
303      LAMBDA(crown)= .56819      % STRESS RELEASE= 18.11519
304
305      DEPTH  SETTLEMENT
306      .00000  11.22517
307      2.70000  12.34806
308      5.40000  13.77740
309      8.10000  15.74633
310      10.80000 18.93281
311

```

312 9. SURFACE SETTLEMENTS
313
314 WITHOUT HEAVE
315 % STRESS RELEASE= 18.27444
316 Ko= .80 PHI= 30.00 C/ Gamma/D= .00
317 DISTANCE SETTLEMENT
318 .00000 11.33222
319 2.41106 11.10782
320 4.82212 10.46095
321 7.23318 9.46546
322 9.64424 8.22888
323 12.05530 6.87334
324 14.46637 5.51598
325 16.87743 4.25311
326 19.28849 3.15078
327 21.69955 2.24263
328 24.11061 1.53365
329 MAX. DISTORTION= 1/ 1755.46
330
331 WITH HEAVE
332 % STRESS RELEASE= 18.11519
333 Ko= .80 PHI= 30.00 C/ Gamma/D= .00
334 DISTANCE SETTLEMENT
335 .00000 11.22517
336 2.41106 11.00290
337 4.82212 10.36214
338 7.23318 9.37605
339 9.64424 8.15115
340 12.05530 6.80841
341 14.46637 5.46388
342 16.87743 4.21293
343 19.28849 3.12102
344 21.69955 2.22145
345 24.11061 1.51916
346 MAX. DISTORTION= 1/ 1772.20
347
348
349 Remark: Units
350 Dimensions:.....m
351 Soil Density:.....kN/m³
352 c:.....kPa
353 Phi:.....degree
354 P(atmospheric):.....kPa (=101.325)
355 Soil movements:.....mm
356 Soil Modulus(Et):.....MPa
357 Liner Modulus(Es):.....GPa
358 Liner Thickness(As):.....m²/m
359 Liner Inertia(Is):.....1E-05 m⁴/m
360 Stresses:.....kPa
361 Forces:.....kN/m
362 Moments:.....kN.m/m
363

```

1  IMPLICIT REAL* 8 (A-H, O-Z)
2  CHARACTER* 40 TITLE
3  COMMON /GL/ HD, XKO, IPLACE, S1INI( 3), S3INI( 3)
4  COMMON /VAR/ P1( 12,4), P2( 40,2), P3( 40,2),
5  *      P4( 47), XLL2I( 3),
6  *      ETI( 3), UR( 3), U( 3), ALF6( 3), ALF8( 3), AU6( 3),
7  *      AU8( 3), AU1( 3), ALF( 3), AU( 3), UU( 3), XL( 3),
8  *      XLL( 3), XL1( 3), XLL1( 3), XL2( 3), XLL2( 3),
9  *      SIGMA( 3), ET( 3), ALFX( 3), URF( 3), PP( 82)
10 COMMON/S/ PP2(180)
11 COMMON/TT/ PP3(36)
12 COMMON/NEW/ XGAM2( 3), XKO2( 3), XGAMA2, XKAV
13 *      , XNSR( 3), XNRO( 3), XN3D
14 CALL RIN( TITLE, XH, XD, XGAMA, XKO, XC, XFI, RF, XK
15 *      , XN, PA, XNU, XG, XLINER, XES, XNUS, XAS
16 *      , XIS, RL, IWRIT, NITE)
17 C *** Read input data and transfer it in their actual values
18 XHO= ( XH+ XD/2)/( XD/2)
19 HD= XH/ XD
20 IND= 1
21 CALL RDATA
22 C
23 DO 10 I= 1,3
24     IPLACE= I
25
26     CALL MYSHLD( XG, XLINER, XNU, XKO, XHO, I, IWRIT)
27 C *** Evaluate the stress ratio,  $\sigma_r$  and surface displacement
28 C      related to the construction method
29     CALL CHECK( XFI, XC, XH, XD, XGAMA, XKO, I, IWRIT)
30 C *** Check that the shear stresses do not violate the failure
31 C      criterion
32     CALL EHYPER( XFI, XC, XK, XN, PA, RF, I, IWRIT, XGAMA, XH)
33 C *** Evaluate the modulus of deformation according to the
34 C      Hyperbolic model
35     XALFA= ALFA( XES, XNU, XGAMA, ETI( I), X, XNUS)
36     XBETA= BETA( XES, XNU, XGAMA, I( I), XD, XNUS, XIS)
37     CALL ABC( A, B, C, D, XALFA, XBETA, XNU, XHO, I, IWRIT)
38 C *** Calculate A, B, C, and D values
39     CALL NEWSTS( A, B, C, D, XH, XD, XKO, I, IWRIT)
40 C *** Calculate the new gamma and Ko related to the construction
41 C      method
42     CALL CHECK2
43 C *** Check that the calculated value of Ko is within the
44 C      applicable range
45     10 CONTINUE
46 C
47 DO 20 I= 1, 3
48     IPLACE= I
49     CALL HARIMAN( XALFA, XBETA, XH, I, XD
50 *      , XNU, SRO, SFIO, IWRIT)
51 C *** Calculate radial and tangential stresses at the
52 C      three points of the liner
53     CALL GSIGMA( SRO, XH, XD, XGAMA, XKO, I)
54 C *** Calculate the amount of stress reduction at the three points

```

Appendix E: FORTRAN Program for Design of Shallow Tunnels constructed using Pressurized Shield Methods

```

55 C           of the liner
56   20       CONTINUE
57 C
58   CALL GREF( XH, XD, XFI, XC, RF, IND)
59 C *** Calculate reference values for the shear strength parameters at
60 C           the three points of the liner
61   CALL GLMDA
62 C *** Calculate the twice normalized stress relief parameters (lambda)
63 C           the three points of the liner
64   CALL CHECK2
65 C ***       Check that the calculated value of Lambda is within the
66 C           applicable range
67   CALL DLAMDA
68 C *** Calculate the twice normalized Stiffness change parameters
69 C           (Derivative lambda) at the three points of the liner
70   CALL GUU( IND)
71 C *** Back substitute to calculate the normalized displacement at the
72 C           tunnel circumference
73   CALL WOUT( TITLE, XH, XGAMA, XC, XFI, RF, XK
74   *           , XN, PA, XNU, XG, XLINER, PL, XES, XNUS, XAS, XIS)
75 C *** Write output data related to the initial step
76   IND= 0
77   CALL NEGROS( TITLE, XH, XD, XGAMA, XKO, XC, XFI, RF
78   *           , XK, XN, PA, XNU, XG, XLINER, PL, XES, XNUS, XAS
79   *           , XIS, RL, NITE)
80 C *** For the given circumferencial displacement estimate the straining
81 C           actions at the liner and the surface displacement after the
82 C           ground liner interaction
83   STOP
84   END
85 C
86 C
87 C
88   SUBROUTINE CHECK( XFI, XC, XH, XD, XGAMA, XKO, IPLACE, IPRINT)
89   IMPLICIT REAL* 8 (A-H, O-Z)
90   COMMON/STS/ZETA, RO, S1( 3), S3( 3)
91   COMMON/NEW/XGAM2( 3), XKO2( 3), XGAMA2, XKAV, XNSR( 3), XNRO( 3)
92   *           , XN3D
93 C
94   ICRRCT= 0
95   HO= XH+ XD/2
96   PI= 2* DASIN(1.)
97 C
98   ZETAO= XGAMA* (XH+ ( IPLACE-1)*(XD/2))*(1+2*XKO)/DSQRT(3.)
99   ZETA= XNSR( IPLACE)* ZETAO
100  RO= XNRO( IPLACE)* XGAMA* HO
101 C
102  SIGMA3= ZETA/DSQRT(3.)- RO/DSQRT(6.)
103  S3( IPLACE)= SIGMA3
104  S1( IPLACE)= SIGMA3+ RO/DSQRT(2./3.)
105  IF( XFI.EQ. 0) GOTO 100
106 C
107  IF( XC. EQ. 0) THEN
108  XFIA= XFI

```

Appendix E: FORTRAN Program for Design of Shallow Tunnels constructed using Pressurized Shield Methods (continued)


```

109         GOTO 10
110         ENDIF
111         XFIA= DASIN(( 1+ SIGMA3* DTAN( XFI)/ XC)/
112         *      ( 1+ SIGMA3/ DCOS( XFI)/ XC))
113 10 DUMMY= 3*RO/(RO+2*DSQRT(2)*ZETA)
114         IF( DUMMY.LT.-1 .OR. DUMMY.GT.1) THEN
115             XFI2= PI/2
116             GOTO 20
117         ENDIF
118         XFI2= DASIN( DUMMY)
119 20 IF( XFI2. GT. XFIA) ICRRCT= 1
120         IF( ICRRCT. EQ.1) THEN
121             RONEW= DSQRT( 2/3)* DSIN( XFIA)*
122             *      ( S1( IPLACE)+ S3( IPLACE))
123             XNRO( IPLACE)= RONEW/XGAMA/HO
124         ENDIF
125         GOTO 200
126 100 XC2= ( S1( IPLACE)-S3( IPLACE))/2
127         IF( XC2. GT. XC) THEN
128             RONEW= DSQRT( 8/3)* XC
129             XNRO( IPLACE)= RONEW/XGAMA/HO
130         ENDIF
131         IF( IWRIT.EQ. 1) WRITE( 7, 1000) XNRO( IPLACE), XNSR( IPLACE)
132 1000 FORMAT( 2X, 'XSR, XRO= ',/, 2X, 3G20.5)
133         200 RETURN
134         END
135 C
136 C
137 C
138 C
139         SUBROUTINE ABC( A, B, C, D, XALF, XBET, XXNU, XHR, IPLACE, IWRIT)
140         IMPLICIT REAL*8 (A-H, O-Z)
141         COMMON/HRTABC/ AC(6,9), BC(4,9), CC(8,9), DC(8,9)
142         *      , AS(6,9), BS(4,9), CS(8,9), DS(8,9)
143         *      , AF(6,9), BF(4,9), CF(8,9), DF(8,9)
144         OPEN( 4, FILE= 'ABC.DAT', STATUS= 'OLD')
145 C
146         READ( 4,*) ( ( AC( I, J), J= 1, 9), I= 1,6)
147         READ( 4,*) ( ( BC( I, J), J= 1, 9), I= 1,4)
148         READ( 4,*) ( ( CC( I, J), J= 1, 9), I= 1,8)
149         READ( 4,*) ( ( DC( I, J), J= 1, 9), I= 1,8)
150         READ( 4,*) ( ( AS( I, J), J= 1, 9), I= 1,6)
151         READ( 4,*) ( ( BS( I, J), J= 1, 9), I= 1,4)
152         READ( 4,*) ( ( CS( I, J), J= 1, 9), I= 1,8)
153         READ( 4,*) ( ( DS( I, J), J= 1, 9), I= 1,8)
154         READ( 4,*) ( ( AF( I, J), J= 1, 9), I= 1,6)
155         READ( 4,*) ( ( BF( I, J), J= 1, 9), I= 1,4)
156         READ( 4,*) ( ( CF( I, J), J= 1, 9), I= 1,8)
157         READ( 4,*) ( ( DF( I, J), J= 1, 9), I= 1,8)
158 C
159         CALL CALC( A, B, C, D, IPLACE, XALF, XBET, XXNU , XHR)
160         CLOSE( 4)
161         IF( IWRIT.EQ. 1) WRITE( 7, 1000) A, B, C, D
162         IF( IWRIT.EQ. 1) WRITE( 7, 1010) XALF, XBET

```

Appendix E: FORTRAN Program for Design of Shallow Tunnels constructed using Pressurized Shield Methods (continued)

```

163 1000 FORMAT( 2X, 'A, B, C, D= ',/, 2X, 4G20.5)
164 1010 FORMAT( 2X, 'ALFA, BETA= ',/, 2X, 4G20.5)
165 RETURN
166 END
167 C
168 C
169 C
170 SUBROUTINE CALC( XA, XB, XC, XD, IPLACE, XALF, XBET, XNU, XHR)
171 IMPLICIT REAL*8 (A-H, O-Z)
172 COMMON/HRTABC/ AC(6,9), BC(4,9), CC(8,9), DC(8,9)
173 * , AS(6,9), BS(4,9), CS(8,9), DS(8,9)
174 * , AF(6,9), BF(4,9), CF(8,9), DF(8,9)
175 DIMENSION A(6,9), B(4,9), C(8,9), D(8,9)
176 IF( IPLACE. EQ. 1) THEN
177 DO 50 J= 1, 9
178 DO 10 I= 1, 6
179 10 A(I,J)= AC(I,J)
180 DO 20 I= 1, 4
181 20 B(I,J)= BC(I,J)
182 DO 30 I= 1, 10
183 30 C(I,J)= CC(I,J)
184 DO 40 I= 1, 8
185 40 D(I,J)= DC(I,J)
186 50 CONTINUE
187 ELSEIF( IPLACE. EQ. 2) THEN
188 DO 100 J= 1, 9
189 DO 60 I= 1, 6
190 60 A(I,J)= AS(I,J)
191 DO 70 I= 1, 4
192 70 B(I,J)= BS(I,J)
193 DO 80 I= 1, 10
194 80 C(I,J)= CS(I,J)
195 DO 90 I= 1, 8
196 90 D(I,J)= DS(I,J)
197 100 CONTINUE
198 ELSE
199 DO 150 J= 1, 9
200 DO 110 I= 1, 6
201 110 A(I,J)= AF(I,J)
202 DO 120 I= 1, 4
203 120 B(I,J)= BF(I,J)
204 DO 130 I= 1, 10
205 130 C(I,J)= CF(I,J)
206 DO 140 I= 1, 8
207 140 D(I,J)= DF(I,J)
208 150 CONTINUE
209 ENDIF
210 C
211
212 A1= A(1,1)+ A(1,2)* XALF+ A(1,3)* XBET+ A(1,4)* XNU
213 * + A(1,5)* XALF* XBET+ A(1,6)* XALF* XNU
214 * + A(1,7)* XBET* XNU+ A(1,8)* XALF* XBET* XNU
215 IF( A(1,9). EQ.1) A1= A1/ XHR
216 A2= A(2,1)+ A(2,2)* XALF+ A(2,3)* XBET+ A(2,4)* XNU

```

Appendix E: FORTRAN Program for Design of Shallow Tunnels constructed using Pressurized Shield Methods (continued)

```

217 * + A(2,5)* XALF* XBET
218 * + A(2,6)* XALF* XNU+ A(2,7)* XBET* XNU
219 * + A(2,8)* XALF* XBET* XNU
220 A3= A(3,1)+ A(3,2)* XALF+ A(3,3)* XBET+ A(3,4)* XNU
221 * + A(3,5)* XALF* XBET
222 * + A(3,6)* XALF* XNU+ A(3,7)* XBET* XNU
223 * + A(3,8)* XALF* XBET* XNU
224 IF( A(3,9). EQ.1) A3= A3/ XHR
225 A4= A(4,1)+ A(4,2)* XALF+ A(4,3)* XBET
226 * + A(4,4)* XNU+ A(4,5)* XALF* XBET
227 * + A(4,6)* XALF* XNU+ A(4,7)* XBET* XNU
228 * + A(4,8)* XALF* XBET* XNU
229 A5= A(5,1)+ A(5,2)* XALF+ A(5,3)* XBET+ A(5,4)* XNU
230 * + A(5,5)* XALF* XBET
231 * + A(5,6)* XALF* XNU+ A(5,7)* XBET* XNU
232 * + A(5,8)* XALF* XBET* XNU
233 IF( A(5,9). EQ.1) A5= A5/ XHR
234 A6= A(6,1)+ A(6,2)* XALF+ A(6,3)* XBET+ A(6,4)* XNU
235 * + A(6,5)* XALF* XBET
236 * + A(6,6)* XALF* XNU+ A(6,7)* XBET* XNU
237 * + A(6,8)* XALF* XBET* XNU
238 B1= B(1,1)+ B(1,2)* XALF+ B(1,3)* XBET+ B(1,4)* XNU
239 * + B(1,5)* XALF* XBET
240 * + B(1,6)* XALF* XNU+ B(1,7)* XBET* XNU
241 * + B(1,8)* XALF* XBET* XNU
242 IF( B(1,9). EQ.1) B1= B1/ XHR
243 B2= B(2,1)+ B(2,2)* XALF+ B(2,3)* XBET+ B(2,4)* XNU
244 * + B(2,5)* XALF* XBET
245 * + B(2,6)* XALF* XNU+ B(2,7)* XBET* XNU
246 * + B(2,8)* XALF* XBET* XNU
247 B3= B(3,1)+ B(3,2)* XALF+ B(3,3)* XBET+ B(3,4)* XNU
248 * + B(3,5)* XALF* XBET
249 * + B(3,6)* XALF* XNU+ B(3,7)* XBET* XNU
250 * + B(3,8)* XALF* XBET* XNU
251 IF( B(3,9). EQ.1) B3= B3/ XHR
252 B4= B(4,1)+ B(4,2)* XALF+ B(4,3)* XBET+ B(4,4)* XNU
253 * + B(4,5)* XALF* XBET
254 * + B(4,6)* XALF* XNU+ B(4,7)* XBET* XNU
255 * + B(4,8)* XALF* XBET* XNU
256 C1= C(1,1)+ C(1,2)* XALF+ C(1,3)* XBET+ C(1,4)* XNU
257 * + C(1,5)* XALF* XBET
258 * + C(1,6)* XALF* XNU+ C(1,7)* XBET* XNU
259 * + C(1,8)* XALF* XBET* XNU
260 IF( C(1,9). EQ.1) C1= C1/ XHR
261 C2= C(2,1)+ C(2,2)* XALF+ C(2,3)* XBET+ C(2,4)* XNU
262 * + C(2,5)* XALF* XBET
263 * + C(2,6)* XALF* XNU+ C(2,7)* XBET* XNU
264 * + C(2,8)* XALF* XBET* XNU
265 C3= C(3,1)+ C(3,2)* XALF+ C(3,3)* XBET+ C(3,4)* XNU
266 * + C(3,5)* XALF* XBET
267 * + C(3,6)* XALF* XNU+ C(3,7)* XBET* XNU
268 * + C(3,8)* XALF* XBET* XNU
269 IF( C(3,9). EQ.1) C3= C3/ XHR
270 C4= C(4,1)+ C(4,2)* XALF+ C(4,3)* XBET+ C(4,4)* XNU

```

```

271 * + C(4,5)* XALF* XBET
272 * + C(4,6)* XALF* XNU+ C(4,7)* XBET* XNU
273 * + C(4,8)* XALF* XBET* XNU
274 C5= C(5,1)+ C(5,2)* XALF+ C(5,3)* XBET+ C(5,4)* XNU
275 * + C(5,5)* XALF* XBET
276 * + C(5,6)* XALF* XNU+ C(5,7)* XBET* XNU
277 * + C(5,8)* XALF* XBET* XNU
278 IF( C(5,9). EQ.1) C5= C5/ XHR
279 C6= C(6,1)+ C(6,2)* XALF+ C(6,3)* XBET+ C(6,4)* XNU
280 * + C(6,5)* XALF* XBET
281 * + C(6,6)* XALF* XNU+ C(6,7)* XBET* XNU
282 * + C(6,8)* XALF* XBET* XNU
283 C7= C(7,1)+ C(7,2)* XALF+ C(7,3)* XBET+ C(7,4)* XNU
284 * + C(7,5)* XALF* XBET
285 * + C(7,6)* XALF* XNU+ C(7,7)* XBET* XNU
286 * + C(7,8)* XALF* XBET* XNU
287 IF( C(7,9). EQ.1) C7= C7/ XHR
288 C8= C(8,1)+ C(8,2)* XALF+ C(8,3)* XBET
289 * + C(8,4)* XNU+ C(8,5)* XALF* XBET
290 * + C(8,6)* XALF* XNU+ C(8,7)* XBET* XNU
291 * + C(8,8)* XALF* XBET* XNU
292 D1= D(1,1)+ D(1,2)* XALF+ D(1,3)* XBET+ D(1,4)* XNU
293 * + D(1,5)* XALF* XBET
294 * + D(1,6)* XALF* XNU+ D(1,7)* XBET* XNU
295 * + D(1,8)* XALF* XBET* XNU
296 IF( D(1,9). EQ.1) D1= D1/ XHR
297 D2= D(2,1)+ D(2,2)* XALF+ D(2,3)* XBET+ D(2,4)* XNU
298 * + D(2,5)* XALF* XBET
299 * + D(2,6)* XALF* XNU+ D(2,7)* XBET* XNU
300 * + D(2,8)* XALF* XBET* XNU
301 D3= D(3,1)+ D(3,2)* XALF+ D(3,3)* XBET+ D(3,4)* XNU
302 * + D(3,5)* XALF* XBET
303 * + D(3,6)* XALF* XNU+ D(3,7)* XBET* XNU
304 * + D(3,8)* XALF* XBET* XNU
305 IF( D(3,9). EQ.1) D3= D3/ XHR
306 D4= D(4,1)+ D(4,2)* XALF+ D(4,3)* XBET+ D(4,4)* XNU
307 * + D(4,5)* XALF* XBET
308 * + D(4,6)* XALF* XNU+ D(4,7)* XBET* XNU
309 * + D(4,8)* XALF* XBET* XNU
310 D5= D(5,1)+ D(5,2)* XALF+ D(5,3)* XBET
311 * + D(5,4)* XNU+ D(5,5)* XALF* XBET
312 * + D(5,6)* XALF* XNU+ D(5,7)* XBET* XNU
313 * + D(5,8)* XALF* XBET* XNU
314 IF( D(5,9). EQ.1) D5= D5/ XHR
315 D6= D(6,1)+ D(6,2)* XALF+ D(6,3)* XBET+ D(6,4)* XNU
316 * + D(6,5)* XALF* XBET
317 * + D(6,6)* XALF* XNU+ D(6,7)* XBET* XNU
318 * + D(6,8)* XALF* XBET* XNU
319 D7= D(7,1)+ D(7,2)* XALF+ D(7,3)* XBET+ D(7,4)* XNU
320 * + D(7,5)* XALF* XBET
321 * + D(7,6)* XALF* XNU+ D(7,7)* XBET* XNU
322 * + D(7,8)* XALF* XBET* XNU
323 IF( D(7,9). EQ.1) D7= D7/ XHR
324 D8= D(8,1)+ D(8,2)* XALF+ D(8,3)* XBET+ D(8,4)* XNU

```

```

325      * + D(8,5)* XALF* XBET
326      * + D(8,6)* XALF* XNU+ D(8,7)* XBET* XNU
327      * + D(8,8)* XALF* XBET* XNU
328      C
329      C
330      C
331      XA= A1/A2+ A3/A4+ A5/A6
332      XB= B1/B2+ B3/B4
333      XC= C1/C2+ C3/C4+ C5/C6+ C7/C8
334      XD= D1/D2+ D3/D4+ D5/D6+ D7/D8
335      RETURN
336      END
337      C
338      C
339      C
340      SUBROUTINE NEWSTS( A, B, C, D, XH, XD, XKO, IPLACE, IWRT)
341      IMPLICIT REAL* 8 (A-H, O-Z)
342      COMMON/STS/ZETA, RO, S1( 3), S3( 3)
343      COMMON/NEW/XGAM2( 3), XKO2( 3), XGAMA2, XKAV
344      *      , XNSR( 3), XNRO( 3), XNGD
345      HO= XH+ XD/2
346      SUM= S1( IPLACE)+ S3( IPLACE)
347      DIF= DABS( S1( IPLACE)- S3( IPLACE))
348      XGAM12= (B* DIF- D* SUM)/( B* C- A*D)/ HO
349      XKO12= SUM/B/XGAM12/HO- A/B
350      DIF= -DIF
351      XGAM2( IPLACE)= (B* DIF- D* SUM)/( C- A*D)/ HO
352      XKO2( IPLACE)= SUM/B/XGAM2( IPLACE) - A/B
353      IF( DABS(XKO12- XKO). LT. DABS( XKO - XKO)
354      *      . OR. XKO2( IPLACE). LT. 0 . OR. XGAM2( IPLACE). LT. 0)
355      *      THEN
356          XKO2( IPLACE)= XKO12
357          XGAM2( IPLACE)= XGAM12
358      *      ENDIF
359      IF( IPLACE. EQ. 3) THEN
360          XGAMA2= ( XGAM2( 1)+ 2* XGAM2( 2)+ XGAM2( 3))/4
361          XKAV= ( XKO2( 1)+ 2* XKO2( 2)+ XKO2( 3))/4
362      *      ENDIF
363      IF( IWRT.EQ. 1) WRITE( 7, 1000) XGAM2( IPLACE), XKO2( IPLACE)
364      1000 FORMAT( 2X, 'CAMA NEW, KO= ',/, 2X, 3G20.5)
365      RETURN
366      END
367      C
368      C
369      C
370      FUNCTION ALFA( XES, XAS, XNU, XET, D, XNUS)
371      IMPLICIT REAL* 8 (A-H, O-Z)
372      R= D/2
373      ALFA= XES*XAS*(1+XNU)/XET/R/(1-XNUS*XNUS)
374      END
375      C
376      C
377      C
378      FUNCTION BETA( XES, XNU, XET, D, XNUS, XIS)

```

```

379      IMPLICIT REAL* 8 (A-H, O-Z)
380      R= D/2
381      BETA= XES*XIS*(1+XNU)/XET/R**3/(1-XNUS*XNUS)
382      END
383      C
384      C
385      C
386      SUBROUTINE HARTMAN( ALF, BET, XH, IPLACE
387      *                   , XD, XNU, SRO, SFIO, IWRIT)
388      IMPLICIT REAL* 8 (A-H, O-Z)
389      COMMON/NEW/XGAM2( 3), XKO2( 3), XGAMA2, XKAV, XNSR( 3), XNRO( 3)
390      *           , XN3D
391      C
392      XK= XKO2( IPLACE)
393      GAMA= XGAM2( IPLACE)
394      PI= 2* DASIN( 1.)
395      R= XD/2
396      Z= XH+ R
397      IF( IPLACE. EQ. 1) FI= PI
398      IF( IPLACE. EQ. 2) FI= PI/2
399      IF( IPLACE. EQ. 3) FI= 0
400      C
401      SRO= SR( XK, ALF, BET, GAMA, Z, FI, R, XNU)
402      SFIO= SFI( XK, ALF, BET, GAMA, Z, FI, R, XNU)
403      IF( IWRIT.EQ. 1) WRITE( 7, 1000) SRO, SFIO
404      RETURN
405      1000 FORMAT( 'SIGMA RO AND SIGMA FI= ', /, 5X, 2F10.5)
406      END
407      C
408      C
409      C
410      FUNCTION SR(XK,ALF, BET, GAMA, Z, FI, R, XNU)
411      IMPLICIT REAL* 8 (A-H, O-Z)
412      SR= ( 1+ XK)* ( ALF+ BET)* GAMA* Z/ 2/ ( 1+ ALF+ BET)+
413      *   ( 1+ XK)* ALF* GAMA* R* DCOS( FI)/ 4/ (1+ ALF)-
414      *   ( 1- XK)* ( 3- 4* XNU)*( ALF- 9* BET- 12* ALF* BET)*
415      *   GAMA* Z* DCOS( 2* FI)/2/(1+ ALF* (3- 2* XNU)+ 3* BET*
416      *   (5- 6* XNU+4* ALF*(3- 4* XNU)))-
417      *   (1- XK)* (3- 4* XNU)* (ALF- 32* BET- 72* ALF* BET)*
418      *   GAMA* R* DCOS( 3* FI)/4/(1+ ALF* (5- 4* XNU)+ 8* BET*
419      *   (7- 8* XNU+ 9* ALF* ( 3- 4* XNU)))
420      END
421      C
422      C
423      C
424      FUNCTION SFI(XK,ALF, BET, GAMA, Z, FI, R, XNU)
425      IMPLICIT REAL* 8 (A-H, O-Z)
426      SFI= ( 1+ XK)* ( 2+ ALF+ BET)* GAMA* Z/ 2/ ( 1+ ALF+ BET)+
427      *   ( 2+ ALF+ (XK- XNU- XK* XNU)*(4+3* ALF))*
428      *   GAMA* R* DCOS( FI)/ 4/ (1-XNU)/ (1+ ALF)-
429      *   ( 1- XK)* (4+ ALF* (3+ 4* XNU)+ 3* BET*( 11- 12*
430      *   XNU+ 4* ALF* (3- 4* XNU)))*
431      *   GAMA* Z* DCOS( 2* FI)/2/(1+ ALF* (3- 2* XNU)+ 3* BET*
432      *   (5- 6* XNU+4* ALF*(3- 4* XNU)))-

```

```

433      *      (1- XK)* (4+ ALF* (5+ 4* XNU)+ 8* BET*
434      *      ( 16- 16* XNU+ 9* ALF* ( 3-4 * XNU)))*)
435      *      GAMA* R* DCOS( 3* FI)/4/(1+ ALF* (5- 4* XNU)+ 8* BET*
436      *      (7- 8* XNU+ 9* ALF* ( 3- 4* XNU)))
437      END
438      C
439      C
440      C
441      FUNCTION RTSEC( Y, X1, X2, XACC)
442      IMPLICIT REAL*8 (A-H, O-Z)
443      PARAMETER ( MAXIT= 30)
444      COMMON /GL/ HD, XKO, IPLACE, S1INI( 3), S3INI( 3)
445      FL= GLAMDA( X1)-Y
446      F= GLAMDA( X2)-Y
447      IF( ABS( FL) .LT. ABS( F)) THEN
448          RTSEC= X1
449          XL= X2
450          SWAP= FL
451          FL= F
452          F= SWAP
453      ELSE
454          XL= X1
455          RTSEC= X2
456      ENDIF
457      DO 11 J= 1, MAXIT
458          DX= (XL-RTSEC)*F/( F- FL)
459          XL= RTSEC
460          FL= F
461          RTSEC= RTSEC+DX
462          F= GLAMDA( RTSEC)-Y
463          IF( ABS( DX) . LT. XACC. OR. F. EQ. 0) THEN
464              RETURN
465          ENDIF
466      11 CONTINUE
467      END
468      C
469      C
470      C
471      FUNCTION GLAMDA( XUJ)
472      IMPLICIT REAL*8 ( A-H, O-Z)
473      DIMENSION XXL( 3), XXL1( 3), XXL2( 3)
474      COMMON /GL/ HD, XKO, IPLACE, S1INI( 3), S3INI( 3)
475      COMMON /VAR/ P1( 12,4), P2( 40,2), P3( 40,2), P4( 47), XLL2I( 3),
476      *      ETI( 3), UR( 3), U( 3), ALF6( 3), ALF8( 3), AU6( 3),
477      *      AU8( 3), AU1( 3), ALF( 3), AU( 3), UU( 3), XL( 3),
478      *      XLL( 3), XL1( 3), XLL1( 3), XL2( 3), XLL2( 3),
479      *      SIGMA( 3), ET( 3), ALFX( 3), U*F( 3), PP( 82)
480      I= IPLACE
481          DO 80 J= 1,3
482              DO 70 K=1,3
483                  KK= K+9*J+3*I-7
484                  XXL(K)= F4(P2(KK,1), P2(KK,2), P3(KK,1),
485      *      P3(KK,2), P4(KK), XUJ)
486      70          CONTINUE

```

Appendix E: FORTRAN Program for Design of Shallow Tunnels constructed using Pressurized Shield Methods (continued)

```

487             XXL1(J)= F6(XXL(1),XXL(2),XXL(3),P4(36),P4(37),
488 *             P4(38),HD)
489 80          CONTINUE
490             XXL2(I)= F6( XXL1(1), XXL1(2), XXL1(3),
491 *             P4(33),P4(34),P4(35),XKO)
492             GLAMDA= XXL2( I)
493             END
494 C
495 C
496 C
497 SUBROUTINE MYSHLD( XG, XL, XN, XKO, XHO, IPLACE, IWRTT)
498 IMPLICIT REAL*8 (A-H,O-Z)
499 COMMON/SHLD/ A(2,3,3,6), A2(2,3), A3( 4,3)
500 COMMON/NEW/XGAM2( 3), XKO2( 3), XGAMA2, XKAV, XNSR( 3), XNRO( 3)
501 *           , XN3D
502 OPEN( 4, FILE= 'SHLD2.DAT', STATUS='OLD')
503 DO 40 I= 1, 2
504     DO 30 J= 1, 3
505         DO 20 K= 1, 3
506             READ (4, *)
507 *             ( A( I, J, K, II), II= 1, 6)
508 20          CONTINUE
509 30          CONTINUE
510 40          CONTINUE
511 DO 50 K= 1, 2
512     READ (4, *) ( A2( K, II), II= 1,3)
513 50          CONTINUE
514 DO 60 K= 1, 4
515     READ (4, *) ( A3( K, II), II= 1,3)
516 60          CONTINUE
517 CALL SHLD2 ( XSR, XRO, XG, XL, XN, XKO, XHO, IPLACE)
518 CALL SHLD3 ( XS3D, XG, XL, XN, XKO, XHO)
519 XNSR( IPLACE)= XSR
520 XNRO( IPLACE)= XRO
521 XN3D= - XS3D
522 CLOSE ( 4)
523 IF( IWRTT.EQ. 1) WRITE( 7, 1000) XSR, XRO, XS3D
524 1000 FORMAT( 2X, 'XSR, XRO, XS3D= ',/, 2X, 3G20.5)
525 END
526 C
527 C
528 C
529 SUBROUTINE SHLD2 (XSR,XRO,XG,XL,XN,XKO,XHO, IPLACE)
530 IMPLICIT REAL*8 (A-H,O-Z)
531 COMMON/SHLD/ A(2,3,3,6), A2(2,3), A3( 4,3)
532 AG= POLY2( XHO, A(1, IPLACE, 1, 1), A(1, IPLACE, 2, 1)
533 *         , A(1, IPLACE, 3, 1))
534 AL= POLY2( XHO, A(1, IPLACE, 1, 2), A(1, IPLACE, 2, 2)
535 *         , A(1, IPLACE, 3, 2))
536 AN2= POLY2( XHO, A(1, IPLACE, 1, 3), A(1, IPLACE, 2, 3)
537 *         , A(1, IPLACE, 3, 3))
538 AN1= POLY2( XHO, A(1, IPLACE, 1, 4), A(1, IPLACE, 2, 4)
539 *         , A(1, IPLACE, 3, 4))
540 AK= POLY2( XHO, A(1, IPLACE, 1, 5), A(1, IPLACE, 2, 5)

```

Appendix E: FORTRAN Program for Design of Shallow Tunnels constructed using
Pressurized Shield Methods (continued)


```

541      *           , A(1, IPLACE, 3, 5))
542      AC= POLY2( XHO, A(1, IPLACE, 1, 6), A(1, IPLACE, 2, 6)
543      *           , A(1, IPLACE, 3, 6))
544      AH= A2(1, IPLACE)
545      XSR= AG* XG+AL* XL+AN2* XN* XN+AN1* XN+AK/ XKO+AH/ XHO+AC
546      AG2= POLY2( XHO, A(2, IPLACE, 1, 1), A(2, IPLACE, 2, 1)
547      *           , A(2, IPLACE, 3, 1))
548      AG1= POLY2( XHO, A(2, IPLACE, 1, 2), A(2, IPLACE, 2, 2)
549      *           , A(2, IPLACE, 3, 2))
550      AN2= POLY2( XHO, A(2, IPLACE, 1, 3), A(2, IPLACE, 2, 3)
551      *           , A(2, IPLACE, 3, 3))
552      AN1= POLY2( XHO, A(2, IPLACE, 1, 4), A(2, IPLACE, 2, 4)
553      *           , A(2, IPLACE, 3, 4))
554      AK= POLY2( XHO, A(2, IPLACE, 1, 5), A(2, IPLACE, 2, 5)
555      *           , A(2, IPLACE, 3, 5))
556      AC= POLY2( XHO, A(2, IPLACE, 1, 6), A(2, IPLACE, 2, 6)
557      *           , A(2, IPLACE, 3, 6))
558      AH= A2(2, IPLACE)
559      XRO= AG2* XG* XG+AG1* XG+AN2* XN* XN+AN1* XN+AK/ XKO+AH+AC
560      RETURN
561      END
562      C
563      C
564      C
565      FUNCTION POLY2( X, A, B, C)
566      IMPLICIT REAL*8 (A-H,O-Z)
567      POLY2= A*X*X+B*X+C
568      RETURN
569      END
570      C
571      C
572      C
573      SUBROUTINE SHLD3 ( XS3D, XG, XL, XN, XKO, XHO)
574      IMPLICIT REAL*8 (A-H,O-Z)
575      COMMON/SHLD/ A(2,3,3,6), A2(2,3), A3( 4,3)
576      AG= POLY2( XHO, A3(2,1), A3( 3,1), A3(4,1))
577      AL= POLY2( XHO, A3(2,2), A3( 3,2), A3(4,2))
578      C= POLY2( XHO, A3(2,3), A3( 3,3), A3(4,3))
579      XS3D= ( A3(1,1)* XN+ A3( 1,2)/XKO+ A3( 1,3))/XHO/XHO+
580      * ( AG* XG+ AL* XL+ C)/XHO
581      RETURN
582      END
583      C
584      C
585      C
586      C
587      C
588      C
589      FUNCTION F1( A, B, C, D, X)
590      IMPLICIT REAL*8 ( A-H, O-Z)
591      F1= ( A+ B* X)/ ( C+ D* X)
592      RETURN
593      END
594      C

```

Appendix E: FORTRAN Program for Design of Shallow Tunnels constructed using Pressurized Shield Methods (continued)

```

595 C
596 C
597 FUNCTION F2( A, B, C, D, E, X)
598 IMPLICIT REAL*8 ( A-H, O-Z)
599 F2= A+ B* X+ C* X* X+ D* X** 3+ E* X** 4
600 RETURN
601 END
602 C
603 C
604 C
605 FUNCTION F3( A, B, C, D, E, X)
606 IMPLICIT REAL*8 ( A-H, O-Z)
607 F3= ( A+ B* X+ C* X* X)/ ( D+ E* X)
608 RETURN
609 END
610 C
611 C
612 C
613 FUNCTION F4( A, B, C, D, E, X)
614 IMPLICIT REAL*8 ( A-H, O-Z)
615 F4= 1- X/ ( A+ B* X+ 1/ ( C+ D* X+ E* X* X))
616 RETURN
617 END
618 C
619 C
620 C
621 FUNCTION F5( A, B, C, D, E, X)
622 IMPLICIT REAL*8 ( A-H, O-Z)
623 F5= 1/( A+ B* X+ 1/ ( C+ D* X+ E* X* X))-
624 * X/( A+ B* X+1/ ( C+ D* X+ E* X* X))** 2*
625 * ( B- ( D+ 2* E* X)/ ( C+ D* X+ E* X* X) ** 2)
626 RETURN
627 END
628 C
629 C
630 C
631 FUNCTION F6( A, B, C, AA, BB, CC, X)
632 IMPLICIT REAL*8 ( A-H, O-Z)
633 F6= ( X- BB)* ( X- CC)* A/ ( AA- BB)/
634 * ( AA- CC)+ ( X- AA)* ( X- CC)* B/
635 * ( BB- AA)/ ( BB- CC)+ ( X- AA)*
636 * ( X- BB)* C/ ( CC- AA)/ ( CC- BB)
637 RETURN
638 END
639 C
640 C
641 C
642 SUBROUTINE RDATA
643 IMPLICIT REAL*8 ( A-H, O-Z)
644 COMMON /VAR/ P1( 12,4), P2( 40,2),P3( 40,2), P4( 47), XLL2I( 3),
645 * ETI( 3), UR( 3), U( 3), ALF6( 3), ALF8( 3), AU6( 3),
646 * AU8( 3), AU1( 3), ALF( 3), AU( 3), UU( 3), XL( 3),
647 * XLL( 3), XL1( 3), XLL1( 3), XL2( 3), XLL2( 3),
648 * SIGMA( 3), ET( 3), ALFX( 3), URF( 3), PP( 82)

```

Appendix E: FORTRAN Program for Design of Shallow Tunnels constructed using
Pressurized Shield Methods (continued)

```

649      COMMON/S/ PP2(180)
650      COMMON/TT/ PP3(36)
651      OPEN( 4, FILE= 'NDATA', STATUS= 'OLD')
652      READ( 4,1025) ( ( P1( I,J), I=1,12), J= 1,4)
653      READ( 4,1025) ( ( P2( I,J), I=1,40), J= 1,2)
654      READ( 4,1025) ( ( P3( I,J), I=1,40), J= 1,2)
655      READ( 4,1025) ( P4( I), I= 1,47)
656      READ( 4,1025) ( PP( I), I= 1, 82)
657      READ( 4,1025) ( PP2( I), I= 1, 180)
658      READ( 4,1025) ( PP3( I), I= 1, 36)
659      CLOSE( 4)
660      RETURN
661      1025 FORMAT (5F15.10)
662      END
663      C
664      C
665      C
666      SUBROUTINE RIN( TITLE, H, D, GAM, XKO, C, PH, RF, XK
667      *           , XN, PA, XNU, XG, XL, ES, XNUS, AS, XIS
668      *           , RL, IWRT, NITE)
669      IMPLICIT REAL*8 ( A-H, O-Z)
670      CHARACTER* 40 TITLE
671      OPEN( 3, FILE= 'SHIELD.IN', STATUS= 'OLD')
672      READ( 3,1010) TITLE
673      READ( 3,*) H, D
674      READ( 3,*) GAM, XKO, C, PH, RF
675      READ( 3,*) XK, XN, PA, XNU
676      READ( 3,*) XG, XL
677      READ( 3,*) XS
678      READ( 3,*) ES, XNUS, AS, XIS
679      READ( 3,*) RL
680      READ( 3,*) NITE
681      READ( 3,*) IWRT
682      IF( IWRT. EQ. 1)
683      *   OPEN( 7, FILE= 'SHIELD3.OUT', STATUS= 'UNKNOWN')
684      CLOSE ( 3)
685      ES= ES* 1000000D0
686      XIS= XIS* 0.00001
687      PI= 2* DASIN(1.)
688      PH= PH* PI/180
689      RETURN
690      1010 FORMAT( 2X, 20A)
691      END
692      C
693      C
694      C
695      SUBROUTINE WOUT( TITLE, H, GAM, C, PH, RF, XK
696      *           , XN, PA, XNU, XG, XLINER, RL, ES, XNUS, AS, XIS)
697      IMPLICIT REAL*8 ( A-H, O-Z)
698      CHARACTER* 1 Q( 3)
699      CHARACTER* 13 RX( 3)
700      CHARACTER* 40 TITLE
701      DIMENSION A( 3), B( 3)
702      COMMON /VAR/ P1( 12,4), P2( 40,2), P3( 40,2)

```

```

703      *           , P4( 47), XLL2I( 3),
704      *           ETI ( 3), UR( 3), U( 3), ALF6( 3), ALF8( 3), AU6( 3),
705      *           AU8( 3), AU1( 3), ALF( 3), AU( 3), UU( 3), XL( 3),
706      *           XLL( 3), XL1( 3), XLL1( 3), XL2( 3), XLL2( 3),
707      *           SIGMA( 3), ET( 3), ALFX( 3), URF( 3), PP( 82)
708      COMMON/OUT/SIGMA3, PHIA, PHIE, XM
709      COMMON/GL/ HD, XKO, IPLACE, S1INI( 3), S3INI( 3)
710      COMMON/STS/ZETA, RO, S1( 3), S3( 3)
711      COMMON/NEW/XGAM2( 3), XKO2( 3), XGAMA2, XKAV, XNSR( 3), XNRO( 3)
712      *           , XN3D
713      PI= DASIN( 1)* 2
714      RX( 1)= '1/2 D ABOVE C'
715      RX( 2)= '   AT S   '
716      RX( 3)= '1/2 D BELOW F'
717      Q( 1)= 'C'
718      Q( 2)= 'S'
719      Q( 3)= 'F'
720      OPEN( 4, FILE= 'SHIELD.OUT', STATUS= 'UNKNOWN')
721      D= H/ HD
722      HO= H+ D/2
723      ES= ES* 0.000001
724      XIS= XIS* 100000
725      ETAV= ( ETI(1)+ 2* ETI( 2)+ ETI( 3))/4
726      DO 20 I= 1, 3
727          A(I)= SIGMA( I)* GAM* (H+ D*0.5*( I-1))
728          IF( I. EQ. 2) A( I)= A( I)* XKO
729          B( I)= D* A( I)/ ETI( I)
730          UR( I)= B( I)* U( I)
731      20    CONTINUE
732      XXN3D= XN3D*D*GAM*HO/ ETAV
733      C
734      WRITE( 4, 1000) TITLE, H, D, RL, GAM, XKO, C, PH*180/PI
735      *           , XK, XN, XNU, PA, RF
736      *           , XG*100, XLINER*100
737      *           , ES, XNUS, AS, XIS
738      WRITE( 4, 1010) PHIA*180/PI, PHIE*180/PI, XM
739      *           , ( Q( I), XNSR( I)*100, XNRO( I)*100, I= 1, 3)
740      *           , ( Q( I), XGAM2( I), XKO2( I), I= 1, 3)
741      *           , XGAMA2, XKAV
742      *           , ( Q(I), S1( I), S3(I), ETI(I)*.001
743      *           , I= 1, 3)
744      WRITE( 4,1020) ETAV* 0.001, XXN3D
745      *           , ( Q( I), ALF( I), AU( I), URF( I), I= 1, 3)
746      *           , ( Q( I), XL2( I), XLL2( I), I= 1, 3)
747      WRITE( 4, 1030) ( Q(I), UU( I), U(I), A( I), B( I)
748      *           , UR(I)*1000, I= 1, 3)
749      WRITE( 4, 1100)
750      CLOSE ( 4)
751      RETURN
752      C
753      1000 FORMAT( 30X, 'Design Method', /
754      *           , 26X, 'for Tunnels Constructed', /
755      *           , 25X, 'using Pressurized Shields', /, /, /
756      *           , T6, 'A. L. ...', /, /

```

Appendix E. FORTRAN Program for Design of Shallow Tunnels constructed using Pressurized Shield Methods (continued)

```

757 *      , T11, '1. Title:', 5X, A20, /, /
758 *      , T11, '2. Geometry:', /
759 *      , T16, 'H= ', T21, F7.3, T31, 'D= ', T36, F7.3
760 *      , T46, 'Rl= ', T51, F7.3, /, /
761 *      , T11, '3. Ground Properties', /
762 *      , T16, 'Gama=', T26, F7.3, T36, 'Ko= ', T46, F7.3, /
763 *      , T16, 'c= ', T26, F7.3, T36, 'Phi= ', T46, F7.3, /
764 *      , T11, 'Hyperbolic Parameters:', /
765 *      , T16, 'K= ', T26, F7.3, T36, 'n= ', T46, F7.3, /
766 *      , T16, 'mu= ', T26, F7.3, /
767 *      , T16, 'Pa= ', T26, F7.3, T36, 'Rf= ', T46, F7.3, /, /
768 *      , T11, '4. Construction Method:', /
769 *      , T16, 'G.R. (%) =', T26, F7.3, T36, 'L.R. (%) ='
770 *      , T46, F7.3, /, /
771 *      , T11, '5. Liner Properties:', /
772 *      , T16, 'E= ', T26, F7.3, T36, 'mu= ', T46, F7.3, /
773 *      , T16, 't= ', T26, F7.3, T36, 'I= ', T46, F7.3, /, /)
774 1010 FORMAT( T11, '6. Modified Shear Strength Parameters:', /
775 *      , T16, 'Phi (a)= ', T26, F7.3, T36, 'Phi (e)= '
776 *      , T46, F7.3, /
777 *      , T16, ' m-1 = ', T26, F7.3, /, /, /
778 *      , T6, 'B. Stress Changes due to Three '
779 *      , 'Dimensional Effect:', /, /
780 *      , T11, '1. Stress Changes:', /
781 *      , T16, 1X, T26, ' S.R. (%) ', T36, 'D.S.R. (%)', /
782 *      , 3( T16, 2X, 1A, 2X, T26, F10.4, T36, F10.4, /), /
783 *      , T11, '2. Modified Stress Field:', /
784 *      , T16, 1X, T26, 'Gama (mod)', T36, ' Ko (mod) ', /
785 *      , 3( T16, 2X, A, 2X, T26, F10.4, T36, F10.4, /)
786 *      , T26, ' _____', ' _____', /
787 *      , T16, ' Average', T26, F10.4, T36, F10.4, /, /
788 *      , T11, '3. Modified Stiffness:', /
789 *      , T16, 1X, T26, ' Sigma 1 ', T36, ' Sigma 3 '
790 *      , T46, ' Et/1000 ', /
791 *      , 3( T16, 2X, A, 2X, T26, F10.4, T36, F10.4
792 *      , T46, F10.4, /)
793 *      , T46, ' _____', /)
794 1020 FORMAT( T16, ' Average', T46, F10.4, /, /
795 *      , T11, '4. Surface Displacement:', /
796 *      , T16, 'S3D= ', T26, F7.3, /, /, /
797 *      , T6, 'C. Stress Changes in Plane Stain Condition:'
798 *      , /, /
799 *      , T11, '1. Reference Values:', /
800 *      , T16, 1X, T26, ' Alfa ref ', T36, 'Alfa/U ref'
801 *      , T46, ' Uref ', /
802 *      , 3( T16, 2X, A, 2X, T26, F10.4, T36, F10.4
803 *      , T46, F10.4, /), /
804 *      , T11, '2. Twice Normalized Ground Reaction Curve:', /
805 *      , T26, ' Lambda ', T36, 'Deriv. Lambda', /
806 *      , 3( T18, A1, T26, F10.4, T36, F10.4, /), /)
807 1030 FORMAT( T11, '3. Equivalent Deformations at the Tunnel:', /
808 *      , T16, 1X, T26, ' U/Uref ', T36, ' U '
809 *      , T46, ' Sigma ', T56, 'D(Sigma)/E'
810 *      , T66, ' ur ', /

```

```

811      *      , 3( T18, A1, T26, F10.4, T36, F10.4
812      *      , T46, F10.4, T56, F10.4, T66, F10.4, /))
813 1100 F. AMAT( /, 8X, '_____ ',
814      *      /, 8X, 'Remark: Units',
815      *      /, 8X, 'Dimensions:.....m',
816      *      /, 8X, 'Soil Density:.....kN/m^3',
817      *      /, 8X, 'c:.....kPa',
818      *      /, 8X, 'Phi:.....degree',
819      *      /, 8X, 'P( atmospheric):.....kPa (=101.325)',
820      *      /, 8X, 'Soil movements:.....mm',
821      *      /, 8X, 'Soil Modulus( Et):.....MPa',
822      *      /, 8X, 'Liner Modulus( Es):.....GPa',
823      *      /, 8X, 'Liner Thickness( As):.....m^2/m',
824      *      /, 8X, 'Liner Inertia( Is):.....1E-05 m4/m',
825      *      /, 8X, 'Stresses:.....kPa',
826      *      /, 8X, 'Forces:.....kN/m',
827      *      /, 8X, 'Moments:.....kN.m/m',/,/,/)
828      END
829      C
830      C
831      C
832      SUBROUTINE EHYPER( PHI, C, XK, XN, PA, RF, I, IWRIT, GAMA, H)
833      IMPLICIT REAL*8 ( A-H, O-Z)
834      COMMON /VAR/ P1( 12,4), P2( 40,2), P3( 40,2), P4( 47), XLL2I( 3),
835      *      ETI( 3), UR( 3), U( 3), ALF6( 3), ALF8( 3), AU6( 3),
836      *      AU8( 3), AU1( 3), ALF( 3), AU( 3), UU( 3), XL( 3),
837      *      XLL( 3), XLI( 3), XLL1( 3), XL2( 3), XLL2( 3),
838      *      SIGMA( 3), ET( 3), ALFX( 3), URF( 3), PP( 82)
839      COMMON /GL/ HD, XKO, IPLACE, SLINI( 3), S3INI( 3)
840      COMMON/STS/ZETA, RO, S1( 3), S3( 3)
841      D= H/ HD
842      HO= H+ D/2
843      SLINI( I)= GAMA*( HO+ (I-2) *D)
844      S3INI( I)= SLINI( I)* XKO
845      IF( SLINI( I). LT. S3INI( I)) THEN
846          SWAP= SLINI( I)
847          SLINI( I)= S3INI( I)
848          S3INI( I)= SWAP
849      ENDIF
850      ETI( I)= YOUNG( S1( I), S3( I), PHI, C, XK, XN, PA, RF)
851      IF( IWRIT.EQ. 1) WRITE( 7, 1000) ( ETI( I), I= 1, 3)
852 1000 FORMAT( 2X, 'ETI= ',/, 2X, 3G20.5)
853      RETURN
854      END
855      C
856      C
857      C
858      FUNCTION YOUNG( S1, S3, PHI, C, XK, XN, PA, RF)
859      IMPLICIT REAL*8 ( A-H, O-Z)
860      E= 1-(RF*(1-DSIN(PHI))* (S1-S3))/
861      *      (2*C*DCOS(PHI)+2*S3*DSIN(PHI))
862      YOUNG= E*E*XK*PA*(S3/PA)**XN
863      END
864      C

```

Appendix E: FORTRAN Program for Design of Shallow Tunnels constructed using
Pressurized Shield Methods (continued)

```

865 C
866 C
867 SUBROUTINE GUU( IND)
868 IMPLICIT REAL*8 ( A-H, O-Z)
869 COMMON /VAR/ P1( 12,4), P2( 40,2), P3( 40,2), P4( 47), XLL2I( 3),
870 *      ETI ( 3), UR( 3), U( 3), ALF6( 3), ALF8( 3), AU6( 3),
871 *      AU8( 3), AU1( 3), ALF( 3), AU( 3), UU( 3), XL( 3),
872 *      XLL( 3), XL1( 3), XLL1( 3), XL2( 3), XLL2( 3),
873 *      SIGMA( 3), ET( 3), ALFX( 3), URF( 3), PP( 82)
874 X1= 0
875 X2= 5
876 XACC= 0.001
877 DO 10 IPLACE= 1,3
878     UU( IPLACE)= RTSEC( XL2(IPLACE), X1, X2, XACC)
879     IF( IND.EQ. 1) U( IPLACE)= UU( IPLACE)* URF( IPLACE)
880 10 CONTINUE
881 RETURN
882 END
883 C
884 C
885 C
886 SUBROUTINE GREF( H, D, PHI, C, RF, IND)
887 IMPLICIT REAL*8 ( A-H, O-Z)
888 COMMON /VAR/ P1( 12,4), P2( 40,2), P3( 40,2), P4( 47), XLL2I( 3),
889 *      ETI ( 3), UR( 3), U( 3), ALF6( 3), ALF8( 3), AU6( 3),
890 *      AU8( 3), AU1( 3), ALF( 3), AU( 3), UU( 3), XL( 3),
891 *      XLL( 3), XL1( 3), XLL1( 3), XL2( 3), XLL2( 3),
892 *      SIGMA( 3), ET( 3), ALFX( 3), URF( 3), PP( 82)
893 COMMON/STS/ZETA, RO, S1( 3), S3( 3)
894 COMMON/OUT/SIGMA3, PHIA, PHIE, XM
895 COMMON/NEW/XGAM2( 3), XKO2( 3), XGAMA2, XKAV
896 *      , XNSR( 3), XNRO( 3), XN3D
897 SIGMA3= S3( 2)
898 XKO= XKAV
899 HD= H/D
900 IF( C.EQ.0) THEN
901     PHIA= PHI
902     PHIE= PHI
903     GOTO 6
904 ENDIF
905 PHIA= DASIN(( 1+ SIGMA3* DTAN( PHI)/ C)/
906 *      ( 1+ SIGMA3/ DCOS( PHI)/ C))
907 PHIE= DASIN(1/(1-RF+RF/DSIN(PHIA)))
908 6 CONTINUE
909 XM= 2*DSIN(PHIE)/(1-DSIN(PHIE))
910 CALL ALPHA( XM, HD, XKO, IND)
911 RETURN
912 END
913 C
914 C
915 C
916 SUBROUTINE ALPHA( XM, HD, XKO, IND)
917 IMPLICIT REAL*8 ( A-H, O-Z)
918 COMMON /VAR/ P1( 12,4), P2( 40,2), P3( 40,2), P4( 47), XLL2I( 3),

```

Appendix E: FORTRAN Program for Design of Shallow Tunnels constructed using Pressurized Shield Methods (continued)

```

919      *      ETI ( 3), UR( 3), U( 3), ALF6( 3), ALF8( 3), AU6( 3),
920      *      AU8( 3), AU1( 3), ALF( 3), AU( 3), UU( 3), XL( 3),
921      *      XLL( 3), XLL1( 3), XLL2( 3), XL2( 3), XLL2( 3),
922      *      SIGMA( 3), ET( 3), ALFX( 3), URF( 3), PP( 82)
923      ALF1= F1(P1(5,1),P1(5,2),P1(5,3),P1(5,4),XM)
924      AU6(1)= F3(P2(2,1),P2(2,2),P3(2,1),P3(2,2),P4(2),HD)
925      AU6(2)= 1.3
926      AU6(3)= 1.95
927      AU8(1)= F3(P2(3,1),P2(3,2),P3(3,1),P3(3,2),P4(3),HD)
928      AU8(2)= 1.12
929      AU8(3)= 2
930      AU1(1)= F3(P2(4,1),P2(4,2),P3(4,1),P3(4,2),P4(4),HD)
931      AU1(2)= 1.05
932      AU1(3)= F3(P2(5,1),P2(5,2),P3(5,1),P3(5,2),P4(5),HD)
933      DO 50 I= 1,3
934          J= I+6
935          L= I+9
936          ALF6( I)= F1(P1(J,1),P1(J,2),P1(J,3),P1(J,4),XM)
937      50      ALF8( I)= F1(P1(L,1),P1(L,2),P1(L,3),P1(L,4),XM)
938      DO 60 I= 1,3
939          ALF(I)= F6(ALF6(I),ALF8(I),ALF1,P4(33),P4(34),P4(35),XKO)
940          AU(I)= F6(AU6(I),AU8(I),AU1(I),P4(33),P4(34),P4(35),XKO)
941          URF(I)= ALF(I)/AU(I)
942          IF( IND.NE. 1) UU(I)= U(I)/URF(I)
943      60      CONTINUE
944      RETURN
945      END
946      C
947      C
948      C
949      SUBROUTINE GSIGMA( SRO, H, D, GAMA, XKO, IPLACE)
950      IMPLICIT REAL*8 ( A-H, O-Z)
951      COMMON /VAR/ P1( 12,4), P2( 40,2),P3( 40,2), P4( 47), XLL2I( 3),
952      *      ETI ( 3), UR( 3), U( 3), ALF6( 3), ALF8( 3), AU6( 3),
953      *      AU8( 3), AU1( 3), ALF( 3), AU( 3), UU( 3), XL( 3),
954      *      XLL( 3), XLL1( 3), XLL2( 3), XL2( 3), XLL2( 3),
955      *      SIGMA( 3), ET( 3), ALFX( 3), URF( 3), PP( 82)
956      SINI= GAMA* ( H+ 0.5* D* (IPLACE- 1))
957      IF( IPLACE.EQ.2) SINI= SINI*XKO
958      SIGMA( IPLACE)= SRO/SINI
959      RETURN
960      END
961      C
962      C
963      C
964      SUBROUTINE GLMDA
965      IMPLICIT REAL*8 ( A-H, O-Z)
966      COMMON /VAR/ P1( 12,4), P2( 40,2),P3( 40,2), P4( 47), XLL2I( 3),
967      *      ETI ( 3), UR( 3), U( 3), ALF6( 3), ALF8( 3), AU6( 3),
968      *      AU8( 3), AU1( 3), ALF( 3), AU( 3), UU( 3), XL( 3),
969      *      XLL( 3), XLL1( 3), XLL2( 3), XL2( 3), XLL2( 3),
970      *      SIGMA( 3), ET( 3), ALFX( 3), URF( 3), PP( 82)
971      DO 10 I= 1,3
972          SIGREF= 1- ALF( I)

```

Appendix E: FORTRAN Program for Design of Shallow Tunnels constructed using Pressurized Shield Methods (continued)


```

973      XL2( I)= (SIGMA( I)- SIGREF)/( 1- SIGREF)
974      10      CONTINUE
975      RETURN
976      END
977      C
978      C
979      C
980      C
981      C
982      SUBROUTINE CHECK2
983      IMPLICIT REAL*8 ( A-H, O-Z)
984      COMMON /VAR/ P1( 12,4), P2( 40,2), P3( 40,2)
985      *      , P4( 47), XLL2I( 3),
986      *      ETI ( 3), UR( 3), U( 3), ALF6( 3), ALF8( 3), AU6( 3),
987      *      AU8( 3), AU1( 3), ALF( 3), AU( 3), UU( 3), XL( 3),
988      *      XLL( 3), XL1( 3), XLL1( 3), XL2( 3), XLL2( 3),
989      *      SIGMA( 3), ET( 3), ALFX( 3), URF( 3), PP( 82)
990      COMMON/NEW/XGAM2( 3), XKO2( 3), XGAMA2
991      *      , XKAV, XNSR( 3), XNRO( 3), XN3D
992      DO 10 I= 1, 3
993      IF( XL2( I). GT. 1.1) XL2( I)= 1.1
994      IF( UU( I). LT. -0.5) UU( I)= -0.5
995      IF( XKO2( I). LT. 0.55) XKO2( I)= 0.55
996      IF( XKO2( I). GT. 1.10) XKO2( I)= 1.10
997      10      CONTINUE
998      XKAV= ( XKO2( 1)+ 2* XKO2( 2)+ XKO2( 3))/4
999      RETURN
1000     END
1001     C
1002     C
1003     SUBROUTINE DLAMDA
1004     IMPLICIT REAL*8 ( A-H, O-Z)
1005     COMMON /VAR/ P1( 12,4), P2( 40,2),P3( 40,2), P4( 47), XLL2I( 3),
1006     *      ETI ( 3), UR( 3), U( 3), ALF6( 3), ALF8( 3), AU6( 3),
1007     *      AU8( 3), AU1( 3), ALF( 3), AU( 3), UU( 3), XL( 3),
1008     *      XLL( 3), XL1( 3), XLL1( 3), XL2( 3), XLL2( 3),
1009     *      SIGMA( 3), ET( 3), ALFX( 3), URF( 3), PP( 82)
1010     COMMON /GL/ HD, XKO, IPLACE, S1INI( 3), S3INI( 3)
1011     DO 90 I= 1,3
1012     DO 80 J= 1,3
1013     DO 70 K=1,3
1014     KK= K+9*J+3*I-7
1015     70      XLL(K)= F5(P2(KK,1),P2(KK,2),P3(KK,1),
1016     *      P3(KK,2),P4(KK),UU(I))
1017     80      XLL1(J)= F6(XLL(1),XLL(2),XLL(3),P4(36),
1018     *      P4(37),P4(38),HD)
1019     XLL2(I)= F6(XLL1(1),XLL1(2),XLL1(3),P4(33),
1020     *      P4(34),P4(35),XKO)
1021     90      CONTINUE
1022     RETURN
1023     END
1024     C
1025     C
1026     C

```

Appendix E: FORTRAN Program for Design of Shallow Tunnels constructed using Pressurized Shield Methods (continued)

```

1027 C
1028 SUBROUTINE NEGROS( TITLE, H, D, GAM, XKO, C, PHI, RF
1029 *           , XK, XN, PA, XNU, ES, XNUS, AS
1030 *           , XIS, RL, NITE)
1031 IMPLICIT REAL*8 ( A-H, O-Z)
1032 CHARACTER* 1 Q( 3)
1033 CHARACTER* 13 RX( 3)
1034 CHARACTER* 40 TITLE
1035 DIMENSION XNOR( 38), XMOM( 38), XQ( 38)
1036 COMMON /VAR/ P1( 12,4), P2( 40,2),P3( 40,2), P4( 47), XLL2I( 3),
1037 *           ETI ( 3), UR( 3) , U( 3), ALF6( 3), ALF8( 3), AU6( 3),
1038 *           AU8( 3), AU1( 3), ALF( 3), AU( 3), UU( 3), XL( 3),
1039 *           XLL( 3), XL1( 3), XLL1( 3), XL2( 3), XLL2( 3),
1040 *           SIGMA( 3), ET( 3), ALFX( 3), URF( 3), PP( 82)
1041 COMMON/S/ PP2(180)
1042 COMMON/TT/ PP3(36)
1043 COMMON/NEW/XGAM2( 3), XKO2( 3), XGAMA2, XKAV
1044 *           , XNSR( 3), XNRO( 3), XN3D
1045 C
1046 Q( 1)= 'C'
1047 Q( 2)= 'S'
1048 Q( 3)= 'F'
1049 RX( 1)= '1/2 D ABOVE C'
1050 RX( 2)= ' AT S '
1051 RX( 3)= '1/2 D BELOW F'
1052 C
1053 PI= 3.1415927
1054 OPEN( 4, FILE= 'SHIELD.OUT', STATUS= 'UNKNOWN')
1055 CALL FEND( 4)
1056 ES= ES* 1000000
1057 XIS= XIS* 0.00001
1058 WRITE( 4,1000)
1059 WRITE( 4,1010) TITLE
1060 C
1061 C GROUND PROPERTIES
1062 C
1063 IIE= 0
1064 IET= 1
1065 PH= PHI* 180/PI
1066 Z= H+ D* 0.5
1067 SIGMA1= GAM* ( H+ D* 0.5)
1068 SIGMA3= SIGMA1* XKAV
1069 IF( C.EQ.0) THEN
1070 PHIA= PHI
1071 PHIE= PHI
1072 GOTO 6
1073 ENDIF
1074 PHIA= DASIN(( 1+ SIGMA3* DTAN( PHI)/ C)/
1075 *           ( 1+ SIGMA3/ DCOS( PHI)/ C))
1076 PHIE= DASIN(1/(1-RF+RF/DSIN(PHIA)))
1077 6 PHA= PHIA*180/PI
1078 PHE= PHIE*180/PI
1079 XM= 2*DSIN(PHIE)/(1-DSIN(PHIE))
1080 RO= ( D-AS)* 0.5

```

Appendix E: FORTRAN Program for Design of Shallow Tunnels constructed using
Pressurized Shield Methods (continued)

```

1081      HD= H/D
1082      CD= C/GAM/D
1083      WRITE (4,1030)
1084      WRITE (4,1040) H,D,HD
1085      WRITE (4,1050)
1086      WRITE (4,1060) GAM, XKAV
1087      WRITE (4,1070) SIGMA3, C, PH, RF
1088      WRITE (4,1080) PHA, PHE
1089      WRITE (4,1090) XM
1090      WRITE (4,1100) XK, XN, PA, XNU
1091      WRITE (4,1110)
1092      DO 10 I= 1,3
1093          S1= GAM*(H+(2*I-3)*D*0.5)
1094          S3= S1*XKAV
1095          IF(IET.EQ.1) GOTO 7
1096          E= 1-(RF*(1-DSIN(PHI))*(S1-S3))/
1097      *      (2*C*DCOS(PHI)+2*S3*DSIN(PHI))
1098          ETI(I)= E*E*XK*PA*(S3/PA)**XN
1099          WRITE (4,1120) RX(I),S3, S1, ETI(I)*.001
1100      10  CONTINUE
1101      WRITE (4,1270)
1102      65 CALL CHECK2
1103      CALL LAMDA( H, XKAV, ITE, SIGAV, GAM, GAMA, ETAV, Q)
1104      IF( ITE.NE.0) THEN
1105          IF( IT2.EQ.0) ET1=ETAV
1106          IF( IT2.EQ.1) ET2=ETAV
1107          GOTO 130
1108      ENDIF
1109      ET1= ETAV
1110      ET2= ETAV
1111  C
1112  C      7. GROUND LINING INTERACTION
1113  C
1114      WRITE (4,1350) Z, RO, RL, ETAV/1000, XNU, GAMA, XKAV,
1115      *      ES* 0.000001, XNUS, AS, XIS* 10000000
1116      ITE= 1
1117      111 DO 112 I=1,3
1118          CALL HRIMN ( I, Z, RO, ETAV, XNU, GAMA, XKAV, ES, XNUS,
1119      *      AS, XIS, VVR, ALFAX, BETAX, VR, S, RL)
1120          ALF6(I)= -VR
1121      112  ALF8(I)= S
1122          WRITE (4,1360) ITE
1123          DO 113 I=1,3
1124      113  AU6(I)= 0.0
1125          IT2=0
1126          WRITE (4,1370)
1127          WRITE (4,1375) ET1/1000,ALFAX,BETAX
1128      115 WRITE (4,1380)
1129          DO 120 I=1,3
1130              AN6(I)= UR(I)+ALF6(I)+AU6(I)
1131              SR6= GAM* (H+D*0.5*(I-1))*(1+(XKAV-1)*DSIN((I-1)*0.5*PI))
1132              U(I)= AU6(I)*ETI(I)/D/SRO
1133      120  UU(I)= U(I)/URF(I)
1134          GOTO 65

```

Appendix E: FORTRAN Program for Design of Shallow Tunnels constructed using Pressurized Shield Methods (continued)

```

1135 130 DO 135 I= 1,3
1136 135 WRITE (4,1390) Q(I),UR(I)*1000,ALF6(I)*1000,
1137 * AU6(I)*1000, U(I),UU(I),
1138 * XLL2(I),ET(I)/1000,ALF8(I)
1139 WRITE( 4,1385) ETAV*0.001D0
1140 AU6(1)= VVR
1141 AU6(2)= 0.
1142 AU6(3)= -VVR
1143 IF( IT2.EQ.1) GOTO 140
1144 IF( ITE.EQ.NITE) THEN
1145 DO 136 I= 1, 19
1146 ANGL= ( I-1)* 10.D0
1147 CALL HRT2 ( ANGL, Z, RO, ETAV, XNU, GAMA, XKAV, ES,
1148 * XNUS, AS, XIS, ALFAX, BETAX, XMOM( I),
1149 * XNOR( I), XQ( I))
1150 136 CONTINUE
1151 CALL SETL((1-SIGMA( 1)), XKO, PH, HD, SS1, SS2, SS3, SS4, SS5)
1152 SS6= (ALF6( 1)+ UR( 1))
1153 SS7= UU( 1)
1154 SS8= XL2(1)
1155 SS9= (1-SIGMA( 1))
1156 ENDIF
1157 WRITE (4,1420)
1158 WRITE (4,1375) ET2/1000,ALFAX,BETAX
1159 ETAV= ET2
1160 IT2= IT2+1
1161 GOTO 115
1162 140 WRITE( 4,1430) -VVR*1000.
1163 ITE= ITE+1
1164 IF (ITE.LE.NITE) GOTO 111
1165 DO 141 I= 20, 38
1166 ANGL= ( I-20)* 10.0D0
1167 CALL HRT2 ( ANGL, Z, RO, ETAV, XNU, GAMA, XKAV, ES,
1168 * XNUS, AS, XIS, ALFAX, BETAX, XMOM( I),
1169 * XNOR( I), XQ( I))
1170 141 CONTINUE
1171 WRITE( 4,1490)
1172 WRITE( 4,1370)
1173 WRITE( 4,1500)
1174 DO 142 I= 1, 19
1175 ANGL= ( I-1)* 10.0D0
1176 IF( ANGL.EQ.0) THEN
1177 WRITE( 4,1520) Q( 3), ANGL, XNOR( I),
1178 * XQ( I), XMOM( I)
1179 GOTO 142
1180 ENDIF
1181 IF( ANGL.EQ.90) THEN
1182 WRITE( 4,1520) Q( 2), ANGL, XNOR( I),
1183 * XQ( I), XMOM( I)
1184 GOTO 142
1185 ENDIF
1186 IF( ANGL.EQ.180) THEN
1187 WRITE( 4,1520) Q( 1), ANGL, XNOR( I),
1188 * XQ( I), XMOM( I)

```

Appendix E: FORTRAN Program for Design of Shallow Tunnels constructed using
Pressurized Shield Methods (continued)

```

1189             GOTO 142
1190             ENDIF
1191             WRITE( 4,1510) ANGL, XNOR( I), XQ( I), XMOM( I)
1192 142 CONTINUE
1193             WRITE( 4,1420)
1194             WRITE( 4,1500)
1195             DO 143 I= 20, 38
1196                 ANGL= ( I-20)* 10.0D0
1197                 IF( ANGL.EQ.0) THEN
1198                     WRITE( 4,1520) Q( 3), ANGL, XNOR( I),
1199 *                     XQ( I), XMOM( I)
1200                     GOTO 143
1201                     ENDIF
1202                 IF( ANGL.EQ.90) THEN
1203                     WRITE( 4,1520) Q( 2), ANGL, XNOR( I),
1204 *                     XQ( I), XMOM( I)
1205                     GOTO 143
1206                     ENDIF
1207                 IF( ANGL.EQ.180) THEN
1208                     WRITE( 4,1520) Q( 1), ANGL, XNOR( I),
1209 *                     XQ( I), XMOM( I)
1210                     GOTO 143
1211                     ENDIF
1212                 WRITE( 4,1510) ANGL, XNOR( I), XQ( I), XMOM( I)
1213 143 CONTINUE
1214             CALL SETL((1-SIGMA( 1)), XKO, PH, HD, SS10, SS11,
1215 *             SS12, SS13, SS14)
1216                 SS15= (ALF6( 1)+ UR( 1)+ AU6( 1))
1217                 SS16= UU( 1)
1218                 SS17= XL2(1)
1219                 SS18= (1-SIGMA( 1))
1220             WRITE( 4,1440)
1221             WRITE( 4,1370)
1222             CALL PROFL( SS1, SS2, SS3, SS4, SS5, SS6, SS7, SS8, SS9, H)
1223             WRITE( 4,1420)
1224             CALL PROFL( SS10, SS11, SS12, SS13, SS14, SS15,
1225 *             SS16, SS17, SS18, H)
1226             WRITE( 4,1450)
1227             WRITE( 4,1370)
1228             WRITE( 4,1460) SS9* 100, XKO, PH, CD
1229             CALL TRIH( PH, HD, CD, XKO, PPL)
1230             DO 150 I= 1, 11
1231                 Y= PPL* ( I-1)* 0.2D0
1232                 YY= DEXP( -1* Y*Y/2/PPL/PPL)*SS1*SS6
1233                 WRITE( 4, 1470) Y* D, YY* 1000
1234 150 CONTINUE
1235                 DIST= PPL* D/ 0.606/ SS1/ SS6
1236                 WRITE( 4, 1480) DIST
1237             WRITE( 4,1420)
1238             WRITE( 4,1460) SS18* 100, XKO, PH, CD
1239             DO 160 I= 1, 11
1240                 Y= PPL* ( I-1)* 0.2D0
1241                 YY= DEXP( -1* Y*Y/2/PPL/PPL)*SS10*SS15
1242                 WRITE( 4, 1470) Y* D, YY* 1000

```

Appendix E: FORTRAN Program for Design of Shallow Tunnels constructed using
Pressurized Shield Methods (continued)

```

1243     160 CONTINUE
1244         DIST= PPL* D/ 0.606/ SS10/ SS15
1245         WRITE( 4, 1480) DIST
1246         WRITE( 4, 1530)
1247     C
1248     C             FORMATS
1249     C
1250     1000 FORMAT (20X, 'EISENSTEIN- NEGRO METHOD FOR GROUND',/,
1251     *           18X, 'REACTION PREDICTION OF SHALLOW TUNNELLING',/)
1252     1010 FORMAT (20A)
1253     1015 FORMAT (10I5)
1254     1020 FORMAT (8F10.5)
1255     1025 FORMAT (5F15.10)
1256     1030 FORMAT (2X, '1. GEOMETRY')
1257     1040 FORMAT (5X, 'H= ', 4X, F10.4, 5X, 'D= ', 4X, F10.4, 5X, 'H/D= ', 2X, F10.4,/)
1258     1050 FORMAT (2X, '2. GROUND PROPERTIES')
1259     1060 FORMAT (5X, 'GAMA= ', 1X, F10.4, 5X, 'KO= ', 3X, F10.4)
1260     1070 FORMAT (5X, 'SIGMA3= ', F7.3, 5X, 'C= ', 4X, F10.4, 5X, 'PHI= '
1261     *           , 2X, F10.4, 5X, 'RF= ', 3X, F10.4)
1262     1080 FORMAT (5X, 'PHI A= ', F10.4, 5X, 'PHI E= ', F10.4)
1263     1090 FORMAT (5X, 'M-1= ', 2X, F10.4)
1264     1100 FORMAT (5X, 'F = ', 4X, F7.3, 5X, 'N= ', 4X, F10.4,
1265     *           5X, 'A= ', 3X, F7.3, 5X, 'NU= ', 3X, F10.4,/)
1266     1110 FORMAT (8X, 'LOCATION', 12X, 'SIGMA3', 4X, 'SIGMA1', 4X, ' ETI ')
1267     1120 FORMAT (8X, A13, 7X, F7.3, 3X, F7.3, 3X, F10.4)
1268     1130 FORMAT (I5)
1269     1150 FORMAT (2X, '3. TUNNEL CLOSURE AT LINING ACTIVATION')
1270     1160 FORMAT (5X, 'X= ', 4X, F10.4, 5X, 'X/D= ', 2X, F10.4, 5X
1271     *           , 'KO= ', 3X, F10.4, 5X)
1272     1170 FORMAT (8X, 'LOCATION', 4X, 'U', 7X, 'SRO', 7X, 'D SRO/ETI ', 2X, 'UR')
1273     1180 FORMAT (11X, A1, 6X, F10.4, 3X, F7.3, 3X, F10.4, 3X, F10.4)
1274     1210 FORMAT (2X, '4. REFERENCE VALUES')
1275     1220 FORMAT (5X, 'H/D', 2X, F10.4, 5X, 'KO= ', 3X, F10.4, 5X, 'M-1= ', 2X, F10.4)
1276     1230 FORMAT (23X, 'ALFA REF', 7X, '(ALFA/U)REF', 4X, 'U REF')
1277     1240 FORMAT (15X, A1, 7X, F10.4, 8X, F10.4, 8X, F10.4)
1278     1270 FORMAT (2X, '5. STRESS RELEASE AND STIFFNESS CHANGE',/, 7X,
1279     *           'AT LINING ACTIVATION',/, 18X, 'U', 9X, 'U/U(REF)',
1280     *           2X, 'LAMEDA', 4X, 'LAMBDA')
1281     1350 FORMAT (2X, '7. LINING GROUND INTERACTION'
1282     *           ,/, 5X, 'ZO= ', 3X, F10.4, 5X,
1283     *           'RO= ', 3X, F10.4, 5X, 'RL= ', 3X
1284     *           , F10.4,/, 5X, 'ET AV.= ', F10.4, 5X,
1285     *           'NU= ', 3X, F10.4, 5X, 'GAMA RED.= '
1286     *           , F10.4,/, 5X, 'KO= ', 3X, F10.4,/,
1287     *           5X, 'ES= ', 3X, F10.4, 5X, 'NU, S= ', 1X
1288     *           , F10.4, 5X, 'AS= ', 3X, F10.4,/,
1289     *           5X, 'IS= ', 3X, F10.4)
1290     1360 FORMAT (/, 8X, 'ITERATION N. ', I3)
1291     1370 FORMAT (/, 8X, 'WITHOUT HEAVE')
1292     1375 FORMAT( 8X, 'ET AV.= ', F10.4, 5X, 'ALFA= ',
1293     *           1X, F10.4, 5X, 'BETA= ', 1X, F10.4,/)
1294     1380 FORMAT (13X, 'UR', 4X, 'D(UR)', 4X, 'URF', 6X, 'U', 4X, 'U/U REF', 2X,
1295     *           'LAMBDA', 3X, 'ET', 4X, 'SIGMA R')
1296     1385 FORMAT( 8X, 'NEW ET AV.= ', F8.4)

```

Appendix E: FORTRAN Program for Design of Shallow Tunnels constructed using
Pressurized Shield Methods (continued)

```

1297 1390 FORMAT (5X,A1,4X,3(F8.3),3(F8.4),2(F8.3))
1298 1420 FORMAT (/, 8X, 'WITH HEAVE')
1299 1430 FORMAT ( 8X, 'UPWARD HEAVE= ', F8.3)
1300 1440 FORMAT ( /, 8X, '8. SUBSURFACE SETTLEMENTS')
1301 1450 FORMAT ( /, 8X, '9. SURFACE SETTLEMENTS')
1302 1460 FORMAT( 8X, '% STRESS RELEASE=', F10.5, /, 8X, 'Ko=',
1303 * F7.2, 5X, 'PHI=', F7.2, 5X, 'C/ Gamma/D=', F7.2, /,
1304 * 8X, 1X, 'DISTANCE', 1X, 'SETILEMENT')
1305 1470 FORMAT( 8X, 2F10.5)
1306 1480 FORMAT( 8X, 'MAX. DISTORTION= 1/', F8.2)
1307 1490 FORMAT( /, 8X, 'STRAINING ACTIONS', F8.2)
1308 1500 FORMAT( 8X, 2X, 'ANGLE', 3X, 3X, 'NORMAL F.', 3X, 2X,
1309 * 'SHEAR FORCE', 2X, 5X, 'MOMENT')
1310 1510 FORMAT( 8X, F10.2, 3E15.8)
1311 1520 FORMAT( 8X, A1, F9.2, 3E15.8)
1312 1530 FORMAT( /, 8X, '_____'),
1313 * /, 8X, 'Remark: Units',
1314 * /, 8X, 'Dimensions:.....m',
1315 * /, 8X, 'Soil Density:.....kN/m^3',
1316 * /, 8X, 'c:.....kPa',
1317 * /, 8X, 'Phi:.....degree',
1318 * /, 8X, 'P( atmospheric):.....kPa (=101.325)',
1319 * /, 8X, 'Soil movements:.....mm',
1320 * /, 8X, 'Soil Modulus( Et):.....MPa',
1321 * /, 8X, 'Liner Modulus( Es):.....GPa',
1322 * /, 8X, 'Liner Thickness( As):....m^2/m',
1323 * /, 8X, 'Liner Inertia( Is):.....1E-05 m4/m',
1324 * /, 8X, 'Stresses:.....kPa',
1325 * /, 8X, 'Forces:.....kN/m',
1326 * /, 8X, 'Moments:.....kN.m/m')
1327 STOP
1328 END
1329 C
1330 C
1331 C
1332 C HARMANN'S SOLUTION
1333 SUBROUTINE HRIMN ( I, ZO, RO, ET, XNU, GAMA, XKO, ES, XNUS, AS,
1334 * XIS, VRR1, ALFAX, BETAX, VR, S, RL)
1335 IMPLICIT REAL*8 ( A-H, O-Z)
1336 PI= 3.14159265
1337 IF( RL.EQ.0.D0) RL= ZO
1338 X1= 1+XKO
1339 X2= 1-XKO
1340 X3= 3-4*XNU
1341 X4= 5-4*XNU
1342 VRR1= (1+XNU)*X3*GAMA*RO*RO*DLOG(RO/RL)/ET/(1-XNU)/4
1343 ALFAX= ES*AS*(1+XNU)/ET/RO/(1-XNUS*XNUS)
1344 BETAX= ES*XIS*(1+XNU)/ET/RO**3/(1-XNUS*XNUS)
1345 IF (I.EQ.1) PHI= PI
1346 IF (I.EQ.2) PHI= PI*0.5
1347 IF (I.EQ.3) PHI= 0.0
1348 CALL VRR ( X1, X2, X3, X4, GAMA, ZO, RO, ALFAX,
1349 * BETAX, PHI, XNU, ET, VR)
1350 CALL SIGMA ( X1, X2, X3, X4, ALFAX,

```

Appendix E: FORTRAN Program for Design of Shallow Tunnels constructed using
Pressurized Shield Methods (continued)

```

1351      *          GAMA, BETAX, PHI, ZO, RO, XNU, S)
1352      RETURN
1353      STOP
1354      END
1355      C
1356      C
1357      C
1358      C
1359      C
1360      C
1361      SUBROUTINE VRR ( X1, X2, X3, X4, GAMA, ZO, RO, ALFAX,
1362      *          BETAX, PHI, XNU, ET, VR)
1363      IMPLICIT REAL*8 ( A-H, O-Z)
1364      VR1= X1*GAMA*ZO*RO/2/(1+ALFAX+BETAX)
1365      VR2= X1*GAMA*RO*RO*DCOS(PHI)/8/(1+ALFAX)
1366      VR31= X2*X3*(1+2*ALFAX)*GAMA*ZO*RO*DCOS(2*PHI)
1367      VR32= 2*(1+(3-2*XNU)*ALFAX+3*BETAX*(5-6*XNU+4*X3*ALFAX))
1368      VR3= VR31/VR32
1369      VR41= X2*X3*(1+3*ALFAX)*GAMA*RO*RO*DCOS(3*PHI)
1370      VR42= 8*(1+X4*ALFAX+8*BETAX*(7-8*XNU-9*X3*ALFAX))
1371      VR4= VR41/VR42
1372      VR5= -1*(1+XNU)/ET
1373      VR= VR5*(VR1+VR2+VR3+VR4)
1374      RETURN
1375      END
1376      C
1377      C
1378      C
1379      C
1380      C
1381      C
1382      SUBROUTINE SIGMA( X1, X2, X3, X4, ALFAX, GAMA,
1383      *          BETAX, PHI, ZO, RO, XNU, S)
1384      IMPLICIT REAL*8 ( A-H, O-Z)
1385      S1= X1*(ALFAX+BETAX)*GAMA*ZO/2/(1+ALFAX+BETAX)
1386      S2= X1*ALFAX*GAMA*RO*DCOS(PHI)/4/(1+ALFAX)
1387      S31= X2*X3*(ALFAX-9*BETAX-12*ALFAX*BETAX)*GAMA*ZO*DCOS(2*PHI)
1388      S32= 2*(1+ALFAX*(3-2*XNU)+3*BETAX*(5-6*XNU+4*ALFAX*X3))
1389      S3= (-1)*S31/S32
1390      S41=X2*X3*(ALFAX-32*BETAX-72*ALFAX*BETAX)*GAMA*RO*DCOS(3*PHI)
1391      S42= 4*(1+ALFAX*X4+8*BETAX*(7-8*XNU+9*ALFAX*X3))
1392      S4= (-1)*S41/S42
1393      S=S1+S2+S3+S4
1394      RETURN
1395      END
1396      C
1397      C
1398      C
1399      C
1400      C
1401      FUNCTION F7( A, B, C, D, AA, BB, CC, DD, X)
1402      IMPLICIT REAL*8 ( A-H, O-Z)
1403      F7= (X-BB)*(X-CC)*(X-DD)*A/(AA-BB)/(AA-CC)/(AA-DD)+
1404      *      (X-AA)*(X-CC)*(X-DD)*B/(BB-AA)/(BB-CC)/(BB-DD)+

```

Appendix E: FORTRAN Program for Design of Shallow Tunnels constructed using
Pressurized Shield Methods (continued)


```

1405      *      (X-AA) * (X-BB) * (X-DD) * C / (CC-AA) / (CC-BB) / (CC-DD) +
1406      *      (X-AA) * (X-BB) * (X-CC) * D / (DD-AA) / (DD-BB) / (DD-CC)
1407      RETURN
1408      END
1409      C
1410      C
1411      C
1412      FUNCTION FP1( A, B, C, X)
1413      IMPLICIT REAL*8 ( A-H, O-Z)
1414      FP1= C+ 1/ ( A* X+ B)
1415      RETURN
1416      END
1417      C
1418      C
1419      C
1420      FUNCTION FP2( A, B, C, X)
1421      IMPLICIT REAL*8 ( A-H, O-Z)
1422      FP2= A* X** 3+ B* X* X+ C* X
1423      RETURN
1424      END
1425      C
1426      C
1427      C
1428      FUNCTION FP3( A, B, AA, BB, X)
1429      IMPLICIT REAL*8 ( A-H, O-Z)
1430      FP3= ( X-AA) * ( B-A) / ( BB-AA) + A
1431      RETURN
1432      END
1433      C
1434      C
1435      C
1436      FUNCTION FUNC( A, B, C, X)
1437      IMPLICIT REAL*8 ( A-H, O-Z)
1438      FUNC= A* DLOG( B+ C*X)
1439      RETURN
1440      END
1441      C
1442      C
1443      C
1444      SUBROUTINE LAMDA( HD, XKO, ITE, SIGAV, GAM, GAMA, ETAV, Q)
1445      IMPLICIT REAL*8 ( A-H, O-Z)
1446      CHARACTER* 1 Q( 3)
1447      COMMON /VAR/ P1( 12,4), P2( 40,2), P3( 40,2), P4( 47), XLL2I( 3),
1448      *      ETI( 3), UR( 3), U( 3), ALF6( 3), ALF8( 3), AU6( 3),
1449      *      AU8( 3), AU1( 3), ALF( 3), AU( 3), UU( 3), XL( 3),
1450      *      XLL( 3), XL1( 3), XLL1( 3), XL2( 3), XLL2( 3),
1451      *      SIGMA( 3), ET( 3), ALFX( 3), URF( 3), PP( 82)
1452      SIGAV= 0.0
1453      ETAV= 0.0
1454      DO 90 I= 1,3
1455          DO 80 J= 1,3
1456              DO 70 K=1,3
1457                  KK= K+9*J+3*I-7
1458                  XL(K)= F4(P2(KK,1), P2(KK,2), P3(KK,1),

```

Appendix E: FORTRAN Program for Design of Shallow Tunnels constructed using
Pressurized Shield Methods (continued)

```

1459      *                P3(KK,2),P4(KK),UU(I)
1460      70                XLL(K)= F5(P2(KK,1),P2(KK,2),P3(KK,1),
1461      *                P3(KK,2),P4(KK),UU(I))
1462                XL1(J)= F6(XL(1),XL(2),XL(3),P4(36),P4(37),
1463      *                P4(38),HD)
1464      80                XLL1(J)= F6(XLL(1),XLL(2),XLL(3),P4(36),
1465      *                P4(37),P4(38),HD)
1466                XL2(I)= F6(XL1(1),XL1(2),XL1(3),P4(33),P4(34),P4(35),XKO)
1467                XLL2(I)= F6(XLL1(1),XLL1(2),XLL1(3),P4(33),
1468      *                P4(34),P4(35),XKO)
1469                SIGMA(I)= 1-(1-XL2(I))*ALF(I)
1470                IF (ITE.EQ.0) WRITE (4,1180) Q(I),U(I),UU(I),XL2(I),XLL2(I)
1471      90                SIGAV= SIGAV+ SIGMA(I)/4
1472                SIGAV= SIGAV+ SIGMA(2)/4
1473                GAMA= GAM*SIGAV
1474                IF (ITE.NE.0) GOTO 105
1475                WRITE (4,1280)
1476                DO 100 I= 1,3
1477                    ALFX(I)= 1-XL2(I)
1478      100                WRITE (4,1180) Q(I),ALFX(I),SIGMA(I)
1479                WRITE (4,1290) SIGAV,1-SIGAV,GAMA
1480                DO 106 I= 1,3
1481                    J= 56+ ( I-1)* 9
1482                    XL6= F6( PP(J), PP(J+1), PP(J+2), 6.D0, 3.D0, 1.5D0, HD)
1483                    XL8= F6( PP(J+3), PP(J+4), PP(J+5), 6.D0, 3.D0, 1.5D0, HD)
1484                    XL10= F6( PP(J+6), PP(J+7), PP(J+8), 6.D0, 3.D0, 1.5D0, HD)
1485      106                XLL2I(I)= F6( XL6, XL8, XL10, 0.6D0, 0.8D0, 1.0D0, XKO)
1486      105 DO 110 I= 1,3
1487                    ET(I)= XLL2(I)*ETI(I)/XLL2I(I)
1488                    IF (ITE.NE.0) GOTO 110
1489                    WRITE (4,1240) Q(I),XLL2I(I),ETI(I)*0.001D0/XLL2I(I),
1490      *                    ET(I)*0.001D0
1491      110                ETAV= ETAV+ ET(I)/4
1492                ETAV= ETAV+ ET(2)/4
1493                IF (ITE.NE.0) RETURN
1494                WRITE (4,1300) ETAV*0.001D0
1495      1180 FORMAT (11X,A1,6X,F10.4,3X,F7.3,3X,F10.4,3X,F10.4)
1496      1240 FORMAT (15X,A1,7X,F10.4,8X,F10.4,8X,F10.4)
1497      1280 FORMAT (5X,'STRESSES: SIGMA= 1-(1-LAMBDA)*ALFA REF.',/,
1498      *            18X,'1-LAMBDA',2X,'SIGMA')
1499      1290 FORMAT (5X,'SIGMA AV.= (SIGMA(C)+2 SIGMA(S)+SIGMA(F))/4=',F10.4,/,
1500      *            5X,'ALFA AV. = 1- SIGMA AV.',F10.4,/,5X,'GAMA REDUCED=',
1501      *            'GAMA* SIGMA AV. =',F10.4,/,5X,'STIFFNESS: ET= (LAMBDA`',
1502      *            'LAMBDA` (I) *ETI',/,18X,'LAMBDA` (I)',5X,'ETI/LAMBDA` (I)',
1503      *            9X,'ET')
1504      1300 FORMAT (5X,'ET(AV.)= (ET(C)+2 ET(S)+ET(F))/4= ',F10.4)
1505                RETURN
1506                END
1507      C
1508      C
1509      C
1510      C
1511      C
1512                SUBROUTINE SETL( STR, XKO, PH, HD, S1, S2, S3, S4,S5)

```

Appendix E: FORTRAN Program for Design of Shallow Tunnels constructed using Pressurized Shield Methods (continued)

```

1513      IMPLICIT REAL*8 ( A-H, O-Z)
1514      COMMON/S/ PP2(180)
1515      DIMENSION S(5), X(5)
1516      PI= 3.1415927D0
1517      T2O= DTAN( 20* PI/ 180)
1518      T3O= DTAN( 30* PI/ 180)
1519      T4O= DTAN( 40* PI/ 180)
1520      TPH= DTAN( PH* PI/ 180)
1521      DO 10 I= 1, 5
1522          X(I)= (I-1)* 0.2
1523          IF( PH.EQ.0D0) THEN
1524              P111= FUNC(PP2( 1), PP2( 2), PP2( 3), X(I))
1525              P112= FUNC(PP2( 4), PP2( 5), PP2( 6), X(I))
1526              P113= FUNC(PP2( 7), PP2( 8), PP2( 9), X(I))
1527              P1211= FUNC(PP2(10), PP2(11), PP2(12), X(I))
1528              P1212= FUNC(PP2(13), PP2(14), PP2(15), X(I))
1529              P122= FUNC(PP2(16), PP2(17), PP2(18), X(I))
1530              P1231= FUNC(PP2(19), PP2(20), PP2(21), X(I))
1531              P1232= FUNC(PP2(22), PP2(23), PP2(24), X(I))
1532              P1311= FUNC(PP2(25), PP2(26), PP2(27), X(I))
1533              P1312= FUNC(PP2(28), PP2(29), PP2(30), X(I))
1534              P132= FUNC(PP2(31), PP2(32), PP2(33), X(I))
1535              P1331= FUNC(PP2(34), PP2(35), PP2(36), X(I))
1536              P1332= FUNC(PP2(37), PP2(38), PP2(39), X(I))
1537              P121= FP3(P1211, P1212, .1D0, .6D0, STR)
1538              P123= FP3(P1231, P1232, .7D0, .1D0, STR)
1539              P131= FP3(P1311, P1312, .1D0, .6D0, STR)
1540              P133= FP3(P1331, P1332, .3D0, .1D0, STR)
1541              P11= F6( P111, P112, P113, 1.5D0, 3.D0, 6.D0, HD)
1542              P12= F6( P121, P122, P123, 1.5D0, 3.D0, 6.D0, HD)
1543              P13= F6( P131, P132, P133, 1.5D0, 3.D0, 6.D0, HD)
1544              P1= F6( P11, P12, P13, 2.5D0, 1.25D0, 0.625D0, CD)
1545              S(I)= P1
1546      C
1547          ELSE
1548              P1111= FUNC(PP2( 40), PP2( 41), PP2( 42), X(I))
1549              P1112= FUNC(PP2( 43), PP2( 44), PP2( 45), X(I))
1550              P1121= FUNC(PP2( 46), PP2( 47), PP2( 48), X(I))
1551              P1122= FUNC(PP2( 49), PP2( 50), PP2( 51), X(I))
1552              P1131= FUNC(PP2( 52), PP2( 53), PP2( 54), X(I))
1553              P1132= FUNC(PP2( 55), PP2( 56), PP2( 57), X(I))
1554              P1211= FUNC(PP2( 58), PP2( 59), PP2( 60), X(I))
1555              P1212= FUNC(PP2( 61), PP2( 62), PP2( 63), X(I))
1556              P1221= FUNC(PP2( 64), PP2( 65), PP2( 66), X(I))
1557              P1222= FUNC(PP2( 67), PP2( 68), PP2( 69), X(I))
1558              P123 = FUNC(PP2( 70), PP2( 71), PP2( 72), X(I))
1559              P131 = FUNC(PP2( 73), PP2( 74), PP2( 75), X(I))
1560              P1321= FUNC(PP2( 76), PP2( 77), PP2( 78), X(I))
1561              P1322= FUNC(PP2( 79), PP2( 80), PP2( 81), X(I))
1562              P1331= FUNC(PP2( 82), PP2( 83), PP2( 84), X(I))
1563              P1332= FUNC(PP2( 85), PP2( 86), PP2( 87), X(I))
1564              P2111= FUNC(PP2( 88), PP2( 89), PP2( 90), X(I))
1565              P2112= FUNC(PP2( 91), PP2( 92), PP2( 93), X(I))
1566              P2121= FUNC(PP2( 94), PP2( 95), PP2( 96), X(I))

```

Appendix E: FORTRAN Program for Design of Shallow Tunnels constructed using
Pressurized Shield Methods (continued)

```

1567 P2122= FUNC(PP2( 97), PP2( 98), PP2( 99), X(I))
1568 P2131= FUNC(PP2(100), PP2(101), PP2(102), X(I))
1569 P2132= FUNC(PP2(103), PP2(104), PP2(105), X(I))
1570 P2211= FUNC(PP2(106), PP2(107), PP2(108), X(I))
1571 P2212= FUNC(PP2(109), PP2(110), PP2(111), X(I))
1572 P2221= FUNC(PP2(112), PP2(113), PP2(114), X(I))
1573 P2222= FUNC(PP2(115), PP2(116), PP2(117), X(I))
1574 P223 = FUNC(PP2(118), PP2(119), PP2(120), X(I))
1575 P231 = FUNC(PP2(121), PP2(122), PP2(123), X(I))
1576 P232 = FUNC(PP2(124), PP2(125), PP2(126), X(I))
1577 P233 = FUNC(PP2(127), PP2(128), PP2(129), X(I))
1578 P3111= FUNC(PP2(130), PP2(131), PP2(132), X(I))
1579 P3112= FUNC(PP2(133), PP2(134), PP2(135), X(I))
1580 P3121= FUNC(PP2(136), PP2(137), PP2(138), X(I))
1581 P3122= FUNC(PP2(139), PP2(140), PP2(141), X(I))
1582 P3131= FUNC(PP2(142), PP2(143), PP2(144), X(I))
1583 P3132= FUNC(PP2(145), PP2(146), PP2(147), X(I))
1584 P3211= FUNC(PP2(148), PP2(149), PP2(150), X(I))
1585 P3212= FUNC(PP2(151), PP2(152), PP2(153), X(I))
1586 P3221= FUNC(PP2(154), PP2(155), PP2(156), X(I))
1587 P3222= FUNC(PP2(157), PP2(158), PP2(159), X(I))
1588 P3231= FUNC(PP2(160), PP2(161), PP2(162), X(I))
1589 P3232= FUNC(PP2(163), PP2(164), PP2(165), X(I))
1590 P3311= FUNC(PP2(166), PP2(167), PP2(168), X(I))
1591 P3312= FUNC(PP2(169), PP2(170), PP2(171), X(I))
1592 P3321= FUNC(PP2(172), PP2(173), PP2(174), X(I))
1593 P3322= FUNC(PP2(175), PP2(176), PP2(177), X(I))
1594 P333 = FUNC(PP2(178), PP2(179), PP2(180), X(I))
1595 P111= FP3 (P1111, P1112, .5D0, .1D0, STR)
1596 P112= FP3 (P1121, P1122, .5D0, .1D0, STR)
1597 P113= FP3 (P1131, P1132, .5D0, .1D0, STR)
1598 P121= FP3 (P1211, P1212, .7D0, .1D0, STR)
1599 P122= FP3 (P1221, P1222, .7D0, .1D0, STR)
1600 P132= FP3 (P1321, P1322, .9D0, .1D0, STR)
1601 P133= FP3 (P1331, P1332, .9D0, .1D0, STR)
1602 P211= FP3 (P2111, P2112, .1D0, .4D0, STR)
1603 P212= FP3 (P2121, P2122, .1D0, .4D0, STR)
1604 P213= FP3 (P2131, P2132, .1D0, .4D0, STR)
1605 P221= FP3 (P2211, P2212, .1D0, .6D0, STR)
1606 P222= FP3 (P2221, P2222, .1D0, .6D0, STR)
1607 P311= FP3 (P3111, P3112, .1D0, .2D0, STR)
1608 P312= FP3 (P3121, P3122, .1D0, .2D0, STR)
1609 P313= FP3 (P3131, P3132, .1D0, .2D0, STR)
1610 P321= FP3 (P3211, P3212, .1D0, .5D0, STR)
1611 P322= FP3 (P3221, P3222, .1D0, .5D0, STR)
1612 P323= FP3 (P3231, P3232, .1D0, .5D0, STR)
1613 P331= FP3 (P3311, P3312, .1D0, .7D0, STR)
1614 P332= FP3 (P3321, P3322, .1D0, .7D0, STR)
1615 P11= F6( P111, P112, P113, 1.5D0, 3.D0, 6.D0, HD)
1616 P12= F6( P121, P122, P123, 1.5D0, 3.D0, 6.D0, HD)
1617 P13= F6( P131, P132, P133, 1.5D0, 3.D0, 6.D0, HD)
1618 P21= F6( P211, P212, P213, 1.5D0, 3.D0, 6.D0, HD)
1619 P22= F6( P221, P222, P223, 1.5D0, 3.D0, 6.D0, HD)
1620 P23= F6( P231, P232, P233, 1.5D0, 3.D0, 6.D0, HD)

```

Appendix E: FORTRAN Program for Design of Shallow Tunnels constructed using
Pressurized Shield Methods (continued)

```

1621          P31= F6( P311, P312, P313, 1.5D0, 3.D0, 6.D0, HD)
1622          P32= F6( P321, P322, P323, 1.5D0, 3.D0, 6.D0, HD)
1623          P33= F6( P331, P332, P333, 1.5D0, 3.D0, 6.D0, HD)
1624          P1= F6( P11, P12, P13, T20, T30, T40,TPH)
1625          P2= F6( P21, P22, P23, T20, T30, T40,TPH)
1626          P3= F6( P31, P32, P33, T20, T30, T40,TPH)
1627          S(I)= F6(P1, P2, P3, 1.0D0, .8D0, .6D0, XK0)
1628          ENDIF
1629 10 CONTINUE
1630      S1= S(1)
1631      S2= S(2)
1632      S3= S(3)
1633      S4= S(4)
1634      S5= S(5)
1635      RETURN
1636      END
1637  C
1638  C
1639  C
1640  C
1641  C
1642  C
1643      SUBROUTINE PROFL( SS1, SS2, SS3, SS4, SS5
1644 *          , SS6, SS7, SS8, SS9, H)
1645      IMPLICIT REAL*8 ( A-H, O-Z)
1646      WRITE( 4, 1000) SS6* 1000.D0, SS7, SS8, SS9*100D0
1647      WRITE( 4, 1010)
1648          WRITE(4, 1020) 0.D0, SS1*SS6* 1000D0
1649          WRITE(4, 1020) 0.2D0* H, SS2*SS6* 1000D0
1650          WRITE(4, 1020) 0.4D0* H, SS3*SS6* 1000D0
1651          WRITE(4, 1020) 0.6D0* H, SS4*SS6* 1000D0
1652          WRITE(4, 1020) 0.8D0* H, SS5*SS6* 1000D0
1653 1000 FORMAT( ,X, 'CROWN SETTL.=', F10.5, 6X, 'U/Uref=', F10.5, /, 8X,
1654 *          'LAMBDA(crown)=', F10.5, 6X, '% STRESS RELEASE=', F10.5)
1655 1010 FORMAT( /, 8X, 2X, 'DEPTH', 3X, 'SETTLEMENT')
1656 1020 FORMAT( 8X, 2F10.5)
1657      RETURN
1658      END
1659  C
1660  C
1661  C
1662      SUBROUTINE TRIH( PH, HD, CD, XK0, P)
1663      IMPLICIT REAL*8 ( A-H, O-Z)
1664      COMMON/ TT/ PP3( 36)
1665      PI= 3.1415927D0
1666      IF( PH.EQ.0) THEN
1667          P1= F6( PP3( 1), PP3( 2), PP3( 3), 1.5D0, 3.0D0, 6.0D0, HD)
1668          P2= F6( PP3( 4), PP3( 5), PP3( 6), 1.5D0, 3.0D0, 6.0D0, HD)
1669          P3= F6( PP3( 7), PP3( 8), PP3( 9), 1.5D0, 3.0D0, 6.0D0, HD)
1670          P = F6( P1, P2, P3, 2.5D0, 1.25D0, 0.625D0, CD)
1671      ELSE
1672          T20= DTAN( 20* PI/ 180)
1673          T30= DTAN( 30* PI/ 180)
1674          T40= DTAN( 40* PI/ 180)

```

Appendix E: FORTRAN Program for Design of Shallow Tunnels constructed using
Pressurized Shield Methods (continued)

```

1675      TPH= DTAN( PHI* PI/ 180)
1676      P11= F6( PP3(10), PP3(11), PP3(12), 1.5D0, 3.0D0, 6.0D0, HD)
1677      P12= F6( PP3(13), PP3(14), PP3(15), 1.5D0, 3.0D0, 6.0D0, HD)
1678      P13= F6( PP3(16), PP3(17), PP3(18), 1.5D0, 3.0D0, 6.0D0, HD)
1679      P21= F6( PP3(19), PP3(20), PP3(21), 1.5D0, 3.0D0, 6.0D0, HD)
1680      P22= F6( PP3(22), PP3(23), PP3(24), 1.5D0, 3.0D0, 6.0D0, HD)
1681      P23= F6( PP3(25), PP3(26), PP3(27), 1.5D0, 3.0D0, 6.0D0, HD)
1682      P31= F6( PP3(28), PP3(29), PP3(30), 1.5D0, 3.0D0, 6.0D0, HD)
1683      P32= F6( PP3(31), PP3(32), PP3(33), 1.5D0, 3.0D0, 6.0D0, HD)
1684      P33= F6( PP3(34), PP3(35), PP3(36), 1.5D0, 3.0D0, 6.0D0, HD)
1685      P1= F6( P11, P12, P13, T20, T30, T40, TPH)
1686      P2= F6( P21, P22, P23, T20, T30, T40, TPH)
1687      P3= F6( P31, P32, P33, T20, T30, T40, TPH)
1688      P= F6( P1, P2, P3, 1.D0, 0.8D0, 0.6D0, XKO)
1689      ENDIF
1690      RETURN
1691      END
1692      C
1693      C
1694      C
1695      C
1696      HARTIMANN'S SOLUTION- FORCES
1697      SUBROUTINE HRT2 ( PHI, ZO, RO, ET, XNU, GAMA, XKO, ES, XNUS, AS,
1698      *                XIS, ALFAX, BETAX, XM, XN, Q)
1699      IMPLICIT REAL*8 ( A-H, O-Z)
1700      PI= 3.14159265
1701      PHI= PHI* PI/ 180.0D0
1702      X1= 1+XKO
1703      X2= 1-XKO
1704      X3= 3-4*XNU
1705      X4= 5-4*XNU
1706      ALFAX= ES* AS* ( 1+ XNU) / ET/ RO/ ( 1- XNUS* XNUS)
1707      BETAX= ES* XIS* ( 1+ XNU) / ET / RO** 3/ ( 1- XNUS* XNUS)
1708      XN11= X1* ( ALFAX+ BETAX)* GAMA* ZO* RO
1709      XN12= 2* ( 1+ ALFAX+ BETAX)
1710      XN1= XN11/ XN12
1711      XN21= X1* ALFAX* GAMA* RO* RO* DCOS( PHI)
1712      XN22= 4* ( 1+ ALFAX)
1713      XN2= XN21/ XN22
1714      XN31= X2* X3* ( ALFAX+ 3* BETAX+ 12* ALFAX* BETAX)*
1715      * GAMA* ZO* RO* DCOS( 2* PHI)
1716      XN32= 2* ( 1+ ( 3- 2* XNU)* ALFAX+ 3* BETAX* ( 5- 6* XNU+
1717      * 4* X3* ALFAX))
1718      XN3= XN31/ XN32
1719      XN41= X2* X3* ( ALFAX+ 4* BETAX+ 36* ALFAX* BETAX)*
1720      * GAMA* RO* RO* DCOS( 3* PHI)
1721      XN42= 4* ( 1+ X5* ALFAX+ 8* BETAX* ( 7- 8* XNU+
1722      * 9* X3* ALFAX))
1723      XN4= XN41/ XN42
1724      XN= XN1+ XN2+ XN3+ XN4
1725      XM11= X1* BETAX* GAMA* ZO* RO* RO
1726      XM12= 2* ( 1+ ALFAX+ BETAX)
1727      XM1= XM11/ XM12
1728      XM21= 3* X2* X3* ( 1+ 2* ALFAX)* BETAX* GAMA* ZO* RO* RO*
      * DCOS( 2* PHI)

```

Appendix E: FORTRAN Program for Design of Shallow Tunnels constructed using Pressurized Shield Methods (continued)

```

1729      XM22= 2* ( 1+ ( 3- 2* XNU)* ALFAX+ 3* BETAX*
1730      *      ( 5- 6* XNU- 4* X3* ALFAX) )
1731      XM2= XM21/ XM22
1732      XM31= X2* X3* ( 1+ 3* ALFAX)* BETAX* GAMA* RO* RO* RO*
1733      *      DCOS( 3* PHI)
1734      XM32= 1+ X4* ALFAX+ 8* BETAX* ( 7- 8* XNU+ 9* X3* ALFAX)
1735      XM3= XM31/ XM32
1736      XM= XM1+ XM2+ XM3
1737      Q11= -3* X2* X3* ( 1+ 2* ALFAX)* BETAX* GAMA* ZO*
1738      *      RO* DSIN( 2* PHI)
1739      Q12= 1+ ( 3- 2* XNU)* ALFAX+ 3* BETAX*
1740      *      ( 5- 6* XNU+ 4* X3* ALFAX)
1741      Q1= Q11/ Q12
1742      Q21= -3* X2* X3* ( 1+ 3* ALFAX)* BETAX* GAMA* RO*
1743      *      RO* DSIN( 3* PHI)
1744      Q22= 1+ X4* ALFAX+ 8* BETAX* ( 7- 8* XNU+ 9* X3* ALFAX)
1745      Q2= Q21/ Q22
1746      Q= Q1+ Q2
1747      RETURN
1748      END
1749      C
1750      C
1751      C
1752      C
1753      C
1754      SUBROUTINE FEND (N)
1755      IMPLICIT REAL*8 ( A-H, O-Z)
1756      C
1757      10 READ (N, 1000, END= 20)
1758      GOTO 10
1759      20 BACKSPACE (4)
1760      RETURN
1761      1000 FORMAT( 1X)
1762      END
1763      C
1764
1765      File NDATA.DAT
1766
1767      .1600026000      .0971421500      .0640636700      .0592716900      -.0033647150
1768      .0492345400      -.9177321000      -.1857097000      .1491511000      .0079954570
1769      -.1388935000      .5325237000      1.8112280000      .8289432000      1.3517440000
1770      .8405021000      .7932231000      .8506255000      1.2848020000      .4296901000
1771      .1701946000      .7270666000      .6566916000      .2262355000      .4266736000
1772      .4625817000      .2834676000      .4032087000      1.5251480000      .3593762000
1773      .1607589000      1.7069250000      1.9932610000      1.1167590000      1.3589120000
1774      1.5750390000      1.4398360000      1.2560210000      1.6143270000      1.2732060000
1775      .5620248000      1.4717130000      2.0291620000      .2964059000      .1500671000
1776      .7334012000      .5007696000      .3249731000
1777      .0330000000      1.8033490000      1.9939660000      .1636050000      2.8217980000
1778      .7863000000      .7592000000      .5830000000      .3270000000      .3262000000
1779      .3173000000      .7550000000      .8201000000      .8312000000      .5480000000
1780      .5055000000      .5052000000      .4223000000      .4197000000      .4096000000
1781      .7230000000      .7328000000      .7171000000      .4274000000      .4097000000
1782      .3575000000      .4416000000      .4484000000      .4207000000      .4323000000

```

Appendix E: FORTRAN Program for Design of Shallow Tunnels constructed using Pressurized Shield Methods (continued)

1783	.4574000000	.4258000000	.6814800000	.4015783000	-.2994168000
1784	-7.7340090000	.3283183000	.1609817000	-.1156048000	.2130000000
1785	-.1314524000	1.3523570000	.8068070000	1.5835410000	1.7262410000
1786	.1643000000	.1959000000	.3175000000	.5378000000	.5428000000
1787	.5517000000	.0791000000	.0558000000	.0476000000	.3849000000
1788	.4191000000	.4630000000	.5317000000	.5380000000	.5500000000
1789	.2316000000	.2234000000	.2256000000	.5208000000	.5446000000
1790	.6118000000	.4977000000	.5015000000	.5227000000	.5090000000
1791	.4914000000	.4880000000	-.0429246700	-.0128745000	.0584250000
1792	.3244609000	-.0346085000	-.1485150000	.0163935200	.2880000000
1793	.2505000000	-.0464058400	-.0498460900	-.0157630900	.0066380460
1794	5.8485000000	5.5995000000	2.9017000000	2.2039000000	2.3007000000
1795	2.2334000000	4.2389000000	6.3141000000	6.4333000000	3.0527000000
1796	2.8752000000	3.6081000000	3.4086000000	3.4339000000	3.4225000000
1797	3.5999000000	3.8938000000	3.6040000000	4.2706000000	4.4999000000
1798	5.1904000000	4.0454000000	4.6854000000	4.0515000000	4.0270000000
1799	4.3206000000	3.2546000000	.0016708800	.0003243900	-.0028200000
1800	1.0058190000	.0015922270	.0006477335	-.0007881364	.1660000000
1801	-.1183333000	2.7573700000	3.2514890000	1.4487560000	1.7869470000
1802	-.9192000000	-1.8853000000	1.5671000000	1.3714000000	1.1162000000
1803	1.0538000000	-2.7928000000	-6.6624000000	-5.5703000000	2.9276000000
1804	3.6904000000	5.5775000000	3.2167000000	2.6640000000	2.1201000000
1805	-2.8499000000	-3.9446000000	-3.8964000000	4.9524000000	5.3435000000
1806	5.6765000000	5.6946000000	3.7948000000	4.5578000000	5.0692000000
1807	4.2243000000	4.6773000000	-.0000249300	.0000000000	.0000462000
1808	2.1419250000	-.0000259000	-.0000101000	.0000126900	.0170000000
1809	.0142857100	.6974082000	.2395345000	1.4913750000	1.2995820000
1810	15.2721000000	18.2108000000	5.6710000000	4.4509000000	4.9612000000
1811	5.0694000000	4.6785000000	8.7052000000	7.8069000000	9.9043000000
1812	6.8780000000	17.3331000000	12.6102000000	14.5739000000	15.7848000000
1813	14.5303000000	15.8681000000	11.6415000000	9.1674000000	10.7461000000
1814	17.2042000000	6.1024000000	10.6789000000	8.2557000000	7.6430000000
1815	10.4066000000	3.4674000000	.6000000000	.8000000000	1.0000000000
1816	6.0000000000	3.0000000000	1.5000000000	.2204000000	.7935000000
1817	1.4106000000	.1820000000	.4914000000	.1443000000	.2174000000
1818	.1259000000	.1401000000			
1819	-9.5471227000	-2.4957755000	0.4006770700	-5.4803145000	-6.1540912000
1820	0.1624935300	-0.0020076933	0.1781538500	-0.0388845910	-0.4494333000
1821	-0.7638702100	1.3091229000	-0.3833905500	-1.2088930000	0.8272030900
1822	-0.0004895650	0.0966155300	-0.4179649700	-0.0030983044	-0.0131409240
1823	0.6508545300	0.0016025580	-0.0240384130	0.4262819500	-0.0473290600
1824	0.4657051300	-1.2260684000	-0.0902883360	0.9022919500	-2.7735421000
1825	-0.0071693440	0.3188258300	2.4413799000	0.0054824583	-0.0570820370
1826	2.7218781000	-1.3544891000	2.3026316000	-1.9735843000	-0.0328947250
1827	0.3405571600	0.4237619300	-0.5998454700	-0.0548245810	0.6056503000
1828	-1.5724977000	0.1006194100	-0.0164473770	0.2563855500	-1.3738394000
1829	-2.4767770000	-0.0164473470	0.2292955000	-1.3428789000	-0.7120745200
1830	1.0446000000	1.0663000000	1.0780000000	1.1421000000	1.1719000000
1831	1.2782000000	1.5116000000	1.5825000000	1.8176000000	1.2808000000
1832	1.3143000000	1.3071000000	1.3973000000	1.4066000000	1.4249000000
1833	1.4518000000	1.5110000000	1.4981000000	1.0092000000	1.0210000000
1834	1.0135000000	0.9992000000	1.0105000000	1.0055000000	1.4692000000
1835	1.4517000000	1.3641000000			
1836	-0.2599895800	0.2308981400	-0.2095397000	-0.1771655400	0.1843268400

Appendix E: FORTRAN Program for Design of Shallow Tunnels constructed using
Pressurized Shield Methods (continued)


```

1837 -0.1807897100 -0.1362154900 0.2391451800 -0.2384959800 -0.3408626400
1838 0.3581488600 -0.3049507800 -0.2633070700 0.2137655600 -0.1913465700
1839 -0.1365293400 0.1013794000 -0.1007201700 -0.0864084870 0.3093141300
1840 -0.3093047100 -0.0864084870 0.3093141300 -0.3093047100 -0.2564090500
1841 0.2316548200 -0.2114132801 -0.2525884500 0.1715301400 -0.1524481300
1842 -0.1623711300 0.1548313900 -0.1527164600 -0.0944292880 0.2147555100
1843 -0.2147303400 -0.1385947100 0.2392142000 -0.2399532900 -0.2068508000
1844 0.2328729300 -0.2249214900 -0.2180963900 0.1726191900 -0.1624167600
1845 -0.1185318800 0.1637530400 -0.1435362400 -0.1419165200 0.1261511600
1846 -0.1252806200 -0.0777089230 0.1152511200 -0.1152636900 -0.1514671500
1847 0.2782268500 -0.2768693300 -0.136.842700 0.1134090700 -0.1127549500
1848 -0.2279160600 0.1847054700 -0.1722746500 -0.1052505300 0.1093720700
1849 -0.1092973100 -0.1374113600 0.1099709300 -0.1092803700 -0.1013802800
1850 0.1456717200 -0.1457237400 -0.2168584100 0.1706481600 -0.1607093100
1851 -0.0835275820 0.3849797800 -0.3849734700 -0.1130720000 0.0623857160
1852 -0.0622603330 -0.0864084870 0.3444204600 -0.3444110500 -0.0977428830
1853 0.1099518900 -0.1099158500 -0.1988161500 0.1134227100 -0.1070824100
1854 -0.1959146200 0.0477350760 -0.0416642730 -0.1334392000 0.0939446540
1855 -0.0945673140 -0.1515380600 0.0586890080 -0.0573272820 -0.1026269100
1856 0.1244547900 -0.1244061500 -0.2370878800 0.4245396700 -0.4098093200
1857 -0.1905470800 0.1046179500 -0.0993601680 -0.1894143200 0.0616430790
1858 -0.0565477540 -0.1674795900 0.1622017200 -0.1596497100 -0.1795693100
1859 0.1283403300 -0.1245255800 -0.1127211600 0.1301777500 -0.1303180900
1860 -0.1833120500 0.0775280830 -0.0732539710 -0.1292328700 0.0732272120
1861 -0.0727912560 -0.1343475400 0.1992923500 -0.1987070400 -0.1998708500
1862 0.0958218610 -0.0891056480 -0.1740926900 0.0275971850 -0.0243954630
1863 -0.1586941900 0.1254674600 -0.1236337800 -0.1403407700 0.0442715920
1864 -0.0434672720 -0.1027215700 0.1248252500 -0.1248844200 -0.1322233500
1865 0.1292973900 -0.1287780600 -0.2391261700 0.1431943700 -0.1309247900
1866 -0.1614086100 0.0171498090 -0.0151111360 -0.1339638000 0.0863529130
1867 -0.0869258680 -0.1821441000 0.0892996710 -0.0851724820 -0.1071733200
1868 0.1384235600 -0.1385122200 -0.1530956800 0.1659843800 -0.1645280900
1869 -0.1998708500 0.0958218610 -0.0891056480 -0.2203687100 0.0675911200
1870 -0.0568947340 -0.1337843000 0.0863665100 -0.0869337560 -0.1509702600
1871 0.0643983020 -0.0630699570 -0.1346623700 0.1755088400 -0.1761044200
1872 2.2660000000 3.1250000000 4.5310000000 2.3050000000 2.9590000000
1873 4.2970000000 2.0120000000 2.7340000000 4.5310000000 1.5430000000
1874 2.9690000000 4.6480000000 1.8750000000 2.5000000000 4.6880000000
1875 1.9530000000 3.0470000000 4.5310000000 1.4460000000 2.3440000000
1876 3.7890000000 1.4650000000 2.4220000000 3.9060000000 1.4850000000
1877 2.5390000000 4.0630000000 1.2110000000 2.1090000000 3.5160000000
1878 1.2110000000 2.1880000000 3.5160000000 1.2170000000 2.1880000000
1879 3.5160000000
1880
1881 File ABC.DAT
1882
1883 -1. 0. 0. 2. 0. 0. 0. 0. 1.
1884 2. 0. 0. -2. 0. 0. 0. 0. 0.
1885 -1. 0. 12. 0. 36. -2. -18. -48. 0.
1886 1. 3. 15. 0. 36. -2. -18. -48. 0.
1887 1. 2. 8. 0. 0. 0. 0. 0. 1.
1888 1. 5. 56. 0. 216. -4. -64. -288. 0.
1889 3. 6. 18. 0. 36. -2. -18. -48. 0.
1890 1. 3. 15. 0. 36. -2. -18. -48. 0.

```

Appendix E: FORTRAN Program for Design of Shallow Tunnels constructed using
Pressurized Shield Methods (continued)

1891	-2.	-7.	-64.	0.	-216.	4.	64.	288.	1.
1892	1.	5.	56.	0.	216.	-4.	-64.	-288.	0.
1893	-1.	0.	0.	0.	0.	0.	0.	0.	0.
1894	1.	1.	1.	0.	0.	0.	0.	0.	0.
1895	1.	0.	0.	-2.	0.	-1.	0.	0.	1.
1896	2.	2.	0.	-2.	0.	-2.	0.	0.	0.
1897	2.	0.	30.	0.	36.	4.	-36.	-48.	0.
1898	1.	3.	15.	0.	36.	-2.	-18.	-48.	0.
1899	-2.	-1.	-112.	0.	-216.	-4.	128.	288.	1.
1900	2.	10.	112.	0.	432.	-8.	-128.	-576.	0.
1901	-1.	0.	0.	0.	0.	0.	0.	0.	0.
1902	1.	1.	1.	0.	0.	0.	0.	0.	0.
1903	2.	1.	0.	0.	0.	0.	0.	0.	1.
1904	2.	2.	0.	0.	0.	0.	0.	0.	0.
1905	-2.	0.	-30.	0.	-36.	-4.	36.	48.	0.
1906	1.	3.	15.	0.	36.	-2.	-18.	-48.	0.
1907	2.	1.	112.	0.	216.	4.	-128.	-288.	1.
1908	2.	10.	112.	0.	432.	-8.	-128.	-576.	0.
1909	3.	3.	45.	0.	72.	2.	-54.	-96.	0.
1910	1.	3.	15.	0.	36.	-2.	-18.	-48.	0.
1911	0.	0.	0.	0.	0.	0.	0.	0.	0.
1912	1.	0.	0.	0.	0.	0.	0.	0.	0.
1913	0.	0.	0.	0.	0.	0.	0.	0.	0.
1914	1.	0.	0.	0.	0.	0.	0.	0.	0.
1915	-1.	3.	-15.	0.	0.	-6.	18.	0.	0.
1916	1.	3.	15.	0.	36.	-2.	-18.	-48.	0.
1917	0.	0.	0.	0.	0.	0.	0.	0.	0.
1918	1.	0.	0.	0.	0.	0.	0.	0.	0.
1919	-1.	0.	0.	0.	0.	0.	0.	0.	0.
1920	1.	1.	1.	0.	0.	0.	0.	0.	0.
1921	0.	0.	0.	0.	0.	0.	0.	0.	0.
1922	1.	0.	0.	0.	0.	0.	0.	0.	0.
1923	-2.	0.	-30.	0.	-36.	-4.	36.	48.	0.
1924	1.	3.	15.	0.	36.	-2.	-18.	-48.	0.
1925	0.	0.	0.	0.	0.	0.	0.	0.	0.
1926	1.	0.	0.	0.	0.	0.	0.	0.	0.
1927	-1.	0.	0.	0.	0.	0.	0.	0.	0.
1928	1.	1.	1.	0.	0.	0.	0.	0.	0.
1929	0.	0.	0.	0.	0.	0.	0.	0.	0.
1930	1.	0.	0.	0.	0.	0.	0.	0.	0.
1931	2.	0.	30.	0.	36.	4.	-36.	-48.	0.
1932	1.	3.	15.	0.	36.	-2.	-18.	-48.	0.
1933	0.	0.	0.	0.	0.	0.	0.	0.	0.
1934	1.	0.	0.	0.	0.	0.	0.	0.	0.
1935	1.	0.	0.	-2.	0.	0.	0.	0.	1.
1936	2.	0.	0.	-2.	0.	0.	0.	0.	0.
1937	-1.	0.	12.	0.	36.	-2.	-18.	-48.	0.
1938	1.	3.	15.	0.	36.	-2.	-18.	-48.	0.
1939	-1.	-2.	-8.	0.	0.	0.	0.	0.	1.
1940	1.	5.	56.	0.	216.	-4.	-64.	-288.	0.
1941	3.	6.	18.	0.	36.	-2.	-18.	-48.	0.
1942	1.	3.	15.	0.	36.	-2.	-18.	-48.	0.
1943	2.	7.	64.	0.	216.	-4.	-64.	-288.	1.
1944	1.	5.	56.	0.	216.	-4.	-64.	-288.	0.

Appendix E: FORTRAN Program for Design of Shallow Tunnels constructed using
Pressurized Shield Methods (continued)

1945	-1.	0.	0.	0.	0.	0.	0.	0.	0.
1946	1.	1.	1.	0.	0.	0.	0.	0.	0.
1947	-1.	0.	0.	2.	0.	1.	0.	0.	1.
1948	2.	2.	0.	-2.	0.	-2.	0.	0.	0.
1949	2.	0.	30.	0.	36.	4.	-36.	-48.	0.
1950	1.	3.	15.	0.	36.	-2.	-18.	-48.	0.
1951	2.	1.	112.	0.	216.	4.	-128.	-288.	1.
1952	2.	10.	112.	0.	432.	-8.	-128.	-576.	0.
1953	-1.	0.	0.	0.	0.	0.	0.	0.	0.
1954	1.	1.	1.	0.	0.	0.	0.	0.	0.
1955	-2.	-1.	0.	0.	0.	0.	0.	0.	1.
1956	2.	2.	0.	0.	0.	0.	0.	0.	0.
1957	-2.	0.	-30.	0.	-36.	-4.	36.	48.	0.
1958	1.	3.	15.	0.	36.	-2.	-18.	-48.	0.
1959	-2.	-1.	-112.	0.	-216.	-4.	128.	288.	1.
1960	2.	10.	112.	0.	432.	-8.	-128.	-576.	0.

1961

1962 **File SHLD2.DAT**

1963

1964	.00616	-.00181	-2.28144	1.12211	-.00212	-.12194
1965	-.10359	.02620	28.03099	-13.79419	.03186	1.49905
1966	.95832	-.16238	-17.00942	6.61744	-.37099	.81395
1967	-.00201	.00092	.00799	-.00300	.00045	.00209
1968	.02515	-.01076	-.07240	.02428	-.00777	-.01449
1969	.24377	-.12438	2.39077	-1.24705	.25403	.86398
1970	-.00318	.00067	.42832	-.20628	.00137	.02422
1971	.04770	-.01162	-5.20009	2.50583	-.02357	-.27437
1972	.11534	-.09141	9.74742	-5.15029	-.28405	1.82854
1973	-.01091	.01772	-.08418	.04630	.00356	-.01867
1974	.12149	-.20369	1.36650	-.75088	-.05798	.27039
1975	.27407	-.15983	4.31583	-2.18276	-.10053	.06359
1976	-.01927	.03915	.00076	-.00257	-.00016	.00010
1977	.16655	-.37289	-.01565	.04439	.00207	-.01117
1978	-.06886	-.05009	-2.02813	.61858	.10331	-.07736
1979	-.02747	.03307	-.00464	.00520	-.00151	-.04069
1980	.29106	-.33326	.07563	-.08470	.02772	.54930
1981	-.12815	-.17694	-2.79076	1.14892	-.65811	-1.01871
1982	-.09751	-.05836	.18202			
1983	.37507	.78064	.56610			
1984	1356.01683	-306.45943	-607.02338			
1985	-4.58077	2.80582	1.20644			
1986	10.27782	-22.17239	-9.91671			
1987	303.22511	-24.96859	-75.47406			
1988						